

# Université de Lille

Faculté des Sciences et Technologies

Ecole Doctorale 104 – Sciences de la Matière, du Rayonnement, et de  
l'Environnement

et

**V. N. Karazine Université Nationale de Kharkiv (Ukraine)**

Faculté de Chimie

## Thèse de Doctorat en Cotutelle

par

**Yevhenii VAKSLER**

pour l'obtention du titre de

**Docteur de l'Université de Lille**

Discipline: Chimie théorique, physique, analytique

Synthèse, structure et propriétés des modifications polymorphiques de molécules bioactives

A soutenir le 28 Mai 2021 devant le jury:

<b>Yury BUDKOV</b> <i>Professeur, G.A. Krestov Institut de la Chimie des Solutions (Russie)</i>	<b>Rapporteur</b>
<b>Thierry TASSAING</b> <i>Professeur, Université de Bordeaux</i>	<b>Rapporteur</b>
<b>Abdenacer IDRISSE</b> <i>Professeur, Université de Lille</i>	<b>Directeur de thèse</b>
<b>Svitlana SHISHKINA</b> <i>HDR, V. N. Karazine Université Nationale de Kharkiv (Ukraine)</i>	<b>Co-directrice de thèse</b>
<b>Frédéric AFFOUARD</b> <i>Professeur, Université de Lille</i>	<b>Président</b>
<b>Natalia CORREIA</b> <i>HDR, Université de Lille</i>	<b>Examineur</b>
<b>Francesca INGROSSO</b> <i>HDR, Université de Lorraine</i>	<b>Examineur</b>
<b>Oleg KALUGIN</b> <i>Professeur, V. N. Karazine Université Nationale de Kharkiv (Ukraine)</i>	<b>Examineur</b>
<b>Sergiy KOVALENKO</b> <i>Professeur, V. N. Karazine Université Nationale de Kharkiv (Ukraine)</i>	<b>Examineur</b>



# University of Lille

Faculty of Sciences and Technologies

Doctoral School 104 – Science of the Matter, of the Radiation, and of  
the Environment

and

**V.N. Karazin Kharkiv National University (Ukraine)**

Chemical Faculty

## Co-tutorial Doctoral Thesis

by

**Yevhenii VAKSLER**

to obtain the degree of

**Doctor of the University of Lille**

Discipline: Theoretical, physical, analytical chemistry

Synthesis, structure and properties of polymorphic modifications of bioactive molecules
---

To be defended on 28 May 2021 before the jury:

<b>Yury BUDKOV</b> <i>Professor, G.A. Krestov Institute of Solution Chemistry (Russia)</i>	<b>Referee</b>
<b>Thierry TASSAING</b> <i>Professor, University of Bordeaux</i>	<b>Referee</b>
<b>Abdenacer IDRISSI</b> <i>Professor, University of Lille</i>	<b>Supervisor</b>
<b>Svitlana SHISHKINA</b> <i>Assistant Professor, V.N. Karazin Kharkiv National University (Ukraine)</i>	<b>Co-supervisor</b>
<b>Frédéric AFFOUARD</b> <i>Professor, University of Lille</i>	<b>President</b>
<b>Natalia CORREIA</b> <i>Assistant Professor, University of Lille</i>	<b>Examiner</b>
<b>Francesca INGROSSO</b> <i>Assistant Professor, University of Lorraine</i>	<b>Examiner</b>
<b>Oleg KALUGIN</b> <i>Professor, V.N. Karazin Kharkiv National University (Ukraine)</i>	<b>Examiner</b>
<b>Sergiy KOVALENKO</b> <i>Professor, V.N. Karazin Kharkiv National University (Ukraine)</i>	<b>Examiner</b>



## ACKNOWLEDGEMENTS

This work was done in the framework of co-tutorial agreement between the University of Lille and V. N. Karazin Kharkiv National University, namely, the laboratory LASIRE, headed by Prof. Hervé VEZIN, and the Department of Inorganic Chemistry, headed by Prof. Ivan VYUNNIK, on par with Chemical Faculty, headed by Prof. Oleg KALUGIN. Hereby I thank these institutions for providing me with a chance to pursue my PhD studies. I am grateful to all the sources of financial support, namely, the Ukrainian government for the basic doctoral scholarship, the Embassy of France in Ukraine and the Campus France for the co-tutorial PhD scholarship, French and Ukrainian governments for the “ERASMUS+” scholarship, as well as Campus France itself and program “PHC Kolmogorov” for short-term research visits to G.A. Krestov Institute of Solution Chemistry (RAS, Russia).

I thank my supervisors, Prof. Abdenacer IDRISSE and Asst. Prof. Svitlana SHISHKINA, which allowed this fusion of scientific topics to come true. I express my gratitude to both of them for doing their best in the creation of a pleasant scientific atmosphere, for their wise and methodical guidance and advice. Their different views let me see many sides of the research topic and I appreciate the possibility to study from them.

The referees of this thesis, Profs. Yury BUDKOV and Thierry TASSAING, are gratefully acknowledged for taking their time and efforts to examine my thesis.

Thanks should be given to the research teams I belong to, specifically, of the laboratory LASIRE from the University of Lille and the Department of X-ray Diffraction Studies and Quantum Chemistry from the Institute for Single Crystals (NAS, Ukraine), as well as to the Laboratory 1-2 of “NMR-spectroscopy and numerical investigation methods of liquids” from G.A. Krestov Institute of Solution Chemistry (RAS, Russia). I am especially grateful to Asst. Prof. Roman OPARIN for scientific guidance. Many thanks

should be said to Frederic CAPET, Florence DANEDE, Isabelle DE WAELE, Alexey DYSHIN, Michael KISELEV, Myriam MOREAU, Jean-Pierre VERWAERDE and Oleg ZHIKOL for their help in my researches.

Finally, my deepest gratitude is given to my family and beloved Anastasiya for their support and warm attitude.

# RESUME

Les ingrédients pharmaceutiques actifs peuvent conserver leurs propriétés indéfiniment à l'état solide. En conséquence, de nombreux médicaments sont produits et stockés dans la phase solide la plus stable parmi celles connues. Cependant, plus de 50% des médicaments à l'état solide peuvent avoir plus d'une modification polymorphe. Différentes formes polymorphiques du même composé peuvent posséder des propriétés différentes, qui affectent de manière significative l'efficacité d'un médicament, ses capacités à être fabriqué et stocké. Le contrôle du polymorphisme des ingrédients pharmaceutiques actifs est un problème relativement nouveau, dont les réglementations commencent à peine à se développer. Pour parvenir à une surveillance efficace des propriétés lors de la production et des caractéristiques prévisibles des formes posologiques, il est nécessaire de contrôler les causes profondes du polymorphisme. Il s'agit d'un changement de conformation de la molécule et / ou de la formation d'un nouvel ensemble d'interactions intermoléculaires.

Dans la première partie de cette thèse, deux méthodes expérimentales du contrôle de la composition polymorphe des ingrédients pharmaceutiques actifs et de leur cristallisation sélective à partir du dioxyde de carbone supercritique sont présentées. Le premier est le suivi des conformations de molécules bioactives par spectroscopies infrarouges et Raman *in situ*. Les relations entre les conformations en solution et les modifications polymorphes recristallisées sont illustrées dans l'exemple de l'acide méfénamique et de la carbamazépine, substances particulièrement sensibles au polymorphisme. La deuxième méthode complémentaire permet de cultiver des monocristaux d'haute qualité directement à partir de la solution dans le dioxyde de carbone, de déterminer leur structure par diffraction des rayons X sur monocristaux et, par conséquent, d'établir précisément une référence pour des méthodes rapides d'analyse de composition polymorphe (analyse vibrationnelle, thermique, etc.). Il est étudié pour un co-cristal d'acide méfénamique et de nicotinamide (vitamine B3).

Dans la deuxième partie de la thèse, l'approche est proposée pour l'analyse de la réponse mécanique des formes polymorphiques individuelles et de la probabilité de leurs transformations sous des influences extérieures (pression, broyage, etc.) et en cas de faible stabilité d'une forme cristalline. C'est une méthode multi-étape où les calculs des énergies d'interaction par paires dans les cristaux permettent d'identifier les fragments les plus fortement liés d'arrangements cristallins (unités de construction, colonnes, couches, etc.). L'unité de construction et une partie de la couche voisine sont utilisés comme système modèle pour l'étude ultérieure. Les directions probables du cisaillement des couches moléculaires sont supposées à partir de l'analyse topologique. La dernière étape consiste en des calculs quantiques et chimiques précis des profils d'énergie de décalage et des barrières pour le déplacement des couches dans ces directions. Cette approche est appliquée aux médicaments populaires: l'aspirine, le paracétamol et l'ibuprofène.



# RESUME

Active pharmaceutical ingredients can retain their properties indefinitely in a solid state. As a result, numerous drugs are produced and stored in the most stable solid phase among the known ones. However, more than 50% of solid-state drugs may have more than one polymorphic modification. Different polymorphic forms of the same compound can possess different properties, which affect significantly the effectiveness of a drug, its abilities to be manufactured and stored. The control of polymorphism in active pharmaceutical ingredients is a relatively new approaching problem, whose regulations just start to develop. To achieve effective monitoring of the properties during the production and dosage forms predictable characteristics, it is necessary to control the root causes of polymorphism. They are a molecule conformational change and / or the formation of a new set of intermolecular interactions.

In the first part of this thesis, two experimental methods for the control over the polymorphic composition of the active pharmaceutical ingredients and their selective crystallization from the supercritical carbon dioxide are presented. The first is the monitoring of the conformations of bioactive molecules with *in situ* infrared and Raman spectroscopies. The relationships between conformations in solution and recrystallized polymorphic modifications are shown in the example of mefenamic acid and carbamazepine, substances especially susceptible to polymorphism. The second complementary method allows one to grow high-quality single crystals directly from the solution in carbon dioxide, to determine their structure by single-crystal X-ray diffraction and, as a result, to clearly establish a reference for fast methods of analysis of polymorphic composition (vibrational, thermal analysis, etc.). It is studied for a co-crystal of mefenamic acid and nicotinamide (vitamin B3).

In the second part of the current thesis, the approach for the analysis of mechanical response of individual polymorphic forms and the probability of their transformations under external influences (pressure, milling, etc.) and in case of low stability of a crystalline form is proposed. It is a multi-step method, where calculations of the pairwise interaction energies in crystals allow to identify the most strongly bound fragments of crystalline arrangements (building units, columns, layers, etc.). The building unit and a part of the neighboring layer are used as a model system for the further study. The probable directions of molecular layers shear are assumed from topological analysis. The final step is precise quantum-chemical calculations of shift energy profiles and barriers for the layers displacement in these directions. This approach is applied to popular drugs: aspirin, paracetamol and ibuprofen.



# TABLE OF CONTENTS

<b>CHAPTER 1. GENERAL INTRODUCTION .....</b>	<b>14</b>
1.1. State of a problem.....	15
1.2. Solid-state classification .....	21
1.3. Formation and transformation of crystalline forms .....	28
1.4. Methods for solid forms synthesis.....	34
1.5. Crystallization from supercritical fluids.....	37
1.6. Mechanically induced polymorphic transformations .....	40
1.7. Methods for the identification of polymorphic forms .....	45
1.8. Quantum-chemical modelling of properties in the solid state .....	48
1.9. Conclusions .....	59
1.10. References for Chapter 1 .....	61
<b>CHAPTER 2. EXPERIMENTAL AND COMPUTATIONAL DETAILS .....</b>	<b>84</b>
2.1. Objects of the investigation .....	85
2.2. Vibrational analysis .....	92
2.2.1. <i>In situ</i> infrared spectroscopy.....	92
2.2.2. <i>In situ</i> Raman spectroscopy .....	96
2.2.3. Micro infrared spectroscopy .....	97
2.2.4. Diffuse reflectance infrared Fourier transform spectroscopy .....	97
2.2.5. Micro Raman spectroscopy .....	98
2.3. Microscopic observations of sample changes.....	99
2.4. Single-crystal X-ray diffraction .....	100
2.5. Powder X-ray diffraction.....	101
2.6. Quantum-chemical calculations .....	101
2.6.1. Conformation analysis and frequency assignment .....	101
2.6.2. Analysis of polymorphic modifications structure .....	103
2.6.2.1. Crystal structure analysis from the energetic viewpoint .....	103
2.6.2.2. Comparison of experimental and optimized in solid state structures.....	105
2.7. References for Chapter 2 .....	107
<b>CHAPTER 3. CONTROL OF THE POLYMORPHISM OF ACTIVE PHARMACEUTICAL INGREDIENTS CRYSTALLIZING FROM SUPERCRITICAL CO<sub>2</sub>.....</b>	<b>117</b>
3.1. Polymorphism and conformations of mefenamic acid in supercritical carbon dioxide .....	118
3.1.1. Recrystallization of mefenamic acid through sublimation .....	118
3.1.2. Recrystallization of mefenamic acid being in contact with supercritical CO <sub>2</sub> phase: <i>in situ</i> Raman spectroscopy .....	119
3.1.3. Choice of analytical spectral domains for <i>in situ</i> infrared spectroscopy .....	122
3.1.4. Assignment of spectral contributions .....	125

3.1.5. Analysis of mefenamic acid conformers in CO <sub>2</sub> phase: <i>in situ</i> infrared spectroscopy.....	129
3.1.6. Analysis of crystalline mefenamic acid obtained by crystallization from a binary mixture of [mefenamic acid - supercritical CO <sub>2</sub> ].....	137
<b>3.2. High-temperature recrystallization of carbamazepine in supercritical CO<sub>2</sub>: a way to obtain pure polymorph I.....</b>	<b>139</b>
3.2.1. Visual analysis of the changes in the carbamazepine sample.....	140
3.2.2. Assignment of spectral contributions and analytical spectral domains .....	141
3.2.3. Analysis of carbamazepine conformers in CO <sub>2</sub> phase: <i>in situ</i> infrared spectroscopy .....	145
3.2.3.1. Temperature range of 110-150°C.....	145
3.2.3.2. Temperature range of 150-170°C.....	148
3.2.3.1. Temperature range of 170-200°C.....	149
3.2.4. Micro Raman spectroscopy analysis .....	151
<b>3.3. Supercritical fluids for the synthesis of single crystals .....</b>	<b>154</b>
3.3.1. High-pressure high-temperature reactor.....	154
3.3.2. Effect of temperature, solid mixture composition and time duration of the co-crystallization process.....	156
3.3.3. Comparison with the rapid expansion of supercritical solution experiment .....	159
3.3.4. Synthesis of single crystals of the mefenamic acid : nicotinamide co-crystal.....	161
<b>3.4. Conclusions .....</b>	<b>165</b>
<b>3.5. References for Chapter 3 .....</b>	<b>167</b>
<b>CHAPTER 4. ANALYSIS OF SOLID-SOLID POLYMORPHIC TRANSFORMATIONS .....</b>	<b>170</b>
<b>4.1. Quantum-chemical modeling of mechanical properties of aspirin polymorphic modifications.....</b>	<b>171</b>
4.1.1. The crystal packing analysis based on the study of pairwise interaction energies between building units.....	171
4.1.2. Modeling of the slip deformation in the crystals.....	178
4.1.2.1. Details on calculations.....	178
4.1.2.2. Formation of the method .....	179
4.1.3. Verification of the proposed model by the study of a slip deformation in the aspirin polymorphic structures I and II .....	182
4.1.4. Prediction of a slip deformation in polymorphic structure IV of aspirin.....	185
<b>4.2. High-pressure polymorphic transition in piracetam crystals: studying by quantum-chemical methods .....</b>	<b>187</b>
4.2.1. Preliminary assessment of the possibility of displacement of strongly bound crystal fragments.....	188

4.2.2. Characterization of the crystal structure .....	191
4.2.3. Study of the initial crystal structure of piracetam using quantum-chemical methods .....	194
4.2.3.1. Crystal structure analysis from the pairwise interaction energies viewpoint .....	194
4.2.3.2. Modeling of a shear deformation by quantum-chemical methods .....	198
4.2.4. Study of the pressure influence on piracetam crystal structures using quantum-chemical methods .....	201
4.2.4.1. The analysis of crystal structures under different pressures from the energetic viewpoint .....	202
4.2.4.2. Modeling of shear deformation in the crystal structures under different pressures .....	207
4.2.4.3. The study of interaction energy components using the Localized Molecular Orbital Energy Decomposition Analysis .....	208
<b>4.3. Computational analysis of pressure-induced shear in R,S-ibuprofen .....</b>	<b>212</b>
4.3.1. Comparison of experimental and optimized in solid state structures .....	212
4.3.2. Analysis of basic structural motives from an energetic viewpoint .....	218
4.3.3. Topological analysis of molecular shear in crystals of ibuprofen .....	226
4.3.4. Quantum-chemical calculation of shear probability .....	238
<b>4.4. Conclusions .....</b>	<b>244</b>
<b>4.5. References for Chapter 4 .....</b>	<b>247</b>
<b>4.6. Chapter 4 Appendix .....</b>	<b>249</b>
<b>CONCLUSIONS AND PERSPECTIVES .....</b>	<b>352</b>

# Chapter 1. General introduction

## 1.1. State of a problem

Bioactive molecules are kind of chemicals that have actions in the human body promoting good health. Usually, small amounts of them can be found in plants, fungi or other living organisms, but they can be collected and concentrated producing active pharmaceutical ingredients (APIs). Such ingredients are the substances used in drugs and intended to furnish pharmacological activity or to otherwise have direct effect in the diagnosis, cure, mitigation, treatment or prevention of disease, or to have direct effect in restoring, correcting or modifying physiological functions in human beings. The drugs made of APIs with other excipients can be delivered in numerous forms: solutions, aerosols or even gaseous mixtures, but the vast majority of drugs are delivered in the solid form [1]. Recent assessments [2, 3] have shown that more than 70% of all the APIs are used in a solid state.

It seems logical, that the solids are the most used among all the possibilities to produce and spread the medications. They seem the most stable and easy to handle, but the solids same from the first glance may not coincide in structure and, thus, in properties. Time to time differences in structure may also cause differences in solids exterior. This effect is not reliable and cannot be used to signal the presence of differences [4-6], but in 1832 this phenomenon was observed in practice by F. Wöhler and J. von Liebig for benzamide [7] creating a question of “miraculous transformations of crystals”. The causes of the issue remained unclear until in 1916 L. Vegard experimentally showed the existence of the different modifications of  $\text{TiO}_2$ : rutile, anatase and brookite [8]. The ability of substances to form more than one crystalline phase with varying long-range order was proved and later called polymorphism (or allotropy, when referred to a chemical element). For a long time, the APIs polymorphism was not a subject of investigations. Differences in the properties of solid drugs have

not been considered as the consequences of distinctions in crystalline arrangements of basic APIs.

Aspirin, an anti-inflammatory drug, became the first object [9], of investigations that show that the polymorphic modifications (forms) of APIs are possible as for other substances (TiO<sub>2</sub>, benzamide, etc.), but their analysis for APIs is more complex. These investigations attracted the attention to polymorphism and proved the thought of W.C. McCrone that "...the number of forms known for that compound is proportional to the time and money spent in research on that compound." [10]. The discussion of the possibility of a transition between two crystalline arrangements for this wide-spread medication continued until the next incident triggered the interest of manufacturers. Carbamazepine, an anti-epileptic drug, became the first pointer, which showed that the substance released at the market can possess an unstable crystal structure and have drawbacks caused by molecular arrangement in a solid phase. The slow dissolution rate of the new solid form caused the incomplete digestion and seriously decreased the dose of medication delivered with the pill. The reason for this was attributed to the hydration of anhydrous carbamazepine [11, 12]. Further, the European Pharmacopoeia issued new rules to prohibit the use of any solid phases of carbamazepine, except for polymorphic modification III (CRS) [13].

Finally, the significant growth of interest in the question of crystal polymorphism in the pharmaceutical industry started in 1995. This is due to several litigations and the first big problem around ranitidine hydrochloride (Zantac®). The most popular drug on the market (\$3.45 billion / year) [14], ranitidine hydrochloride had 2 polymorphic modifications patented by Glaxo company in 1978 [15] and in 1985/1987 [16, 17], respectively. In 1995 the patent defense of the form I had to end. Novopharm company tried to reproduce the polymorphic modification I, but did not succeed to get rid of the polymorph II and suffered the first financial losses associated with polymorphism [18].

Further, the most famous polymorphism-based case of financial losses happened. Ritonavir (Norvir®) is a drug for the treatment of Acquired Immunodeficiency Syndrome (AIDS), which has been sold in solid form from 1996 till its withdrawal from the market in 1998 [19]. The appearance of a new undesirable polymorphic modification II of the API caused a sudden drop in the solubility of the ready drug product by near 400% of the solubility inherent to the metastable form I [20]. Large amount of the formulated medication was recalled [21]. This case was the first strongly associated with the changes in solubility caused by polymorphism and stimulated the interest in the polymorphs as a tool for the manipulation of drugs properties. Some other cases including a few major incidents happened in the next years (Figure 1.1), but they were just consequences of insufficient preliminary researches or production control.

During the latest years, the problems of an occurrence and distinctions in properties of various solid phases of one component, along with the issues of an acquisition, purification and characterization of individual polymorphic modifications, have become fundamental in any pharmaceutical research [23]. The polymorphism is an option strictly controlled before the release of an API on the market by European Pharmacopoeia beginning from its fifth edition (2004). The number of publications and patents in the field grows very quickly [14] and the quantity of the indexed articles has increased by near 2 times during the latest decade, from 2010 till 2020 (Figure 1.2), according to the Scopus database. In an analogous way, the number of patents in the field of polymorphism of drugs has grown from around 11100 issues to 24800 worldwide according to the data from Espacenet [24].

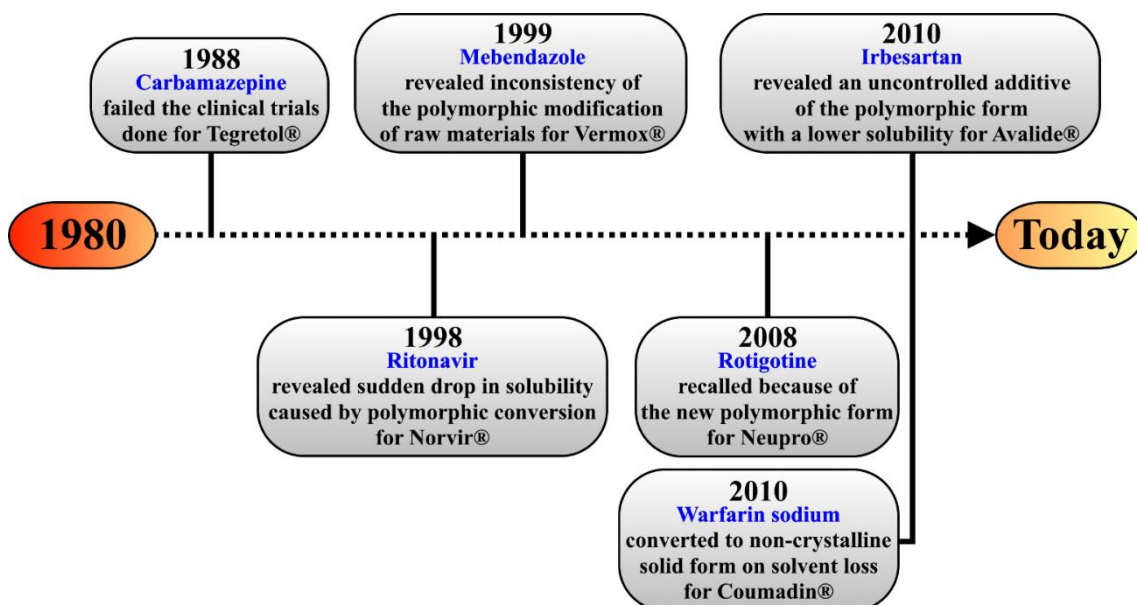


Figure 1.1. A timeline of the most famous pharmaceutical accidents concerning polymorphism led to financial loss (adapted from [22]).

Noteworthy, that in spite of all the regulations and the efforts to control the polymorphism there were still at least 30% of APIs with undefined crystal structures among the non-protein part of the top 200 in the world pharmaceutical products by retail sales in 2018 [25]. The same situation repeats for example for the Ukrainian industry. There are 13 drugs used in the solid state among the top 20 brands (Table 1.1) by pharmacy sales in monetary terms [26]. In their composition, 20 individual APIs were found and just for 11 of them the question of polymorphism was studied according to available data. Multiple structures were obtained just for 6 out of 20 individual APIs according to the data of the Cambridge Crystallographic Data Center (CCDC) and published papers. Since the modern assessments show, that more than 50% of all the bioactive compounds can have more than 1 solid form [27], it is possible to speak about the serious incompleteness of the data available for wide-spread medications. The properties have been studied for an even smaller number of polymorphic forms.

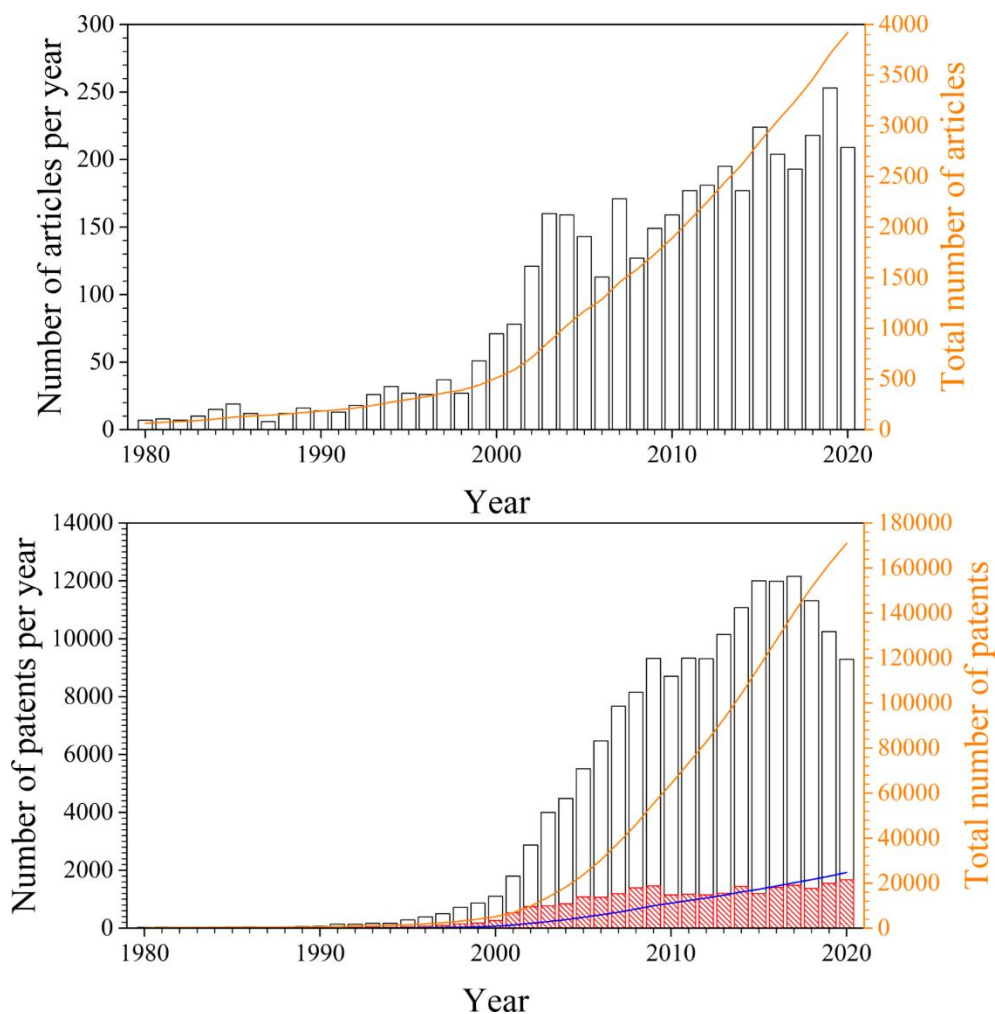


Figure 1.2. Number of publications (top) and patents (bottom) concerning polymorphism according to the data from Scopus and Espacenet, relatively. For patents worldwide (red bars and blue line) and summary for all the countries (black bars and orange line) sections are highlighted.

Table 1.1. Example of polymorphism problem for the solid dosage forms among the top 20 drug brands in Ukraine by pharmacy sales in monetary terms.

Rating	Brand name	API	Action	DrugBank IDs	RefCodes CCDC	Number of polymorphic modifications	
						CCDC	Literature
1	Nurofen®	Ibuprofen	NSAID*	DB01050	IBPRAC	2 [28, 29]	2+NC** [30]
2	Xarelto®	Rivaroxaban	Anticoagulant	DB06228	LEMSOO	1 [31]	4+NC [32-35]

Table 1.1 Continued.

Rating	Brand name	API	Action	DrugBank IDs	RefCodes CCDC	Number of polymorphic modifications	
						CCDC	Literature
3	Nimesil®	Nimesulide	NSAID	DB04743	WINWUL	2 [36, 37]	2+NC [38]
6	Spazmalgon®	Metamizole sodium	NSAID-like	DBSALT000332	METMIZ	1 [39]	1
		Fenpiverinium bromide	Anticholinergic, antispasmodic	DB13759	-	0	0
		Pitofenone	Antispasmodic	-	-	0	1 [40]
8	Tivortin®	L-Arginine L-aspartate	Antihypoxic, cytoprotective, antioxidant	DB00125, DB00128	NAGLYB	1 [41]	1
10	No-spa®	Drotaverine hydrochloride	Antispasmodic	DB06751	-	0	4 [42, 43]
11	ACC®	Acetylcysteine	Mucolytic	DB06151	NALCYS	2 [44, 45]	2
13	Valsacor®	Valsartan	Blocker of angiotensin II	DB00177	KIPLIG	1 [46]	13+NC [47]
15	Novirin®	Inosine	Neuroprotector, cardioprotector, anti-inflammatory, immunomodulatory	DB04335	INOSIN	2 [48, 49]	2
		Acedoben	<i>Undefined</i>	DB04500	DIXFAR	1 [50]	1
		Dimepranol	<i>Undefined</i>	-	-	0	0
16	Citramon®	Caffeine	CNS stimulant	DB00201	NIWFEE	3 [51-53]	4+NC [54-56]
		Paracetamol	Antipyretic, pain reliever	DB00316	COTZAN, HXACAN	6 [57-62]	9+NC [62, 63]
		Acetylsalicylic acid	NSAID	DB00945	ACSALA	3 [64-66]	4+NC [67, 68]
18	Fervex®	Paracetamol	Antipyretic, pain reliever	DB00316	COTZAN, HXACAN	5	9+NC
		Ascorbic acid	Vitamin C	DB00126	LASCAC, COFKOA	1 [69]	1
		Pheniramine	Antihistamine, anticholinergic	DB01620	-	0	0

Table 1.1 Continued.

Rating	Brand name	API	Action	DrugBank IDs	RefCodes CCDC	Number of polymorphic modifications	
						CCDC	Literature
20	Pulmicort®	Budesonide	Corticosteroid, antispasmodic, anti-inflammatory, antihistamine	DB01222	RHBUXP	1 [70]	1+NC [71]

\* NSAID (NonSteroidal Anti-Inflammatory Drug) is a drug class that reduces pain, decreases fever, prevents blood clots and, in higher doses, decreases inflammation.

\*\* NC (Non-Crystalline or amorphous form) is a form of solids that lacks the periodicity appearing in crystals.

## 1.2. Solid-state classification

Properties of the drugs can differ depending on the molecular arrangement and conformation in a solid state, but what actually underlies the phenomenon of polymorphism? To answer this question, it is necessary to look at the classification of all the solids. It has been an object of controversy and confusion for a long time [21, 72-81]. Different goals were pursued from the creation of universal processing and description procedures for the compounds used in the pharmaceutical industry to the prediction of some properties (like bioavailability, stability, tableting, etc.) for substances by the principle of similarity [82-84]. Some consensus has been reached in recent years regarding the classification of the pharmaceutical compounds, but it still remains a subject of controversy. The most comprehensive classification systems were proposed by Grothe et al. [85] and Cruz-Cabeza et al. [14].

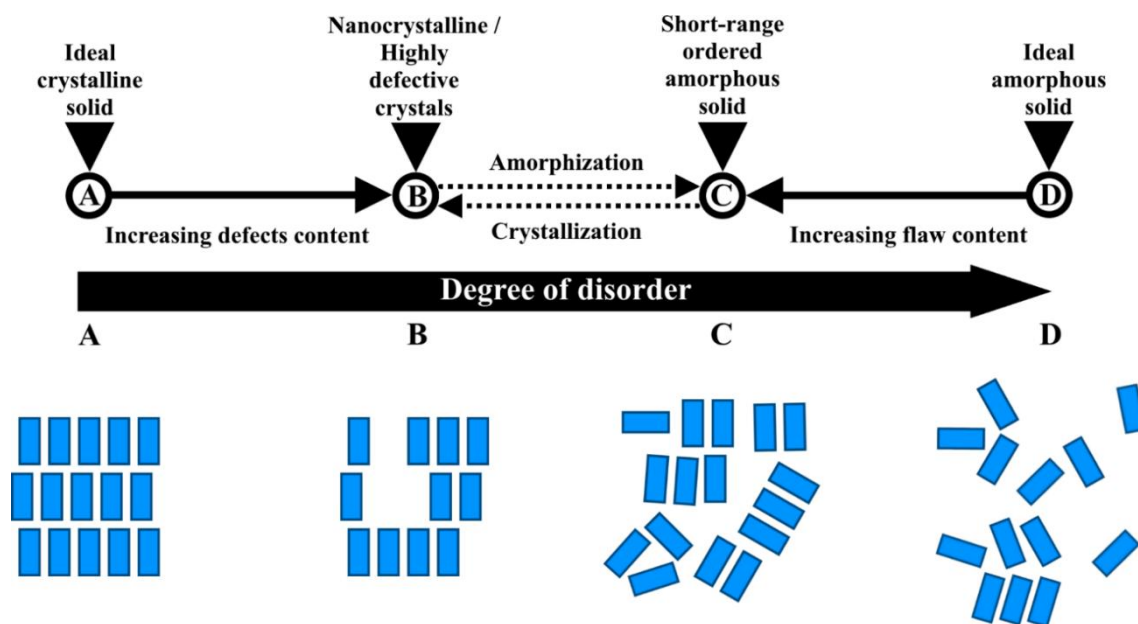


Figure 1.3. Schematic drawing representing the connection between the degree of disorder in pharmaceutical solids and their classification. Adapted from [89, 90].

At first, the two large groups can be distinguished according to the degree of ordering or, more precisely, according to the presence of a strong periodicity. Every solid consists of atoms or molecules. If their positions are known at one point, the place of each nucleus can be foretold with high accuracy in case if periodicity takes place. Expectably, the number of possible arrangements is infinite [86, 87], but just very few of them are capable to exist long enough to be detected, studied and used. Thus, the crystals are defined as the first group. They have such characteristic sets of crystalline lattices, where the atoms constituting the solid phase are distributed regularly. These sets are the polymorphic modifications, so formally they are the patterns of atoms distribution in some ideal crystals. However, defects always are present. With an increase in their number, periodicity is more and more violated and a transition to short-range order occurs. It operates on the probability distribution of several nearest neighbors in a structure, but the distance of prediction is limited [86, 87]. The second group is amorphous solids and polyamorphic modifications, respectively (Figure 1.3). Since the real border between the crystalline and amorphous states

is blurred, earlier, polymorphism was considered as polymorphism of highly disordered defective crystals [88], but, in the present time, amorphous solid phases are defined as a separate class [89].

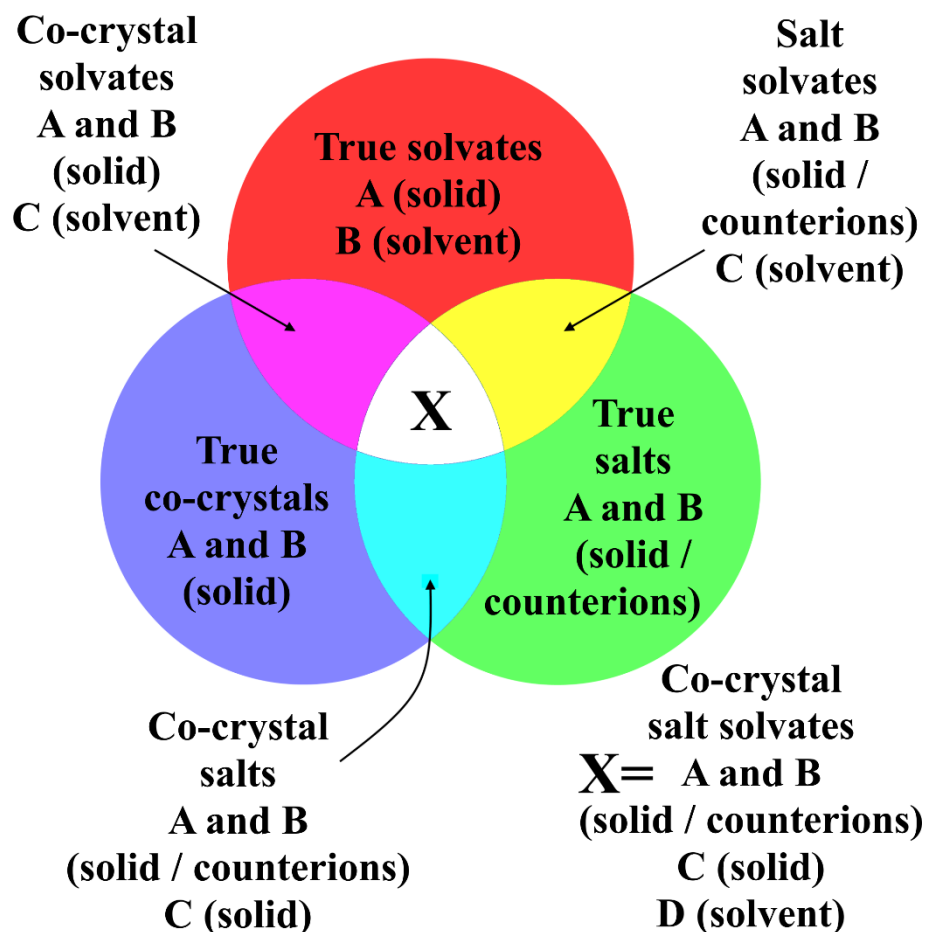


Figure 1.4. Visualization of the classification scheme for multicomponent crystalline organic pharmaceutical solid forms combining molecules from different initial phases. Adapted from [85].

Further, it is common for the pharmaceutical compounds to divide the aforementioned groups into subclasses by the number and type of the structural units that build them up. Single- and multicomponent systems can be distinguished first. All of them can possess polymorphic forms. However, the additional separation of the most significant classes of compounds is considered for multicomponent systems in the pharmaceutical industry. These classes are salts, solvates and co-crystals [80, 85]. They are not mutually exclusive and any

of the aforementioned true or mixed subclasses may possess more than one form to crystallize (Figure 1.5) [78]. Such a classification is problematic for the amorphous solids because of their disorder [91]. Some similarity can be observed between the subclasses of crystalline solids presented below and polyamorphs [92], but their classification is in development and not yet specified.

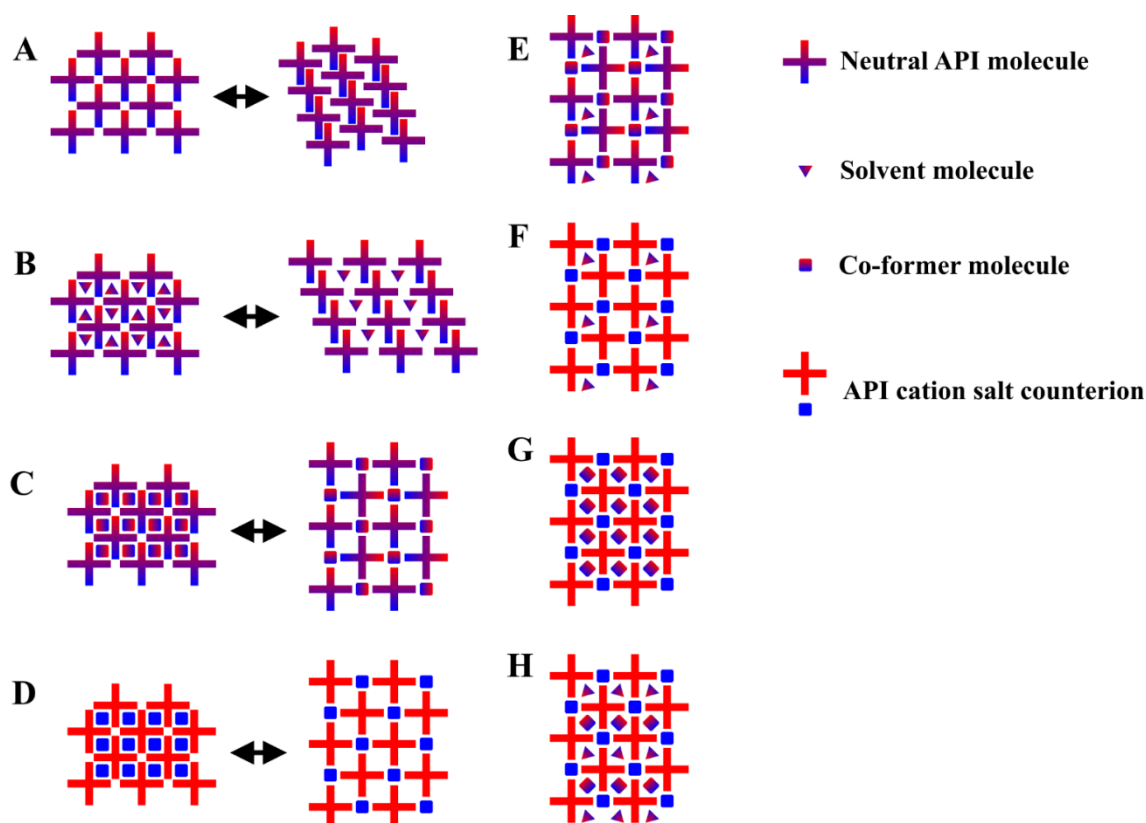


Figure 1.5. General options for crystallization of active pharmaceutical ingredients. A-D are the examples of polymorphism appearance for the pure subclasses of pharmaceutical solid forms: single-component crystals based on neutral molecules (A), solvates (B), cocrystals (C) and salts (D). The examples of crystal structures for the mixed subclasses (E-H) are offered to introduce the breadth of possibilities for the formation of molecular crystals.

The two types of differences in the crystal structure are expectable. They can be orientational (inducing packing polymorphism) or both conformational and orientational at the same time (inducing conformational polymorphism)

[18]. As it is seen, the reasons for the polymorphism types are not mutually exclusive, so it can be difficult to make a perfect distinction basing on the crystallographic definition. Thereby, the phenomenon of polymorphism should be formulated in terms of the energy and stability of different crystal forms. The total energy of a crystal form consists of two main terms. They are the internal energy of structural units involved in a crystal and the energy of their interactions. The orientational polymorphic modifications differ mostly in the mutual arrangement of the molecules, but not in their conformation, the interactions between the structural units have the main influence on the diversity of polymorphic forms. On one hand, the Gibbs free energy of two orientational polymorphic modifications may differ, on the other hand, it is not obligatory and may be close to zero [93-95]. For the second type of the differences between the polymorphic forms, the definition of conformation should be given, because it can cause significant differences in total energy. According to A. J. Cruz-Cabeza and J. Bernstein [96], the new conformation occurs if the conformational change goes through a potential energy barrier into a different minimum on the potential energy surface. It means that any conformational change cannot take place without the appearance of the two energetically favorable conformations of a molecule in a crystal. The definition can be extended with the fact that barriers may be close or of the same order at RT [97-101]. Thereby, the final formulation of the polymorphism may be given mixed geometric-energetic.

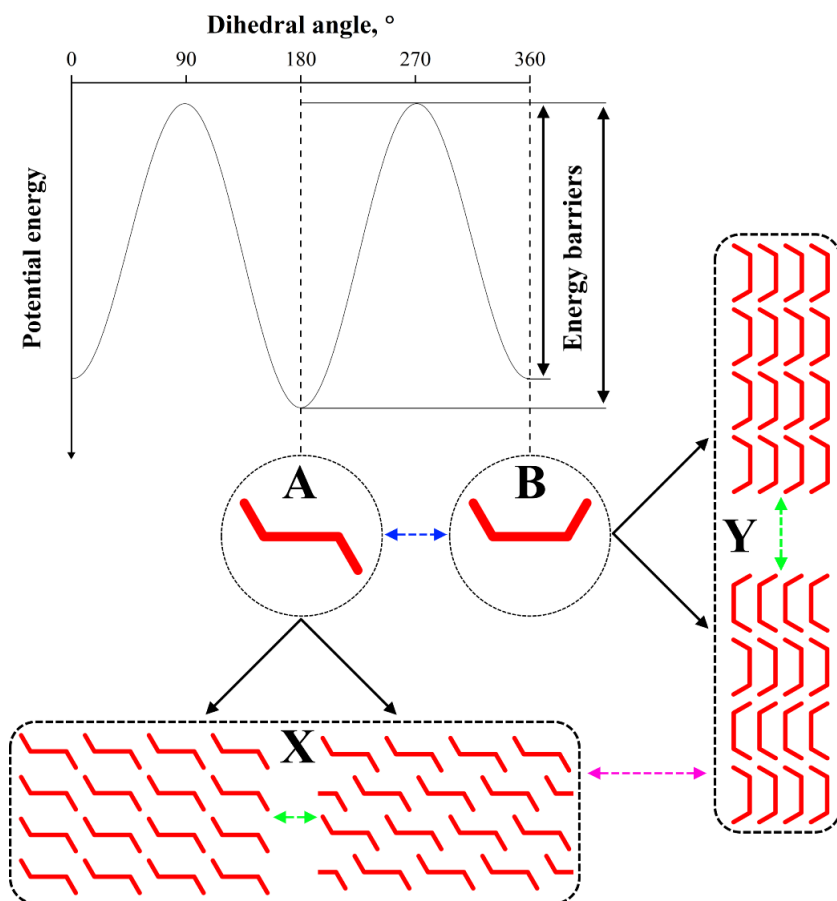


Figure 1.6. The visualization of the polymorphism classification, where the conformers A and B can exist in the solid state as pairs of orientational polymorphs (X and Y), which are conformational in relation to each other (any of X to any of Y). The conformers can transform mutually after overcoming the corresponding energetic barriers (blue arrow) as well as the conformational and orientational polymorphs between each other (green and magenta arrows for changes in packing and conformation respectively).

Polymorphism is then the ability of crystalline material to form more than one arrangement with different mutual orientations of molecules, including the possibility for them to change their conformation from one energetically favorable through overcoming energy barrier (Figure 1.6). The different polymorphic modifications are correlated with the fact that the positions of molecules (orientation and conformation) may explore different local minima of the potential energy surface in crystal.

The difference in energy for polymorphic modifications is usually small and can often only be detected using state-of-art computational methods. Commonly the assessment of the energy is limited to the enthalpy (or lattice energy) without taking into account the effects of temperature and pressure. It may lead to contradictions [102]. Even so, the energy difference between the polymorphic modifications is shown to be less than 10 kJ/mol for the most of molecular crystals [103-105]. According to J. Nyman and G. M. Day, this number can be even lowered to 2 kJ/mol for near 50% of tested molecular crystals or 7.2 kJ/mol for 95% respectively [102]. While S.L. Price postulates [106] that “the energy differences between polymorphic forms are of the order of 1 kJ/mol”, which is a rather small value. Among all the numerous minima on the potential energy surface only limited number of the polymorphic forms are known for a given substance [106-109]. For example, there are just 13 compounds with a high amount of studied polymorphic forms registered in CCDC out of 64 active pharmaceutical ingredients registered in Ukraine (Figure 1.7). Thereby, the following questions arise:

1. Why is the number of detected polymorphic modifications so small with such vast possibilities?
2. How the suitable polymorphs can be chosen for the pharmaceutical industry during the research?

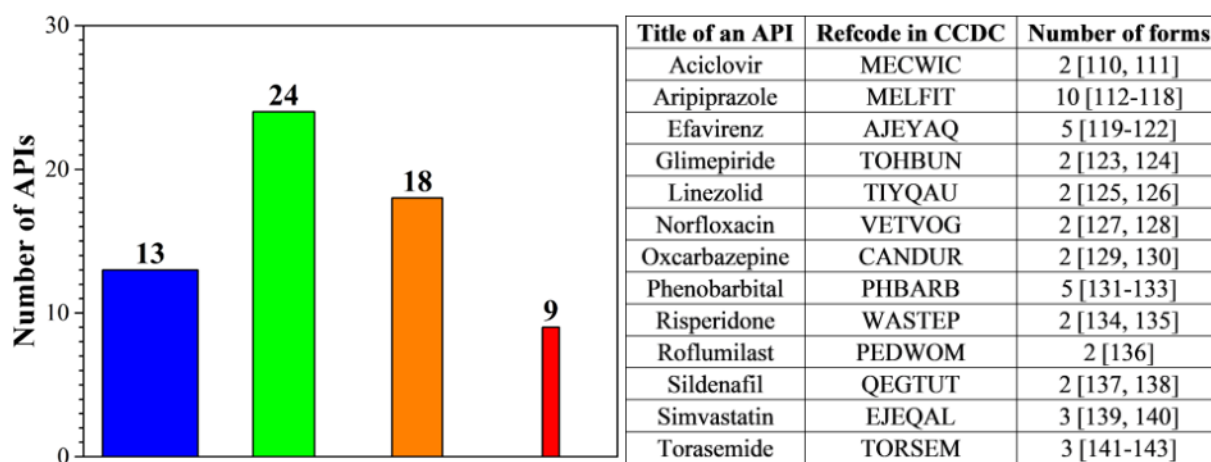


Figure 1.7. APIs registered in Ukraine from well-studied to an undefined structure. The amount of the APIs with a few (in blue) and sole (in green) polymorphic modification, of the ones, whose structure is studied just for derivatives of original compounds (in orange), and of non-studied ones (in red) is represented as a histogram (on the left). The width of bars is scaled following the amount of the polymorphic modifications appearing in CCDC (equals 1 for the non-studied compounds). Table of compounds with a few polymorphic modifications whose structure is studied with their Refcodes is shown to the right.

### 1.3. Formation and transformation of crystalline forms

To answer both questions on polymorphism, many factors should be considered, but in particular the metastability of crystalline forms. In 1899 W. Ostwald wrote: “Almost every substance can exist in two or more solid phases provided the experimental conditions are suitable” [144]. Then Kuhnert-Brandstatter stated that “...probably every substance is potentially polymorphous. The only question is, whether it is possible to adjust the external conditions in such a way that polymorphism can be realized or not...” [87]. These statements lead to the obvious conclusion that the conditions of experiment and storage should be optimized to obtain a specific polymorphic form and to preserve it for long enough time for its analysis and application. So, amount of observable polymorphic modifications is bound to their stability under specific conditions.

In 1897, a general rule of the relative stability of polymorphic modifications was formulated from thermodynamic principles. It is known as the Ostwald rule of stages: “If a reaction can result in several products, it is not the most stable state with the least amount of free energy that is initially obtained, but the least stable one, lying nearest to the original state in free energy” [145]. In the current sense, it predetermines that the system, leaving any state, seeks to achieve an equilibrium, thereby passing into the state of minimum free energy. However, a jump-like conversion is usually not possible, therefore the system passes into the phase with the lowest free energy available at a given time and undergoes a series of transformations to reach the most thermodynamically favorable state (Figure 1.8). The probability of this transformation to occur is determined by the energy barrier value, i.e. the energy required for the system to overcome the unfavorable configurations lying between the structures from local minima of the free energy. If this barrier is too high, then a transformation is not possible without the breakage of periodicity and a new arrangement of the molecules occurs as a new solid form. The time steps required for such transformations depend on a substance and the conditions of its formation and storage. They can last from very short periods of time to months or even years [146-149].

The last point in the issue of the relatively small number of polymorphic modifications is about the formation and reorganization of crystals at the stage of nucleation. The classical theory of nucleation from the solution or melt can be used to understand this fact. According to it, the nucleation rates of stable and metastable forms per unit volume can be derived from the Arrhenius equation [150-153]:

$$J = K_v(T) * \exp \left[ -\frac{W + E_a}{k_B T} \right] = K_v(T) \exp \left( -\frac{W}{k_B T} \right) \exp \left( -\frac{E_a}{k_B T} \right) \quad (1.1)$$

$$K_v(T) = nN_0v \left( \frac{r_a^2 \gamma}{Wk_B T} \right)^{1/2} \quad (1.2)$$

$$r_a = \frac{-2\gamma}{\Delta G_v} \quad (1.3)$$

$$\Delta G_v = (G_s - G_l)\Delta T = \left( \frac{S_s - S_l}{V_M} \right) \Delta T = \left( \frac{S_s - S_l}{V_M} \right) (T - T_M) \quad (1.4)$$

where  $J$  is a nucleation rate;  $k_B$  - Boltzmann constant;  $T$  - absolute temperature;  $W$  - diffusion energy barrier caused by redissolution of nuclei;  $E_a$  - activation energy barrier for nucleation;  $K_v(T)$  - pre-exponent kinetic factor showing empirical dependence between temperature and frequency of molecules attachment to solid nuclei;  $n$  - number of molecules on the surface of transforming nuclei;  $N_0$  - number of molecules per unit volume;  $v$  - molecules attachment frequency;  $r_a$  - critical solid nucleus size at which the nucleation occurs;  $\gamma$  - interfacial tension;  $\Delta G_v$  - the energy required for the formation of a new phase and a difference between the Gibbs energies of a solid phase,  $G_s$ , and a solution containing these forming crystals,  $G_l$ , per molar volume,  $V_M$ ;  $S_s$  and  $S_l$  - entropies of solid and liquid phases, respectively;  $T_M$  - melting temperature of a new solid phase.

According to the equation 1.1, the two opposing processes take part in the crystallization: formation and redissolution of the nuclei [150]. Redissolution values are usually small (Figure 1.8), but it affects significantly the initial nuclei formation giving enough time for reorientation and conformational changes to occur [106]. So, the crystal structures unstable under the crystallization conditions change to more stable ones.

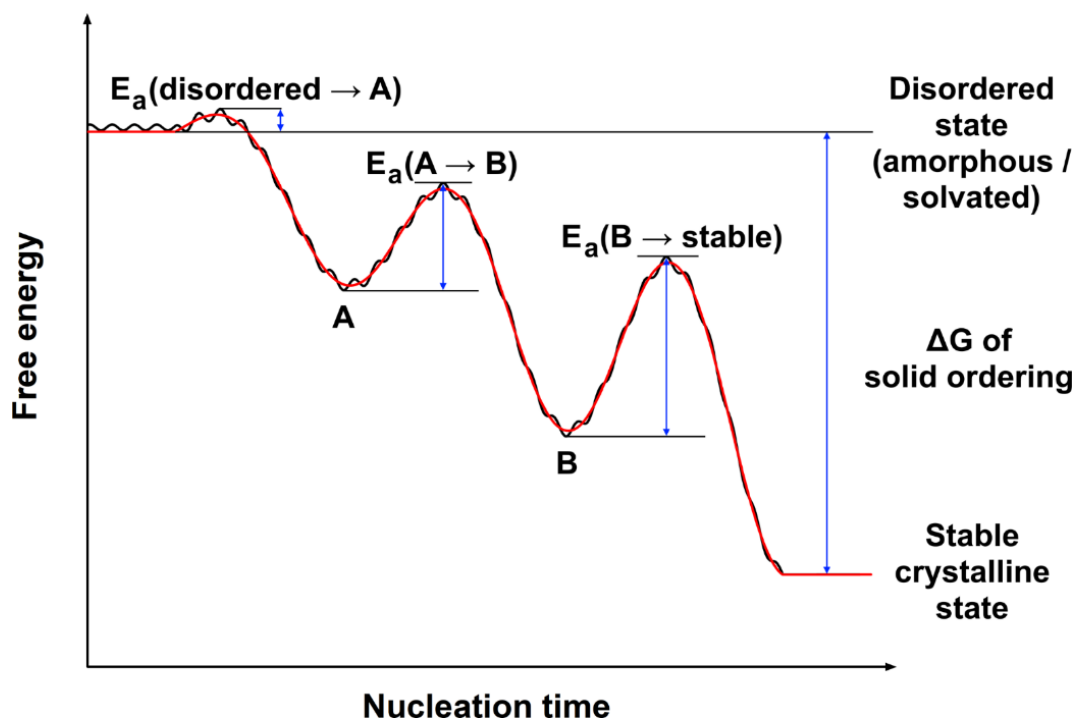


Figure 1.8. Schematic drawing of Ostwald rule of stages with (black) and without (red) the implementation of nuclei redissolution correction from classic nucleation theory showing the process of the formation of the most thermodynamically stable form from the disordered state through intermediate ones (A and B). Adapted from [162, 163].

At least two popular methods, which allow to decrease the amount of observable polymorphic modifications, are based on the avoidance of redissolution. They are the introduction of seeds to bypass the redissolution process [154] or the slow formation of thermodynamically favorable crystals [155-157]. However, the polymorphic forms can still disappear [148, 158] and emerge [159] occasionally in the pharmaceutical production processes. All the aforementioned facts show that the best way to the application of specific crystalline forms in pharmaceutical application is by the choice and maintenance of correct conditions for their synthesis and storage [5, 146, 160, 161].

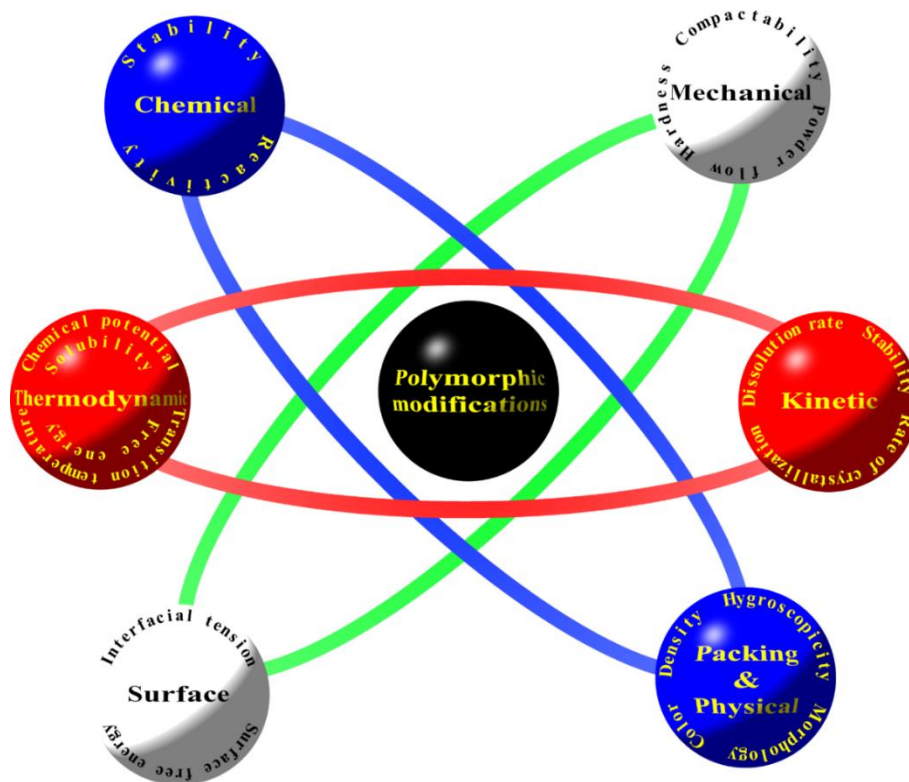


Figure 1.9. Properties capable to change for different polymorphic modifications of the same API. Adapted from [22].

Numerous metastable polymorphic modifications of drugs possess other properties (Figure 1.9) than their stable analogs. Since the Gibbs free energy of their formation is lower than the ones of stable forms, the intermediate solid forms can dissolve much faster [20, 164, 165] showing higher bioavailability [164, 166] for active pharmaceutical ingredients belonging to the groups II and IV according to the biopharmaceutical drug classification [167]. Thus, the solubilization of drugs can be reached through manipulations on polymorphic modifications for at least 25% of orally administered drugs with respect to the analysis made for the Essential Medicines of the World Health Organization [168]. The powder flow, tableability and hardness also can be affected [169-173]. The preparation of metastable form of paracetamol [174] and of  $\beta$ -lactose [175] helped to overcome their incompressibility during their tableting process. It also can improve the hygroscopicity [176, 177] and the surface area and morphology of drug [178, 179]. However, only the most stable

forms of drugs are often used and sometimes they are even solely permitted by the Pharmacopoeia or other regulations as in the cases of carbamazepine [180], indometacin [181], chloramphenicol palmitate [182] and doxazosin mesilate [183]. Changes in properties are especially problematic for substances acting on the central nervous system (CNS), such as antipsychotics, pain relievers and anesthetics, etc. [22, 184-186], whose higher bioavailability or faster dissolution potentially may cause a transition from a therapeutic to a toxic or even lethal dose. It counters the efficiency, but the usage of metastable forms without stringent control of their synthesis, formulation in ready dosage forms and storage is dangerous. Thereby, the issues of the control of synthesis conditions and the stabilization for the subsequent storage of such polymorphic forms and formulations made of them are of primary importance.

Returning to the classical theory of nucleation, the other useful conclusion done from equations 1.1-1.4 is that the transformation to the structure with the smaller entropy is preferable. It follows the rule of stages, but also numerous questions appear, among which the most interesting for us is “How the equation will change and will it work for the cases other than crystallization from the solution or melt?” It can be solved partially by the addition of empirical coefficients analogous to strain coefficients for solid-solid transformations. However, the above equations and in particular the calculation of a critical nucleus size becomes dependent on the form of contact of solid phases during the transition and molecules specific positions in crystals of both phases [187], which is difficult to solve:

$$\left. \frac{d\Delta G(r)}{dr} \right|_r = 0 = 4\pi r^2(\Delta G_v + \Delta G_{strain}) + 8\pi r\gamma \quad (1.5)$$

where  $r$  is a radius of a particle of a new phase and  $\Delta G_{strain}$  - strain energy per unit volume.

It should be noted as well that the interfacial tension, strain coefficient and particles radii are not the same parameters for all the parts of the crystal. They change significantly even for different faces of molecular crystals and have to be actually represented as tensors even if we exclude the conformational flexibility of the majority of bioactive molecules. The effects of pressure and surrounding solvent should also be taken into account with the fact that they are distributed unevenly in crystal. Thus, the multilayer correlations between variables complicate the analysis and the prediction of the stability and mechanisms of transformation of drug polymorphic modifications. Thus, it is difficult to assess the possibilities of polymorphs formation in fluids and almost impossible to do it for solid-solid phase transitions, i.e. polymorphic transformations in the classical meaning.

To conclude, new techniques are required for the synthesis and storage, which will give a possibility to produce and to keep for a relatively long time the polymorphic modification of interest other than the most stable ones. Thus, the new methods for the control and analysis of these processes are needed, as well as for the search of possible but not observed polymorphic forms.

#### **1.4. Methods for solid forms synthesis**

Stabilization of polymorphic modifications begins already at the stage of synthesis. There are many methods for its implementation and their number continues to grow. They include both classical and new methods created for the improved control over the crystallization process and, as a result, the composition of the final product. In the former group, these methods are recrystallization from solution or melt, sublimation and evaporation-based methods, freezing, anti-solvent methods, various types of grinding, granulation and compression [188-192]. In the latter group, 3 methods are often discussed. The first one is growing crystals in a confined space, which is gaining popularity and has proven its efficiency for such popular objects as aspirin [66] and

paracetamol [62], the second one is based on laser processing (nucleation) of solutions [193, 194] and the third one is based on the templating with the addition of solid matrices for crystallization [179, 195] or additives similar to dissolved substance [189]. All of these 3 methods can be divided into several groups according to 3 characteristics: duration; initial phases of the components used in the formation of a new solid phase; and the type of the process that is the cause of a new solid phase formation.

It has been noted that the synthesis methods with the highest duration suit better for the formation of the most stable phases. The same principle works in the opposite direction. It is generally accepted that the preparation of metastable polymorphic modifications of APIs is more successful in the case of rapid synthesis methods [179, 190, 196]. According to [190, 191], sublimation, anti-solvent methods and various techniques based on supercooled phases containing APIs could be called the most productive for obtaining metastable forms (Figure 1.10). Recrystallization and grinding go next, although their popularity is much higher. This may be explained in 2 ways. Firstly, thermal methods associated with the melting or evaporation of APIs are often characterized by thermal destruction of some fraction of bioactive molecules [197-200]. This is unacceptable for the pharmaceutical industry [201-203], since the degradation products of the API may exhibit biological activity themselves [204, 205]. Secondly, the probability of finding a new polymorphic modification is high when large range of synthesis conditions for its detection can be varied, i.e. the greater the variability of the conditions available for the method and the wider the thermodynamic stability zone of the desired modification [192]. These two restrictions, along with the requirement to control strictly the conditions of the acquisition of solid forms, limit the use of the fastest methods from the sides of both low and high temperature.

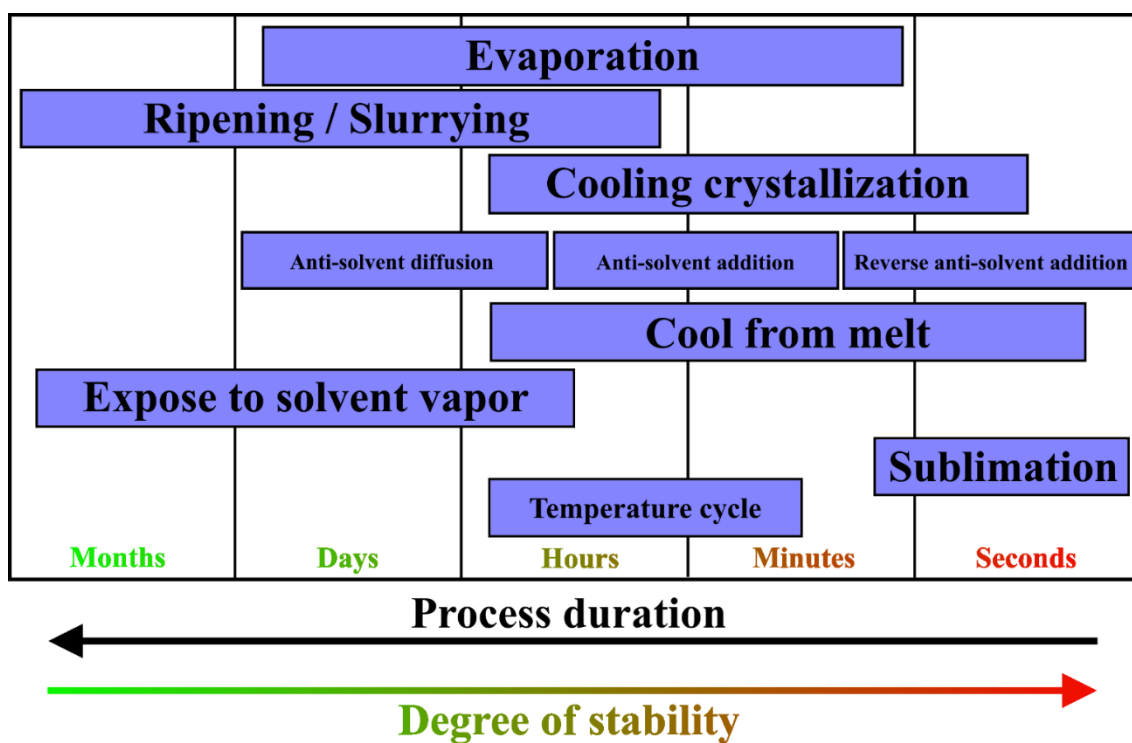


Figure 1.10. Timescales of crystallization experiments and the dependence of the processing time from the probability of metastable form acquisition. Adapted from [190].

Recrystallization, as one of the most wide-spread and accessible methods in the pharmaceutical industry, allows also to vary easily the conditions of synthesis. Thus, it has been chosen for this work, but a few difficulties required resolution. Molecules do not remain in the solid state during recrystallization, it is a complex process consisting of at least 2 phases: the dissolution of an initial polymorphic modification and its crystallization into a new crystalline arrangement. Thereby, the control of composition should be realized at every phase (initial and final solids, intermediate solution) and stage (dissolution and crystallization).

During recrystallization, it is usual to control just the composition and the temperature of the solution [189]. However, the control of just these parameters doesn't ensure the reproducibility of the polymorphic forms as it is shown in the literature data [148, 158, 166]. The polymorphic modifications may re-dissolve during storage [5, 206] and even small impurities in the cavities of crystals may be the reason for changes in polymorphic form as well as the desolvation, which

leads to the disruption of crystallinity [207]. Therefore, if it is necessary to obtain the desired polymorphic modification, the interaction of the API with the environment should be taken into account, as well as the possibility of "drying" of the solvated forms in a dry environment. The metastable polymorphic modification should be purified from the solvent during the synthesis [192]. Thus, a new method that would give the possibility to control a large number of conditions without the complexity associated with subsequent storage. It is the synthesis of solid forms in supercritical fluids (SCF). Closed reaction chamber together with the ability to maintain constant pressure and temporary convert gases to fluids gives it a significant advantage, while the principle of method operation remains almost the same. Thus, supercritical fluid technology has shown itself to be the most suitable candidate as a method for the synthesis of metastable polymorphic modifications increasing their lifetime, as well as the study of conformational changes inherent to molecules in the fluid phase [208].

### **1.5. Crystallization from supercritical fluids**

Liquids (water, ethanol, etc.) or gases (carbon dioxide, ammonia, ethane, etc.) acquire unusual properties partially similar to liquid and gaseous phases when exposed to specific temperatures and pressures (Figure 1.11) [209]. In particular, these are density, viscosity and diffusion coefficient [210, 211]. These critical pressure and temperature are proportionally interdependent [211]. Thus, the variation of the thermodynamic parameters can be used to control the density of the solvent and the solubility of API in SCF [213, 214]. However, a critical point exists for each material, although its position varies in a complicated way for multicomponent systems [215]. The smallest fluctuations of temperature and pressure close to that point affect significantly the properties of SCF. Range of the method performance is somewhat limited then, but only in the low-temperature region. The high-temperature formation of polymorphic modifications and the conversion of conformations in the solution can still be

studied because the solubility of APIs increases with temperature [216]. Pressure is the main factor leading to the compounds dissolution [217] and the miscibility of SCF with other solvents is extremely high [209], making it possible to use anti-solvent methods in tandem with supercritical technology. It should also be noted that high diffusion coefficients make it possible to avoid the local overheating of the API and, consequently, its destruction [210]. The last and the most important argument in favor of the synthesis of polymorphic modifications in SCF is the possibility of fast depressurization of the system which allows the formation of a solid phase from a solution [218].

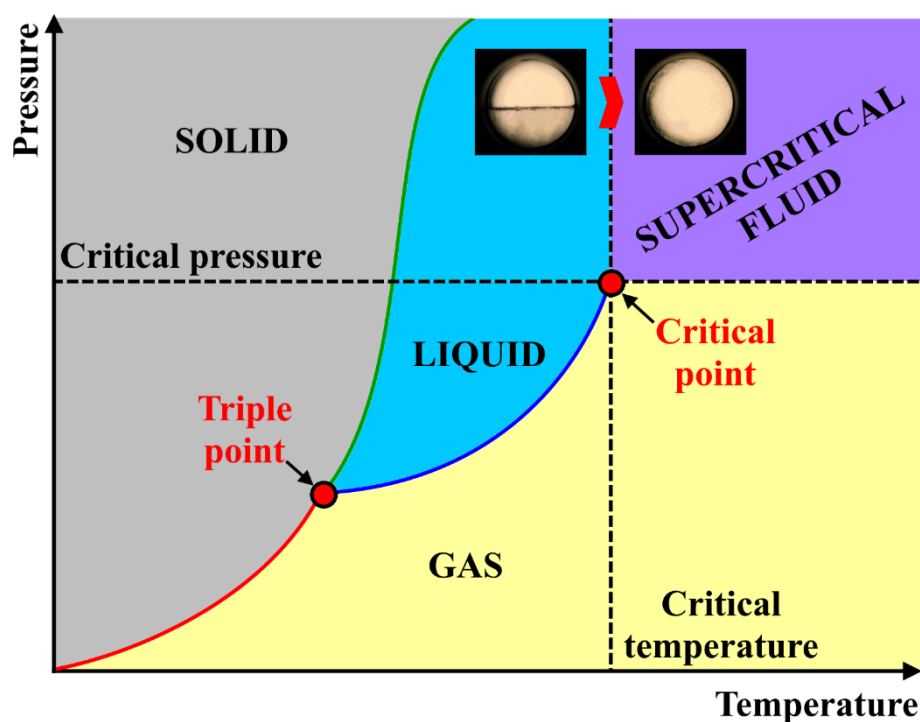


Figure 1.11. Example of a liquid-gas critical point on a pressure-temperature phase diagram with the photos of the liquid-gas interphase (at the top-left) transforming to the supercritical CO<sub>2</sub> (at the top-right).

The application of fast crystallization through depressurization or slow recrystallization depends on a chosen method of synthesis and solvent. Firstly, the huge number of solvents suitable for APIs treatment under supercritical conditions exists. Water and carbon dioxide are popular, safe for human and

environment friendly [219], so the methods based on them are to be explained. Water is characterized by mean acidity and oxidizing properties in the supercritical state [220], which makes it reactive in relation to APIs and corrosive to reactors containing water-based solutions. Carbon dioxide is non-flammable, non-toxic and cheap (up to 0.15 €/kg for industrial needs in France [221]). It is also an extremely popular "green" solvent because it is chemically inert and can be completely removed from the most of solid APIs by depressurization. Rather low critical temperature of 304.2 K [222] allows it to be used for the treatment of thermolabile molecules [206]. Role of carbon dioxide can change in this case. Three groups of techniques based on this role can be distinguished. In the first case, CO<sub>2</sub> acts as an additive, as in the case of supercritical-assisted atomization or spray-drying, particle formation from gas-saturated solutions, etc. In the second case, it is an anti-solvent (gas anti-solvent, supercritical anti-solvent, etc.). Finally, carbon dioxide is a solvent in several methods that seem to be the most interesting for the pharmaceutical industry due to the production of solvent-free crystals with a high shelf life and ease of handling [223]. Varieties of rapid expansion of supercritical solutions (RESS) and the crystallization from supercritical solution (CSS) [224] can be assigned to this group. In the former method takes full advantage of supercritical CO<sub>2</sub> (scCO<sub>2</sub>). The API of interest is dissolved in a supercritical fluid under high pressure in an autoclave. The mixture is then rapidly expanded through the autoclave nozzle to collect the fine powder. This expansion causes instant supersaturation of the supercritical fluid, whereby a rapid formation of microcrystalline powder occurs. However, crystallization occurs during depressurization. It is not an equilibrium process and, therefore, the control of conditions is reduced without giving advantages in reproducibility at the post-expansion stage. In the later method, CSS provides the same capabilities for controlling liquid and solid phases during the pre-expansion stage as in the RESS method, without the aforementioned problem, because, in essence, CSS is

the evaporative recrystallization with uncommon solvent. The product in CSS is not only a dissolved part of an API but also the solid phase that does not come into solution constantly and stays in equilibrium with it. There is also a limitation for RESS similar to usual recrystallization techniques but more problematic than for CSS, for example. Just part of bioactive molecules can be dissolved in scCO<sub>2</sub> well enough for a significant fraction of API to remain in the solution. It makes CSS a more convenient method for *in situ* control over the phase composition of APIs and inherent conformational equilibria.

Experiments using RESS and CSS methods have been performed on many APIs [223-226]. However, most of them have undergone only micronization, which, although useful for increasing solubility, is not a manifestation of polymorphism. Several compounds can be identified as the most interesting from the viewpoint of polymorphs formation. From RESS experiments, these are carbamazepine [227] and tolbutamide [228], for which, 4 and 3 polymorphic modifications were obtained through different crystallization routes, as well as mefenamic acid and paracetamol, whose processing showed ambiguous results according to powder X-ray diffraction [229] at temperatures up to 353 K. CSS is applied usually to co-crystallize mediations [223, 224], so the results received for the pure drugs treated with scCO<sub>2</sub> are very few. These are the acquisition of the pure polymorphic form II of paracetamol after processing [230] and the amorphization of ibuprofen [231].

### **1.6. Mechanically induced polymorphic transformations**

The stability of a polymorphic modification of an API during and after production should also be controlled. The post- processing to ready formulations can easily cause transformations [5, 164, 196, 232-237]. For example, the compaction takes place at elevated pressure (typically 40-200 MPa) during a short period of time ( $\leq 1$  sec) [238]. However, this is often enough to induce

phase transformations affecting significantly the final product performance [5, 22, 232, 239, 240].

Indeed, the pressure has an effect in the process of recrystallization of bioactive molecules from scCO<sub>2</sub> too, but its contribution is not exactly defined there and affects the solution as well as solid. It is currently not possible to determine the effect of pressure on the solid and fluid phases and, as a consequence, on the mechanism of the formation of crystalline phases. Thus, the orientational changes of molecules are mixed with strong conformational changes coming from the solution phase, especially at the elevated temperature. Their joint analysis is too complicated for the initial stage of characterization of polymorphic transformations. On the other hand, the pressure becomes a key process in multistage mechanical deformation of API crystals and solid-solid transformations, which suit much better for modelling.

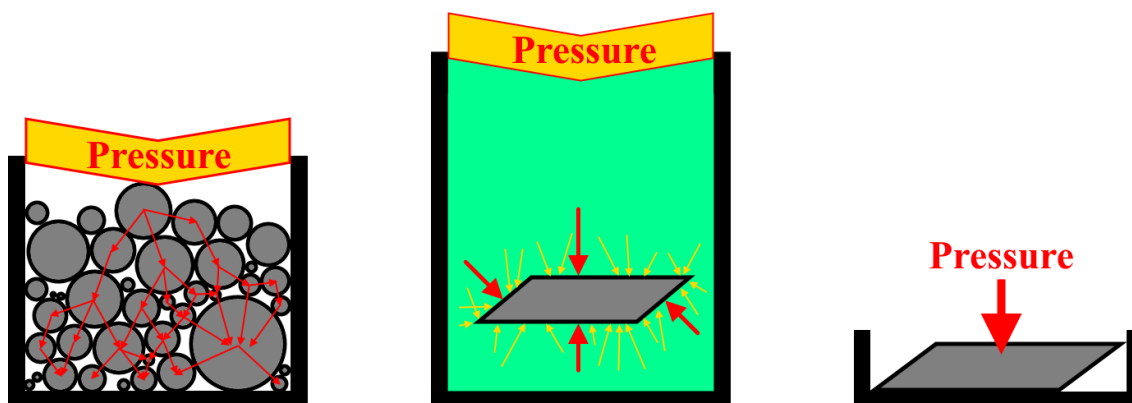


Figure 1.12. Pressure transmission during the different types of mechanical treatment. From the left to the right: grinding, DAC, nanoindentation. Examples of instant impetus vectors appearing due to the pressure are shown in red, instant vectors of individual particles before collisions - in yellow.

There are many ways to transfer mechanical energy to the solid phase [241-243], but only a few of them are suitable for studying molecular interactions and are wide-spread enough to use the experimental data acquired with them to build theoretical models of polymorphic transformations. To

estimate the probability of polymorphic transformations 3 practical methods are usually used: classical dry grinding, compression in the diamond anvil cell [244, 245] and nanoindentation [246, 247]. They all can lead to polymorphic transitions through the application of pressure to a solid phase. Their main differences are in fact the efficiency of energy transfer and the orientation of the impetus vector to the surface (Figure 1.12), which radically affects the anisotropy of the interactions and, as a consequence, the mechanical response of materials [6]. It is possible to put the previously mentioned methods in a row according to these factors as follow in order to simplify the construction of a physical model for the description of solid-solid transformations:

- Pressure is transmitted to polycrystalline samples in the direction changing with time affecting different particles and crystalline faces during the dry grinding. It is somewhat similar to a movement of molecules or large structural units in a crystal in different directions [248]. The pressure here affects the solid phase, whose crystals are disoriented relatively to walls of vessel containing them and a compression element, as well as the faces of neighbors [249]. Formally, very fine powders can be assumed as ideally disoriented, so the pressure will be applied simultaneously to all the faces [250] in the same way as in the case of preferential orientation in powder X-ray diffraction [251]. However, this approximation is questionable. Powders are usually analyzed before and after such treatment, and only recently rapid *in situ* control techniques started to emerge [252-255].
- Directed pressure on all the faces of a crystal or a powder [245, 256] at the same time occurs in the case of compression in a diamond anvil cell (DAC). An inert liquid carrier is used in it to transfer impetus from the moving parts of a DAC to a sample whose properties are measured. The transfer, in fact, occurs in a chaotic manner, depending on the collisions of the carrier molecules with the ones of the sample onto the surfaces of

crystal(s) faces. Its probability depends on a large number of factors (the pressure value, molecular and crystal structures of the analyte and the carrier, the possibility and intensity of their interaction, the crystal habit(s), etc.). Nevertheless, the probabilities of collisions per unit of surface area can be brought to almost the same values, when operating within the hydrostatic pressure diapason [257]. Therefore, the contribution of pressure on each face of the single crystal becomes proportional to their areas. The method of compression in a DAC allows the creation of constant pressure for an unlimited period of time, so it is often combined with X-ray diffraction for better control of crystal structure. So, then the structure and the structure-to-pressure relationship can be described in details.

- Directed pressure on one of the faces of a single crystal is created with a special probe (Berkovich, Vickers or Knoop probe [241]) during the nanoindentation, which is the simplest method to describe. Compression is performed for given face-direction combinations, and the pressure is often detected *in situ* directly from the probe itself using an atomic force microscope. Concomitant techniques of spectral analysis are also available and the structural deformation caused by local stress can be assessed before and after the experiment. Thus, the data received from this method is abundant, but it is not suitable specifically for the synthesis of new polymorphic forms in its current form, which is confirmed by the almost complete absence of articles on this topic [258]. This technique is often used to analyze the mechanical properties of single crystals [259-261], which can be called a step prior to some polymorphic transformations [5, 262, 263]. Thus, it lays at the junction of methods for the studies of polymorphic transitions and mechanical properties.

Over the years of research, numerous experiments to study the mechanical response of crystals [241, 247, 258, 260, 261, 264], their flexibility [263, 265-

270], as a transitional stage between mechanical deformation and polymorphic transformation, as well as polymorphic transformations have been carried out. A significant amount of data has been collected for transformations by grinding and under pressure, as well as for the substances that do not undergo transformations under the influence of the aforementioned techniques according to data from CCDC and published articles (Figure 1.13). The largest number of published structures and individual compounds registered in the DrugBank database was found for the DAC method with an observed polymorphic transformation (844 and 48, respectively). Particular attention is paid to the classes of natural amino acids (total 275 structures), saccharides (65 structures) and APIs not related to these 2 groups (220 structures). The compounds that affect CNS and so susceptible to polymorphism under pressure can be distinguished. These are aspirin [66, 271], salicylamide [272] and phenylbutazone [273] as NSAIDs, paracetamol [274-276] as NSAID-like API, caffeine [277, 278] as a psychoactive drug and the group of nootropic drugs and cognitive enhancers: piracetam [279], glycine [280-283] and sarcosine [284]. The number of data is significantly less for the transformations of compounds registered in the DrugBank database during grinding (234 and 23) and for processed APIs without transformations in response to pressure (172 and 11). Carbamazepine [285-287] as an anticonvulsant, aspirin [288], diflunisal [289], ibuprofen [290], indomethacin [291], nimesulide [37] and sulindac [292] as NSAIDs can be separated out from the first group. Ibuprofen is also noted in the literature as a drug unable to transformations during the processing in DAC [293], similar to halothane [294], which is an anesthetic.

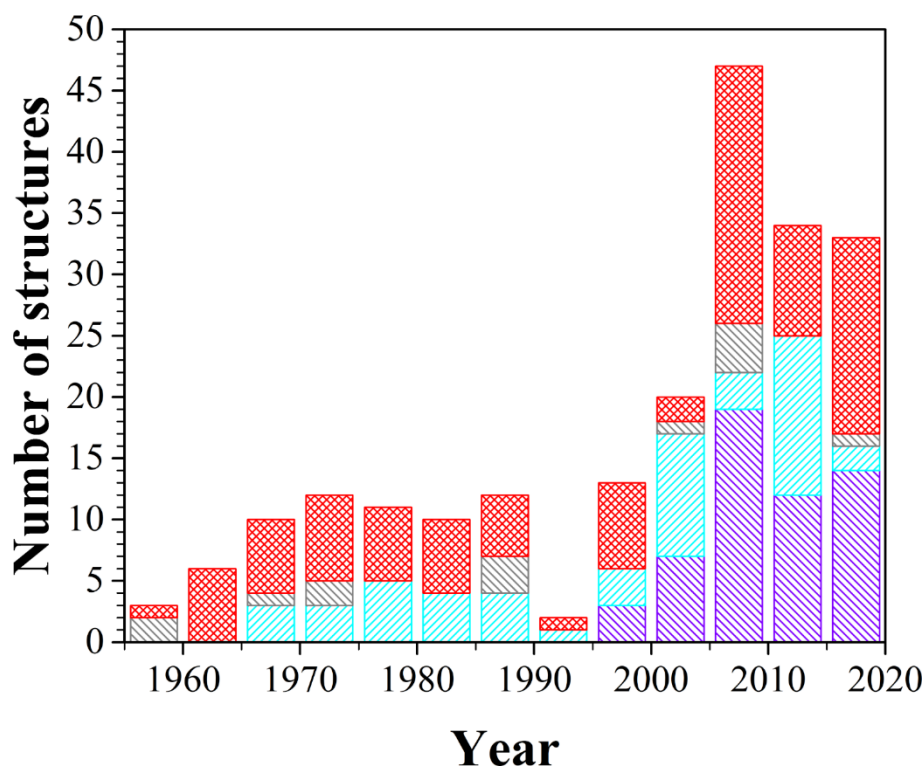


Figure 1.13. Number of polymorphic modifications by years for the compounds, which proved the conversion under the increased pressure as in DAC (in violet), during grinding (in cyan) or whose transition was denied during the mechanical treatment (gray), together with the number of their polymorphic forms non-studied with aforementioned methods (red).

### 1.7. Methods for the identification of polymorphic forms

Individual polymorphic forms of APIs obtained at the stage of synthesis or after storage and processing should be identified and compared with the modification documented and permitted in technological processes. Many methods are suitable for laboratory needs, but only a small number of them are approved for use in industry. The European Pharmacopoeia of the 10th edition for 2019 allows the following [295]:

- X-ray diffraction of powders;
- X-ray diffraction of single crystals;
- thermal analysis (differential scanning calorimetry, thermogravimetry, thermomicroscopy);

- microcalorimetry;
- moisture absorption analysis;
- moisture absorption analysis;
- solid-state nuclear magnetic resonance;
- infrared (IR) absorption spectrophotometry;
- Raman spectroscopy;
- measurement of solubility and intrinsic dissolution rate;
- density measurement.

It is noted as well that these techniques are often complementary and it is indispensable to use several of them to study polymorphism. Multi-stage analysis is usually required at the stage of an analytical methodology approval when the structure and properties of dosage forms are determined or during the identification of problems appearing at different stages of pharmaceutical production. It is completely unsuitable for express control of the product and related processes. Thermal analysis and vibrational spectroscopy (in particular IR absorption and Raman spectroscopies) are the most popular for the control of polymorphism in batches on line or at line. However, they all have a number of drawbacks that limit their use to polymorphic modifications of substances present in the reference data libraries. They have a stated limit of the accuracy of 2 molar percent of the sample for differential scanning calorimetry [296] or even lower for spectral methods [297, 298], which depends on experimental conditions. Also, thermal analysis methods themselves are capable of causing polymorphic transitions and it is not sufficient to ensure the initial formation of the most stable polymorphic form [299]. So, they are not suitable for non-destructive testing. Raman measurements are capable of this, but they are susceptible to changes in spectra caused by fluorescence, differences in sample geometry, size, shape and packing density of API particles (for example, in tablets) [300].

Spectral data libraries such as AIST [301] often contain conceived spectrum-substance pairs, but not data for individual polymorphic modifications. Thus, it is common practice to measure reference spectra, which require verification by methods capable of revealing the crystal structure of the analyzed solid phases or at least to distinguish analyte structures unambiguously. Only methods based on X-ray diffraction are capable of this among the listed common techniques. Therefore, spectra or heating profiles of individual polymorphic modifications can be used for *in situ* control only if the X-ray structural or powder X-ray analysis was performed on the same samples at least once and the corresponding curves were compared.

Application of the fast methods belonging to *in situ* process analytical technology is widely known though [299, 300, 302-329]. Raman spectroscopy is the most convenient technique for the pharmaceutical industry among them, because measurements can be performed directly on the production line through the packaging or even through the outer shell of the pills [318] using the spatially offset Raman spectroscopy [315]. Batch-to-batch variations of the product may be controlled then [300]. It is also useful at the stage of crystal formation when the shape and morphology of solid particles are monitored using a low-frequency Raman probe [324-326, 328]. A popular technique is the combination of synthesis and on-line analysis in closed-loop process control [302, 311, 313]. Connection of the control over the intensity of certain reference peaks in the spectra of solid particles with a programmable logic controller makes it possible to create a self-calibrating procedure for selecting the synthesis conditions for a given polymorphic modification [322]. The other advantage of Raman spectroscopy is the capability to measure only symmetric vibrations when the polarizability changes. It allows to use the analysis to a broader range of solvents than it is for IR absorption. For example, Raman scattering is easily measured in water, as the most popular industrial solvent [305, 312]. In its turn, IR spectroscopy [303, 306, 316] and thermal analysis

[304, 320] are spread more as in line techniques. Despite this, the IR absorption spectroscopy is still widely used to mother liquors, i.e. solutions of APIs [330, 331], making it the second method after Raman measurements able to on line control of the batches in drug production (reactions and conformations of ingredients), but not their polymorphism directly. Thereby, the Raman and, in some extent, IR spectroscopy can be used on line for mass control of the manufacturing process of APIs and dosage forms.

### **1.8. Quantum-chemical modelling of properties in the solid state**

Polymorphic transformations and the preceding changes in crystals are of great interest, as well as their mutual influence on the properties of solid APIs. Their analysis and prediction are not new and can be performed by a variety of methods, ranging from molecular dynamics [332, 333] and statistical Monte Carlo methods [334-336] to neural networks [337] and ab initio quantum-chemical calculations. At the moment, the latter group is able to give the state-of-art level of results accuracy with minimal discrepancy between the predicted and experimental data and the error of methods themselves at the sub-kJ/mol level in the case of energy [103, 338, 339], which is sensitive parameter related directly to the square of the wavefunction of a system [340]. Thus, it becomes possible to calculate accurately the data of relative stability at 0 K and the Gibbs free energy [338, 341], as well as many others options [341-343], if the appropriate level of theory for electron-electron and electron-nuclear interactions, in particular, exchange-correlation interactions, was taken into account. However, so high accuracy is available only when using large computing power, therefore, quantum-chemical calculations, even more than the other types of theoretical methods, require balancing the spent resources and the required accuracy.

This is especially true for calculations performed in systems infinite from a quantum-chemical point of view, like crystals. Solid-state computational

methods based on Bloch's plane wave theorem [344] use the periodicity of crystals and, therefore, the periodicity of the change in the wavefunctions that describe it (Equations 1.6-1.7). They allow to reduce the time required for calculating the properties of quasiperiodic structures and fundamentally make the calculations for an infinite number of electrons possible at the current level of computational technology [345]. Plane-wave calculations are the most common method for the search of polymorphic transformations of APIs.

However, they are based on discrete sampling in the same way as classical quantum-chemical methods, though the way they are applied is different (Figure 1.14). Bloch's theorem is based on the fact that electrons, the same as atoms in a crystal structure, are periodically distributed. In this case, the wavefunction becomes equal to itself at the starting point at any other point distant from the original by a distance that is a multiple of a parameter  $a$  (Equation 1.6), which is the reciprocal lattice constant of the crystal [344, 346]. Molecules or atoms located at the knots of the crystalline lattice are tens of thousands of times more massive than electrons (so the lattice parameters are) [347-349] and their movements are much slower according to the Born-Oppenheimer approximation [350]. This makes possible the replacement of real electronic potentials with their pseudopotential analogs without errors because of the edge effects or the nuclei motion [340]. Thus, an electron or, more precisely, a set of electrons lying in the plane of propagation of a plane wave is described by the product of the multiplication of the periodic function ( $u_k(x)$ ) and a particular case of the standing wave equation in periodic systems (Equation 1.7).

$$V(x + n * a) = V(x) \quad (1.6)$$

$$\varphi(x) = e^{ikx} u_k(x) \quad (1.7)$$

where  $x$  is a coordinate (for one-dimensional case);  $n$  - any integer;  $a$  - a reciprocal lattice parameter;  $\varphi$  - electron wavefunction;  $e$  - Euler's number;  $i$  - imaginary unit.

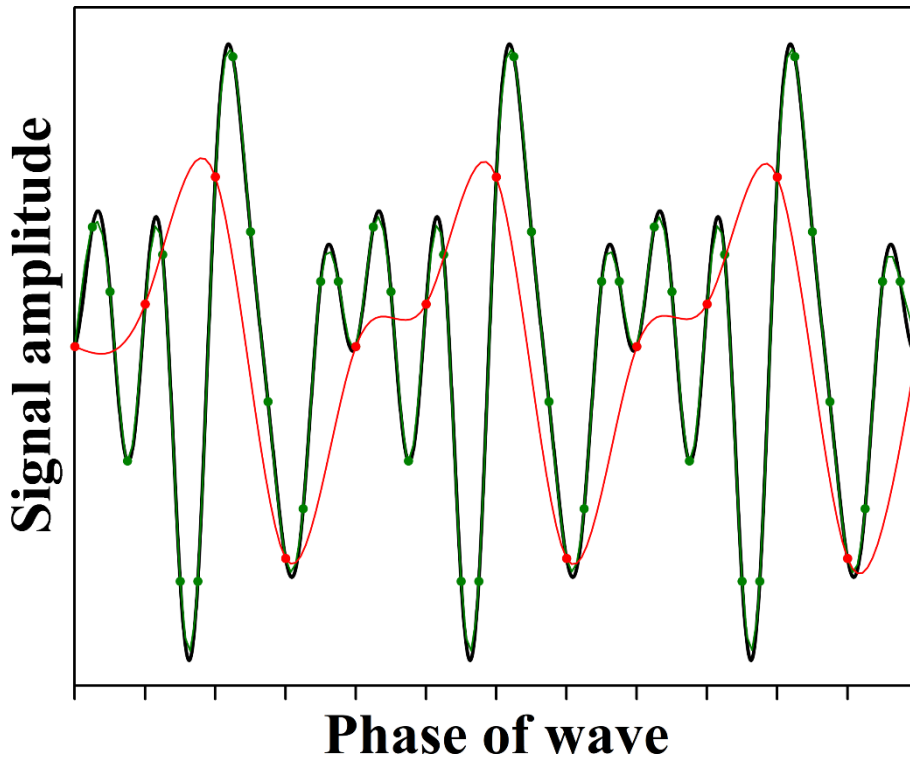


Figure 1.14. Problem of wavefunction sampling in plane waves-based calculations: the real signal (in black) and the signals reproducing it with good (in green) and bad (in red) sampling.

Here, the quasi-vector parameter  $\vec{k}$  is used to describe phases of wavefunction sets inherent to certain planes (plane waves / sets of electrons). This approach is equivalent to a statement that the quasi-momentum of each electron is proportional to its quasi-vector, and therefore the crystal momentum ( $\vec{p}_{crystal}$ ) is proportional to it (Equation 1.8). This is fundamentally wrong because the crystal momentum is periodic up to the parameter  $a$  in contrast to the regular moment in its classical understanding [346] and cannot be estimated with greater accuracy so as not to contradict 2<sup>nd</sup> Noether's theorem (law of conservation of momentum).

$$\vec{p}_{crystal} = \hbar \vec{k} \quad (1.8)$$

where  $\hbar$  is reduced Planck's constant.

This would introduce a significant error in the calculation of any crystal parameters, but a method was invented to partially circumvent this problem. According to the Nyquist-Shannon theorem, any function consisting of waves with frequencies from 0 to  $f$  can be precisely understood probing it with timestep less than  $1/(2f)$  seconds [351]. Thus, the continuous distribution of electrons can be described with an accuracy higher than the lattice parameter by discrete measurement of the phase at several points of the reciprocal lattice of a crystal using  $k$ -vectors [352]. To avoid their aliasing, the required frequency of measurements, i.e. the Nyquist frequency, should be the higher, the stronger the fluctuations of wavefunctions within the crystalline cell. Indeed, the increase in the frequency of sampling causes a proportional growth of the required computational power and time required to study the properties of molecular crystals. The size and descension in the symmetry of molecules in crystals affect the requirements as well [353]. The required discretization in plane-wave calculations on par with their high demand for computational resources makes it possible to apply to molecular crystals methods based on classical aperiodic quantum-chemical calculations as well.

There are just very few methods that could be applied for a wide range of API crystals to assess their stability and the possibility of polymorphic transformations. They can be conditionally divided into those that are used to calculate properties directly from the wavefunction of the system, and those that are based on the distribution of energy in crystals.

Screening for polymorphic modifications and the calculation of the Cauchy stress tensor can be assigned to the first group. Despite the obvious success of screening [14, 23, 99, 107, 108, 196, 354-359], it works without taking into account real experimental structures of API polymorphic forms and often based on the prediction of both conformations and orientations of molecules in crystals or on their pseudo-random change in order to obtain energetically favorable solid forms [354, 355]. Thus, it has a considerable

chance of discrepancy [354, 360]. In turn, the combination of the optimization of a real structure obtained from the X-ray diffraction experiment with the calculation of the Cauchy stress tensor can give results close to the true ones or at least it shows similar trends [355, 361]. However, the lower the conformational flexibility of molecules, the higher the similarity. This is due to the calculation method itself. It performs finite distortions of the lattice in different directions and subsequently calculates the stress and strain followed by the decomposition of the corresponding changes in the lattice parameters into components along the main crystallographic directions [362]. The method is designed to work with ions at the knots of the crystal lattice, i.e. inorganic crystals, therefore, it did not take into account the possibility of changes in the conformation of the contents of the knots of the crystalline cell with the distortion [363]. Therefore, the second group of computational methods, based on calculations of the energies of pair interactions in crystals, is often preferred.

The structure of crystals from the energetic point of view can be described by two approaches: static and dynamic. The first approach implies operations on the initial experimental structure of API crystals, the second - measurements in dynamics. The foundations of the static approach were laid by Kitaygorodskii [364] with the calculations of pairwise atom-atomic potentials. As a matter of fact, a cheaper option than the computations on whole molecules, this technique definitely required improvements. It could not take into account covalent bonding. The periodicity of the crystals was also disregarded, i.e. the influence of the environment on the molecule in the solid phase. However, it could predict stability for molecules like benzene, its annelated analogs, adamantane, etc. [365]

In parallel, the attachment energy model was developed so by Hartman and Perdok [366]. This mechanistic model was based on the fact that the attachment of a new layer of a given thickness to any of the crystal faces with Miller indices (hkl), similarly to the attachment of a molecule, will require some

energy  $E_{hkl}^{att}$ . However, the attachment of layers, unlike molecules, will not depend on the relative position of the attached part and the crystal, or the number of molecules already connected to the surface. The energy of the crystal lattice ( $E_{latt}$ ) in this case is equal to the sum of the attachment (between layers) and slice (in layers) energy ( $E_{hkl}^{slice}$ ):

$$E_{latt} = E_{hkl}^{att} + E_{hkl}^{slice} \quad (1.9)$$

This method allowed to analyze the anisotropy of the energy distribution in molecular crystals, to estimate the relative form stability [18] and to search for the planes potentially capable of deformation under mechanical action [367]. An unpleasant moment is that the definition of the planes for which the calculation will be made is based on visual analysis or topology, or the theory of supramolecular synthons [368, 369]. Therefore, non-obvious options for the locations of planes may be overlooked [370].

New technique able to reveal the anisotropy of the distribution of interaction energy in a crystal with the data solely on its structure without additional assumptions was required. Prof. Gavezzotti solved this by proposing the PIXEL model [371, 372]. Its idea is the possibility to split the electron density of any structure, for example, a group of molecules in a crystal, into infinitesimal parts relative to the size of interacting objects, i.e. pixels. These pixels can be thought of as point dipoles. Consequently, the calculations of the energy of attraction, repulsion, polarization, charge transfer and even empirical dispersion in a London-type inverse sixth-power formulation can be made explicitly. PIXEL model is capable of working with any electron density, including that obtained from high-resolution X-ray diffraction experiments [372] or, theoretically, from plane-wave calculations, giving an idea of the spatial distribution of various energy components in three-dimensional space [373]. The ease of adaptation of the algorithm to the available computing power is also an

advantage of this method because pixels a priori could be agglomerated into enlarged super-pixels. The method of Gavezotti gives a good accuracy in the assessment of the stability of solid forms and, in some cases, of the prerequisites for polymorphic transformations [374-377]. This model is extremely fast due to the parameterization of pixel-pixel, pixel-core and core-core interactions, but its accuracy drops significantly with the appearance of heavy atoms (from the 3<sup>rd</sup> period) and core electrons. This is not an absolute problem for most APIs, since their molecules usually contain just light atoms. However, the systematic underestimation of the energy of hydrogen-bonded crystals and symmetry errors in the polar point groups are [378].

Ab initio quantum-chemical methods do not have such problems. Group of Prof. Shishkin drew attention to this and proposed the newest of the widespread methods to assess the energetic structure of crystals [379]. The general idea of this approach is a logical continuation of the Kitaygorodsky method of atom-atom potentials. It is based on the calculation of the pairwise interaction energies between molecules in a crystal. This is achieved through the formation of the first coordination spheres of each of the molecules in the asymmetric unit to account the non-valence binding of each of them with each neighbor significant from the point of view of the interaction energy. Initially, the first coordination sphere was formed using the Voronoi-Dirichlet triangulation algorithm [380, 381], but it has been replaced by a faster empirical criterion similar to that used in the software package “Mercury” [382]. Molecule belongs to the “Molecular Shell” of the other one just if the distance between at least one pair of their atoms is less than the sum of corresponding van der Waals radii plus 1 Å [383]. Thus, insignificant pairs of molecules are not taken into account, and due to the juxtaposition of the crystal symmetry, the number of necessary calculations can be further reduced [384], making it as computationally cheap as possible.

The high variability of the levels of theory together with the relative cheapness of calculations (depending on the functionals) makes this method extremely popular [385-389]. At the moment, it has been used to study various types of interactions and anisotropy of their distribution, as well as to substantiate the stability of polymorphic forms [160, 385, 390-392], mechanical [392-394] and biological properties [395, 396] of crystals. The method for calculating the pairwise interaction energies in crystals was also combined with the supramolecular theory of synthons. Which states, “supramolecular synthons are structural units within supermolecules which can be formed and / or assembled by known or conceivable synthetic operations involving intermolecular interactions” [397]. It examines all the directional interactions in crystals and allows one to form an idea of the most strongly bound fragments in them (building units) and how the fragments are interconnected (structural motives). However, this applies only to directional interactions, and a quantitative estimate of the binding strength cannot be given on the basis of geometric characteristics alone. Quantum-chemical calculations correct these shortcomings and allow the formulation of numerical criteria for the definition of building units (BU) and basic structural motives (BSM) [383]. Four types of molecular crystals have been identified based on numerous calculations (Figure 1.15):

- Isotropic, where interactions are distributed approximately evenly in all directions.
- Columnar containing BU chains.
- Layered, whose structure is approximately homogeneous in BU layers.
- Columnar-layered crystals, combining anisotropy both within the layers and between them.

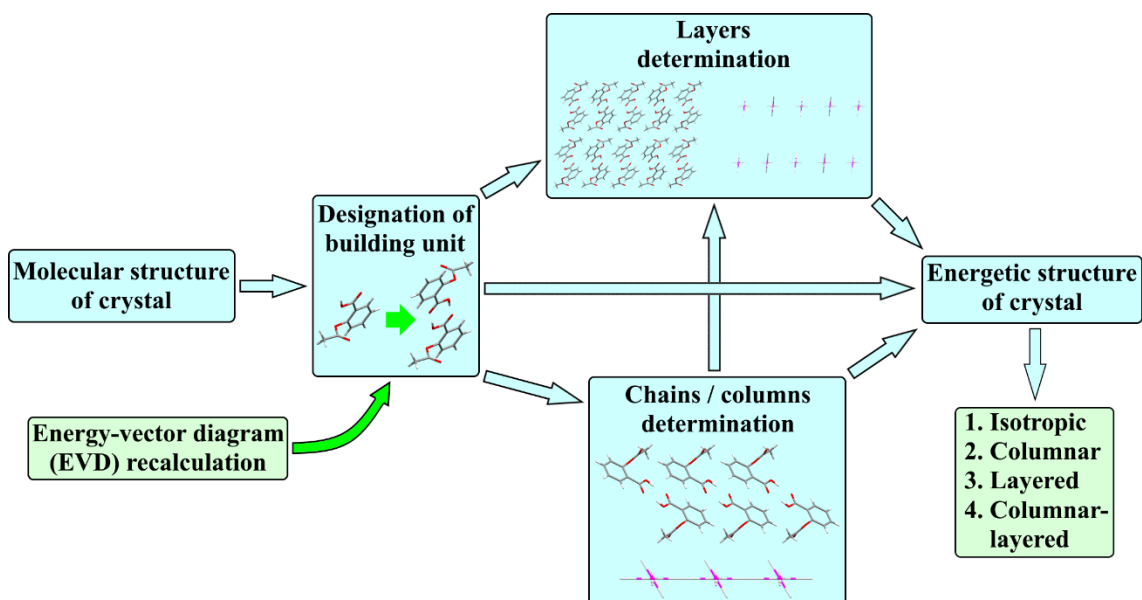


Figure 1.15. Scheme of the identification of basic structural motives from molecular to the energetic structure.

This classification, or more precisely the possibility of an unambiguous choice of crystal fragments resistant to external influence, gives a possibility to advance further in the study of relative stability using an experimentally determined crystal lattice and the possibility of its transformation under mechanical action in a static form.

Of course, mechanical transformations of the crystal lattice during storage or processing cannot be fully modeled on a static model. The dynamics of the displacement should be estimated as well on the base of distortions similar to those discussed for the plane wave calculations of the Cauchy stress tensor. Only two such approaches were found: Burger's vectors [398] with the Peierls-Nabarro slip barriers [399, 400] from the inorganic dislocation theory, as well as the calculation of the contours for the interfacial shear-sliding [401].

Burger's vectors rely on the assumption that the motion of molecules in a crystal is similar to the motion of dislocations, i.e. linear defects. A special closed contour of arbitrary shape surrounding a dislocation in a real crystal can be built by connecting the knots of the crystal lattice. If we then project it onto an ideal crystal, it will be seen that the endpoints of the contour bordering the

dislocation will not be connected. The translation vector connecting the ends of such a contour is called the Burger's vector. Its values in molecular crystals coincide with the distances between the mean planes passing through the centers of inertia of molecules from neighboring layers oriented along the shear direction [402-404]. The smaller it is, the closer the layers and the lower the probability of such movement are. Burger's vectors are still used by themselves [404-406] because layers with high interlayer separation obviously have shown themselves to be plastic and capable of polymorphic transformations [393, 394, 402, 403]. However, the calculation of the Peierls-Nabarro slip barriers based on these vectors is more informative [407-410]. Barriers are not formally dynamic, because for their calculation, the movement of molecules is still not taken into account, and the resistance of materials to mechanical stress is estimated using the thermodynamic approach. This method postulates that the quantitative characteristic of deformation / transformation will be the energy difference between the final and initial states. It is proportional to the maximum possible force  $\sigma_{pn}b$  acting on the body during the normal deviation from the plane of motion by the maximum distance, i.e. Burger's vector  $b$ , and is expressed by the following harmonic potential [411]:

$$U(y) = \frac{\sigma_{pn}ba}{2\pi} \left[ 1 - \cos\left(\frac{2\pi y}{a}\right) \right] - \sigma by \quad (1.10)$$

where  $\sigma_{pn}$  is the stress of the pinning (Peierls stress);  $a$  - lattice parameter in the direction of shear;  $y$  - the dislocation displacement in a slip plane;  $\sigma by$  is the additional external stress affecting the crystal in the direction of molecular movement on compression.

It is seen that this potential is unapplicable to crystals whose knots are occupied by non-point charges. Superposition of multiple harmonic potentials

can help to some extent, but the shape of molecules is neglected in Peierls-Nabarro displacement barriers [410, 411].

A relatively new method, which makes not only the causes and mechanisms of polymorphic transitions understandable but also gives a possibility to predict their occurrence, was proposed by Prof. Chaoyang Zhang [400]. However, its application at the moment is limited to the response of energetic materials to mechanical action [401, 412-417]. The logic of the method is as follows:

1. Layers of molecules in the (hkl) plane can be distinguished on the basis of visual observations and the theory of synthons in a crystal.
2. Adjacent crystalline layers are capable of shifting relative to each other in this plane, up to positions identical to the original one.
3. The crystal structure is optimized after each displacement step and the interaction energy analogous to the attachment one is calculated.
4. The maximum energy required for a molecule to move to a new position through all intermediate points is estimated and compared with the activation energy of the decomposition of a polymorphic modification.

Obviously, the method requires some improvements, in particular, it should be combined with the method of pairwise interaction energies in crystals to reduce the excessively high costs of computational time for multiple calculations of the attachment energy. Optimization at every point also puts questions. On the one hand, it allows one to get rid of the problem of rigid conformations and take into account the ability of the molecules themselves to deform during shear. On the other hand, it also makes the calculation many times more expensive, if at all possible (depending on the convergence of the wavefunction), and causes changes in the geometry of molecules from the experimentally determined one.

Thereby, a new method that would combine static and dynamic assessment of stability and the possibility of structural transformations in the crystals of APIs. The criteria for its effectiveness are:

- Workability under normal conditions and the influence of mechanical stress.
- Capability to work on a structure as close as possible to the experimentally determined by X-ray diffraction methods.
- Consideration of the real conformation of molecules
- The maximum possible ratio of price-quality-information content in the analysis of the structures of polymorphic modifications of APIs.

### **1.9. Conclusions**

Combining all the mentioned above, crystal polymorphism is indeed a problem for the pharmaceutical industry. It can create challenges at any stages of APIs manufacturing and already led to the numerous accidents in the latest 40 years (Section 1.1). Among the many ways for a drug to change, namely, polymorphism is the most difficult to control and analyze, because it can happen to any class of pharmaceutical solid forms without the variation of a crystal chemical composition. Thus, the orientation and conformation of the molecules have to be analyzed to characterize crystalline structures and to understand the mechanism of the polymorphs formation during the manufacturing (Section 1.2).

As shown in Section 1.3, the current theory of nucleation becomes inefficient for the description of the polymorphs formation from fluids and transformations in solid phases. Thereby, the improvement should be introduced to the theory for the both cases to synthesize the polymorphic modifications of interest and to preserve them during further processing and storage.

The most spread experimental methods used for the synthesis of desired polymorphic modifications do not allow the complete control of the polymorphs

formation processes (Section 1.4). Thus, the pressure, for example, is out of control in most experimental techniques. The recrystallization of the drugs as the well-known crystallization pathway does not allow it too, but it can be improved with the introduction of the supercritical technology. It is shown in Section 1.5 that the two methods fit best for APIs. They are the rapid expansion of supercritical solutions and the crystallization from supercritical solution. The supercritical CO<sub>2</sub> is used for the both of them, however, solely the CSS works in equilibrium conditions and so allows to reproduce perfectly the conditions of polymorphs formation. CSS is the method, which will be discussed a lot in Chapter 3 of the thesis and used on par with the in situ analytical techniques (Section 1.7) in order to analyze the relationship of conformations in solution and resulting polymorphic forms.

The other family of methods used to reach polymorphic transformations is the mechanical processing of APIs. It can be used as for the synthesis, as for the analysis showing the proximity of practical and theoretical approaches. A lot of data is available on the most known methods: grinding, DAC and nanoindentation (Section 1.6). This data, especially the experimental crystalline structures received under pressure, will be used by us to create a new computational approach for the analysis and prediction of the mechanical properties and polymorphic transformations of the crystal structure. The crucial criteria for the new method able to analyze the orientational changes of molecules in crystals during the mechanical treatment are formulated in Section 1.8 from the comprehensive analysis of the existing computational approaches. The application of the technique will be discussed in details in Chapter 4.

## 1.10. References for Chapter 1

- (1) Karimi-Jafari, M.; Padrela, L.; Walker, G.M.; Croker, D.M. Creating cocrystals: A review of pharmaceutical cocrystal preparation routes and applications. *Crystal Growth & Design* **2018**. *18* (10), 6370-6387.
- (2) Béchar, S.; Mouget, Y.: Libs for the analysis of pharmaceutical materials. In *Laser induced breakdown spectroscopy*; Miziolek, A.W., Schechter, I., Palleschi, V. Eds.; Cambridge University Press: Cambridge, 2006, pp. 314-331.
- (3) Gadade, D.D.; Pekamwar, S.S. Pharmaceutical cocrystals: Regulatory and strategic aspects, design and development. *Advanced Pharmaceutical Bulletin* **2016**. *6* (4), 479-494.
- (4) Tiwary, A.K. Modification of crystal habit and its role in dosage form performance. *Drug Development and Industrial Pharmacy* **2001**. *27* (7), 699-709.
- (5) Sood, J.; Sapra, B.; Bhandari, S.; Jindal, M.; Tiwary, A.K. Understanding pharmaceutical polymorphic transformations I: Influence of process variables and storage conditions. *Therapeutic Delivery* **2014**. *5* (10), 1123-1142.
- (6) Hadjittofis, E.; Isbell, M.A.; Karde, V.; Varghese, S.; Ghoroi, C., *et al.* Influences of crystal anisotropy in pharmaceutical process development. *Pharmaceutical Research* **2018**. *35* (5), 100 (1-22).
- (7) Wöhler; Liebig Untersuchungen über das radikal der benzoessäure. *Annalen der Pharmacie* **1832**. *3* (3), 249-282.
- (8) Vegard, L. VI. Results of crystal analysis. *The London, Edinburgh, and Dublin Philosophical Magazine and Journal of Science* **1916**. *32* (187), 65-96.
- (9) Tawashi, R. Aspirin: Dissolution rates of two polymorphic forms. *Science* **1968**. *160* (3823), 76.
- (10) McCrone, W.C.: Polymorphism. In *Physics and chemistry of the organic solid state*; Fox, D.; Labes, M.M.; Weissberger, A. Eds.; Wiley-Interscience: New York, 1965, pp. 725-767.
- (11) Gilman, J.T.; Duchowny, M.S.; Resnick, T.J.; Hershorin, E.R. Carbamazepine malabsorption: A case report. *Pediatrics* **1988**. *82* (3), 518-519.
- (12) Kok, W.J.J.; Vrijhof, W.P. Impairment of carbamazepine tablet disintegration in patients. *International Journal of Pharmaceutics* **1992**. *86* (2), 259-262.
- (13) Rustichelli, C.; Gamberini, G.; Ferioli, V.; Gamberini, M.C.; Ficarra, R., *et al.* Solid-state study of polymorphic drugs: Carbamazepine. *Journal of Pharmaceutical and Biomedical Analysis* **2000**. *23* (1), 41-54.
- (14) Cruz-Cabeza, A.J.; Reutzel-Edens, S.M.; Bernstein, J. Facts and fictions about polymorphism. *Chemical Society Reviews* **2015**. *44* (23), 8619-8635.
- (15) Bradshaw, J.; Clitherow, J.W.; Price, B.J. US4128658A. Aminoalkyl furan derivatives, **1978**.
- (16) Crookes, D.L. US4521431A. Aminoalkyl furan derivative, **1985**.
- (17) Crookes, D.L. US4672133A. Process for forming form 2 ranitidine hydrochloride, **1987**.
- (18) Bernstein, J. *Polymorphism in molecular crystals*; Oxford University Press: Oxford, 2002, pp. 297-307.
- (19) Chemburkar, S.R.; Bauer, J.; Deming, K.; Spiwek, H.; Patel, K., *et al.* Dealing with the impact of ritonavir polymorphs on the late stages of bulk drug process development. *Organic Process Research & Development* **2000**. *4* (5), 413-417.
- (20) Bauer, J.; Spanton, S.; Henry, R.; Quick, J.; Dziki, W., *et al.* Ritonavir: An extraordinary example of conformational polymorphism. *Pharmaceutical Research* **2001**. *18* (6), 859-866.

- (21) Santos, O.M.M.; Reis, M.E.D.; Jacon, J.T.; Lino, M.E.D.S.; Simões, J.S., *et al.* Polymorphism: An evaluation of the potential risk to the quality of drug products from the farmácia popular rede própria. *Brazilian Journal of Pharmaceutical Sciences* **2014**. *50*, 1-24.
- (22) Lee, A.Y.; Erdemir, D.; Myerson, A.S. Crystal polymorphism in chemical process development. *Annual Review of Chemical and Biomolecular Engineering* **2011**. *2 (1)*, 259-280.
- (23) Abramov, Y.A.: Computational pharmaceutical solid-state chemistry. In *Computational pharmaceutical solid state chemistry*; Abramov, Y.A. Ed.; John Wiley & Sons: Hoboken, New Jersey, 2016, pp. 1-13.
- (24) European Patent Office, Espacenet, 2021, [Online] <https://worldwide.espacenet.com>
- (25) Andrews, P. *Top 200 drugs in the csd*, 2020, [Online] <https://www.ccdc.cam.ac.uk/Community/blog/2020-04-15-top-200-drugs-in-the-csd>
- (26) Kirsanov, D. Pharmacy market of ukraine according to the results of the 1st quarter 2019: Helicopter view [Translated from Russian], 2019, [Online] <https://www.apteka.ua/article/498776>
- (27) Raza, K. Polymorphism: The phenomenon affecting the performance of drugs. *SOJ Pharmacy & Pharmaceutical Sciences* **2014**. *1 (2)*, 1-10.
- (28) Shankland, N.; Florence, A.J.; Cox, P.J.; Sheen, D.B.; Love, S.W., *et al.* Crystal morphology of ibuprofen predicted from single-crystal pulsed neutron diffraction data. *Chemical Communications* **1996** (7), 855-856.
- (29) Derollez, P.; Dudognon, E.; Affouard, F.; Danede, F.; Correia, N.T., *et al.* Ab initio structure determination of phase II of racemic ibuprofen by X-ray powder diffraction. *Acta Crystallographica Section B* **2010**. *66 (1)*, 76-80.
- (30) Johari, G.P.; Kim, S.; Shanker, R.M. Dielectric relaxation and crystallization of ultraviscous melt and glassy states of aspirin, ibuprofen, progesterone, and quinidine. *Journal of Pharmaceutical Sciences* **2007**. *96 (5)*, 1159-1175.
- (31) Shen, J.; Tang, G.-P.; Hu, X.-R. Crystal structure of (S)-5-chloro-N-({2-oxo-3-[4-(3-oxomorpholin-4-yl)phenyl]oxazolidin-5-yl}methyl)thiophene-2-carboxamide. *Acta Crystallographica Section E* **2018**. *74 (1)*, 51-54.
- (32) Bodhuri, P.; Weeratunga, G. WO2010075631A1. Polymorphic form of 5-chloro-n-{{(5s)-2-oxo-3-{{4-(3-oxomorpholin-4-yl)phenyl}oxa-zolidin-5-yl}-methyl}thiophene-2-carboxamide, **2010**.
- (33) Grunenber, A.; Lenz, J.; Braun, G.A.; Keil, B.; Thomas, C.R. WO2007039132A1. Novel polymorphous form and the amorphous form of 5-chloro-n-{{(5s)-2-oxo-3[4-(3-oxo-4-morpholinyl(-phenyl)]-1,3-oxazolidine-5-yl}-methyl)-2-thiophene carboxamide, **2006**.
- (34) Xu, Y.; Wu, S.-P.; Liu, X.-J.; Zhang, L.-J.; Lu, J. Crystal characterization and transformation of the forms I and II of anticoagulant drug rivaroxaban. *Crystal Research and Technology* **2017**. *52 (3)*, 1600379.
- (35) Zupancic, S.; Benkic, P. EP3309158A1. Crystalline form k of rivaroxaban and process for its preparation, **2018**.
- (36) Dupont, L.; Pirotte, B.; Masereel, B.; Delarge, J.; Geczy, J. Nimesulide. *Acta Crystallographica Section C* **1995**. *51 (3)*, 507-509.
- (37) Sanphui, P.; Sarma, B.; Nangia, A. Phase transformation in conformational polymorphs of nimesulide. *Journal of Pharmaceutical Sciences* **2011**. *100 (6)*, 2287-2299.
- (38) Wang, X.; Zhang, J. CN105384664A. Novel crystal habit of nimesulide, **2015**.
- (39) Krishna Murthy, H.M.; Brehm, L. Structural studies of analgesics and their interactions. V. The crystal and molecular structure of metamizol monohydrate. *Acta Crystallographica Section B* **1979**. *35 (3)*, 612-615.

- (40) Popeneciu, H.G. **2018**, *Study of pharmaceutical compound involved in environmental pollution*, PhD thesis, Babes-Bolyai University, Cluj-Napoca.
- (41) Salunke, D.M.; Vijayan, M. L-arginine L-aspartate. *Acta Crystallographica Section B* **1982**. *38* (4), 1328-1330.
- (42) Chen, L.; Guo, W.; Guo, Z.; Wang, Z.; Ye, Y. CN103694171A. Drotaverine hydrochloride crystal form III and crystal form IV and preparation method thereof, **2013**.
- (43) Chen, L.; Guo, W.; Guo, Z.; Wang, Z.; Ye, Y. CN103664781A. Drotaverine hydrochloride crystal form I and crystal form II and preparation method, **2013**.
- (44) Takusagawa, F.; Koetzle, T.F.; Kou, W.W.H.; Parthasarathy, R. Structure of N-acetyl-L-cysteine: X-ray (T = 295 K) and neutron (T = 16 K) diffraction studies. *Acta Crystallographica Section B* **1981**. *37* (8), 1591-1596.
- (45) Kumar, S.S.; Nangia, A. A new conformational polymorph of N-acetyl-L-cysteine. The role of S-H...O and C-H...O interactions. *CrystEngComm* **2013**. *15* (33), 6498-6505.
- (46) Wang, J.-R.; Wang, X.; Lu, L.; Mei, X. Highly crystalline forms of valsartan with superior physicochemical stability. *Crystal Growth & Design* **2013**. *13* (7), 3261-3269.
- (47) Aronhime, J.; Flyaks, E.; Koltai, T.; Rukhman, I. WO2004083192A1. Polymorphs of valsartan, **2004**.
- (48) Munns, A.R.I.; Tollin, P. The crystal and molecular structure of inosine. *Acta Crystallographica Section B* **1970**. *26* (8), 1101-1113.
- (49) Subramanian, E. Inosine. *Crystal Structure Communications* **1979**. *8*, 777.
- (50) Kashino, S.; Matsushita, T.; Iwamoto, T.; Yamaguchi, K.; Haisa, M. Structure of N-aromatic amides. II. XC6H4NHC(O)Y. *Acta Crystallographica Section C* **1986**. *42* (4), 457-462.
- (51) G. M. Edwards, H.; Lawson, E.; de Matas, M.; Shields, L.; York, P. Metamorphosis of caffeine hydrate and anhydrous caffeine. *Journal of the Chemical Society, Perkin Transactions 2* **1997** (10), 1985-1990.
- (52) Derollez, P.; Correia, N.T.; Danede, F.; Capet, F.; Affouard, F., *et al.* Ab initio structure determination of the high-temperature phase of anhydrous caffeine by X-ray powder diffraction. *Acta Crystallographica Section B* **2005**. *61* (3), 329-334.
- (53) Enright, G.D.; Terskikh, V.V.; Brouwer, D.H.; Ripmeester, J.A. The structure of two anhydrous polymorphs of caffeine from single-crystal diffraction and ultrahigh-field solid-state <sup>13</sup>C NMR spectroscopy. *Crystal Growth & Design* **2007**. *7* (8), 1406-1410.
- (54) Shi, X.; Wong, S.Y.; Yang, X.; Myerson, A.S. Concomitant cocrystallization on engineered surfaces. *CrystEngComm* **2013**. *15* (37), 7450-7455.
- (55) Dichi, E.; Legendre, B.; Sghaier, M. Physico-chemical characterisation of a new polymorph of caffeine. *Journal of Thermal Analysis and Calorimetry* **2014**. *115* (2), 1551-1561.
- (56) Schleinitz, M., **2016**, *Oxalic acid – phase behavior of a cocrystal and hydrate forming component*, Master thesis, Technical University of Dortmund, Dortmund.
- (57) Perrin, M.-A.; Neumann, M.A.; Elmaleh, H.; Zaske, L. Crystal structure determination of the elusive paracetamol form III. *Chemical Communications* **2009** (22), 3181-3183.
- (58) Stone, K.H.; Lapidus, S.H.; Stephens, P.W. Implementation and use of robust refinement in powder diffraction in the presence of impurities. *Journal of Applied Crystallography* **2009**. *42* (3), 385-391.
- (59) Chan, E.J.; Goossens, D.J. Study of the single-crystal X-ray diffuse scattering in paracetamol polymorphs. *Acta Crystallographica Section B* **2012**. *68* (1), 80-88.
- (60) Anitha, R.; Gunasekaran, M.; Kumar, S.S.; Athimoolam, S.; Sridhar, B. Single crystal XRD, vibrational and quantum chemical calculation of pharmaceutical drug paracetamol: A new synthesis form. *Spectrochimica Acta Part A: Molecular and Biomolecular Spectroscopy* **2015**. *150*, 488-498.

- (61) Reiss, C.A.; Mechelen, J.B.V.; Goubitz, K.; Peschar, R. Reassessment of paracetamol orthorhombic form III and determination of a novel low-temperature monoclinic form III-m from powder diffraction data. *Acta Crystallographica Section C* **2018**. *74* (3), 392-399.
- (62) Shtukenberg, A.G.; Tan, M.; Vogt-Maranto, L.; Chan, E.J.; Xu, W., *et al.* Melt crystallization for paracetamol polymorphism. *Crystal Growth & Design* **2019**. *19* (7), 4070-4080.
- (63) Martino, P.D.; Palmieri, G.F.; Martelli, S. Molecular mobility of the paracetamol amorphous form. *Chemical and Pharmaceutical Bulletin* **2000**. *48* (8), 1105-1108.
- (64) Bond, A.D.; Boese, R.; Desiraju, G.R. On the polymorphism of aspirin: Crystalline aspirin as intergrowths of two “polymorphic” domains. *Angewandte Chemie International Edition* **2007**. *46* (4), 618-622.
- (65) Bond, A.D.; Boese, R.; Desiraju, G.R. On the polymorphism of aspirin. *Angewandte Chemie International Edition* **2007**. *46* (4), 615-617.
- (66) Shtukenberg, A.G.; Hu, C.T.; Zhu, Q.; Schmidt, M.U.; Xu, W., *et al.* The third ambient aspirin polymorph. *Crystal Growth & Design* **2017**. *17* (6), 3562-3566.
- (67) Fukuoka, E.; Makita, M.; Nakamura, Y. Glassy state of pharmaceuticals. V. Relaxation during cooling and heating of glass by differential scanning calorimetry. *Chemical & Pharmaceutical Bulletin* **1991**. *39* (8), 2087-2090.
- (68) Crowell, E.L.; Dreger, Z.A.; Gupta, Y.M. High-pressure polymorphism of acetylsalicylic acid (aspirin): Raman spectroscopy. *Journal of Molecular Structure* **2015**. *1082*, 29-37.
- (69) Hvoslef, J. The crystal structure of L-ascorbic acid, 'vitamin C'. II. The neutron diffraction analysis. *Acta Crystallographica Section B* **1968**. *24* (11), 1431-1440.
- (70) Albertsson, J.; Oskarsson, A.; Svensson, C. X-ray study of budesonide: Molecular structures and solid solutions of the (22S) and (22R) epimers of 11 $\beta$ ,21-dihydroxy-16 $\alpha$ ,17 $\alpha$ -propylmethylenedioxy-1,4-pregnadiene-3,20-dione. *Acta Crystallographica Section B* **1978**. *34* (10), 3027-3036.
- (71) Descamps, M.; Willart, J.F.; Dudognon, E.; Caron, V. Transformation of pharmaceutical compounds upon milling and comilling: The role of Tg. *Journal of Pharmaceutical Sciences* **2007**. *96* (5), 1398-1407.
- (72) Kuhnert-Brandstätter, M.; Grimm, H. Zur unterscheidung von lösungsmittelhaltigen pseudopolymorphen kristallformen und polymorphen modifikationen bei steroidhormonen. I. *Microchimica Acta* **1968**. *56* (1), 115-126.
- (73) Halebian, J.; McCrone, W. Pharmaceutical applications of polymorphism. *Journal of Pharmaceutical Sciences* **1969**. *58* (8), 911-929.
- (74) Pfeiffer, R.R.; Yang, K.S.; Tucker, M.A. Crystal pseudopolymorphism of cephaloglycin and cephalixin. *Journal of Pharmaceutical Sciences* **1970**. *59* (12), 1809-1814.
- (75) Bettinetti, G.P. X-ray diffractometry in the analysis of drugs and pharmaceutical forms. *Bollettino Chimico Farmaceutico* **1989**. *128* (5), 149-62.
- (76) Byrn, S.R.; Pfeiffer, R.R.; Stephenson, G.; Grant, D.J.W.; Gleason, W.B. Solid-state pharmaceutical chemistry. *Chemistry of Materials* **1994**. *6* (8), 1148-1158.
- (77) Carstensen, J.T. *Advanced pharmaceutical solids*; Taylor & Francis: Boca Raton, 2000, pp. 134-157.
- (78) Desiraju, G.R. Polymorphism: The same and not quite the same. *Crystal Growth & Design* **2008**. *8* (1), 3-5.
- (79) Aaltonen, J.; Allesø, M.; Mirza, S.; Koradia, V.; Gordon, K.C., *et al.* Solid form screening – a review. *European Journal of Pharmaceutics and Biopharmaceutics* **2009**. *71* (1), 23-37.

- (80) Aitipamula, S.; Banerjee, R.; Bansal, A.K.; Biradha, K.; Cheney, M.L., *et al.* Polymorphs, salts, and cocrystals: What's in a name? *Crystal Growth & Design* **2012**. *12* (5), 2147-2152.
- (81) Gosar, A.; Hussain, D.; Shaikh, T. Polymorphism and polymorph characterisation in pharmaceuticals. *Journal of Biomedical and Pharmaceutical Research* **2019**. *8* (5), 52-59.
- (82) Leane, M.; Pitt, K.; Reynolds, G. A proposal for a drug product manufacturing classification system (MCS) for oral solid dosage forms. *Pharmaceutical Development and Technology* **2015**. *20* (1), 12-21.
- (83) Leane, M.; Pitt, K.; Reynolds, G.K.; Dawson, N.; Ziegler, I., *et al.* Manufacturing classification system in the real world: Factors influencing manufacturing process choices for filed commercial oral solid dosage formulations, case studies from industry and considerations for continuous processing. *Pharmaceutical Development and Technology* **2018**. *23* (10), 964-977.
- (84) Bryant, M.J.; Black, S.N.; Blade, H.; Docherty, R.; Maloney, A.G.P., *et al.* The CSD drug subset: The changing chemistry and crystallography of small molecule pharmaceuticals. *Journal of Pharmaceutical Sciences* **2019**. *108* (5), 1655-1662.
- (85) Grothe, E.; Meekes, H.; Vlieg, E.; Ter Horst, J.H.; de Gelder, R. Solvates, salts, and cocrystals: A proposal for a feasible classification system. *Crystal Growth & Design* **2016**. *16* (6), 3237-3243.
- (86) Verma, A.R.; Verma, Q.R.; Krishna, P. *Polymorphism and polytypism in crystals*; John Wiley & Sons: New York, 1966, 362 p.
- (87) Kuhnert-Brandstätter, M. Polymorphie bei arzneistoffen. *Pharmazie in unserer Zeit* **1975**. *4* (5), 131-137.
- (88) Cheng, Y.-T.; Johnson, W.L. Disordered materials: A survey of amorphous solids. *Science* **1987**. *235* (4792), 997-1002.
- (89) Stachurski, Z.H. On structure and properties of amorphous materials. *Materials* **2011**. *4* (9), 1564-1598.
- (90) Bellantone, R.A.: Fundamentals of amorphous systems: Thermodynamic aspects. In *Amorphous solid dispersions: Theory and practice*; Shah, N.; Sandhu, H.; Choi, D.S.; Chokshi, H.; Malick, A.W. Eds.; Springer New York: New York, 2014, pp. 3-34.
- (91) Wei, D.; Yang, J.; Jiang, M.-Q.; Dai, L.-H.; Wang, Y.-J., *et al.* Assessing the utility of structure in amorphous materials. *The Journal of Chemical Physics* **2019**. *150* (11), 114502 (1-11).
- (92) Stoler, E.; Warner, J.C. Non-covalent derivatives: Cocrystals and eutectics. *Molecules* **2015**. *20* (8), 14833-14848.
- (93) Bauer-Brandl, A.; Marti, E.; Geoffroy, A.; Poso, A.; Suurkuusk, J., *et al.* Comparison of experimental methods and theoretical calculations on crystal energies of 'isoenergetic' polymorphs of cimetidine. *Journal of Thermal Analysis and Calorimetry* **1999**. *57* (1), 7-22.
- (94) Cherukuvada, S.; Thakuria, R.; Nangia, A. Pyrazinamide polymorphs: Relative stability and vibrational spectroscopy. *Crystal Growth & Design* **2010**. *10* (9), 3931-3941.
- (95) Reilly, A.M.; Tkatchenko, A. Seamless and accurate modeling of organic molecular materials. *The Journal of Physical Chemistry Letters* **2013**. *4* (6), 1028-1033.
- (96) Cruz-Cabeza, A.J.; Bernstein, J. Conformational polymorphism. *Chemical Reviews* **2014**. *114* (4), 2170-2191.
- (97) Price, S.L. Predicting crystal structures of organic compounds. *Chemical Society Reviews* **2014**. *43* (7), 2098-2111.
- (98) Thompson, H.P.G.; Day, G.M. Which conformations make stable crystal structures? Mapping crystalline molecular geometries to the conformational energy landscape. *Chemical Science* **2014**. *5* (8), 3173-3182.

- (99) Anwar, J.; Zahn, D. Polymorphic phase transitions: Macroscopic theory and molecular simulation. *Advanced Drug Delivery Reviews* **2017**. *117*, 47-70.
- (100) Surov, A.O.; Manin, A.N.; Voronin, A.P.; Churakov, A.V.; Perlovich, G.L., *et al.* Weak interactions cause packing polymorphism in pharmaceutical two-component crystals. The case study of the salicylamide cocrystal. *Crystal Growth & Design* **2017**. *17* (3), 1425-1437.
- (101) Zaczek, A.J.; Catalano, L.; Naumov, P.; Korter, T.M. Mapping the polymorphic transformation gateway vibration in crystalline 1,2,4,5-tetrabromobenzene. *Chemical Science* **2019**. *10* (5), 1332-1341.
- (102) Nyman, J.; Day, G.M. Static and lattice vibrational energy differences between polymorphs. *CrystEngComm* **2015**. *17* (28), 5154-5165.
- (103) Reilly, A.M.; Tkatchenko, A. Understanding the role of vibrations, exact exchange, and many-body van der waals interactions in the cohesive properties of molecular crystals. *The Journal of Chemical Physics* **2013**. *139* (2), 024705 (1-13).
- (104) Dolgonos, G.A.; Hoja, J.; Boese, A.D. Revised values for the X23 benchmark set of molecular crystals. *Physical Chemistry Chemical Physics* **2019**. *21* (44), 24333-24344.
- (105) Stein, M.; Heimsaat, M. Intermolecular interactions in molecular organic crystals upon relaxation of lattice parameters. *Crystals* **2019**. *9* (12), 665 (1-17).
- (106) Price, S. Why don't we find more polymorphs? *Acta Crystallographica Section B* **2013**. *69* (4), 313-328.
- (107) Price, S.L.; Braun, D.E.; Reutzel-Edens, S.M. Can computed crystal energy landscapes help understand pharmaceutical solids? *Chemical Communications* **2016**. *52* (44), 7065-7077.
- (108) Mortazavi, M.; Hoja, J.; Aerts, L.; Quéré, L.; van de Streek, J., *et al.* Computational polymorph screening reveals late-appearing and poorly-soluble form of rotigotine. *Communications Chemistry* **2019**. *2* (1), 70 (1-7).
- (109) Yang, M.; Dybeck, E.; Sun, G.; Peng, C.; Samas, B., *et al.* Prediction of the relative free energies of drug polymorphs above zero kelvin. *Crystal Growth & Design* **2020**. *20* (8), 5211-5224.
- (110) Tutughamiarso, M.; Wagner, G.; Egert, E. Cocrystals of 5-fluorocytosine. I. Cofomers with fixed hydrogen-bonding sites. *Acta Crystallographica Section B* **2012**. *68* (4), 431-443.
- (111) Terada, K.; Kurobe, H.; Ito, M.; Yoshihashi, Y.; Yonemochi, E., *et al.* Polymorphic and pseudomorphic transformation behavior of acyclovir based on thermodynamics and crystallography. *Journal of Thermal Analysis and Calorimetry* **2013**. *113* (3), 1261-1267.
- (112) Tessler, L.; Goldberg, I. Crystal structures of aripiprazole, a new anti-psychotic drug, and of its inclusion compounds with methanol, ethanol and water. *Journal of inclusion phenomena and macrocyclic chemistry* **2006**. *55* (3), 255-261.
- (113) Braun, D.E.; Gelbrich, T.; Kahlenberg, V.; Tessadri, R.; Wieser, J., *et al.* Conformational polymorphism in aripiprazole: Preparation, stability and structure of five modifications. *Journal of Pharmaceutical Sciences* **2009**. *98* (6), 2010-2026.
- (114) Nanubolu, J.B.; Sridhar, B.; Babu, V.S.P.; Jagadeesh, B.; Ravikumar, K. Sixth polymorph of aripiprazole - an antipsychotic drug. *CrystEngComm* **2012**. *14* (14), 4677-4685.
- (115) Delaney, S.P.; Pan, D.; Yin, S.X.; Smith, T.M.; Korter, T.M. Evaluating the roles of conformational strain and cohesive binding in crystalline polymorphs of aripiprazole. *Crystal Growth & Design* **2013**. *13* (7), 2943-2952.
- (116) Delaney, S.P.; Smith, T.M.; Pan, D.; Yin, S.X.; Korter, T.M. Low-temperature phase transition in crystalline aripiprazole leads to an eighth polymorph. *Crystal Growth & Design* **2014**. *14* (10), 5004-5010.

- (117) Zeidan, T.A.; Trotta, J.T.; Tilak, P.A.; Oliveira, M.A.; Chiarella, R.A., *et al.* An unprecedented case of dodecamorphism: The twelfth polymorph of aripiprazole formed by seeding with its active metabolite. *CrystEngComm* **2016**. *18* (9), 1486-1488.
- (118) Tyler, A.R.; Ragbirsingh, R.; McMonagle, C.J.; Waddell, P.G.; Heaps, S.E., *et al.* Encapsulated nanodroplet crystallization of organic-soluble small molecules. *Chem* **2020**. *6* (7), 1755-1765.
- (119) Cuffini, S.; Howie, R.A.; Tiekink, E.R.T.; Wardell, J.L.; Wardell, S.M.S.V. (S)-6-chloro-4-cyclopropylethynyl-4-trifluoromethyl-1H-3,1-benzoxazin-2(4H)-one. *Acta Crystallographica Section E* **2009**. *65* (12), o3170-o3171.
- (120) Ravikumar, K.; Sridhar, B. Molecular and crystal structure of efavirenz, a potent and specific inhibitor of HIV-1 reverse transcriptase, and its monohydrate. *Molecular Crystals and Liquid Crystals* **2009**. *515* (1), 190-198.
- (121) Mahapatra, S.; Thakur, T.S.; Joseph, S.; Varughese, S.; Desiraju, G.R. New solid state forms of the anti-HIV drug efavirenz. Conformational flexibility and high Z' issues. *Crystal Growth & Design* **2010**. *10* (7), 3191-3202.
- (122) De Melo, A.C.C.; de Amorim, I.F.; Cirqueira, M.D.L.; Martins, F.T. Toward novel solid-state forms of the anti-HIV drug efavirenz: From low screening success to cocrystals engineering strategies and discovery of a new polymorph. *Crystal Growth & Design* **2013**. *13* (4), 1558-1569.
- (123) Iwata, M.; Nagase, H.; Endo, T.; Ueda, H. Glimepiride. *Acta Crystallographica Section C* **1997**. *53* (3), 329-331.
- (124) Endo, T.; Iwata, M.; Nagase, H.; Shiro, M.; Ueda, H. Polymorphism of glimepiride: Crystallographic study, thermal transitions behavior and dissolution study. *S.T.P. Pharma Sciences* **2003**. *13*, 281-286.
- (125) Maccaroni, E.; Alberti, E.; Malpezzi, L.; Masciocchi, N.; Vladiskovic, C. Polymorphism of linezolid: A combined single-crystal, powder diffraction and NMR study. *International Journal of Pharmaceutics* **2008**. *351* (1), 144-151.
- (126) Tanaka, R.; Hirayama, N. Crystal structure of linezolid. *Analytical Sciences: X-ray Structure Analysis Online* **2008**. *24*, x43-x44.
- (127) Basavoju, S.; Boström, D.; Velaga, S.P. Pharmaceutical cocrystal and salts of norfloxacin. *Crystal Growth & Design* **2006**. *6* (12), 2699-2708.
- (128) Barbas, R.; Prohens, R.; Puigjaner, C. A new polymorph of norfloxacin. *Journal of Thermal Analysis and Calorimetry* **2007**. *89* (3), 687-692.
- (129) Hempel, A.; Camerman, N.; Camerman, A.; Mastropaolo, D. Oxcarbazepine: Structure and anticonvulsant activity. *Acta Crystallographica Section E* **2005**. *61* (5), o1313-o1315.
- (130) Lutker, K.M.; Matzger, A.J. Crystal polymorphism in a carbamazepine derivative: Oxcarbazepine. *Journal of Pharmaceutical Sciences* **2010**. *99* (2), 794-803.
- (131) Williams, P. Polymorphism of phenobarbitone. II. The crystal structure of modification III. *Acta Crystallographica Section B* **1974**. *30* (1), 12-17.
- (132) Platteau, C.; Lefebvre, J.; Hemon, S.; Baetz, C.; Danede, F., *et al.* Structure determination of forms I and II of phenobarbital from X-ray powder diffraction. *Acta Crystallographica Section B* **2005**. *61* (1), 80-88.
- (133) Roy, S.; Goud, N.R.; Matzger, A.J. Polymorphism in phenobarbital: Discovery of a new polymorph and crystal structure of elusive form V. *Chemical Communications* **2016**. *52* (23), 4389-4392.
- (134) Peeters, O.M.; Blaton, N.M.; de Ranter, C.J. Structure of 3-{2-[4-(6-fluoro-1,2-benzisoxazol-3-yl)piperidino]ethyl}-6,7,8,9-tetrahydro-2-methyl-4H-pyrido[1,2-a]pyrimidin-4-one (risperidone). *Acta Crystallographica Section C* **1993**. *49* (9), 1698-1700.

- (135) Wang, D.-H.; Zhou, M.-H.; Hu, X.-R. Crystalline form B of risperidone. *Acta Crystallographica Section E* **2006**. *62* (8), o3527-o3528.
- (136) Viertelhaus, M.; Holst, H.C.; Volz, J.; Hummel, R.-P. Roflumilast – a reversible single-crystal to single-crystal phase transition at 50°C. *Journal of Molecular Structure* **2013**. *1031*, 254-262.
- (137) Stepanovs, D.; Mishnev, A. Molecular and crystal structure of sildenafil base. *Zeitschrift für Naturforschung B* **2012**. *67* (5), 491-494.
- (138) Barbas, R.; Font-Bardia, M.; Prohens, R. Polymorphism of sildenafil: A new metastable desolvate. *Crystal Growth & Design* **2018**. *18* (7), 3740-3746.
- (139) Cejka, J.; Kratochvíl, B.; Cisarova, I.; Jegorov, A. Simvastatin. *Acta Crystallographica Section C* **2003**. *59* (8), o428-o430.
- (140) Hušák, M.; Kratochvíl, B.; Jegorov, A.; Brus, J.; Maixner, J., *et al.* Simvastatin: Structure solution of two new low-temperature phases from synchrotron powder diffraction and SS-NMR. *Structural Chemistry* **2010**. *21* (3), 511-518.
- (141) Dupont, L.; Campsteyn, H.; Lamotte, J.; Vermeire, M. Structure d'une seconde variété de la torasemide. *Acta Crystallographica Section B* **1978**. *34* (8), 2659-2662.
- (142) Dupont, L.; Lamotte, J.; Campsteyn, H.; Vermeire, M. Structure cristalline et moléculaire d'un diurétique dérivé de l'alkyl-1 [(phenylamino-4 pyridyl-3)sulfonyl]-3 urée: La torasemide (C<sub>16</sub>H<sub>20</sub>N<sub>4</sub>SO<sub>3</sub>). *Acta Crystallographica Section B* **1978**. *34* (4), 1304-1310.
- (143) Bartolucci, G.; Bruni, B.; Coran, S.A.; Di Vaira, M. 4-(3-methylanilino)-N-[N-(1-methylethyl)carbamoyl]pyridinium-3-sulfonamide (torasemide T-N): A low temperature redetermination. *Acta Crystallographica Section E* **2009**. *65* (5), o972-o973.
- (144) Ostwald, W. *Grundriss der allgemeinen chemie*; Verlag Von Wilhelm Engelmann: Leipzig, 1899; 414 p.
- (145) Ostwald, W. Studien über die bildung und umwandlung fester körper. *Zeitschrift für Physikalische Chemie* **1897**. *22U* (1), 289-330.
- (146) Dematos, L.L.; Williams, A.C.; Booth, S.W.; Petts, C.R.; Taylor, D.J., *et al.* Solvent influences on metastable polymorph lifetimes: Real-time interconversions using energy dispersive X-ray diffractometry. *Journal of Pharmaceutical Sciences* **2007**. *96* (5), 1069-1078.
- (147) Yu, L. Survival of the fittest polymorph: How fast nucleator can lose to fast grower. *CrystEngComm* **2007**. *9* (10), 847-851.
- (148) Bučar, D.-K.; Lancaster, R.W.; Bernstein, J. Disappearing polymorphs revisited. *Angewandte Chemie International Edition* **2015**. *54* (24), 6972-6993.
- (149) Sun, W.; Ceder, G. Induction time of a polymorphic transformation. *CrystEngComm* **2017**. *19* (31), 4576-4585.
- (150) Turnbull, D.; Fisher, J.C. Rate of nucleation in condensed systems. *The Journal of Chemical Physics* **1949**. *17* (1), 71-73.
- (151) Kashchiev, D.; Van Rosmalen, G.M. Review: Nucleation in solutions revisited. *Crystal Research and Technology* **2003**. *38* (7-8), 555-574.
- (152) Shelby, J.E. *Introduction to glass science and technology*; 2<sup>nd</sup> Ed.; Royal Society of Chemistry: Cambridge, 2005; 291 p.
- (153) Li, Q.; Jun, Y.-S. The apparent activation energy and pre-exponential kinetic factor for heterogeneous calcium carbonate nucleation on quartz. *Communications Chemistry* **2018**. *1* (1), 56.
- (154) Parambil, J.V.; Heng, J.Y.Y.: Seeding in crystallisation. In *Engineering crystallography: From molecule to crystal to functional form*; Roberts, K.J., Docherty, R., Tamura, R. Eds.; Springer Netherlands: Dordrecht, 2017, pp. 235-245.
- (155) Cote, A.; Zhou, G.; Stanik, M. A novel crystallization methodology to ensure isolation of the most stable crystal form. *Organic Process Research & Development* **2009**. *13* (6), 1276-1283.

- (156) Bonn, D.; Shahidzadeh, N. Multistep crystallization processes: How not to make perfect single crystals. *Proceedings of the National Academy of Sciences* **2016**. *113* (48), 13551.
- (157) Abramov, Y.A.; Zhang, P.; Zeng, Q.; Yang, M.; Liu, Y., *et al.* Computational insights into kinetic hindrance affecting crystallization of stable forms of active pharmaceutical ingredients. *Crystal Growth & Design* **2020**. *20* (3), 1512-1525.
- (158) Dunitz, J.D.; Bernstein, J. Disappearing polymorphs. *Accounts of Chemical Research* **1995**. *28* (4), 193-200.
- (159) Bernstein, J.; Davey, R.J.; Henck, J.-O. Concomitant polymorphs. *Angewandte Chemie International Edition* **1999**. *38* (23), 3440-3461.
- (160) Brittain, H.G. *Polymorphism in pharmaceutical solids*, 2<sup>nd</sup> Ed.; Informa: New York, 2009; 640 p.
- (161) Chistyakov, D.; Sergeev, G. The polymorphism of drugs: New approaches to the synthesis of nanostructured polymorphs. *Pharmaceutics* **2020**. *12* (1), 34 (1-9).
- (162) Zhang, T.H.; Liu, X.Y. Nucleation: What happens at the initial stage? *Angewandte Chemie International Edition* **2009**. *48* (7), 1308-1312.
- (163) Schmelzer, J.W.P.; Abyzov, A.S.: How do crystals nucleate and grow: Ostwald's rule of stages and beyond. In *Thermal physics and thermal analysis: From macro to micro, highlighting thermodynamics, kinetics and nanomaterials*; Šesták, J., Hubík, P., Mareš, J.J. Eds.; Springer International Publishing: Cham, 2017, pp. 195-211.
- (164) Censi, R.; Di Martino, P. Polymorph impact on the bioavailability and stability of poorly soluble drugs. *Molecules* **2015**. *20* (10), 18759-18776.
- (165) Nicoud, L.; Licordari, F.; Myerson, A.S. Estimation of the solubility of metastable polymorphs: A critical review. *Crystal Growth & Design* **2018**. *18* (11), 7228-7237.
- (166) Singhal, D.; Curatolo, W. Drug polymorphism and dosage form design: A practical perspective. *Advanced Drug Delivery Reviews* **2004**. *56* (3), 335-347.
- (167) Food and Drug Administration. Guidance for industry: Waiver of in vivo bioavailability and bioequivalence studies for immediate-release solid oral dosage forms based on a biopharmaceutics classification system. Food and Drug Administration, 2000, [Online] <https://www.fda.gov/media/70963>
- (168) Lindenberg, M.; Kopp, S.; Dressman, J.B. Classification of orally administered drugs on the world health organization model list of essential medicines according to the biopharmaceutics classification system. *European Journal of Pharmaceutics and Biopharmaceutics* **2004**. *58* (2), 265-278.
- (169) Rasenack, N.; Müller, B.W. Crystal habit and tableting behavior. *International Journal of Pharmaceutics* **2002**. *244* (1), 45-57.
- (170) Gohel, M.C.; Jogani, P.D. A review of co-processed directly compressible excipients. *Journal of Pharmacy and Pharmaceutical Sciences* **2005**. *8* (1), 76-93.
- (171) Rojas, J.: Effect of polymorphism on the particle and compaction properties of microcrystalline cellulose. In *Cellulose*; van de Ven, T.G.M. Ed.; IntechOpen, 2013, pp. 27-46.
- (172) Vanhoorne, V.; Bekaert, B.; Peeters, E.; de Beer, T.; Remon, J.P., *et al.* Improved tableability after a polymorphic transition of delta-mannitol during twin screw granulation. *International Journal of Pharmaceutics* **2016**. *506* (1), 13-24.
- (173) Alsirawan, M.B.; Paradkar, A.: Impact of the polymorphic form of drugs/NCEs on preformulation and formulation development. In *Innovative dosage forms*; Bachav Y. Ed.; Wiley-VCH Verlag GmbH & Co. KGaA : Weinheim, 2019, pp. 1-47.
- (174) Di Martino, P.; Guyot-Hermann, A.M.; Conflant, P.; Drache, M.; Guyot, J.C. A new pure paracetamol for direct compression: The orthorhombic form. *International Journal of Pharmaceutics* **1996**. *128* (1), 1-8.

- (175) Ilić, I.; Kása, P.; Dreu, R.; Pintye-Hódi, K.; Srčić, S. The compressibility and compactibility of different types of lactose. *Drug Development and Industrial Pharmacy* **2009**. *35* (10), 1271-1280.
- (176) Yoshinari, T.; Forbes, R.T.; York, P.; Kawashima, Y. Moisture induced polymorphic transition of mannitol and its morphological transformation. *International Journal of Pharmaceutics* **2002**. *247* (1), 69-77.
- (177) Lu, J.; Rohani, S. Polymorphic crystallization and transformation of the anti-viral/HIV drug stavudine. *Organic Process Research & Development* **2009**. *13* (6), 1262-1268.
- (178) Bhargavi, N.; Chavan, R.B.; Shastri, N.R. Hollow crystal generation through polymorphic transformation – a case study of flufenamic acid. *CrystEngComm* **2018**. *20* (3), 275-279.
- (179) Banerjee, M.; Brettmann, B. Combining surface templating and confinement for controlling pharmaceutical crystallization. *Pharmaceutics* **2020**. *12* (10), 995 (1-19).
- (180) Council of Europe: Carbamazepine. In *European pharmacopoeia*, 10<sup>th</sup> Ed.; Deutscher Apotheker Verlag: Strasbourg, 2019, pp. 2078-2080.
- (181) Council of Europe: Indometacin. In *European pharmacopoeia*, 10<sup>th</sup> Ed.; Deutscher Apotheker Verlag: Strasbourg, 2019, pp. 2936-2938.
- (182) Council of Europe: Chloramphenicol palmitate. In *European pharmacopoeia*, 10<sup>th</sup> Ed.; Deutscher Apotheker Verlag: Strasbourg, 2019, pp. 2168-2170.
- (183) Council of Europe: Doxazosin mesilate. In *European pharmacopoeia*, 10<sup>th</sup> Ed.; Deutscher Apotheker Verlag: Strasbourg, 2019, pp. 2468-2470.
- (184) Zencirci, N.; Griesser, U.J.; Gelbrich, T.; Apperley, D.C.; Harris, R.K. Crystal polymorphs of barbital: News about a classic polymorphic system. *Molecular Pharmaceutics* **2014**. *11* (1), 338-350.
- (185) Paczkowska, M.; Wiergowska, G.; Miklaszewski, A.; Krause, A.; Mroczkowska, M., *et al.* The analysis of the physicochemical properties of benzocaine polymorphs. *Molecules* **2018**. *23* (7), 1737 (1-13).
- (186) Chung, S.; Kim, J.; Ban, E.; Yun, J.; Park, B., *et al.* Solution-mediated phase transformation of aripiprazole: Negating the effect of crystalline forms on dissolution and oral pharmacokinetics. *Journal of Pharmaceutical Sciences* **2020**. *109* (12), 3668-3677.
- (187) Singh, R. *Applied Welding Engineering: Processes, Codes, and Standards*; Butterworth-Heinemann: Oxford, 2016, pp. 13-26.
- (188) Mullin, J.W. *Crystallization*; Elsevier Science: Amsterdam, 2001, 600 p.
- (189) Rodríguez-Spong, B.; Price, C.P.; Jayasankar, A.; Matzger, A.J.; Rodríguez-Hornedo, N.R. General principles of pharmaceutical solid polymorphism: A supramolecular perspective. *Advanced Drug Delivery Reviews* **2004**. *56* (3), 241-274.
- (190) Llinàs, A.; Goodman, J.M. Polymorph control: Past, present and future. *Drug Discovery Today* **2008**. *13* (5), 198-210.
- (191) Gao, Z.; Rohani, S.; Gong, J.; Wang, J. Recent developments in the crystallization process: Toward the pharmaceutical industry. *Engineering* **2017**. *3* (3), 343-353.
- (192) Kwokal, A.: Preparation, stabilisation and advantages of metastable polymorphs. In *Engineering crystallography: From molecule to crystal to functional form*; Roberts, K.J., Docherty, R., Tamura, R. Eds.; Springer Netherlands: Dordrecht, 2017, pp. 247-260.
- (193) Ikni, A.; Clair, B.; Scoufflaire, P.; Veessler, S.; Gillet, J.-M., *et al.* Experimental demonstration of the carbamazepine crystallization from non-photochemical laser-induced nucleation in acetonitrile and methanol. *Crystal Growth & Design* **2014**. *14* (7), 3286-3299.
- (194) Li, W.; Ikni, A.; Scoufflaire, P.; Shi, X.; El Hassan, N., *et al.* Non-photochemical laser-induced nucleation of sulfathiazole in a water/ethanol mixture. *Crystal Growth & Design* **2016**. *16* (5), 2514-2526.

- (195) Parambil, J.V.; Poornachary, S.K.; Heng, J.Y.Y.; Tan, R.B.H. Template-induced nucleation for controlling crystal polymorphism: From molecular mechanisms to applications in pharmaceutical processing. *CrystEngComm* **2019**. *21* (28), 4122-4135.
- (196) Lee, E.H. A practical guide to pharmaceutical polymorph screening & selection. *Asian Journal of Pharmaceutical Sciences* **2014**. *9* (4), 163-175.
- (197) Wesołowski, M.; Konarski, T. General remarks on the thermal decomposition of some drugs. *Journal of thermal analysis* **1995**. *43* (1), 279-289.
- (198) Sovizi, M.R. Thermal behavior of drugs. *Journal of Thermal Analysis and Calorimetry* **2010**. *102* (1), 285-289.
- (199) Alharbi, L.; El-Mossalamy, E.-S.; Obaid, A.; El-Ries, M. Thermal decomposition of some cardiovascular drugs (telmisartane, cilazapril and terazosin HCL). *American Journal of Analytical Chemistry* **2013**. *04* (07), 337-342.
- (200) Shamsipur, M.; Pourmortazavi, S.M.; Beigi, A.a.M.; Heydari, R.; Khatibi, M. Thermal stability and decomposition kinetic studies of acyclovir and zidovudine drug compounds. *AAPS PharmSciTech* **2013**. *14* (1), 287-293.
- (201) European Medicines Agency, ICH topic Q5C quality of biotechnological products: Stability testing of biotechnological/biological products, 1996, [Online] [https://www.ema.europa.eu/en/documents/scientific-guideline/ich-topic-q-5-c-quality-biotechnological-products-stability-testing-biotechnological/biological-products\\_en.pdf](https://www.ema.europa.eu/en/documents/scientific-guideline/ich-topic-q-5-c-quality-biotechnological-products-stability-testing-biotechnological/biological-products_en.pdf)
- (202) European Medicines Agency, ICH topic Q6B specifications: Test procedures and acceptance criteria for biotechnological/biological products, 1999, [Online] [https://www.ema.europa.eu/en/documents/scientific-guideline/ich-q-6-b-test-procedures-acceptance-criteria-biotechnological/biological-products-step-5\\_en.pdf](https://www.ema.europa.eu/en/documents/scientific-guideline/ich-q-6-b-test-procedures-acceptance-criteria-biotechnological/biological-products-step-5_en.pdf)
- (203) European Medicines Agency, ICH topic Q6A specifications: Test procedures and acceptance criteria for new drug substances and new drug products: Chemical substances, 2000, [Online] [https://www.ema.europa.eu/en/documents/scientific-guideline/ich-q-6-test-procedures-acceptance-criteria-new-drug-substances-new-drug-products-chemical\\_en.pdf](https://www.ema.europa.eu/en/documents/scientific-guideline/ich-q-6-test-procedures-acceptance-criteria-new-drug-substances-new-drug-products-chemical_en.pdf)
- (204) Alsante, K.M.; Ando, A.; Brown, R.; Ensing, J.; Hatajik, T.D., *et al.* The role of degradant profiling in active pharmaceutical ingredients and drug products. *Advanced Drug Delivery Reviews* **2007**. *59* (1), 29-37.
- (205) Tamizi, E.; Jouyban, A. Forced degradation studies of biopharmaceuticals: Selection of stress conditions. *European Journal of Pharmaceutics and Biopharmaceutics* **2016**. *98*, 26-46.
- (206) Chakravarty, P.; Famili, A.; Nagapudi, K.; Al-Sayah, M.A. Using supercritical fluid technology as a green alternative during the preparation of drug delivery systems. *Pharmaceutics* **2019**. *11* (12), 629 (1-34).
- (207) Zhang, G.G.Z.; Law, D.; Schmitt, E.A.; Qiu, Y. Phase transformation considerations during process development and manufacture of solid oral dosage forms. *Advanced Drug Delivery Reviews* **2004**. *56* (3), 371-390.
- (208) Daintree, L.S.; Kordikowski, A.; York, P. Separation processes for organic molecules using SCF technologies. *Advanced Drug Delivery Reviews* **2008**. *60* (3), 351-372.
- (209) Taylor, L.T. *Supercritical fluid extraction*, 1<sup>st</sup> Ed.; John Wiley & Sons: New York, 1996; 181 p.
- (210) Baiker, A. Supercritical fluids in heterogeneous catalysis. *Chemical Reviews* **1999**. *99* (2), 453-474.
- (211) Noyori, R. Supercritical fluids: Introduction. *Chemical Reviews* **1999**. *99* (2), 353-354.
- (212) Saeki, S. Empirical equation of state for supercritical fluids. *The Journal of Supercritical Fluids* **1995**. *8* (1), 30-45.

- (213) Henczka, M.; Djas, M.; Krzysztoforski, J.: Supercritical fluids in green technologies. In *Practical aspects of chemical engineering: Selected contributions from paic 2017*, 1<sup>st</sup> Ed.; Ochwiak, M., Doligalski, M., Woziwodski, S., Mitkowski, P.T. Eds.; Springer International Publishing: Cham, Switzerland, 2018, pp. 137-149.
- (214) Kostrzewa, D.; Dobrzyńska-Inger, A.; Turczyn, A. Experimental data and modelling of the solubility of high-carotenoid paprika extract in supercritical carbon dioxide. *Molecules* **2019**. *24* (22), 4174 (1-13).
- (215) Ivanov, D.Y., *Critical behavior of non-ideal systems*; Wiley-VCH: Berlin, 2008; 257 p.
- (216) Ploetz, E.A.; Smith, P.E. Gas or liquid? The supercritical behavior of pure fluids. *The Journal of Physical Chemistry B* **2019**. *123* (30), 6554-6563.
- (217) McHugh, M.A.; Krukoni, V.J.: 3 - phase diagrams for supercritical fluid–solute mixtures. In *Supercritical fluid extraction*; 2<sup>nd</sup> Ed.; McHugh, M.A., Krukoni, V.J. Eds.; Butterworth-Heinemann: Boston, 1994, pp. 27-84.
- (218) Bagheri, H.; Hashemipour, H. *Investigation the nucleation process in rapid expansion of supercritical solution (RESS) process*; 2<sup>th</sup> national conference on nanostructures, nanoscience and nanoengineering, Kashan, Iran, 14 February, **2018**.
- (219) Machida, H.; Takesue, M.; Smith, R.L. Green chemical processes with supercritical fluids: Properties, materials, separations and energy. *The Journal of Supercritical Fluids* **2011**. *60*, 2-15.
- (220) Galli, G.; Pan, D. A closer look at supercritical water. *Proceedings of the National Academy of Sciences* **2013**. *110* (16), 6250-6251.
- (221) Clercq, S., **2019**, *Etude des mécanismes de cristallisation en milieu supercritique. Application à des principes actifs pharmaceutiques*, PhD thesis, Université Aix-Marseille: Marseille.
- (222) Efremova, G.D.; Shvarts, A.V. Higher-order critical phenomena in ternary systems. The methanol-carbon dioxide-ethane system. *Russian Journal of Physical Chemistry* **1972**. *46*, 237-239.
- (223) Pando, C.; Cabañas, A.; Cuadra, I.A. Preparation of pharmaceutical co-crystals through sustainable processes using supercritical carbon dioxide: A review. *RSC Advances* **2016**. *6* (75), 71134-71150.
- (224) Padrela, L.; Rodrigues, M.A.; Duarte, A.; Dias, A.M.A.; Braga, M.E.M., *et al.* Supercritical carbon dioxide-based technologies for the production of drug nanoparticles/nanocrystals – a comprehensive review. *Advanced Drug Delivery Reviews* **2018**. *131*, 22-78.
- (225) Chiou, A.H.-J.; Yeh, M.-K.; Chen, C.-Y.; Wang, D.-P. Micronization of meloxicam using a supercritical fluids process. *The Journal of Supercritical Fluids* **2007**. *42* (1), 120-128.
- (226) Pasquali, I.; Bettini, R.; Giordano, F. Supercritical fluid technologies: An innovative approach for manipulating the solid-state of pharmaceuticals. *Advanced Drug Delivery Reviews* **2008**. *60* (3), 399-410.
- (227) Gosselin, P.M.; Thibert, R.; Preda, M.; McMullen, J.N. Polymorphic properties of micronized carbamazepine produced by res. *International Journal of Pharmaceutics* **2003**. *252* (1), 225-233.
- (228) Shinozaki, H.; Oguchi, T.; Suzuki, S.; Aoki, K.; Sako, T., *et al.* Micronization and polymorphic conversion of tolbutamide and barbital by rapid expansion of supercritical solutions. *Drug Development and Industrial Pharmacy* **2006**. *32* (7), 877-891.
- (229) Türk, M.; Bolten, D. Polymorphic properties of micronized mefenamic acid, nabumetone, paracetamol and tolbutamide produced by rapid expansion of supercritical solutions (RESS). *The Journal of Supercritical Fluids* **2016**. *116*, 239-250.

- (230) Oparin, R.D.; Moreau, M.; de Walle, I.; Paolantoni, M.; Idrissi, A., *et al.* The interplay between the paracetamol polymorphism and its molecular structures dissolved in supercritical CO<sub>2</sub> in contact with the solid phase: In situ vibration spectroscopy and molecular dynamics simulation analysis. *European Journal of Pharmaceutical Sciences* **2015**. *77*, 48-59.
- (231) Oparin, R.D.; Vorobei, A.M.; Kiselev, M.G. Polymorphism of micronized forms of ibuprofen obtained by rapid expansion of a supercritical solution. *Russian Journal of Physical Chemistry B* **2019**. *13* (7), 1139-1146.
- (232) Chan, H.K.; Doelker, E. Polymorphic transformation of some drugs under compression. *Drug Development and Industrial Pharmacy* **1985**. *11* (2-3), 315-332.
- (233) Otsuka, M.; Onoe, M.; Matsuda, Y. Physicochemical stability of phenobarbital polymorphs at various levels of humidity and temperature. *Pharmaceutical Research* **1993**. *10* (4), 577-582.
- (234) Brits, M.; Liebenberg, W.; De Villiers, M.M. Characterization of polymorph transformations that decrease the stability of tablets containing the who essential drug mebendazole. *Journal of Pharmaceutical Sciences* **2010**. *99* (3), 1138-1151.
- (235) Baviskar, S.R.; Patil, S.H. Solid phase transformation considerations during process development and manufacture of solid oral dosage forms – a review. *International Journal of PharmTech Research* **2014**. *6*, 1963-1969.
- (236) Juban, A.; Briancon, S.; Puel, F. Processing-induced-transformations (PITs) during direct compression: Impact of compression speeds on phase transition of caffeine. *Drug Development and Industrial Pharmacy* **2016**. *42* (11), 1857-1864.
- (237) Thakral, N.K.; Thakral, S.; Stephenson, G.A.; Sedlock, R.; Suryanarayanan, R. Compression-induced polymorphic transformation in tablets: Role of shear stress and development of mitigation strategies. *Journal of Pharmaceutical Sciences* **2019**. *108* (1), 476-484.
- (238) Thakral, S.; Govindarajan, R.; Suryanarayanan, R.: Processing-induced phase transformations and their implications on pharmaceutical product quality. In *Polymorphism in the pharmaceutical industry: Solid form and drug development*; Hilfiker, R., Von Raumer, M. Eds.; John Wiley & Sons: Weinheim, 2019; pp. 329-369.
- (239) Joksimović, T.; Baumgartner, S. Tableting of pressure-sensitive materials. *Farmaceutski Vestnik* **2008**. *59* (4), 193-199.
- (240) Wildfong, P.: Effects of pharmaceutical processing on the solid form of drug and excipient materials. In *Polymorphism in pharmaceutical solids*; Informa Healthcare: New York, 2009, pp. 510-559.
- (241) Li, X.; Bhushan, B. A review of nanoindentation continuous stiffness measurement technique and its applications. *Materials Characterization* **2002**. *48* (1), 11-36.
- (242) Bauer, J.D.; Haussühl, E.; Winkler, B.; Arbeck, D.; Milman, V., *et al.* Elastic properties, thermal expansion, and polymorphism of acetylsalicylic acid. *Crystal Growth & Design* **2010**. *10* (7), 3132-3140.
- (243) Kang, K., **2011**, *Microcantilever (MC) based nanomechanical sensor for detection of molecular interactions*, PhD thesis, Iowa State University: Ames, Iowa.
- (244) Katrusiak, A. High-pressure X-ray diffraction studies on organic crystals. *Crystal Research and Technology* **1991**. *26* (5), 523-531.
- (245) Piermarini, G.J. High pressure X-ray crystallography with the diamond cell at NIST/NBS. *Journal of research of the National Institute of Standards and Technology* **2001**. *106* (6), 889-920.
- (246) Kalei, G.N. Some results of microhardness test using the depth of impression. *Mashinovedenie* **1968**. *4* (3), 105-107.

- (247) Varughese, S.; Kiran, M.S.R.N.; Ramamurty, U.; Desiraju, G.R. Nanoindentation in crystal engineering: Quantifying mechanical properties of molecular crystals. *Angewandte Chemie International Edition* **2013**. *52* (10), 2701-2712.
- (248) Shimizu, J.; Zhou, L.; Eda, H. Molecular dynamics simulation of effect of grinding wheel stiffness on nanogrinding process. *International Journal of Abrasive Technology* **2008**. *1*, 316-326.
- (249) Denkena, B.; Bouabid, A.; Kroedel, A. Single grain grinding: A novel approach to model the interactions at the grain/bond interface during grinding. *The International Journal of Advanced Manufacturing Technology* **2020**. *107* (11), 4811-4822.
- (250) Ericson, F.; Schweitz, J.-A.: Mechanical properties of materials in microstructure technology. In *Handbook of micro/nano tribology*; 2<sup>nd</sup> Ed.; Bhushan, B. Ed.; CRC Press: London, 2020, pp. 763-796.
- (251) Smith, D.K.; Barrett, C.S.: Special handling problems in X-ray diffractometry. In *Twenty-Seventh Annual Conference on Applications of X-ray Analysis*; McCarthy, G.J. Ed.; Cambridge University Press: Cambridge, 1978, p. 1-12.
- (252) Kim, B.; Kwon, M.; Ha, J.; Lee, K. An in-situ monitoring system on the grinding process. *Optical Metrology and Inspection for Industrial Applications* **2010**. 7855, 785525 (1-8).
- (253) Gracin, D.; Štrukil, V.; Friščić, T.; Halasz, I.; Užarević, K. Laboratory real-time and in situ monitoring of mechanochemical milling reactions by Raman spectroscopy. *Angewandte Chemie International Edition* **2014**. *53* (24), 6193-6197.
- (254) Katsenis, A.D.; Puškarić, A.; Štrukil, V.; Mottillo, C.; Julien, P.A., *et al.* In situ X-ray diffraction monitoring of a mechanochemical reaction reveals a unique topology metal-organic framework. *Nature Communications* **2015**. *6* (1), 6662 (1-8).
- (255) Tireli, M.; Juribašić Kulcsár, M.; Cindro, N.; Gracin, D.; Biliškov, N., *et al.* Mechanochemical reactions studied by in situ Raman spectroscopy: Base catalysis in liquid-assisted grinding. *Chemical Communications* **2015**. *51* (38), 8058-8061.
- (256) Yamanaka, T.; Fukuda, T.; Hattori, T.; Sumiya, H. New diamond anvil cell for single-crystal analysis. *Review of Scientific Instruments* **2001**. *72* (2), 1458-1462.
- (257) Anzellini, S.; Boccatto, S. A practical review of the laser-heated diamond anvil cell for university laboratories and synchrotron applications. *Crystals* **2020**. *10* (6), 459 (1-28).
- (258) Manimunda, P.; Syed Asif, S.A.; Mishra, M.K. Probing stress induced phase transformation in aspirin polymorphs using Raman spectroscopy enabled nanoindentation. *Chemical Communications* **2019**. *55* (62), 9200-9203.
- (259) Govedarica, B.; Škarabot, M.; Ilić, I.; Planinšek, O.; Mušević, I., *et al.* Mapping the local elastic properties of pharmaceutical solids using atomic force microscopy. *Procedia Engineering* **2011**. *10*, 2857-2866.
- (260) Egart, M.; Janković, B.; Srčić, S. Application of instrumented nanoindentation in preformulation studies of pharmaceutical active ingredients and excipients. *Acta Pharmaceutica* **2016**. *66* (3), 303-330.
- (261) Gabriele, B.P.A.; Williams, C.J.; Lauer, M.E.; Derby, B.; Cruz-Cabeza, A.J. Nanoindentation of molecular crystals: Lessons learned from aspirin. *Crystal Growth & Design* **2020**. *20* (9), 5956-5966.
- (262) Zahn, D.; Anwar, J. Collective displacements in a molecular crystal polymorphic transformation. *RSC Advances* **2013**. *3* (31), 12810-12815.
- (263) Ahmed, E.; Karothu, D.P.; Warren, M.; Naumov, P. Shape-memory effects in molecular crystals. *Nature Communications* **2019**. *10* (1), 3723.
- (264) Fischer-Cripps, A.C. Critical review of analysis and interpretation of nanoindentation test data. *Surface and Coatings Technology* **2006**. *200* (14), 4153-4165.

- (265) Reddy, C.M.; Gundakaram, R.C.; Basavoju, S.; Kirchner, M.T.; Padmanabhan, K.A., *et al.* Structural basis for bending of organic crystals. *Chemical Communications* **2005**. *31*, 3945-3947.
- (266) Bag, P.P.; Chen, M.; Sun, C.C.; Reddy, C.M. Direct correlation among crystal structure, mechanical behaviour and tableability in a trimorphic molecular compound. *CrystEngComm* **2012**. *14* (11), 3865-3867.
- (267) Raju, K.B.; Ranjan, S.; Vishnu, V.S.; Bhattacharya, M.; Bhattacharya, B., *et al.* Rationalizing distinct mechanical properties of three polymorphs of a drug adduct by nanoindentation and energy frameworks analysis: Role of slip layer topology and weak interactions. *Crystal Growth & Design* **2018**. *18* (7), 3927-3937.
- (268) Khandavilli, U.B.R.; Lusi, M.; Frawley, P.J. Plasticity in zwitterionic drugs: The bending properties of pregabalin and gabapentin and their hydrates. *IUCrJ* **2019**. *6* (4), 630-634.
- (269) Reddy, C. Plasticity enhancement in pharmaceutical drugs by water of crystallization: Unusual slip planes. *IUCrJ* **2019**. *6* (4), 505-506.
- (270) Wang, K.; Mishra, M.K.; Sun, C.C. Exceptionally elastic single-component pharmaceutical crystals. *Chemistry of Materials* **2019**. *31* (5), 1794-1799.
- (271) Bond, A.D.; Solanko, K.A.; Parsons, S.; Redder, S.; Boese, R. Single crystals of aspirin form II: Crystallisation and stability. *CrystEngComm* **2011**. *13* (2), 399-401.
- (272) Johnstone, R.D.L.; Lennie, A.R.; Parker, S.F.; Parsons, S.; Pidcock, E., *et al.* High-pressure polymorphism in salicylamide. *CrystEngComm* **2010**. *12* (4), 1065-1078.
- (273) Targett, J.; Cockcroft, J.K. CCDC 755086: Experimental Crystal Structure Determination, **2013**.
- (274) Boldyreva, E.V.; Shakhshneider, T.P.; Vasilchenko, M.A.; Ahsbahs, H.; Uchtmann, H. Anisotropic crystal structure distortion of the monoclinic polymorph of acetaminophen at high hydrostatic pressures. *Acta Crystallographica Section B* **2000**. *56* (2), 299-309.
- (275) Smith, S.J.; Bishop, M.M.; Montgomery, J.M.; Hamilton, T.P.; Vohra, Y.K. Polymorphism in paracetamol: Evidence of additional forms IV and V at high pressure. *The Journal of Physical Chemistry A* **2014**. *118* (31), 6068-6077.
- (276) Ward, M.R.; Oswald, I.D.H. Antisolvent addition at extreme conditions. *CrystEngComm* **2019**. *21* (30), 4437-4443.
- (277) Pirttimäki, J.; Laine, E.; Ketolainen, J.; Paronen, P. Effects of grinding and compression on crystal structure of anhydrous caffeine. *International Journal of Pharmaceutics* **1993**. *95* (1), 93-99.
- (278) Mazel, V.; Delplace, C.; Busignies, V.; Faivre, V.; Tchoreloff, P., *et al.* Polymorphic transformation of anhydrous caffeine under compression and grinding: A re-evaluation. *Drug Development and Industrial Pharmacy* **2011**. *37* (7), 832-840.
- (279) Fabbiani, F.P.A.; Allan, D.R.; David, W.I.F.; Davidson, A.J.; Lennie, A.R., *et al.* High-pressure studies of pharmaceuticals: An exploration of the behavior of piracetam. *Crystal Growth & Design* **2007**. *7* (6), 1115-1124.
- (280) Boldyreva, E.V.; Ivashevskaya, S.N.; Sowa, H.; Ahsbahs, H.; Weber, H.P. Effect of high pressure on crystalline glycine: A new high-pressure polymorph. *Doklady Physical Chemistry* **2004**. *396* (1), 111-114.
- (281) Boldyreva, E.; Ivashevskaya, S.; Sowa, H.; Ahsbahs, H.; Weber, H.P. Effect of hydrostatic pressure on the  $\gamma$ -polymorph of glycine 1. A polymorphic transition into a new  $\delta$ -form. *Zeitschrift Fur Kristallographie* **2005**. *220*, 50-57.
- (282) Dawson, A.; Allan, D.R.; Belmonte, S.A.; Clark, S.J.; David, W.I.F., *et al.* Effect of high pressure on the crystal structures of polymorphs of glycine. *Crystal Growth & Design* **2005**. *5* (4), 1415-1427.

- (283) Tumanov, N.A.; Boldyreva, E.V.; Ahsbahs, H. Structure solution and refinement from powder or single-crystal diffraction data? Pros and cons: An example of the high-pressure  $\beta'$ -polymorph of glycine. *Powder Diffraction* **2012**. *23* (4), 307-316.
- (284) Kapustin, E.A.; Minkov, V.S.; Boldyreva, E.V. Effect of pressure on methylated glycine derivatives: Relative roles of hydrogen bonds and steric repulsion of methyl groups. *Acta Crystallographica Section B* **2014**. *70* (3), 517-532.
- (285) Kala, H.; Haack, U.; Wenzel, U.; Zessin, G.; Pollandt, P. Phase transformation of carbamazepine by the milling process. *Pharmazie* **1986**. *41* (11), 777-781.
- (286) Lefebvre, C.; Guyot-Hermann, A.M.; Dragnet-Brughmans, M.; Bouché, R.; Guyot, J.C. Polymorphic transitions of carbamazepine during grinding and compression. *Drug Development and Industrial Pharmacy* **1986**. *12* (11-13), 1913-1927.
- (287) Patterson, J.E.; James, M.B.; Forster, A.H.; Lancaster, R.W.; Butler, J.M., *et al.* The influence of thermal and mechanical preparative techniques on the amorphous state of four poorly soluble compounds. *Journal of Pharmaceutical Sciences* **2005**. *94* (9), 1998-2012.
- (288) Varughese, S.; Kiran, M.S.R.N.; Solanko, K.A.; Bond, A.D.; Ramamurty, U., *et al.* Interaction anisotropy and shear instability of aspirin polymorphs established by nanoindentation. *Chemical Science* **2011**. *2* (11), 2236-2242.
- (289) Pallipurath, A.R.; Civati, F.; Sibik, J.; Crowley, C.; Zeitler, J.A., *et al.* A comprehensive spectroscopic study of the polymorphs of diflunisal and their phase transformations. *International Journal of Pharmaceutics* **2017**. *528* (1), 312-321.
- (290) Malfait, B.; Correia, N.T.; Ciotonea, C.; Dhainaut, J.; Dacquin, J.-P., *et al.* Manipulating the physical states of confined ibuprofen in SBA-15 based drug delivery systems obtained by solid-state loading: Impact of the loading degree. *The Journal of Chemical Physics* **2020**. *153*, 154506 (1-14).
- (291) Sharma, P.; Denny, W.A.; Garg, S. Effect of wet milling process on the solid state of indomethacin and simvastatin. *International Journal of Pharmaceutics* **2009**. *380* (1), 40-48.
- (292) Latreche, M.; Willart, J.-F.; Paccou, L.; Guinet, Y.; Hédoux, A. Polymorphism versus devitrification mechanism: Low-wavenumber Raman investigations in sulindac. *International Journal of Pharmaceutics* **2019**. *567*, 118476 (1-6).
- (293) Ostrowska, K.; Kropidłowska, M.; Katrusiak, A. High-pressure crystallization and structural transformations in compressed R,S-ibuprofen. *Crystal Growth & Design* **2015**. *15* (3), 1512-1517.
- (294) Olejniczak, A.; Katrusiak, A.; Metrangolo, P.; Resnati, G. Molecular association in 2-bromo-2-chloro-1,1,1-trifluoroethane (halothane). *Journal of Fluorine Chemistry* **2009**. *130* (2), 248-253.
- (295) Council of Europe: Polymorphism. In *European pharmacopoeia*, 10<sup>th</sup> Ed.; Deutscher Apotheker Verlag: Strasbourg, 2019, pp. 759.
- (296) Council of Europe: Thermal analysis. In *European pharmacopoeia*, 10<sup>th</sup> Ed.; Deutscher Apotheker Verlag: Strasbourg, 2019, pp. 61-63.
- (297) Council of Europe: Absorption spectrophotometry. In *European pharmacopoeia*, 10<sup>th</sup> Ed.; Deutscher Apotheker Verlag: Strasbourg, 2019, pp. 39-42.
- (298) Council of Europe: Raman spectroscopy. In *European pharmacopoeia*, 10<sup>th</sup> Ed.; Deutscher Apotheker Verlag: Strasbourg, 2019, pp. 92-94.
- (299) Yu, Z.Q.; Chew, J.W.; Chow, P.S.; Tan, R.B.H. Recent advances in crystallization control: An industrial perspective. *Chemical Engineering Research and Design* **2007**. *85* (7), 893-905.
- (300) Févotte, G. In situ raman spectroscopy for in-line control of pharmaceutical crystallization and solids elaboration processes: A review. *Chemical Engineering Research and Design* **2007**. *85* (7), 906-920.

- (301) Spectral database for organic compounds, SDBS, 2021, [Online] <https://sdb.sdb.aist.go.jp>
- (302) Braatz, R.D. Advanced control of crystallization processes. *Annual Reviews in Control* **2002**. *26 (1)*, 87-99.
- (303) Févotte, G. On line monitoring of batch pharmaceutical crystallization using ATR FTIR spectroscopy. *IFAC Proceedings Volumes* **2002**. *35 (1)*, 259-264.
- (304) Giron, D. Applications of thermal analysis and coupled techniques in pharmaceutical industry. *Journal of Thermal Analysis and Calorimetry* **2002**. *68 (2)*, 335-357.
- (305) Yu, L.X.; Lionberger, R.A.; Raw, A.S.; D'costa, R.; Wu, H., *et al.* Applications of process analytical technology to crystallization processes. *Advanced Drug Delivery Reviews* **2004**. *56 (3)*, 349-369.
- (306) Pöllänen, K.; Häkkinen, A.; Reinikainen, S.-P.; Rantanen, J.; Karjalainen, M., *et al.* IR spectroscopy together with multivariate data analysis as a process analytical tool for in-line monitoring of crystallization process and solid-state analysis of crystalline product. *Journal of Pharmaceutical and Biomedical Analysis* **2005**. *38 (2)*, 275-284.
- (307) Shen, L.; Jayawickrama, D.; Wethman, R.; Hung, V. Application of Raman and FBRM techniques in the development of pharmaceutical crystallization processes. The annual meeting, Cincinnati, 2005, [Online] <https://aiche.confex.com/aiche/2005/techprogram/P28431.HTM>
- (308) Chan, K.L.A.; Kazarian, S.G.; Vassou, D.; Gionis, V.; Chryssikos, G.D. In situ high-throughput study of drug polymorphism under controlled temperature and humidity using FT-IR spectroscopic imaging. *Vibrational Spectroscopy* **2007**. *43 (1)*, 221-226.
- (309) Hu, Y.; Wikström, H.; Byrn, S.R.; Taylor, L.S. Estimation of the transition temperature for an enantiotropic polymorphic system from the transformation kinetics monitored using Raman spectroscopy. *Journal of Pharmaceutical and Biomedical Analysis* **2007**. *45 (4)*, 546-551.
- (310) Strachan, C.J.; Rades, T.; Gordon, K.C.; Rantanen, J. Raman spectroscopy for quantitative analysis of pharmaceutical solids. *Journal of Pharmacy and Pharmacology* **2007**. *59 (2)*, 179-192.
- (311) Alatalo, H.; Kohonen, J.; Qu, H.; Hatakka, H.; Reinikainen, S.-P., *et al.* In-line monitoring of reactive crystallization process based on ATR-FTIR and Raman spectroscopy. *Journal of Chemometrics* **2008**. *22 (11-12)*, 644-652.
- (312) Caillet, A.; Puel, F.; Fevotte, G. Quantitative in situ monitoring of citric acid phase transition in water using raman spectroscopy. *Chemical Engineering and Processing: Process Intensification* **2008**. *47 (3)*, 377-382.
- (313) Nagy, Z.K.; Chew, J.W.; Fujiwara, M.; Braatz, R.D. Comparative performance of concentration and temperature controlled batch crystallizations. *Journal of Process Control* **2008**. *18 (3)*, 399-407.
- (314) Lu, J.; Rohani, S. Polymorphism and crystallization of active pharmaceutical ingredients (APIs). *Current Medicinal Chemistry* **2009**. *16 (7)*, 884-905.
- (315) Aina, A.; Hargreaves, M.D.; Matousek, P.; Burley, J.C. Transmission raman spectroscopy as a tool for quantifying polymorphic content of pharmaceutical formulations. *Analyst* **2010**. *135 (9)*, 2328-2333.
- (316) Heinz, A.; Strachan, C.J.; Gordon, K.C.; Rades, T. Analysis of solid-state transformations of pharmaceutical compounds using vibrational spectroscopy. *Journal of Pharmacy and Pharmacology* **2010**. *61 (8)*, 971-988.
- (317) Gilpin, R.K.; Gilpin, C.S. Pharmaceuticals and related drugs. *Analytical Chemistry* **2011**. *83 (12)*, 4489-4507.

- (318) Olds, W.J.; Jaatinen, E.; Fredericks, P.; Cletus, B.; Panayiotou, H., *et al.* Spatially offset Raman spectroscopy (SORS) for the analysis and detection of packaged pharmaceuticals and concealed drugs. *Forensic Science International* **2011**. *212 (1)*, 69-77.
- (319) Zhao, Y.; Yuan, J.; Ji, Z.; Wang, J.; Rohani, S. Combined application of in situ FBRM, ATR-FTIR, and Raman on polymorphism transformation monitoring during the cooling crystallization. *Industrial & Engineering Chemistry Research* **2012**. *51 (38)*, 12530-12536.
- (320) Huang, J.; Dali, M. Evaluation of integrated Raman-DSC technology in early pharmaceutical development: Characterization of polymorphic systems. *Journal of Pharmaceutical and Biomedical Analysis* **2013**. *86*, 92-99.
- (321) Jednačák, T.; Hodzic, A.; Scheibelhofer, O.; Marijan, M.; Khinast, J.G., *et al.* Fast real-time monitoring of entacapone crystallization and characterization of polymorphs via Raman spectroscopy, statistics and SWAXS. *Acta Pharmaceutica* **2014**. *64 (1)*, 1-13.
- (322) Simon, L.L.; Pataki, H.; Marosi, G.; Meemken, F.; Hungerbühler, K., *et al.* Assessment of recent process analytical technology (PAT) trends: A multiauthor review. *Organic Process Research & Development* **2015**. *19 (1)*, 3-62.
- (323) Takeguchi, K.; Obitsu, K.; Hirasawa, S.; Orii, R.; Ieda, S., *et al.* Strategy for controlling polymorphism of di(arylamino) aryl compound ASP3026 and monitoring solution structures via Raman spectroscopy. *Organic Process Research & Development* **2015**. *19 (12)*, 1966-1972.
- (324) Andrea, E. Application of vibrational spectroscopy to study solid-state transformations of pharmaceuticals. *Current Pharmaceutical Design* **2016**. *22 (32)*, 4883-4911.
- (325) Inoue, M.; Hisada, H.; Koide, T.; Carriere, J.; Heyler, R., *et al.* In situ monitoring of crystalline transformation of carbamazepine using probe-type low-frequency Raman spectroscopy. *Organic Process Research & Development* **2017**. *21 (2)*, 262-265.
- (326) Inoue, M.; Hisada, H.; Koide, T.; Fukami, T.; Roy, A., *et al.* Transmission low-frequency Raman spectroscopy for quantification of crystalline polymorphs in pharmaceutical tablets. *Analytical Chemistry* **2019**. *91 (3)*, 1997-2003.
- (327) Camí, G.E.; Brusau, E.V.; Narda, G.E.; Maggio, R.M. Dual approach for concomitant monitoring of dissolution and transformation at solid-state. Mebendazole salts case study. *Journal of Drug Delivery Science and Technology* **2020**. *55*, 101344.
- (328) Nomura, K.; Titapiwatanakun, V.; Hisada, H.; Koide, T.; Fukami, T. In situ monitoring of the crystalline state of active pharmaceutical ingredients during high-shear wet granulation using a low-frequency Raman probe. *European Journal of Pharmaceutics and Biopharmaceutics* **2020**. *147*, 1-9.
- (329) Pallipurath, A.R.; Flandrin, P.-B.; Wayment, L.E.; Wilson, C.C.; Robertson, K. In situ non-invasive Raman spectroscopic characterisation of succinic acid polymorphism during segmented flow crystallisation. *Molecular Systems Design & Engineering* **2020**. *5 (1)*, 294-303.
- (330) Perro, A.; Lebourdon, G.; Henry, S.; Lecomte, S.; Servant, L., *et al.* Combining microfluidics and FT-IR spectroscopy: Towards spatially resolved information on chemical processes. *Reaction Chemistry & Engineering* **2016**. *1 (6)*, 577-594.
- (331) Tiernan, H.; Byrne, B.; Kazarian, S.G. ATR-FTIR spectroscopy and spectroscopic imaging for the analysis of biopharmaceuticals. *Spectrochimica Acta Part A: Molecular and Biomolecular Spectroscopy* **2020**. *241*, 118636.
- (332) Schettino, V.; Bini, R. *Materials under extreme conditions: Molecular crystals at high pressure*; Imperial College Press: London, 2014; 354 p.
- (333) Weng, J.; Huang, Y.; Hao, D.; Ji, Y. Recent advances of pharmaceutical crystallization theories. *Chinese Journal of Chemical Engineering* **2020**. *28 (4)*, 935-948.

- (334) Heinz, H.; Ramezani-Dakhel, H. Simulations of inorganic–bioorganic interfaces to discover new materials: Insights, comparisons to experiment, challenges, and opportunities. *Chemical Society Reviews* **2016**. *45* (2), 412-448.
- (335) Katiyar, R.S.; Jha, P.K. Molecular simulations in drug delivery: Opportunities and challenges. *WIREs Computational Molecular Science* **2018**. *8* (4), e1358 (1-18).
- (336) Fermeglia, M.; Mio, A.; Aulic, S.; Marson, D.; Laurini, E., *et al.* Multiscale molecular modelling for the design of nanostructured polymer systems: Industrial applications. *Molecular Systems Design & Engineering* **2020**. *5* (9), 1447-1476.
- (337) Syed Ausaf, A.; Md. Imtaiyaz, H.; Asimul, I.; Faizan, A. A review of methods available to estimate solvent-accessible surface areas of soluble proteins in the folded and unfolded states. *Current Protein & Peptide Science* **2014**. *15* (5), 456-476.
- (338) Tajti, A.; Szalay, P.G.; Császár, A.G.; Kállay, M.; Gauss, J., *et al.* Heat: High accuracy extrapolated ab initio thermochemistry. *The Journal of Chemical Physics* **2004**. *121* (23), 11599-11613.
- (339) Otero-de-la-Roza, A.; Johnson, E.R. A benchmark for non-covalent interactions in solids. *The Journal of Chemical Physics* **2012**. *137* (5), 054103 (1-11).
- (340) Sakurai, J.J.; Napolitano, J. *Modern quantum mechanics*; 2<sup>nd</sup> Ed.; Cambridge University Press: Cambridge, UK, 2017, 550 p.
- (341) Baiano, C.; Lupi, J.; Tasinato, N.; Puzzarini, C.; Barone, V. The role of state-of-the-art quantum-chemical calculations in astrochemistry: Formation route and spectroscopy of ethanimine as a paradigmatic case. *Molecules* **2020**. *25* (12), 2873 (1-21).
- (342) Puzzarini, C.; Stanton, J.F.; Gauss, J. Quantum-chemical calculation of spectroscopic parameters for rotational spectroscopy. *International Reviews in Physical Chemistry* **2010**. *29* (2), 273-367.
- (343) Smidstrup, S.; Markussen, T.; Vancraeyveld, P.; Wellendorff, J.; Schneider, J., *et al.* QuantumATK: An integrated platform of electronic and atomic-scale modelling tools. *Journal of Physics: Condensed Matter* **2019**. *32* (1), 015901 (1-37).
- (344) Bloch, F. Über die quantenmechanik der elektronen in kristallgittern. *Zeitschrift für Physik* **1929**. *52* (7), 555-600.
- (345) Piela, L. *Ideas of quantum chemistry*; Elsevier: Amsterdam, 2007, pp. 428-497.
- (346) Adams II, E.N. The crystal momentum as a quantum mechanical operator. *The Journal of Chemical Physics* **1953**. *21* (11), 2013-2017.
- (347) Dehmelt, H. A single atomic particle forever floating at rest in free space: New value for electron radius. *Physica Scripta* **1988**. *T22*, 102-110.
- (348) Haken, H.; Wolf, H.C.; Brewer, W.D. *The physics of atoms and quanta: Introduction to experiments and theory*; Springer Berlin Heidelberg: Berlin, Heidelberg, 2005, pp. 69-80.
- (349) Angeli, I.; Marinova, K.P. Table of experimental nuclear ground state charge radii: An update. *Atomic Data and Nuclear Data Tables* **2013**. *99* (1), 69-95.
- (350) Wang, M.; Audi, G.; Wapstra, A.H.; Kondev, F.G.; Maccormick, M., *et al.* The AME2012 atomic mass evaluation. *Chinese Physics C* **2012**. *36* (12), 1603-2014.
- (351) Nyquist, H. Certain topics in telegraph transmission theory. *Transactions of the American Institute of Electrical Engineers* **1928**. *47* (2), 617-644.
- (352) Chadi, D.J.; Cohen, M.L. Special points in the brillouin zone. *Physical Review B* **1973**. *8* (12), 5747-5753.
- (353) Dovesi, R.; Civalleri, B.; Roetti, C.; Saunders, V.R.; Orlando, R.: Ab initio quantum simulation in solid state chemistry. In *Reviews in computational chemistry*; Lipkowitz, K.B., Larter, R., Cundari, T.R. Eds.; John Wiley & Sons, 2005, pp. 1-125.
- (354) Price, S.L. From crystal structure prediction to polymorph prediction: Interpreting the crystal energy landscape. *Physical Chemistry Chemical Physics* **2008**. *10* (15), 1996-2009.

- (355) Beran, G.J.O. Modeling polymorphic molecular crystals with electronic structure theory. *Chemical Reviews* **2016**. *116* (9), 5567-5613.
- (356) Daniel, P.O.; Melgardt, M.D.V. Solid state concerns during drug discovery and development: Thermodynamic and kinetic aspects of crystal polymorphism and the special cases of concomitant polymorphs, co-crystals and glasses. *Current Drug Discovery Technologies* **2017**. *14* (2), 72-105.
- (357) Jones, W. An appreciation of organic solid-state chemistry and challenges in the field of “molecules, materials, medicines”. *Israel Journal of Chemistry* **2017**. *57* (1-2), 117-123.
- (358) Jaleh, V.; Erfaneh, G.; Saeedeh, A. Crystal engineering for enhanced solubility and bioavailability of poorly soluble drugs. *Current Pharmaceutical Design* **2018**. *24* (21), 2473-2496.
- (359) Mazurek, A.H.; Szeleszczuk, Ł.; Pisklak, D.M. Periodic DFT calculations—review of applications in the pharmaceutical sciences. *Pharmaceutics* **2020**. *12* (5), 415 (1-30).
- (360) Vasileiadis, M.; Pantelides, C.C.; Adjiman, C.S. Prediction of the crystal structures of axitinib, a polymorphic pharmaceutical molecule. *Chemical Engineering Science* **2015**. *121*, 60-76.
- (361) Beran, G.J.O.; Hartman, J.D.; Heit, Y.N. Predicting molecular crystal properties from first principles: Finite-temperature thermochemistry to nmr crystallography. *Accounts of Chemical Research* **2016**. *49* (11), 2501-2508.
- (362) Yu, R.; Zhu, J.; Ye, H.Q. Calculations of single-crystal elastic constants made simple. *Computer Physics Communications* **2010**. *181* (3), 671-675.
- (363) Day, G.M.; Price, S.L.; Leslie, M. Elastic constant calculations for molecular organic crystals. *Crystal Growth & Design* **2001**. *1* (1), 13-27.
- (364) Kitajgorodskij, A.I., *Molecular crystals and molecules*; Academic Press: New York, 1973, 553 p.
- (365) Pertsin, A.J.; Kitaigorodskii, A.I., *The atom-atom potential method. Applications to organic molecular solids*; 1<sup>st</sup> Ed.; Springer-Verlag Berlin Heidelberg: Berlin, 1987, 400 p.
- (366) Hartman, P.; Perdok, W.G. On the relations between structure and morphology of crystals. I. *Acta Crystallographica* **1955**. *8* (1), 49-52.
- (367) Roberts, R.J.; Rowe, R.C.; York, P. The relationship between indentation hardness of organic solids and their molecular structure. *Journal of Materials Science* **1994**. *29* (9), 2289-2296.
- (368) Sun, C.C.; Kiang, Y.H. On the identification of slip planes in organic crystals based on attachment energy calculation. *Journal of Pharmaceutical Sciences* **2008**. *97* (8), 3456-3461.
- (369) Bryant, M.J.; Maloney, A.G.P.; Sykes, R.A. Predicting mechanical properties of crystalline materials through topological analysis. *CrystEngComm* **2018**. *20* (19), 2698-2704.
- (370) Zolotarev, P.N.; Moret, M.; Rizzato, S.; Proserpio, D.M. Searching new crystalline substrates for ombe: Topological and energetic aspects of cleavable organic crystals. *Crystal Growth & Design* **2016**. *16* (3), 1572-1582.
- (371) Gavezzotti, A. Calculation of intermolecular interaction energies by direct numerical integration over electron densities. I. Electrostatic and polarization energies in molecular crystals. *The Journal of Physical Chemistry B* **2002**. *106* (16), 4145-4154.
- (372) Gavezzotti, A. Calculation of intermolecular interaction energies by direct numerical integration over electron densities. 2. An improved polarization model and the evaluation of dispersion and repulsion energies. *The Journal of Physical Chemistry B* **2003**. *107* (10), 2344-2353.
- (373) Bond, A. ProcessPIXEL: A program to generate energy-vector models from Gavezzotti's PIXEL calculations. *Journal of Applied Crystallography* **2014**. *47* (5), 1777-1780.

- (374) Gavezzotti, A. Coulombic and dispersive factors in the molecular recognition of peptides: Pixel calculations on two NNQQ (Asn-Asn-Gln-Gln) crystal polymorphs. *Acta Crystallographica Section D* **2008**. *64* (8), 905-908.
- (375) Braun, D.E.; Griesser, U.J. Why do hydrates (solvates) form in small neutral organic molecules? Exploring the crystal form landscapes of the alkaloids brucine and strychnine. *Crystal Growth & Design* **2016**. *16* (11), 6405-6418.
- (376) Gavezzotti, A.; Rizzato, S.; Lo Presti, L. The taco puzzle: A phase-transition mystery revisited. *Crystal Growth & Design* **2018**. *18* (11), 7219-7227.
- (377) Reeves, M.G.; Wood, P.A.; Parsons, S. MrPIXEL: Automated execution of Pixel calculations via the Mercury interface. *Journal of Applied Crystallography* **2020**. *53* (4), 1154-1162.
- (378) Gavezzotti, A. Calculation of lattice energies of organic crystals: The PIXEL integration method in comparison with more traditional methods. *Zeitschrift für Kristallographie - Crystalline Materials* **2005**. *220* (5-6), 499-510.
- (379) Konovalova, I.S.; Shishkina, S.V.; Paponov, B.V.; Shishkin, O.V. Analysis of the crystal structure of two polymorphic modifications of 3,4-diamino-1,2,4-triazole based on the energy of the intermolecular interactions. *CrystEngComm* **2010**. *12* (3), 909-916.
- (380) Fischer, W.; Koch, E. Geometrical packing analysis of molecular compounds. *Zeitschrift für Kristallographie - Crystalline Materials* **1979**. *150* (1-4), 245-260.
- (381) Baburin, I.A.; Blatov, V.A. Sizes of molecules in organic crystals: The Voronoi-Dirichlet approach. *Acta Crystallographica Section B* **2004**. *60* (4), 447-452.
- (382) Macrae, C.F.; Sovago, I.; Cottrell, S.J.; Galek, P.T.A.; McCabe, P., *et al.* Mercury 4.0: From visualization to analysis, design and prediction. *Journal of Applied Crystallography* **2020**. *53* (1), 226-235.
- (383) Shishkin, O.V.; Dyakonenko, V.V.; Maleev, A.V. Supramolecular architecture of crystals of fused hydrocarbons based on topology of intermolecular interactions. *CrystEngComm* **2012**. *14* (5), 1795-1804.
- (384) Turner, M.J.; Grabowsky, S.; Jayatilaka, D.; Spackman, M.A. Accurate and efficient model energies for exploring intermolecular interactions in molecular crystals. *The Journal of Physical Chemistry Letters* **2014**. *5* (24), 4249-4255.
- (385) Mackenzie, C.F.; Spackman, P.R.; Jayatilaka, D.; Spackman, M.A. Crystalexplorer model energies and energy frameworks: Extension to metal coordination compounds, organic salts, solvates and open-shell systems. *IUCrJ* **2017**. *4* (5), 575-587.
- (386) Shishkina, S.V. Using of quantum-chemical calculations to molecular crystals studying. *Structural Chemistry* **2019**. *30* (5), 1565-1577.
- (387) Varadwaj, P.R.; Varadwaj, A.; Marques, H.M. Halogen bonding: A halogen-centered noncovalent interaction yet to be understood. *Inorganics* **2019**. *7* (3), 40 (1-63).
- (388) Rychkov, D.A. A short review of current computational concepts for high-pressure phase transition studies in molecular crystals. *Crystals* **2020**. *10* (2), 81 (1-12).
- (389) Konovalova, I.S.; Muzyka, E.N.; Urzhuntseva, V.V.; Shishkina, S.V. Role of intermolecular interactions in formation of mono- and diaminopyridine crystals: Study from the energetic viewpoint. *Structural Chemistry* **2021**. *32* (1), 235-257.
- (390) Rubeš, M.; Bludský, O. Intermolecular  $\pi$ - $\pi$  interactions in solids. *Physical Chemistry Chemical Physics* **2008**. *10* (19), 2611-2615.
- (391) Dunitz, J.D.; Gavezzotti, A. How molecules stick together in organic crystals: Weak intermolecular interactions. *Chemical Society Reviews* **2009**. *38* (9), 2622-2633.
- (392) Turner, M.J.; Thomas, S.P.; Shi, M.W.; Jayatilaka, D.; Spackman, M.A. Energy frameworks: Insights into interaction anisotropy and the mechanical properties of molecular crystals. *Chemical Communications* **2015**. *51* (18), 3735-3738.

- (393) Reddy, C.M.; Rama Krishna, G.; Ghosh, S. Mechanical properties of molecular crystals—applications to crystal engineering. *CrystEngComm* **2010**. *12* (8), 2296-2314.
- (394) Shishkin, O.V.; Medvediev, V.V.; Zubatyuk, R.I. Supramolecular architecture of molecular crystals possessing shearing mechanical properties: Columns versus layers. *CrystEngComm* **2013**. *15* (1), 160-167.
- (395) Shishkina, S.V.; Levandovskiy, I.A.; Ukrainets, I.V.; Sidorenko, L.V.; Grinevich, L.A., *et al.* Polymorphic modifications of a 1H-pyrrolo[3,2,1-ij]quinoline-5-carboxamide possessing strong diuretic properties. *Acta Crystallographica Section C* **2018**. *74* (12), 1759-1767.
- (396) Ukrainets, I.V.; Burian, A.A.; Baumer, V.N.; Shishkina, S.V.; Sidorenko, L.V., *et al.* Synthesis, crystal structure, and biological activity of ethyl 4-methyl-2,2-dioxo-1H-2λ6,1-benzothiazine-3-carboxylate polymorphic forms. *Scientia Pharmaceutica* **2018**. *86* (2), 21 (1-17).
- (397) Desiraju, G.R. Supramolecular synthons in crystal engineering—a new organic synthesis. *Angewandte Chemie International Edition* **1995**. *34* (21), 2311-2327.
- (398) Burgers, J.M. Some considerations on the fields of stress connected with dislocations in a regular crystal lattice. *Proceedings of the Koninklijke Nederlandse Akademie van Wetenschappen* **1939**. *42*, 293-325.
- (399) Peierls, R. The size of a dislocation. *Proceedings of the Physical Society* **1940**. *52* (1), 34-37.
- (400) Nabarro, F.R.N. Dislocations in a simple cubic lattice. *Proceedings of the Physical Society* **1947**. *59* (2), 256-272.
- (401) Zhang, C.; Wang, X.; Huang, H.  $\pi$ -stacked interactions in explosive crystals: Buffers against external mechanical stimuli. *Journal of the American Chemical Society* **2008**. *130* (26), 8359-8365.
- (402) Lei, L.; Koslowski, M. Mesoscale modeling of dislocations in molecular crystals. *Philosophical Magazine* **2011**. *91* (6), 865-878.
- (403) Chattoraj, S.; Shi, L.; Chen, M.; Alhalaweh, A.; Velaga, S., *et al.* Origin of deteriorated crystal plasticity and compaction properties of a 1:1 cocrystal between piroxicam and saccharin. *Crystal Growth & Design* **2014**. *14* (8), 3864-3874.
- (404) Zeng, Y.; Alzate-Vargas, L.; Li, C.; Graves, R.; Brum, J., *et al.* Mechanically induced amorphization of small molecule organic crystals. *Modelling and Simulation in Materials Science and Engineering* **2019**. *27* (7), 074005.
- (405) Lee, M.K.; Kim, M.Y.; Kim, S.; Lee, J. Cryoprotectants for freeze drying of drug nano-suspensions: Effect of freezing rate. *Journal of Pharmaceutical Sciences* **2009**. *98* (12), 4808-4817.
- (406) Lei, L.; Carvajal, T.; Koslowski, M. Defect-induced solid state amorphization of molecular crystals. *Journal of Applied Physics* **2012**. *111* (7), 073505.
- (407) Mathew, N.; Picu, C.R.; Chung, P.W. Peierls stress of dislocations in molecular crystal cyclotrimethylene trinitramine. *The Journal of Physical Chemistry A* **2013**. *117* (25), 5326-5334.
- (408) Pal, A.; Picu, C.R. Peierls–Nabarro stresses of dislocations in monoclinic cyclotetramethylene tetranitramine ( $\beta$ -HMX). *Modelling and Simulation in Materials Science and Engineering* **2018**. *26* (4), 045005 (1-22).
- (409) Khan, M.; Picu, C.R. Dislocation cross slip in molecular crystal cyclotetramethylene tetranitramine ( $\beta$ -HMX). *Journal of Applied Physics* **2019**. *126* (15), 155105 (1-10).
- (410) Zhang, S.H.; Legut, D.; Zhang, R.F. PNADIS: An automated Peierls–Nabarro analyzer for dislocation core structure and slip resistance. *Computer Physics Communications* **2019**. *240*, 60-73.

- (411) Petukhov, B. Dislocation dynamics in a crystal lattice (Peierls-Nabarro) relief. *Crystal Lattice Defects and Dislocation Dynamics*. Preprint arXiv:0704.1714. **2007**. 1-39.
- (412) Zhang, C. Understanding the desensitizing mechanism of olefin in explosives versus external mechanical stimuli. *The Journal of Physical Chemistry C* **2010**. *114 (11)*, 5068-5072.
- (413) Ma, Y.; Zhang, A.; Xue, X.; Jiang, D.; Zhu, Y., *et al.* Crystal packing of impact-sensitive high-energy explosives. *Crystal Growth & Design* **2014**. *14 (11)*, 6101-6114.
- (414) Zhou, X.; Lu, Z.; Zhang, Q.; Chen, D.; Li, H., *et al.* Mechanical anisotropy of the energetic crystal of 1,1-diamino-2,2-dinitroethylene (FOX-7): A study by nanoindentation experiments and density functional theory calculations. *The Journal of Physical Chemistry C* **2016**. *120 (25)*, 13434-13442.
- (415) Lu, Z.; Zeng, Q.; Xue, X.; Zhang, Z.; Nie, F., *et al.* Does increasing pressure always accelerate the condensed material decay initiated through bimolecular reactions? A case of the thermal decomposition of TKX-50 at high pressures. *Physical Chemistry Chemical Physics* **2017**. *19 (34)*, 23309-23317.
- (416) Bu, R.; Xie, W.; Zhang, C. Heat-induced polymorphic transformation facilitating the low impact-sensitivity of 2,2-dinitroethylene-1,1-diamine (FOX-7). *The Journal of Physical Chemistry C* **2019**. *123 (26)*, 16014-16022.
- (417) Bu, R.; Xiong, Y.; Zhang, C.  $\pi$ - $\pi$  stacking contributing to the low or reduced impact sensitivity of energetic materials. *Crystal Growth & Design* **2020**. *20 (5)*, 2824-2841.

## **Chapter 2. Experimental and computational details**

## 2.1. Objects of the investigation

The objects of investigation in this work were selected so as to cover a larger number of problems arising in the process of obtaining the desired polymorphic modification during pharmaceutical production. They were divided into two groups depending on the stage when control is especially necessary.

APIs crystallizing in various polymorphic modifications or their mixture, whose structure is difficult to identify and control, are assigned to the first group. It is composed of mefenamic acid (MFA) and carbamazepine (CBZ), as well as a co-crystal of mefenamic acid with nicotinamide (NA). These crystalline phases are studied experimentally at the stages of *in situ* crystallization from scCO<sub>2</sub> using the CSS method and post-processing in Chapter 3. The general view of their molecular structures is presented in Figure 2.1.

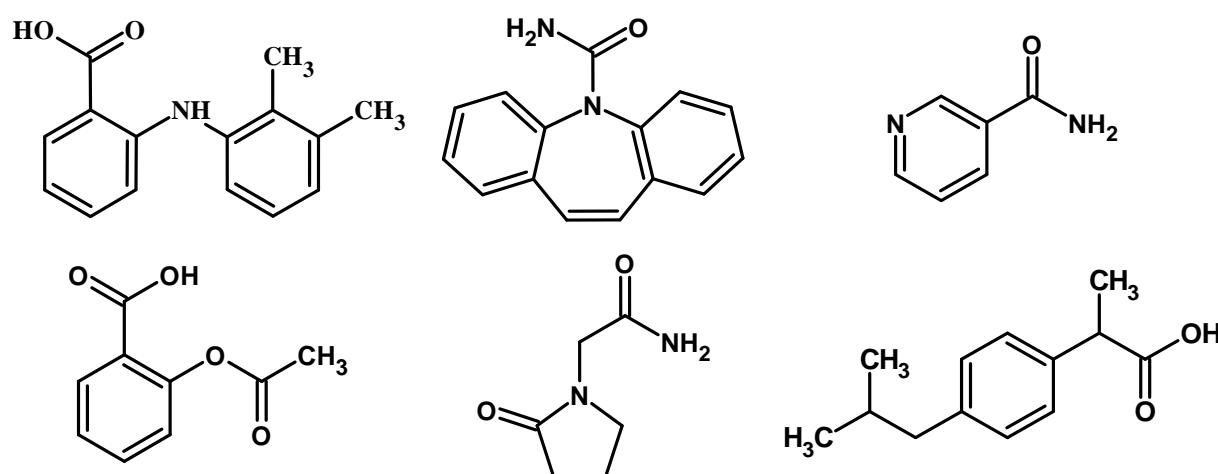


Figure 2.1. Chemical structures of six APIs whose crystal structures were studied with experimental (at the top) and theoretical (at the bottom) methods. Top: mefenamic acid (on the left), carbamazepine (in the middle) and nicotinamide (on the right). Bottom: aspirin (on the left), piracetam (in the middle) and ibuprofen (on the right).

Mefenamic acid is a well-known analgesic-antipyretic agent belonging to the fenamates class (anthranilic acid derivatives) of NSAIDs and is used to treat

mild to moderate pain. Four polymorphic forms [1-4] of MFA have been discovered and the properties of the first two have been characterized. The third form has very low stability and, moreover, cannot be obtained by direct crystallization [3]. Just the structure is known for the fourth form, while its preparation and stability are not described in the literature. It has been shown that the second form has a higher dissolution rate [5, 6]. However, the ratio of polymorphs in commercial forms of MFA is not usually specified and this influences significantly the measured values of the relative concentration of MFA in blood plasma. This is illustrated by the enormous dispersion of the reported data which range between 28 and 86% [7]. It should be mentioned that this ratio also is not available when quantifying the solubility of MFA [6, 8-15] and the solubility of the ready dosage form of MFA in water at normal conditions has an extremely low value (the molar fraction is lower than  $10^{-4}$ ) [14].

In order to control the formation of specific polymorphic form, thermal conversion upon heating above  $155^{\circ}\text{C}$  at ambient pressure [10] and recrystallization from polar aprotic solvents [5, 16, 17], among which dimethylformamide is the most popular [13, 18], have been proposed. However, there are three issues, which significantly limit the use of these methods: high speed of sublimation, which is faster than the conversion between crystalline forms [10], the toxicity of DMF and incomplete conversion from the first polymorph into the second one [13, 19] and finally, the second polymorph form is not stable in the wet state, which is a drawback during both its synthesis and long-term storage [20, 21]. Nevertheless, it was shown that when MFA is kept in the dry state, the back-transformation of the second form to the first one does not occur even within 90 days [21, 22]. Thereby, the mefenamic acid seems to be problematic during the crystallization and storage.

Carbamazepine is the second compound to study. It can crystallize in five different polymorphs [23-28], four of which can be easily obtained in

recrystallization [29]. They differ only in the orientation of the molecules in the crystal structures and have rather low conformational flexibility. Polymorph III of CBZ is the only one used in pharmaceuticals nowadays as the most stable at room temperature [24]. However, polymorph I that is less stable at room temperature [29], could be more interesting pharmacologically. The possibility of polymorphic control of carbamazepine at the crystallization stage is very problematic, but it is of great interest.

As the last system, the API mefenamic acid and nicotinamide, vitamin B3, an extremely popular co-former and API with 9 polymorphic modifications [30], was chosen. Co-crystallization is a widely used method to improve the chemical properties of the targeted active pharmaceutical ingredient such as its aqueous solubility, bioavailability, dissolution rate, melting point and stability [31-33] by obtaining its joint crystal with a co-former. It may be carried out in scCO<sub>2</sub> that allows synthesizing co-crystals of high purity in a single step process with the possibility to handle thermosensitive APIs [34-53] as MFA or CBZ. Application of scCO<sub>2</sub> can solve most of the drawbacks of synthesizing the co-crystal with commonly used mechano-chemical and solution-based methods [54, 55]. Specifically, when compared with conventional methods (solid-based or solution mediated ones), the utilization of scCO<sub>2</sub> helps to control the thermodynamic parameters (temperature, pressure) and to achieve the repeatability of the proposed process [56-59]. However, using scCO<sub>2</sub>, co-crystals have been synthesized mostly as microcrystalline powders, the structure of which is determined by powder X-ray diffraction (PXRD). It is well established that the structure determination using PXRD is a powerful auxiliary implement to single-crystal X-ray diffraction (SCXRD). Whereas, the structure determination using PXRD is more challenging than single-crystal X-ray diffraction, in particular in the case of organic molecular materials with a large number of atoms in an asymmetric unit cell [60, 61]. Furthermore, because of the impossibility to obtain single crystals of sufficient size, it was not possible to

determine the structure of many synthesized samples [62, 63]. The growth of a defect-free single crystal using scCO<sub>2</sub> was demonstrated only for acetylated carbohydrates [64]. The validation of co-crystals structure is rather difficult and the acquisition of its single crystals from scCO<sub>2</sub> will simplify it significantly.

MFA:NA co-crystal was already synthesized as a powder using conventional methods and gas anti-solvent process [46, 65, 66]. The solubility of MFA from such a co-crystal in water was declared to be near 1.5 times higher in comparison with that of the pure API [66] making it an alternative for obtaining a metastable polymorphic form II. However, numerous experimental results have shown that, in the co-crystallization process in a solvent, the large difference in solubility existing between the API and the co-former in that solvent is an incompatibility factor, which makes the formation of the co-crystal incomplete [67]. For the NA the solubility in water is more than 10<sup>5</sup> times higher than for the MFA under normal conditions [68, 69]. Their solubility in scCO<sub>2</sub> is relatively close [70, 71], but the validation of co-crystals purity is complex because of the presence of at least 3 phases: API, co-former and co-crystal, each of which can exhibit polymorphism. The spectral methods are hardly capable of this. Thereby, the important task was to obtain the single crystal of MFA:NA co-crystal from scCO<sub>2</sub>, to determine its structure with SCXRD and, as a consequence, to receive the reference spectra and PXRD patterns for the express control of any powder samples. The details of the crystallization process, as well as the principal device scheme, will be discussed in Chapter 3 as an object of modifications.

All the used powders of APIs were purchased from “Sigma-Aldrich”. The CAS numbers are 61-68-7, 298-46-4 and 98-92-0 for the mefenamic acid, carbamazepine and nicotinamide respectively. The purity of components in the same order corresponds to >98%, 99% and 99.5%. In order to characterize the MFA initial form used in the experiment, the IR spectra of three MFA samples in KBr tablets were measured. The analysis of these spectra presented in Figure

2.2 in the wavenumber range corresponding to the N-H stretching vibrations region ( $3250\text{-}3400\text{ cm}^{-1}$ ) has revealed the presence of a small spectral contribution related to polymorph II. It means that the initial commercial form of MFA used in this study is not pure polymorph I, and it contains a small amount of polymorph II. This is in good agreement with the results of [10, 15]. Moreover, a quantitative analysis of these three spectra in the N-H stretching vibrations region has shown that the average percentage of polymorph II is 13.6% that is commensurable with the value of 10% given in [10]. The commercial CBZ was not checked as a one meeting the testing specifications of Pharmacopoeia (pure form III), as well as NA, whose polymorphic modification I is the sole stable under ambient conditions according to [72]. The  $\text{CO}_2$  gas (99.99% purity) was purchased from “The Linde Group”.

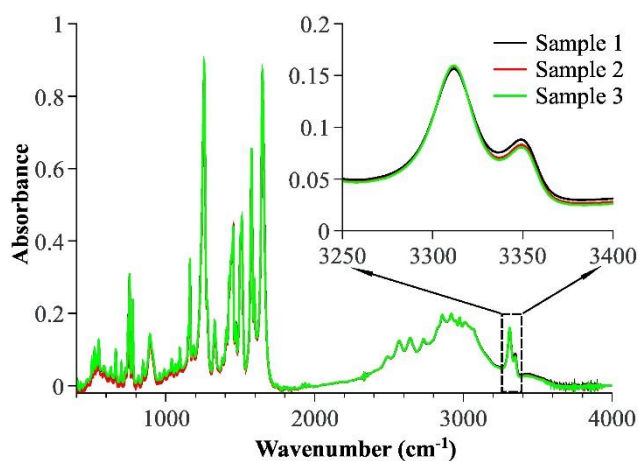


Figure 2.2. IR spectra of three samples of crystalline mefenamic acid commercial form. The area limited by a rectangle shows the N-H stretching vibration region and corresponds to the insert.

The second group consists of the following APIs: aspirin, paracetamol and ibuprofen. Their processing after the crystallization and storage is the bottleneck for the pharmaceutical production, so the studies were aimed at the analysis of polymorphic transformations and solid-state changes accompanying

them. The creation of a new theoretical model will be based on the molecules represented in Figure 2.1 and will be discussed in Chapter 4 of the current thesis.

Polymorphic modifications of the aspirin were chosen as a very suitable object for the development of a new method for modeling the mechanical properties of molecular crystals using quantum-chemical calculations. Aspirin is a well-studied drug, so the results obtained within a new approach can be compared with the available experimental and theoretical data. For a very long time, the existence of aspirin polymorphs remained questionable [73-78]. The crystal structure of the polymorph II was obtained only in 2005 by Zaworotko and co-workers [79]. However, the very subtle difference between polymorphs I and II as well as the low quality of the experimental data required additional evidence. Further studies of the new crystal form of aspirin showed that it was not a twin or a mixture of form I and form II but it was an intergrown crystal containing domains of both forms I and II [80, 81]. After crystallization of form II as a pure phase [82], both polymorphic modifications were thoroughly studied by experimental [83-87] and theoretical methods [88-91]. Particular attention was paid to the study of possible polymorphic transitions of aspirin polymorphs [86]. The transition of the less stable form II into the form I was proven under grinding [85]. The existence of polymorph III obtained at the pressure above  $\sim 2$  GPa from the polymorph I was assumed based on Raman spectroscopy data [86]. Unfortunately, the structure of this polymorph was not proven reliably. The newest ambient polymorph of aspirin (form IV according to the original publication [92]) was found only in 2017 and turned out to be metastable so its properties are still not studied. It should be mentioned that the mechanical properties of polymorphic structures I and II as the interconvertible ones are still unclear are the directions for the easiest deformation, which can be important during the treatment, were determined ambiguously [84, 85]. Thereby, the mechanical response and any possibilities of conversion between the polymorphic modifications I, II and IV of aspirin are of great interest.

The further development of the computational method and its application to the polymorphic transformations will be discussed in the example of piracetam. This simple molecule possesses low conformational flexibility and can form different sets of intermolecular interactions due to the presence of two strong proton donors and two strong proton acceptors. The structures of four polymorphic modifications of this API have been identified and characterized using the X-ray diffraction method [93]. Most of them are capable to transform mutually under pressure, such as during tableting or grinding. However, just for one transition from polymorph II to form V pressure was described as the dominant and sole factor necessary for the transformation without the need of a solvent. It is characterized as reversible and occurs at the pressure near 0.70 GPa, while the crystal behavior is described in detail till the pressure of 4.00 GPa [94]. However, driving forces and reasons for this transformation have not been described. Together the aforementioned characteristics make the polymorphic transition of piracetam polymorphic modification II to V an ideal object to test the new technique.

The latest object for theoretical studies is ibuprofen. Ibuprofen belongs to class II according to BCS [95] and has a low solubility under normal conditions (0.143 g / l) [96]. The increase in its solubility is an important unsolved task for the pharmaceutical industry. During the search for a solution, the amorphous form of the API [97] and its polymorphic modification II [98] were found, as well as that solubility has a clear relationship with the shape (habit) of crystals [99-101]. It should be noted that the amorphous form and the polymorphic modification II of ibuprofen are metastable and prone to a transition to form I [102, 103], which prompts the search for transformation mechanisms and possible stabilization of these forms. Mechanical processing of ibuprofen produced ambiguous results. From one side, the compression of this drug till 4.00 GPa did not lead to significant changes in the experiment [104]. At the same time, the amorphous form can be partially stabilized by the grinding with

the mesoporous silica [105]. It makes the polymorphic transformation of ibuprofen an interesting object for the theoretical study of its polymorphic transformations and mechanical properties.

The polymorphic structures of aspirin (whose Refcodes are ACSALA14 [81], ACSALA15 [80] and ACSALA23 [92]), piracetam (BISMEV [106], BISMEV06-BISMEV10 [94]) and ibuprofen (IBPRAC04 [98], IBPRAC05-IBPRAC15 [104]) have been extracted from the Cambridge Crystal Structure Database [107].

## 2.2. Vibrational analysis

### 2.2.1. *In situ* infrared spectroscopy

The control over the process of crystallization requires constant monitoring of the conformational equilibria in the fluid phase. This control is usually performed in the pharmaceutical industry inside of the flow-reactors [108, 109] and allows to crystallize selectively the solid phases of interest [110]. The conformational equilibria of MFA and CBZ were studied in the scCO<sub>2</sub> pre-expansional phase which was in contact with the excess of the corresponding API crystalline form (with respect to the expected solubility in scCO<sub>2</sub>), the same experimental setup as described in detail in [111] was used. The experiments were held under isochoric heating conditions to avoid the influence of the scCO<sub>2</sub> density and so the corresponding changes in APIs concentrations. The high-pressure high-temperature (HPHT) optical cell with a variable optical path length [112] was improved. This cell allows reaching the equilibrium concentration of the solute in scCO<sub>2</sub> relatively fast and to record spectra with a high resolution as well as with a high signal-to-noise ratio in a wide range of thermodynamic parameters of state. The general and sectional views of this cell are shown in Figure 2.3a,b. In this cell, the optical windows with an effective working diameter of 8 mm and thickness of 9 mm to stand the high pressure up

to 1000 bar were used. The windows made of silicon allowed one to measure the IR spectra in the wavenumber range of 1000-7000  $\text{cm}^{-1}$ . The isolation of cell is done with graphite packing rings. The sample of initial (commercial) crystalline form of MFA with a diameter of 9 mm and thickness of 7 mm was placed into a sample holder in the bottom part of the cell (Figure 2.3b). In order to avoid the contamination of the initial sample by the residuals of atmospheric components (in particular, water and oxygen), the HPHT cell was pumped out to a residual pressure of 0.1 mbar. After that, the cell was filled with dry  $\text{CO}_2$  through a stainless-steel capillary connected to a high-pressure setup allowing the adjustment of the pressure with an accuracy of  $\pm 0.5$  bar. The cell was heated by means of four cartridge heaters disposed in its body corners. Three thermocouples were used for temperature control. One of them was located in the vicinity of one of the four cartridge heaters and was connected to a proportional-integral-derivative (PID) controller allowing controlling the temperature with an accuracy of about  $\pm 1^\circ\text{C}$ . The second thermocouple was located in the upper part of the cell body close to the fluid solution phase and the third one was located in the bottom part of the cell containing the crystalline form of MFA. By choosing the thermocouple positions it is possible to control the temperature gradient between the bottom and the fluid phases. In the experiments with MFA and CBZ, this gradient did not exceed  $3^\circ\text{C}$  even at the highest temperature studied.

The measured mid IR spectra corresponded to the  $\text{CO}_2$  phase of a binary [MFA- $\text{scCO}_2$ ] mixture (the sectional view in Figure 2.3b). These spectra were obtained using a FTIR spectrometer Bruker Vertex 80 equipped with a deuterated triglycine sulfate detector in the wavenumber range of 1000-4000  $\text{cm}^{-1}$ . The choice of temperature ranges was based on the melting points of the APIs under pressure in  $\text{scCO}_2$  and the temperatures of conformational transitions in the bioactive molecules the APIs built of. It was 80-220 $^\circ\text{C}$  and 110-200 $^\circ\text{C}$  for MFA and CBZ respectively. The temperature step

of 10°C was used. The density of scCO<sub>2</sub> and the optical path were adapted to avoid the oversaturation of the analytical spectral bands of APIs in scCO<sub>2</sub>. For the MFA, the density corresponded to  $\rho=1.1*\rho_{\text{critical}}(\text{CO}_2)$ , where  $\rho_{\text{critical}}(\text{CO}_2)=10.625 \text{ mol}\cdot\text{L}^{-1}$  is the critical density of carbon dioxide, and the two optical path lengths were used: 1.600 mm in the temperature range of 80-160°C when the solubility of MFA is low and 0.137 mm in the temperature range of 150-220°C. CBZ absorbance was lower, so the density was increased to coincide with the isochore of  $1.3*\rho_{\text{critical}}(\text{CO}_2)$  and the optical path length of 1.000 mm was used. For these isochores, the pressure varied in the ranges of 172-459 bar and 289-539 bar for MFA and CBZ respectively. At each temperature, the initial spectrum was measured immediately when the temperature reached the target value. Since it takes some time to achieve the equilibrium concentration of APIs in the scCO<sub>2</sub> phase (when the intensity of the spectra remains constant in the last 3-4 measurements), the dynamic spectra were recorded every 30 minutes to get information on the dissolution of APIs in the scCO<sub>2</sub> phase at a given temperature during the equilibration process. It took the following times to reach the equilibration:

- MFA: 6 hours for the temperatures in the range of 80-170°C, 24 hours at T=180°C, 48 hours at T=190°C, and 12 hours for the temperatures in the range of 200-220°C.
- CBZ: 110°C - 12 hours, 120°C - 30 hours, 130°C - 6 hours, 140°C - 30 hours, 150°C - 30 hours, 160°C - 15 hours, 170°C - 12 hours, 180°C - 5 hours, 190°C - 5 hours, 200°C - 5 hours.

Thereby, the IR spectra of the scCO<sub>2</sub>-rich phase (SCF solution phase) of two-phases systems of “API solid - SCF solution” or “API melt - SCF solution” depending on parameters of state were measured.

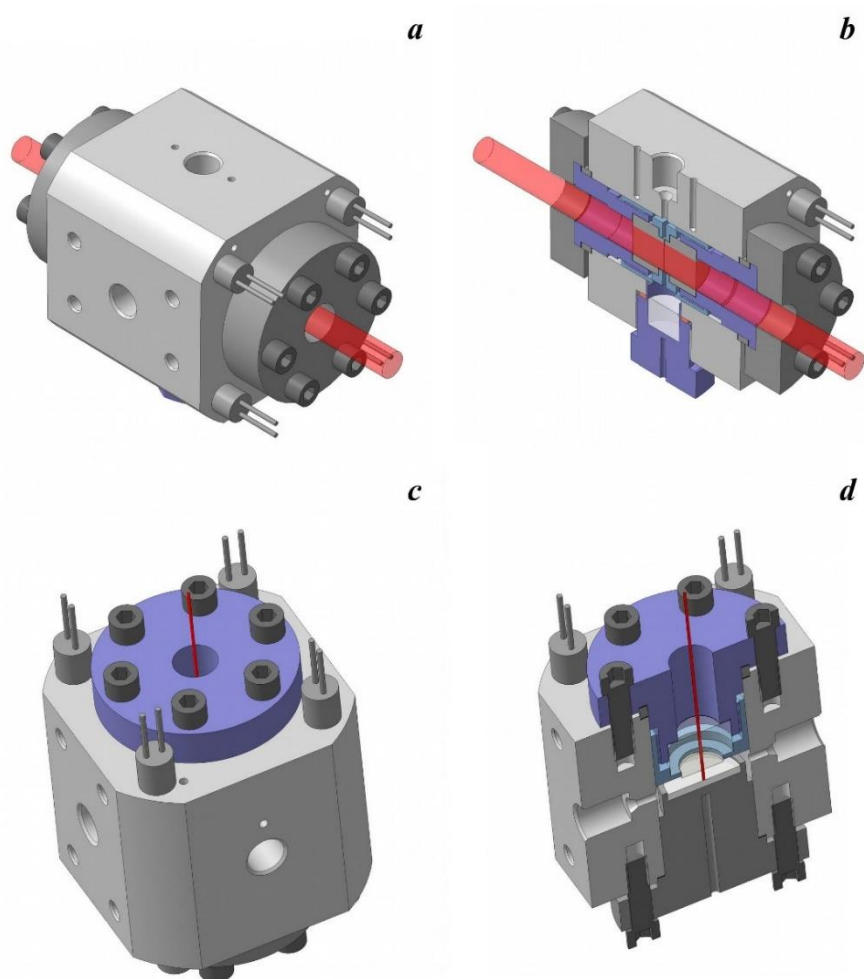


Figure 2.3. (a) Schematic representation of the experimental HPHT optical cell for IR spectroscopy with a variable optical path length; (c) Schematic representation of the experimental HPHT optical cell for Raman spectroscopy; (b,d) Cells sectional views showing their internal geometry and position of the IR beam or excitation red laser beam relative to the bottom part of the cell containing the sample solid phase.

Since the single-beam spectrometer was used in experiments, the influence of the atmosphere components (in particular, water vapor) caught in the path of the infrared beam outside the cell has to be excluded. Thus, the dry air was continuously pumped through the sample spectrometer chamber where the optical cell was positioned. For each temperature, the spectra of the empty cell (the silicon windows spectra) and the spectra of the cell filled only with CO<sub>2</sub> were recorded. Finally, the spectra were recorded from the binary mixture where API was placed in the bottom part of the cell (Figure 2.3b) filled with CO<sub>2</sub>. All

these spectra were measured with a resolution of  $1\text{ cm}^{-1}$ . For each spectrum, 128 interferograms were recorded and averaged out to increase the signal-to-noise ratio. The resulting spectra of API diluted in  $\text{scCO}_2$  were calculated by direct subtraction of the spectra measured for the cell filled only with  $\text{CO}_2$  from the spectra of the binary mixture. The final spectra were corrected by baseline subtraction.

### 2.2.2. *In situ* Raman spectroscopy

The same changes followed with *in situ* IR technique can be analyzed as well with the Raman measurements. In this case, the analyzed phase is not the fluid, but the solid phase of the API. It gives a possibility to select the synthesis conditions looking directly at the changes in the vibrational structure of a solid and to see the correlation between the conformations observed in the supercritical solution and the polymorphic composition. As well, it allows one to follow up the changes occurring on the surface of an API crystalline sample.

To achieve this, the samples of MFA and CBZ with linear sizes of 14 mm in diameter and 3 mm thick (the sectional view in Figure 2.3d) were placed in the sample holder in contact with the  $\text{scCO}_2$  fluid phase. The inox Raman cell equipped with the sapphire window and packed with graphite rings (Figure 2.3c) was heated in the same manner as the one for IR measurements, but the analyzed temperature ranges changed for MFA and CBZ to 80-190°C and 40, 110-120°C respectively, to exclude the work on molten APIs. A He-Ne laser ( $\lambda = 632.81\text{ nm}$ ) with an output power of about 18 mW was connected to an optical fiber directing the laser beam into the specific module “Power Head” [113]. This module was used to ensure the remote collection of the Raman scattering with optimal sensitivity. The laser beam was focused on the sample by a lens with a focal length of 40 mm. The laser beam power at the focal point was about 10mW. The Raman light was collected in the backscattering mode by the same lens and then was focused inside the module at the entrance of the

collecting optical fiber connected to a visible Raman spectrometer LabRAM HR Evolution (produced by HORIBA Jobin Yvon, France). The spectra were registered in the wavenumber range of 50-4000  $\text{cm}^{-1}$ . The diffraction gratings of 600 and 1800 grooves/mm were used for MFA and CBZ respectively. The acquisition time and the number of accumulations were adapted to optimized to get spectra with a good signal-to-noise ratio.

### 2.2.3. Micro infrared spectroscopy

The IR analysis of crystalline samples after the crystallization can be done in many ways. The most popular techniques which do not require any sample treatment are the attenuated total reflectance IR and micro IR spectroscopies. However, just the second gives well-resolved spectral data for solids. In this work, the micro IR reflectance spectra of the MFA crystalline forms were recorded using a Vertex 70 spectrometer equipped with a liquid nitrogen-cooled Mercury-Cadmium-Telluride (MCT) detector. This spectrometer was coupled with a Hyperion 3000 FT-IR confocal microscope (produced by Bruker Optik GmbH) equipped with a 15x magnifying objective and was operated in the reflectance mode using an aperture size of 160x160  $\mu\text{m}$ . In order to obtain the spectra with a good signal-to-noise ratio, 256 interferograms were recorded and averaged out for each measurement. Then the resulting absorption spectra in the wavenumber range of 800-3600  $\text{cm}^{-1}$  with a 1  $\text{cm}^{-1}$  spectral resolution were derived from the recorded reflectance spectra by applying the Kramers-Kronig transformation algorithm [114]. It helped in the identification of the polymorphic forms of MFA by the comparison with reference spectra represented in [15].

### 2.2.4. Diffuse reflectance infrared Fourier transform spectroscopy

The alternative algorithm for studies of solids is to work in diffuse-reflection mode and diffuse reflectance infrared Fourier transform spectroscopy

(DRIFTS) is a good variant for mass analysis of the crystallized APIs because it allows to collect high amount of reflected IR waves and to obtain good signal practically without sample treatment [115]. Thus, the vibrational spectra of MFA:NA co-crystal were registered using Bruker Vertex 70V infrared spectrometer equipped with liquid nitrogen cooled MCT detector in the spectral range from 700 to 4000  $\text{cm}^{-1}$  with the resolution of 2  $\text{cm}^{-1}$  (256 scans per spectrum). For the DRIFTS a Harrick Scientific Diffuse reflectance attachment “Praying Mantis” combined with the cell equipped with  $\text{CaF}_2$  windows was applied. Further data manipulation including Kubelka-Munk transformation [116] was performed in OPUS Bruker software. The samples for DRIFTS were used in two ways: as is and milled in an agate mortar. It was done to decrease the Mie scattering, but both analytes showed the same spectral pattern, demonstrating that the samples received through the crystallization in  $\text{scCO}_2$  are very fine powders (diameter of crystals less than 5  $\mu\text{m}$  [115]). All samples of MFA:NA co-crystal were mixed with KBr to receive the final percentage of analyzed powder  $\leq 5$  molar per cent and loosely packed in the sample holder.

#### 2.2.5. Micro Raman spectroscopy

The micro Raman spectroscopy is also an effective and wide-spread method for the analysis of solid phases. Recording of the inelastically Raman-scattered photons has a serious advantage in comparison to IR-based methods when the crystals are analyzed. The cross-section of inelastic Stokes scattering basic for Raman spectroscopy is usually from  $10^{-8}$  times smaller than that for Rayleigh scattering [117], so the oversaturation is hardly reached without purpose. Thus, the powders can be taken as is after the crystallization.

Two measurement methods based on micro Raman spectroscopy were applied in this work: conventional analysis of powders and *in situ* measurement with heating (no  $\text{CO}_2$ ). The MFA samples were studied using heating without  $\text{scCO}_2$  to check for the possibility to obtain the other polymorphic modifications

from the form I. For this, the add-on Linkam THMS600, which allows studying the solid phase under heating and cooling in the temperature range from  $-196^{\circ}\text{C}$  to  $600^{\circ}\text{C}$  with an accuracy of  $0.1^{\circ}\text{C}$  was applied. Raman spectra of the MFA crystalline forms were obtained using the same visible Raman spectrometer as for *in situ* measurements in  $\text{CO}_2$ , combined with a confocal microscope (10-100x magnifying objectives were used), in the back-scattering geometry in the spectral range of  $50\text{-}3600\text{ cm}^{-1}$ . A He-Ne laser ( $\lambda = 632.81\text{ nm}$ ) with the energy of 15 mW at the sample was applied for excitation. The Raman signal was collected with a CCD-detector ( $1024*256$  pixels) placed after a diffraction grating (1800 grooves/mm) giving the final spectral resolution of about  $0.3\text{ cm}^{-1}$ . The spectra were accumulated in each single scan with the exposure time of 300 s per each orientation of the grating that assured the spectra with a good signal-to-noise ratio.

The spectra measured for CBZ were done to reveal polymorphism in the final product, so they were measured using conventional micro Raman spectroscopy under ambient conditions with the same LabRAM HR Evolution Raman spectrometer combined with a confocal microscope. The objective with a magnifying power of 100x was used. The acquisition times, the number of accumulations and laser beam power were varied according to the orientation and thickness of the sample in order to avoid its burning-out and to improve the signal-to-noise ratio.

### **2.3. Microscopic observations of sample changes**

The thermal changes in the APIs surface permanently contacting with their saturated solution in  $\text{scCO}_2$  were visually observed with the help of the system specially designed for this work. It is based on a digital long-focus optical microscope. This microscope is united with a universal High-Pressure High-Temperature optical cell via a precise positioning system. Moreover, the microscope is also equipped with coaxial brightening that allows making a

bright image of a target placed deep inside the optical cell. The HPHT cell is equipped with an optically transparent sapphire window enabling one to take a photo of the API surface inside the cell. Its thickness of 9 mm in combination with a small diameter (the external diameter is 12 mm and the effective working diameter is 8 mm) allows one to work at pressures of up to 1 kbar inside the cell. The detailed descriptions of the optical cell and experimental setup for the control of temperature and pressure of the reaction medium are given in Sections 2.2.1. “*In situ* IR spectroscopy” and 2.2.2. “*In situ* Raman spectroscopy”. The photos of the API surface permanently contacting with API saturated solution in scCO<sub>2</sub> were made with an optical resolution of 2 megapixels. The images were obtained for a number of temperatures along the chosen isochores.

#### **2.4. Single-crystal X-ray diffraction**

SCXRD experiment was performed on the co-crystal of MFA and NA to prove that its structure corresponds to one obtained earlier and to generate the reference PXRD pattern and DRIFT spectra for the express unambiguous determination of the co-crystal during synthesis. Reflection data and unit cell parameters of the synthesized crystals were measured at the temperature of 100 K using an Apex II CCD 4K Bruker diffractometer ( $\lambda = 0.71073 \text{ \AA}$ ). Correction for Lorentz polarization was performed in SAINT software [118]. Empirical absorption corrections introduced in SADABS software [119]. The structure was solved by a direct method using the SHELXTL program package [120, 121]. Hydrogen atoms bonded to carbon were placed at geometrically calculated positions. The other H atoms were revealed from the Fourier difference map. The refinement was done in the riding model with Uiso values scaled to the ones of the parental heavy atoms. OLEX2 program [122] was used for visualization and data processing. Previously the structure of the co-crystal with 1:2 MFA:NA ratio was determined from powder X-ray data using not an easily accessible

synchrotron source of radiation [123], so it was used for the comparison with the current data.

## **2.5. Powder X-ray diffraction**

PXRD analysis of the MFA:NA co-crystal was carried out at room temperature and humidity using a BRUKER AXS D8 ADVANCE diffractometer (Bragg-Brentano geometry) equipped with a 1D PSD detector (Lynx-Eye). Copper ( $K\alpha$ ) radiation was used for the measurements over the  $2\theta$ -range from  $4^\circ$  to  $60^\circ$  with a scan rate of  $0.02^\circ/\text{sec}$  (goniometer continuous mode). The X-ray source operated at the generator voltage of 40 kV and the tube current of 40 mA. Match! Software [124] was used on powder X-ray data to assess semi-quantitatively the phase composition of the synthesized solid.

## **2.6. Quantum-chemical calculations**

### **2.6.1. Conformation analysis and frequency assignment**

The assignment of the spectral contributions of the different conformers of bioactive molecules in the supercritical fluid phase required to perform the conformational search and vibrational spectra calculations with GAUSSIAN 09 software package [125]. To do so the preliminary optimization of the geometry and calculations of vibration frequencies were performed using the density functional theory hybrid Becke three-parameter functional B3LYP [126] for MFA and Austin-Frisch-Petersson functional with dispersion APFD [127] for CBZ molecules. The split-valence triple zeta basis set with diffuse functions for all atoms and the additional sets of p- and d-type polarization functions 6-311++g(2d,p) [128-130] was used. The conformational search was based on the analysis of the potential energy surface scans. The potential energy profiles were calculated along with the three dihedral angles, which determine the rotations of the carboxylic group and two aromatic fragments of the molecule,

respectively. The search for all possible conformers was based on the analysis of the potential energy surface scan. The preliminary scanning of the hyper-surface of potential energy was performed by semi-empirical method PM3 [131, 132] and the obtained set of conformers was further optimized using the same functionals and basis sets as for preliminary calculations. The dihedral angles scanned for MFA and CBZ are shown in Figure 2.4. The structure of each conformer corresponded to the local minimum of potential energy, which was confirmed by frequency calculations.

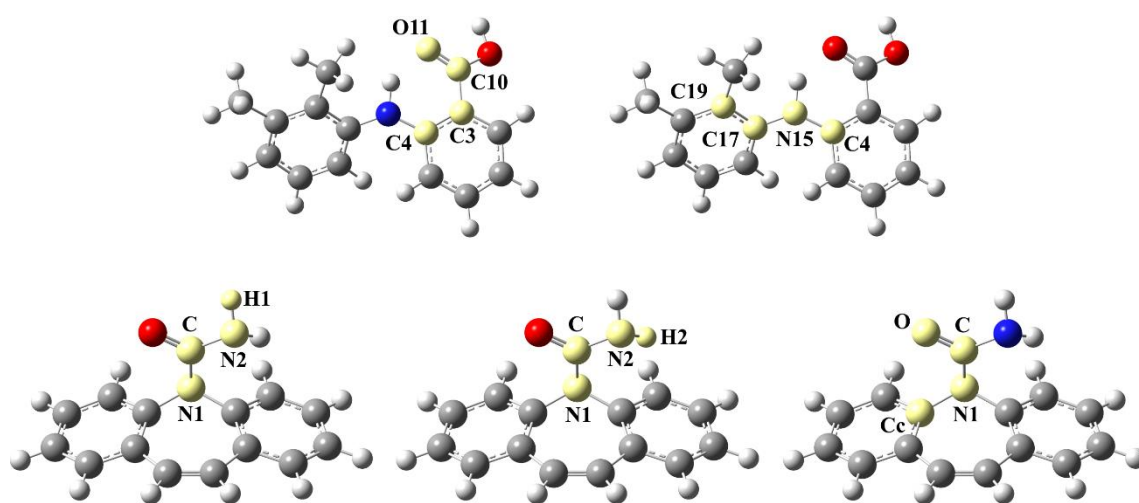


Figure 2.4. Schematic representation of the MFA and CBZ molecules with atoms forming the scanned dihedral angles.

Sixteen MFA conformers have been identified, but only the four most stable conformers were further taken into account. CBZ demonstrated four probable conformers for the conformer corresponding to the form I in solution among which two mirror pairs were found, so only two conformers were considered. Sole conformer occurs after the dissolution of the modification III  $scCO_2$ . The other molecules, namely conformer appearing in fluid phase after polymorphic form III dissolution, iminostilbene (IMST), its protonated form (IMST- $H^+$ ) and isocyanic acid (ICA), discussed in details in [133] were

optimized as well. Their vibrational spectra were calculated using all the same routines as for conformers search.

## 2.6.2. Analysis of polymorphic modifications structure

### 2.6.2.1. Crystal structure analysis from the energetic viewpoint

The crystal structure analysis was performed within the approach based on quantum-chemical calculations of pairwise interaction energies between molecules in a crystal [134, 135]. According to the proposed method, any molecule (simple or monomeric building unit) or strongly bound dimer of molecules (complex or dimeric building unit) may be considered as a basic building unit and its first coordination sphere can be constructed using standard procedure within the Mercury program [136]. This option allows one to determine all molecules (in the case of monomeric BU) or dimers (in the case of dimeric BU) for which the distance between atoms of the basic  $BU_0$  and its symmetrically equivalent  $BU_i$  is shorter than the corresponding van der Waals radii sum plus 1 Å at least for one pair of atoms. Usually, the van der Waals radii proposed by A. Bondi [137] for all the atoms except the hydrogen ones were used [138]. The fragment of a crystal packing containing the basic  $BU_0$  (monomeric or dimeric) and all the  $BU_i$  belonging to its first coordination sphere was divided into dimers  $BU_0$ - $BU_i$  without any change in their geometry. The pairwise interaction energies for  $BU_0$ - $BU_i$  dimers were calculated using B97D3 [139, 140] density functional method with the 3rd version of the empirical correction of dispersion interactions (D3) proposed by Grimme (including Becke-Johnson damping) [141] and Karlsruhe triple zeta valence polarized def2-TZVP basic set [142, 143]. All the energies were corrected for a basis set superposition error by the counterpoise method [144]. The choice of the calculation method was based on the benchmark study of accurate estimation of pairwise interaction energies described in details in [145]. All the single-point calculations were performed within the Gaussian09 software.

The energy vector diagrams (EVD) were used for the visualization of the obtained data [135, 146]. The calculated interaction energy between two building units takes on vector properties if it originates the geometrical center of the basic  $BU_0$  and is directed toward the geometrical center of symmetrically equivalent  $BU_i$ . The use of such an assumption to the calculated pairwise interaction energies between  $BU_0$  and each of the  $BU_i$  belonging to its first coordination sphere makes it possible to visualize the interaction energies in a crystal as a set of such vectors ( $L_i$ ) originated the geometrical center of a basic BU. The length of each energy vector  $L_i$  is calculated using the following equation:

$$L_i = \frac{R_i E_i}{2E_{str}} \quad (2.1)$$

where  $R_i$  is the distance between the geometric centers of the building units in pair,  $E_i$  is the interaction energy between the basic building unit and its  $i^{\text{th}}$  neighbor and  $E_{str}$  is the energy of the strongest interaction between the basic building unit and its neighbor from the first coordination sphere.

Replacing the basic  $BU_0$  with such a vector image and applying all symmetry operations to it result in the visualization of a crystal packing in terms of interaction energies between molecules. This method allows one to define the most strongly bound fragments of a crystal packing such as primary basic structural motif ( $BSM_1$ ) or secondary basic structural motif ( $BSM_2$ ) according to [135].

To understand the driving forces of the polymorphic transition, the contributions of different types of interactions to the total interaction energy in piracetam (Section 4.2) were studied. For this purpose, the modified method of Morokuma and Kitaura [147] namely Localized Molecular Orbital Energy Decomposition Analysis (LMOEDA) [148] implemented in the GAMESS-US

software package [149] was used. The geometry applied during these calculations was chosen identically to the one described above. The calculations were carried out using the B97 method with the 2nd version empirical correction of the dispersion interactions (D2) proposed by Grimme [150] and triple zeta valence polarized TZVP basis set [151, 152] and corrected for basis set superposition error by the counterpoise method. The accuracy of the DFT grid [153] was increased to ultrafine (99 radial shells with 590 Lebedev points in each) similar to that used in the current Gaussian09. Pulay's direct inversion of the iterative subspace (DIIS) interpolation [154, 155] was used in these calculations to increase the convergence speed.

The contribution of the dispersion term (DISP) was separated within this method while the hydrogen bond contribution is approximated as the sum of electrostatic (ES), polarization (POL), and charge transfer terms. These parameters were described as the most appropriate in numerous sources [156-159].

The interaction energies calculated in the GAMESS-US software package were compared with those calculated in the Gaussian09 software package to justify the change of the functional and basis set for LMOEDA calculations.

#### 2.6.2.2. Comparison of experimental and optimized in solid state structures

The metastable polymorphic modification II of ibuprofen was obtained from the Rietveld powder refinement technique and required additional optimization step for further application of its structure in the analysis. However, this action must be justified.

Thereby, the first step to apply the optimization was the comparison of experimental and optimized in solid state structures. The experimental crystalline structure of the polymorphic modification I at ambient pressure was

optimized using the variable cell relaxation (“vc-relax” subroutine) in Quantum Espresso 6.3 software package [160, 161] at the pressures coinciding with the ones studied experimentally in [104] with the maximal deviation of pressure equal  $\pm 0.05$  GPa (or  $+0.05$  GPa for the initial structure obtained at ambient pressure). Projector augmented-wave pseudopotentials (namely H.pbe-kjpaw\_psl.1.0.0.UPF, C.pbe-n-kjpaw\_psl.1.0.0.UPF and O.pbe-n-kjpaw\_psl.1.0.0.UPF) were used in combination with Perdew-Burke-Ernzerhof PBE density functional theory method [162] corrected with the parametrized three-body (D3) dispersion correction (including Becke-Johnson damping). The total energy and force convergence thresholds for ionic minimizations were  $10^{-4}$  and  $10^{-3}$  Ry/atom, respectively. The convergence threshold for self-consistent calculations was set to  $10^{-6}$  Ry/atom. The kinetic energy cutoff for the wavefunctions and for charge density and potential were set to 80 and 640 Ry, respectively, as the ones required for good reproducibility in [163, 164]. Monkhorst-Pack k-point samplings of a  $1 \times 3 \times 2$  grid were applied to check the Brillouin zone with a minimal resolution of  $0.05 \text{ \AA}^{-1}$ . Molecular arrangements in experimental and optimized structures of polymorphic modification I were compared with the corresponding experimental ones in order to understand the applicability of the solid-state optimization for ibuprofen. Besides the lengths of the principal crystallographic axes, the volume of the unit cell, the lengths and angles of hydrogen bonds occurring in crystals were studied. The volume of crystal voids [165] under different pressure was computed using Crystal Explorer 17.5 software [166]. The crystals density after the optimization was calculated with Platon software [167].

The second step, i.e. the optimization of the polymorphic modification II of ibuprofen, was to apply a very similar strategy to the one used for its checking. However, the variable cell relaxation was not applied to prevent any changes in experimentally defined data and according to the comparison, which will be given in Section 4.3.

## 2.7. References for Chapter 2

- (1) McConnell, J.F.; Company, F.Z. Mefenamic acid. *Crystal Structure Communications* **1976**. *5*, 861.
- (2) Lee, E.H.; Byrn, S.R.; Carvajal, M.T. Additive-induced metastable single crystal of mefenamic acid. *Pharmaceutical Research* **2006**. *23* (10), 2375-2380.
- (3) Seethalekshmi, S.; Guru Row, T.N. Conformational polymorphism in a non-steroidal anti-inflammatory drug, mefenamic acid. *Crystal Growth & Design* **2012**. *12* (8), 4283-4289.
- (4) Mague, J.; Ouzidan, Y. CCDC 1585883: Experimental Crystal Structure Determination, **2017**.
- (5) Aguiar, A.J.; Zelmer, J.E. Dissolution behavior of polymorphs of chloramphenicol palmitate and mefenamic acid. *Journal of Pharmaceutical Sciences* **1969**. *58* (8), 983-987.
- (6) Romero, S.; Escalera, B.; Bustamante, P. Solubility behavior of polymorphs I and II of mefenamic acid in solvent mixtures. *International Journal of Pharmaceutics* **1999**. *178* (2), 193-202.
- (7) Shinkuma, D.; Hamaguchi, T.; Yamanaka, Y.; Mizuno, N. Correlation between dissolution rate and bioavailability of different commercial mefenamic acid capsules. *International Journal of Pharmaceutics* **1984**. *21* (2), 187-200.
- (8) Rawashdeh, N.M.; Najib, N.M.; Jalal, I.M. Comparative bioavailability of two capsule formulations of mefenamic acid. *International Journal of Clinical Pharmacology and Therapeutics* **1997**. *35* (8), 329-333.
- (9) Adam, A.; Schrimpl, L.; Schmidt, P.C. Some physicochemical properties of mefenamic acid. *Drug Development and Industrial Pharmacy* **2000**. *26* (5), 477-487.
- (10) Gilpin, R.K.; Zhou, W. Infrared studies of the thermal conversion of mefenamic acid between polymorphic states. *Vibrational Spectroscopy* **2005**. *37* (1), 53-59.
- (11) Gilpin, R.K.; Zhou, W. Infrared studies of the polymorphic states of the fenamates. *Journal of Pharmaceutical and Biomedical Analysis* **2005**. *37* (3), 509-515.
- (12) Bapurao, T.; Ashokraaj, Y.; Panchagnula, R.; Pillai, P. Mefenamic acid: New polymorph or crystal defect? *Pharmaceutical Technology Europe* **2006**. *18* (10).
- (13) Nicholson, C.E.; Cooper, S.J. Crystallization of mefenamic acid from dimethylformamide microemulsions: Obtaining thermodynamic control through 3D nanoconfinement. *Crystals* **2011**. *1* (3), 195-205.
- (14) Abdul Mudalip, S.K.; Abu Bakar, M.R.; Jamal, P.; Adam, F. Solubility and dissolution thermodynamic data of mefenamic acid crystals in different classes of organic solvents. *Journal of Chemical & Engineering Data* **2013**. *58* (12), 3447-3452.
- (15) Abbas, N.; Oswald, I.D.H.; Pulham, C.R. Accessing mefenamic acid form II through high-pressure recrystallisation. *Pharmaceutics* **2017**. *9* (2), 16-27.
- (16) Panchagnula, R.; Sundaramurthy, P.; Pillai, O.; Agrawal, S.; Raj, Y.A. Solid-state characterization of mefenamic acid. *Journal of Pharmaceutical Sciences* **2004**. *93* (4), 1019-1029.
- (17) Abdul Mudalip, S.K.; Abu Bakar, M.R.; Jamal, P.; Adam, F.; Che Man, R., *et al.* Effects of solvents on polymorphism and shape of mefenamic acid crystals. *MATEC Web of Conferences* **2018**. *150*, 02004 (1-6).
- (18) Cesur, S.; Gokbel, S. Crystallization of mefenamic acid and polymorphs. *Crystal Research and Technology* **2008**. *43* (7), 720-728.
- (19) Bodnár, K.; Hudson, S.P.; Rasmuson, Å.C. Stepwise use of additives for improved control over formation and stability of mefenamic acid nanocrystals produced by antisolvent precipitation. *Crystal Growth & Design* **2017**. *17* (2), 454-466.

- (20) Otsuka, M.; Kato, F.; Matsuda, Y. Effect of temperature and kneading solution on polymorphic transformation of mefenamic acid during granulation. *Solid State Ionics* **2004**. *172* (1), 451-453.
- (21) Kato, F.; Otsuka, M.; Matsuda, Y. Kinetic study of the transformation of mefenamic acid polymorphs in various solvents and under high humidity conditions. *International Journal of Pharmaceutics* **2006**. *321* (1), 18-26.
- (22) Dixit, M.; Kini, A.; Kulkarni, P. Enhancing the dissolution of polymorphs I and II of mefenamic acid by spray drying. *Turkish Journal of Pharmaceutical Sciences* **2012**. *9*, 13-26.
- (23) Lowes, M.M.J.; Caira, M.R.; Lötter, A.P.; Van Der Watt, J.G. Physicochemical properties and X-ray structural studies of the trigonal polymorph of carbamazepine. *Journal of Pharmaceutical Sciences* **1987**. *76* (9), 744-752.
- (24) Rustichelli, C.; Gamberini, G.; Ferioli, V.; Gamberini, M.C.; Ficarra, R., *et al.* Solid-state study of polymorphic drugs: Carbamazepine. *Journal of Pharmaceutical and Biomedical Analysis* **2000**. *23* (1), 41-54.
- (25) Lang, M.; Kampf, J.W.; Matzger, A.J. Form IV of carbamazepine. *Journal of Pharmaceutical Sciences* **2002**. *91* (4), 1186-1190.
- (26) Fernandes, P.; Shankland, K.; Florence, A.J.; Shankland, N.; Johnston, A. Solving molecular crystal structures from X-ray powder diffraction data: The challenges posed by  $\gamma$ -carbamazepine and chlorothiazide N,N-dimethylformamide (1/2) solvate. *Journal of Pharmaceutical Sciences* **2007**. *96* (5), 1192-1202.
- (27) Arlin, J.-B.; Price, L.S.; Price, S.L.; Florence, A.J. A strategy for producing predicted polymorphs: Catemeric carbamazepine form V. *Chemical Communications* **2011**. *47* (25), 7074-7076.
- (28) Sovago, I.; Gutmann, M.J.; Senn, H.M.; Thomas, L.H.; Wilson, C.C., *et al.* Electron density, disorder and polymorphism: High-resolution diffraction studies of the highly polymorphic neuralgic drug carbamazepine. *Acta Crystallographica Section B* **2016**. *72* (1), 39-50.
- (29) Grzesiak, A.L.; Lang, M.; Kim, K.; Matzger, A.J. Comparison of the four anhydrous polymorphs of carbamazepine and the crystal structure of form I. *Journal of Pharmaceutical Sciences* **2003**. *92* (11), 2260-2271.
- (30) Li, X.; Ou, X.; Wang, B.; Rong, H.; Wang, B., *et al.* Rich polymorphism in nicotinamide revealed by melt crystallization and crystal structure prediction. *Communications Chemistry* **2020**. *3* (1), 152.
- (31) Shan, N.; Zaworotko, M.J. The role of cocrystals in pharmaceutical science. *Drug Discovery Today* **2008**. *13* (9), 440-446.
- (32) Aakeröy, C.B.; Forbes, S.; Desper, J. Using cocrystals to systematically modulate aqueous solubility and melting behavior of an anticancer drug. *Journal of the American Chemical Society* **2009**. *131* (47), 17048-17049.
- (33) Smith, A.J.; Kavuru, P.; Wojtas, L.; Zaworotko, M.J.; Shytle, R.D. Cocrystals of quercetin with improved solubility and oral bioavailability. *Molecular Pharmaceutics* **2011**. *8* (5), 1867-1876.
- (34) Vemavarapu, C.; Mollan, M.J.; Needham, T.E. Crystal doping aided by rapid expansion of supercritical solutions. *AAPS PharmSciTech* **2002**. *3* (4), 17.
- (35) Padrela, L.; Rodrigues, M.A.; Velaga, S.P.; Matos, H.A.; de Azevedo, E.G. Formation of indomethacin-saccharin cocrystals using supercritical fluid technology. *European Journal of Pharmaceutical Sciences* **2009**. *38* (1), 9-17.
- (36) Vemavarapu, C.; Mollan, M.J.; Needham, T.E. Coprecipitation of pharmaceutical actives and their structurally related additives by the res process. *Powder Technology* **2009**. *189* (3), 444-453.

- (37) Shikhar, A.; Bommana, M.M.; Gupta, S.S.; Squillante, E. Formulation development of carbamazepine–nicotinamide co-crystals complexed with  $\gamma$ -cyclodextrin using supercritical fluid process. *The Journal of Supercritical Fluids* **2011**. *55* (3), 1070-1078.
- (38) Ober, C.A.; Gupta, R.B. Formation of itraconazole–succinic acid cocrystals by gas antisolvent cocrystallization. *AAPS PharmSciTech* **2012**. *13* (4), 1396-1406.
- (39) Ober, C.A.; Montgomery, S.E.; Gupta, R.B. Formation of itraconazole/L-malic acid cocrystals by gas antisolvent cocrystallization. *Powder Technology* **2013**. *236*, 122-131.
- (40) Tiago, J.M.; Padrela, L.; Rodrigues, M.A.; Matos, H.A.; Almeida, A.J., *et al.* Single-step co-crystallization and lipid dispersion by supercritical enhanced atomization. *Crystal Growth & Design* **2013**. *13* (11), 4940-4947.
- (41) Padrela, L.; Rodrigues, M.A.; Tiago, J.; Velaga, S.P.; Matos, H.A., *et al.* Tuning physicochemical properties of theophylline by cocrystallization using the supercritical fluid enhanced atomization technique. *The Journal of Supercritical Fluids* **2014**. *86*, 129-136.
- (42) Erriguible, A.; Neurohr, C.; Revelli, A.L.; Laugier, S.; Fevotte, G., *et al.* Cocrystallization induced by compressed CO<sub>2</sub> as antisolvent: Simulation of a batch process for the estimation of nucleation and growth parameters. *The Journal of Supercritical Fluids* **2015**. *98*, 194-203.
- (43) Müllers, K.C.; Paisana, M.; Wahl, M.A. Simultaneous formation and micronization of pharmaceutical cocrystals by rapid expansion of supercritical solutions (RESS). *Pharmaceutical Research* **2015**. *32* (2), 702-713.
- (44) Padrela, L.; Rodrigues, M.A.; Tiago, J.; Velaga, S.P.; Matos, H.A., *et al.* Insight into the mechanisms of cocrystallization of pharmaceuticals in supercritical solvents. *Crystal Growth & Design* **2015**. *15* (7), 3175-3181.
- (45) Cuadra, I.A.; Cabañas, A.; Cheda, J.a.R.; Martínez-Casado, F.J.; Pando, C. Pharmaceutical co-crystals of the anti-inflammatory drug diflunisal and nicotinamide obtained using supercritical CO<sub>2</sub> as an antisolvent. *Journal of CO<sub>2</sub> Utilization* **2016**. *13*, 29-37.
- (46) Hiendrawan, S.; Veriansyah, B.; Widjojokusumo, E.; Soewandhi, S.; Wikarsa, S., *et al.* Simultaneous cocrystallization and micronization of paracetamol-dipicolinic acid cocrystal by supercritical antisolvent (SAS). *International Journal of Pharmacy and Pharmaceutical Sciences* **2016**. *8* (2), 89-98.
- (47) Neurohr, C.; Erriguible, A.; Laugier, S.; Subra-Paternault, P. Challenge of the supercritical antisolvent technique SAS to prepare cocrystal-pure powders of naproxen-nicotinamide. *Chemical Engineering Journal* **2016**. *303*, 238-251.
- (48) Pando, C.; Cabañas, A.; Cuadra, I.A. Preparation of pharmaceutical co-crystals through sustainable processes using supercritical carbon dioxide: A review. *RSC Advances* **2016**. *6* (75), 71134-71150.
- (49) Cuadra, I.A.; Cabañas, A.; Cheda, J.A.R.; Pando, C. Polymorphism in the co-crystallization of the anticonvulsant drug carbamazepine and saccharin using supercritical CO<sub>2</sub> as an anti-solvent. *The Journal of Supercritical Fluids* **2018**. *136*, 60-69.
- (50) Padrela, L.; Rodrigues, M.A.; Duarte, A.; Dias, A.M.A.; Braga, M.E.M., *et al.* Supercritical carbon dioxide-based technologies for the production of drug nanoparticles/nanocrystals – a comprehensive review. *Advanced Drug Delivery Reviews* **2018**. *131*, 22-78.
- (51) Wichianphong, N.; Charoenchaitrakool, M. Statistical optimization for production of mefenamic acid–nicotinamide cocrystals using gas anti-solvent (GAS) process. *Journal of Industrial and Engineering Chemistry* **2018**. *62*, 375-382.
- (52) Cuadra, I.A.; Cabañas, A.; Cheda, J.a.R.; Türk, M.; Pando, C. Cocrystallization of the anticancer drug 5-fluorouracil and cofomers urea, thiourea or pyrazinamide using

- supercritical CO<sub>2</sub> as an antisolvent (SAS) and as a solvent (CSS). *The Journal of Supercritical Fluids* **2020**. *160*, 104813 (1-12).
- (53) Maceachern, L.; Kermanshahi-Pour, A.; Mirmehrabi, M. Supercritical carbon dioxide for pharmaceutical co-crystal production. *Crystal Growth & Design* **2020**. *20* (9), 6226-6244.
- (54) Brittain, H.G., *Polymorphism in pharmaceutical solids*; 2<sup>nd</sup> Ed.; Informa: New York, 2009; 640 p.
- (55) Duarte, Í.; Andrade, R.; Pinto, J.F.; Temtem, M. Green production of cocrystals using a new solvent-free approach by spray congealing. *International Journal of Pharmaceutics* **2016**. *506* (1), 68-78.
- (56) Uchida, H.; Manaka, A.; Matsuoka, M.; Takiyama, H. Growth phenomena of single crystals of naphthalene in supercritical carbon dioxide. *Crystal Growth & Design* **2004**. *4* (5), 937-942.
- (57) Llinàs, A.; Goodman, J.M. Polymorph control: Past, present and future. *Drug Discovery Today* **2008**. *13* (5), 198-210.
- (58) Stolar, T.; Lukin, S.; Tireli, M.; Sović, I.; Karadeniz, B., *et al.* Control of pharmaceutical cocrystal polymorphism on various scales by mechanochemistry: Transfer from the laboratory batch to the large-scale extrusion processing. *ACS Sustainable Chemistry & Engineering* **2019**. *7* (7), 7102-7110.
- (59) Sarve, A.; George, J.; Agrawal, S.; Jasra, R.V.; Munshi, P. Unidirectional growth of organic single crystals of naphthalene, anthracene and pyrene by isothermal expansion of supercritical CO<sub>2</sub>. *RSC Advances* **2020**. *10* (38), 22480-22486.
- (60) Thompson, J.M.T.; Tremayne, M. The impact of powder diffraction on the structural characterization of organic crystalline materials. *Philosophical Transactions of the Royal Society of London. Series A: Mathematical, Physical and Engineering Sciences* **2004**. *362* (1825), 2691-2707.
- (61) Harris, K.D.M.; Williams, P.A.: Structure determination of organic molecular solids from powder x-ray diffraction data: Current opportunities and state of the art. In *Advances in organic crystal chemistry: Comprehensive reviews 2015*; Tamura, R., Miyata, M. Eds.; Springer Japan: Tokyo, 2015, pp. 141-166.
- (62) Przybyłek, M.; Ziółkowska, D.; Mroczyńska, K.; Cysewski, P. Propensity of salicylamide and ethenzamide cocrystallization with aromatic carboxylic acids. *European Journal of Pharmaceutical Sciences* **2016**. *85*, 132-140.
- (63) Ribas, M.M.; Sakata, G.S.B.; Santos, A.E.; Dal Magro, C.; Aguiar, G.P.S., *et al.* Curcumin cocrystals using supercritical fluid technology. *The Journal of Supercritical Fluids* **2019**. *152*, 104564 (1-7).
- (64) Raveendran, P.; Blatchford, M.A.; Hurrey, M.L.; White, P.S.; Wallen, S.L. Crystallization and processing of carbohydrates using carbon dioxide. *Green Chemistry* **2005**. *7* (3), 129-131.
- (65) Utami, D.; Nugrahani, I.; Ibrahim, S. Formation and characterization of mefenamic acid-nicotinamide cocrystal during co-milling based on X-ray powder diffraction analysis. *Journal of Applied Pharmaceutical Science* **2016**. *6*, 075-081.
- (66) Utami, D.; Nugrahani, I.; Ibrahim, S. Mefenamic acid-nicotinamide co-crystal synthesized by using melt crystallization method and its solubility study. *Asian Journal of Pharmaceutical and Clinical Research* **2017**. *10* (5), 135-139.
- (67) Greenhalgh, D.J.; Williams, A.C.; Timmins, P.; York, P. Solubility parameters as predictors of miscibility in solid dispersions. *Journal of Pharmaceutical Sciences* **1999**. *88* (11), 1182-1190.
- (68) Yalkowsky, S.H.; Dannenfelser, R.M., *Aquasol database of aqueous solubility*; 5<sup>th</sup> Ed.; College of Pharmacy, University of Arizona: Tucson, 1992.

- (69) Van Arnum, S.D.: Niacin, nicotinamide, and nicotinic acid. In *Kirk-othmer encyclopedia of chemical technology*; Kirk, R.E., Othmer, D.F. Eds.; John Wiley & Sons, Inc.: New York, 2000, pp. 83-99.
- (70) Kotnik, P.; Škerget, M.; Knez, Ž. Solubility of nicotinic acid and nicotinamide in carbon dioxide at T = (313.15 to 373.15) K and P = (5 to 30) MPa: Experimental data and correlation. *Journal of Chemical & Engineering Data* **2011**. *56* (2), 338-343.
- (71) Zeinolabedini Hezave, A.; Khademi, M.H.; Esmaeilzadeh, F. Measurement and modeling of mefenamic acid solubility in supercritical carbon dioxide. *Fluid Phase Equilibria* **2012**. *313*, 140-147.
- (72) Li, J.; Bourne, S.A.; Caira, M.R. New polymorphs of isonicotinamide and nicotinamide. *Chemical Communications* **2011**. *47* (5), 1530-1532.
- (73) Tawashi, R. Aspirin: Dissolution rates of two polymorphic forms. *Science* **1968**. *160* (3823), 76.
- (74) Kildsig, D.O.; Denbo, R.; Peck, G.E. Structural differences in solutions derived from polymorphic modifications of aspirin. *Journal of Pharmacy and Pharmacology* **1971**. *23* (5), 374-376.
- (75) Mitchell, A.G.; Milaire, B.L.; Saville, D.J.; Griffiths, R.V. Aspirin dissolution: Polymorphism, crystal habit or crystal defects. *Journal of Pharmacy and Pharmacology* **1971**. *23* (7), 534-535.
- (76) Mulley, B.A.; Rye, R.M.; Shaw, P. Further evidence on the question of polymorphism in aspirin. *Journal of Pharmacy and Pharmacology* **1971**. *23* (11), 902-904.
- (77) Schwartzman, G. Does aspirin exist in polymorphic states? *Journal of Pharmacy and Pharmacology* **1972**. *24* (2), 169-170.
- (78) Watanabe, A.; Yamaoka, Y.; Takada, K. Crystal habits and dissolution behavior of aspirin. *Chemical and Pharmaceutical Bulletin* **1982**. *30* (8), 2958-2963.
- (79) Vishweshwar, P.; McMahon, J.A.; Oliveira, M.; Peterson, M.L.; Zaworotko, M.J. The predictably elusive form II of aspirin. *Journal of the American Chemical Society* **2005**. *127* (48), 16802-16803.
- (80) Bond, A.D.; Boese, R.; Desiraju, G.R. On the polymorphism of aspirin: Crystalline aspirin as intergrowths of two "polymorphic" domains. *Angewandte Chemie International Edition* **2007**. *46* (4), 618-622.
- (81) Bond, A.D.; Boese, R.; Desiraju, G.R. On the polymorphism of aspirin. *Angewandte Chemie International Edition* **2007**. *46* (4), 615-617.
- (82) Bond, A.D.; Solanko, K.A.; Parsons, S.; Redder, S.; Boese, R. Single crystals of aspirin form II: Crystallisation and stability. *CrystEngComm* **2011**. *13* (2), 399-401.
- (83) Bauer, J.D.; Haussühl, E.; Winkler, B.; Arbeck, D.; Milman, V., *et al.* Elastic properties, thermal expansion, and polymorphism of acetylsalicylic acid. *Crystal Growth & Design* **2010**. *10* (7), 3132-3140.
- (84) Olusanmi, D.; Roberts, K.J.; Ghadiri, M.; Ding, Y. The breakage behaviour of aspirin under quasi-static indentation and single particle impact loading: Effect of crystallographic anisotropy. *International Journal of Pharmaceutics* **2011**. *411* (1), 49-63.
- (85) Varughese, S.; Kiran, M.S.R.N.; Solanko, K.A.; Bond, A.D.; Ramamurty, U., *et al.* Interaction anisotropy and shear instability of aspirin polymorphs established by nanoindentation. *Chemical Science* **2011**. *2* (11), 2236-2242.
- (86) Crowell, E.L.; Dreger, Z.A.; Gupta, Y.M. High-pressure polymorphism of acetylsalicylic acid (aspirin): Raman spectroscopy. *Journal of Molecular Structure* **2015**. *1082*, 29-37.
- (87) Mittal, A.; Malhotra, D.; Jain, P.; Kalia, A.; Shunmugaperumal, T. Studies on aspirin crystals generated by a modified vapor diffusion method. *AAPS PharmSciTech* **2016**. *17* (4), 988-994.

- (88) Wen, S.; Beran, G.J.O. Accidental degeneracy in crystalline aspirin: New insights from high-level ab initio calculations. *Crystal Growth & Design* **2012**. *12* (5), 2169-2172.
- (89) Reilly, A.M.; Tkatchenko, A. Role of dispersion interactions in the polymorphism and entropic stabilization of the aspirin crystal. *Physical Review Letters* **2014**. *113* (5), 055701 (1-5).
- (90) Adhikari, K.; Flurchick, K.M.; Valenzano, L. A hybrid density functional study on the effects of pressure on paracetamol and aspirin polymorphs. *Computational and Theoretical Chemistry* **2015**. *1062*, 90-98.
- (91) Leblanc, L.M.; Otero-de-la-Roza, A.; Johnson, E.R. Evaluation of shear-slip transitions in crystalline aspirin by density-functional theory. *Crystal Growth & Design* **2016**. *16* (12), 6867-6873.
- (92) Shtukenberg, A.G.; Hu, C.T.; Zhu, Q.; Schmidt, M.U.; Xu, W., *et al.* The third ambient aspirin polymorph. *Crystal Growth & Design* **2017**. *17* (6), 3562-3566.
- (93) Fabbiani, F.P.A.; Allan, D.R.; Parsons, S.; Pulham, C.R. An exploration of the polymorphism of paracetamol using high pressure. *CrystEngComm* **2005**. *7* (29), 179-186.
- (94) Fabbiani, F.P.A.; Allan, D.R.; David, W.I.F.; Davidson, A.J.; Lennie, A.R., *et al.* High-pressure studies of pharmaceuticals: An exploration of the behavior of paracetamol. *Crystal Growth & Design* **2007**. *7* (6), 1115-1124.
- (95) European Medicines Agency, Ibuprofen product-specific bioequivalence guidance, 2018, [Online] <https://www.ema.europa.eu/en/ibuprofen-product-specific-bioequivalence-guidance>
- (96) Manrique, J.; Martínez, F. Solubility of ibuprofen in some ethanol + water cosolvent mixtures at several temperatures. *Latin American Journal of Pharmacy* **2007**. *26*, 344-354.
- (97) Brás, A.R.; Noronha, J.P.; Antunes, A.M.M.; Cardoso, M.M.; Schönhals, A., *et al.* Molecular motions in amorphous ibuprofen as studied by broadband dielectric spectroscopy. *The Journal of Physical Chemistry B* **2008**. *112* (35), 11087-11099.
- (98) Derollez, P.; Dudognon, E.; Affouard, F.; Danede, F.; Correia, N.T., *et al.* Ab initio structure determination of phase II of racemic ibuprofen by X-ray powder diffraction. *Acta Crystallographica Section B* **2010**. *66* (1), 76-80.
- (99) Gavrilin, M.; Fat'yanova, E.; Lukashova, L.; Kompantseva, E.; Ziep, C. Effect of crystallization conditions on the solubility of ibuprofen. *Pharmaceutical Chemistry Journal* **2000**. *34*, 555-557.
- (100) Rasenack, N.; Müller, B.W. Properties of ibuprofen crystallized under various conditions: A comparative study. *Drug Development and Industrial Pharmacy* **2002**. *28* (9), 1077-1089.
- (101) Nokhodchi, A.; Amire, O.; Jelvehgari, M. Physico-mechanical and dissolution behaviours of ibuprofen crystals crystallized in the presence of various additives. *Daru : Journal of Faculty of Pharmacy, Tehran University of Medical Sciences* **2010**. *18* (2), 74-83.
- (102) Williams, P.A.; Hughes, C.E.; Harris, K.D.M. New insights into the preparation of the low-melting polymorph of racemic ibuprofen. *Crystal Growth & Design* **2012**. *12* (12), 5839-5845.
- (103) Lee, S.Y.; Yu, G.; Kim, I.W. Effects of polymeric additives on the crystallization and release behavior of amorphous ibuprofen. *Journal of Nanomaterials* **2013**. *2013*, 503069 (1-7).
- (104) Ostrowska, K.; Kropidłowska, M.; Katrusiak, A. High-pressure crystallization and structural transformations in compressed R,S-ibuprofen. *Crystal Growth & Design* **2015**. *15* (3), 1512-1517.
- (105) Malfait, B.; Correia, N.T.; Ciotonea, C.; Dhainaut, J.; Dacquin, J.-P., *et al.* Manipulating the physical states of confined ibuprofen in SBA-15 based drug delivery

- systems obtained by solid-state loading: Impact of the loading degree. *The Journal of Chemical Physics* **2020**. 153, 154506 (1-14).
- (106) Admiraal, G.; Eikelenboom, J.C.; Vos, A. Structures of the triclinic and monoclinic modifications of (2-oxo-1-pyrrolidiny)acetamide. *Acta Crystallographica Section B* **1982**. 38 (10), 2600-2605.
- (107) Groom, C.R.; Bruno, I.J.; Lightfoot, M.P.; Ward, S.C. The cambridge structural database. *Acta Crystallographica Section B* **2016**. 72 (2), 171-179.
- (108) Zhao, Y.; Yuan, J.; Ji, Z.; Wang, J.; Rohani, S. Combined application of in situ FBRM, ATR-FTIR, and Raman on polymorphism transformation monitoring during the cooling crystallization. *Industrial & Engineering Chemistry Research* **2012**. 51 (38), 12530-12536.
- (109) Tiernan, H.; Byrne, B.; Kazarian, S.G. ATR-FTIR spectroscopy and spectroscopic imaging for the analysis of biopharmaceuticals. *Spectrochimica Acta Part A: Molecular and Biomolecular Spectroscopy* **2020**. 241, 118636 (1-11).
- (110) Kitamura, M. Strategy for control of crystallization of polymorphs. *CrystEngComm* **2009**. 11 (6), 949-964.
- (111) Oparin, R.D.; Idrissi, A.; Fedorov, M.V.; Kiselev, M.G. Dynamic and static characteristics of drug dissolution in supercritical CO<sub>2</sub> by infrared spectroscopy: Measurements of acetaminophen solubility in a wide range of state parameters. *Journal of Chemical & Engineering Data* **2014**. 59 (11), 3517-3523.
- (112) Oparin, R.D.; Ivlev, D.V.; Vorobei, A.M.; Idrissi, A.; Kiselev, M.G. Screening of conformational polymorphism of ibuprofen in supercritical CO<sub>2</sub>. *Journal of Molecular Liquids* **2017**. 239, 49-60.
- (113) Grignard, B.; Gilbert, B.; Malherbe, C.; Jérôme, C.; Detrembleur, C. Online monitoring of heterogeneous polymerizations in supercritical carbon dioxide by Raman spectroscopy. *ChemPhysChem* **2012**. 13 (11), 2666-2670.
- (114) Bruzzoni, P.; Carranza, R.M.; Collet Lacoste, J.R.; Crespo, E.A. Kramers–Kronig transforms calculation with a fast convolution algorithm. *Electrochimica Acta* **2002**. 48 (4), 341-347.
- (115) Larkin, P.: Chapter 3 - instrumentation and sampling methods. In *Infrared and Raman spectroscopy*; Larkin, P. Ed.; Elsevier: Oxford, 2011, pp. 27-54.
- (116) Kubelka, P.; Munk, F. Ein Beitrag zur Optik der Farbanstriche. *Zeitschrift für Technische Physik* **1931**. 12, 593-601.
- (117) Cialla-May, D.; Schmitt, M.; Popp, J. Theoretical principles of Raman spectroscopy. *Physical Sciences Reviews* **2019**. 4 (6).
- (118) Bruker, SAINT, Bruker AXS Inc., Madison, Wisconsin, USA, **2014**
- (119) Bruker, SADABS, Bruker AXS Inc., Madison, Wisconsin, USA, **2014**.
- (120) Sheldrick, G. SHELXT - integrated space-group and crystal-structure determination. *Acta Crystallographica Section A* **2015**. 71 (1), 3-8.
- (121) Sheldrick, G. Crystal structure refinement with SHELXL. *Acta Crystallographica Section C* **2015**. 71 (1), 3-8.
- (122) Dolomanov, O.V.; Bourhis, L.J.; Gildea, R.J.; Howard, J.a.K.; Puschmann, H. Olex2: A complete structure solution, refinement and analysis program. *Journal of Applied Crystallography* **2009**. 42 (2), 339-341.
- (123) Fábíán, L.; Hamill, N.; Eccles, K.S.; Moynihan, H.A.; Maguire, A.R., *et al.* Cocrystals of fenamic acids with nicotinamide. *Crystal Growth & Design* **2011**. 11 (8), 3522-3528.
- (124) H. Putz, K. Brandenburg, Match! - Phase Identification from Powder Diffraction, Crystal Impact, GbR Kreuzherrenstr, Bonn, Germany, **2019**.
- (125) Frisch, M.J.; Trucks, G.W.; Schlegel, H.B.; Scuseria, G.E.; Robb, M.A., *et al.*, *Gaussian 09, Revision D.09*. **2016**, Gaussian, Inc.: Wallingford CT.

- (126) Becke, A.D. Density-functional exchange-energy approximation with correct asymptotic behavior. *Physical Review A* **1988**. *38* (6), 3098-3100.
- (127) Austin, A.; Petersson, G.A.; Frisch, M.J.; Dobek, F.J.; Scalmani, G., *et al.* A density functional with spherical atom dispersion terms. *Journal of Chemical Theory and Computation* **2012**. *8* (12), 4989-5007.
- (128) Wachters, A.J.H. Gaussian basis set for molecular wavefunctions containing third-row atoms. *The Journal of Chemical Physics* **1970**. *52* (3), 1033-1036.
- (129) Hay, P.J. Gaussian basis sets for molecular calculations. The representation of 3D orbitals in transition-metal atoms. *The Journal of Chemical Physics* **1977**. *66* (10), 4377-4384.
- (130) Raghavachari, K.; Trucks, G.W. Highly correlated systems. Excitation energies of first row transition metals Sc–Cu. *The Journal of Chemical Physics* **1989**. *91* (2), 1062-1065.
- (131) Stewart, J.J.P. Optimization of parameters for semiempirical methods II. Applications. *Journal of Computational Chemistry* **1989**. *10* (2), 221-264.
- (132) Stewart, J.J.P. Optimization of parameters for semiempirical methods I. Method. *Journal of Computational Chemistry* **1989**. *10* (2), 209-220.
- (133) Oparin, R.D.; Kurskaya, M.V.; Krestyaninov, M.A.; Idrissi, A.; Kiselev, M.G. Correlation between the conformational crossover of carbamazepine and its polymorphic transition in supercritical CO<sub>2</sub>: On the way to polymorph control. *European Journal of Pharmaceutical Sciences* **2020**. *146*, 105273 (1-8).
- (134) Konovalova, I.S.; Shishkina, S.V.; Paponov, B.V.; Shishkin, O.V. Analysis of the crystal structure of two polymorphic modifications of 3,4-diamino-1,2,4-triazole based on the energy of the intermolecular interactions. *CrystEngComm* **2010**. *12* (3), 909-916.
- (135) Shishkin, O.V.; Dyakonov, V.V.; Maleev, A.V. Supramolecular architecture of crystals of fused hydrocarbons based on topology of intermolecular interactions. *CrystEngComm* **2012**. *14* (5), 1795-1804.
- (136) Macrae, C.F.; Sovago, I.; Cottrell, S.J.; Galek, P.T.A.; McCabe, P., *et al.* Mercury 4.0: From visualization to analysis, design and prediction. *Journal of Applied Crystallography* **2020**. *53* (1), 226-235.
- (137) Bondi, A. Van der Waals volumes and radii. *The Journal of Physical Chemistry* **1964**. *68* (3), 441-451.
- (138) Rowland, R.S.; Taylor, R. Intermolecular nonbonded contact distances in organic crystal structures: Comparison with distances expected from van der Waals radii. *The Journal of Physical Chemistry* **1996**. *100* (18), 7384-7391.
- (139) Becke, A.D. Density-functional thermochemistry. V. Systematic optimization of exchange-correlation functionals. *The Journal of Chemical Physics* **1997**. *107* (20), 8554-8560.
- (140) Schmider, H.L.; Becke, A.D. Optimized density functionals from the extended G2 test set. *The Journal of Chemical Physics* **1998**. *108* (23), 9624-9631.
- (141) Grimme, S.; Ehrlich, S.; Goerigk, L. Effect of the damping function in dispersion corrected density functional theory. *Journal of Computational Chemistry* **2011**. *32* (7), 1456-1465.
- (142) Weigend, F.; Ahlrichs, R. Balanced basis sets of split valence, triple zeta valence and quadruple zeta valence quality for H to Rn: Design and assessment of accuracy. *Physical Chemistry Chemical Physics* **2005**. *7* (18), 3297-3305.
- (143) Weigend, F. Accurate Coulomb-fitting basis sets for H to Rn. *Physical Chemistry Chemical Physics* **2006**. *8* (9), 1057-1065.
- (144) Boys, S.F.; Bernardi, F. The calculation of small molecular interactions by the differences of separate total energies. Some procedures with reduced errors. *Molecular Physics* **1970**. *19* (4), 553-566.

- (145) Shishkina, S.V. Using of quantum-chemical calculations to molecular crystals studying. *Structural Chemistry* **2019**. *30* (5), 1565-1577.
- (146) Shishkin, O.V.; Zubatyuk, R.I.; Maleev, A.V.; Boese, R. Investigation of topology of intermolecular interactions in the benzene–acetylene co-crystal by different theoretical methods. *Structural Chemistry* **2014**. *25* (5), 1547-1552.
- (147) Kitaura, K.; Morokuma, K. A new energy decomposition scheme for molecular interactions within the hartree-fock approximation. *International Journal of Quantum Chemistry* **1976**. *10* (2), 325-340.
- (148) Su, P.; Li, H. Energy decomposition analysis of covalent bonds and intermolecular interactions. *The Journal of Chemical Physics* **2009**. *131* (1), 014102 (1-16).
- (149) Schmidt, M.W.; Baldridge, K.K.; Boatz, J.A.; Elbert, S.T.; Gordon, M.S., *et al.* General atomic and molecular electronic structure system. *Journal of Computational Chemistry* **1993**. *14* (11), 1347-1363.
- (150) Grimme, S. Semiempirical GGA-type density functional constructed with a long-range dispersion correction. *Journal of Computational Chemistry* **2006**. *27* (15), 1787-1799.
- (151) Schäfer, A.; Horn, H.; Ahlrichs, R. Fully optimized contracted gaussian basis sets for atoms Li to Kr. *The Journal of Chemical Physics* **1992**. *97* (4), 2571-2577.
- (152) Schäfer, A.; Huber, C.; Ahlrichs, R. Fully optimized contracted gaussian basis sets of triple zeta valence quality for atoms Li to Kr. *The Journal of Chemical Physics* **1994**. *100* (8), 5829-5835.
- (153) Lebedev, V.I.; Laikov, D.N. A quadrature formula for the sphere of the 131st algebraic order of accuracy. *Doklady Mathematics* **1999**. *59* (3), 477-481.
- (154) Pulay, P. Convergence acceleration of iterative sequences. The case of scf iteration. *Chemical Physics Letters* **1980**. *73* (2), 393-398.
- (155) Pulay, P. Improved scf convergence acceleration. *Journal of Computational Chemistry* **1982**. *3* (4), 556-560.
- (156) Morokuma, K.; Kitaura, K.: Energy decomposition analysis of molecular interactions. In *Chemical applications of atomic and molecular electrostatic potentials: Reactivity, structure, scattering, and energetics of organic, inorganic, and biological systems*; Politzer, P., Truhlar, D.G. Eds.; Springer US: Boston, MA, 1981, pp. 215-242.
- (157) Thellamurege, N.; Hirao, H. Water complexes of cytochrome P450: Insights from energy decomposition analysis. *Molecules* **2013**. *18* (6), 6782-6791.
- (158) Liu, M.-X.; Zhuo, H.-Y.; Li, Q.-Z.; Li, W.-Z.; Cheng, J.-B. Theoretical study of the cooperative effects between the triel bond and the pnictogen bond in  $\text{BF}_3 \cdots \text{NCXH}_2 \cdots \text{Y}$  ( $\text{X} = \text{P, As, Sb}$ ;  $\text{Y} = \text{H}_2\text{O, NH}_3$ ) complexes. *Journal of Molecular Modeling* **2015**. *22* (1), 10 (1-7).
- (159) Alkorta, I.; Mata, I.; Molins, E.; Espinosa, E. Charged versus neutral hydrogen-bonded complexes: Is there a difference in the nature of the hydrogen bonds? *Chemistry – A European Journal* **2016**. *22* (27), 9226-9234.
- (160) Giannozzi, P.; Baroni, S.; Bonini, N.; Calandra, M.; Car, R., *et al.* Quantum ESPRESSO: A modular and open-source software project for quantum simulations of materials. *Journal of Physics: Condensed Matter* **2009**. *21* (39), 395502 (1-20).
- (161) Giannozzi, P.; Andreussi, O.; Brumme, T.; Bunau, O.; Buongiorno Nardelli, M., *et al.* Advanced capabilities for materials modelling with Quantum ESPRESSO. *Journal of Physics: Condensed Matter* **2017**. *29*, 465901 (1-31).
- (162) Perdew, J.P.; Burke, K.; Ernzerhof, M. Generalized gradient approximation made simple. *Physical Review Letters* **1996**. *77* (18), 3865-3868.
- (163) Lejaeghere, K.; Bihlmayer, G.; Björkman, T.; Blaha, P.; Blügel, S., *et al.* Reproducibility in density functional theory calculations of solids. *Science* **2016**. *351* (6280), aad3000 (1-7).

- (164) Prandini, G.; Marrazzo, A.; Castelli, I.E.; Mounet, N.; Marzari, N. Precision and efficiency in solid-state pseudopotential calculations. *npj Computational Materials* **2018**. *4* (1), 72 (1-13).
- (165) Turner, M.J.; Mckinnon, J.J.; Jayatilaka, D.; Spackman, M.A. Visualisation and characterisation of voids in crystalline materials. *CrystEngComm* **2011**. *13* (6), 1804-1813.
- (166) Turner, M.J.; McKinnon, J.J.; Wolff, S.K.; Grimwood, D.J.; Spackman, P.R., *et al.* *CrystalExplorer17*. 2017, University of Western Australia: University of Western Australia.
- (167) Spek, A. Structure validation in chemical crystallography. *Acta Crystallographica Section D* **2009**. *65* (2), 148-155.

# Chapter 3. Control of the polymorphism of active pharmaceutical ingredients crystallizing from supercritical CO<sub>2</sub>

*The material presented in this chapter forms the basis of publications*

Oparin, R. D.; Vaksler, Ye. A.; Krestyaninov, M. A.; Idrissi, A.; Shishkina, S. V.; Kiselev, M.G. Polymorphism and conformations of mefenamic acid in supercritical carbon dioxide. **J. Supercrit. Fluids** 2019, 152, 104547 (1-15).

Oparin, R. D.; Vaksler, Ye. A.; Krestyaninov, M. A.; Idrissi, A.; Kiselev, M.G. High temperature polymorphic conversion of carbamazepine in supercritical CO<sub>2</sub>: A way to obtain pure polymorph I. **J. Mol. Liq.** 2021, 323, 114630 (1-10).

Vaksler, Ye. A.; Benedis, D.; Dyshin, A. A.; Oparin, R. D.; Correia, N. T.; Capet F.; Shishkina, S. V.; Kiselev, M.G.; Idrissi, A. Spectroscopic characterization of single co-crystal of mefenamic acid and nicotinamide using supercritical CO<sub>2</sub>. **J. Mol. Liq.** 2021, 334, 116117 (1-7).

Control over the crystallization and its products is the key prerequisite in obtaining the pure polymorphic modifications of the APIs. We propose the methods based on recrystallization from scCO<sub>2</sub>. They are usually associated with fast and uncontrolled crystal formation, but the techniques proposed in this chapter allowed us to obtain forcefully the required polymorphic modifications. We divide the process of recrystallization into pre-expansion and expansion stages, as well as the stage of product analysis and make a detailed assessment of the possibility of simplifying the control over the production of pure polymorphic forms. We give suggestions on the monitoring of conformations and the interfaces of the APIs (MFA and CBZ) with the solution in scCO<sub>2</sub> during the pre-expansion stage, as well as on the equilibria between phases during the recrystallization. Different approaches to the control of the product after crystallization are shown for the selected APIs. As well as a new way to easily obtain the crystal structure through single-crystal X-ray diffraction and, as a consequence, the reference spectra and powder patterns of individual polymorphic modifications demonstrated for MFA:NA co-crystal.

### **3.1. Polymorphism and conformations of mefenamic acid in supercritical carbon dioxide**

#### 3.1.1. Recrystallization of mefenamic acid through sublimation

The sublimation of MFA at different temperatures was studied specially to obtain the reference patterns of API pure polymorphic forms and to compare with the ones proved by X-ray diffraction experiment, as well as to choose the spectral domains for unambiguous determination of the polymorphic modifications. To do this we continuously measured the Raman spectra of single crystals of MFA that were placed in temperature-controlled plate of Linkam system. These measurements were fulfilled in fast mode when the acquisition time was 5 sec and only one orientation of the grating was used. The wavenumber range of 1300-1360  $\text{cm}^{-1}$  was used as analytical. Indeed, in the case of polymorph I (PI) it contains one spectral contribution whereas for polymorph II (PII) two spectral contributions are observed (Figure 3.1). This figure also shows the differences between Raman spectra of a single crystal of the MFA initial form and a single crystal of the obtained MFA polymorph II in two spectral domains (50-1800  $\text{cm}^{-1}$  and 2700-3600  $\text{cm}^{-1}$ ).

We have found that the sublimation of polymorph I into polymorph II begins at a temperature slightly above 160°C. However, the rate of this process is slow and depends on the crystal size. Though the transition of small crystals occurs faster, nevertheless it may take hours. Finally, we have found that the fast phase transition occurs in the temperature range of 180-190°C. In this temperature range irrespective of crystal size the sublimation of polymorphic form II from I takes minutes. This fact is in good agreement with the results of [1], where the authors showed that starting from the temperature of 150°C, the sublimation of MFA from polymorph I into polymorph II is observed, but the dynamics of this process is extremely slow. Nevertheless, these authors did not

succeed in achieving the full transformation of the sample to polymorphic form II at this temperature even after 140 hours, and the full recrystallization of the polymorphic modification II was reached by us only at 160°C, after 35 hours.

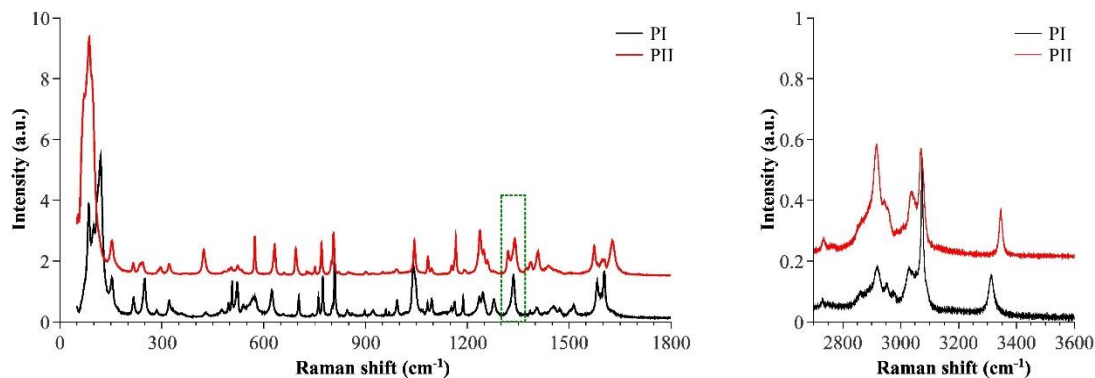


Figure 3.1. Comparison of Raman spectra of single crystals of mefenamic acid polymorph I and polymorph II in two spectral domains of 50-1800  $\text{cm}^{-1}$  and 2700-3600 $\text{cm}^{-1}$ . The area limited by a rectangle corresponds to the spectral band used as an indicator of recrystallization through sublimation of polymorph I to polymorph II during measurements.

### 3.1.2. Recrystallization of mefenamic acid being in contact with $\text{scCO}_2$ phase: *in situ* Raman spectroscopy

We have also studied the thermal transformation of the MFA crystalline form being in contact with a  $\text{scCO}_2$  phase under isochoric heating. We have measured a set of Raman spectra of the crystalline MFA sample surface in the bottom part of the cell at different temperatures. Figure 3.2a,b shows the temperature evolution of these spectra. Here we monitored the polymorphic transformation on the base of observation of spectral bands change in three wavenumber ranges ( $50\text{-}200\text{ cm}^{-1}$ ,  $1300\text{-}1360\text{ cm}^{-1}$ , and  $3300\text{-}3400\text{ cm}^{-1}$ ). It has been found that in the temperature range  $80\text{-}140^\circ\text{C}$  the obtained spectra correspond to polymorph I. Further, at the temperature of  $160^\circ\text{C}$ , the spectral signature reveals the transformation of polymorph I to polymorph II. However, the rate of this process is slow as in the case of the sublimation of MFA without

the  $\text{scCO}_2$  phase. Finally, the full polymorphic transformation has been found at the temperature of  $190^\circ\text{C}$ .

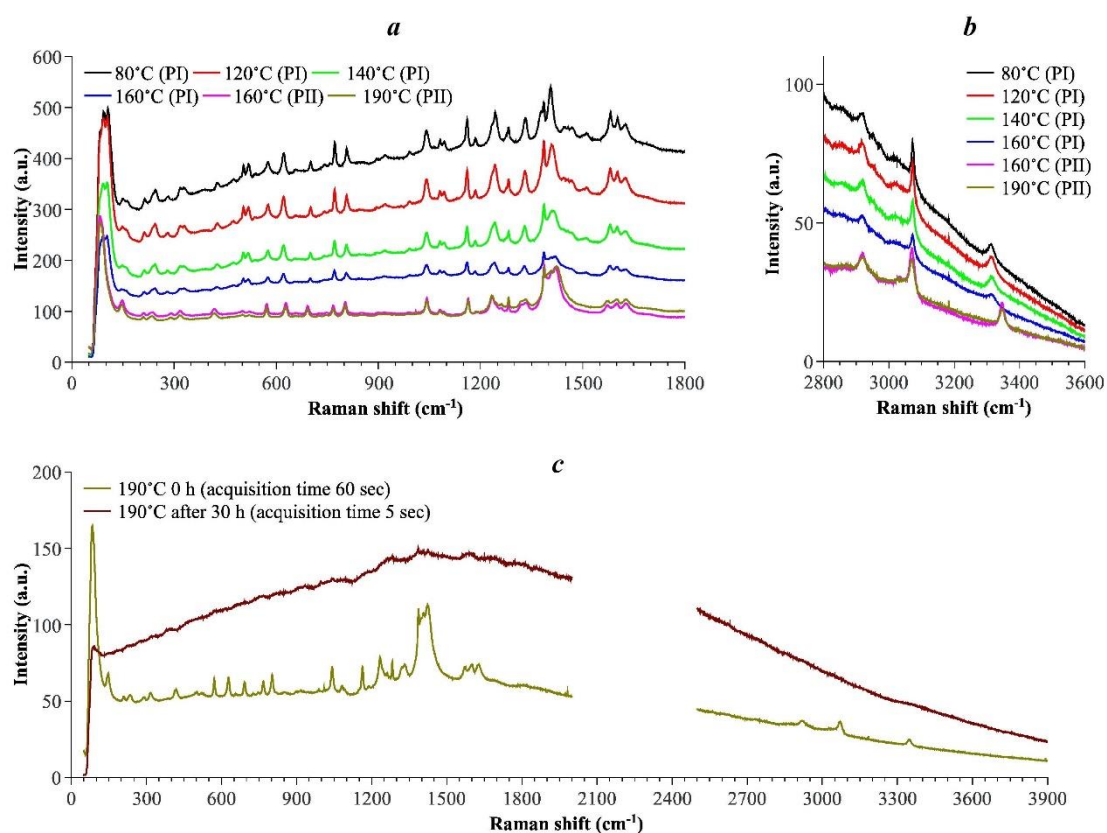


Figure 3.2. Thermal evolution of Raman spectra in wavenumber ranges of  $50\text{-}1800\text{ cm}^{-1}$  (a) and  $2800\text{-}3600\text{ cm}^{-1}$  (b) of crystalline mefenamic acid being in contact with  $\text{scCO}_2$  phase under isochoric heating. Comparison of Raman spectra of crystalline mefenamic acid and its melted phase (c).

Moreover, the visual inspection of the crystalline MFA surface being in contact with a  $\text{scCO}_2$  phase also allowed detecting the changes in the sample at  $160^\circ\text{C}$ . The emergence of dark domains on a bright background (Figure 3.3) may indicate the beginning of this transition. Then, the full change of color of the sample surface has been found at the temperature of  $170^\circ\text{C}$ . Nevertheless, this visual analysis has not allowed us to state the fact of a polymorphic transformation in the sample bulk and gives only a general idea about the temperature range of this polymorphic transition. It has also been discovered

that after 30 hours when the temperature was maintained at 190°C, the crystalline sample was melted and became transparent (the last photo in Figure 3.3). As a result, strong fluorescence appears and gives contribution into the Raman spectrum (Figure 3.2c). This fluorescence occurs because of the interaction of the laser beam with the metal alloy of the sample holder.

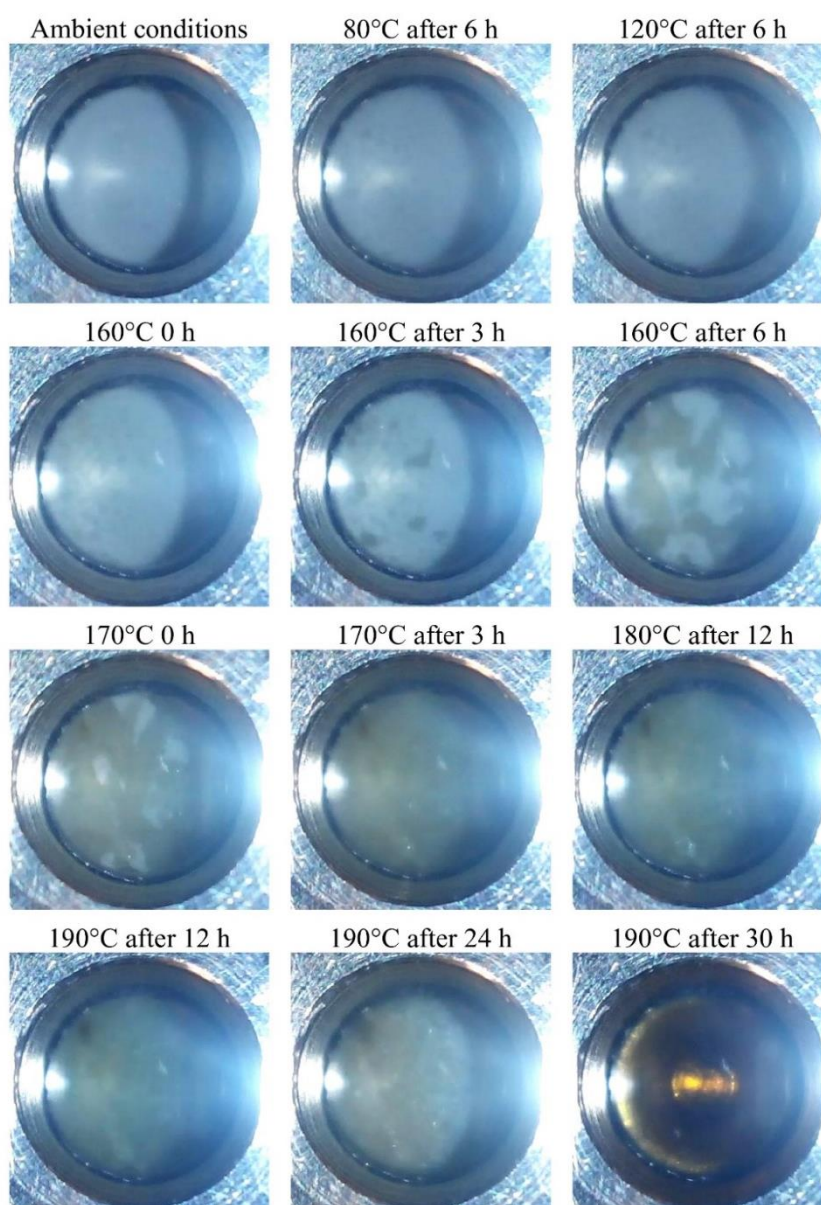


Figure 3.3. Photos of the powder of mefenamic acid in the sample holder of an optical cell being in contact with  $\text{scCO}_2$  under isochoric heating conditions for various temperatures and for various time ranges. The last photo shows the melted transparent phase of mefenamic acid.

According to various literature data [2-4] the MFA melting point of polymorph II is expected in the temperature range of 230-233°C, however, in the case of a binary system of [MFA-scCO<sub>2</sub>] under isochoric heating conditions, the MFA melting point is reached at 190°C under the pressure of 459 bar. Indeed, this is in good agreement both with the previous findings of our research group, namely for a binary system of [Ibuprofen-scCO<sub>2</sub>] [5] and with the literature data [6-8], where the authors noted the depression of melting temperatures of organic solids by high-pressure CO<sub>2</sub>.

### 3.1.3. Choice of analytical spectral domains for *in situ* infrared spectroscopy

In order to analyze the experimental IR spectra, two spectral domains were chosen as analytical. These domains are located in the wavenumber ranges of 1400-1550 cm<sup>-1</sup> and 3250-3500 cm<sup>-1</sup> (Figure 3.4). The first spectral domain is associated with complex vibrations that include the vibrations of the MFA molecule aromatic system and rocking vibration of the N-H group; the second wavenumber range is associated with the stretching vibration of the N-H group. This choice is linked with the fact that changing the MFA conformations induces a direct change in the N-H vibrations because the amino-group can be directly involved in the formation of intramolecular hydrogen bonds with hydroxyl or carbonyl oxygen of carboxyl fragment depending on its orientation. Thus, the change in the parameters of these bonds as a consequence of conformational transition will directly affect the vibration parameters of the N-H group itself. On the other hand, conformational changes affect the vibration of atoms of aromatic fragments indirectly, namely by means of electronic density redistribution, because of their close positions to the MFA functional groups (in particular, C=O, N-H, O-H) that are sensitive to the conformation changes. Therefore, the emergence of a new spectral contribution in this spectral domain

that is induced, for instance, by the change in the thermodynamic conditions, is a signature of the change in the MFA conformation. In the recent works of our research group [9, 5], the advantage of using the spectral domain of 1400-1550  $\text{cm}^{-1}$  associated with the aromatic ring for screening the conformational transitions of pharmaceutical molecules diluted in  $\text{scCO}_2$  has also been shown.

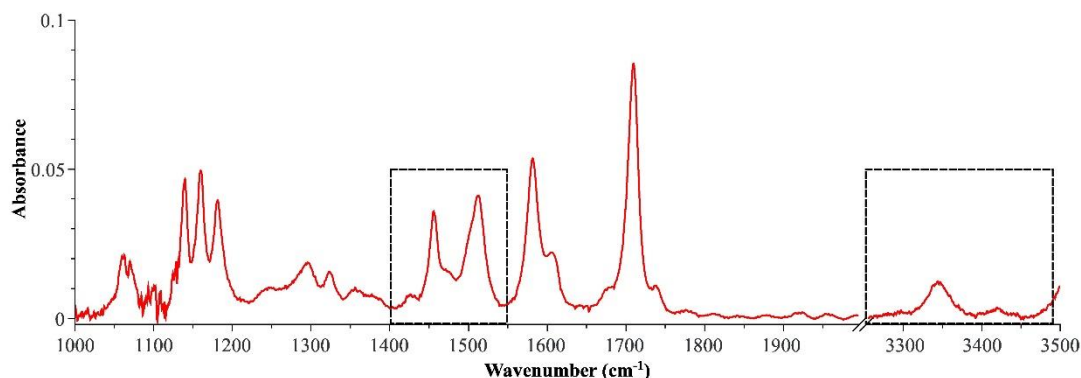


Figure 3.4. Analytical spectral domains in the wavenumber ranges of 1400-1550  $\text{cm}^{-1}$  and 3250-3500  $\text{cm}^{-1}$  of mefenamic acid IR spectrum measured at 170°C in  $\text{scCO}_2$  phase as an example.

Another reason to choose the N-H stretching vibration mode as analytical is associated with differences in its behavior in the various polymorphs of MFA. Indeed, the spectral domain of 3300-3350  $\text{cm}^{-1}$  was successfully used for screening the polymorphic transformation of crystalline MFA as has been shown above in the text and in a number of works [1, 10]. The authors of these works have shown that the appreciable change in the N-H stretching band position that occurs in the range of 3300-3350  $\text{cm}^{-1}$  allows distinguishing between polymorphs I and II. As a result of the transformation from polymorph I to polymorph II, the position of this band shifts from 3312  $\text{cm}^{-1}$  to a higher frequency of 3353  $\text{cm}^{-1}$ . Such behavior is consistent with the crystallographic results. For polymorph I, the proton of the N-H group is involved in relatively strong interaction with the carbonyl oxygen (the intramolecular hydrogen bond).

Indeed, in this case, the N...O distance is 2.636(2) Å [11]. However, the transformation to polymorph II, because of the changes in the molecular geometry, changes this distance too (Figure 3.5). Thus, for two different configurations of polymorph II, the N...O distance increases up to 2.67(1) Å and 2.72(2) Å, respectively [12] (these distances were measured in the Mercury program [13]). It is logical that the N-H bond length also decreases upon this polymorphic transformation. All these changes indicate the change in the parameters of the intramolecular hydrogen bond as a consequence of the polymorphic transformation, namely the weakening of the interaction between the proton of the amino-group and the carbonyl oxygen. This shifts the amino-group vibration toward higher energies (the blue shift of the N-H stretching band). Furthermore, the IR and Raman spectroscopic studies and computational studies of the MFA polymorphic forms point out the noticeable difference in the position of the N-H stretching spectral band [14, 4].

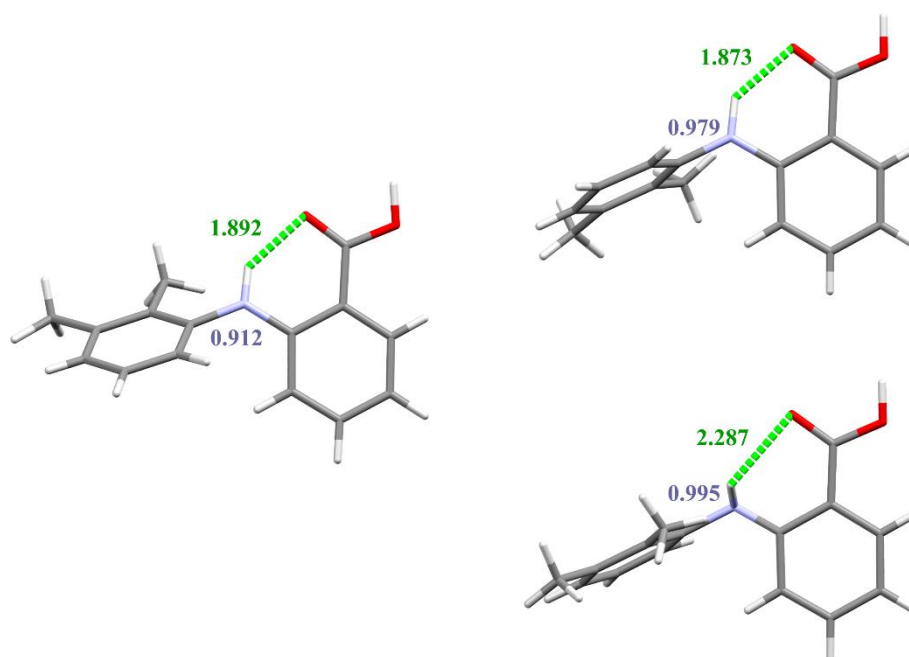


Figure 3.5. Conformations of MFA molecules in crystals of its polymorphic form I (on the left) and disordered modification II (on the right). The lengths of covalent N-H (in blue) and intramolecular hydrogen N-H...O (in olive) bonds are shown in angstroms.

### 3.1.4. Assignment of spectral contributions

In order to assign the spectral contributions of the analytical spectral domains presented in Figure 3.4 to the different MFA conformers, we relied on the results of the quantum-chemical calculations. It is been said in Chapter 2 that the four most stable conformers were taken into account. These conformers, named Ia, Ib, IIa, IIb, are schematically presented in Figure 3.6. They can be realized through the variation of two dihedral angles of  $\tau_1$  and  $\tau_2$ , which correspond to  $\angle(\text{C4-C3-C10-O11})$  and  $\angle(\text{C4-N15-C17-C19})$  respectively (Figure 2.4). The values of these angles for the given conformers are presented in Table 3.1.

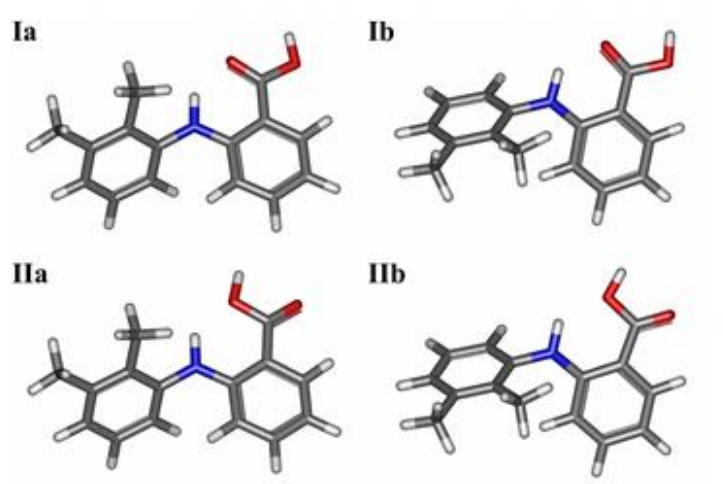


Figure 3.6. Schematic representation of the four most stable conformers of mefenamic acid obtained by quantum-chemical calculations.

Table 3.1. Values of the dihedral angles of  $\tau_1$  and  $\tau_2$ , N-H bond length in the molecule amino-group, and potential energy for 4 most stable conformers in comparison to the most stable one obtained by quantum-chemical calculations.

Parameter	conformer Ia	conformer Ib	conformer IIa	conformer IIb
$\tau_1, ^\circ$	4	-2	180	177
$\tau_2, ^\circ$	135	77	135	77
d(N-H), Å	1.02	1.02	1.02	1.01
$\Delta E, \text{kJ}\cdot\text{mol}^{-1}$	0	1.5	16.1	16.7

For these conformers, it has been found (Figure 3.7) that the energy barriers quantifying the conformational transition (that are related to the variation of dihedral angle  $\tau_1$ ) Ia $\rightarrow$ IIa and Ib $\rightarrow$ IIb are high ( $>33$  kJ/mol). This definitively excludes the possibility of a spontaneous thermal transition between the conformers within these pairs even at the highest investigated temperature ( $RT_{493K}=4.1$  kJ/mol). However, as shown in Figure 3.7, the energy barriers of the conformational transitions Ia $\rightarrow$ Ib and IIa $\rightarrow$ IIb that are related to the variation of dihedral angle  $\tau_2$  do not exceed 1.5 kJ/mol. Thus, because of the fact that these barriers are lower than the thermal fluctuations even at room temperature ( $RT_{298K}=2.5$  kJ/mol), the formation of each conformer within these pairs is equiprobable over the whole investigated temperature range. Consequently, these conformers may be grouped into two pairs, namely Ia-Ib and IIa-IIb; and each of these pairs may be considered as a single conformer. These two conformers were named conformer I and conformer II, respectively.

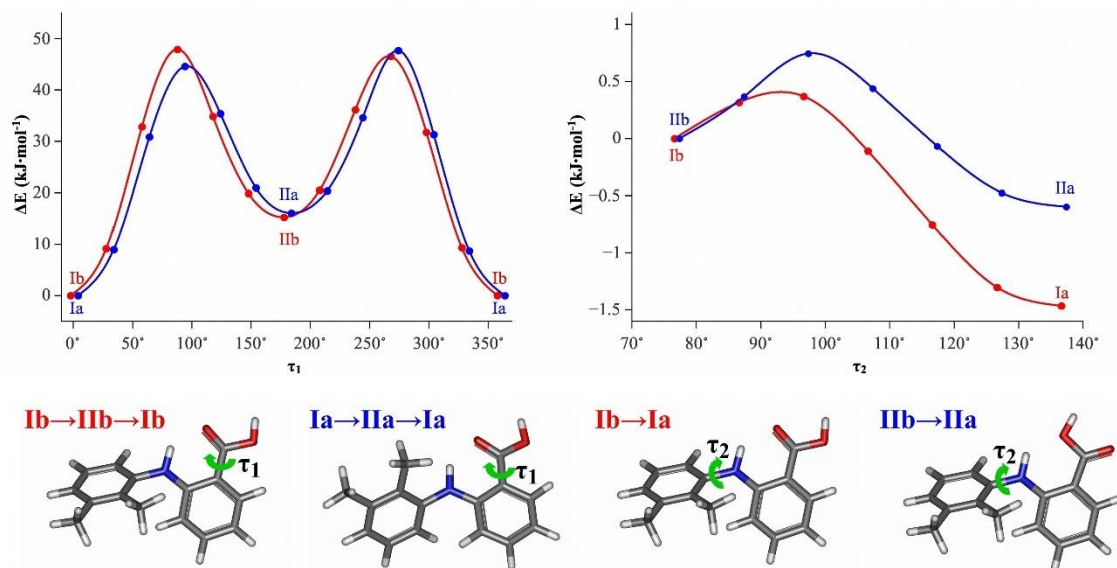


Figure 3.7. Energy barriers of conformational transitions within pairs Ia $\rightarrow$ IIa $\rightarrow$ Ia and Ib $\rightarrow$ IIb $\rightarrow$ Ib that are related to the variation of dihedral angle  $\tau_1$  and within pairs Ib $\rightarrow$ Ia and IIb $\rightarrow$ IIa that are related to the variation of dihedral angle  $\tau_2$ .

In order to analyze the changes in the experimental spectra and to get information on the conformational state of the MFA molecules in the  $scCO_2$  phase, we have also calculated the IR spectra for these conformers within the quantum-chemical calculations. These spectra are presented in Figure 3.8a.

It is obvious from these spectra that the N-H band positions for conformers IIa and IIb are blue-shifted relative to those calculated for conformers Ia and Ib. Therefore, taking into account this difference in the N-H band positions, which correlates with its behavior during the transformation from polymorph I to polymorph II [1, 10], the difference in the potential energies for these conformers as well as the difference in the N-H bond lengths for these conformers (Table 3.1), we have made a hypothesis that the conformational pair of Ia-Ib may be related to polymorph I, while that of IIa-IIb may be related to polymorph II. However, it is obvious that the MFA molecules geometry for conformers IIa and IIb in vacuum differs from that of the conformers in polymorph II. Indeed, according to the analysis of the dihedral angle values presented in Table 3.1 for MFA conformers IIa and IIb, the carbonyl oxygen is directed to the opposite side of the amino-group proton, whereas in the crystalline forms of polymorph II the carbonyl oxygen is directed toward the amino-group proton as in polymorph I [12]. These discrepancies may be explained by the constrained geometry of the molecules in the crystal, where it is defined by intramolecular bonds as well as intermolecular weak bonding. However, the molecule release from crystal to the solution, where at low concentrations the molecule exists as a monomer, is accompanied by the relaxation of the aforementioned constrained geometry, which leads the molecule to the closest local energy minimum.

Because according to our statement that each of the pairs of Ia-Ib and IIa-IIb may be considered as a single conformer, we summarized the spectra of conformers within these pairs. These summarized spectra, named Ia+Ib and IIa+IIb are also presented in Figure 3.8b for the wavenumber range of

1390-1610  $\text{cm}^{-1}$  and in Figure 3.8c for the wavenumber range of 3200-4000  $\text{cm}^{-1}$ . The spectra shown in Figure 3.8c demonstrate an appreciable shift in the N-H stretching band from 3480  $\text{cm}^{-1}$  to a higher frequency of 3600  $\text{cm}^{-1}$  at the transition from conformer I to conformer II. This change is consistent with the N-H stretching band position shift during the MFA crystalline polymorphic transformation. Additionally, in the wavenumber range associated with the vibrations of the aromatic system, we may also clearly distinguish different conformers, each of which gives two separated spectral contributions to the summarized spectrum (Figure 3.8b).

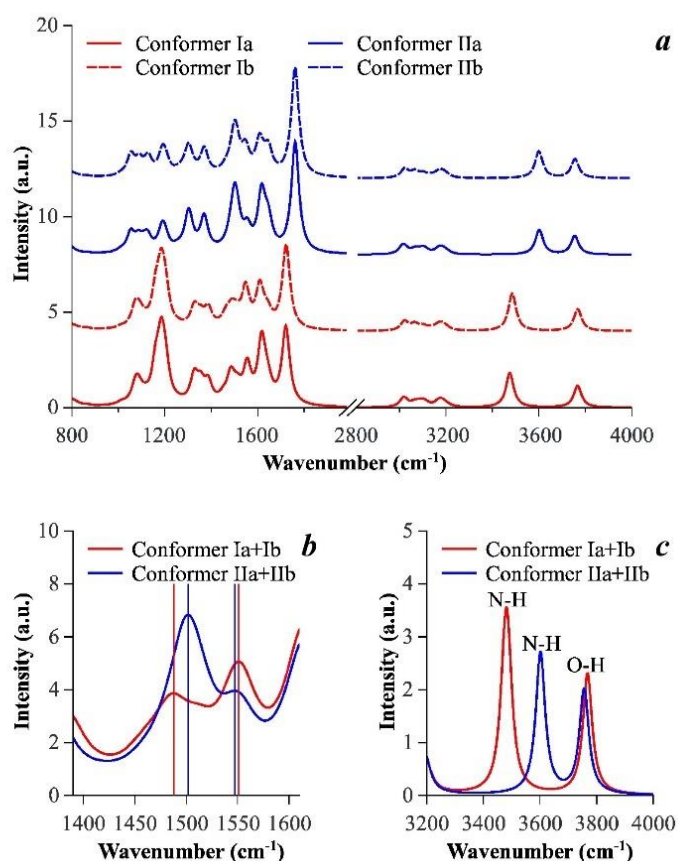


Figure 3.8. (a) IR spectra for the four most stable conformers Ia, Ib, IIa, IIb obtained by quantum-chemical calculations. (b,c) Sums of the IR spectra for pairs of conformers Ia and Ib (Conformer Ia+Ib) and conformers IIa and IIb (Conformer IIa+IIb).

### 3.1.5 Analysis of mefenamic acid conformers in CO<sub>2</sub> phase: *in situ* infrared spectroscopy

Figure 3.9a,b demonstrates the evolution of experimental spectra (the two analytical spectral domains) of MFA in the scCO<sub>2</sub> phase with a temperature increase in the range of 80-160°C. These spectra correspond to the equilibrium state at each temperature. The spectral bands intensity increase is related to the increase in the MFA concentration in the scCO<sub>2</sub> phase with the temperature increase. However, the spectral band shape is not affected. The analysis of the experimental spectra in the wavenumber ranges of 1400-1550 cm<sup>-1</sup> and 3250-3500 cm<sup>-1</sup> shows that in the first spectral domain two spectral contributions (at 1456 and 1515 cm<sup>-1</sup>) and in the second spectral domain the spectral contribution at 3346 cm<sup>-1</sup> are predominant. According to the calculated spectra (Figure 3.9b,c), we can assign these contributions to MFA conformer I. Nevertheless, the experimental spectra contain very small contributions at 1475 and 3436 cm<sup>-1</sup>, which we can attribute to MFA conformer II, even at these temperatures.

In the previous works of our research group [9, 5], it is been shown for pharmaceutical substances possessing different types of polymorphism that a polymorphic transformation of crystalline form being in contact with a fluid solution (scCO<sub>2</sub> phase) leads to a conformational transition of the molecules of these pharmaceutical substances in the fluid phase. Moreover, in the equilibrium conditions between the solid and fluid phases, the molar ratios of the polymorphs in the solid phase are correlated with the molar ratios of the conformers in the fluid solution phase. Therefore, in the case of the interface between the bottom phase containing the crystalline initial form of MFA and the CO<sub>2</sub> phase containing molecules of diluted MFA, the presence of MFA conformer II in the scCO<sub>2</sub> phase is an indicator of the presence of polymorph II in the initial commercial crystalline MFA as it was discussed in Section 2.1.

This is also in good agreement with results of [15] where authors on the basis of results of NMR spectroscopy have shown that in a saturated solution of commercial MFA in DMSO being in equilibrium with the solid phase of MFA, mainly two stable conformers exist. Moreover, the molar fractions of these conformers correspond to molar fractions of MFA polymorphs in its solid phase, where the fraction of the first polymorph is prevailing. The analysis of the spectra presented in Figure 3.9a,b also shows that the intensities associated with conformers I and II increases, while their ratio remains constant. It means that in this temperature range the percentages of these conformers do not change. Thus, we may assume that in this temperature range the polymorphic transformation from polymorph I into II in the MFA crystalline phase does not occur.

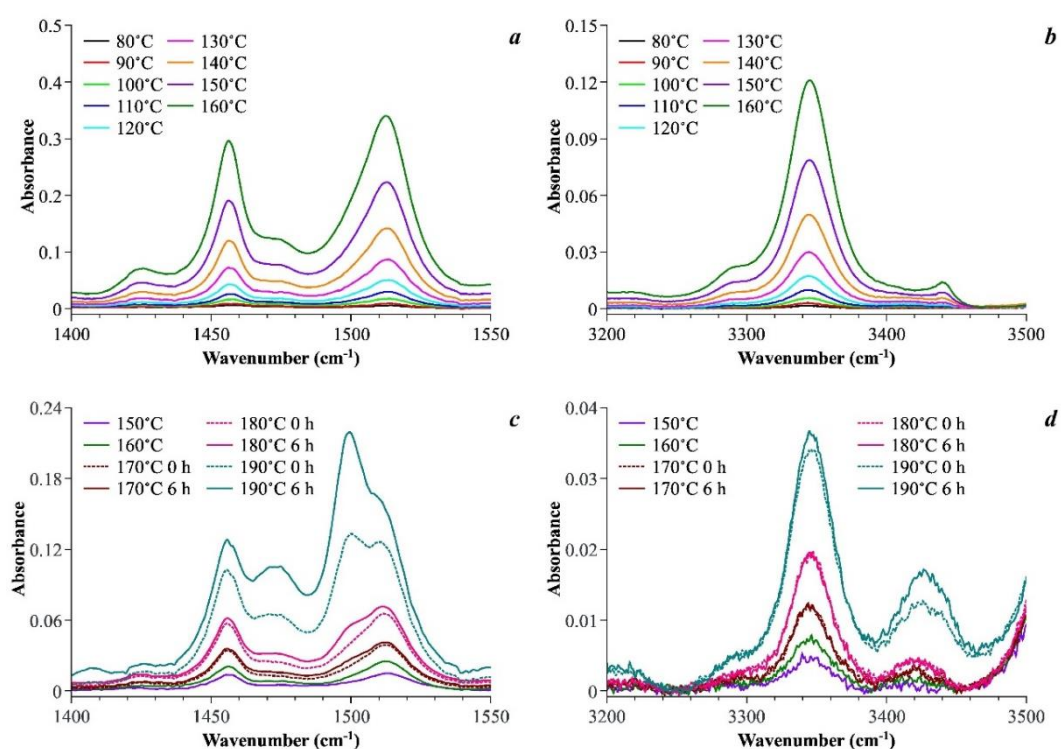


Figure 3.9. IR spectra of mefenamic acid diluted in  $scCO_2$  phase measured in the temperature range of 80-160°C: (a,b) in two analytical spectral domains 1400-1550  $cm^{-1}$  and 3200-3500  $cm^{-1}$ , respectively (the spectra were measured at the sample optical path length of 1.6 mm); and measured in the temperature range of 150-190°C: (c,d) in the same wavenumber ranges (here the sample optical path length was of 0.137 mm).

Figure 3.9c,d shows the spectra of MFA diluted in the scCO<sub>2</sub> phase for the two analytical spectral domains in the temperature range of 150-190°C. For each temperature in the range of 170-190°C both spectra that were measured immediately after reaching the targeted temperature and those after 6 hours of equilibration are presented. Examining the spectra that are presented in Figure 3.9c,d, we can observe that starting from the temperature of 170°C the spectral contributions, which are attributed to MFA conformer II and located at 1475, 1500 and 3436 cm<sup>-1</sup>, increase appreciably. It has also been found that the rate of increasing these contributions is higher than the rate of increasing contributions that are related to conformer I (at 1456, 1515 and 3346 cm<sup>-1</sup>). We interpret this behavior as an indication of the transition from conformer I to conformer II.

After that, we compared the intensity changes in these spectral contributions at the temperatures of 170°C, 180°C and 190°C over the first 6 hours and found that with the temperature increase, the rate of transition of conformer I to conformer II also increase. Therefore, the highest rate of conformational transitions was found at 190°C. This behavior may be attributed to the beginning of the fast polymorphic transformation of the MFA crystalline phase in the bottom part of the cell. This is in good agreement with the results of [1] and our finding mentioned in Sections 3.1.1 and 3.1.2 of this work.

In order to confirm this hypothesis, we examined in detail and compared the dynamics of the changes in the MFA IR spectra in the phase of scCO<sub>2</sub> at two temperatures (180 and 190°C). For the temperature of 180°C, the spectra were measured every 30 minutes over 24 hours and for the temperature of 190°C, the spectra were also measured every 30 minutes over 48 hours. The results of these measurements are summarized in Figures 3.10 and 3.11 where the dynamics of the MFA spectral changes in the scCO<sub>2</sub> phase as a function of time at the temperature of 180°C and 190°C are presented, respectively.

It is obvious from Figure 3.10 that the MFA concentration in  $scCO_2$  increases. The analysis of these spectra shows that the intensities of the spectral bands located at 1475, 1500 and 3436  $cm^{-1}$  attributed to MFA conformer II increase faster than those located at 1456, 1515 and 3346  $cm^{-1}$  attributed to conformer I. Such behavior testifies the increase in the percentage of conformer II. Nevertheless, even after 24 hours, the spectral bands that were attributed to conformer I were still observed in the spectrum. It means that over 24 hours the full transition of conformer I to conformer II is not achieved, though we might expect the full transition because according to the aforementioned finding polymorphic transformation at this temperature should take less time.

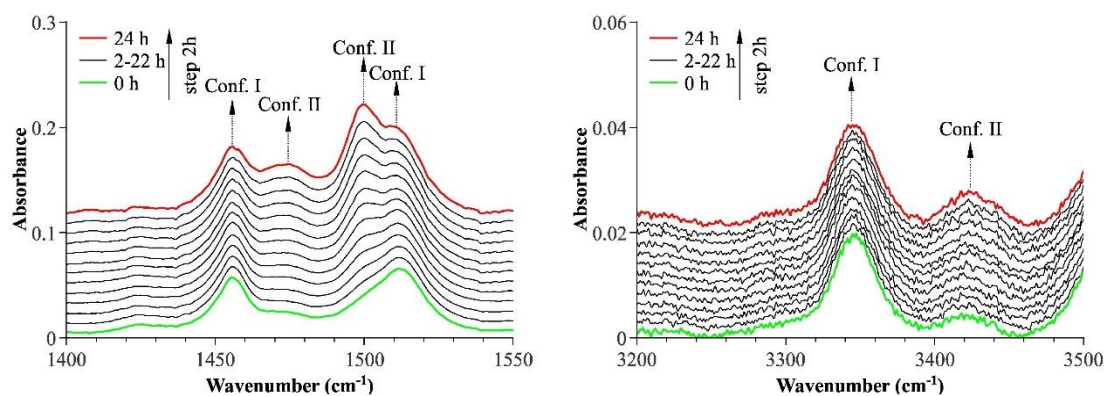


Figure 3.10. Dynamics of spectral changes in spectral domains of 1400-1550  $cm^{-1}$  and 3200-3500  $cm^{-1}$  of IR spectra of mefenamic acid in  $scCO_2$  phase kept at the temperature of 180°C for 24 hours.

Figure 3.11 shows the dynamics of MFA spectral changes in the  $scCO_2$  phase as a function of time at the temperature of 190°C. It has been found that in the first 19 hours, the spectral contributions intensities that are related to MFA conformer II (at 1475, 1500 and 3436  $cm^{-1}$ ) are higher than the rise of intensities of the spectral contributions that are attributed to conformer I (1456, 1515 and 3346  $cm^{-1}$ ). This leads to an increase in the molar fraction of conformer II. In the time range of 19-21.5 hours the intensity of the spectral band that is related to the N-H stretching vibration of conformer I reaches its maximum.

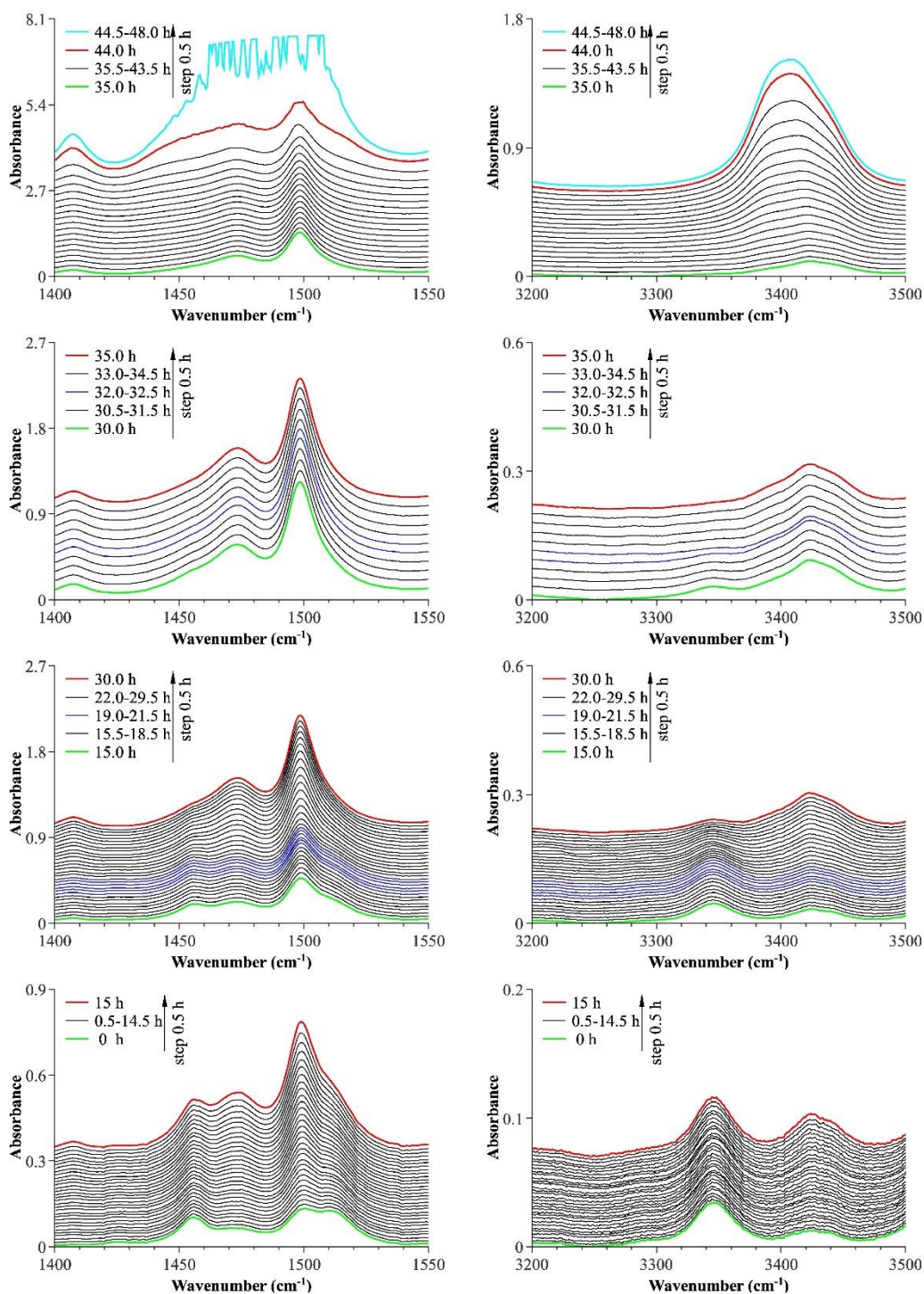


Figure 3.11. Dynamics of spectral changes in spectral domains of  $1400\text{--}1550\text{ cm}^{-1}$  and  $3200\text{--}3500\text{ cm}^{-1}$  of IR spectra of mefenamic acid in  $\text{scCO}_2$  phase kept at the temperature of  $190^\circ\text{C}$  for 48 hours. Different colors show certain key time ranges.

Further, in the time range of 22–32 hours all the spectral components that are related to this conformer considerably decrease, while the intensities of the

spectral bands associated with conformer II continue rising. As a result, after 32 hours it becomes impossible to detect the spectral signatures of conformer I. Therefore, we may hypothesize that at 190°C the full transition of conformers I to conformers II occurs. However, the spectra at 190°C behave in an interesting way in the time interval of 35-48 hours. Namely, in both analytical spectral domains, we observe an avalanche-like increase in the spectral bands integral intensities. Indeed, in the wavenumber range of 1400-1550  $\text{cm}^{-1}$ , the spectral bands become wider and reach their oversaturation after 44.5 hours. Though we might expect an exponentially-damped increase in their integral intensities with time at a constant temperature (due to the limit of the MFA solubility in the  $\text{scCO}_2$  phase spectral intensity asymptotically reaches maximum value within a certain time and remains constant), on the contrary, we observe the acceleration of the integral intensities increase.

The same scheme of changes is also observed in the N-H vibration mode, where the spectral band that is associated with conformer II also broadens, and it is accompanied by the simultaneous appearance of a pronounced contribution on its low-frequency slope (3380-3400  $\text{cm}^{-1}$ ), whereas its integral intensity increases exponentially. This unusual change is correlated with the occurrence of critical phenomena that induce the change in the extinction coefficients of these spectral bands.

Indeed, as it was shown before, the melting of MFA polymorph II occurs at 190°C and this is the first-order phase transition [16] that may be traced back to the appearance of critical opalescence in the  $\text{scCO}_2$  fluid phase being in contact with the MFA solid phase. This is also confirmed by the behavior of the raw spectra (without baseline correction) of MFA in the  $\text{scCO}_2$  phase which demonstrate an increase in the spectral intensity accompanied by spontaneous growth in the spectral background at 190°C (Figure 3.12).

Such a phenomenon is due to the increasing of continuous absorption induced by a large density fluctuation of the MFA molecules in the  $\text{scCO}_2$

phase. It is precisely this fact that explains the occurrence of nonlinearity in the behavior of the extinction coefficient. Of course, it results in the non-equilibrium state of the system that is characterized by the presence of transient MFA molecular clusters. This may also be confirmed by the considerable change in the absorption of the solvent itself. At the same time, we observe a considerable decrease in the integral intensities of the CO<sub>2</sub> combination spectral bands ( $2\nu_2\nu_3$  and  $\nu_1\nu_3$ ), which are both red-shifted and narrowed (Figure 3.13a).

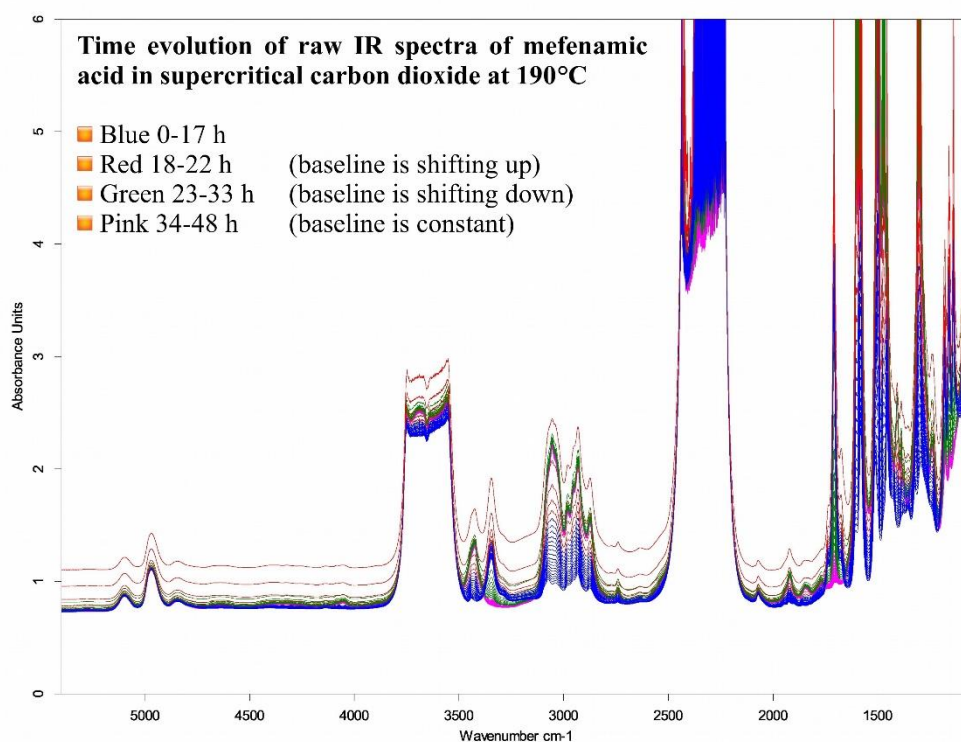


Figure 3.12. Time-evolution of raw experimental IR spectra of mefenamic acid in scCO<sub>2</sub> phase at 190°C without subtraction of silicon and CO<sub>2</sub> contributions as well as without baseline correction (the screenshot was obtained from OPUS software interface).

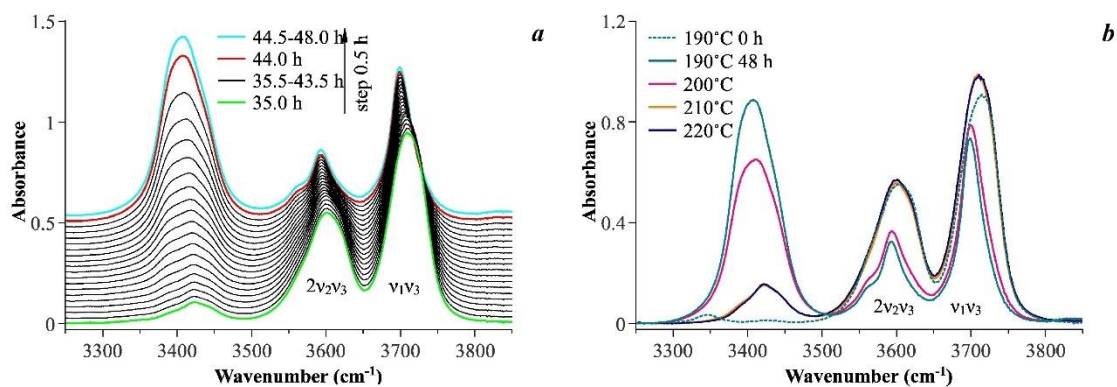


Figure 3.13. IR spectra of binary [MFA-CO<sub>2</sub>] mixture in the wavenumber range that are related to the N-H stretching vibration of a mefenamic acid molecule and combinational bands ( $2\nu_2\nu_3$  and  $\nu_1\nu_3$ ) of CO<sub>2</sub>: (a) time-evolution of spectra at 190°C in the range of 35-48 hours, (b) the spectra obtained in the temperature range of 200-220°C in comparison with the spectra obtained at 190°C at 0 hours and after 48 hours.

These critical phenomena are expected to disappear when the temperature is increased further (above 190°C). Indeed, the subsequent heating to 200°C and further to 210°C and 220°C leads again to an appreciable decrease in the integral intensities and narrowing of the spectral contributions in the wavenumber range of 1400-1550 cm<sup>-1</sup> (Figure 3.14a). The spectral band associated with the N-H stretching vibration of conformer II loses its low-frequency shoulder and its total integral intensity also decreases considerably. Nevertheless, these changes do not result in the reappearance of an N-H stretching band that is related to conformer I. Finally, the spectra of MFA and CO<sub>2</sub> (combination bands) again become similar to the spectra recorded at 190°C in the time range before the avalanche-like increase in the spectral intensity occurs (Figures 3.14b and 3.13b). Furthermore, the similarity between the MFA spectra at the temperatures of 210-220°C and those at 190°C that were measured in the time interval from 30 to 35 hours allows us to state that even at such high-temperatures no thermal decomposition of MFA takes place.

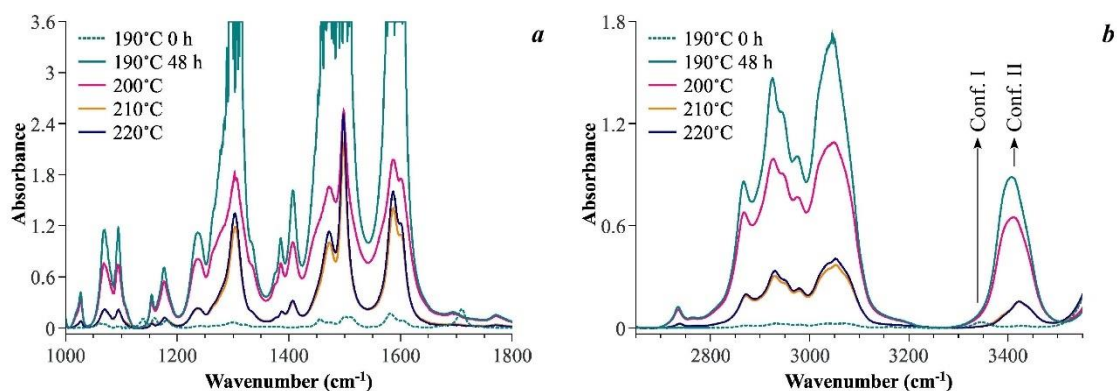


Figure 3.14. IR spectra of mefenamic acid diluted in  $\text{scCO}_2$  phase in the temperature range of 190-220°C in two spectral domains: (a) 1000-1800  $\text{cm}^{-1}$  and (b) 2650-3550  $\text{cm}^{-1}$ . The spectra were measured at the sample optical path length of 0.137 mm.

Taking into account the full transition of MFA conformer I to conformer II at 190°C in the  $\text{scCO}_2$  phase being in contact with the MFA crystalline phase, we may suppose that, in the bottom phase, the total recrystallization of polymorph I into polymorph II also takes place. Therefore, it might be expected that after a fast cooling down of the cell, pure polymorph II can be obtained. To confirm this hypothesis we subtracted the recrystallized MFA obtained from the binary mixture of  $[\text{MFA}-\text{scCO}_2]$  and analyzed it.

### 3.1.6. Analysis of crystalline mefenamic acid obtained by crystallization from a binary mixture of [mefenamic acid - supercritical $\text{CO}_2$ ]

We have analyzed two processed MFA samples obtained after cooling down the optical cell and the subsequent evacuation of  $\text{CO}_2$ . The first sample was extracted from the bottom part of the cell that contained an excess of MFA, whereas the second one was collected from the upper part of the cell, which corresponded to the phase of  $\text{scCO}_2$  (Figure 3.13b). This sample was obtained as a deposit on the cell walls as a result of recrystallization from a fluid solution upon its fast cooling down. The main difference between these two samples was in their particles sizes. Thus, the sample obtained from the  $\text{scCO}_2$  phase was

microcrystalline. Then, we recorded full range micro Raman and micro IR spectra of these two samples and compared them with the spectra of MFA of PII form (Figure 3.15). It has been found that for these samples, both the IR and Raman spectra totally correspond to the spectra of pure polymorph II. Indeed, the main signature of polymorph II is located in the N-H stretching region, whereas the signature of polymorph I in this region is totally absent. At the same time, there are also a number of spectral peculiarities in the wavenumber ranges of 50-1800  $\text{cm}^{-1}$  for Raman spectra and 800-1800  $\text{cm}^{-1}$  for IR spectra, which clearly prove that the MFA samples obtained after processing in the experimental cell are pure polymorph II.

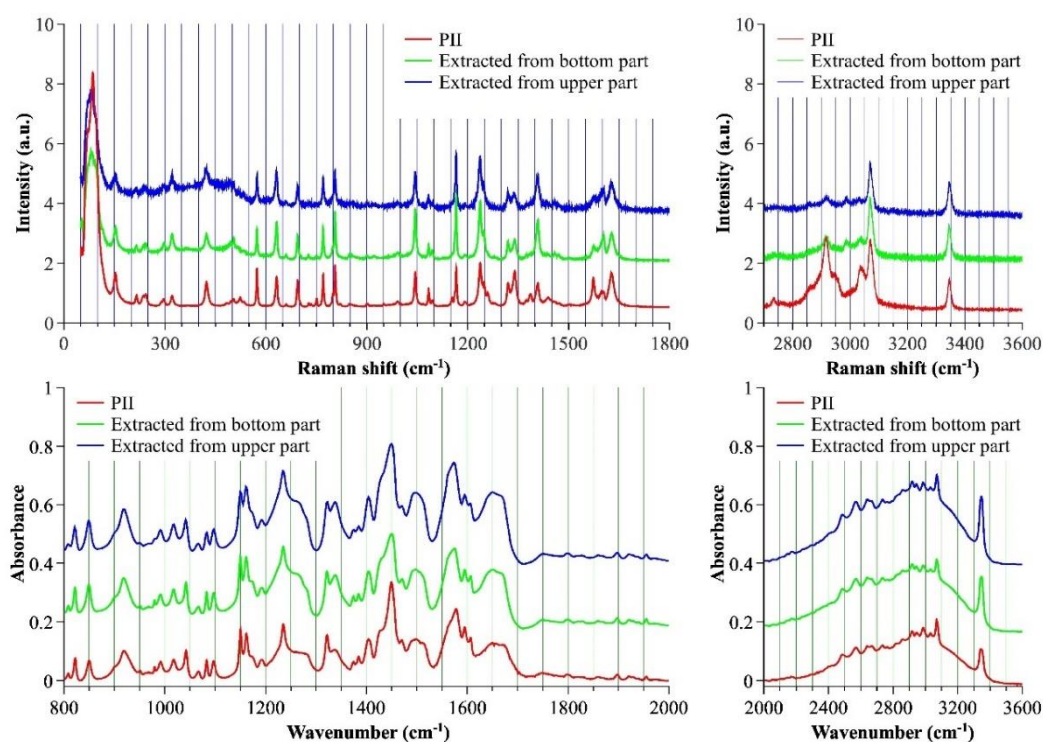


Figure 3.15. Comparison of Raman and IR spectra of the mefenamic acid samples obtained after processing in an experimental cell (the first sample was extracted from the bottom part of the cell that always contained an excess of MFA, the second sample was collected from the upper part of the cell, where it was obtained as a deposit on the cell walls as a result of crystallization from a fluid solution upon its fast cooling down) with spectra of mefenamic acid polymorph II obtained via sublimation of polymorph I using the Linkam system with a temperature-controlled plate.

Therefore, we may assert that, on the one hand, there are correlations between the conformational state of MFA molecules in the scCO<sub>2</sub> phase and the polymorphism of the crystalline phase being in contact with each other. On the other hand, we can also expect the correlations between the polymorphism of the MFA form obtained by crystallization from the fluid phase and the conformational state of its molecules in the scCO<sub>2</sub> phase, from which this form was crystallized.

### **3.2. High-temperature recrystallization of carbamazepine in supercritical CO<sub>2</sub>: a way to obtain pure polymorph I**

Crystallization of polymorph II of mefenamic acid has been a success in obtaining pure polymorphic forms from scCO<sub>2</sub>. In a similar way, we decided to study the possibility of obtaining a pure metastable form I of carbamazepine. It was previously shown that melting of II, III and IV forms of carbamazepine leads to the formation of polymorphic modification I [17]. However, these transformations can be associated with a number of problems, the largest of which is the undesirable thermal decomposition of CBZ at high temperatures 153.75°C [18]. By itself, the appearance of an impurity changes in an unpredictable way the bioavailability of drugs based on CBZ. In addition, iminostilbene, which is a product of this thermal decomposition, has an antiepileptic activity itself [19].

Preliminary studies of the ratio of forms after recrystallization at different densities of the scCO<sub>2</sub> phase and temperature were published by our group earlier [20]. The acquisition of the polymorphic modification I of CBZ from scCO<sub>2</sub> showed high efficiency. Despite this, the probability of the appearance of an impurity of the initial form is high, therefore, it was necessary to refine the methodology and to circumvent the thermal decomposition. Our suggestions will be described below.

### 3.2.1. Visual analysis of the changes in the carbamazepine sample

The photos made by us using microscope is represented in Figure 3.16. By their analysis, three temperature ranges were identified. In the temperature range of 70-110°C, no changes are observed at the CBZ surface. However, at the temperature of 120°C, the surface takes on a yellow tint, the intensity of which considerably increases while this temperature is maintained. In the temperature range of 120-150°C, the surface color remains unchanged. The yellow color of the CBZ surface is the evidence of CBZ thermal degradation, with solid iminostilbene (IMST) and volatile isocyanic acid (ICA) formed as a result of the deamidation process (Figure 3.17). This is one of the most probable pathways of CBZ degradation described in the literature [21-24].

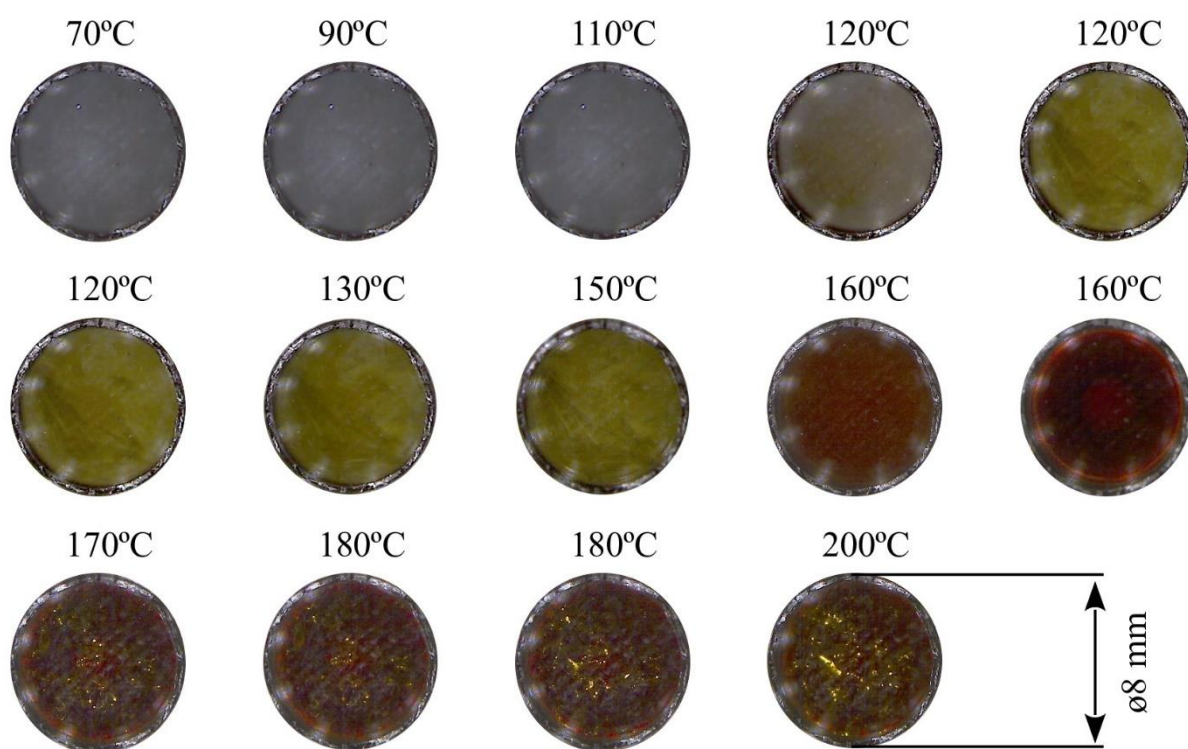


Figure 3.16. Photos of the thermal change's evolution in the CBZ surface permanently contacting with CBZ saturated solution in scCO<sub>2</sub> when heated along the chosen isochore. The photos correspond to the equilibrium state. For the key temperatures of 120, 160, 180°C we presented the series of photos with a time step of 12 hours to demonstrate the dynamics of the changes.

The heating to 160°C considerably changes the color of the CBZ surface, while maintaining this temperature for another 12 hours leads to the total melting of the CBZ crystalline phase. It is also important to note that this temperature is lower than the melting temperature of polymorph III as was shown above. Such a decrease in the melting temperature of pharmaceuticals occurred for MFA and was mentioned in the previous work of our group [5]. This fact is in good agreement with works [6-8], where the authors noted the reduction in the melting temperatures of organic solids in a high-pressure CO<sub>2</sub> medium. They attributed this to the increase in the CO<sub>2</sub> dissolution capacity with an increase in its density. Further heating from 160°C to 200°C results in the crystallization of small yellow crystals of IMST. Along with this in the temperature range of 160-200°C melt CBZ phase remains stable and its crystallization does not occur.

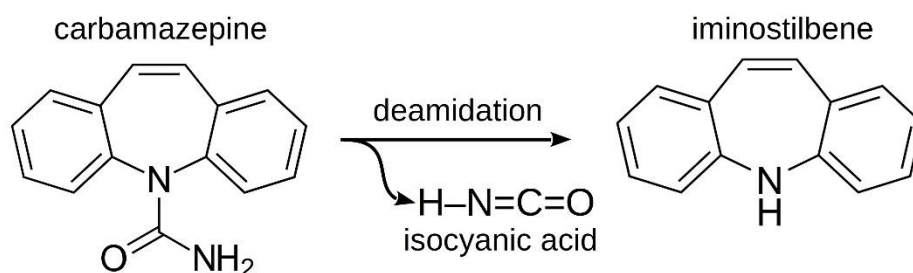


Figure 3.17. CBZ degradation pathway leading to the formation of IMST and ICA.

### 3.2.2. Assignment of spectral contributions and analytical spectral domains

The spectra obtained from the bioactive molecules solution in scCO<sub>2</sub> are presented in Figure 3.18. Their preliminary analysis in combination with the aforementioned data of visual observations allowed us to identify 3 key temperature ranges: 110-150°C, 150-170°C, and 170-200°C, where the character of the spectral changes is different. Moreover, we determined the spectral domains: 1350-1850 cm<sup>-1</sup> and 3250-3550 cm<sup>-1</sup>, which will be used as analytical

ones in the conformational analysis. On par with quantum-chemical calculations it will be used in the studies directed towards conformational analysis of drug molecules in CO<sub>2</sub> phase.

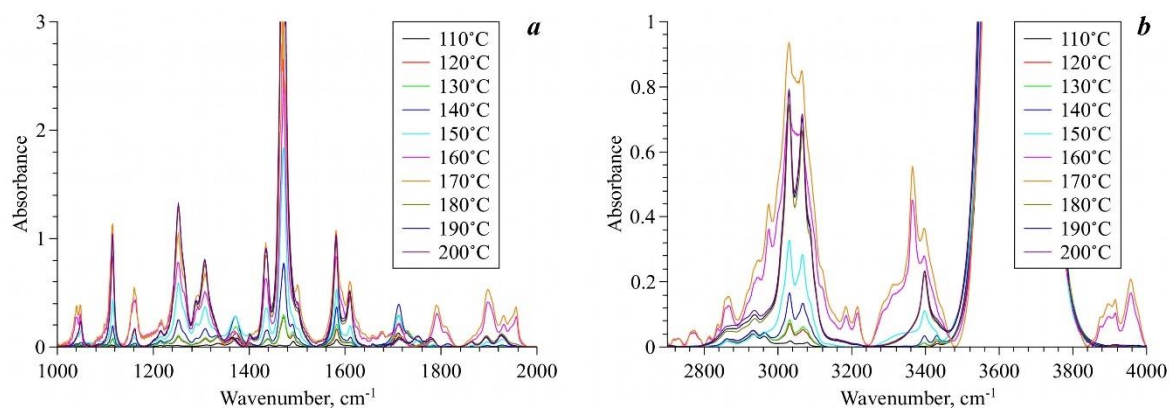


Figure 3.18. IR spectra of CBZ dissolved in the scCO<sub>2</sub> phase permanently contacting with an excess of CBZ in isochoric heating conditions in the temperature range of 110-200°C ( $\Delta T=10^{\circ}\text{C}$ ) along the chosen isochore for two spectral ranges: (a) 1000-2000 cm<sup>-1</sup> and (b) 2700-4000 cm<sup>-1</sup>.

The quantum-chemical calculations in this work are based on the results that were performed in the previous research of our group [20]. The two most stable conformers of CBZ were determined in that work. However, they are important in the current research, so their geometric parameters, determined by the dihedral angles of  $\tau_1$ ,  $\tau_2$  and  $\tau_3$ , are collected in Table 3.2. It was shown that the first conformer has lower energy, and the energy difference between these two conformers is 1.5 kJ·mol<sup>-1</sup>. For them we calculated the IR spectra and identified the key analytical IR spectral bands, whose behavior is sensitive to the conformational transitions of the CBZ molecule. Taking into account the CBZ thermal degradation, leading to the formation of IMST, and applying the same calculation approach, as described in [20], in the present work we additionally optimized the geometry and calculated the vibration frequencies for IMST and for its protonated form (IMST-H<sup>+</sup>). Moreover, relying on the possibility of the

CBZ tautomerization that should occur via proton transfer in the carboxamide group from the amide nitrogen to carbonyl oxygen [22], we also performed calculations for the most probable CBZ tautomer (Figure 3.19). To perform an assignment of the spectral bands during the further analysis of *in situ* IR data the vibrational frequencies, intensities and types of motions for each calculated molecule were collected to Table 3.3.

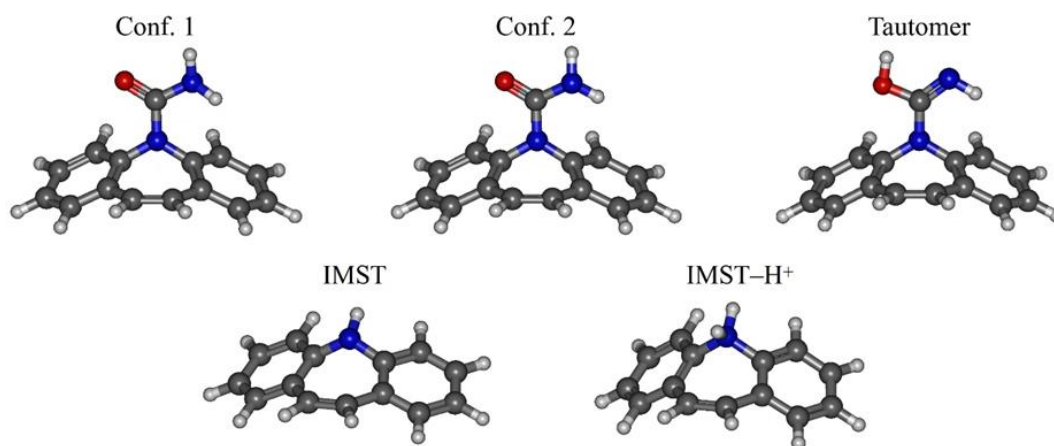


Figure 3.19. The optimized molecular structures of two CBZ conformers (Conf. 1 and Conf. 2) with different orientation of the hydrogen atoms of the amide group, CBZ tautomeric form, iminostilbene (IMST), and its protonated form (IMST-H<sup>+</sup>).

Table 3.2. Values of dihedral angles  $\tau_1$ ,  $\tau_2$  and  $\tau_3$  for two CBZ conformers as obtained by quantum-chemical calculations.

	$\tau_1$	$\tau_2$	$\tau_3$
Conf. I	-166°	-24°	-7°
Conf. II	167°	16°	-10°

The vibration bands obtained from the quantum-chemical calculations were described with a set of Lorentzian functions with arbitrary dispersion and represented in Figure 3.20 for easier comparison with the experimental spectra.

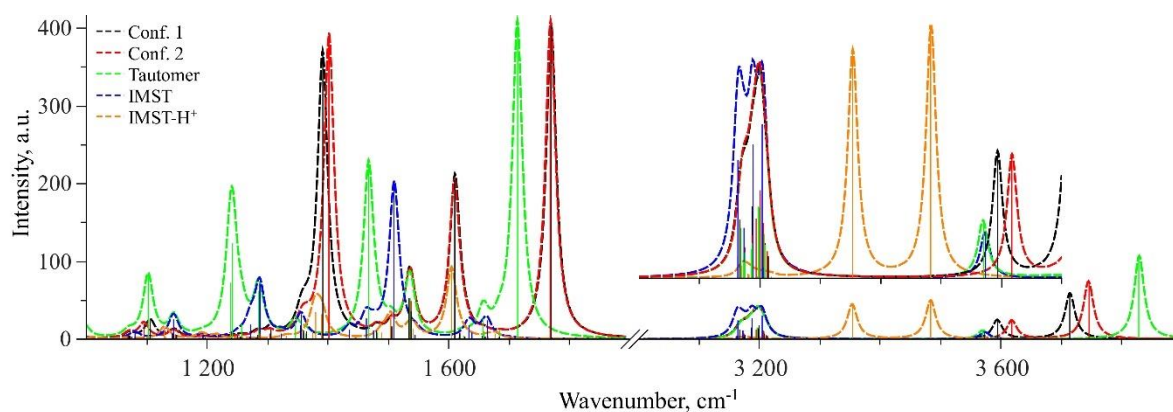


Figure 3.20. The set of vibrational bands calculated via quantum-chemical calculations (straight vertical lines) for two CBZ conformers (Conf. 1 and Conf. 2), CBZ tautomeric form, IMST, and IMST-H<sup>+</sup>. The insertion shows the scaled spectral domain in the range of 3000-3700 cm<sup>-1</sup>.

Table 3.3. Peak maximum positions (frequency, cm<sup>-1</sup>), intensities and assignments of the analytical spectral bands for molecular structures (Figure 3.19).

Conf. 1	Conf. 2	Tautomer	IMST	IMST-H <sup>+</sup>
1390.96 cm <sup>-1</sup>	1401.59 cm <sup>-1</sup>			
366.68	390.26			
δ(C-N-H1)	δ(C-N-H1)			
		1467.06 cm <sup>-1</sup>		
		223.11		
		δ(C-O-H)+		
		δ(C=N-H)		
			1509.42 cm <sup>-1</sup>	
			200.23	
			aromatic + ρ(N-H)	
				1604.28 cm <sup>-1</sup>
				91.64
				δ(H-N-H <sup>+</sup> )
		1713.21 cm <sup>-1</sup>		
		407.54		
		ν(C=N)		
1769.17 cm <sup>-1</sup>	1768.10 cm <sup>-1</sup>			
402.99	408.77			
ν(C=O)	ν(C=O)			
			3164.06 cm <sup>-1</sup>	
			23.33	
			ν(C-H)	
			3187.88 cm <sup>-1</sup>	
			26.29	
			ν(C-H)	
		3569.67 cm <sup>-1</sup>	3573.27 cm <sup>-1</sup>	
		11.17	8.99	
		ν(N-H)	ν(N-H)	

Table 3.3 Continued.

Conf. 1	Conf. 2	Tautomer	IMST	IMST-H+
3593.76 cm <sup>-1</sup>	3617.83 cm <sup>-1</sup>			3353.73 cm <sup>-1</sup>
24.68	24.00			44.92
$\nu_s(\text{H-N-H})$	$\nu_s(\text{H-N-H})$			$\nu_s(\text{H-N-H}^+)$
3713.97 cm <sup>-1</sup>	3744.68 cm <sup>-1</sup>			3483.57 cm <sup>-1</sup>
59.15	74.56			50.05
$\nu_{as}(\text{H-N-H})$	$\nu_{as}(\text{H-N-H})$			$\nu_{as}(\text{H-N-H}^+)$
		3828.53 cm <sup>-1</sup>		
		107.40		
		$\nu(\text{O-H})$		

Here we denoted the different types of vibration as follows:  $\delta$  - scissoring;  $\nu$  - stretching;  $\nu_s$  - symmetric stretching;  $\nu_{as}$  - antisymmetric stretching;  $\delta(\text{C-O-H})+\delta(\text{C=N-H})$  - antiphase scissoring; aromatic+ $\rho(\text{N-H})$  - complex vibration.

### 3.2.3. Analysis of carbamazepine conformers in CO<sub>2</sub> phase: *in situ* infrared spectroscopy

#### 3.2.3.1. Temperature range of 110-150°C

Figure 3.21 illustrates the thermal evolution of the IR spectra of CBZ dissolved in the scCO<sub>2</sub> phase in the temperature range of 110-150°C. Based on the IR spectra obtained by quantum-chemical calculations we determined the key analytical spectral bands. The assignments of these spectral bands (Table 3.4) were performed based on the data presented in Table 3.3.

An analysis of the thermal evolution of the spectra presented in Figure 3.21 allowed us to identify the appearance of the CBZ tautomeric form in the scCO<sub>2</sub> phase beginning from 120°C. Further heating up to 140°C reduces the spectral contributions related to CBZ Conf. 1, whereas the intensity of the spectral contributions related to the CBZ tautomeric form considerably increases. Moreover, at this stage two points related to the thermal degradation of CBZ deserve to be also clarified. The analysis of the IR spectra didn't allow us to identify the spectral signatures of IMST, despite the appearance of yellow tint (associated with IMST) at the surface of the CBZ solid form beginning from

120°C as shown in Figure 3.16. It means that IMST is not present in the scCO<sub>2</sub> phase.

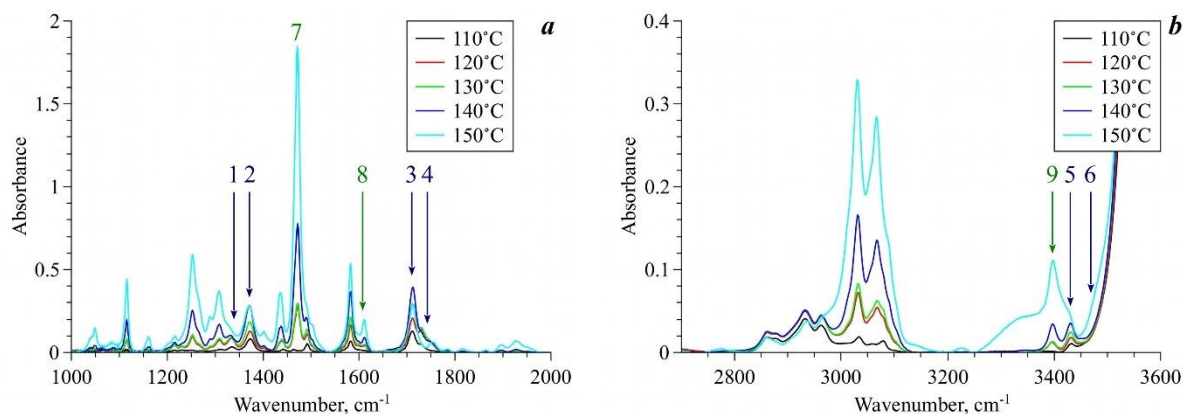


Figure 3.21. IR spectra of CBZ dissolved in the scCO<sub>2</sub> phase permanently contacting with an excess of CBZ in isochoric heating conditions in the temperature range of 110-150°C ( $\Delta T=10^\circ\text{C}$ ) along the chosen isochore for two spectral ranges: (a) 1000-2000 cm<sup>-1</sup> and (b) 2700-3600 cm<sup>-1</sup>. The arrows with numbers show the analytical spectral bands determined by quantum-chemical calculations.

Table 3.4. The assignment of the spectral bands in two analytical spectral domains (1350-1850 cm<sup>-1</sup> and 3250-3550 cm<sup>-1</sup>) of the experimental spectra based on the results of quantum-chemical calculations presented in Table 3.3.

1350-1850 cm <sup>-1</sup>		3250-3550 cm <sup>-1</sup>	
1 -	$\delta(\text{C-N-H1})$ of Conf. 1	5 -	$\nu_s(\text{H-N-H})$ of Conf. 1
2 -	$\delta(\text{C-N-H1})$ of Conf. 2	6 -	$\nu_s(\text{H-N-H})$ of Conf. 2
3 -	$\nu(\text{C=O})$ of Conf. 2	9 -	$\nu(\text{N-H})$ of Tautomer
4 -	$\nu(\text{C=O})$ of Conf. 1		
7 -	$\delta(\text{C-O-H})+\delta(\text{C=N-H})$ of Tautomer		
8 -	$\nu(\text{C=N})$ of Tautomer		

Concerning the ICA component, we will discuss in more details the problems we were faced to prove its presence in the scCO<sub>2</sub> phase. According to the quantum-chemical calculations, the most intensive spectral bands related to the vibrations of gaseous ICA (boiling point  $T_b=23.5^\circ\text{C}$  [25]) are either situated beyond the transmission band of silicon ( $\sim 1000\text{-}8300\text{ cm}^{-1}$ ), the material the

optical windows of the IR cell are made of, or totally overlap with the spectral bands of the other component of the system. The first case is related to the  $\delta(\text{C}=\text{N}-\text{H})$  spectral band of ICA having a maximum at  $812.46 \text{ cm}^{-1}$  (Table 3.3). In the second case, the spectral band of  $\nu_{\text{as}}(\text{O}=\text{C}=\text{N})$  (maximum at  $2344.96 \text{ cm}^{-1}$ ) for the ICA molecule is completely overlapped by the oversaturated spectral band of  $\nu_3(\text{CO}_2)$  lying in the wavenumber range of  $2100\text{-}2600 \text{ cm}^{-1}$ . Another spectral band of  $\nu(\text{N}-\text{H})$  (with the maximum at  $3703.26 \text{ cm}^{-1}$ ) for the ICA molecule is completely overlapped by the intensive spectral band of the  $\text{CO}_2$  combinational dyad ( $2\nu_2\nu_3+\nu_1\nu_3$ ) lying in the wavenumber range of  $3500\text{-}3850 \text{ cm}^{-1}$  (Figure 3.18).

Nevertheless, according to [26, 27], a tautomeric equilibrium between ICA and cyanic acid (CA) is possible ( $\text{H}-\text{N}=\text{C}=\text{O} \leftrightarrow \text{N}\equiv\text{C}-\text{O}-\text{H}$ ), where ICA is more stable, as shown by the quantum-chemical calculations [28]. Thus, we can expect the appearance of CA bands on the IR spectrum along with ICA spectral bands. Indeed, starting from  $120^\circ\text{C}$  two spectral bands centered at  $1088 \text{ cm}^{-1}$  and  $1231 \text{ cm}^{-1}$  appear on the IR spectrum. According to our calculations and database [29], these two bands can be assigned to  $\delta(\text{C}-\text{O}-\text{H})$  and  $\nu(\text{C}-\text{O})$  of CA. Also, two more spectral bands related to CA can be subtracted from the calculations, namely  $\nu(\text{N}\equiv\text{C})$  with a maximum at  $2389.32 \text{ cm}^{-1}$  and  $\nu(\text{O}-\text{H})$  with a maximum at  $3810.36 \text{ cm}^{-1}$ . However, as it was shown above, these two bands cannot be observed in the spectrum due to their overlapping with  $\nu_3$  spectral mode of  $\text{CO}_2$  and the combinational dyad ( $2\nu_2\nu_3+\nu_1\nu_3$ ) of  $\text{CO}_2$ , respectively.

Starting from  $150^\circ\text{C}$ , the intensity of the spectral contributions that are related to CBZ Conf. 1 reaches the lower identification threshold. Along with this, the total spectral intensity increases. It is accompanied by the appearance of a wide shoulder on the low-frequency slope of the  $\nu(\text{N}-\text{H})$  spectral band of the CBZ tautomeric form. Such a drastic change in the spectral behavior is associated with the criticality phenomena, more specifically, with the

appearance of the critical opalescence in the CO<sub>2</sub> phase. Similar behavior was explained for MFA.

### 3.2.3.2. Temperature range of 150-170°C

Subsequent increase in the temperature from 150 to 170°C results in a strong increase in the total spectral intensity of CBZ dissolved in the scCO<sub>2</sub> phase (Figure 3.22). This behavior is related to the phase transition region, namely, the melting of crystalline CBZ contacting the CO<sub>2</sub> phase. It is also proved by the results of visual control presented in Figure 3.16 that show CBZ melting at 160°C.

Moreover, one of the interesting peculiarities characterizing the spectra of the CBZ-scCO<sub>2</sub> binary mixture in this temperature range is the appearance of new spectral contributions related to the CBZ thermal degradation products (Figure 3.22). These new contributions were identified in both analytical spectral domains and were attributed to the vibrations of the functional groups of IMST and IMST-H<sup>+</sup> (Table 3.5). It is also necessary to note that the complex band related to the  $\nu(\text{C-H})$  vibrations has an obvious difference for CBZ and IMST in the spectral domain of 2800-3225 cm<sup>-1</sup>. Namely, when IMST appears in the system, two additional intensive spectral contributions arise at the low-frequency side of the CBZ  $\nu(\text{C-H})$  band (Figure 3.20).

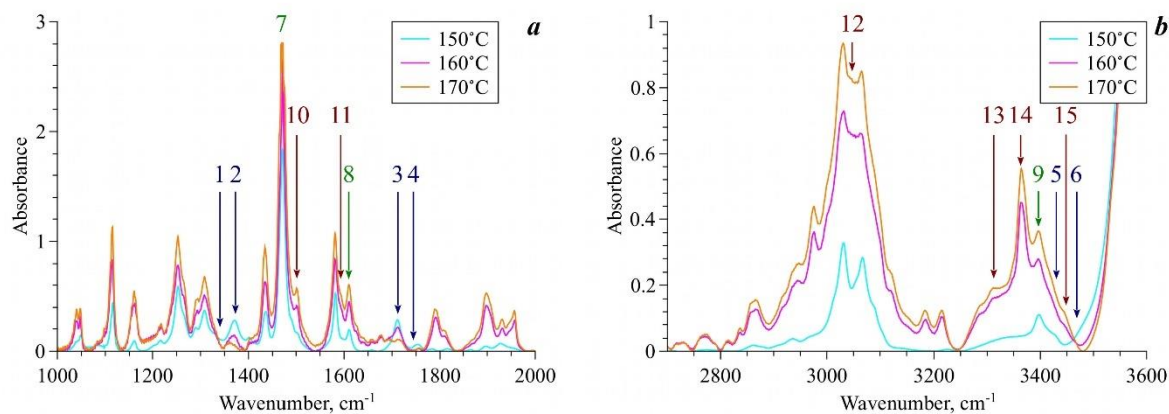


Figure 3.22. IR spectra of CBZ dissolved in the  $scCO_2$  phase permanently contacting with an excess of CBZ in isochoric heating conditions in the temperature range of 150-170°C ( $\Delta T=10^\circ C$ ) along the chosen isochore for two spectral ranges: (a) 1000-2000  $cm^{-1}$  and (b) 2700-3600  $cm^{-1}$ . The arrows with numbers show the analytical spectral bands determined by the quantum-chemical calculations. The assignments of these spectral bands are presented in Table 3.5.

Table 3.5. The assignments of the experimental spectral bands related to the vibrations of the functional groups of IMST and IMST- $H^+$  in two analytical spectral domains (1350-1850  $cm^{-1}$  and 3250-3550  $cm^{-1}$ ) based on the computational results are presented in Table 3.3. The additional spectral domain of 2800-3225  $cm^{-1}$  shows a set of unique spectral contributions of  $\nu(C-H)$  that exist only in the IMST spectrum (Figure 3.20 and Table 3.3).

1350-1850 $cm^{-1}$	2800-3225 $cm^{-1}$	3250-3550 $cm^{-1}$
10 - aromatic system vibration + $\rho(N-H)$ of IMST	12 - $\nu(C-H)$ of IMST	13 - $\nu_s(HN-H^+)$ IMST- $H^+$
11 - $\delta(H-N-H^+)$ of IMST- $H^+$		14 - $\nu_{as}(H-N-H^+)$ IMST- $H^+$
		15 - $\nu_s(N-H)$ of IMST

### 3.2.3.3. Temperature range of 170-200°C

The analysis of the spectral changes in the temperature range of 170-180°C (Figure 3.23) showed a considerable decrease in the total spectral intensity. Along with this, the spectral bands, which are related to the vibrations of IMST and IMST- $H^+$  completely disappear. The wide shoulder on the low-frequency slope of the  $\nu(N-H)$  spectral band of the CBZ tautomeric form as well

as the spectral contributions related to Conf. 2 also vanished. As a result, the CBZ tautomeric form prevailed in the scCO<sub>2</sub> phase.

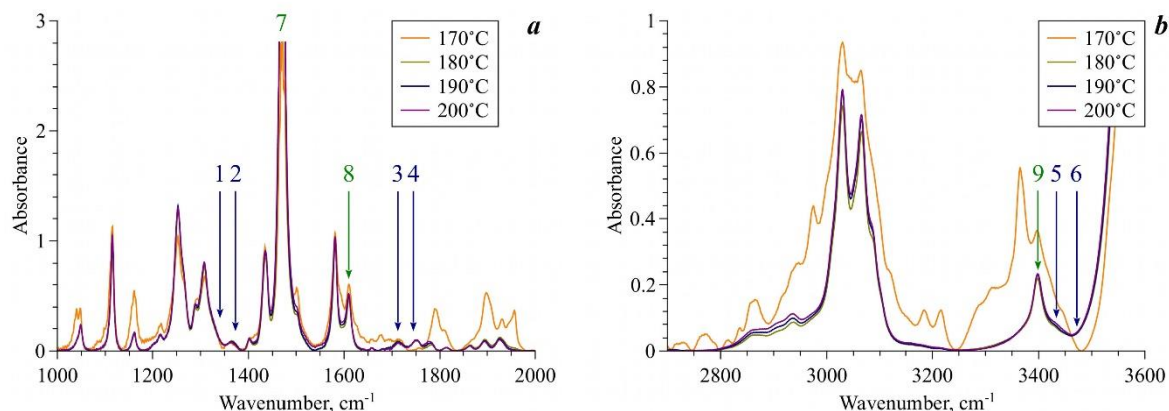


Figure 3.23. IR spectra of CBZ dissolved in the scCO<sub>2</sub> phase permanently contacting with an excess of CBZ in isochoric heating conditions in the temperature range of 170-200°C ( $\Delta T=10^\circ\text{C}$ ) along the chosen isochore for two spectral ranges: (a) 1000-2000 cm<sup>-1</sup> and (b) 2700-3600 cm<sup>-1</sup>. The arrows with numbers show the analytical spectral bands determined by quantum-chemical calculations.

Further heating from 180 to 200°C the spectral changes become monotonous that is generally typical of the thermal evolution of the equilibrium spectra. This behavior is the evidence of the CBZ concentration increase in the CO<sub>2</sub> phase, at that it is not accompanied by CBZ conformational transitions. The same as it was demonstrated for MFA in the CO<sub>2</sub> phase.

It is important to note that the disappearance of the spectral contributions related to IMST and IMST-H<sup>+</sup> correlates with crystallization from the scCO<sub>2</sub> phase of the yellow IMST crystals, the appearance of which is observed on the optical window surface at the temperature 170°C and above (Figure 3.16). Therefore, as far as only CBZ in the tautomeric form is present in the scCO<sub>2</sub> phase in the temperature range of 180-200°C, it may be expected that the

crystallization from such a SCF solution should lead to the formation of pure CBZ polymorph I.

Analyzing the data obtained for two systems: where solid-fluid equilibrium (CBZ solid - SCF solution) and liquid-fluid equilibrium (CBZ melt - SCF solution) are realized, we can assume that from a pharmaceutical perspective, especially in terms of fundamental understanding of such systems, the crystallization of pure polymorph I is more preferable from scCO<sub>2</sub> phase being in contact with CBZ melt. Indeed, taking into account the results obtained for the MFA, one can see that in the case of CBZ melt - SCF solution system, in scCO<sub>2</sub> phase there is only one CBZ conformer, and crystallization from such solution will lead to formation of polymorph I. On the contrary, when the CBZ solid - SCF solution interface exists, in scCO<sub>2</sub> phase there is conformational equilibrium that can shift toward certain conformer depending on parameters of state, and it will lead to change of polymorphic modification of drug solid being crystallized.

#### 3.2.4. Micro Raman spectroscopy analysis

In order to prove the aforementioned hypothesis, we analyzed the crystalline phase that was obtained by cooling the experimental cell (from 200°C to the ambient temperature) with subsequent depressurization and removal of the residual CO<sub>2</sub>. The crystalline sample extracted from the cell was a mixture of two crystalline structures (Figure 3.24): relatively large rhombic crystals (up to 0.5 mm) and long needle crystals (0.1×1 mm). These crystalline samples were studied by the micro Raman spectroscopy technique.

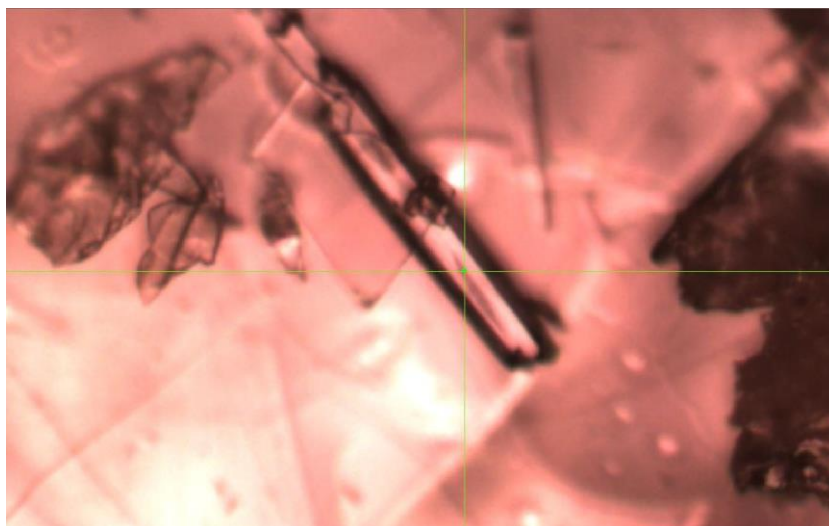


Figure 3.24. The micro-photo of the crystalline sample that was extracted from the experimental cell after its slow cooling down with the subsequent slow depressurization and removal of the residual CO<sub>2</sub>.

The obtained Raman spectra were compared to that of pure CBZ polymorph III, as well as to the spectra measured from the crystalline CBZ surface permanently contacting with CBZ saturated solution in scCO<sub>2</sub> at the temperatures of 40, 110, and 120°C [20] (Figure 3.25).

The spectral range (3300-3600 cm<sup>-1</sup>), that is associated with the stretching N-H vibrations, is more convenient for analyzing CBZ polymorphic forms. Indeed, in this spectral domain the characteristic spectral bands are well resolved and do not overlap each other (Figure 3.25b). An analysis of these spectra allowed us to conclude that the large rhombic crystals are IMST (the characteristic spectral band of  $\nu(\text{N-H})$  has a maximum at 3363 cm<sup>-1</sup>), whereas the long needle crystals have spectral signatures of both IMST and CBZ polymorph I, whose characteristic spectral band of  $\nu_s(\text{H-N-H})$  has a maximum at 3487 cm<sup>-1</sup> (see the spectrum «120°C CBZ in CO<sub>2</sub>» measured at 120°C from the CBZ surface permanently contacting with CO<sub>2</sub> [20]). Moreover, the spectrum of the needle crystals does not show the spectral signatures of CBZ polymorph III, whose characteristic spectral band of  $\nu_s(\text{H-N-H})$  has a maximum at 3468 cm<sup>-1</sup> (see the spectra: «Initial CBZ room T», «40°C CBZ in CO<sub>2</sub>» and «40°C CBZ in

CO<sub>2</sub>» [20]). This fact means that the CBZ, which presents at 200°C preferably in tautomeric form, crystallizes into polymorph I when cooling down.

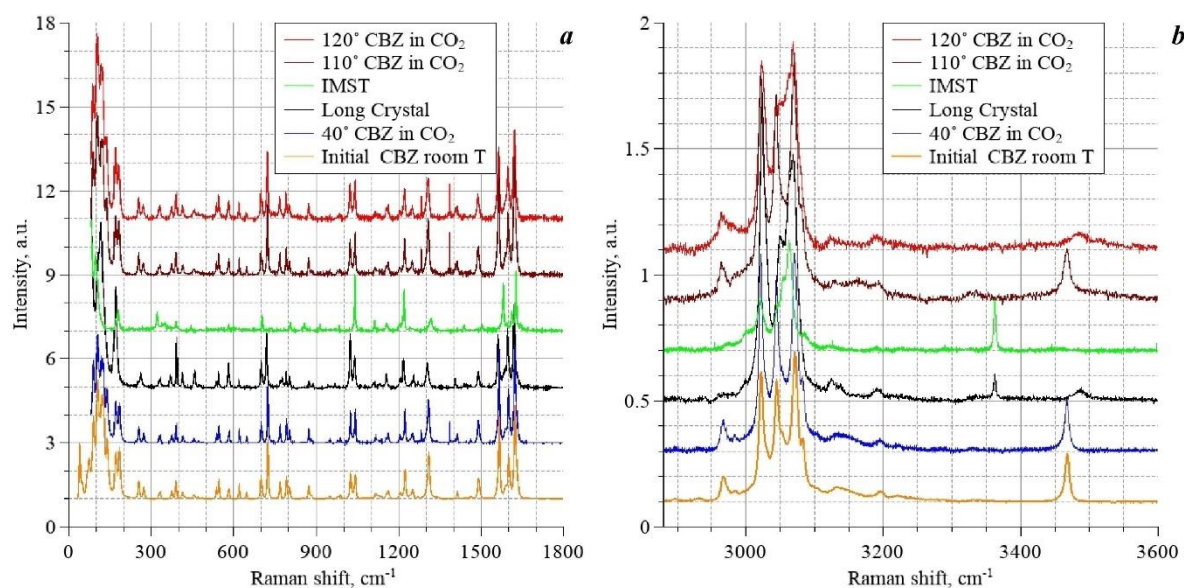


Figure 3.25. The Raman spectra in two wavenumber ranges (0–1800 cm<sup>-1</sup> and 2875–3600 cm<sup>-1</sup>) of the crystalline sample extracted from the experimental cell (Long Crystal and IMST), as compared to that of pure CBZ polymorph III (initial CBZ form), as well as compared to the Raman spectra measured from the crystalline CBZ surface permanently contacting with CBZ saturated solution in scCO<sub>2</sub> at the temperatures of 40, 110, and 120°C [20] along the same isochore.

Thus, the obtained results showed that though the initial CBZ being in bottom phase of two-phase system partially decomposes with formation of IMST, the last has not been found in scCO<sub>2</sub> phase in the temperature range of (180-200°C). Such phenomenon is mainly related to the difference of CBZ and IMST solubilities in scCO<sub>2</sub> (solubility of IMST is much lower that is related to its molecular structure), as well as to the difference of their melting temperatures ( $T_{\text{melt}}(\text{CBZ III}) < 170^\circ\text{C}$ ,  $T_{\text{melt}}(\text{IMST}) = 197^\circ\text{C}$ ). Consequently, dissolution of CBZ in scCO<sub>2</sub> phase will lead to the IMST crystallization from solution (salting out effect) without its melting. Therefore, one can suppose that if the RESS procedure is realized directly from the scCO<sub>2</sub> phase containing only the CBZ

molecules existing in its tautomeric form, pure crystalline CBZ polymorph I (without an IMST admixture) can be obtained. Moreover, the probable admixture of ICA dissolved in scCO<sub>2</sub> will be also removed from the target product along with CO<sub>2</sub>, upon their transition into the gaseous phase at adiabatic expansion.

### **3.3. Supercritical fluids for the synthesis of single crystals**

Recrystallization from scCO<sub>2</sub> showed itself an effective way to crystallize the desired polymorphic modifications. However, the method based on the control over the conformations of bioactive molecules gives a possibility to monitor exactly just the solution phase. At this time, the solid, which is important during the crystallization, stays out of observation and so it is controlled indirectly. Of course, the *in situ* Raman spectroscopy partly helps to solve this issue, but without the reference spectra of individual polymorphic modifications the unambiguous determination of qualitative and, moreover, the quantitative composition of the product of recrystallization is almost impossible.

We decided to modify the method of recrystallization from scCO<sub>2</sub> proposed in the previous two sections of this thesis for obtaining the crystalline phase difficult to analyze with Raman spectroscopy, the co-crystal of MFA and NA. Using the powder and single-crystal X-ray diffraction, as well as DRIFTS, we searched for the optimal condition of the synthesis and formed the set of reference powder patterns and IR spectra for the MFA-NA co-crystal for further express analysis. The effect of RESS was checked as it was proposed for carbamazepine and its yield was compared with our method.

#### **3.3.1. High-pressure high-temperature reactor**

For this work, the special high-pressure high-temperature was applied in combination with a magnetic stirrer with heater. To start the experiment, the initial component, namely MFA and NA, were dried under vacuum equal to

$10^{-4}$  bar at  $60^{\circ}\text{C}$ . Further, they were introduced in the high-pressure high-temperature reactor and were further mixed with  $\text{CO}_2$  in the system shown at the Figure 3.26. The reactor was isolated with graphite packing rings and pumped for 24h to reduce the impact of the moisture at the solid mixture of MFA and NA-fluid interface. Then the reactor was refilled with  $\text{CO}_2$  and slowly heated ( $1^{\circ}\text{C}/\text{min}$ ) by a cuff-heater to a constant temperature ( $40$  or  $90^{\circ}\text{C}$ ) below the melting temperature of the initial powders or the co-crystal and, in particular, below the melting point of NA. The contents of the HTHP were compressed to a pressure corresponding to 1.1 critical density of  $\text{CO}_2$  (equal to  $11.687 \text{ mol}\cdot\text{L}^{-1}$  according to NIST database [30]). The pressure in the reactor was 91 and 193 bars at  $40$  and  $90^{\circ}\text{C}$ , respectively, according to isochoric conditions. The reactor was isolated during the whole duration of the synthesis (4 days or 3 weeks) with constant stirring (300 rpm). MFA:NA mixing ratios of 2:1, 1:1 and 1:2 were tested.

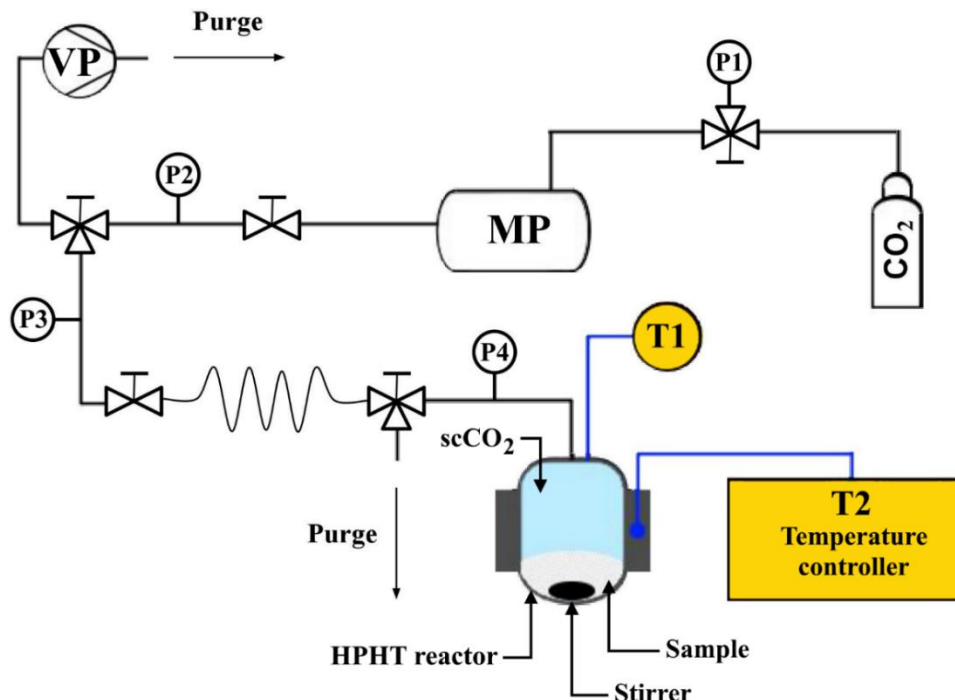


Figure 3.26. The experimental setup used for the synthesis of the MFA:NA co-crystal: P1-P4 are the pressure sensors; T1 - temperature in-cell sensor; T2 - temperature sensor-controller of the cuff-heater; MP - manual press; VP - vacuum pump.

### 3.3.2. Effect of temperature, solid mixture composition and time duration of the co-crystallization process

In the first stage of our work, we analyzed the effect of the temperature (40°C and 90°C), the mixture composition (MFA:NA mixing molar ratio of 2:1, 1:1 and 1:2) and the time duration (4 days and three weeks) on the co-crystallization process. We have then systematically analyzed the composition of the synthesized solid form. Our analysis was based on comparing the X-ray diffraction patterns of the synthesized solids at the different temperatures, mixture compositions and duration times of the co-crystallization process with that measured for the corresponding physical mixture of the initial components without co-crystallization and the one calculated, using the Mercury program, for the co-crystallized sample (single crystal data).

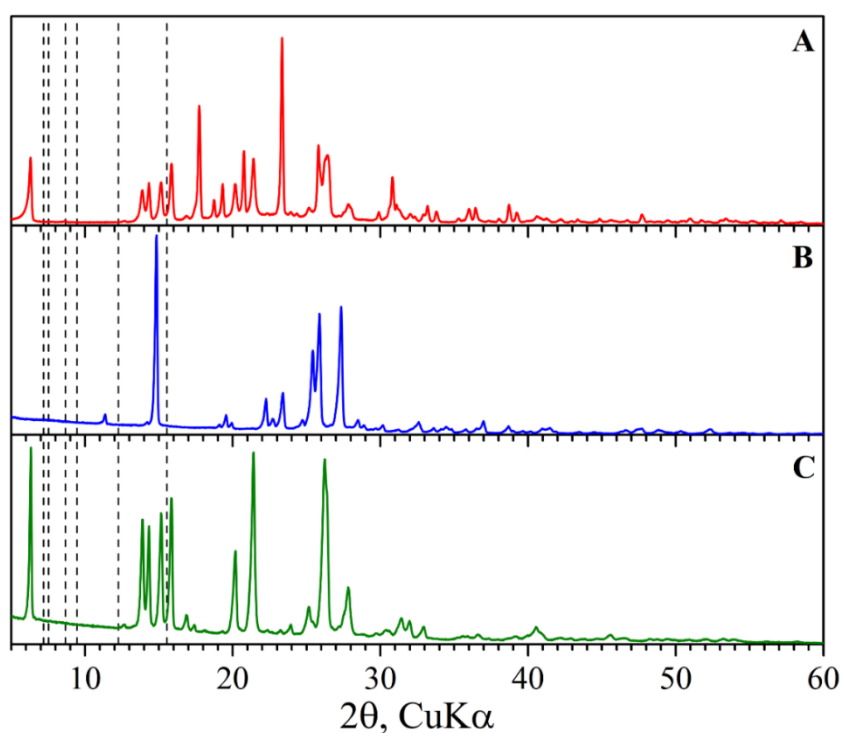


Figure 3.27. Comparison of the experimental X-ray diffraction patterns of the synthesized powder obtained at 40°C with an acquisition time of 3 weeks (A) and the ones for the initial NA (B) and MFA (C). The characteristic peaks appearing on co-crystallization are marked with dashed lines.

The results of PXRD analysis showed that the synthesis was not successful at 40°C for all the ratio of initial components and for both duration times. Indeed, as it is illustrated, for the 1:2 mixture in Figure 3.27, the obtained powder X-ray diffraction patterns did not correspond to the 1:2 co-crystal but coincide to larger extent with that of the initial compounds. However, at 90°C, as it is shown in Figure 3.28, the emergence of new peaks in the X-ray powder patterns at  $2\theta$  angles of 7.20°, 7.52°, 8.68°, 9.44°, 12.26°, 15.54° evidences the formation of a powder co-crystal phase. More precisely, the semi-quantitative analysis of PXRD data showed that uniquely the co-crystal with stoichiometry 1:2 of MFA to NA was formed.

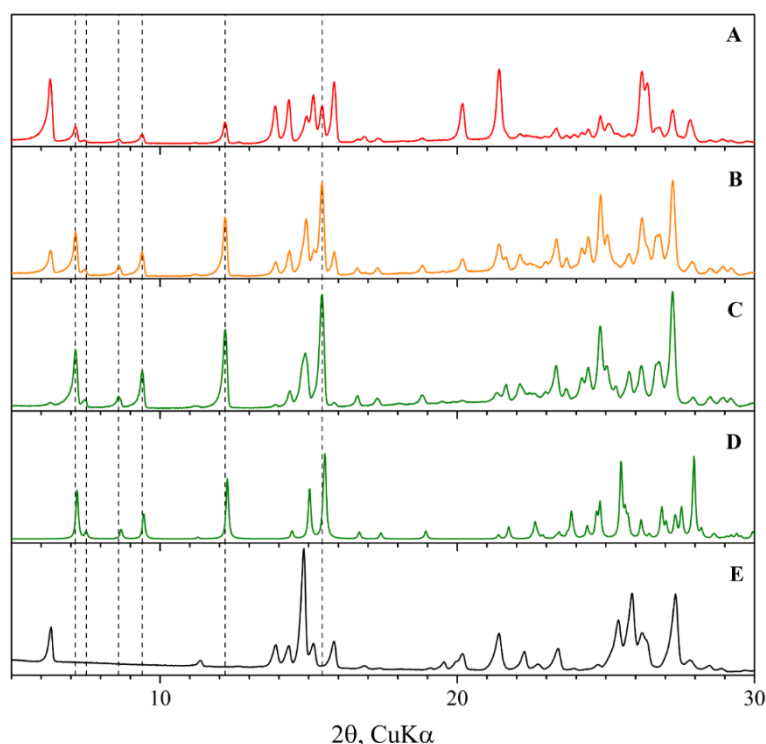


Figure 3.28. Comparison between the experimental X-ray powder diffraction patterns of the synthesized powder at 90°C with the acquisition time of 4 days in the cases where mefenamic acid and nicotinamide are mixed in the ratio 2:1 (A), 1:1 (B), 1:2 (C) and the sum of the diffractograms of the initial components mixed physically without co-crystallization in the 1:2 ratio (E). The calculated X-ray powder pattern of the synthesized single co-crystal with the 1:2 ratio of MFA:NA (D). The characteristic peaks appearing on co-crystallization are marked with dashed lines.

The estimation of the co-crystal yield at different temperatures and acquisition times showed no significant difference between the 4 days and 3 weeks (the powder part of the obtained sample) durations. As shown in Table 3.6, the co-crystal yield estimation at 90°C is obviously high, of about 90%, when the initial mixing ratio of MFA and NA is 1:2. The residual quantity of the MFA varies from sample to sample with the 1:2 MFA:NA ratio, but stays less than 10% (weight) on average. It indicates some incompleteness of co-crystallization within 4 days.

Table 3.6. The initial ratio of MFA and NA, the residual polymorphic form I of MFA in the product and the yields (%) of the co-crystal according to the semi-quantitative analysis of the PXRD data that were obtained at 90°C and the acquisition time of 4 days.

Initial molar ratio of the components (MFA:NA)	$\omega(\text{MFA}), \%$	$\omega(\text{co-crystal}), \%$
2:1	75	25
1:1	33	67
1:2*	>10	90

\*The traces of initial NA were found together with MFA, but their quantification was impossible due to low values.

The changes in the interactions during the powder co-crystal formation are another point of interest. Thus, we recorded the DRIFT spectra of the synthesized powder co-crystal and we compared them with those of the corresponding initial no processed MFA and NA powders (Figure 3.29). Our results show that there are no significant changes in the position of MFA vibration modes (less than  $5 \text{ cm}^{-1}$ ). On the contrary, the shifts of the NA vibration modes positions [31-33] in the DRIFT spectra is considered a spectral signature of the formation of new intermolecular hydrogen bonds in the obtained co-crystal (Table 3.7). Thus, the DRIFT spectra can be used for the quick identification of co-crystal formation.

Table 3.7. Wavenumbers ( $\text{cm}^{-1}$ ) of the peaks in DRIFTS shifted during the powder co-crystal formation (secondary peaks constituents are put in brackets).

Vibration type	Co-crystal	NA	MFA
	3307	-	3311
N-H stretch	3165	3157	-
	3386 (3402)	3361	-
N-H bend	1577 (1591)	-	1576
C=O stretch	1649	-	1647
	1684	1674	-

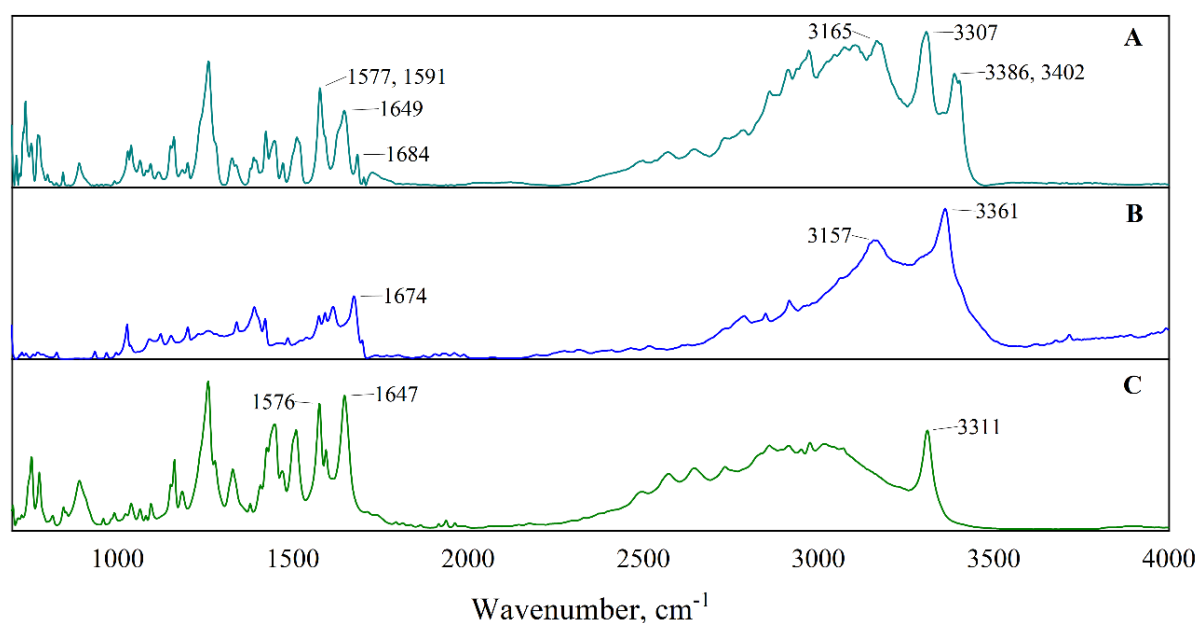


Figure 3.29. DRIFT spectra of MFA-NA powder co-crystal (A) as well as the initial components: NA (B) and MFA (C). The changes in the positions of the peaks during the co-crystal formation are marked (the main component position is followed by the secondary constituent in the case of the complex peaks in co-crystal).

### 3.3.3. Comparison with the rapid expansion of supercritical solution experiment

As the second step of this work, we aimed to compare the obtained powder co-crystal of MFA:NA in the ratio 1:2 at  $90^{\circ}\text{C}$ , the pressure of 193 bars and the duration of 4 days with that obtained using RESS experiment in the same thermodynamic conditions. To this purpose, the extraction unit of the

RESS set up was filled with the initial MFA and NA mixture with molar ratio 1:2 and CO<sub>2</sub> was kept under the constant pressure of 193 bars at a temperature of 90°C for 24 hours for the initial conversion of MFA-NA mixture to co-crystal phase. The supercritical solution was expanded through a 100 μm sapphire nozzle into the dry expansion chamber by cycles: 5 pulverizations of 20 seconds each followed by a break for dissolution within 2 hours. The temperature of the nozzle was set to 50°C. The detailed experimental scheme is shown in Figure 3.30.

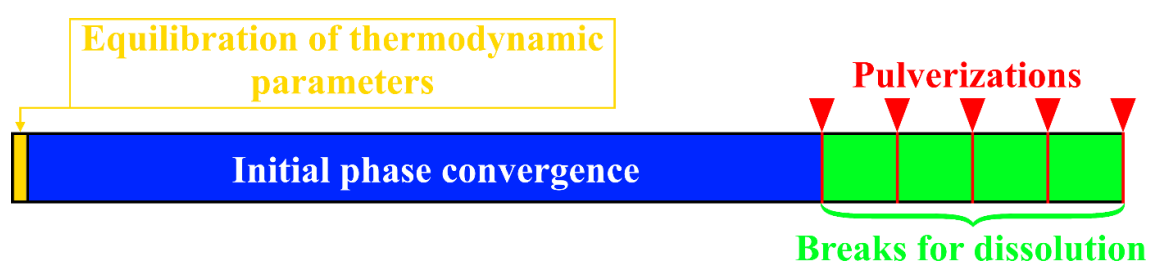


Figure 3.30. Stages of the RESS experiment for MFA-NA (1:2) mixture.

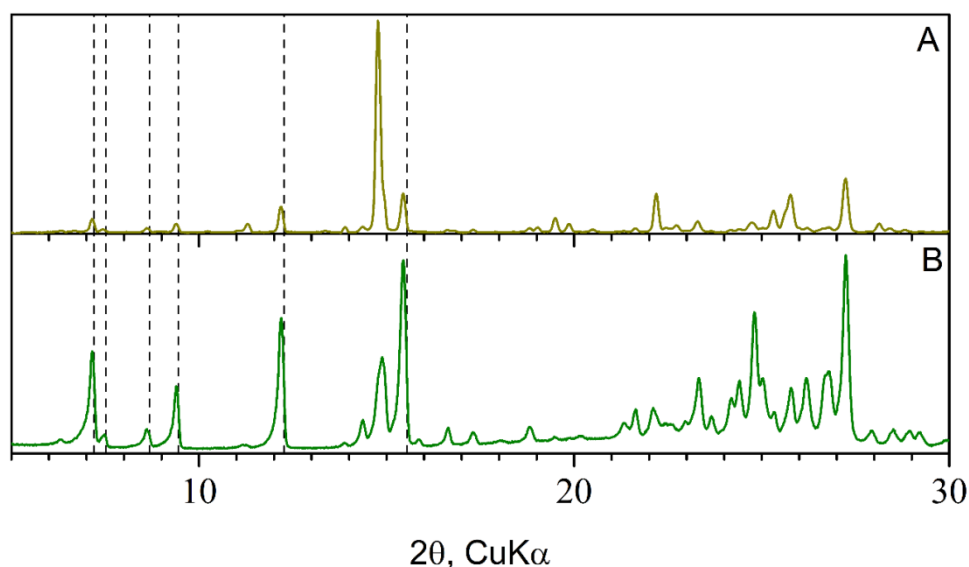


Figure 3.31. Comparison between the experimental powder X-ray diffraction patterns of the synthesized co-crystal of mefenamic acid and nicotinamide using the RESS experiment (A) and the HPHT reactor (B). The characteristic peaks appearing on transformation are marked with dashed lines.

The X-ray diffraction patterns of the powders obtained by the two methods are compared in Figure 3.31. Their semi-quantitative analysis indicates that near 20% of the initial components mixture was converted into the co-crystal using the RESS technique while with the method using the HPHT reactor about 90% was transformed in the co-crystal even in a relatively short 4 days experiment. This demonstrates the efficiency of our methodology in comparison with the classical fast kinetically controlled method without the addition of any non-ecofriendly solvent. It shows that the quick kinetically controlled RESS method, which worked exactly on the solution phase, may result in the formation of the phase different than the one obtained during continuous crystallization in the HPHT reactor. Thereby, the question stays open as for the current experiment, as for the experiments on conformational control of the MFA and CBZ described in the previous sections of this chapter about the mechanism of solid phase formation.

#### 3.3.4. Synthesis of single crystals of the mefenamic acid : nicotinamide co-crystal

The last point discussed in this section is our main finding, namely it is the synthesis of the single crystal of MFA:NA co-crystal. As it is shown in Figure 3.32, after processing the MFA and NA raw powders for two test duration times: 4 days and 3 weeks, the single crystals were grown only at 90°C with the acquisition time of 3 weeks. For the shorter duration, as it is seen (Figure 3.32a), the product obtained is a powdery mass due to the large excess of initial components, however, in the long-term synthesis (Figure 3.32b) thin needle-shaped crystals up to 2 cm length and to 1 mm width were grown.



Figure 3.32. The morphology changes due to different acquisition times: a powdery product from 4-days (A) and crystals from 3-weeks (B) experiments obtained at 90°C with the 1:2 initial ratio of MFA to NA.

Table 3.8. Comparison of the crystallographic data received by us from SCXRD and powder synchrotron experiment [35].

	Current work	L. Fábíán [et al.]
Formula	$C_{15}H_{15}NO_2, 2(C_6H_6N_2O)$	$C_{27}H_{27}N_5O_4$
formula weight	485.54	485.54
crystal system	triclinic	Triclinic
space group	P-1	P-1
a (Å)	3.9660(3)	4.064104(14)
b (Å)	12.4578(9)	12.50989(5)
c (Å)	23.9391(14)	24.08865(10)
$\alpha$ (°)	100.041(3)	99.8930(4)
$\beta$ (°)	91.621(3)	90.7285(4)
$\gamma$ (°)	91.820(4)	92.4340(4)
V (Å <sup>3</sup> )	1163.38(14)	1205.154(8)
Z	2	2
$D_c$ (g*cm <sup>-3</sup> )	1.386	1.338
$\lambda$ (Å)	0.71073	1.0002
T (K)	100.05	295
2 $\theta$ range (°)	3.322 – 60.942	2 – 60
data / parameters / restraints	7047 / 351 / 0	15388/240/206
R indices (all data)	$R_1 = 0.0648$ $wR_2 = 0.1259$	$R_p = 0.004, R_{wp} = 0.006,$ $R_{exp} = 0.004$
goodness of fit	S = 1.028	$\chi^2 = 2.574$
largest diff. peak and hole (e Å <sup>-3</sup> )	0.401 / -0.233	0.33/0.33

Their structure has been determined by SCXRD (Table 3.8). The numbering of atoms is displayed in Figure 3.33. It is shown that the benzene fragments are turned relative to each other by  $52^\circ$ . This twist is probably caused by steric repulsion between them (the shortened intramolecular contacts are C6...C10 (2.39 Å), H6...C10 (2.82 Å), C6...H10 (2.58 Å), C1...H10 (2.67 Å) as compared to van der Waals radii sum [34] C...C (2.42 Å) and H...C (2.87 Å)). The formation of the N1-H1...O1 intramolecular hydrogen bond (Table. 3.9) between the carboxyl and amino groups causes the coplanarity of the carboxyl group to the aromatic cycle as well as the stronger conjugation of the nitrogen lone pair with carboxyl substituted benzene ring leading to non-equivalence of the N1-C9 and N1-C1 bonds (1.370(2) Å and 1.409(2) Å respectively). As a result, the molecular conformation change of the MFA molecule can occur only due to the rotation around the C1-N1 bond. The carbamide groups of both NA molecules, found in the unit cell asymmetric part, are noticeably turned relative to the pyridine planes (the  $C_{ar}-C_{ar}-C_{sp^2}=O$  torsion angles are  $15^\circ$  and  $24^\circ$  for molecules A and B, respectively) despite a conjugation between the carbonyl group and aromatic system. It may be presumed that such a non-planarity is caused by the influence of intermolecular hydrogen bonds formation.

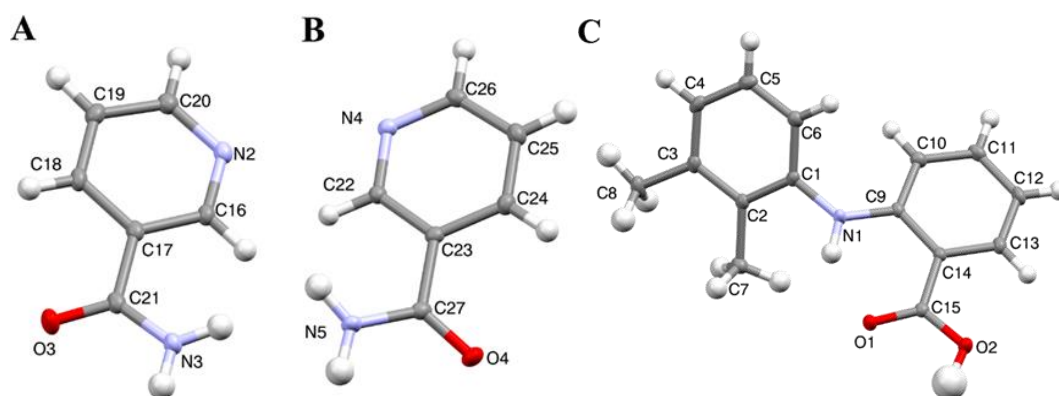


Figure 3.33. Structure of the molecules involved in the MFA:NA co-crystal: A - NA (A), B - NA (B), C - MFA.

The analysis of intermolecular interactions (Table 3.9) in the co-crystal has revealed that two NA molecules differ by their arrangements and role in the crystal structure formation. NA (B) is bound with MFA molecule due to the O2-H2...N4 intermolecular linear hydrogen bond as well as with NA (A) due to the N5-H5A...N2 linear hydrogen bond. On contrary, NA (A) is bound with two NA molecules: with NA (A) through the N3-H3B...O3 intermolecular centrosymmetric hydrogen bond and with NA (B) through the above mentioned N5-H5A...N2 linear hydrogen bond. As a result, hexamer (Figure 3.34) containing two MFA and four NA molecules may be separated out as some structural fragment of the co-crystal. The MFA molecules form a sole hydrogen bond, O2-H2...N4, which may explain the previously stated higher availability of MFA in co-crystal in comparison with the pure component.

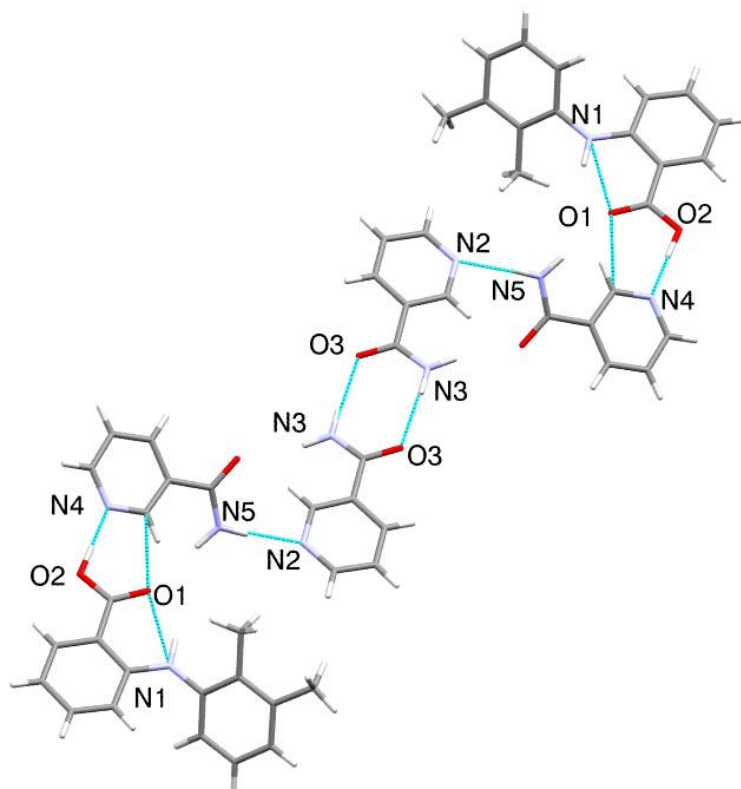


Figure 3.34. Hexameric building unit formed by intermolecular hydrogen bonds in the structure of the MFA:NA co-crystal. The atoms involved in the hydrogen bonds are marked.

Table 3.9. Geometric characteristics of hydrogen bonds involved in the 1:2 MFA:NA co-crystal.

Hydrogen bond	Symmetry operation	d(H...A), Å	∠(D-H...A), °
N1-H1...O1	x,y,z	1.91(2)	140(2)
O2-H2...N4	-x,1-y,1-z	1.63(3)	175(2)
N5-H5B...O1	1-x,1-y,1-z	2.18(2)	171(2)
N5-H5A...N2	2-x,1-y,1-z	2.04(2)	175(2)
N3-H3A...O4	1-x,1-y,1-z	2.21(2)	172(2)
N3-H3B...O3	-x,-y,2-z	2.04(2)	172(2)

### 3.4. Conclusions

The conformational equilibria were studied for MFA and CBZ molecules in their saturated solutions in supercritical carbon dioxide being in contact with bottom phase containing different polymorphs of APIs, under isochoric heating conditions in the temperature ranges of 80-220°C and 110-200°C respectively. In order to understand the conversion mechanism between the conformations in solution and, as a consequence, crystallization of different polymorphic modifications of the aforementioned drugs, the two new methods of *in situ* control were applied:

- *In situ* IR spectroscopy was used and supplemented with quantum-chemical calculations to analyze the fluid phase.
- *In situ* Raman spectroscopy was applied for the solid phase characterization.

The correlations were found between the polymorphic modifications of the crystalline forms and the conformers of bioactive molecules in the CO<sub>2</sub> rich phase, which occurs as a consequence of equality of chemical potentials of API in the solid phase and the corresponding bioactive molecule conformer in solution. So that the transformation of polymorph leads to change of chemical potential of solid phase which in turn should result in the change of chemical

potential of another phase as follows from conformational transition. The systems «API solid - SCF solution» and «API melt - SCF solution» were studied and the following global suggestion on crystallization conditions was formulated. To prepare the pure polymorphic modification of an API by crystallization from its solution the corresponding bioactive molecules in the CO<sub>2</sub> rich phase should remain in one conformation at the moment of the pressure release. In its turn, this conformation should be strictly defined from the joint studies of the solid or melted API together with its solution.

The method able to simplify the further analysis of the polymorphic composition of the recrystallized product was proposed as well on the example of MFA:NA co-crystal. Based on the fact of growth of the single crystal directly from the API solution in scCO<sub>2</sub>, it allows determining the structure of the acquired solid phase to compute the reference powder pattern and to use it further verification of the other fast analytical techniques discussed in Section 1.6, as DRIFT spectra studied by us.

### 3.5. References for Chapter 3

- (1) Gilpin, R.K.; Zhou, W. Infrared studies of the thermal conversion of mefenamic acid between polymorphic states. *Vibrational Spectroscopy* **2005**. *37* (1), 53-59.
- (2) Cesur, S.; Gokbel, S. Crystallization of mefenamic acid and polymorphs. *Crystal Research and Technology* **2008**. *43* (7), 720-728.
- (3) Zeinolabedini Hezave, A.; Khademi, M.H.; Esmaeilzadeh, F. Measurement and modeling of mefenamic acid solubility in supercritical carbon dioxide. *Fluid Phase Equilibria* **2012**. *313*, 140-147.
- (4) Cunha, V.R.R.; Izumi, C.M.S.; Petersen, P.A.D.; Magalhães, A.; Temperini, M.L.A., *et al.* Mefenamic acid anti-inflammatory drug: Probing its polymorphs by vibrational (IR and Raman) and solid-state NMR spectroscopies. *The Journal of Physical Chemistry B* **2014**. *118* (16), 4333-4344.
- (5) Oparin, R.D.; Ivlev, D.V.; Vorobei, A.M.; Idrissi, A.; Kiselev, M.G. Screening of conformational polymorphism of ibuprofen in supercritical CO<sub>2</sub>. *Journal of Molecular Liquids* **2017**. *239*, 49-60.
- (6) Lemert, R.M.; Johnston, K.P. Solid-liquid-gas equilibria in multicomponent supercritical fluid systems. *Fluid Phase Equilibria* **1989**. *45* (2), 265-286.
- (7) Uchida, H.; Yoshida, M.; Kojima, Y.; Yamazoe, Y.; Matsuoka, M. Measurement and correlation of the solid-liquid-gas equilibria for the carbon dioxide + S-(+)-Ibuprofen and carbon dioxide + RS-(±)-Ibuprofen systems. *Journal of Chemical & Engineering Data* **2005**. *50* (1), 11-15.
- (8) Takebayashi, Y.; Sue, K.; Furuya, T.; Hakuta, Y.; Yoda, S. Near-infrared spectroscopic solubility measurement for thermodynamic analysis of melting point depressions of biphenyl and naphthalene under high-pressure CO<sub>2</sub>. *The Journal of Supercritical Fluids* **2014**. *86*, 91-99.
- (9) Oparin, R.D.; Moreau, M.; de Walle, I.; Paolantoni, M.; Idrissi, A., *et al.* The interplay between the paracetamol polymorphism and its molecular structures dissolved in supercritical CO<sub>2</sub> in contact with the solid phase: In situ vibration spectroscopy and molecular dynamics simulation analysis. *European Journal of Pharmaceutical Sciences* **2015**. *77*, 48-59.
- (10) Abbas, N.; Oswald, I.D.H.; Pulham, C.R. Accessing mefenamic acid form II through high-pressure recrystallisation. *Pharmaceutics* **2017**. *9* (2), 16-27.
- (11) McConnell, J.F.; Company, F.Z. Mefenamic acid. *Crystal Structure Communications* **1976**. *5*, 861.
- (12) Seethalekshmi, S.; Guru Row, T.N. Conformational polymorphism in a non-steroidal anti-inflammatory drug, mefenamic acid. *Crystal Growth & Design* **2012**. *12* (8), 4283-4289.
- (13) Macrae, C.F.; Sovago, I.; Cottrell, S.J.; Galek, P.T.A.; McCabe, P., *et al.* Mercury 4.0: From visualization to analysis, design and prediction. *Journal of Applied Crystallography* **2020**. *53* (1), 226-235.
- (14) Jabeen, S.; Dines, T.J.; Leharne, S.A.; Chowdhry, B.Z. Raman and ir spectroscopic studies of fenamates – conformational differences in polymorphs of flufenamic acid, mefenamic acid and tolfenamic acid. *Spectrochimica Acta Part A: Molecular and Biomolecular Spectroscopy* **2012**. *96*, 972-985.
- (15) Khodov, I.A.; Belov, K.V.; Efimov, S.V.; Batista de Carvalho, L.A.E. Determination of preferred conformations of mefenamic acid in DMSO by NMR spectroscopy and GIAO calculation. *AIP Conference Proceedings* **2019**. *2063* (1), 040007 (1-5).
- (16) Forbes, J.W.: First-order polymorphic and melting phase transitions under shock loading. In *Shock wave compression of condensed matter: A primer*; Springer Berlin Heidelberg: Berlin, Heidelberg, 2012, pp. 201-241.

- (17) Grzesiak, A.L.; Lang, M.; Kim, K.; Matzger, A.J. Comparison of the four anhydrous polymorphs of carbamazepine and the crystal structure of form I. *Journal of Pharmaceutical Sciences* **2003**. *92* (11), 2260-2271.
- (18) Qi, Z.-L.; Zhang, D.-F.; Chen, F.-X.; Miao, J.-Y.; Ren, B.-Z. Thermal decomposition and non-isothermal decomposition kinetics of carbamazepine. *Russian Journal of Physical Chemistry A* **2014**. *88* (13), 2308-2313.
- (19) Schollee, Jennifer, Schymanski, Emma, Stravs, Michael, Gulde, Rebekka, Thomaidis, Nikolaos, & Hollender, Juliane. (2020). S66 | EAWAGTPS | Parent-Transformation Product Pairs from Eawag (Version NORMAN-SLE-S66.0.1.2) [Data set]. Zenodo. <http://doi.org/10.5281/zenodo.3829088>
- (20) Oparin, R.D.; Kurskaya, M.V.; Krestyaninov, M.A.; Idrissi, A.; Kiselev, M.G. Correlation between the conformational crossover of carbamazepine and its polymorphic transition in supercritical CO<sub>2</sub>: On the way to polymorph control. *European Journal of Pharmaceutical Sciences* **2020**. *146*, 105273 (1-8).
- (21) Pinto, M.A.L.; Ambrozini, B.; Ferreira, A.P.G.; Cavaleiro, É.T.G. Thermoanalytical studies of carbamazepine: Hydration/dehydration, thermal decomposition, and solid phase transitions. *Brazilian Journal of Pharmaceutical Sciences* **2014**. *50*, 877-884.
- (22) Tandarić, T.; Vrček, V.; Šakić, D. A quantum chemical study of hocl-induced transformations of carbamazepine. *Organic & Biomolecular Chemistry* **2016**. *14* (46), 10866-10874.
- (23) Tian, L.; Bayen, S.; Yaylayan, V. Thermal degradation of five veterinary and human pharmaceuticals using pyrolysis-gc/ms. *Journal of Analytical and Applied Pyrolysis* **2017**. *127*, 120-125.
- (24) Naguib, I.A.; Elyazeed, N.A.; Elroby, F.A.; El-Ghobashy, M.R. Stability indicating spectrophotometric methods for quantitative determination of carbamazepine and its degradation product, iminostilbene, in pure form and pharmaceutical formulations. *Spectrochimica Acta Part A: Molecular and Biomolecular Spectroscopy* **2019**. *214*, 21-31.
- (25) ChemSRC, Isocyanic acid, [Online] [https://www.chemsrc.com/en/cas/75-13-8\\_401667.html](https://www.chemsrc.com/en/cas/75-13-8_401667.html)
- (26) Jacox, M.E.; Milligan, D.E. Low-temperature infrared study of intermediates in the photolysis of HNCO and DNCO. *The Journal of Chemical Physics* **1964**. *40* (9), 2457-2460.
- (27) Belson, D.J.; Strachan, A.N. Preparation and properties of isocyanic acid. *Chemical Society Reviews* **1982**. *11* (1), 41-56.
- (28) Nguyen Huu, T. Thermokinetic study of the isomerization of isocyanic acid. *Vietnam Journal of Chemistry* **2017**. *55* (4), 1-6.
- (29) NIST, Cyanic acid, [Online] <https://webbook.nist.gov/cgi/cbook.cgi?ID=C420053&Mask=800>
- (30) Span, R.; Wagner, W. A new equation of state for carbon dioxide covering the fluid region from the triple-point temperature to 1100 K at pressures up to 800 MPa. *Journal of Physical and Chemical Reference Data* **1996**. *25* (6), 1509-1596.
- (31) Utami, D.; Nugrahani, I.; Ibrahim, S. Formation and characterization of mefenamic acid-nicotinamide cocrystal during co-milling based on X-ray powder diffraction analysis. *Journal of Applied Pharmaceutical Science* **2016**. *6*, 075-081.
- (32) Utami, D.; Nugrahani, I.; Ibrahim, S. Mefenamic acid-nicotinamide co-crystal synthesized by using melt crystallization method and its solubility study. *Asian Journal of Pharmaceutical and Clinical Research* **2017**. *10* (5), 135-139.
- (33) Wichianphong, N.; Charoenchaitrakool, M. Statistical optimization for production of mefenamic acid-nicotinamide cocrystals using gas anti-solvent (GAS) process. *Journal of Industrial and Engineering Chemistry* **2018**. *62*, 375-382.

- (34) Zefirov, Y.V. Comparative analysis of systems of van der Waals radii. *Crystallography Reports (Kristallografiya)* **1997**. *42 (1)*, 111-116.
- (35) Fábíán, L.; Hamill, N.; Eccles, K.S.; Moynihan, H.A.; Maguire, A.R., *et al.* Cocrystals of fenamic acids with nicotinamide. *Crystal Growth & Design* **2011**. *11 (8)*, 3522-3528.

## Chapter 4. Analysis of solid-solid polymorphic transformations

*The material presented in this chapter forms the basis of publication*

Vaksler, Ye. A.; Idrissi, A.; Urzhuntseva, V. V.; Shishkina, S. V. Quantum chemical modeling of mechanical properties of aspirin polymorphic modifications. **Cryst. Growth Des.** 2021, 21 (4), 2176-2186.

Vaksler, Ye. A.; Idrissi, A.; Shishkina, S. V. High-pressure influence on piracetam crystals: studying by quantum chemical methods. Under review in **Cryst. Growth Des.**

The process of obtaining the dosage form does not end with the crystallization of the polymorphic modification of the API, it is followed by their processing and storage. Polymorphic transformations, i.e. first-order phase transitions according to the modern classification of Yu. Mnyukh [1-3], and in particular solid-solid transitions between polymorphic modifications of APIs, are a widespread phenomenon in the pharmaceutical industry. Along with the crystallization of the desired form, the problem of changing the crystal structure and, as a result, the properties of dosage forms requires a solution.

Obviously, polymorphic transformations during processing and storage (for example, tableting) are associated with the mechanical properties of crystalline APIs, more precisely, with the resistance of the solid phase to external (milling, pressure, etc.) and internal (low stability of a form) influences. The main numerical equivalent of such resistance is the energy required by the system for transformation. Many methods for assessing such barriers based on the unchanged static structure of crystals exist at the moment. However, the more realistic behavior of fragments of the crystal structure (molecules or other building units) during shear has been practically non-studied. In this chapter, we propose a new computational method that allows one to evaluate the mechanical properties and the probability of a polymorphic transformation based on the data of pairwise interactions in a crystal during the mutual movement of its basic structural motifs. This method is based on the experimentally determined crystal structure of the initial polymorphic modification before treatment or storage (like the one for MFA:NA co-crystal). Its effectiveness was assessed using three classical APIs: aspirin, piracetam, and ibuprofen.

## **4.1. Quantum-chemical modeling of mechanical properties of aspirin polymorphic modifications**

4.1.1. The crystal packing analysis based on the study of pairwise interaction energies between building units

The crystal structures of aspirin polymorphs I and II (Figure A 4.1) have been thoroughly studied [4, 5]. However, only hydrogen bonds of various types and their geometric characteristics were discussed and layers of centrosymmetric dimers as a structural motif of the crystal packing were highlighted. Such analysis did not take into account non-directed interactions between molecules like electrostatic, general dispersion, polarization, etc. Also, stacking between  $\pi$ -systems was not mentioned due to the impossibility to describe this interaction unambiguously. The crystal structure of polymorphic form IV proved to be more complicated due to the presence of two molecules in the unit cell asymmetric part. This structure was also characterized as layered [6].

Two types of layers may be visualized in all the studied structures of aspirin (Figure 4.1). There are no specific intermolecular interactions between molecules belonging to the neighboring layers. Therefore, the choice of the plane in which the easiest way of crystal packing deformation may occur can be made on the basis of the interaction energies between strongly bound structural motifs. To evaluate these energies, the analysis of a crystal packing based on the study of pairwise interaction energies between molecules should be applied.

At the first stage of such an analysis, the molecule was considered as a building unit (BU) and its first coordination sphere was constructed. In the case of polymorphic form IV, the first coordination sphere was constructed separately for each of the molecules A and B found in the asymmetric part of the unit cell. The basic molecule is surrounded by 14 neighbors in the polymorphic

form I and only by 13 in polymorphs II and IV (Tables A 4.1-4.3). At that, the total interaction energy of the basic molecule with all the molecules belonging to its first coordination sphere is -63.2 kcal/mol in polymorphic structure I, -64.3 kcal/mol in structure II and -62.2 kcal/mol (the basic molecule A) or -59.3 kcal/mol (the basic molecule B) in structure IV. The basic molecule forms the strongest interaction with only one neighboring molecule due to O-H...O hydrogen bonds in all the aspirin polymorphs. The interaction energy between the molecules in this centrosymmetric dimer is more than three times higher than the interaction energies of the basic molecule with other neighboring ones (Figure A 4.2). Therefore, the building unit of the aspirin polymorphic structures is not a molecule, but a centrosymmetric dimer [7]. It should also be noted that dimers of AA or BB types are the building units in the polymorphic structure IV.

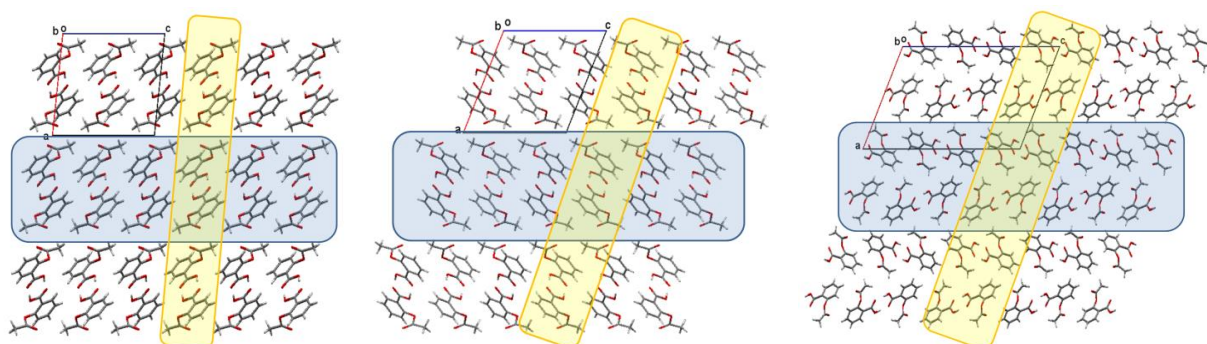


Figure 4.1. Crystal structure of polymorphic forms I (on the left), II (in the middle) and IV (on the right) of aspirin. Layers of centrosymmetric dimers parallel to the (100) crystallographic plane are highlighted blue; layers of centrosymmetric dimers parallel to the (001) crystallographic plane are highlighted yellow.

These dimeric building units were used for further analysis to separate out some structural motifs of a crystal packing and evaluate the interaction energies between them. For this purpose, the first coordination sphere of the dimeric building unit contains 18 neighboring dimers in polymorphic structure I and 16 neighboring ones in structure II. At that, the total energy of building unit

interaction with all the surrounding dimers is equal (-75.3 kcal/mol) in these polymorphic structures (Tables A 4.4-4.6). Each of the AA and BB dimers is surrounded by 16 neighboring dimers of different types, but the total interaction energies of the building unit with its first coordination sphere are slightly different (-79.7 kcal/mol for building unit AA and -78.5 kcal/mol for building unit BB).

Each building unit forms two strongest interactions with equal energies (Tables A 4.4-4.6, Figure A 4.3) between dimers that are located in opposite directions. As a result, the linear column along the direction [010] can be separated out as the primary basic structural motif ( $BSM_1$ ) in all the three polymorphs of aspirin (Figure 4.2). Moreover, the columns containing only dimers AA and the columns of dimers BB are observed in structure IV. Stacking as well as non-specific interactions are found between dimeric building units within these columns. The total interaction energy of the building unit within the column is -26.8 kcal/mol in polymorph I, -26.9 kcal/mol in polymorph II and -35.3 kcal/mol (column A) or -32.9 kcal/mol (column B) in polymorph IV.

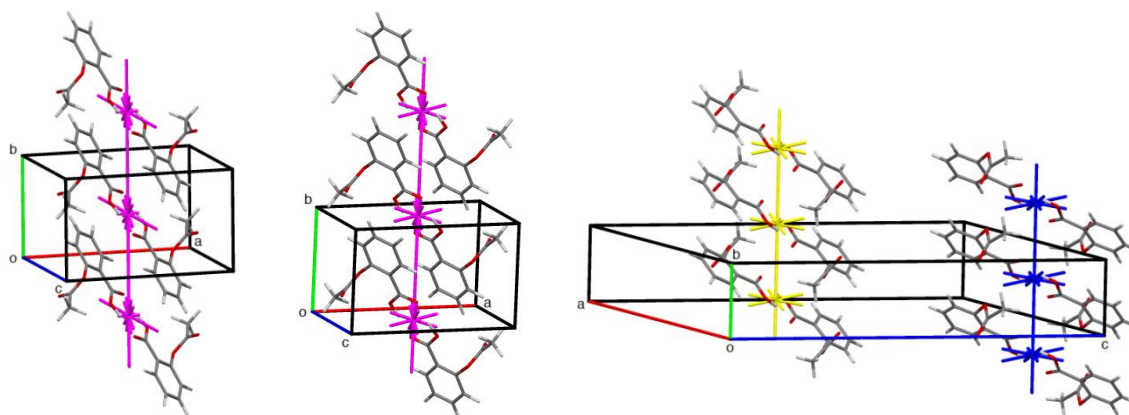


Figure 4.2. Columns along the [010] crystallographic direction as the primary basic structural motif in terms of molecules and energy-vector diagrams in polymorphic structures I (on the left), II (in the middle) and IV (on right). EVD for columns of A and B types are highlighted yellow and blue respectively in structure IV.

Further analysis of the interaction energies between dimeric building units belonging to neighboring columns makes it possible to discuss the formation of layers as the second basic structural motifs in the crystals I, II and IV (Figure 4.3). Each column is surrounded by eight neighboring ones in all the studied crystals. The basic column interacts strongly with two columns lying in opposite directions within the (100) crystallographic plane in crystals I and II. As a result, the layers parallel to the (100) crystallographic plane may be separated out as a secondary basic structural motif ( $BSM_2$ ) in structures I and II. The C-H... $\pi$  and non-specific interactions are found between molecules of the neighboring columns within the layer. Within the  $BSM_2$ , the total interaction energies between the dimeric building unit and the neighboring dimeric ones are almost 8 times higher than the interaction energies between those belonging to the layers parallel to the (100) crystallographic plane (Table 1). It should be noted that the structure of the  $BSM_1$  and  $BSM_2$  (layer parallel to the (100) plane) is the same in polymorphs I and II of aspirin. The main difference between these crystals can be caused by the relative position of the neighboring layers.

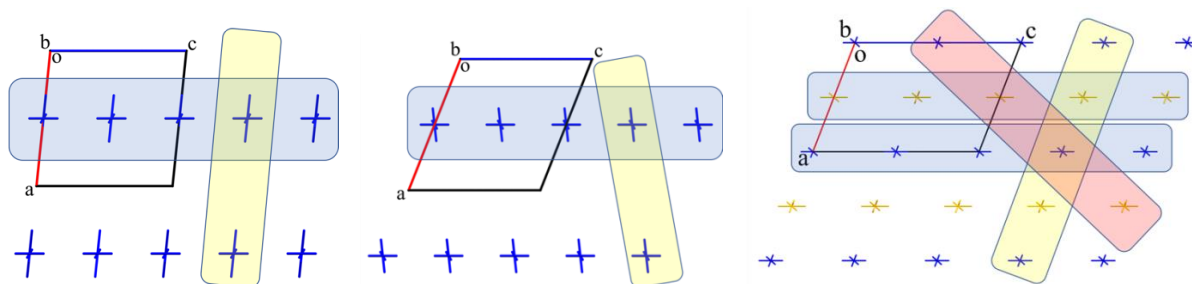


Figure 4.3. The packing of columns in terms of energy-vector diagrams, projection along the [010] crystallographic direction for polymorphic structures I (on the left), II (in the middle) and IV (on the right). Possible layers are highlighted in different colors: layers parallel to the (100) crystallographic plane are blue; layers parallel to the (001) plane in structures I and IV or to (-102) plane in structure II are yellow; a layer parallel to the (-101) plane in structure IV is red.

According to the calculated pairwise interaction energies, the dimeric building unit interacts strongly with two neighboring ones lying in opposite directions within the (001) crystallographic plane in structure I or the (-102) plane in structure II (Figure 4.3, layers are highlighted yellow) which may be considered as an alternative  $BSM_2$ . The interaction energies between  $BSM_1$  within these planes are smaller as compared to those within the (100) planes mentioned above (Table 4.1). It may be caused by the extremely weak C-H...O intermolecular interactions between molecules of the neighboring columns lying in the (001) plane in structure I or the (-102) plane in structure II. Moreover, the relative orientation of centrosymmetric dimers belonging to the neighboring columns within these planes is different (Figure 4.4). Total interaction energies of the dimeric building unit with the neighboring ones within the (001) (structure I) or (-102) (structure II) crystallographic planes as  $BSM_2$  are two times stronger than between them (Table 4.1).

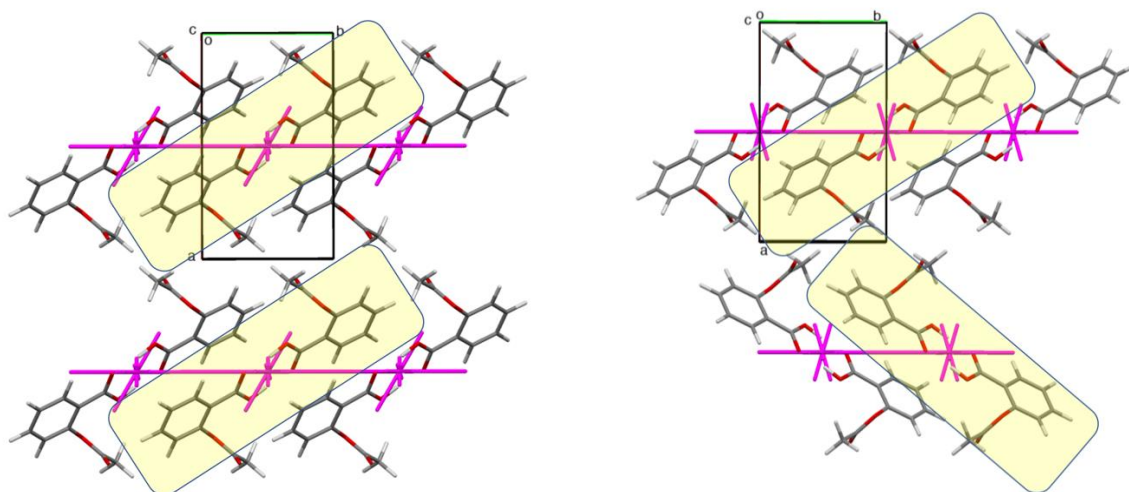


Figure 4.4. Relative positions of centrosymmetric dimers belonging to the neighboring columns within the (001) crystallographic plane in structure I (on the left) and (-102) crystallographic plane in structure II (on the right). Dimeric building units are highlighted yellow.

Comparing the energy ratio inside and between BSM<sub>1</sub> and BSM<sub>2</sub> (Table 4.1), it can be concluded that the polymorphic crystals of aspirin I and II have columnar-layered structure, where layers parallel to the (100) crystallographic plane are the most strongly bound secondary basic structural motifs. The main difference between these polymorphic forms of aspirin is the relative orientation of the dimeric building units belonging to neighboring layers (Figure 4.4). Such a conclusion would not have been possible without the analysis of the energetic structure and strongly bound structural motifs in these crystals.

Table 4.1. The interaction energies (in kcal/mol) between dimeric building units within separated structural motifs and between them.

Structural motif	I		II		IV AA			IV BB		
BSM <sub>1</sub>	-26.8		-26.9		-35.3			-32.9		
	(100)	(001)	(100)	(-102)	(100)	(001)	(-101)	(100)	(001)	(-101)
BSM <sub>1</sub> /BSM <sub>1</sub>	-16.6	-6.5	-16.8	-6.7	-9.9	-8.7	-3.6	-10.5	-8.7	-3.6
BSM <sub>2</sub>	-59.9	-39.0	-60.5	-40.1	-55.0	-52.8	-42.5	-53.8	-50.3	-40.1
BSM <sub>2</sub> /BSM <sub>2</sub>	-7.7	-18.2	-7.4	-17.6	-12.3	-13.5	-18.6	-12.3	-14.1	-19.2

As it was mentioned above, the analysis of polymorphic structure IV is more complicated due to the presence of two molecules in the asymmetric part of the unit cell. Each of the recognized columns AA and BB as the primary basic structural motifs is surrounded by eight neighboring columns. The analysis of interaction energies between dimeric building units belonging to the neighboring columns revealed very close interactions in the directions parallel to the (100) or (001) crystallographic planes and weaker interactions within the diagonal plane (-101) (Table 4.1). Three types of layers parallel to the (100), (001) or (-101) crystallographic planes may be separated out as possible secondary basic structural motifs (Figure 4.3). At that, the layers parallel to the (100)

crystallographic plane contain columns of only one type (layers AA and layers BB) which are alternated. Within these layers, the dimeric building units of the neighboring columns are bound mainly by C-H... $\pi$  interactions. The layers parallel to the (001) plane are mixed and contain columns of both types (layers AB). There are no specific interactions between molecules within these layers. The energy ratios inside and between the layers (100) and (001) are very close (Table 4.1). It may be explained by the balance of two types of interactions: specific and non-specific. Indeed, the interaction energy between the (100) layers is caused mainly by general dispersion due to the absence of any specific interactions and a smaller distance between neighboring planes (7.8 Å). The interaction energy between the (001) layers is caused mainly by C-H... $\pi$  interactions (the distance between layers is 11.1 Å). As a result, the layer of any type as a secondary basic structural motif can't be separated out unambiguously. Therefore, the polymorphic structure IV of aspirin may be classified as columnar.

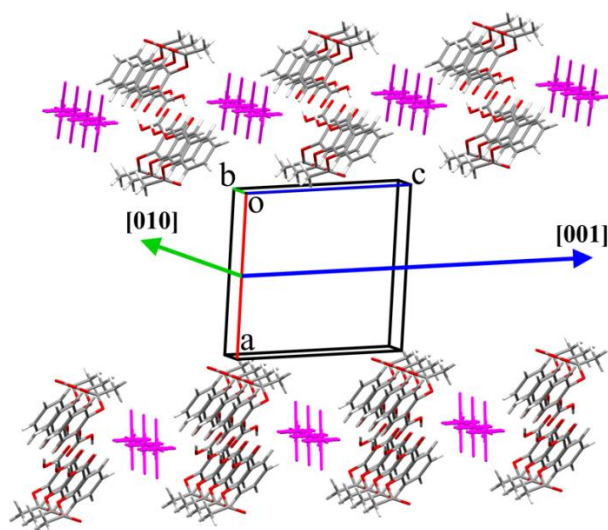


Figure 4.5. Possible directions of the easiest slip deformation along the (100) crystallographic plane in polymorphic crystals I and II.

Summarizing the study of pairwise interaction energies in the polymorphic crystals of I, II and IV, we can conclude that only one plane for the

easiest slip deformation may be recognized in structures I and II, while structure IV can be deformed along two crystallographic planes with close probability. However, the question about the direction of the easiest slip deformation along the plane remains open (Figure 4.5). Another question concerns the fact that the interaction energies between the two visualized types of BSM<sub>2</sub> in structure IV are higher as compared to the interaction energy between BSM<sub>2</sub> in structures I and II (Table 4.1). At that polymorphic structure IV of aspirin proved to be metastable [6]. Therefore, it can be presumed that the stability and ability to mechanical response are caused not only by the interaction energies between the strongly bound fragments of a crystal packing.

#### 4.1.2. Modeling of the slip deformation in the crystals

##### 4.1.2.1. Details on calculations

The results of the crystal structure analysis based on the pairwise interaction energies study were used to model the possible mechanical response of a crystal packing. It was presumed that the shear of the most strongly bound fragments is the most probable and it is not accompanied by the deformation of these fragments themselves.

The fragment of the secondary structural motif used as a fixed part in the modeling and one building unit belonging to the neighboring BSM<sub>2</sub> used as a mobile part were extracted from the crystal structure without any change of atomic coordinates. For the shear simulation, the mobile part of the chosen system was shifted along the fixed part on one crystallographic translation with a step determined as 1/n of this translation. The single point interaction energies between mobile and fixed fragments were calculated in each from n points along the translation trajectory using B97D3 functional and cc-PVDZ basis set [8, 9] within the Gaussian09 software and corrected for basis set superposition error by counterpoise method. The shift energy profile was constructed and the shift

energy barrier was calculated as a difference between the highest and lowest interaction energies between the mobile and fixed parts of the used model fragment of a crystal packing.

#### 4.1.2.2. Formation of the method

To implement an algorithm described above, it is necessary to consider some problems:

1. The minimal size of the mobile part extracted from the experimental data.
2. The optimal size of the fixed part necessary to reproduce the shift energy profile in the chosen point group symmetry.
3. The choice of probable crystallographic directions for the displacements.
4. The optimal step size for the displacement.

Each of these problems was considered using well-studied polymorphic structures I and II of aspirin as model systems.

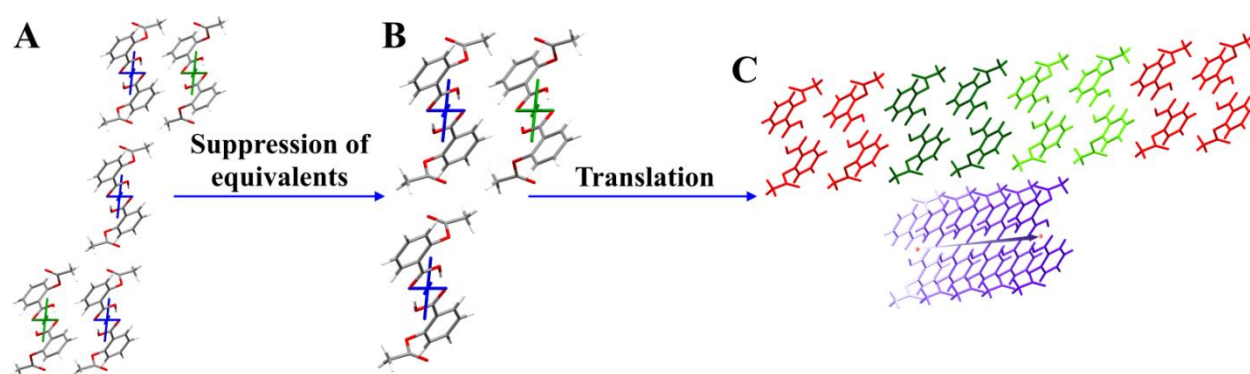


Figure 4.6. Algorithm of a slip deformation modeling: a) fragment of a crystal packing containing two layered parts and a building unit between them; b) fragment of one of the symmetry equivalent layers (fixed part) and building unit (mobile part) belonging to the neighboring layer; c) shift of the building unit in relation to the layer fragment.

The computational costs of quantum-chemical calculations grow exponentially with the number of atoms. Therefore, the mobile part may be minimized up to one building unit. Being bound by symmetry operations, the

two neighboring layers are not necessary for the completeness of the information and the deletion of the equivalents may be done (Figure 4.6a,b, Figure A 4.4). The size of the fixed part ought to satisfy two conditions at the same time: a) to be large enough to represent the layer as best as possible; b) to be small enough so that the calculations of the interaction energies would not be too expensive. Obviously, the fixed part ought to contain all building units belonging to the first coordination sphere of the mobile part (Figure 4.6b). This condition ought to be executed for the moving building unit at all points along the translation trajectory. To do so the fixed part constructed for initial geometry should be repeated at least twice in the direction of the mobile part displacement (light green molecules on Figure 4.6c). Our preliminary modeling of the mobile part translation in the [010] direction within the (100) crystallographic plane have shown the presence of an edge effect. The difference in interaction energies calculated for the building unit equivalent positions in relation to the center and edge of the fixed part was proved to be up to 0.5 kcal/mol (Figure A 4.6). To avoid the edge effect on the calculated energies, the fixed part was expanded by two initial fragments in each direction of the mobile part displacement (red molecules on Figure 4.6c). The final energy deviations due to the edge effect did not overcome 0.2 kcal/mol (Table A 4.7, Figure A 4.5).

As it was mentioned above, the plane of the easiest deformation of a crystal structure may be determined using the analysis of pairwise interaction energies. To choose the direction of the slip deformation within the layer, the minimal interatomic distances between the mobile and fixed parts was estimated along the entire displacement on one crystallographic translation in each of the possible crystallographic directions. If during the translation in a crystallographic direction, an interatomic distance in any point is found to be significantly shorter as compared to the corresponding van der Waals radii sum, this crystallographic direction is excluded from further consideration. Due to the

extreme computational cheapness of such calculations, the distances were found in each one thousandth of a translation (every 0.024 Å in the case of the longest unit cell parameter).

Since the sliding deformation was modeled as the displacement of the mobile part in relation to the layer fragment as a fixed part, it is necessary to determine the step size of such displacement. Being equal to the unit cell parameters, translations in different crystallographic directions within the same structure can have different absolute values (in angstroms). Therefore, it is proposed to define the step size as 1/n part of the corresponding translation. In order to evaluate the effect of step size, energy calculations were performed for a number of geometries where the positions of the mobile part with respect to the fixed part differ by one hundredth of the corresponding translation (Figure A 4.6, Table A 4.8). An error induced by the step size increasing has been defined in comparison to the data obtained within this best approximation. It is only 0.1 kcal/mol in the case of a step size of one twentieth of the corresponding translation length. The decrease of the step size up to one fiftieth of the translation leads to some error increasing. Therefore, one-twentieth part of the translation was identified as the most acceptable step size.

Finally, the shift energy profiles acquired using all the moments mentioned above should be inverted to simulate the relative displacement of layers. In the case of the one-dimensional shift, it is achieved by the reflection of the initial curves in relation to the midpoint of the translation (Figure 4.7). The energy barrier can be calculated as a difference between maximal and minimal interaction energies of the mobile and fixed parts along the translation path.

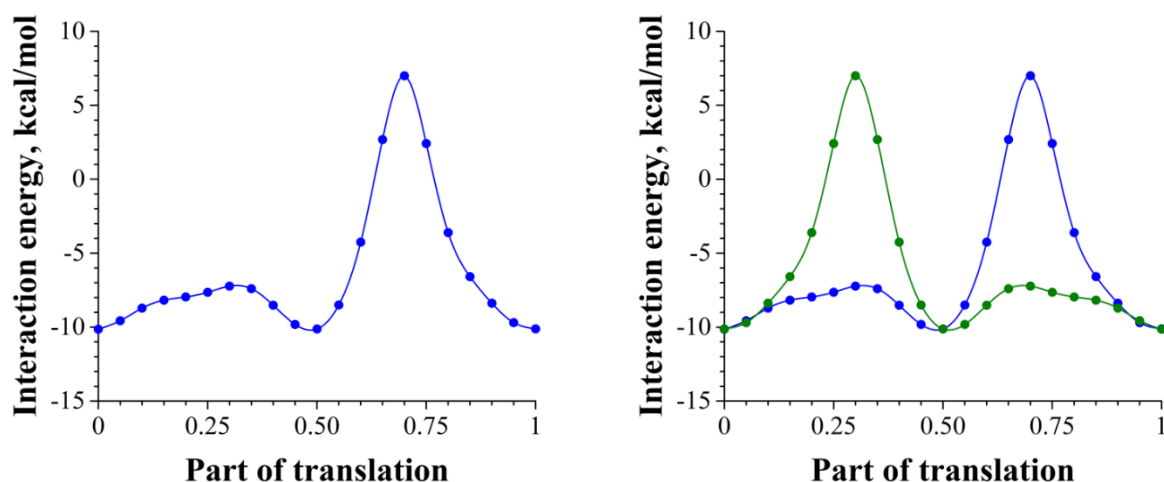


Figure 4.7. The energy profiles for the mobile part displacement in relation to the fixed part along the [001] direction in the (100) crystallographic plane: the case of direct data order (on the left); the overlay of the direct and inverted shift energy profiles (on the right). Data are shown for polymorphic structure I.

#### 4.1.3. Verification of the proposed model by the study of a slip deformation in the aspirin polymorphic structures I and II

To verify the proposed model, it was applied for the study of a slip deformation in the well-studied polymorphic structures of aspirin I and II. The main advantage of these crystals is the availability of many experimental data obtained for them by different methods [10-12].

The (100) crystallographic plane was determined to be the most probable for a slip deformation in aspirin polymorphic structures I and II. The analysis of minimal distances showed that three crystallographic directions for the building unit displacement may be considered within this plane (Table 4.2, Figure A 4.7-4.9). At that, the minimal distances between atoms were observed for the displacement in the [001] crystallographic direction. The displacement in the [010] crystallographic direction within the (100) plane was expected to be more preferable due to the larger values of minimal distances between atoms (Table 4.2) in both polymorphic structures under consideration. The modeling of the dimeric building unit displacement in these crystallographic directions

allowed us to evaluate the shift energy barriers which proved to be somewhat unexpected. The lowest energy barrier was found for the displacement in the [001] crystallographic direction in polymorphic structures I and II where the smallest value of the minimal distances was found (Table 4.2).

Table 4.2. Minimal interatomic distances (Å) and energy barriers (kcal/mol) for the displacement of the building unit in different crystallographic directions in polymorphic crystals I and II of aspirin.

Crystallographic direction	Polymorphic structure I		Polymorphic structure II	
	Minimal distance, Å	Energy barrier, kcal/mol	Minimal distance, Å	Energy barrier, kcal/mol
[010] (100)	1.61	22.1	1.69	20.9
[001] (100)	1.19	17.1	1.26	14.5
[011] (100)	1.46	35.8	1.30	52.4
[100] (001)	1.15	76.1		
[010] (001)	1.41	61.6		
[110] (001)	0.44 *	–		
[010] (-102)			1.41	58.2
[201] (-102)			1.07	91.2
[211] (-102)			0.62 *	–

\* Directions of displacement marked with asterisk are improbable because of the strong reduction in intermolecular distances.

To explain such an unexpected result, a detailed analysis of relative positions of the building unit as a mobile part and molecules belonging to the layer as a fixed fragment along the translation path was performed. It was found that the C-H...O hydrogen bonds were formed during the translation process in both model systems. However, these hydrogen bonds are different. The methyl group of the building unit interacts with the carbonyl group of a molecule belonging to the layer fragment (the H...O shortest distance is 1.95 Å) during the displacement in the [010] crystallographic direction (Figure 4.8a). The displacement of the building unit in the [001] crystallographic direction results

in the formation of the C-H...O hydrogen bonds between the methyl group of a molecule belonging to the layer fragment and the carbonyl group of a molecule belonging to the building unit (the H...O shortest distance is 2.36 Å) (Figure 4.8b). It may be presumed that the formation of stronger hydrogen bonds during the translation along the [010] crystallographic direction results in the higher energy barrier.

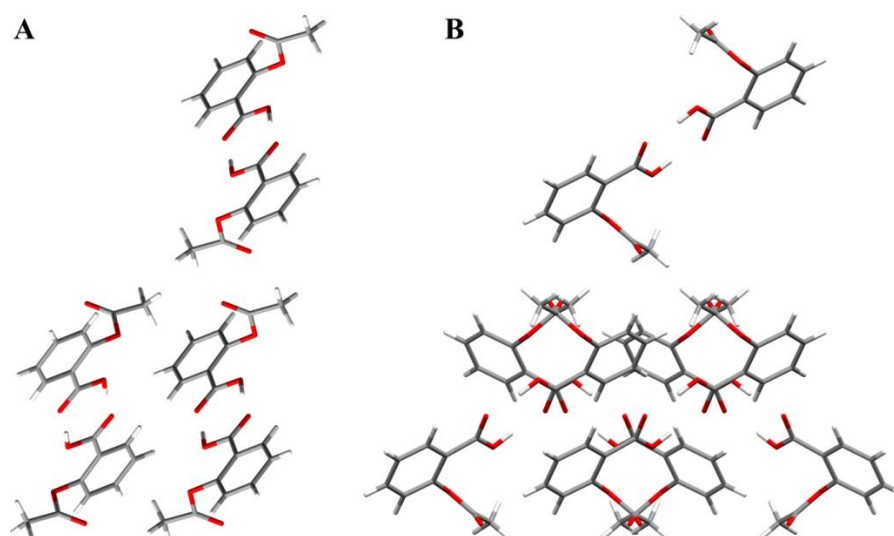


Figure 4.8. The model system for the study of the dimeric building unit displacement in relation to the layer fragment in aspirin polymorphic structures I and II: a) along the [010] crystallographic direction; b) along the [001] crystallographic direction.

Noteworthy is the fact that the systems have positive interaction energies up to 7.0 or 4.4 kcal/mol in some area during the translation of the building unit in the [001] crystallographic direction in structures I and II respectively and 11.7 or 10.5 kcal/mol during the translation in [010] crystallographic direction. The positive interaction energies mean strong repulsion between interacted fragments of a crystal packing. This can be correlated with the low stability of these polymorphic forms of aspirin.

The crystallographic planes (001) and (-102) were identified as alternative BSM<sub>2</sub> in aspirin polymorphic structures I and II (Table 4.1). Therefore, these planes may be considered less preferable but possible for the deformation of

a crystal packing. Usage of the abovementioned method showed that two crystallographic directions are available for a slip deformation within each of these planes. This was based on the data about minimal distances between atoms (Figures A 4.10-4.11). However, energy barriers are very high for the displacement in all these directions (Table 4.2), so a slip deformation is hardly probable within crystallographic planes (001) in polymorph I or (-102) in polymorph II.

It should be noted that the results of our calculations correlate well with the data obtained by the nanoindentation experimental method [10, 11]. Therefore, the proposed method can be used for the prediction of the mechanical properties of a crystal structure.

#### 4.1.4. Prediction of a slip deformation in polymorphic structure IV of aspirin

Polymorphic structure IV proved to be metastable, which complicates the study of its properties by experimental methods. The analysis of pairwise interaction energies allowed to separate out three possible types of BSM<sub>2</sub> (Table 4.1) among which layers parallel to crystallographic planes (100) and (001) are almost equivalent.

Taking into account the presence of two types of building units (AA and BB) in this structure, the calculations for a slip deformation modeling were performed for each of them. The analysis of minimal distances between atoms on the translation path showed a high probability for displacement in the [010] direction within each of the three possible crystallographic planes (Tables 4.3, A 4.9).

The lowest energy barrier (5.4 kcal/mol for AA basic unit or 5.6 kcal/mol for BB basic unit) was calculated for the displacement in the [010] crystallographic direction within the (100) crystallographic plane. The layers

containing only one type of the building units were found to be parallel to this plane. The building unit displacement along the (001) crystallographic plane should overcome the energy barrier which is almost two times higher (9.5 kcal/mol) compared to the lowest energy barrier. Detailed study of two model systems (Figure 4.9) revealed that any directed interactions like hydrogen bonds are not formed during the displacement within the (100) crystallographic plane. The displacement of the building unit within the (001) crystallographic plane results in the formation of a very weak C<sub>ar</sub>-H...O hydrogen bond (the shortest H...O distance is 2.43 Å). It can be presumed that the formation of directional interaction results in increasing of the shift energy barrier.

Table 4.3. Minimal interatomic distances (Å) and energy barriers (kcal/mol) for the displacement of the building unit in different crystallographic directions in polymorphic structure IV of aspirin.

Crystallographic direction	AA basic unit		BB basic unit	
	Minimal distance, Å	Energy barrier, kcal/mol	Minimal distance, Å	Energy barrier, kcal/mol
[010] (100)	1.73	5.4	1.73	5.6
[001] (100)	1.28	22.8	1.28	23.3
[011] (100)	0.86 *	–	0.77 *	–
[100] (001)	0.37 *	–	0.37 *	–
[010] (001)	1.73	9.5	1.73	9.5
[110] (001)	0.32 *	–	0.87 *	–
[010] (-101)	1.82	8.8	1.82	8.4
[101] (-101)	0.32 *	–	0.17 *	–
[111] (-101)	< 0.01 *	–	0.14 *	–

The displacement in the [010] crystallographic direction within the diagonal (-101) crystallographic plane (Figure A 4.12) has the energy barrier which is very close to the one within the (001) crystallographic plane. All the calculated energy barriers in polymorphic structure IV are lower than the smallest energy barrier in structures I and II. Moreover, the highest interaction

energy between the mobile and fixed parts during displacements in the [010] direction within any of the three crystallographic planes is not positive contrary to those found in structures I and II. This means the absence of any steric repulsion during the displacement of the AA or BB columns (separated out as  $BSM_1$ ) in the [010] crystallographic direction. These data confirm our classification of aspirin polymorphic structure IV as columnar and explain the low stability of this crystal form.

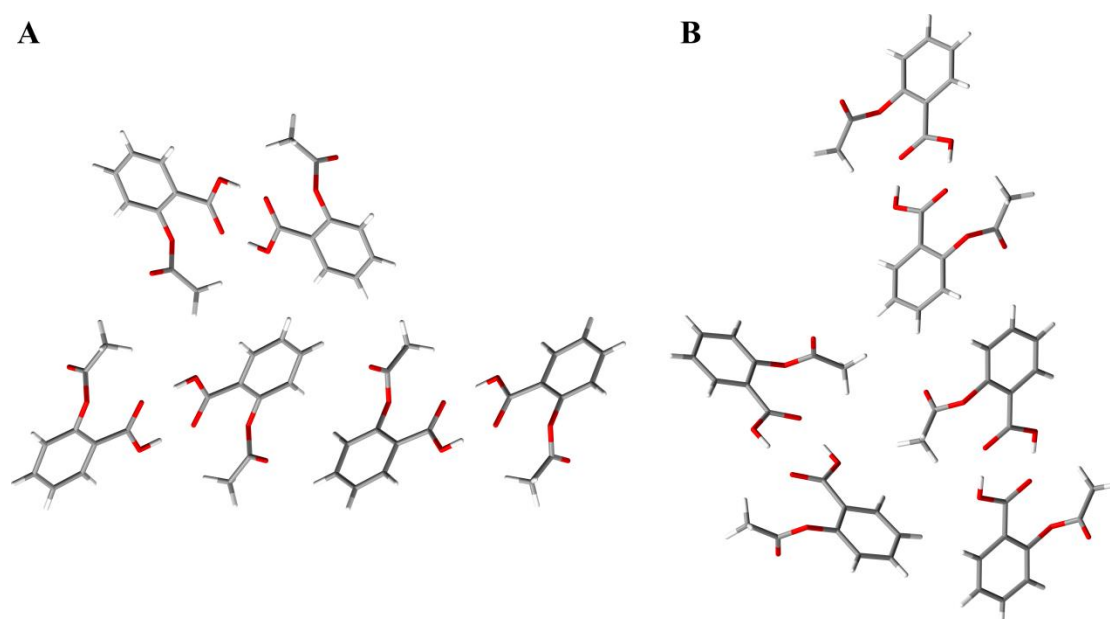


Figure 4.9. The model system for the study of the dimeric building unit displacement along the [010] direction in aspirin polymorphic structure IV: a) within the (100) crystallographic plane; b) within the (001) crystallographic plane.

#### **4.2. High-pressure polymorphic transition in piracetam crystals: studying by quantum-chemical methods**

The previous section was mostly about mechanical properties. The main idea of the current one is to determine the factors that precede the polymorphic transition under pressure and to study the changes that occur during the transformation on the example of polymorphic modifications II and V of

piracetam. The results will help to understand better the polymorphic transformations under the external influence and can be used for their prediction.

#### 4.2.1. Preliminary assessment of the possibility of displacement of strongly bound crystal fragments

As described in the previous section, the easiest deformation of a crystal structure was presumed to be possible due to the displacement of strongly bound fragments (for example, layers as  $\text{BSM}_2$ ) to each other. The next task is the choice of a displacement direction within the layer. To tackle this task, the minimum interatomic distances between molecules belonging to two neighboring  $\text{BSM}_2$  should be estimated along all potential displacement trajectories.

The piracetam molecule is asymmetric, so a simple approximation of particle-accessible voids in a crystal with the use of a spherical probe may be inaccurate [13, 14]. Therefore, a fragment of the crystal structure as a model system was used. For this purpose, the mobile and fixed parts belonging to two neighboring  $\text{BSM}_2$  were defined in the same way as in the method proposed in Section 4.1. The one BU was used as the mobile part in this model system. All BUs of its first coordination sphere belonging to neighboring  $\text{BSM}_2$  were used as the fixed part. The mobile part was shifted along the fixed part on one translation in two crystallographic directions within the plane simultaneously. The step size for the displacement was equal to 1/100 of the corresponding translation (reaching the resolution of 0.117 Å for the longest translation) as soon as different translation paths differ in their absolute length in angstroms. The first coordination sphere was generated at each point of this displacement. Duplicated fragments were excluded.

The main directions for displacements, defining the studied area, were chosen based on the Miller indices corresponding to the selected  $\text{BSM}_2$ .

For planes of the (001) type, coinciding with the principal axes of the crystal lattice, the translation of the mobile part was carried out in the crystallographic directions corresponding to these axes (for example, the directions [100] and [010] along with the layer (001)). For planes parallel to one of the principal axes (whose indices containing one 0), the directions were chosen in such a way that the first one was similar to the principal axis of the crystal structure parallel to this plane and the second direction was identified as orthogonal to this principal axis following the Weiss zone law:

$$hk + ky + lz = 0 \quad (4.1)$$

where  $h, k, l$  are Miller indices of the corresponding plane containing BSM<sub>2</sub> and  $x, y, z$  are indices of assumed direction lying in this plane.

For example, in the case of planes (0kl), the solution with minimized indices is:

$$\begin{cases} x = 0 \\ y = \frac{-l}{GCD(k, l)} \delta \\ z = \frac{k}{GCD(k, l)} \delta \end{cases} \quad (4.2)$$

where  $GCD(k, l)$  is the greatest common divisor of the indices  $k$  and  $l$  and  $\delta = -\frac{kl}{|k||l|}$  is a term removing double negation.

The step size between the points of measurement and so the resolution is proportional to the length of a translation and the number of steps. However, the second parameter cannot be decreased indefinitely and limited by the computational time. It forces us to seek a compromise between the time necessary for the analysis and its accuracy. So in the case, when all the three

indices of the plane containing  $BSM_2$  are not equal to 0, the system of solutions minimizing the lengths of the translations was chosen. The first solution and so the set of the Miller indices belonging to the first shift direction was chosen from orthogonal to the principal axes of the crystal structure laying in the chosen plane:

$$\begin{cases} ky = -lz \\ hx = -lz \\ hx = -ky \end{cases} \quad (4.3)$$

$$dir_1 = \begin{pmatrix} [0, \frac{-l}{GCD(k,l)}, \frac{k}{GCD(k,l)}] \\ [\frac{-l}{GCD(h,l)}, 0, \frac{h}{GCD(h,l)}] \\ [\frac{-k}{GCD(h,k)}, \frac{h}{GCD(h,k)}, 0] \end{pmatrix} \delta \quad (4.4)$$

where  $dir_1$  is the set of indices belonging to the first translation and  $\delta = -\frac{hkl}{|h||k||l|}$  is a term removing double negation.

The one solution was chosen among these three according to the condition of translations lengths minimization described above:

$$D_1 = \sqrt{(x_{dir_1})^2 + (y_{dir_1})^2 + (z_{dir_1})^2} \rightarrow 0 \quad (4.5)$$

where  $D_1$  is the length of the first translation,  $x_{dir_1}$ ,  $y_{dir_1}$  and  $z_{dir_1}$  are its indices.

The second direction was chosen from the residual two solutions in expression 4.4 with the further minimization of its length using the first set of direction indices:

$$dir_2 = \left( \left( \left[ \begin{array}{c} [0, \frac{-l}{GCD(h,k)}, \frac{k}{GCD(h,k)}] \\ [\frac{-l}{GCD(h,l)}, 0, \frac{h}{GCD(h,l)}] \\ [\frac{-k}{GCD(h,k)}, \frac{h}{GCD(h,k)}, 0] \end{array} \right] \setminus dir_1 \right) - Ndir_1 \right) \delta \quad (4.6)$$

where  $dir_2$  is the set of indices belonging to the second translation, which does not coincide with  $dir_1$ ,  $N$  is such an integer, that the condition similar to the expression 4.5 is true for the second direction.

This technique makes it possible to use simple or complex BUs as probes to study the distribution of the minimum interatomic distances between the mobile and fixed parts during their shifts to each other.

#### 4.2.2. Characterization of the crystal structure

Now, when the set of methods required is formulated the analysis of crystal structure may be started (Figure A 4.13-4.14). The crystal-crystal polymorphic transition under pressure has been thoroughly studied in piracetam crystals [15]. This transformation from form II to form V is caused by a very small change in the crystal packing without structure destruction. Also, the pressure influence on form V has been analyzed. All the differences in the crystal structures were considered from the crystallographic and geometric viewpoints. The unit cell parameters (Table 4.4), as well as geometrical characteristics of hydrogen bonds (Table 4.5), were compared in the structures determined under different values of pressure. Such an analysis is hardly analytical and cannot explain the reasons and pre-requisites for a polymorphic transformation.

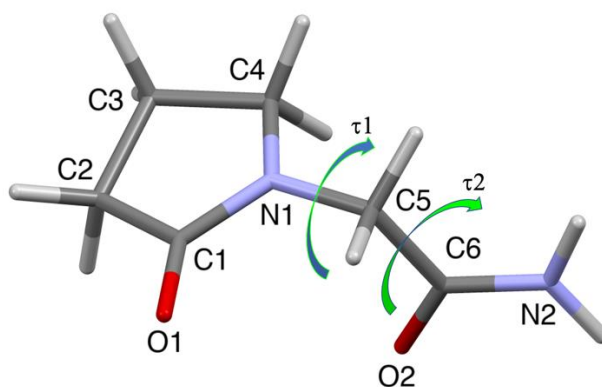


Figure 4.10. The piracetam molecule with possible ways to change its conformation due to rotation around the N1-C5 and C5-C6 bonds (the  $\tau_1$  and  $\tau_2$  torsion angles).

The pressure-mediated polymorphic transformation without destruction of the crystal usually requires the molecules to be conformationally flexible. The piracetam molecule has at least two non-cyclic single bonds around which the rotation is possible (Figure 4.10). However, the geometrical parameters of the molecules in forms II and V at various pressure values are very similar (Table 4.4). Therefore, the pressure mainly affects the arrangement of molecules in the crystal phase.

Table 4.4. The unit cell parameters and  $\tau_1$  and  $\tau_2$  torsion angles of the piracetam molecule in polymorphic forms II and V at various pressure values according to the experimental data.

Parameter	II, ambient	II, 0.45 GPa	V, 0.7 GPa	V, 0.9 GPa	V, 2.5 GPa	V, 4.0 GPa
a	6.403	6.321	6.442	6.3903	6.263	6.169
b	6.618	6.5597	6.353	6.2932	6.2063	6.1602
c	8.556	8.380	8.737	8.6450	8.412	8.287
$\alpha$	79.85	79.82	81.43	81.106	80.77	80.41
$\beta$	102.39	102.34	112.88	113.680	114.69	115.33
$\gamma$	91.09	90.94	91.38	91.295	91.12	91.15
$\tau_1$	91.95	89.65	90.41	91.18	86.77	84.51
$\tau_2$	-27.14	-25.02	-23.47	-21.30	-20.47	-20.67

The piracetam molecules are bound by the N2-H...O2' (the symmetry operation is 1-x,1-y,-z) hydrogen bonds in the crystal phase, forming a centrosymmetric dimer (Figure 4.11). These dimers are bound by the N2-H...O1' (the symmetry operation is 1+x,y,z) hydrogen bonds resulting in the formation of chains/columns in the [100] crystallographic direction. The weak enough C5-H...O1' (the symmetry operation is -x,1-y,-1-z) hydrogen bonds are found between adjacent columns within the (010) crystallographic plane. The comparison of the geometrical characteristics of these hydrogen bonds showed that the weaker C5-H...O1 bonds turned out to be the most sensitive to the pressure influence (Table 4.5).

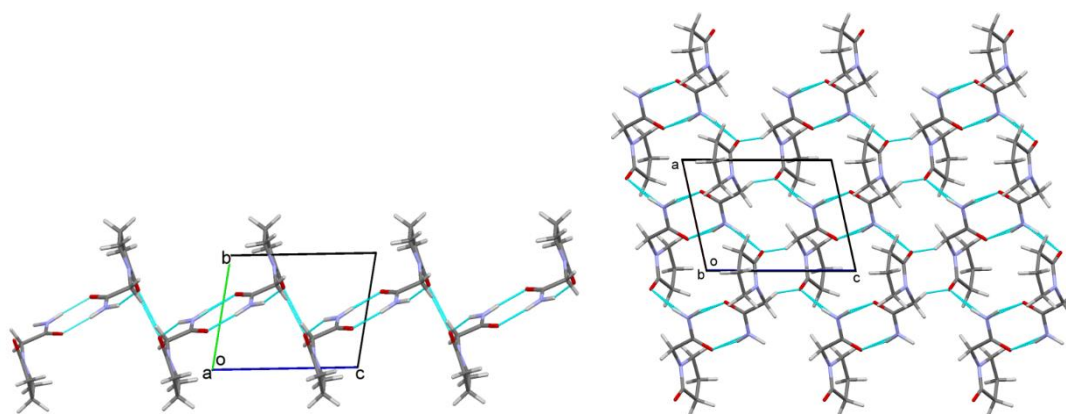


Figure 4.11. The fragment of the crystal packing bound by N-H...O and C-H...O hydrogen bonds: view in the *a* crystallographic direction (on the left); the *ac* crystallographic plane, view in the *b* crystallographic direction (on the right). Hydrogen bonds are shown by cyan lines.

However, this analysis takes into account only the strongest intermolecular interactions in a crystal that is obvious in organic crystal structure analysis [16, 17]. Nevertheless, the recent studies of our research group [18, 19] showed that weak directed interactions and non-directed ones like electrostatic, polarization, dispersion, etc. can also affect crystal packing. To evaluate the contribution of these interactions, the analysis of a crystal structure

based on the study of pairwise interaction energies between molecules [7] can be useful.

Table 4.5. Intermolecular interactions and their geometric characteristics in polymorphic forms II and V under different pressures.

Polymorphic form and pressure (GPa)	N2-H...O2'		N2-H...O1'		C5-H...O1'	
	H...A, Å	D-H...A, deg	H...A, Å	D-H...A, deg	H...A, Å	D-H...A, deg
II (Ambient)	1.95	169	2.00	160	2.33	155
II (0.45)	2.07	165	2.11	151	2.36	153
V (0.7)	2.04	165	2.13	153	2.77	128
V (0.9)	2.02	167	2.14	154	2.71	127
V (2.5)	1.97	164	2.02	152	2.62	123
V (4.0)	1.92	167	2.03	155	2.54	122

#### 4.2.3. Study of the initial crystal structure of piracetam using quantum-chemical methods

##### 4.2.3.1. Crystal structure analysis from the pairwise interaction energies viewpoint

At the first stage, the piracetam molecule was considered as a monomeric building unit and its first coordination sphere containing 13 neighboring molecules was constructed (Table A 4.10, Figure A 4.15a). The total interaction energy of monomeric BU with all the molecules of its first coordination sphere is -73.2 kcal/mol at the ambient pressure. The basic monomeric BU<sub>0</sub> forms the strongest interaction with only one neighbor (Table 4.6). As a result, the centrosymmetric dimer bound by two same N-H...O hydrogen bonds should be used as a complex dimeric building unit for further analysis.

Table 4.6. Symmetry codes, bonding type, the interaction energy of the BU with neighboring ones ( $E_{\text{int}}$ , kcal/mol) with the highest values (more than 5 % of the total interaction energy) and the contribution of this energy to the total interaction energy (%) in piracetam polymorph II under ambient pressure.

Dimer of BUs	Symmetry operation	$E_{\text{int}}$ , kcal/mol	Contribution to the total interaction energy, %	Bonding type
BU is a molecule				
m1	1-x, 1-y, -z	-15.3	20.9	N-H...O (2)
m2	-1+x, y, z	-9.9	13.5	N-H...O
m3	1+x, y, z	-9.9	13.5	N-H...O
m4	-x, -y, -1-z	-8.8	12.0	non-specific
m5	-x, 1-y, -1-z	-7.9	10.8	C-H...O (2)
m6	-x, -y, -z	-7.0	9.6	non-specific
m7	1-x, -y, -z	-4.4	6.0	non-specific
BU is a dimer				
d1	-1+x, y, z	-18.4	17.3	N-H...O (2)
d2	1+x, y, z	-18.4	17.3	N-H...O (2)
d3	x, -1+y, z	-10.4	9.8	non-specific
d4	x, 1+y, z	-10.4	9.8	non-specific
d5	-1+x, -1+y, -1+z	-8.5	8.0	non-specific
d6	1+x, 1+y, 1+z	-8.5	8.0	non-specific
d7	-1+x, -1+y, z	-7.1	6.7	non-specific
d8	1+x, 1+y, z	-7.1	6.7	non-specific
d9	-1+x, y, -1+z	-7.0	6.6	C-H...O (2)
d10	1+x, y, 1+z	-7.0	6.6	C-H...O (2)

The first coordination sphere of a basic dimeric  $\text{BU}_0$  contains 14 dimeric  $\text{BU}_i$  (Table A 4.16, Figure A 4.17a). The total interaction energy of a basic dimeric  $\text{BU}_0$  with all the neighbors is -106.3 kcal/mol. The basic dimeric  $\text{BU}_0$  forms the two strongest interactions in opposite directions parallel to the [100] crystallographic axis (Table 4.6) due to the N-H...O hydrogen bonds. The column of centrosymmetric dimers in the [100] crystallographic direction can be

recognized as the primary basic structural motif of the polymorphic form II (Figure 4.12). The interaction of dimeric  $\text{BU}_0$  with its two neighbors within the column is  $-36.8$  kcal/mol ( $\text{BSM}_1$  in Table 4.7).

Table 4.7. The interaction energies (in kcal/mol) of dimeric  $\text{BU}_0$  with its first coordination sphere, within recognized basic structural motifs ( $\text{BSM}_1$ ,  $\text{BSM}_2$ ) and between them ( $\text{BSM}_1/\text{BSM}_1$ ,  $\text{BSM}_2/\text{BSM}_2$ ) and the distance between two neighboring  $\text{BSM}_2$  (in Å).

Polymorphic form/pressure (GPa)	$E_{\text{int}}$ (total)	$\text{BSM}_1$	Layers position	$\text{BSM}_1/\text{BSM}_1$	$\text{BSM}_2$	$\text{BSM}_2/\text{BSM}_2$	Distance $\text{BSM}_2/\text{BSM}_2$
II (Ambient)	-106.3	-36.8	(001)	-18.0	-72.8	-16.8	8.226
			(010)	-8.2	-53.3	-26.5	6.514
			(0-11)	-8.5	-53.9	-26.2	4.718
II (0.45)	-111.0	-35.9	(001)	-19.2	-74.3	-18.4	8.056
			(010)	-8.8	-53.4	-28.8	6.454
			(0-11)	-9.6	-55.2	-27.9	4.652
V (0.7)	-127.4	-34.6	(001)	-20.4	-75.4	-26.0	7.956
			(010)	-13.2	-60.9	-33.2	6.278
			(0-11)	-12.9	-60.3	-33.5	4.600
V (0.9)	-130.0	-35.2	(001)	-20.1	-75.3	-27.4	7.816
			(010)	-14.1	-63.3	-33.4	6.212
			(0-11)	-13.3	-61.8	-34.1	4.526
V (2.5)	-125.9	-33.7	(001)	-18.6	-71.0	-27.4	7.534
			(010)	-14.8	-63.4	-31.3	6.118
			(0-11)	-12.8	-59.3	-33.3	4.402
V (4.0)	-121.5	-35.0	(001)	-16.0	-67.0	-27.3	7.374
			(010)	-15.2	-65.3	-28.1	6.064
			(0-11)	-12.2	-59.4	-31.0	4.328

The interaction energies of a dimeric  $\text{BU}_0$  with its neighbors belonging to neighboring columns are much smaller than the ones inside them and differ for crystallographic directions. As a result, three types of layers can be recognized as possible secondary basic structural motifs (Figure 4.12). The comparison of

the interaction energies of dimeric  $BU_0$  within the layer ( $BSM_2$  in Table 4.7) and with the neighbors belonging to the neighboring layer ( $BSM_2/BSM_2$ ) showed clearly that the layer parallel to the (001) crystallographic plane can be recognized as the most strongly bound fragment of the crystal packing in piracetam polymorphic form II. Thus, the structure of the polymorphic form II can be characterized as columnar-layered packing of dimeric building units from the viewpoint of interaction energies. It should also be noted that the layers recognized by the analysis of intermolecular interactions (the (010) layer) and those separated by the analysis of the pairwise interaction energies (the (001) layer) do not coincide. Weak C-H...O hydrogen bonds were found between the (001) layers, binding two neighboring  $BSM_2$ .

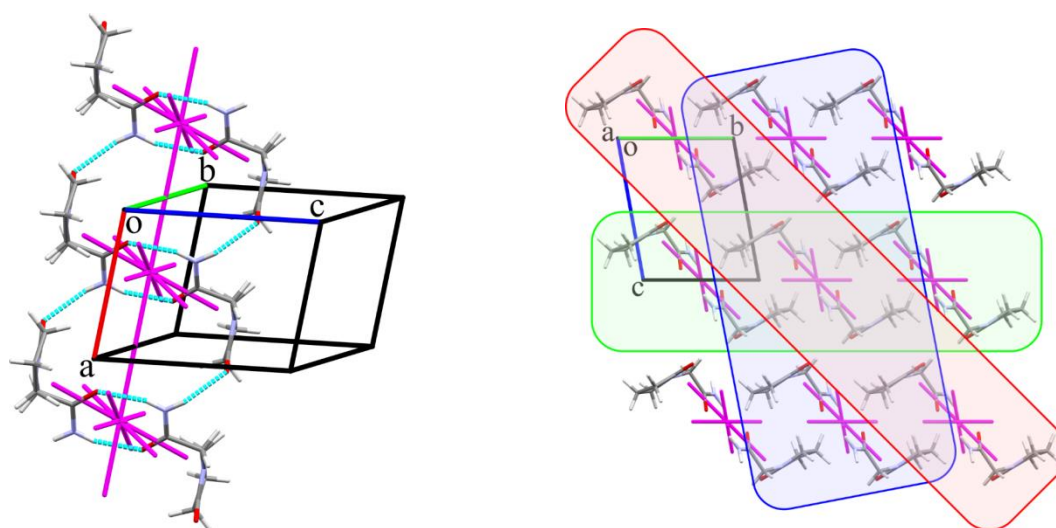


Figure 4.12. The column in the [100] crystallographic direction as a primary basic structural motif in terms of molecules and energy-vector diagrams (in purple) in the polymorphic form II (on the left). The hydrogen bonds stabilized the column are shown in cyan lines. The packing of columns in the polymorphic form II projected in [100] crystallographic direction (on the right). The layers as possible secondary basic structural motifs are highlighted in colors according to their disposition: (001) is in green, (010) - in blue, (0-11) - in red.

#### 4.2.3.2. Modeling of a shear deformation by quantum-chemical methods

According to the approach proposed for aspirin, the choice of the direction of shear deformation in the plane defined by the study of pairwise interaction energies can be made using the results of quantum-chemical modeling. To avoid the modeling of shear deformation in the directions in which a shift of neighboring layers is hindered due to very small distances between atoms, the preliminary assessment was performed. Three model systems based on three types of layers defined from calculations of pairwise interaction energies (Table 4.7) were extracted from the experimental data in the way proposed in Section 4.2.1. 2D-scanning of the mobile part displacement in relation to the fixed part and calculations of the minimal distances between closest atoms belonging to the mobile and fixed parts were performed for each of the model systems. It was already mentioned that the geometric characteristics give just rough estimates, but the preliminary analysis of the 2D-maps of the minimal intermolecular distances between the mobile and fixed parts (Figure 4.13) allows to choose the most probable direction of a crystal deformation.

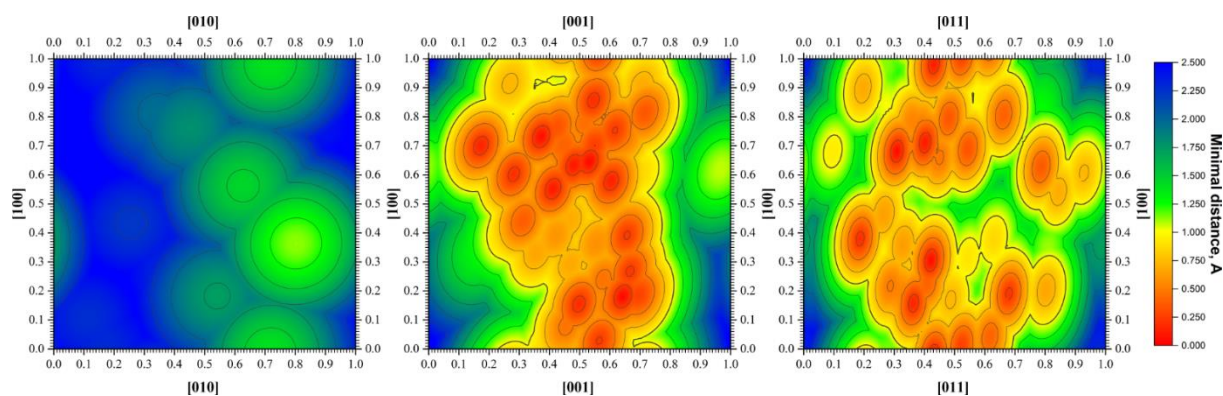


Figure 4.13. 2D-maps of the minimal intermolecular distances ( $\text{\AA}$ ) during the displacement of the dimeric  $\text{BU}_0$  as a mobile part in relation to the fragment of the neighboring layer as a fixed part calculated for three model systems: layers parallel to the (001) crystallographic plane (on the left), layers parallel to the (010) crystallographic plane (in the middle) and layers parallel to the (0-11) crystallographic plane (on the right).

The analysis of the constructed 2D-maps of the minimal intermolecular distances (Figure 4.13) showed clearly that the mobile part displacement only in relation to the (001) crystallographic plane is possible without significant obstacles. At that, the [100] crystallographic direction can be defined as the easiest for a shear deformation along the (001) crystallographic plane (Figure 4.13, on the left). It should also be noted that a 0.125 translation shift in this direction is accompanied by a small increase in the shortest intermolecular distances between the mobile and fixed parts of the model system. (Figure A 4.24).

The next step of shear deformation modeling was the calculations of the interaction energies between the mobile and fixed parts of the model system during the displacement on one crystallographic translation in the chosen direction. Such calculations were performed not only for the displacement in the [100] direction along the (001) crystallographic plane but also for the displacements in the [010] and [110] directions within the same plane as well as displacements in the [100] direction along the (010) or (0-11) crystallographic planes (Table 4.8). The profiles of the interatomic distances used for the crystals of piracetam with the step size of 1/25 of a translation showed the smooth reproduction (the highest divergence of 0.004 Å) of the curves acquired for the shown directions of shear with the step size of 1/1000 of a translation (Table A 4.22). Thus, the energy profiles were calculated with the step size of 1/25 of a translation. The energy barrier for each of the displacements was calculated as the difference of the initial and highest interaction energy between the mobile and fixed parts of the model system. The minimal energy barrier was calculated for the displacement in the [100] crystallographic direction along the (001) crystallographic plane (Table 4.8) as it was presumed by the preliminary assessment based on the analysis of the minimal intermolecular distances in the model system. The displacement of the mobile part in other crystallographic directions required much more energy and proved to be hardly probable.

Table 4.8. Energy barriers (kcal/mol) for the displacements of the dimeric BU<sub>0</sub> as the mobile part relative to the fixed part in different crystallographic directions in three model systems.

Displacement direction	Energy barrier, kcal/mol					
	Form II		Form V			
	Ambient pressure	0.45 GPa	0.7 GPa	0.9 GPa	2.5 GPa	4.0 GPa
[100] (001)	5.2	5.6	7.0	8.1	9.3	10.3
[010] (001)	77.2	117.7	75.8	96.8	166.1	237.7
[110] (001)	98.6	145.0	125.0	158.5	223.3	347.4
[100] (0-11)	163.9	154.4	257.2	308.3	453.2	544.9
[100] (010)	159.7	149.3	255.1	305.1	451.1	542.2

The detailed analysis of the energy profile for the most probable displacement showed some features (Figure 4.14). First of all, the highest interaction energy between the mobile and fixed parts proved to be negative. It means that the system remains stable enough throughout the displacement modeling. This fact may be considered the first pre-requisite for the crystal-crystal polymorphic transformation. The second feature of the energy profile is the small local minima observed just after the first step of the displacement (Figure 4.14, on the left). The next feature is some energy plateau in the transition area of the displacement process. The displacement of almost 10 steps from 0.24 to 0.60 of a translation requires only 0.92 kcal/mol.

The piracetam polymorphic form II has only one symmetry operation, namely the center of symmetry. To reflect the displacement of one layer relative to not one, but two neighboring layers, the calculated energy profile for displacement in the [100] direction must be symmetrized, as shown in Figure 4.14 on the right.

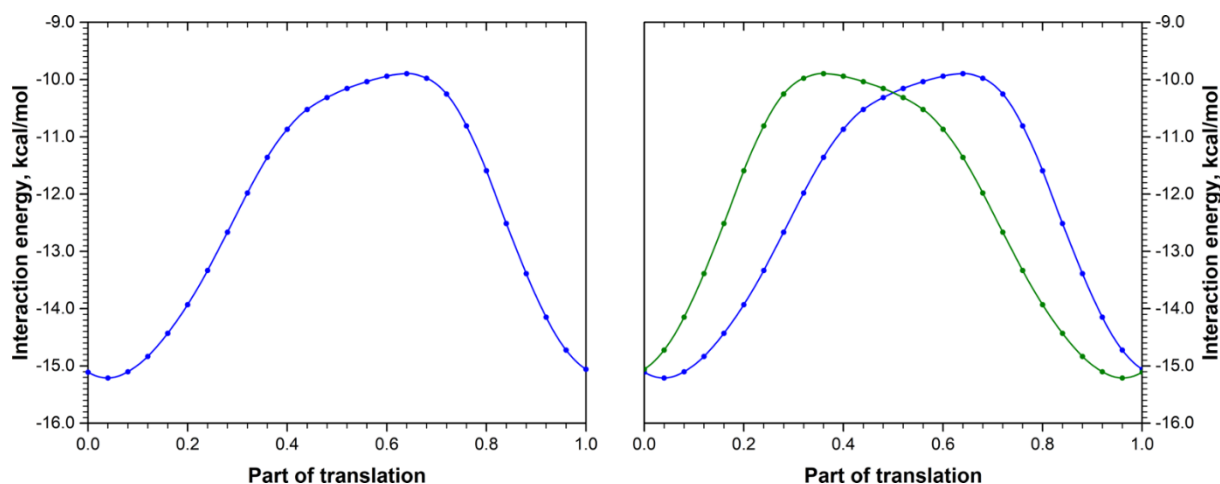


Figure 4.14. The energy profiles for the mobile part displacement in relation to the fixed part in the [100] direction along the (001) crystallographic plane for the polymorphic form II of piracetam under ambient pressure: the case of shear along the layer with lower  $c$ -coordinate (on the left); the overlay for both neighboring layers (on the right).

Thus, the quantum-chemical modeling using the approach proposed for aspirin predicted the possibility of polymorphic transformation of piracetam form II due to the shear deformation in the [100] crystallographic direction along the (001) crystallographic plane.

#### 4.2.4. Study of the pressure influence on piracetam crystal structures using quantum-chemical methods

The aforementioned approach for defining the possible direction of a shear deformation as a way for a possible polymorphic transformation was verified on the example of aspirin polymorphic modifications I and II in Section 4.1.3. Unfortunately, the crystal structure of aspirin after the polymorphic transition remains unknown. The piracetam crystal structure is a very suitable object for the development and verification of the proposed approach due to the existence of X-ray diffraction data for crystal structure after the polymorphic transformation under pressure. Moreover, the comparison of form V at different

pressures gives an opportunity to discuss the mechanism of the pressure influence on a crystal structure.

4.2.4.1. The analysis of crystal structures under different pressures from the energetic viewpoint

Similar to form II at ambient pressure, the piracetam molecule was considered as a monomeric building unit and its first coordination sphere was constructed in all the five structures under pressure. The first coordination sphere includes 13 neighbors in the polymorphic form II (Table A 4.11, Figure A 4.15b). After polymorphic transformation to form V, the number of molecules belonging to the first coordination sphere increases by one at the pressures of 0.7 and 0.9 GPa and by two with a further increase in pressure, reaching 14 and 15 respectively (Tables A 4.12-4.15, Figures A 4.15-4.16). The total interaction energy of the monomeric BU with its first coordination sphere changes nonlinearly with the growth of pressure. It remains almost constant upon the compression of form II (-73.2 kcal/mol at the ambient pressure and -73.0 kcal/mol at 0.45 GPa) and increases abruptly due to the polymorphic transformation to form V. The total interaction energy is -81.6 kcal/mol immediately after the transition and reaches a value of -83.0 kcal/mol with an increase in pressure up to 0.9 GPa. Afterwards, it drops to -79.0 kcal/mol at the pressure of 4.0 GPa.

The detailed analysis of the monomeric BU<sub>0</sub> with all the molecules of its first coordination sphere in five structures under pressure has shown that the pressure changes the ratio in energy between monomeric BUs (Figure 5.15), but the centrosymmetric hydrogen-bonded dimer remains one of the strongest and the steadiest to pressure influence. The interaction energy in this dimer decreases at the pressure of 0.45 GPa as compared to that at ambient pressure, but remains constant during the polymorphic transformation and pressure

increase up to 0.9 GPa. Further increase in pressure causes a slight decrease in the energy of the centrosymmetric hydrogen-bonded dimer. In such a case, this dimer should be considered as a dimeric building unit of the crystal structures under study [7].

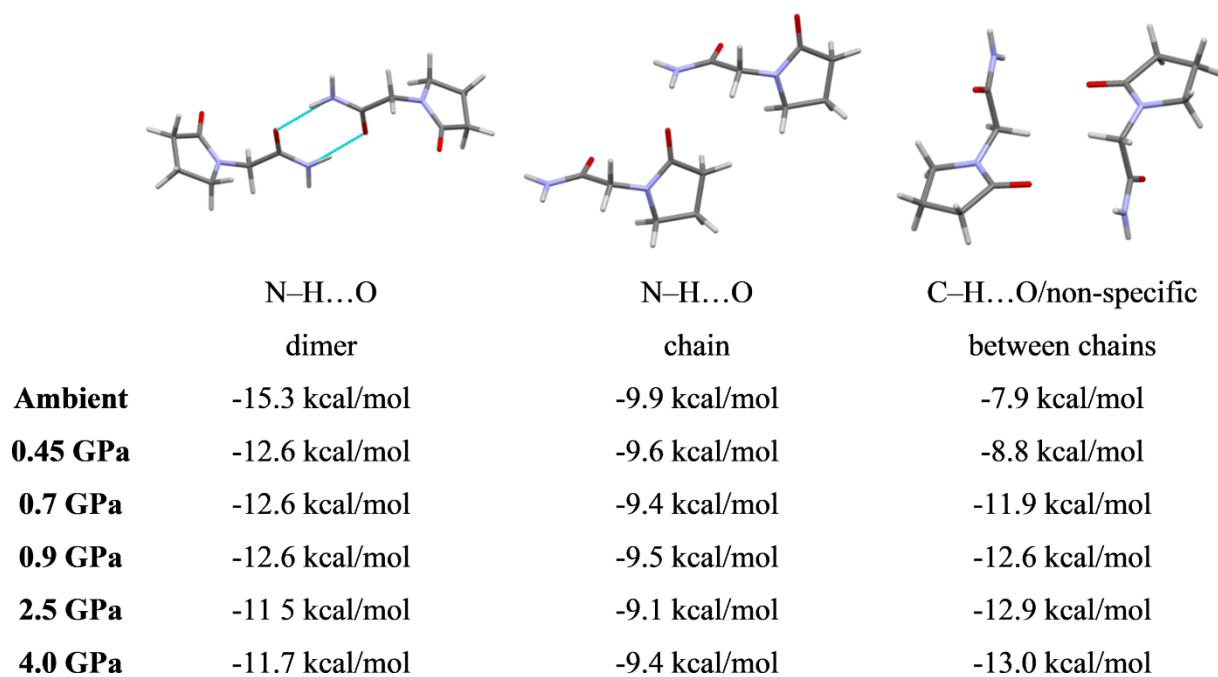


Figure 4.15. The stronger interactions of a basic molecule at different values of pressure in forms II and V.

The first coordination sphere of a dimeric  $BU_0$  contains 14 neighboring dimers in polymorphic structures II or 16 neighboring dimers in structures V (Tables A 4.16-4.21, Figures A 4.17-4.18). The total interaction energy of dimeric  $BU_0$  with all surrounding ones changes nonlinearly with an increase in pressure (Table 4.7). The analysis of the pairwise interaction energies of a dimeric  $BU_0$  with the neighboring dimeric  $BU_i$  in structures under pressure showed the same features as it was found in the structure at ambient pressure. The hydrogen-bonded columns in the [100] crystallographic direction can be defined as the primary basic structural motif and three types of layers can be considered as possible secondary basic structural motifs. Comparison of

distances between the mean planes of these layers at different pressures showed that they decrease almost equidistantly with increasing pressure (Figure 4.16). This confirms the effect of isotropic pressure on the piracetam crystal in the diamond anvil cell [15]. However, the pressure affects the ratio in energy within the structural motifs and between them (Table 4.7).

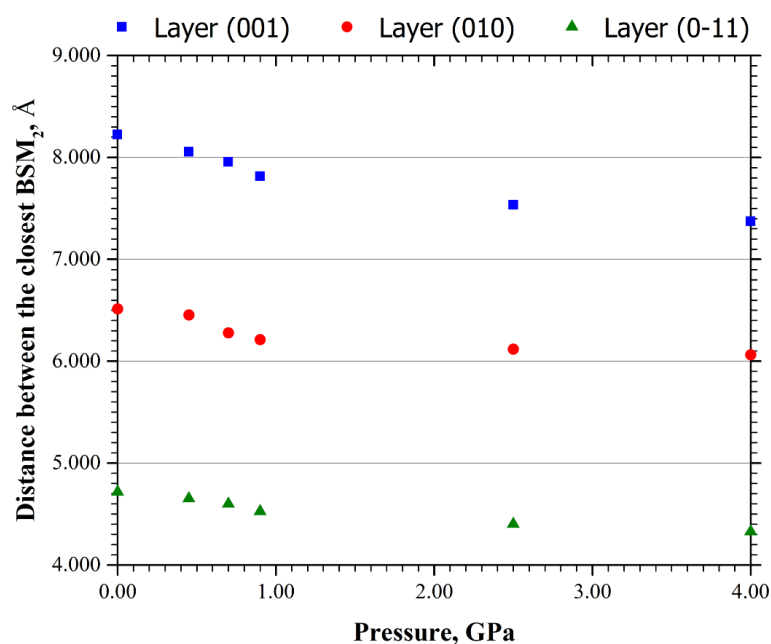


Figure 4.16. Dependence of the distances between planes, determined by the analysis of the pairwise interaction energies, on the pressure value.

The analysis of the energy ratio between structural motifs ( $BSM_1/BSM_1$  and  $BSM_2/BSM_2$ ) showed that the relatively small pressure of 0.45 GPa results in an increase of the interaction energies between all the separated layers almost equally (Figure 4.17). The polymorphic transformation from form II to form V at the pressure between 0.45 and 0.7 GPa causes unequal changes in interaction energy between the layers and columns within the layer. Thus, the interaction energy between the layers parallel to the (001) crystallographic plane increases more than the interaction energy between the layers parallel to the (010) or (0-11) crystallographic planes. On contrary, the interaction energy between the neighboring columns within the (010) or (0-11) layers becomes higher than

the interaction energy between the neighboring columns within the (001) layer (Figure 4.17). It should be noted that the polymorphic transformation is associated with the shift in the [100] crystallographic direction along the layer parallel to the (001) crystallographic plane, as predicted by quantum-chemical modeling and confirmed by comparing structures II and V (Figure 4.18). It also turned out that this shift is accompanied by the destruction of weak C-H...O hydrogen bonds found between these layers.

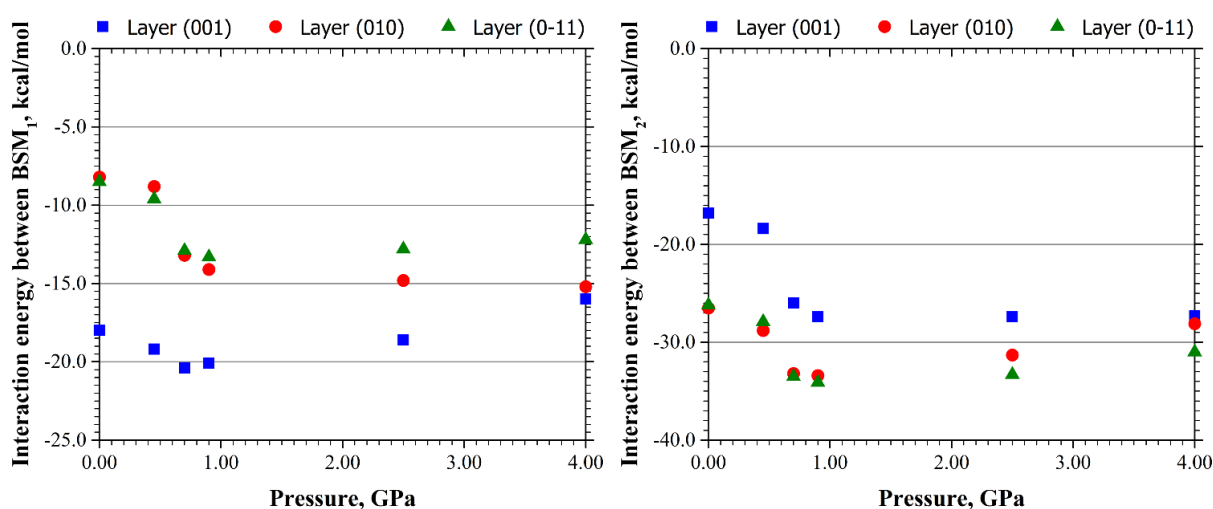


Figure 4.17. Interaction energy between the layers as BSM<sub>2</sub> (on the left) and between the columns as BSM<sub>2</sub> (on the right) at different pressures.

A further increase in pressure leads to a certain redistribution of the interaction energies between primary and secondary structural motifs (Table 4.7). The interaction energy between the layers parallel to the (001) crystallographic plane remains practically unchanged while the interaction energy between the columns within these layers decreases. The opposite situation is found in the case of the layers parallel to the (010) crystallographic plane. The interaction energy between these layers increases, while the interaction energy between adjacent columns within these layers decreases with increasing pressure (Figure 4.17). The interaction energies between the (0-11)

diagonal layers and between the adjacent columns inside them decrease almost equally with increasing pressure. Such a process results in the change of the crystal structure type due to the effect of pressure. The crystal structure of form V can be classified as columnar-layered at the pressure of 0.7 GPa and columnar at the pressure of 4.0 GPa.

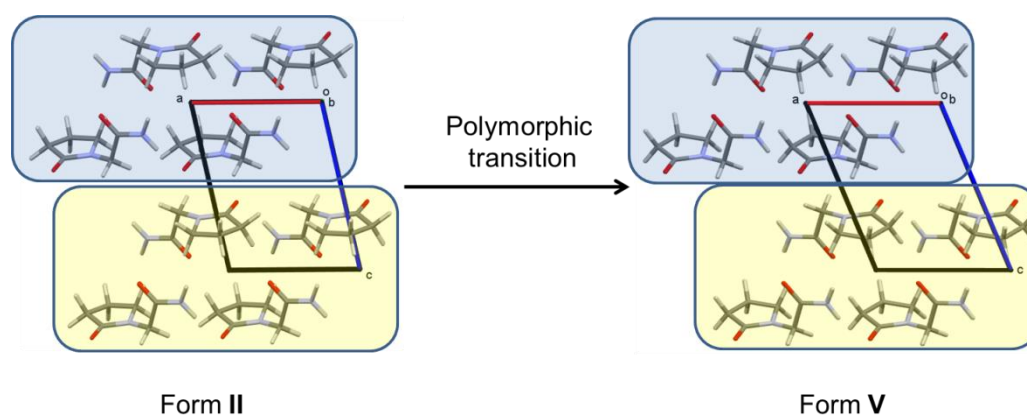


Figure 4.18. The polymorphic transformation from form II to form V under pressure according to the experimental X-ray diffraction data. The layers parallel to the [001] crystallographic plane are highlighted to show their shift.

Thus, the pressure influence on the piracetam crystals can be divided in two stages. At the first stage, the shift of the strongly bound layers recognized as a more probable  $BSM_2$  between which the interaction energy is the weakest causes the polymorphic transformation from form II to form V without the change of the crystal structure type from the energetic viewpoint. At the second stage, the redistribution of the interaction energies between three types of layers and between the columns inside them results in the transition from the columnar-layered type of the crystal structure to the columnar structure without the change of the polymorphic form. It should also be noted that a columnar structure is more isotropic than a columnar-layered one in terms of the interaction energies between molecules. Therefore, it can be presumed that pressure causes a decrease in the anisotropy of molecular crystals.

#### 4.2.4.2. Modeling of shear deformation in the crystal structures under different pressures

To study a possible shear deformation in structures II and V under pressure, quantum-chemical modeling was performed similarly to that was made for form II at ambient pressure. The preliminary assessment of the minimal intermolecular distances during the displacement of the dimeric  $\text{BU}_0$  as the mobile part of the model system along each of the three layers as a fixed part showed the same results as for form II. Comparison of the 2D-maps showed that an increase in pressure causes a decrease in minimal intermolecular distances between dimeric  $\text{BU}_0$  and molecules of the fixed part of the model system (Figures A 4.21-4.23). As a result, the energy barrier for the displacement in all the defined crystallographic directions along the three possible types of layers increases (Figure 4.19, Table 4.8).

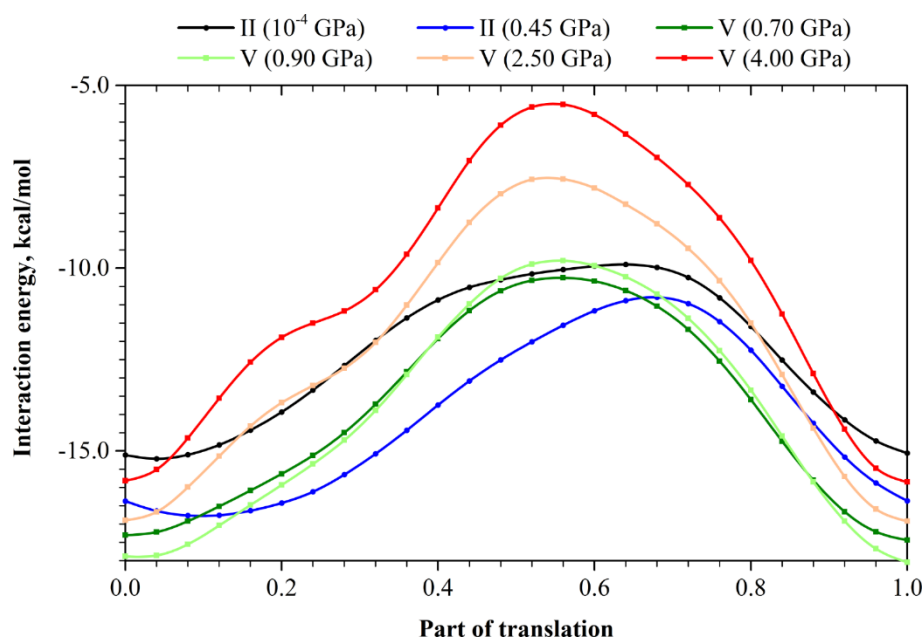


Figure 4.19. The energy profile for the displacement of dimeric  $\text{BU}_0$  as the mobile part in the [100] crystallographic direction along the layer parallel to the (001) crystallographic plane as the fixed part.

The main difference between the energy profiles for the displacement in the most probable [100] crystallographic direction along the layer parallel to the (001) crystallographic plane for forms II and V is the absence of local minima in the area close to the initial state (Figure 4.19). The minimal displacement of the dimeric  $BU_0$  with respect to the fixed part of the model systems extracted from form V at different pressures causes a decrease in the interaction energy between them. At that, the interaction energy between the mobile and fixed parts in the model system remains negative during the displacement trajectory throughout the translation in the [100] crystallographic direction along the (001) plane.

Modeling of shear deformation in other crystallographic directions showed the essential increase in the shift energy barrier with increasing pressure with the exception of the displacement in the [010] crystallographic direction along the (001) crystallographic plane (Table 4.8). The shift energy barrier in this direction is high enough to exclude the possibility of a shear deformation (77.2 kcal/mol) at ambient pressure. The pressure of 0.45 GPa leads to an increase of this barrier up to 117.7 kcal/mol, but the polymorphic transformation into form V causes the decrease of the shift energy barrier almost up to the initial value (75.8 kcal/mol). The displacement in the [010] direction remains improbable at all the pressure values due to a high shift energy barrier and high positive interaction energies between the mobile and fixed parts, but such a decrease in the energy barrier after the polymorphic transformation may indicate a significant reorganization of the crystal structure just in this direction.

#### 4.2.4.3. The study of interaction energy components using the Localized Molecular Orbital Energy Decomposition Analysis

To analyze the intrinsic forces causing the polymorphic transformation under pressure, the energy-vector diagrams for form II at 0.45 GPa and form V

at 0.7 GPa have been compared (Figure 4.20). The strongest interactions in the studied crystals are the N-H...O hydrogen bonds forming a centrosymmetric dimer, the N-H...O hydrogen bonds forming columns as BSM<sub>1</sub> and C-H...O/non-specific interactions found between the layers parallel to the (001) crystallographic plane as BSM<sub>2</sub>. The most essential difference in interaction energy before and after the polymorphic transformation is found in the dimer bound by C-H...O weak hydrogen bond in form II (Figure 4.20).

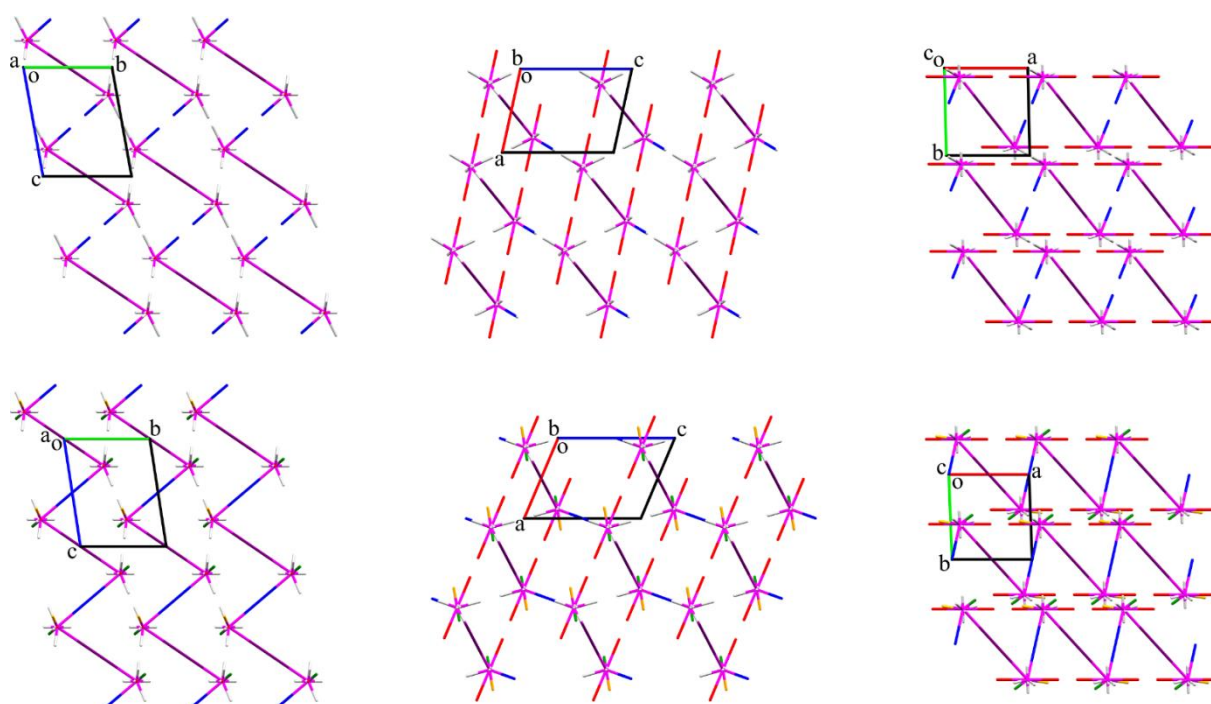


Figure 4.20. Packing of the energy vector diagrams representing the distribution of monomeric building units in the crystals of piracetam polymorphic modifications II (at the top) and V (at the bottom) under pressures of 0.45 and 0.7 GPa, respectively. The vectors connecting the pairs of molecules affecting the structure most of all represented in color: the hydrogen-bonded (N-H...O) dimer - in violet, the ones bonded by N-H...O in BSM<sub>1</sub> - in red, the non-classic hydrogen-bonded (C-H...O) ones and their shifted analogs found between the most probable BSM<sub>2</sub> - in blue. The projections in *a* (on the left), *b* (in the middle), *c* (on the right) crystallographic directions are represented.

An analysis of the components of interaction energy (electrostatic, polarization, dispersion, repulsion and exchange) is the technique that opens

new possibilities to understand the mechanism of polymorphic transformation. Therefore, such an analysis was applied to the study of the strongest interactions in piracetam crystals at different pressures (Tables A 4.10-4.15). The energy of hydrogen bonding approximated as the sum of electrostatic and polarization components (Figures A 4.19-4.20) and the dispersion component are the attractive forces acting in a crystal. The repulsive forces are presented as the sum of exchange and repulsion components. The energy ratio of these forces and their change with increasing pressure are different for the three strongest interactions (Figure 4.21).

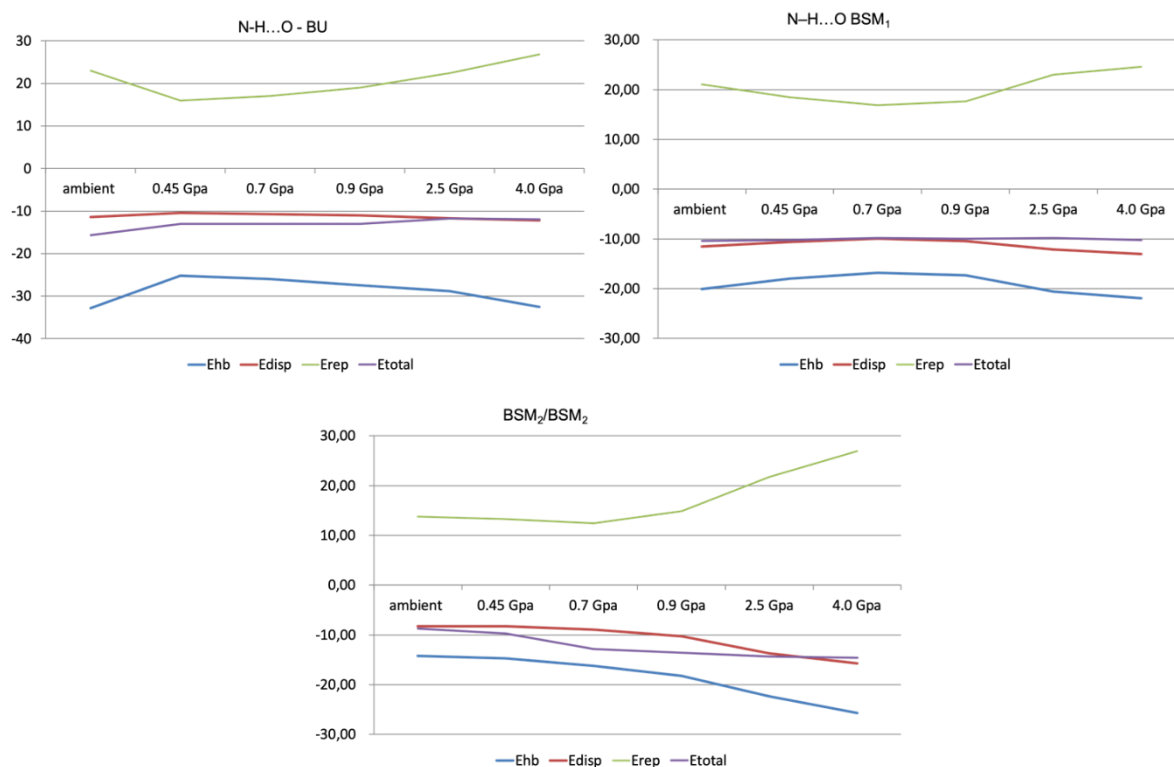


Figure 4.21. Energy of the hydrogen bonding (in blue), dispersive interactions (in red), repulsive interactions (in green) and total interaction energy (in lilac) at different pressures in the centrosymmetric dimer bound by two N-H...O hydrogen bonds and considered as dimeric BU<sub>0</sub> (at the top, on the left); in the linear dimer bound by N-H...O hydrogen bond and formed BSM<sub>1</sub> (at the top, on the right); in the dimer bound by C-H...O or non-specific interactions and provided the interaction between neighboring (001) layers as BSM<sub>2</sub> (at the bottom).

In the case of the centrosymmetric dimer bound by two N-H...O hydrogen bonds, the total interaction energy remains almost unchanged at increasing pressure. This confirms the correctness of the choice of this dimer as a complex building unit in the studied piracetam crystals. Hydrogen bonding is much stronger than dispersive interactions and its change due to pressure increase coincides with the change of the repulsive forces (Figure 4.21). The dispersive component of the total interaction energy does not change almost with increasing pressure.

The N-H...O hydrogen bond forming the column as BSM<sub>1</sub> proved to be not so rigid. The energies of hydrogen bonding and dispersive interactions are closer than those in the centrosymmetric dimer but the energy of hydrogen bonding remains higher. These attractive components of the total interaction energy are changed in the same way (Figure 4.21) and compensated by the change of repulsive interactions. As a result, the total interaction energy of this dimer remains almost unchanged at increasing pressure. It confirms our presumption that the reorganization of the piracetam crystals is caused by the change of interactions between primary basic structural motifs bound by the weakest intermolecular forces.

The components of attractive forces (hydrogen bonding and dispersive interactions) are closest within the dimer bound by C-H...O hydrogen bond in form II or non-specific interactions in form V (Figure 4.21). The relatively small contribution of directed interaction like hydrogen bond into the interaction energy in this dimer can explain the possibility of its shift deformation that results in the single crystal to single-crystal polymorphic transformation. It should be noted that the total interaction energy increases to the highest degree in this dimer with increasing pressure.

Thus, the study of the relative contribution of the components of the interaction energy in total energy in the three most strongly bound dimers showed that the stability of intermolecular interactions to deformation under

pressure influence depends not only upon the value of the energy of the intermolecular interaction, but also the relative contribution of directed and non-directed interactions. Relatively low contribution of hydrogen bonding energy can lead to less rigidity of interaction and to the possibility of shifting molecules relative to each other.

### **4.3. Computational analysis of pressure-induced shear in R,S-ibuprofen**

Now, when it is shown that the reasons and prerequisites of the polymorphic transformation can be successfully studied with the set of methods proposed by us, it is possible to go further and to analyze the probable transitions for the structure, whose inability to transform is questionable. Ibuprofen, popular NSAID, is a profitable candidate for detailed analysis of its crystalline arrangement. On one hand, it does not undergo polymorphic transformation during the compression up to 4.00 GPa (Figures A 4.25-4.27) [20]. On the other hand, it can transform during the grinding experiment showing ambivalence towards the mechanical processing [21]. Structure of the metastable polymorph II is known as well, however, it cannot be obtained directly from the form I allowing one to search for possible mechanism of conversion.

#### 4.3.1. Comparison of experimental and optimized in solid state structures

Usually, experimental crystalline structures of materials can be used for studies of their structure from the energetic viewpoint right away after an X-ray experiment, but in specific cases, like metastability, etc., it is impossible or gives non-realistic values during computations. Ibuprofen is a typical representative of such a situation, the structure of the polymorphic form I is easy to use directly from the experimental data whereas the structure of the polymorphic form II defined from powder X-ray experiment gives improbable result (the hydrogen

bonded dimer has the same energy as a stacking interaction). The additional step of structure optimization is required then. So, the crystalline structures of the polymorphic modification I at different pressures were acquired by us from the initial one at ambient pressure to receive comprehensive information on the resemblance of the optimized and experimental molecular arrangements.

The comparison showed that the mean absolute and relative deviations in parameters  $a$ ,  $b$  and  $c$  between the experimental and vc-relaxed structures are 0.106, 0.045, 0.201 Å and 0.754, 0.596, 1.955 %, respectively, which do not coincide with the experimental ones according to the  $3\sigma$  (99.7%) rule. Their dependencies from pressure have similarities and differences. All of them have an inflection point at the pressure of 1.70 GPa or between 0.88 and 1.70 GPa. For all the main crystallographic directions the relative deviations move at first to the positive area with pressure and further start to fluctuate in a more-less stable way (Figure 4.22a). These stable fluctuations occur around the mean values of absolute and relative deviations of 0.129, 0.022, 0.165 Å and 0.929, 0.304 and 1.656 % for the parameters  $a$ ,  $b$  and  $c$ , respectively. Such a behavior may have two reasons. The first is that the decrease of the relative error in pressure and so the following minimization of the effect of error due to the growth of pressure occurs, but the real deviation of pressure is small for all points except the one under ambient pressure (Figure 4.22b). The second is based on a fact that the pressure growth may cause an abrupt repulsion growth between molecules at some point. For the parameter  $a$ , the value of the relative deviations decrease until the pressure reaches 0.88 GPa, but further suddenly grow at 1.70 GPa. The strange behavior was observed for the parameter  $b$  as well. The deviation for it grows at first, but falls down at 1.70 GPa. It is possible to suppose that the structure changes from strong anisotropy to a more isotropic packing. For example, the length of non-classic hydrogen bonds C-H... $\pi$  becomes shorter with compression, until at 1.70 GPa a new short contacts C...H appear. They lay in the direction opposite to the aforementioned hydrogen bond

(Figure 4.23) and likely is a manifestation of the binding forces counterbalancing these bonds. The parameter  $c$  shows the same behavior, but the deviations for it decrease till the fluctuations begin.

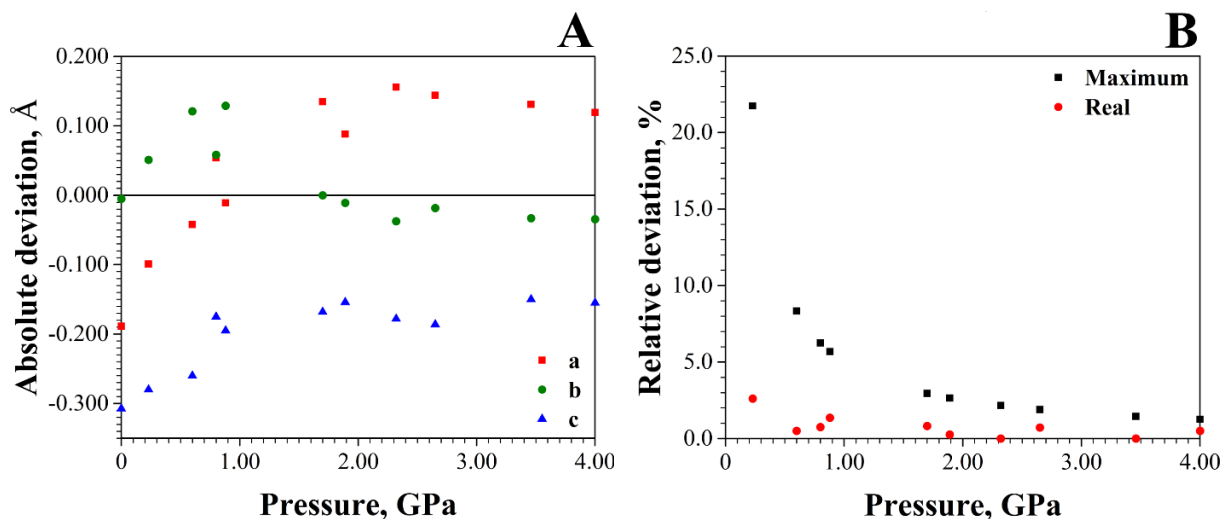


Figure 4.22. The absolute deviations dependency from pressure in the main crystallographic directions  $a$ ,  $b$  and  $c$  between the experimental and optimized structures of the polymorphic modification I of ibuprofen (A). The zero-line is put to see the changes in deviations behavior on pressure. The maximum (with the error initially set in calculation) and really occurred relative deviations in pressure (B).

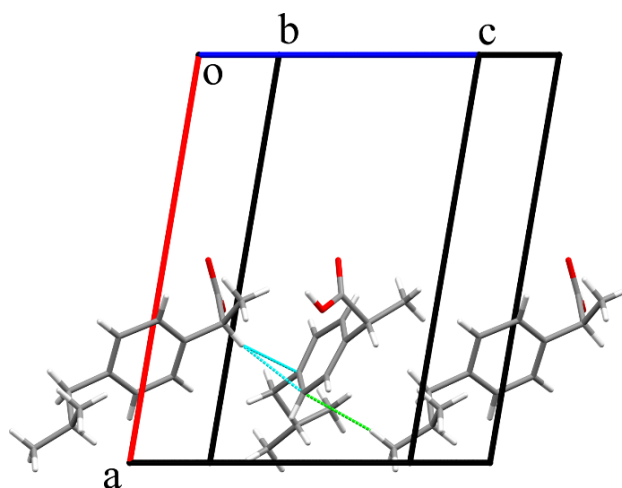


Figure 4.23. Formation of the new short contact C...H (in green) counterbalancing the non-classic hydrogen bonds C-H... $\pi$  (in bright blue) at 1.70 GPa.

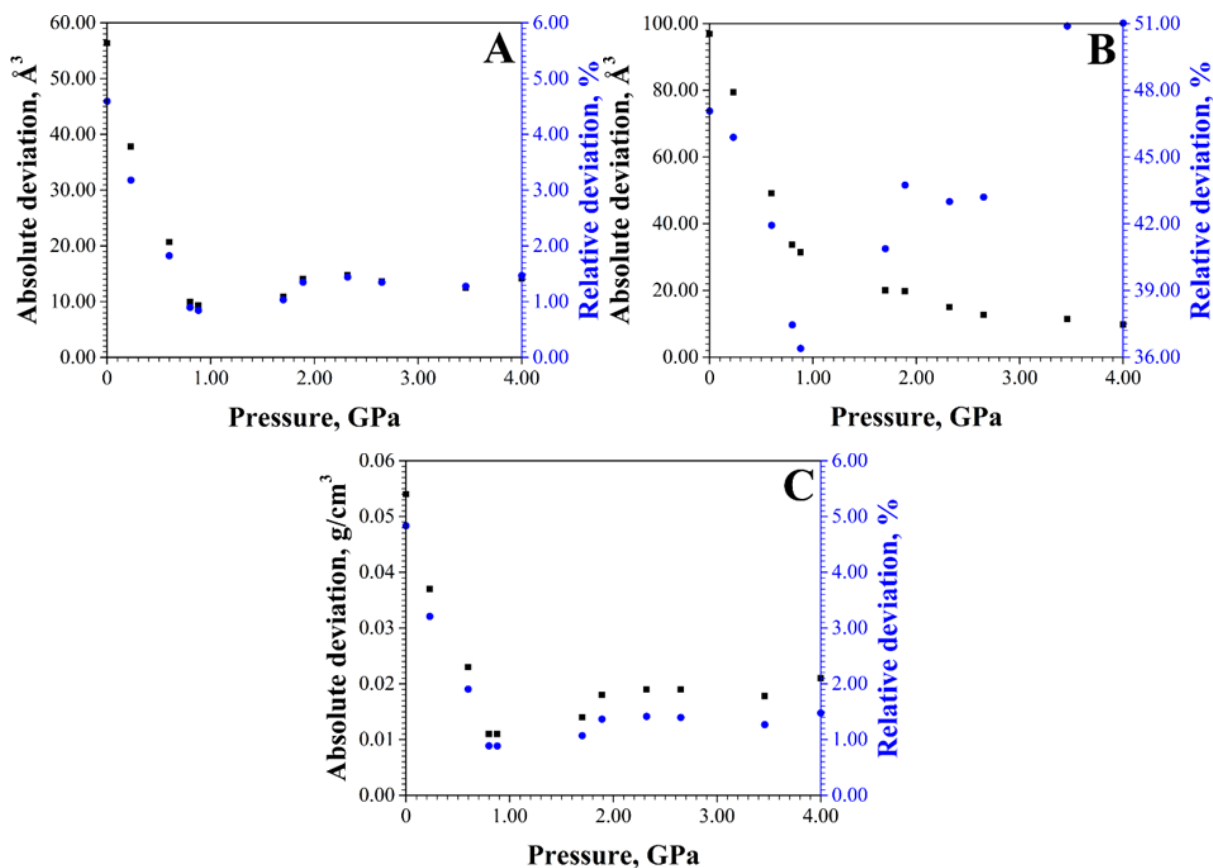


Figure 4.24. Dependencies of the absolute (black) and relative (blue) deviations of the volume (A), void volume (B) and density (C) between the optimized and experimental structures from pressure in the polymorphic modification I of ibuprofen.

Unfortunately, the angle  $\beta$  cannot be compared for the experimental and optimized structures, because the point group symmetry of crystals changes during the optimization to the lowest possible (P1) and the angles  $\alpha$  and  $\gamma$  change from  $90^\circ$ . However, the volume of the unit cell can be. The relative deviations for it seem insignificant, but there is another fact. The volume of the unit cell is smaller after the optimization in all the pressure range and the number of molecules in the unit cell is constant (Figure 4.24a). Literally, it means that the density of the ibuprofen crystals should be overestimated during the computations. Thus, the void volume in crystals and the density for the optimized and experimental structures were calculated as expressed in Chapter 2 (Figure 4.24b,c). Since the same parametrization was applied for all the computations and the point group have no influence in case of ibuprofen, the

comparison of data was done. The absolute and relative deviations of the void volume points out at the same fact of a much denser packing in the optimized structures: 34.48 Å<sup>3</sup> and 43.77 %, respectively. However, the density changes lay in diapason of just 0.054 g/cm<sup>3</sup> or 4.834 % with the mean values of 0.022 g/cm<sup>3</sup> and 1.793 %, respectively. There is a minimum on the curves of deviations more observable for the densities. It may occur because of the fact that in the pressure range from 0.88 to 1.70 GPa the crystal is balancing between the state with low, appearing below 0.88 GPa, and high repulsion, above 0.88 GPa.

Analysis of covalent bonds lengths and the intermolecular hydrogen bonds and corresponding valent angles showed ambiguous results. First, the covalent bonds lengths were compared for the heavy atoms, because the hydrogen atoms positions obviously changed after the optimization from geometrically chosen to the more realistic ones. According to the 3σ (99.7%) rule, the computed structure of the polymorphic modification I of ibuprofen does not correspond to the one received from the experiment under ambient pressure. However, it was an expected result because the minimal pressure for which the convergence could be reached was not 1 bar, but 1 kbar instead using the aforementioned combination of methods. The other structures optimized at the pressures coinciding with the experimental ones showed the good overlap of the data (Table A 4.49). Indeed, the aliphatic parts of the molecule showed the biggest discrepancy, but on a whole the deviation is distributed approximately evenly and did not appear at low pressures.

Three types of hydrogen bonds were found in crystals during the analysis. All their lengths are underestimated during the computations. The deviation with the experimental values is the biggest for the hydrogen bonds O-H...O reaching the mean absolute and relative deviations of 0.27 Å and 15.17 %, respectively, close for all the pressures in range (Figure 4.25). These bonds from the two carboxylic groups form molecular dimers. The dimers are tilted to each other

according to the experimental data and the tilt grows with pressure, however, this effect does not occur after the optimization showing the stable valent angle of  $178^\circ$ . Thus, these angles are totally overestimated and the deviation of their determination growth from  $2^\circ$  under ambient pressure to  $11^\circ$  at the pressure of 4.00 GPa. As well, after the optimization with variable cell routine, the new non-classic hydrogen bonds C-H...O appear already without compression instead of the pressure of 2.32 GPa, when they show up in experimental structures. The difference between the calculated and experimental interatomic distances reaches for it up to  $0.17 \text{ \AA}$ . However, the deviation showed a behavioral gap in the diapason of pressure from 0.88 to 1.70 GPa. At the pressures of 0.88 GPa and below, it decreases gradually with pressure, further the sudden drop in accuracy occur at 1.70 GPa and the consistent decrease in the error prolongs. The angles are very close to the experimental ones (mean absolute error remains constant around  $2^\circ$ ). The latest hydrogen bonds are C-H... $\pi$ . The in their length between the optimized and experimental structures are nearly the same as for C-H...O bonds (mean absolute deviation equals  $0.19 \text{ \AA}$ ), but the changes in deviation are random. The valent angles here differ randomly as well and their mean absolute deviation reaches  $6^\circ$ .

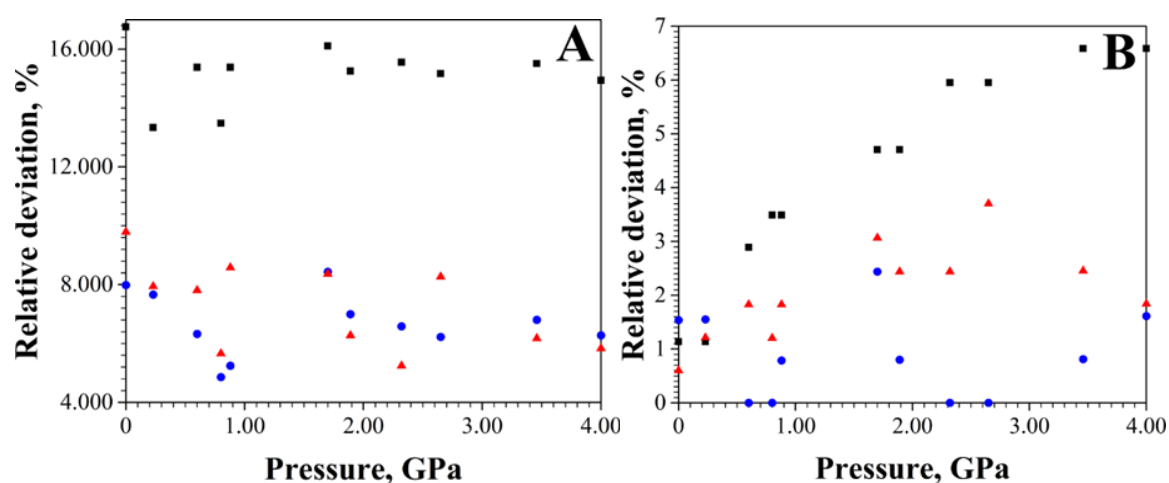


Figure 4.25. Dependencies of the relative deviations of the hydrogen bond lengths (A) and corresponding valent angles (B) between the optimized and experimental structures from pressure in the polymorphic modification I of ibuprofen.

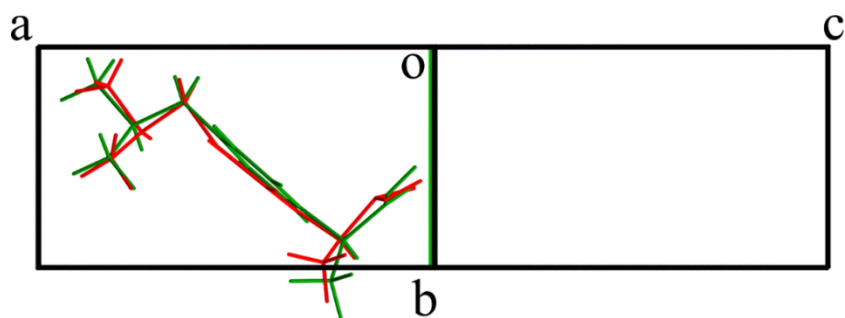


Figure 4.26. Overlap of experimental (in red) and optimized in solid state molecular structures of polymorphic modification II of ibuprofen.

Summarizing all the above mentioned, the variable cell routine will cause more uncertainties than profits in case of the polymorphic modification II of ibuprofen. Its structure was received under ambient pressure, so the conventional relaxation was applied to receive the more appropriate structure quality. It demonstrated significant discrepancies (Figure 4.26) with the initial structure. However, the unit cell parameters remain unchanged and the adequacy of the molecular building is expectable as seen from the preliminary calculations for the form I. Thus, the optimized structure of the polymorphic form II of ibuprofen was applied in the further work instead of the experimental one.

#### 4.3.2. Analysis of basic structural motives from an energetic viewpoint

Search for basic structural motives is complicated (if possible) without the determination of a building unit in the crystal structure. Thus, the first step towards an assessment of ibuprofen's capabilities to a solid-solid shear-based transition is the calculation and analysis of pairwise interaction energies for the individual molecules. This calculation proved to be more accurate than the conventional geometric (visual) analysis of synthons in the crystal structure and obviously gives a possibility to consider more types of cohesive forces (such as non-directional interactions or non-classic hydrogen bonds, being an infeasible component of binding) [22].

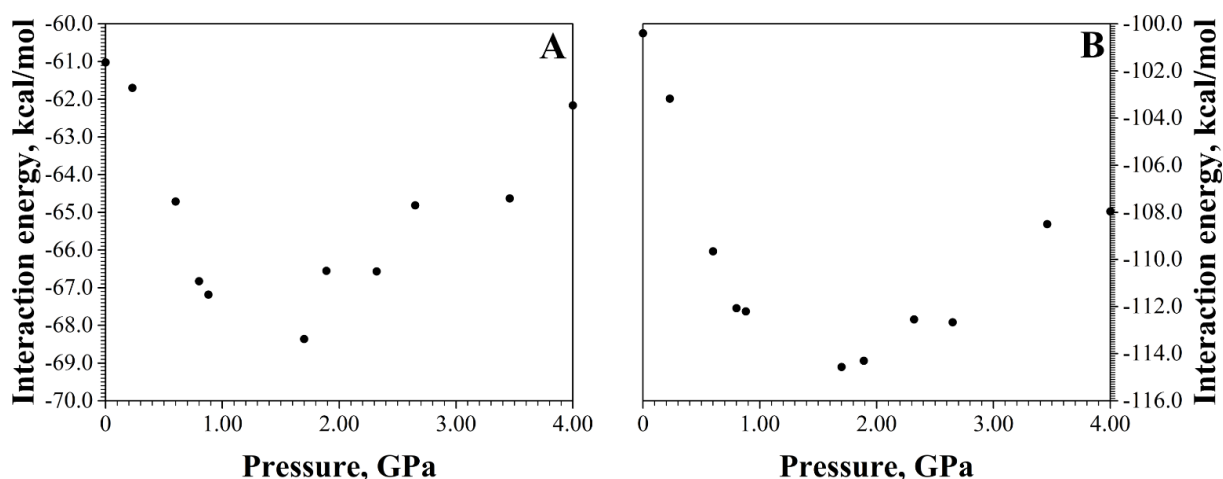


Figure 4.27. The dependence of total pairwise interaction energy of monomeric (A) and dimeric (B) building units with their first coordination spheres from pressure in the polymorphic modification I of ibuprofen.

The pairwise interaction energies were computed and analyzed in the same way as it was done for aspirin and piracetam for both polymorphic modifications of ibuprofen (Tables A 4.23-4.46, Figures A 4.28-4.33). For the form I the calculations were done at every pressure point. The first coordination sphere of a molecule of ibuprofen consists of 14 neighbors for the both forms. The total energies of interaction in the first coordination sphere are equal to -61.0 and -67.8 kcal/mol at ambient pressure for the forms I and II. The higher stability of the polymorphic modification II can be expected than, but according to the experimental data [23] it is metastable, so the building unit in the both polymorphic modifications of ibuprofen is definitely not a molecule.

Speaking of the total interaction energy changes with pressure, the inflection point occurs at the pressure of 1.70 GPa (Figure 4.27a). First, it grows gradually to -68.4 kcal/mol at 1.70 GPa, which can be described with the formation of new interactions and an increase in the stability of the old ones. According to the shortest set of van der Waals radii determined by Y.V. Zefirov and P.M. Zorky [24], the new hydrogen bonds were not found during the compression till 1.70 GPa. The stabilization of the C-H... $\pi$  interactions was observed from the viewpoint of geometric analysis, but the interaction energies

in the corresponding molecular pairs show the exactly opposite behavior (gradual decrease from 10.6% to 9.3% from total). Few new short contacts C...H opposing these non-classic hydrogen bonds were found as well (Figure 4.28a). It is unclear, if the additional stabilization of structure is caused by non-directional interactions or reorder of weak hydrogen bonds, but anyway it causes the slow conversion from anisotropy to more isotropic state. Second, the distances between molecules in the structure become so small, that the repulsion overcomes the effect of stabilization and the significant shortening of contacts between atoms of the same type appear (Figure 4.28b): H...H (2.21 Å at 1.70 GPa), C...C (3.41 Å at 2.65 GPa) and finally O...O in the hydrogen-bonded dimer of molecules (2.57 Å at 3.46 GPa). Two new weak hydrogen bonds appear at the pressures of 1.89 and 4.00 GPa consistently, but their stabilization effect is very low (Figure 4.28c).

Analysis of the individual pairs of molecules has shown that for both modifications and at any pressure up to 4.00 GPa the hydrogen-bonded dimers (Figure 4.28b) prevail by energy over any other molecular pair in the first coordination sphere (Tables A 4.23, 4.25-2.34). Thus, they were chosen as the building units for the second stage of calculations of the pairwise interaction energies. Dimeric building unit can be chosen based on synthon theory [25] as well. According to it, the dimer bonded with the classic hydrogen bonds can be additionally justified as the building unit as the most rigid structure fragment in a view of that the 2 molecular pairs with competitive interaction energy appear at 1.89 GPa in the polymorphic form I (symmetry operations:  $x, 3/2-y, -1/2+z; x, 3/2-y, 1/2+z$ ). Simultaneously, the interaction energy in the aforementioned strongly bound secondary pairs of molecules is reached by non-directional interactions and shows metastable character especially on pressure higher than the 3.46 GPa, while the repulsion growth faster than the attraction and the H...H short contact form instead of C...H ones. The shortening of the interatomic distances in the carboxylic groups of hydrogen-bonded dimers in the

polymorphic modification II show extraordinary values. So, the lengths are only 1.53, 2.27 and 2.43 Å for the hydrogen bond and two short contacts H...H and C...H, respectively. However, the hydrogen-bonded dimers overcome any other pairs in the first coordination of a molecule in the polymorphic modification II sphere by more than 4.5 times and can be chosen as building unit on the base of the interaction energy only.

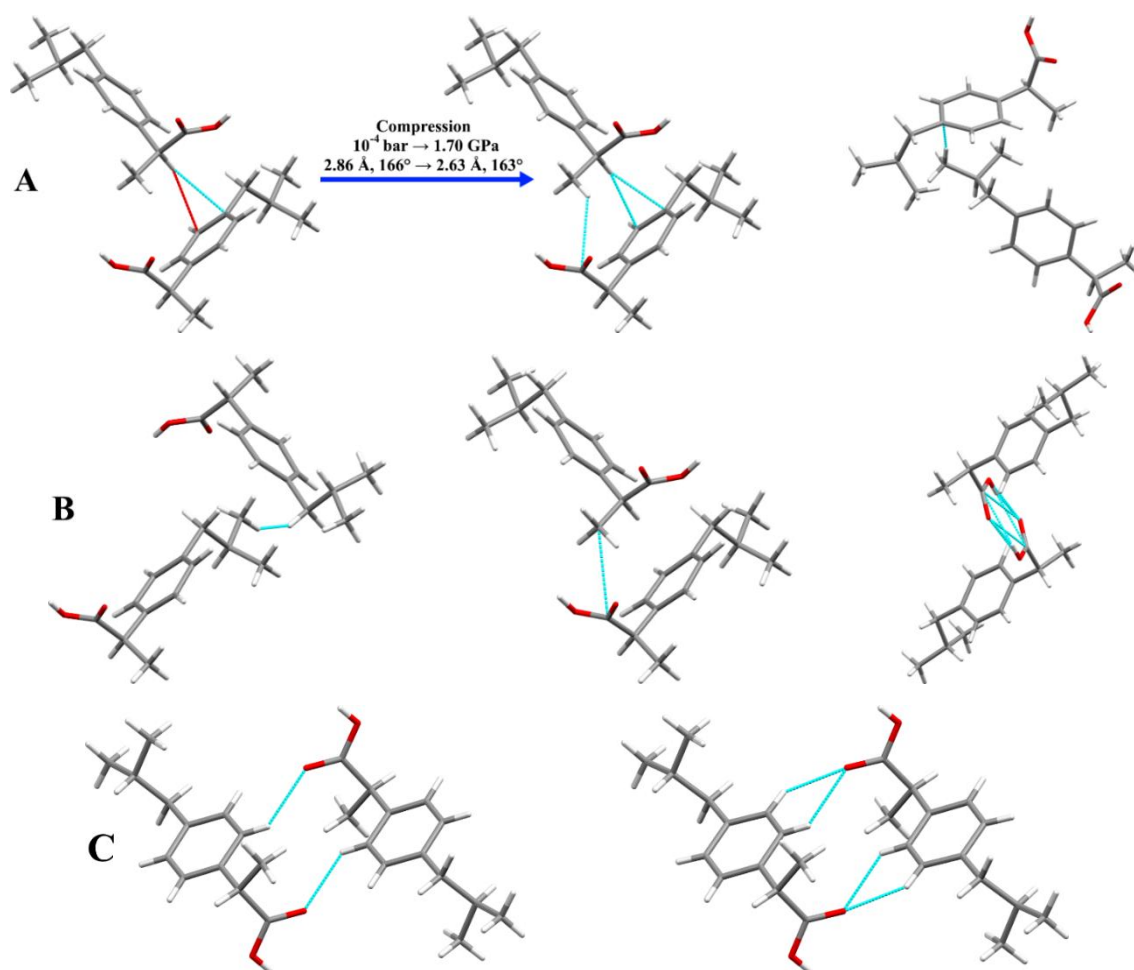


Figure 4.28. Intermolecular contacts, which stabilize the crystal structure till 1.70 GPa (A): changes in C-H... $\pi$  hydrogen bond under pressure (left to center) and the short contacts C...H opposite to it; which indicate a decrease in stability of crystal on further compression: H...H (on the left), C...C (center) and O...O (on the right) short contacts at the pressures of their appearance; which cause an additional stabilization of the structure on compression up to 4.00 GPa: two C-H...O weak hydrogen bonds at 1.89 (on the left) and 4.00 GPa (on the right). The cyan lines represent detected hydrogen bonds and short contacts, red one depicts the short contact involved in C-H... $\pi$  absent under ambient pressure.

The redetermination of the first coordination sphere for the hydrogen-bonded dimers of molecules as building units and the recalculation of the pairwise interaction energies showed that every dimer is surrounded by 18 and 14 neighbors with non-zero interaction energies for the polymorphic modifications I and II, respectively (Tables A 4.35-4.46, Figures A 4.31-4.33). It is already expectable from the fact that the form I is denser than II (1.117 vs 1.077 g/cm<sup>3</sup> under ambient pressure). As well, the energies of dimers interaction in the first coordination sphere have more reasonable values: -100.8 and -81.0 kcal/mol for the polymorphic modifications I and II, respectively. It corresponds to the fact of the form II metastability, since its stabilization is near 20% weaker than that for I. The dependency from pressure found for the total energy of interaction at the first stage of computation repeats for the pairs of dimers as well (Figure 4.27b). The energy growth at first from -100.8 to -114.6 kcal/mol (at 1.70 GPa) and later drops to 108.0 kcal/mol (at 4.00 GPa).

Search for the basic structural motives gave different results for the polymorphic modifications I and II. Solely the secondary basic structural motives were found for the first one, it is layered (Table 4.9). For the orientation of the layers' families, 3 possibilities are available. They are (100), (001) and (102), but just one is satisfactory according to the following criteria:

1. The total energy of interactions in layers is 1.5 or more times higher than that between the layers.
2. The total energy of interactions in layers differs by at least 1.5 times for the two variants of the layer arrangement.

The layers arranged within (100) planes overcome the other ones in energy by more than 2 times as well as the interaction energy between them. They are formed by a network of 4 non-classic hydrogen bonds C-H... $\pi$  (2.86 Å, 166°) and non-directional interactions under normal conditions. The number of bonds and short contacts growth with the increase in pressure (Tables A 4.35-4.46). At the same time, the interaction energy in layers decreases linearly and

increases in between them, but the pressure of 4.00 GPa is not enough for its conversion to isotropic (Figure 4.29). Thereby, the structure of polymorphic form I of ibuprofen remains layered regardless of pressure (Table 4.9).

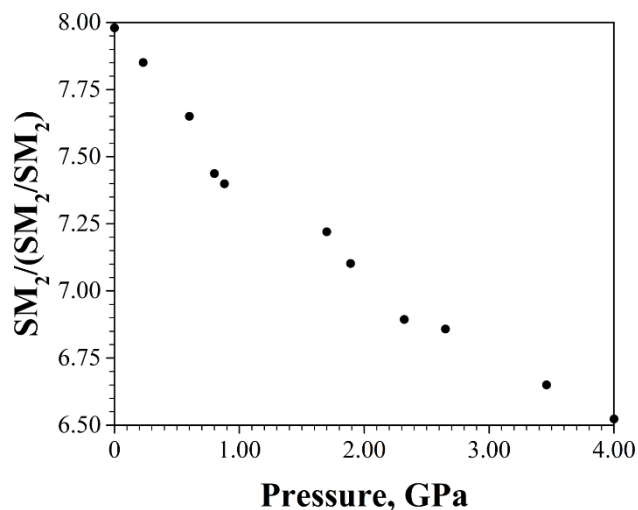


Figure 4.29. The dependency of the ratio of pairwise interaction energy in layer and between them from the measurement pressure.

Table 4.9. The interaction energies (in kcal/mol) of dimeric building units with its first coordination sphere, within the separated out structural motifs and between them in ibuprofen.

Polymorphic form and pressure (GPa)	Interaction energy with the first coordination sphere		Layers position	$SM_2$	$SM_2/SM_2$	Distance $SM_2/SM_2, \text{Å}$
	Monomer BU	Dimer BU				
	I (0.0001)					
-61.4		-100.8	(001)	-32.4	-34.0	5.293
			(102)	-30.2	-35.1	4.724
II (0.0001) *			(100)	-60.0	-21.0 (-33.6) **	12.335
	-67.8	-81.0	(101)	-30.6	-50.4 (-4.2) **	4.851
			(102)	-43.2	-37.8 (-16.8) **	6.868

Table 4.9 Continued.

Polymorphic form and pressure (GPa)	Interaction energy with the first coordination sphere		Layers position	SM <sub>2</sub>	SM <sub>2</sub> / SM <sub>2</sub>	Distance SM <sub>2</sub> / SM <sub>2</sub> , Å
	Monomer	Dimer				
	BU	BU				
I (0.23)	-61.7	-103.2	(100)	-82.2	-10.5	14.322
			(001)	-33.6	-34.8	5.236
			(102)	-30.5	-36.3	4.674
I (0.60)	-64.7	-109.7	(100)	-86.9	-11.4	14.098
			(001)	-35.1	-37.3	5.158
			(102)	-32.5	-38.6	4.596
I (0.80)	-66.8	-112.1	(100)	-88.3	-11.9	13.986
			(001)	-35.7	-38.2	5.079
			(102)	-33.1	-39.5	4.526
I (0.88)	-67.2	-112.2	(100)	-88.3	-11.9	13.974
			(001)	-36.0	-38.1	5.080
			(102)	-33.1	-39.6	4.526
I (1.70)	-68.4	-114.6	(100)	-89.7	-12.4	13.752
			(001)	-36.9	-38.9	4.978
			(102)	-33.3	-40.6	4.434
I (1.89)	-66.6	-114.3	(100)	-89.2	-12.6	13.766
			(001)	-36.5	-38.9	4.951
			(102)	-33.2	-40.5	4.412
I (2.32)	-66.6	-112.5	(100)	-87.2	-12.7	13.684
			(001)	-36.8	-37.9	4.924
			(102)	-33.1	-39.7	4.392
I (2.65)	-64.8	-112.7	(100)	-87.2	-12.7	13.642
			(001)	-36.7	-38.0	4.909
			(102)	-32.7	-40.0	4.376
I (3.46)	-64.6	-108.5	(100)	-83.4	-12.5	13.558
			(001)	-36.6	-36.0	4.843
			(102)	-31.8	-38.3	4.322
I (4.00)	-62.2	-108.0	(100)	-82.6	-12.7	13.522
			(001)	-36.6	-35.7	4.825
			(102)	-31.9	-38.0	4.310

\* Interaction energy in the primary basic structural motives is -26.4 kcal/mol.

\*\* Interaction energy between the primary basic structural motives is put in brackets.

The polymorphic modification II demonstrates the existence of both primary and secondary basic structural motives and it is columnar-layered. The columns in structure are formed by non-directional interactions and should be capable to strain. Each column is surrounded by 6 neighbors. According to their interactions, the possible orientations of the layers' families are limited to 3 possibilities: (100), (102) and (101). The last one is improbable, because the interactions in such layers are near 2 times smaller than the ones in between them, but the other two are prone to appear. The layers formed in parallel to (100) plane are stabilized by 4 non-classic hydrogen bonds C-H... $\pi$  (2.80 Å, 172°) and non-directional interactions (Table A 4.36) very similar to how it happens in form I. However, the pairs of hydrogen atoms belonging to methyl and C2-isobutyl groups cause repulsion because of the shortening of the distances between them to 2.16 Å (0.18 Å shorter than the sum of their van der Waals radii). Thereby, the layers stabilization is influenced not just by the loose structure of the polymorphic form II. The other difference between the forms I and II of ibuprofen is that the interactions between layers parallel to (100) plane are much stronger in the form II ( $\frac{SM_2}{SM_2/SM_2}$  relationship is about 3). It means that the form II is much close to the isotropic structure than the most stable polymorph under ambient pressure. The second possibility for the layers formation is parallel to a plane (102). It is much less profitable. The interaction energy in such layers are just 1.14 times higher than that in between them, so their assignment is questionable.

In summary, the following conclusions can be done from the from the previous steps for the next analysis of shear with topological and quantum-chemical approaches:

1. The possible orientations of layers are (100) in both forms and additionally (102) for the second.

2. The chains, which limit the shear direction to [010], are represented in the polymorphic modification II.
3. The shear should be hindered for the polymorphic form II, because the interlayer interactions are at least 2 times stronger for it than for the first.

#### 4.3.3. Topological analysis of molecular shear in crystals of ibuprofen

Method used for the identification of shear probability in ibuprofen is similar to the one used for piracetam in Section 4.2.1. There we operated with the minimal interatomic distances between the mobile (single building unit) and fixed (specific fragment of a layer neighboring to the mobile building unit) parts. Nevertheless, the application of minimal interatomic distances makes it impossible to consider the nature of interacting atoms in mobile and fixed parts. To introduce the type of atoms involved in interactions without excessive increase in calculation time, van der Waals radii were implemented as proposed in [26]:

$$\delta_{ij} = d_{ij} - vdW_i - vdW_j \quad (4.7)$$

where  $d_{ij}$ ,  $vdW_i$  and  $vdW_j$  are the distance between the atoms  $i$  in mobile part and  $j$  in the fixed part and their van der Waals radii respectively.

The methods used to determine the neighbors and the principal directions of shear based on Miller indices of a slip plane repeats the one proposed for piracetam. The step size left unchanged (0.01 of a translation) and its absolute value correlated with the translation path lengths (reaching the resolution of 0.147 Å for the structure with the longest translation under ambient pressure).

Since the disposition of layers and building units are defined and the change in methodology is discussed, the preliminary topological estimation of the shear probability of building units becomes possible. However, this analysis stays questionable because the data acquired from it requires additional

symmetric transformations to include. In the case of ibuprofen, the polymorphic conversion was modelled. The shear-based transformation was considered as a sole possible. In the current work, two way of conversion will be examined. The first variant is a gradual translation of every layer in crystal beginning from the closest one to surface or the place of the translation initial for polymorphic conversion. The second is the translation of the layer along with both its neighbors at the same time (Figure 4.30). The point group symmetry of both polymorphic modifications of ibuprofen is  $P21/c$  and the building units are dimeric. Thus, the computational approach is similar for the forms of ibuprofen. It differs by an inversion of the data (maps or profiles of the minimal parameter  $\delta$  or the pairwise interaction energy) collected for the case, when a building unit representing one of the layers moves along the fixed part consisting of a fragment of one neighboring layer. In this way, it is possible to include the center of inversion appurtenant to the aforementioned point group symmetry. As defined from the pairwise interaction energy analysis, the layers disposed in the plane (100). They are parallel to the glide plane  $c$ , meaning that the glide plane will be included anyway during the generation of neighboring layers. However, there is an operation left. The 2<sup>nd</sup>-order screw axis laying in parallel to the main direction  $b$  is involved in the generation of the different symmetric equivalents of building units in layers. As a first approximation, it is already included in the neighboring layer(s) / fixed part, but it should be involved as well in the mobile part, which also originally consists of the two different symmetric equivalents of the dimers. Thereby, the second question is to consider that the dimeric building units as the most stable formation in the crystal can move in a disordered way when the different symmetric equivalents in the same layer can move independently from each other, or that they can produce just the coherent shear.

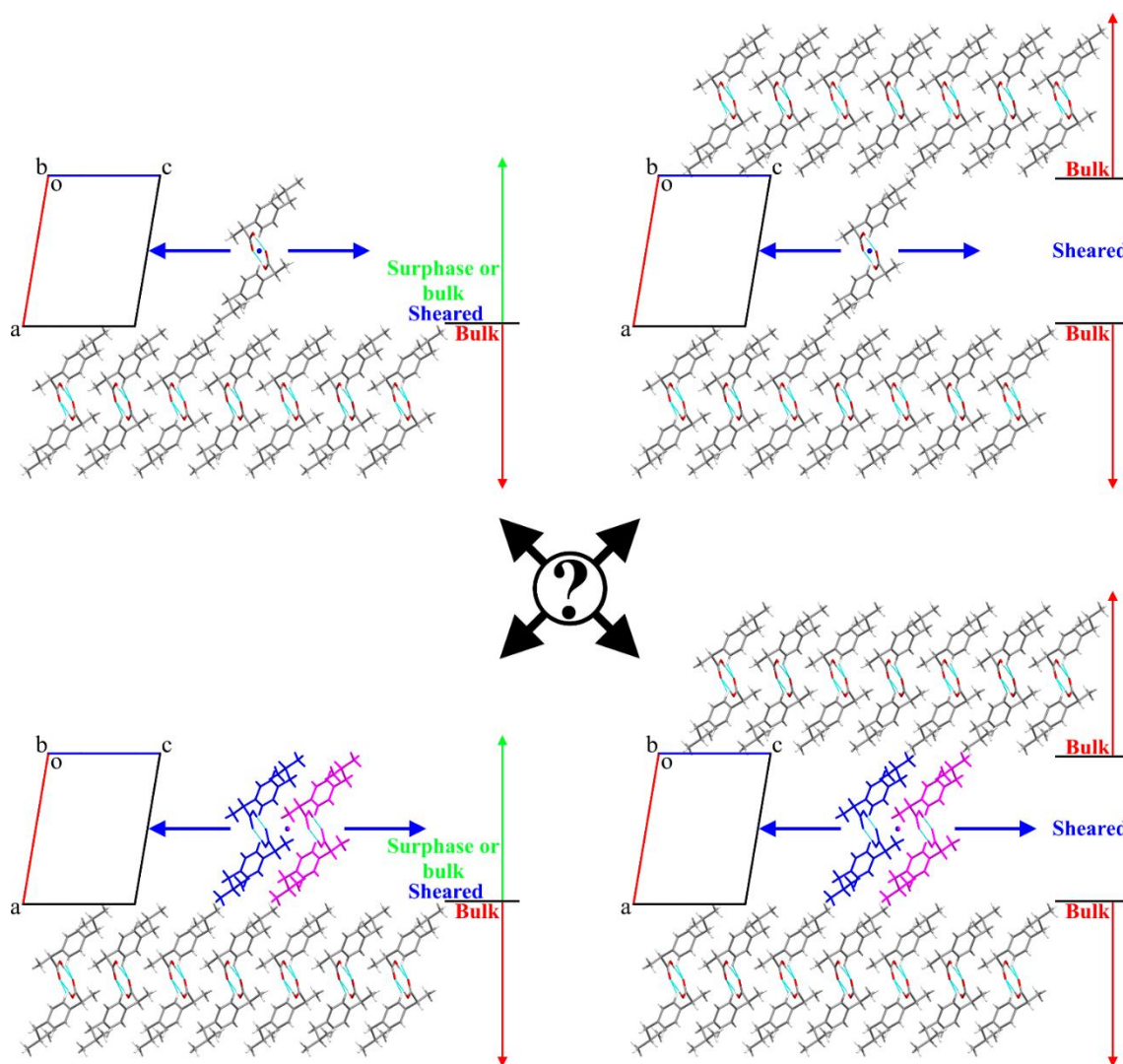


Figure 4.30. Molecular view on the symmetry operations applied to data in the crystals of the polymorphic modification I of ibuprofen: implementation of rotation allowing to reproduce the complete layer with two dimeric building units (top to bottom, “x,y,z” dimer is marked in blue, its equivalent – in magenta), consideration of the sole (to the left) and both (to the right) neighboring fixed layers with the inversion (center of inversion is marked in blue or blue+magenta).

We will consider all the 4 combinations of symmetry elements on the example of the polymorphic order of increase in symmetry (Figure A 4.34-4.46):

1. None of the symmetric transformations is applied to data received for the “x,y,z” (i.e. original) dimer. It is a raw model of shear of independent

dimeric building units along with neighboring layer as during the surface layers gradual destruction in the process of grinding.

2. Data and its inverted version are overlapped and the minimal parameter  $\delta$  at a point is chosen meaning that the maximum approach of molecules relative to the sum of their van der Waals radii is considered. This case is intermediate between the previous and next variants and means the disorder occurring in the bulk phase of the crystal.
3. Data is overlapped with its version rotated around the middle of a translation by the main direction  $b$ . It is noteworthy that normally the data reflection along the main direction  $c$  should be done to simulate the effect of the rotational axis, but it interacts with the center of inversion. Thereby, the double reflection along the  $c$ -axis levels out. This case describes the movement of a part of crystal along a part of the crystal, when the layers stay unchanged themselves.
4. Full symmetric transformation is applied to data, including as the inversion, as the rotation. Conversion of the polymorphic modifications is considered through the move of the layer along with both its neighbors at the same time.

The examination will be started with the polymorphic modification I, whose structure allows shear at some extent and with the least symmetric variant of data transformation as a basic one for other cases. As seen from the Figure 4.31, big void regions exist in structure not just around the initial position of the dimeric building units, but around the local maxima located at ambient pressure at the coordinates (0.12;0.54) or (0.88;0.46) depending on which neighboring layer is considered. It corresponds to the translations along the direction [029]. The translation path to the local maxima lays mostly in the zone with the parameter  $\delta$  bigger than  $-0.250 \text{ \AA}$  at ambient pressure, meaning just a minimum overlap of the van der Waals radii of the atoms in dimers of the mobile and fixed parts. However, in spite the fact that the local maxima remain in structure till the

highest measured pressure, the parameter  $\delta$  decreases much faster on the path with pressure to the minimum showing the value below  $-0.500 \text{ \AA}$  already at 0.60 GPa.

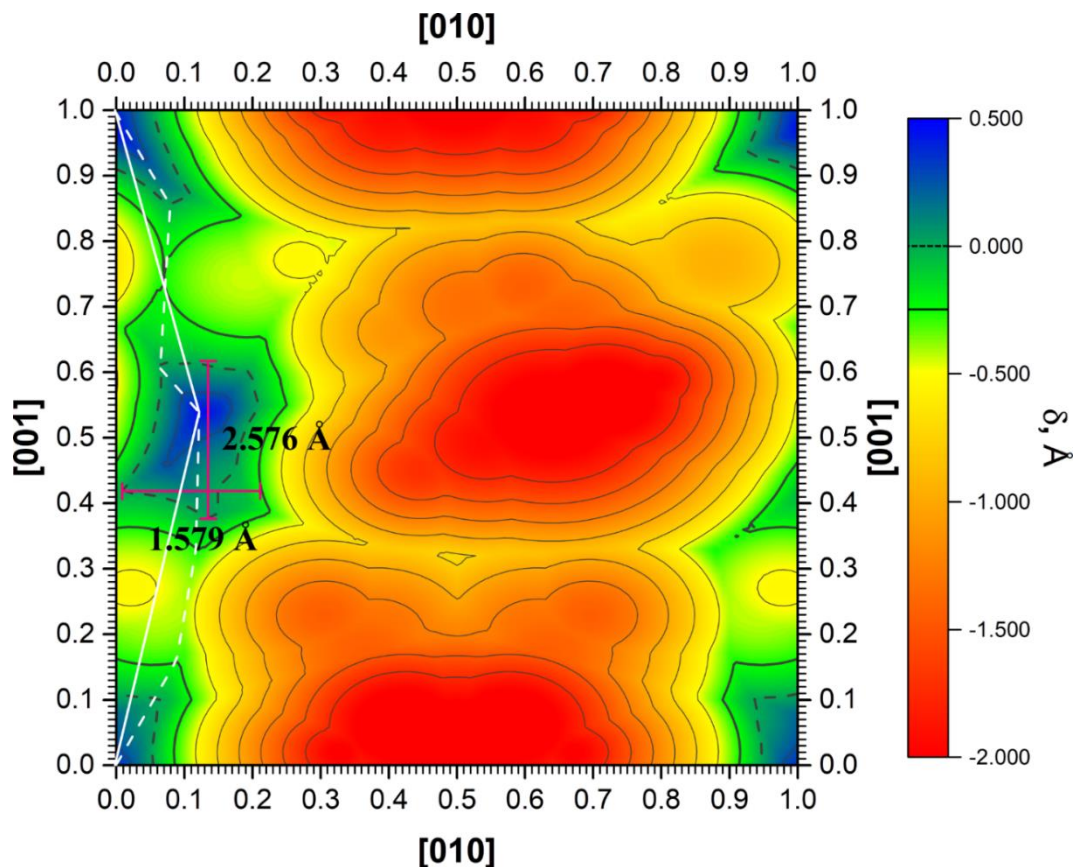


Figure 4.31. Map of parameter  $\delta$  during the shear of the dimeric building unit in relation to neighboring layer with smaller coordinate along the main direction  $a$  parallel to (100) plane in the crystal of ibuprofen polymorphic form I under ambient pressure without symmetric transformations. The probable curvilinear (dashed line) and straightforward (solid line) paths of the building units during the shear are marked with white. The sizes of the void zone (local maximum of parameter  $\delta$ ) in the crystal are marked with pink and black. Dashed contour surrounds the zones without the shortening of interatomic distances below the corresponding sum of van der Waals radii ( $\delta \geq 0$ ). Bold contour surrounds zones with  $\delta$  smaller than  $-0.250 \text{ \AA}$ .

Noteworthy, that solely the straightforward variants of paths were selected, because the curvilinear variants seem questionable in case of DAC

technique, but both ways are probable during the milling. Thus, the possibility to convert should remain at least till the pressure of 0.88 GPa (Figure 4.32). The linear sizes of the zones with positive parameter  $\delta$ , where the van der Waals radii of the parts do not overlap, at ambient pressure, are close to 1.579 and 2.576 Å in directions  $b$  and  $c$ , respectively. The dimeric building unit may shear inside zones without strong repulsion according to our previous study. Besides that, they have a complex inner structure based on van der Waals radii overlap and may contain more than 1 maxima as well as the zones around the original position of dimers in the crystal structure as it was found for piracetam (Figure 4.13).

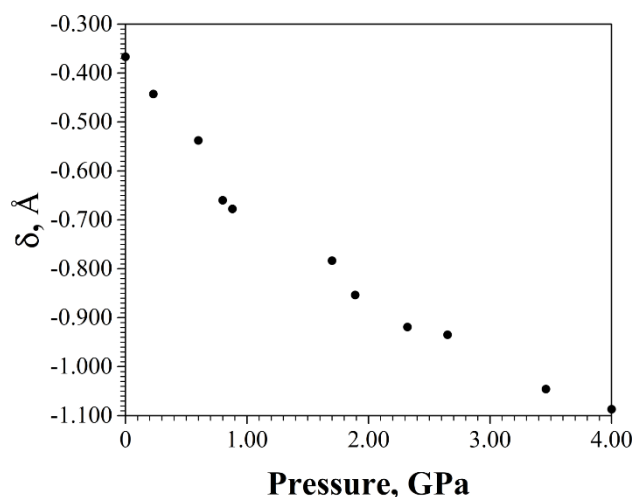


Figure 4.32. The dependency of the parameter  $\delta$  from the measurement pressure at the point, where the closest rapprochement of the dimeric building units of mobile and fixed parts happens during the path from the original dimer position to the biggest local maxima.

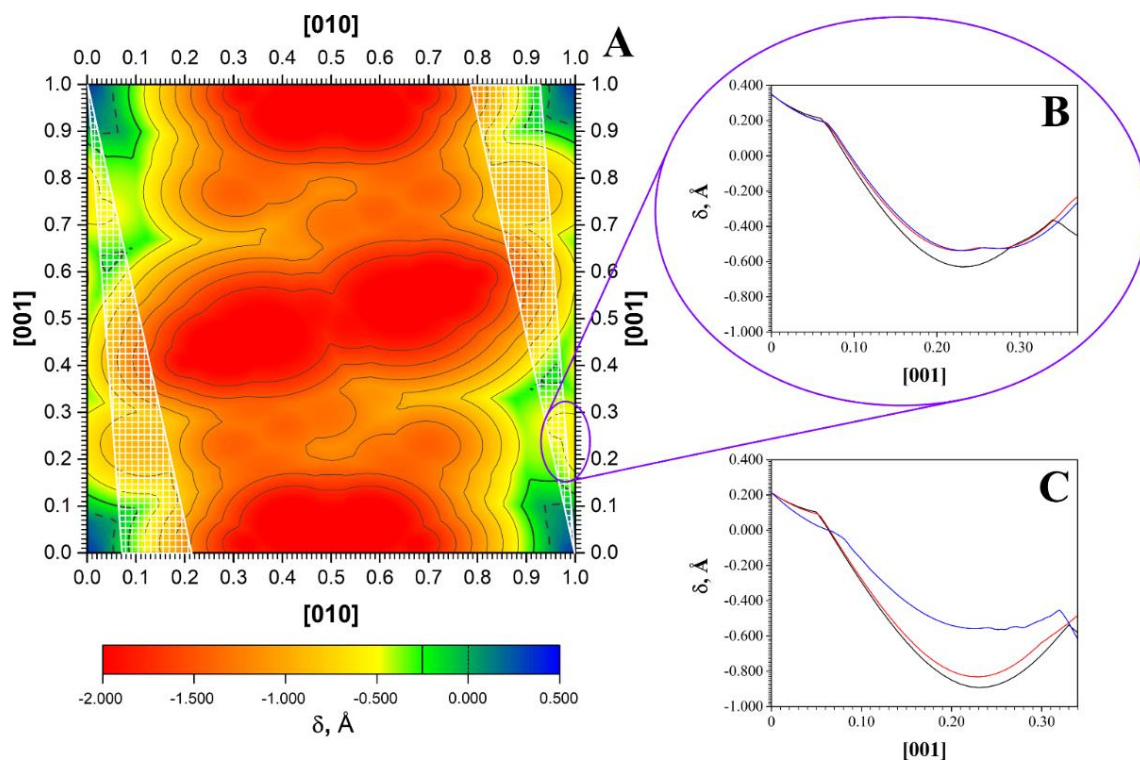


Figure 4.33. Diapason of the directions, for which the shear may lead to some transformations in the structure of ibuprofen polymorphic form I is shown as white net on the map of parameter  $\delta$  during the shear of the dimeric building unit in relation to two neighboring layers (inverted) parallel to (100) plane in crystals under ambient pressure (A). Dashed contour surrounds the zones without the shortening of interatomic distances below the corresponding sum of van der Waals radii ( $\delta \geq 0$ ). Bold contour surrounds zones with  $\delta$  smaller than  $-0.250 \text{ \AA}$ . Profiles of the parameter  $\delta$  during the shear of the layer under ambient pressure (B) and at the pressure of 0.60 GPa (C) along with the main direction  $c$  (in black), the directions  $[0\ 1\ 12]$  (in red) and  $[029]$  (in blue) as the closest and farthest to  $c$ , respectively.

The other positions, which require the accurate quantum-chemical assessment, are just the trails of the aforementioned zones around the local maxima of  $\delta$ . However, they stay actual in all the types of the symmetric transformations excluding just the complete (4th) variant. In case of the inversion, the void regions were detected in two diapasons  $[0.03;0.08]$  by  $x$  and  $[0.60;0.64]$  by  $y$ -axis or  $[0.92;0.97]$  and  $[0.36;0.40]$ , respectively, with the parameter  $\delta$  not higher than  $0.250 \text{ \AA}$ . Since the  $x$ -axis corresponds to  $[010]$  direction and  $y$ -axis to  $[001]$ , respectively, the relocation of the dimeric building

units along the directions laying in diapason from [0 1 12] to [029] may result in some transformations in the crystal structure of polymorphic form I of ibuprofen (Figure 4.33a). It is important to note, that the trails of the local maxima cross the y axis of the topological maps. Thus, we can easily estimate the probability of a relocation of the dimeric building units in the area of the secondary maxima of  $\delta$  with the original quantum-chemical method proposed for aspirin by moving the dimer along the direction [001]. Energy deviations may occur in case of the maps inversion at any pressure because the parameter  $\delta$  differs for the path of dimer from the original position to the void region and the path along the direction [001] (Figure 4.33b,c). However, at the pressure of 0.60, it is easily seen that the most sensitive zone along the direction [001], where the parameter  $\delta$  reaches its maximum, is subjected to the compression much more than the one along the real path to the void region. So, the energy difference between the real path and the one along [001] grows in a non-linear way and have to be taken into account. Nevertheless, the error should not occur, if a part of crystal moves along a part of the crystal (in the 3<sup>rd</sup> variant of the symmetric transformation) because the maximum of parameter  $\delta$  lays exactly on the y-axis. Thus, the energy estimation along the direction [001] will correspond to the direction of the path from the global to local maxima on the map. In both aforementioned cases of symmetric transformations, the path along the direction [001] is sterically hindered and the parameter  $\delta$  reaches the value over  $-0.500 \text{ \AA}$  already under ambient pressure. The sizes of the void domains quickly decrease with pressure and disappear (the parameter  $\delta$  reaches the value over  $-0.500 \text{ \AA}$ ) at the pressure of 2.32 or 1.70 GPa in cases of map inversion or rotation, respectively.

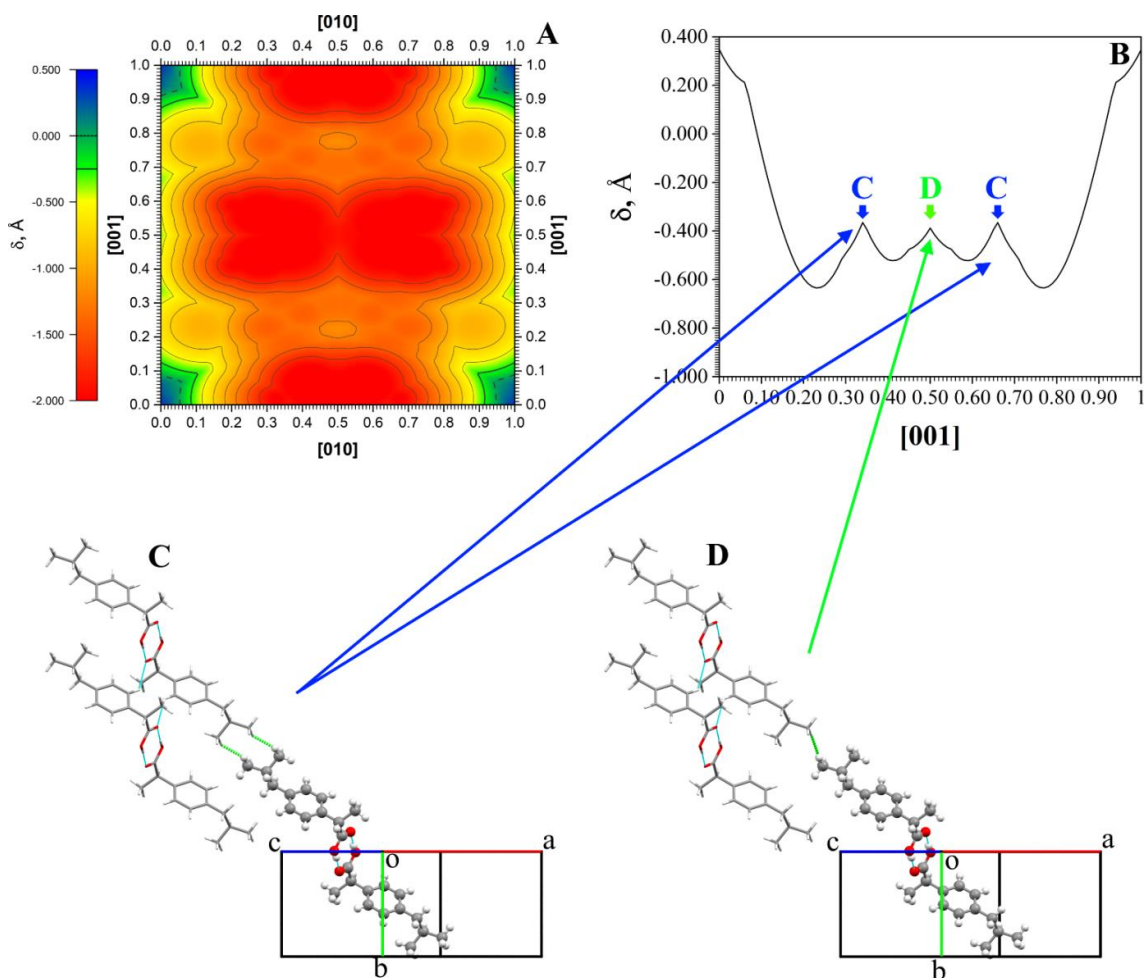


Figure 4.34. The map of parameter  $\delta$  (A) and the shear profile along the main direction  $c$  subtracted from it (B). The map is generated within the shear of the dimeric building unit and its rotated symmetric equivalent in relation to two neighboring layers (inverted) parallel to (100) plane in the crystal of ibuprofen polymorphic form I under ambient pressure (A). Dashed contour surrounds the zones without the shortening of interatomic distances below the corresponding sum of van der Waals radii ( $\delta \geq 0$ ). Bold contour surrounds zones with  $\delta$  smaller than  $-0.250 \text{ \AA}$ . The shifted original dimeric building unit (balls'n'stick model) is shown at the positions of 0.34 or 0.66 (blue arrows) and 0.50 (green arrows) of translation in relation to the closest 2 dimers from the neighboring layer (capped sticks model) with smaller coordinate along the main direction  $a$  parallel to (100) plane. The shortest contacts are shown in green.

The variant of the symmetric transformation, when both of the operations are applied and, so, the shear of a layer within both its neighbors, is the least informative from the point of view of possible maxima of parameter  $\delta$ .

Nevertheless, it shows the void regions and the capabilities to shear, which are the most probable in the crystal structure. As for all the other counted cases of symmetric transformation, the dimeric building units probably can move along just one direction without blocking or cracking, because solely during the translation along with the main direction  $c$  the fixed and mobile parts do not come into close rapprochement at least under the pressure of 0.88 GPa and below (Tables A 4.47-4.48, Figure A 4.38). Whereas, the big local maxima described previously do not appear. Instead of them, the three smaller ones at 0.34, 0.50 and 0.66 exist along with the main direction  $c$ , coinciding with the axis, thus, having the reflections on the pairwise interaction energy curves. The parameter  $\delta$  is greater at 0.34 and 0.66 part of a translation showing the value of  $-0.362 \text{ \AA}$  against  $-0.384 \text{ \AA}$  in the middle of a translation under ambient pressure, but the mutual arrangement of the fixed and mobile parts is characterized by the shortening of the intermolecular distances between the atoms in 2 methylpropyl groups in a dimer-like manner (Figure 4.34). Thus, it is unclear without quantum-chemical calculation which of the local maxima is preferable for the building units.

In spite of the fact, the two orientations for the shifting layers are possible for polymorphic modification II of ibuprofen, it has much less abilities to deform under external influences. The layers family most profitable from the energetic viewpoint according to the static analysis of the crystal structure is parallel to the plane (100) same as for the polymorphic form I. However, the sole significant void region is disposed in the zone hardly reachable during the shear-based transitions in case of the least symmetric transformation of data as seen from Figure 4.35. The exact location of a maximum parameter  $\delta$  can be defined and any internal structure of the void region is absent. It is [0.25;0.47] and the value of the corresponding parameter  $\delta$  is  $-0.224 \text{ \AA}$ . All the straightforward paths are sterically hindered ( $\delta > -2.000 \text{ \AA}$ ) and the curvilinear ones meet the region with  $\delta$  around  $-1.550 \text{ \AA}$ , what is objectively impossible to

pass. The linear move along the main crystallographic directions  $b$  and  $c$  are hindered as well. The compression along  $c$ -axis meets the minimum value of the parameter  $\delta$  less than  $-2.000 \text{ \AA}$ , but along  $b$ -axis it is possible that this movement can be reached with difficulty ( $\delta \approx -1.054 \text{ \AA}$ ).

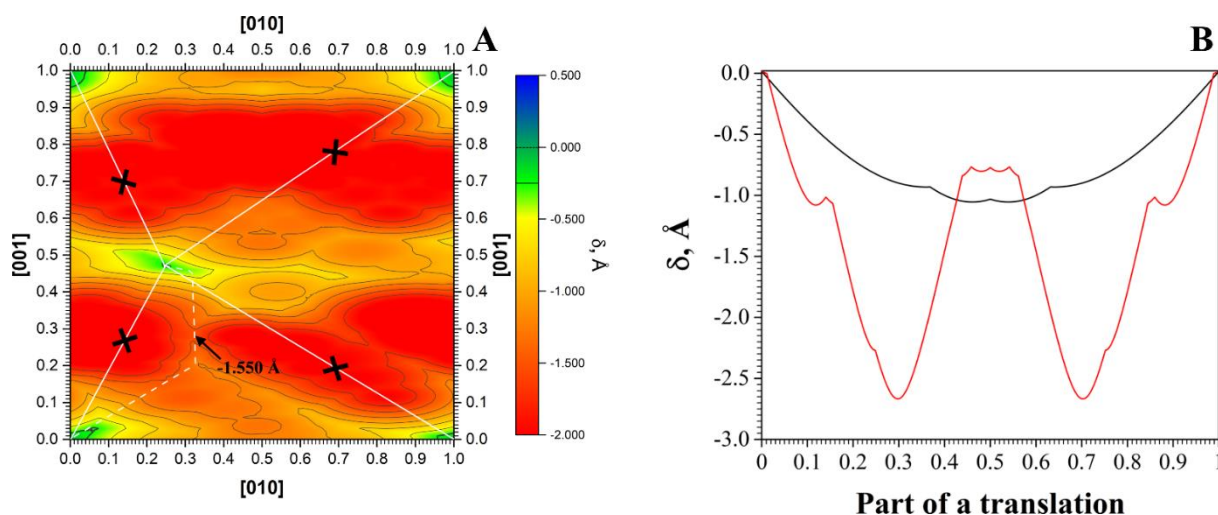


Figure 4.35. The map of parameter  $\delta$  (A) and the shear profiles along the main directions  $b$  (black) and  $c$  (in red) subtracted from it (B). The curvilinear (dash) and straightforward (solid) paths of the building units during the shear are marked with white. The regions preventing shear with strong overlap of van der Waals radii are marked with black on the map. Dashed contour surrounds the zones without the shortening of interatomic distances below the corresponding sum of van der Waals radii ( $\delta \geq 0$ ). Bold contour surrounds zones with  $\delta$  smaller than  $-0.250 \text{ \AA}$ .

The second layers disposition probable according to the energetic structure of crystal is (102). The sole void region was found from 0.95 to 0.28 and from 0.47 to 0.57 of a translation along the directions  $[010]$  and  $[-201]$ . The linear sizes of the corresponding zones with positive parameter  $\delta$ , where the van der Waals radii of the parts do not overlap, are about  $1.938$  and  $3.155 \text{ \AA}$ . It cannot be reached from the initial position of dimer in crystal structure, but rather big and have inner structure (Figure 4.36). The less sterically hindered curvilinear path crosses the diapason of crystal, where the parameter  $\delta$  is about  $-1.500 \text{ \AA}$ , so the layers invariantly come in too close rapprochement on shear. As

for the most probable layers family (100), the sole straightforward path available for the movement of dimers is codirected with the crystallographic axis  $b$  and wherein the minimum parameter  $\delta$  is  $-0.974 \text{ \AA}$ . The smaller overlap of the van der Waals radii of the mobile and fixed parts on movement along the direction [010] makes the disposition of layers in parallel to the plane (102) more preferred for the molecular shear on compression.

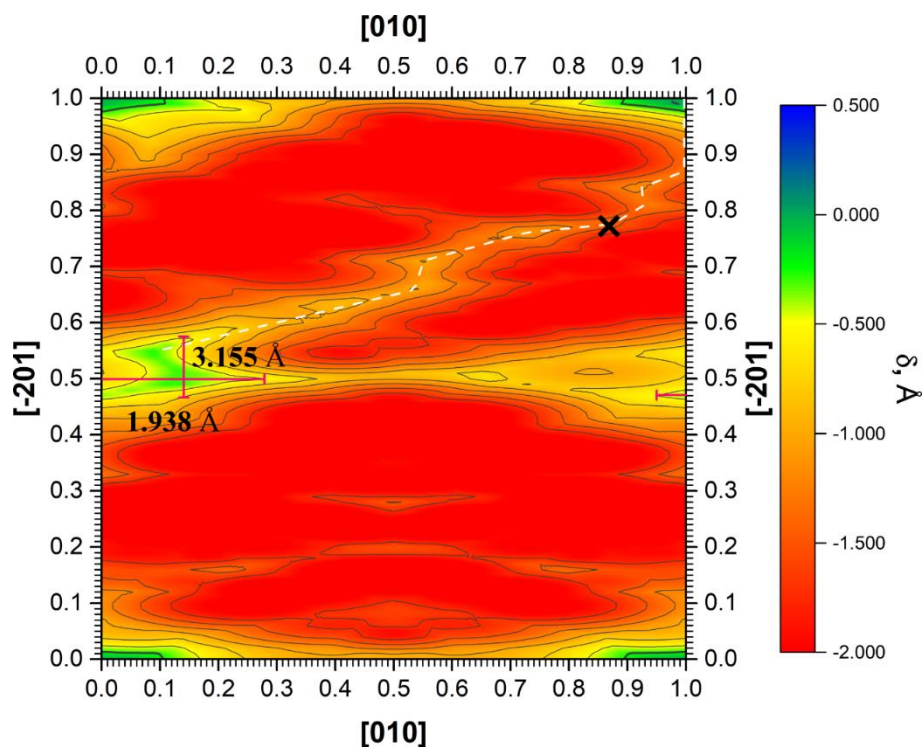


Figure 4.36. Map of parameter  $\delta$  during the shear of the dimeric building unit in relation to neighboring layer with smaller coordinate along the main direction  $a$  parallel to (102) plane in the crystal of ibuprofen polymorphic form II under ambient pressure without symmetric transformations. The sole probable curvilinear path of the building units during the shear is marked with white dash and the region with strong overlap of van der Waals radii is marked with cross on the map. Dashed contour surrounds the zones without the shortening of interatomic distances below the corresponding sum of van der Waals radii ( $\delta \geq 0$ ). Bold contour surrounds zones with  $\delta$  smaller than  $-0.250 \text{ \AA}$ .

The case without any symmetric transformations when solely a building unit moves along one layer showed that the secondary maxima of the parameter

$\delta$  exist in structure for the polymorphic modification II of ibuprofen. It means that the positions alternative to the original one are represented, but not achievable without change in conformation. They disappear, when any symmetric transformations are applied to data except the case of rotation for the layers family parallel to plane (102) and even for this variant the positions cannot be reached without the overcoming the strong steric hindrance ( $\delta > -2.000 \text{ \AA}$ ). Nevertheless, the linear movements on compression along the direction [010] remain possible and noteworthy for further quantum-chemical assessment of the shear energy barriers.

#### 4.3.4. Quantum-chemical calculation of shear probability

Two out of four earlier considered cases of molecular shear have a low possibility of appearance. These are the cases when the sole dimer or the original dimer and its symmetric equivalent are surrounded by the two fixed layers (2<sup>nd</sup> and 4<sup>th</sup> types of symmetric transformation). The first means chaotic movements of the sole dimer in the bulk phase of crystal. It will not be considered in the shear energy profiles. The second is possible, but it is a special case of multiple layers shear during the grinding. This case is not proved to be optimal and its probability is questionable. On the other hand, the initial shear of the sole dimer on the surface and the case of the rotated data, when a part of crystal moves along a part of the crystal, are worthy to assess.

The preliminary assessment of the crystal structure from the energetic and topological viewpoints allowed to separate out just one probable direction for the shear in the polymorphic modification I of ibuprofen. It is [001] for the layers family parallel to plane (100). The rotation of data does not affect this direction, so the shear energy profiles for the polymorphic form I at any pressure remained unchanged during the analysis. However, the shear in the form II has high probability along with the direction [010] for both layers orientations in parallel to (100) and (102). Thus, the rotational axes will require the additional

symmetric transformation of the shear energy curves. The rotated shear energy profiles were overlapped with their own mirror images (curves reflected in relation to the middle of a translation) for the future search of local extrema. Thereby, the 3 cases will be considered:

1. Shear of the original dimeric building unit along with the direction [001] in parallel to neighboring layer (100) for the polymorphic modification I of ibuprofen to model the movement of a dimer on the surface and part to part movement in crystal.
2. Shear of the original dimeric building unit along with the direction [010] in parallel to neighboring layers (100) and (102) for the polymorphic modification II of ibuprofen to simulate the movement of a dimer on the corresponding crystalline facet.
3. Shear of the original dimeric building unit and its symmetric equivalent belonging to the same layer along with the direction [010] in parallel to neighboring layers (100) and (102) to assess the possibility of any part to part movements in crystals of the polymorphic modification II of ibuprofen.

The number of calculated pressure points has been reduced in accordance with the total energy of pairwise interactions in the first coordination sphere of dimeric building units (Figure 4.27b). The range of pressure from 1 bar till 1.70 GPa was considered, because of the attraction growth in crystals of ibuprofen. Further, the structures at maximum pressure (4.00 GPa) and an intermediate one at 2.65 GPa were calculated. Evaluation of the shear probability showed that the topological analysis coincides well with the quantum-chemical data (Figures A 4.47-4.56).

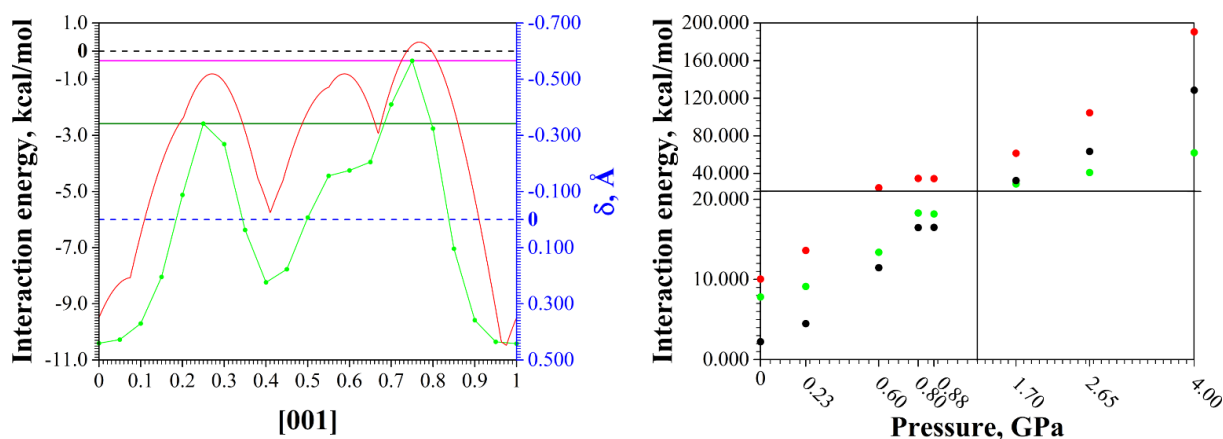


Figure 4.37. Profiles of interaction energy (in bright green) and topological parameter  $\delta$  (in red) occurring during the shear of the dimeric building units along the main crystallographic direction  $c$  in parallel to one neighboring layer (100) with lower coordinate  $a$  in the crystals of the polymorphic modification I of ibuprofen under ambient pressure (to the left). The positions of zeroes are marked with the black and blue dashed lines. The positions of the main and secondary maximum values of the interaction energy used for the calculations of global and local barriers are marked with magenta and olive solid lines. The dependency of the main (in red) and secondary (in bright green) shear energy barriers as well as their difference (in black) from pressure is shown on the right. The breaks on the x- and y-axes are shown with black lines.

Estimation of the shear in the polymorphic modification I of ibuprofen showed that the movement along with the main crystallographic direction  $c$  is possible, but the interaction prevails over the repulsion between the mobile and fixed parts along all the path of a translation just under the ambient pressure. It means that the translation of layers (100) along [001] direction is easy to reach without crystal destruction and the shear from (0;0;0) to (0;0;1) point (in crystallographic coordinates) may occur on mechanical treatment. At the pressures of 0.23 and, probably, 0.60 GPa, the complete translations of the mobile part should be still possible, because the positive components of interaction energy are not too high to limit them (maxima at 2.6 and 12.9 kcal/mol). It means the appearance of the hindrance for movement of the layers (100) shear along [001]. The chances of the complete translations in all the other

points of the diapason of pressures decrease drastically with the growth of the shear energy barriers (Figure 4.37). The shear barrier grows from 10.1 kcal/mol under ambient pressure to 190.7 kcal/mol at 4.00 GPa, reaching the value of 24.9 kcal/mol at 0.60 GPa showing additionally that the movement is hardly possible already at relatively low pressures.

Indeed, the shear energy profiles are not symmetric. This fact did not affect the energy barriers and so meaningless in case of mechanical grinding or the movement of layers on indentation, but the complete translation is not required in case if the possibility of polymorphic transformations is evaluated. It is seen that a local minimum at 0.40 part of a translation is represented in structure of the polymorphic modification I of ibuprofen in all the diapason of pressure. It can be reached through the aforementioned global maximum disposed at the position of 0.75 of a translation or over a smaller one, which lays at 0.25 of a translation. Here the difference between the cases of dimer on the surface and the part to part of crystal movements appear. In the situation, when the dimeric building unit shears onto the surface of crystal, it means that the transmission of the energy bigger than the shear barrier thereto at a tangent to the surface will affect the crystal in different ways. The shear will be already available along one facet, while it will be still hindered on the other one. However, such a situation is difficult to prove and does not take into account the possibility of the distancing of the mobile part from the crystal surface. Everything changes, when the part of crystal moves along the part of crystal. The layers are pressed to each other, so the distances between them cannot increase greatly. Thereby, the transmission of the energy from both sides will lead to the same structure, just the choice of the movable part is different. For example, the compression along the main crystallographic direction  $c$  in case of the polymorphic modification I of ibuprofen will result in a consistent shear of layers (by 0.4 part of a translation) with lower coordinate by the direction  $a$  and vice versa with higher coordinate along  $a$  on pression reverse to  $c$  (Figure 4.38).

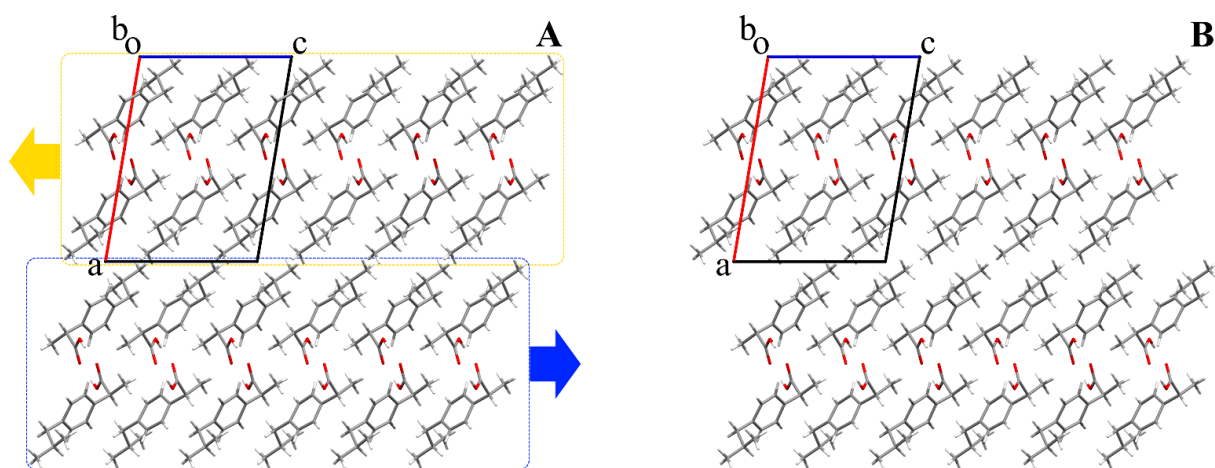


Figure 4.38. Preferred direction of layers shear (A) in cases of compression in the main crystallographic direction *c* (blue) and in the direction reverse to *c* (yellow) in the polymorphic form I of ibuprofen and the resulting structure (B).

Since the final structure of the polymorph after such an incomplete shear is similar in both directions, it is logical to estimate the probability of this movement on the base of the smaller local maximum and local shear energy barrier. On one hand, it grows with pressure as well, proving the inability of the polymorphic modification I of ibuprofen to transform at high pressures. On the other, it extends the diapason of pressures, at which the transformation may occur, to at least 0.23 GPa, where the local maximum lays in the attractive zone (-1.9 kcal/mol) and the shear energy barrier is just 9.1 kcal/mol. In comparison to the previous works, this diapason of pressures can be even extended till 1.70 GPa on condition that the small zone of repulsion may occur between the mobile and fixed parts during the shear. The difference between the global and local energy barriers grows slowly with pressure (Figure 4.39). It means that the difference in behavior of the dimers disposed on the different facets in case of dimeric building unit on the surface or the divergency in energy required for the conversion to some intermediate state and for complete transition in case of part to part movements in crystal become bigger with pressure. However, the absolute values of energy needed for the conversion to the intermediate state increase itself making the high-pressure processing less preferred than low

pressure treatment. It was presumed also from topological analysis that the energy barrier of the transition from the original dimer position to the one in alternative range shown in Figure 4.33 is smaller than the barrier of the analogous transition along the direction  $c$ . On one hand, it allows to make a conclusion that the real conversion barrier is even stronger diverges with the one calculated by us and the shear-based conversion is probable in wider range of pressures. On the other one, it shows that the low-pressure treatment required for the acquisition of the intermediate state from form I should be even easier than it was suggested. It fits well with the fact that the amorphous phase was not obtained in high-pressure experiment, but the grinding with mesoporous silica turned out successful. However, the amorphous state has no stable (periodic) structure, so its comparison of the alternative structure acquired from the calculations of shear is sophisticated.

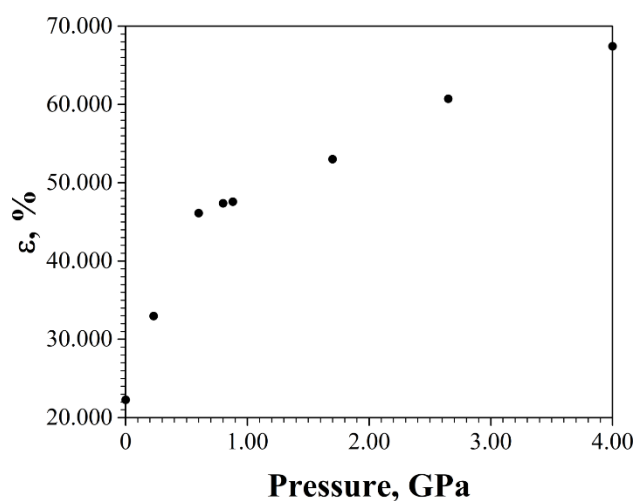


Figure 4.39. The dependency of the relative difference between the global and local shear energy barriers from the measurement pressure in the polymorphic modification I of ibuprofen.

It is been shown that the dimeric building units have more probable directions of the complete transition along translations than the first. However, this conclusion from the topological analysis is untrue and the quantum-

chemical calculations showed that the barriers for the layers shear are extremely high and hardly possible to overcome without the destruction of crystals (Figure A 4.55-4.56). They reach the values of 61.9 and 41.3 kcal/mol for the layers families parallel to planes (100) and (102), respectively, and the maxima to overcome are 51.1 and 21.8 kcal/mol for the same movements. These values are higher than the ones presumed as maximum possible in the polymorph I of ibuprofen. They do not change from symmetric operations. The shear along the main crystallographic direction *b* has more than 2 times higher probability than any other movement of layers in crystals of the form II. Thereby, there is no shear-based transformations available in the polymorphic modification II. Together with the fact that the conformations of the molecules differ between the polymorphs I and II of ibuprofen it coincides well with the experimental results saying that the polymorphic modification II undergoes first the conversion to amorphous state [27].

#### **4.4 Conclusions**

New approach was proposed for assessing the probable mechanical properties of individual polymorphic modifications of APIs and polymorphic transformations in their crystals by calculating the shear energy barriers of molecular layers. It only requires the determination of the crystal structure by any available method as a starting point. Also, this approach is computationally cheap, which is explained by the following set of criteria:

1. By means of a one- or two-stage calculation and analysis of pairwise interaction energies, the bound building units and the most strongly basic structural motives are univocally determined.
2. With the help of topological analysis, improbable directions of displacement of the revealed structural motifs are eliminated according to the principle of excessive shortening of the van der Waals radii of atoms in the shifting layers of molecules.

3. Quantum-chemical evaluation is carried out only in the main directions, which correspond to the pressure on the possible crystal faces.

The proposed approach was used to assess the mechanical properties of aspirin, which revealed that the [001] crystallographic direction within the (100) crystallographic plane is the most likely for a shear deformation for the polymorphic modifications I and II. While the deformation in the [010] direction within the same plane needs more energy due to the necessity to break C-H...O hydrogen bonds formed between the mobile and fixed parts of the model system during the translation. It coincides with the results of nanoindentation experiments. As well, it was found that strong repulsion between the mobile and fixed parts occurs during the displacement in both directions within the (100) crystallographic plane. At the same time, it was revealed for the polymorphic modification IV of aspirin that the most probable direction of a shear deformation is the [010] crystallographic direction within the (100) crystallographic plane. Such shear undergoes without any steric repulsion and it may be used to explain the low stability of polymorphic structure IV.

The same analysis performed for piracetam has shown very similar observation, which proves the conclusions done for aspirin. However, this study was about the possible polymorphic transformation of form II to form V. Forms II and V of piracetam are able to transform reversibly into each other under the pressure of about 0.7 GPa. We found that such a transition from Form II is preceded by the appearance of a local minimum on the shift energy profile in the solely available direction [100] for the (001) layers. We also proposed a method for studying the distribution of interaction energy components in crystals, based on the LMOEDA quantum-chemical approach. It showed that not only the total interaction energy and the ratio of repulsive and attractive forces are important for the possibility of polymorphic transformation, but also the energy ratio of hydrogen bonding and non-specific interactions (like dispersion). Moreover, the most significant was the possibility of breaking the dimer bound by weak

C-H...O hydrogen bonds with its subsequent stabilization by non-specific interactions.

Ibuprofen was the latest subject of research. A solid-phase optimization technique with the least effect on the experimentally determined characteristics was proposed and used for its polymorphic modification II. Its layered or columnar-layered structures for polymorphs I and II respectively are well suited for discussions of the influence of crystal symmetry on the energy profiles of displacement and, as a consequence, on the type of shear inherent to crystals. Four possible types of displacement in the crystal were formulated. For polymorphic modification I, such displacement directions were revealed that they did not coincide with the main directions of the crystal lattice ( $[029]$  and  $[0\ 1\ 12]$  in the (100) plane), which can lead to the impossibility of detecting or overestimating the ability to be deformed by indentation methods or with our quantum-chemical method. Shear in these directions leads to the regions of secondary local minima (distancing of layers) found during the topological analysis. These regions appear as secondary minima on the shift energy profiles at all pressures, but the shift energy barrier increases abruptly at 0.60 GPa showing the decrease in the probability of shear at elevated pressure. They may indicate that the polymorphic modification of ibuprofen has new opportunities for transformation, as well as the possibility of detecting crystal-amorphous phase transitions by our method. At the same time, form II did not show the possibility of transition without the destruction of crystals.

## 4.5. References for Chapter 4

- (1) Mnyukh, Yu.V.; Panfilova, N.A.; Petropavlov, N.N.; Uchvatova, N.S. Polymorphic transitions in molecular crystals - III.: Transitions exhibiting unusual behavior. *Journal of Physics and Chemistry of Solids* **1975**. *36* (3), 127-144.
- (2) Mnyukh, Yu. Second-Order Phase Transitions, L. Landau and His Successors. *American Journal of Condensed Matter Physics* **2013**. *3* (2), 25-30.
- (3) Smets, M.M.H.; Kalkman, E.; Krieger, A.; Tinnemans, P.; Meeke, H.; Vlieg, E.; Cuppen, H.M. On the mechanism of solid-state phase transitions in molecular crystals - the role of cooperative motion in (quasi)racemic linear amino acids. *IUCrJ* **2020**. *7* (2), 331-341.
- (4) Bond, A.D.; Boese, R.; Desiraju, G.R. On the polymorphism of aspirin: Crystalline aspirin as intergrowths of two "polymorphic" domains. *Angewandte Chemie International Edition* **2007**. *46* (4), 618-622.
- (5) Bond, A.D.; Boese, R.; Desiraju, G.R. On the polymorphism of aspirin. *Angewandte Chemie International Edition* **2007**. *46* (4), 615-617.
- (6) Shtukenberg, A.G.; Hu, C.T.; Zhu, Q.; Schmidt, M.U.; Xu, W., *et al.* The third ambient aspirin polymorph. *Crystal Growth & Design* **2017**. *17* (6), 3562-3566.
- (7) Shishkin, O.V.; Zubatyuk, R.I.; Shishkina, S.V.; Dyakonenko, V.V.; Medvediev, V.V. Role of supramolecular synthons in the formation of the supramolecular architecture of molecular crystals revisited from an energetic viewpoint. *Physical Chemistry Chemical Physics* **2014**. *16* (14), 6773-6786.
- (8) Dunning Jr., T.H. Gaussian basis sets for use in correlated molecular calculations. I. The atoms boron through neon and hydrogen. *The Journal of Chemical Physics* **1989**. *90* (2), 1007-1023.
- (9) Davidson, E.R. Comment on "comment on dunning's correlation-consistent basis sets". *Chemical Physics Letters* **1996**. *260* (3), 514-518.
- (10) Olusanmi, D.; Roberts, K.J.; Ghadiri, M.; Ding, Y. The breakage behaviour of aspirin under quasi-static indentation and single particle impact loading: Effect of crystallographic anisotropy. *International Journal of Pharmaceutics* **2011**. *411* (1), 49-63.
- (11) Varughese, S.; Kiran, M.S.R.N.; Solanko, K.A.; Bond, A.D.; Ramamurty, U., *et al.* Interaction anisotropy and shear instability of aspirin polymorphs established by nanoindentation. *Chemical Science* **2011**. *2* (11), 2236-2242.
- (12) Crowell, E.L.; Dreger, Z.A.; Gupta, Y.M. High-pressure polymorphism of acetylsalicylic acid (aspirin): Raman spectroscopy. *Journal of Molecular Structure* **2015**. *1082*, 29-37.
- (13) Barbour, L.J. Crystal porosity and the burden of proof. *Chemical Communications* **2006**. *11*, 1163-1168.
- (14) Turner, M.J.; Mckinnon, J.J.; Jayatilaka, D.; Spackman, M.A. Visualisation and characterisation of voids in crystalline materials. *CrystEngComm* **2011**. *13* (6), 1804-1813.
- (15) Fabbiani, F.P.A.; Allan, D.R.; David, W.I.F.; Davidson, A.J.; Lennie, A.R., *et al.* High-pressure studies of pharmaceuticals: An exploration of the behavior of piracetam. *Crystal Growth & Design* **2007**. *7* (6), 1115-1124.
- (16) Steiner, T. C-H...O hydrogen bonding in crystals. *Crystallography Reviews* **2003**. *9* (2-3), 177-228.
- (17) Vologzhanina, A. Intermolecular interactions in functional crystalline materials: From data to knowledge. *Crystals* **2019**. *9*, 478.
- (18) Shishkina, S.V.; Shishkin, O.V.; Medvediev, V.V.; Omelchenko, I.V.; Ismiev, A.I., *et al.* Weak but strong: Role of weak C-H...X (X=O, N) hydrogen bonds in organization of crystals of (1S,2S,3S,4R,5R,8S)-diethyl 2,4-dicyano-3-(furan-2-yl)-8-morpholino-6-oxobicyclo[3.2.1]octane-2,4-dicarboxylate. *Structural Chemistry* **2016**. *27* (1), 315-321.

- (19) Shishkina, S.V.; Dyakonenko, V.V.; Shishkin, O.V.; Maraval, V.; Chauvin, R. Supramolecular architecture of substituted tetraphenyl-carbo-benzenes from the energetic viewpoint. *ChemPhysChem* **2017**. *18* (18), 2499-2508.
- (20) Ostrowska, K.; Kropidłowska, M.; Katrusiak, A. High-pressure crystallization and structural transformations in compressed R,S-ibuprofen. *Crystal Growth & Design* **2015**. *15* (3), 1512-1517.
- (21) Malfait, B.; Correia, N.T.; Ciotonea, C.; Dhainaut, J.; Dacquin, J.-P., *et al.* Manipulating the physical states of confined ibuprofen in SBA-15 based drug delivery systems obtained by solid-state loading: Impact of the loading degree. *The Journal of Chemical Physics* **2020**. *153*, 154506 (1-14).
- (22) Shishkina, S.V. Using of quantum-chemical calculations to molecular crystals studying. *Structural Chemistry* **2019**. *30* (5), 1565-1577.
- (23) Derollez, P.; Dudognon, E.; Affouard, F.; Danede, F.; Correia, N.T., *et al.* Ab initio structure determination of phase II of racemic ibuprofen by X-ray powder diffraction. *Acta Crystallographica Section B* **2010**. *66* (1), 76-80.
- (24) Zefirov, Y.V.; Zorky, P.M. New applications of van der Waals radii in chemistry. *Russian Chemical Reviews* **1995**. *64* (5), 415-428.
- (25) Desiraju, G.R. Supramolecular synthons in crystal engineering—a new organic synthesis. *Angewandte Chemie International Edition* **1995**. *34* (21), 2311-2327.
- (26) Kaźmierczak, M.; Katrusiak, A. The most loose crystals of organic compounds. *The Journal of Physical Chemistry C* **2013**. *117* (3), 1441-1446.
- (27) Oparin, R.D.; Vorobei, A.M.; Kiselev, M.G. Polymorphism of micronized forms of ibuprofen obtained by rapid expansion of a supercritical solution. *Russian Journal of Physical Chemistry B* **2019**. *13* (7), 1139-1146.

## 4.6. Chapter 4 Appendix

Table A 4.1. Symmetry codes, bonding types, interaction energies of the basic monomeric BU with neighboring ones ( $E_{\text{int}}$ , kcal/mol) and the contribution of these energies to the total interaction energy (%) in the crystal of aspirin form I.

Dimer	Symmetry operation	$E_{\text{int}}$ , kcal/mol	Contribution to the	
			total interaction energy,	Interaction
			%	
d1	$x, 1+y, z$	-4.9	7.7	non-specific
d2	$x, -1+y, z$	-4.9	7.7	non-specific
d3	$1-x, 1/2+y, 5/2-z$	-2.1	3.3	non-specific
d4	$1-x, -1/2+y, 5/2-z$	-2.1	3.3	non-specific
d5	$2-x, 1/2+y, 3/2-z$	-0.6	0.9	non-specific
d6	$2-x, -1/2+y, 3/2-z$	-0.6	0.9	non-specific
d7	$1-x, -y, 2-z$	-19.9	31.5	O-H...O, 1.65 Å, 174°
d8	$1-x, 1-y, 2-z$	-5.5	8.7	Stacking, C...C, 3.32Å
d9	$2-x, -y, 2-z$	-3.6	5.6	non-specific
d10	$2-x, 1-y, 2-z$	-6.0	9.5	non-specific
d11	$x, 1/2-y, 1/2+z$	-3.7	5.9	C-H... $\pi$ , 2.71 Å, 178°
d12	$x, 1/2-y, -1/2+z$	-3.7	5.9	C-H... $\pi$ , 2.71 Å, 178°
d13	$x, 3/2-y, 1/2+z$	-2.8	4.4	non-specific
d14	$x, 3/2-y, -1/2+z$	-2.8	4.4	non-specific

Table A 4.2. Symmetry codes, bonding types, interaction energies of the basic monomeric BU with neighboring ones ( $E_{\text{int}}$ , kcal/mol) and the contribution of these energies to the total interaction energy (%) in the crystal of aspirin form II.

Dimer	Symmetry operation	$E_{\text{int}}$ , kcal/mol	Contribution to the	
			total interaction energy, %	Interaction
d1	$x, 1+y, z$	-4.9	7.6	non-specific
d2	$x, -1+y, z$	-4.9	7.6	non-specific
d3	$-x, 1/2+y, 1/2-z$	-4.8	7.4	non-specific
d4	$-x, -1/2+y, 1/2-z$	-4.8	7.4	non-specific
d5	$1-x, 1/2+y, 3/2-z$	-2.2	3.4	non-specific
d6	$1-x, -1/2+y, 3/2-z$	-2.2	3.4	non-specific
d7	$-x, -y, -z$	-0.6	0.9	non-specific
d8	$1-x, -y, 1-z$	-21.3	33.2	O-H...O, 1.64Å, 176°
d9	$1-x, 1-y, 1-z$	-5.5	8.6	Stacking, C...C, 3.36Å
d10	$x, 1/2-y, 1/2+z$	-3.8	5.9	C-H... $\pi$ , 2.71 Å, 176°
d11	$x, 1/2-y, -1/2+z$	-3.8	5.9	C-H... $\pi$ , 2.71 Å, 176°
d12	$x, 3/2-y, 1/2+z$	-2.8	4.3	non-specific
d13	$x, 3/2-y, -1/2+z$	-2.8	4.3	non-specific

Table A 4.3. Symmetry codes, bonding types, interaction energies of the basic monomeric BUs A and B with neighboring ones ( $E_{\text{int}}$ , kcal/mol) and the contribution of these energies to the total interaction energy (%) in the crystal of aspirin form IV.

Dimer	Symmetry operation	$E_{\text{int}}$ , kcal/mol	Contribution to the		
			total interaction energy, %	Interaction	Neighbor type
Monomers neighboring to molecule A					
d1	2-x,2-y,2-z	-2.7	2.2	non-specific	A
d2	2-x,3-y,2-z	-23.2	19.1	O-H...O, 1.58Å, 171°	A
d3	1-x,1/2+y,3/2-z	-2.1	1.7	C-H... $\pi$ , 2.84 Å, 140°	B
d4	1-x,3/2+y,3/2-z	-1.1	0.9	H...H, 2.11Å	B
d5	2-x,1/2+y,3/2-z	-4.8	4.0	C-H... $\pi$ , 2.66 Å, 162°	A
d6	2-x,1/2+y,3/2-z	-1.8	1.5	non-specific	B
d7	2-x,-1/2+y,3/2-z	-4.8	4.0	C-H... $\pi$ , 2.66 Å, 162°	A
d8	1+x,1/2-y,1/2+z	-1.4	1.1	non-specific	B
d9	1+x,3/2-y,1/2+z	-2.2	1.8	non-specific	B
d10	x,y,z	-0.9	0.7	H...H, 2.28Å	B
d11	x,1+y,z	-7.5	6.1	non-specific	A
d12	x,1+y,z	-2.3	1.9	non-specific	B
d13	x,-1+y,z	-7.5	6.1	non-specific	A

Table A 4.3 Continued.

Dimer	Symmetry operation	$E_{\text{int}}$ , kcal/mol	Contribution to the		
			total interaction energy, %	Interaction	Neighbor type
Monomers neighboring to molecule B					
d14	1-x,-y,1-z	-21.0	17.3	O-H...O, 1.67Å, 170°	B
d15	1-x,1-y,1-z	-1.9	1.6	non-specific	B
d16	1-x,1/2+y,3/2-z	-5.1	4.2	C-H...O, 2.46Å, 130°	B
d17	1-x,-1/2+y,3/2-z	-5.1	4.2	C-H...O, 2.46Å, 130°	B
d18	1-x,-1/2+y,3/2-z	-2.1	1.7	C...H, 2.84Å	A
d19	1-x,-3/2+y,3/2-z	-1.1	0.9	H...H, 2.11Å	A
d20	2-x,-1/2+y,3/2-z	-1.8	1.5	non-specific	A
d21	-1+x,1/2-y,-1/2+z	-1.4	1.1	non-specific	A
d22	-1+x,3/2-y,-1/2+z	-2.2	1.8	non-specific	A
d23	x,y,z	-0.9	0.7	H...H, 2.28Å	A
d24	x,1+y,z	-7.3	6.0	Stacking, C...C, 3.36Å	B
d25	x,-1+y,z	-7.3	6.0	Stacking, C...C, 3.36Å	B
d26	x,-1+y,z	-2.3	1.9	non-specific	A

Table A 4.4. Symmetry codes, bonding types, interaction energies of the basic dimeric BU with neighboring ones ( $E_{\text{int}}$ , kcal/mol) and the contribution of these energies to the total interaction energy (%) in the crystal of aspirin form I.

Dimer of dimers	Symmetry operation	$E_{\text{int}}$ , kcal/mol	Contribution to the total interaction energy, %	Interaction
dd1	$x, 1+y, z$	-13.4	17.8	Stacking, C...C, 3.32Å
dd2	$x, -1+y, z$	-13.4	17.8	Stacking, C...C, 3.32Å
dd3	$1+x, y, z$	-1.6	2.1	non-specific
dd4	$1+x, 1+y, z$	-4.6	6.0	non-specific
dd5	$-1+x, y, z$	-1.6	2.1	non-specific
dd6	$-1+x, -1+y, z$	-4.6	6.0	non-specific
dd7	$-x, 1/2+y, 5/2-z$	-0.8	1.0	non-specific
dd8	$-x, -1/2+y, 5/2-z$	-0.8	1.0	non-specific
dd9	$1-x, 1/2+y, 3/2-z$	-5.5	7.3	C-H... $\pi$ , 2.71 Å, 178°
dd10	$1-x, 1/2+y, 5/2-z$	-5.5	7.3	C-H... $\pi$ , 2.71 Å, 178°
dd11	$1-x, 3/2+y, 3/2-z$	-2.8	3.7	non-specific
dd12	$1-x, 3/2+y, 5/2-z$	-2.8	3.7	non-specific
dd13	$1-x, -1/2+y, 3/2-z$	-5.5	7.3	C-H... $\pi$ , 2.71 Å, 178°
dd14	$1-x, -1/2+y, 5/2-z$	-5.5	7.3	C-H... $\pi$ , 2.71 Å, 178°
dd15	$1-x, -3/2+y, 3/2-z$	-2.8	3.7	non-specific
dd16	$1-x, -3/2+y, 5/2-z$	-2.8	3.7	non-specific
dd17	$2-x, 1/2+y, 3/2-z$	-0.8	1.0	non-specific
dd18	$2-x, -1/2+y, 3/2-z$	-0.8	1.0	non-specific

Table A 4.5. Symmetry codes, bonding types, interaction energies of the basic dimeric BU with neighboring ones ( $E_{\text{int}}$ , kcal/mol) and the contribution of these energies to the total interaction energy (%) in the crystal of aspirin form II.

Dimer of dimers	Symmetry operation	$E_{\text{int}}$ , kcal/mol	Contribution to the total interaction energy, %	Interaction
dd1	$x, 1+y, z$	-13.4	17.8	Stacking, C...C, 3.36Å
dd2	$x, -1+y, z$	-13.4	17.8	Stacking, C...C, 3.36Å
dd3	$1+x, y, 1+z$	-0.8	1.0	non-specific
dd4	$-1+x, y, -1+z$	-0.8	1.0	non-specific
dd5	$-x, 1/2+y, 1/2-z$	-3.3	4.4	non-specific
dd6	$-x, -1/2+y, 1/2-z$	-3.3	4.4	non-specific
dd7	$1-x, 1/2+y, 1/2-z$	-5.6	7.4	C-H... $\pi$ , 2.71 Å, 176°
dd8	$1-x, 1/2+y, 3/2-z$	-5.6	7.4	C-H... $\pi$ , 2.71 Å, 176°
dd9	$1-x, 3/2+y, 1/2-z$	-2.8	3.7	non-specific
dd10	$1-x, 3/2+y, 3/2-z$	-2.8	3.7	non-specific
dd11	$1-x, -1/2+y, 1/2-z$	-5.6	7.4	C-H... $\pi$ , 2.71 Å, 176°
dd12	$1-x, -1/2+y, 3/2-z$	-5.6	7.4	C-H... $\pi$ , 2.71 Å, 176°
dd13	$1-x, -3/2+y, 1/2-z$	-2.8	3.7	non-specific
dd14	$1-x, -3/2+y, 3/2-z$	-2.8	3.7	non-specific
dd15	$2-x, 1/2+y, 3/2-z$	-3.3	4.4	non-specific
dd16	$2-x, -1/2+y, 3/2-z$	-3.3	4.4	non-specific

Table A 4.6. Symmetry codes, bonding types, interaction energies of the basic dimeric BUs AA and BB, based on the corresponding molecules A and B, with neighboring ones ( $E_{\text{int}}$ , kcal/mol) and the contribution of these energies to the total interaction energy (%) in the crystal of aspirin form IV.

Dimer	Symmetry operation	$E_{\text{int}}$ , kcal/mol	Contribution to the		
			total interaction energy, %	Interaction	Neighbor type
Dimers neighboring to AA-BU					
dd1	x,-1+y,z	-17.7	11.2	non-specific	AA
dd2	x,1+y,z	-17.7	11.2	non-specific	AA
dd3	2-x,-0.5+y,1.5-z	-4.9	3.1	C-H... $\pi$ , 2.68 Å, 163°	AA
dd4	2-x,-0.5+y,2.5-z	-4.9	3.1	C-H... $\pi$ , 2.68 Å, 163°	AA
dd5	2-x,0.5+y,1.5-z	-4.9	3.1	C-H... $\pi$ , 2.68 Å, 163°	AA
dd6	2-x,0.5+y,2.5-z	-4.9	3.1	C-H... $\pi$ , 2.68 Å, 163°	AA
dd7	1-x,0.5+y,1.5-z	-2.2	1.4	non-specific	BB
dd8	1-x,1.5+y,1.5-z	-3.0	1.9	non-specific	BB
dd9	1-x,2.5+y,1.5-z	-3.6	2.3	non-specific	BB
dd10	x,y,z	-1.2	0.8	non-specific	BB
dd11	x,1+y,z	-2.4	1.5	non-specific	BB
dd12	2-x,0.5+y,1.5-z	-3.6	2.3	non-specific	BB
dd13	2-x,1.5+y,1.5-z	-2.9	1.9	non-specific	BB
dd14	2-x,2.5+y,1.5-z	-2.2	1.4	non-specific	BB
dd15	1+x,2+y,1+z	-2.4	1.5	non-specific	BB
dd16	1+x,3+y,1+z	-1.2	0.8	non-specific	BB

Table A 4.6 Continued.

Dimer	Symmetry operation	$E_{\text{int}}$ , kcal/mol	Contribution to the		
			total interaction energy, %	Interaction	Neighbor type
Dimers neighboring to BB-BU					
dd17	x,1+y,z	-16.5	10.4	Stacking, C...C, 3.36Å	BB
dd18	x,-1+y,z	-16.5	10.4	Stacking, C...C, 3.36Å	BB
dd19	1-x,0.5+y,0.5-z	-5.2	3.3	non-specific	BB
dd20	1-x,-0.5+y,0.5-z	-5.2	3.3	non-specific	BB
dd21	1-x,0.5+y,1.5-z	-5.2	3.3	non-specific	BB
dd22	1-x,-0.5+y,1.5-z	-5.2	3.3	non-specific	BB
dd23	2-x,-0.5+y,1.5-z	-3.6	2.3	non-specific	AA
dd24	2-x,-1.5+y,1.5-z	-2.9	1.9	non-specific	AA
dd25	2-x,-2.5+y,1.5-z	-2.2	1.4	non-specific	AA
dd26	1-x,-0.5+y,1.5-z	-2.2	1.4	non-specific	AA
dd27	1-x,-1.5+y,1.5-z	-2.9	1.9	non-specific	AA
dd28	1-x,-2.5+y,1.5-z	-3.6	2.3	non-specific	AA
dd29	-1+x,-2+y,-1+z	-2.4	1.5	non-specific	AA
dd30	-1+x,-3+y,-1+z	-1.2	0.8	non-specific	AA
dd31	x,-1+y,z	-2.4	1.5	non-specific	AA
dd32	x,y,z	-1.2	0.8	non-specific	AA

Table A 4.7. Interaction energy differences arising between the terminal positions of the shifts in the different directions due to the edge effect using the fixed part expanded by an initial fragment in each direction of the mobile part displacement.

Shift direction	$\Delta E_{\text{int}}$ , kcal/mol			
	<b>I</b>	<b>II</b>	<b>IV</b> , AA-basic element	<b>IV</b> , BB-basic element
[100] (001)	0.0	-	-	-
[201] (-102)	-	0.0	-	-
[010] (-101)	-	-	0.1	0.0
[010] (001)	0.2	0.1	0.1	0.0
[010] (100)	0.0	0.0	0.1	0.0
[001] (100)	0.0	0.0	0.0	0.0
[011] (100)	0.0	0.0	-	-

Table A 4.8. Interaction energy differences between the barriers extracted from the shift profiles of the (100) layers in the [010] direction with the step sizes 1/50, 1/25, 1/20, 1/10 of a translation and the energy barrier value appearing, when the step size equals 1/100 of a translation.

Step size (in parts of translation)	$\Delta E_{\text{int}}$ , kcal/mol			
	<b>I</b>	<b>II</b>	<b>IV</b> , AA-basic element	<b>IV</b> , BB-basic element
1/50	0.0	0.0	0.0	0.0
1/25	0.0	0.0	0.0	0.0
1/20	0.0	0.1	0.0	0.0
1/10	0.0	0.1	0.2	0.2

Table A 4.9. Minimal interatomic distances occurring for the displacements of the BUs in the different crystallographic directions.

Shift direction	Minimal interatomic distance, Å			
	I	II	IV, AA-basic element	IV, BB-basic element
[010] (100)	1.61	1.69	1.73	1.73
[001] (100)	1.19	1.26	1.28	1.28
[011] (100)	1.46	1.30	0.86*	0.77*
[100] (001)	1.15	-	0.37*	0.37*
[010] (001)	1.41	-	1.73	1.73
[110] (001)	0.44*	-	0.32*	0.87*
[010] (-102)	-	1.41	-	-
[201] (-102)	-	1.07	-	-
[211] (-102)	-	0.62*	-	-
[010] (-101)	-	-	1.82	1.82
[101] (-101)	-	-	0.32*	0.17*
[111] (-101)	-	-	> 0.01**	0.14*

\* Displacements excluded from calculations due to the considerable shortening of the interatomic distances.

\*\* Approaching of the mobile and fixed parts closer than 0.01 Å has been set as the computational limit.

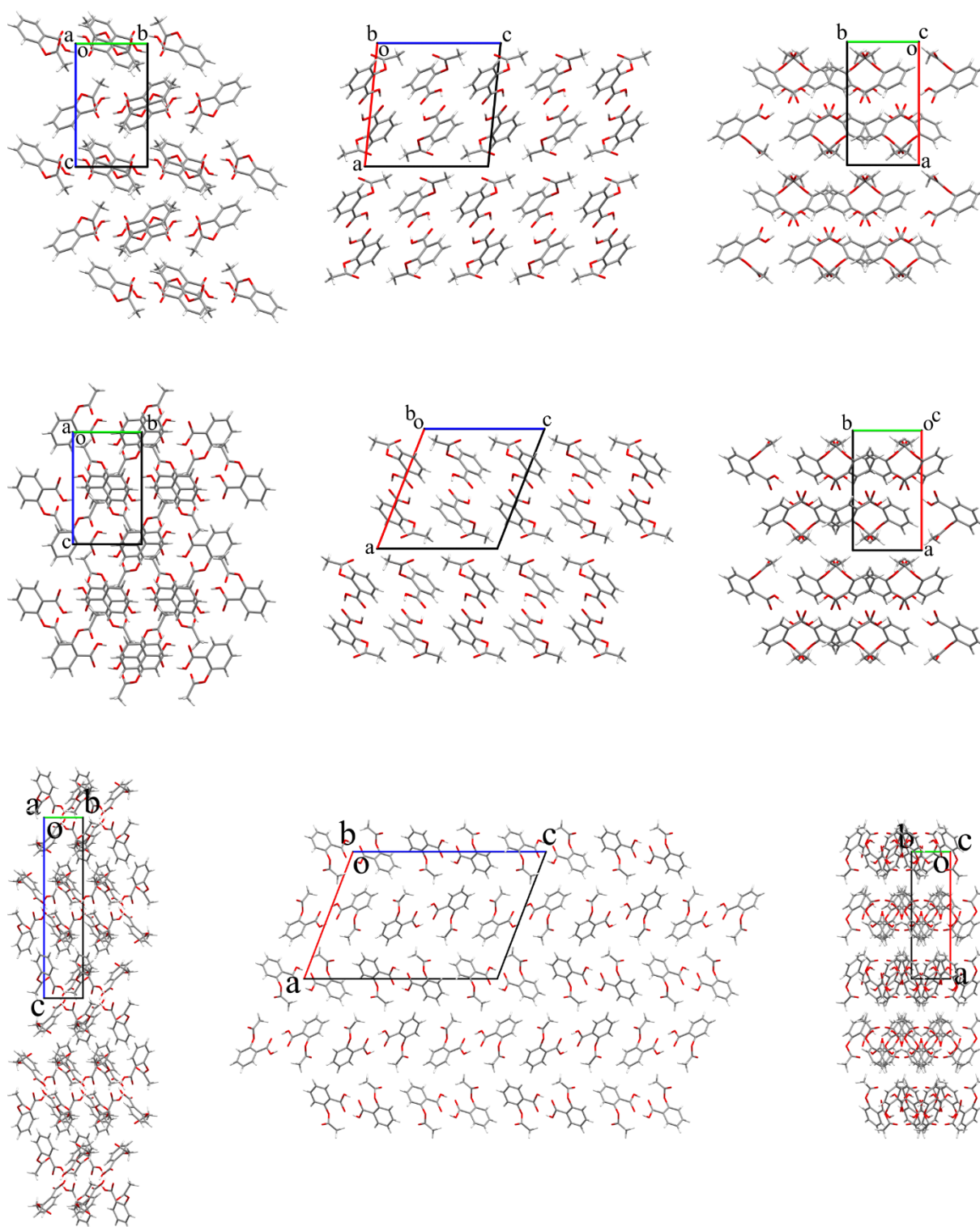


Figure A 4.1. Packing of the molecules in the crystals of aspirin polymorphs I (at the top), II (in the middle), IV (at the bottom). The projections in the  $a$  (on the right),  $b$  (in the middle),  $c$  (on the left) crystallographic directions are represented.

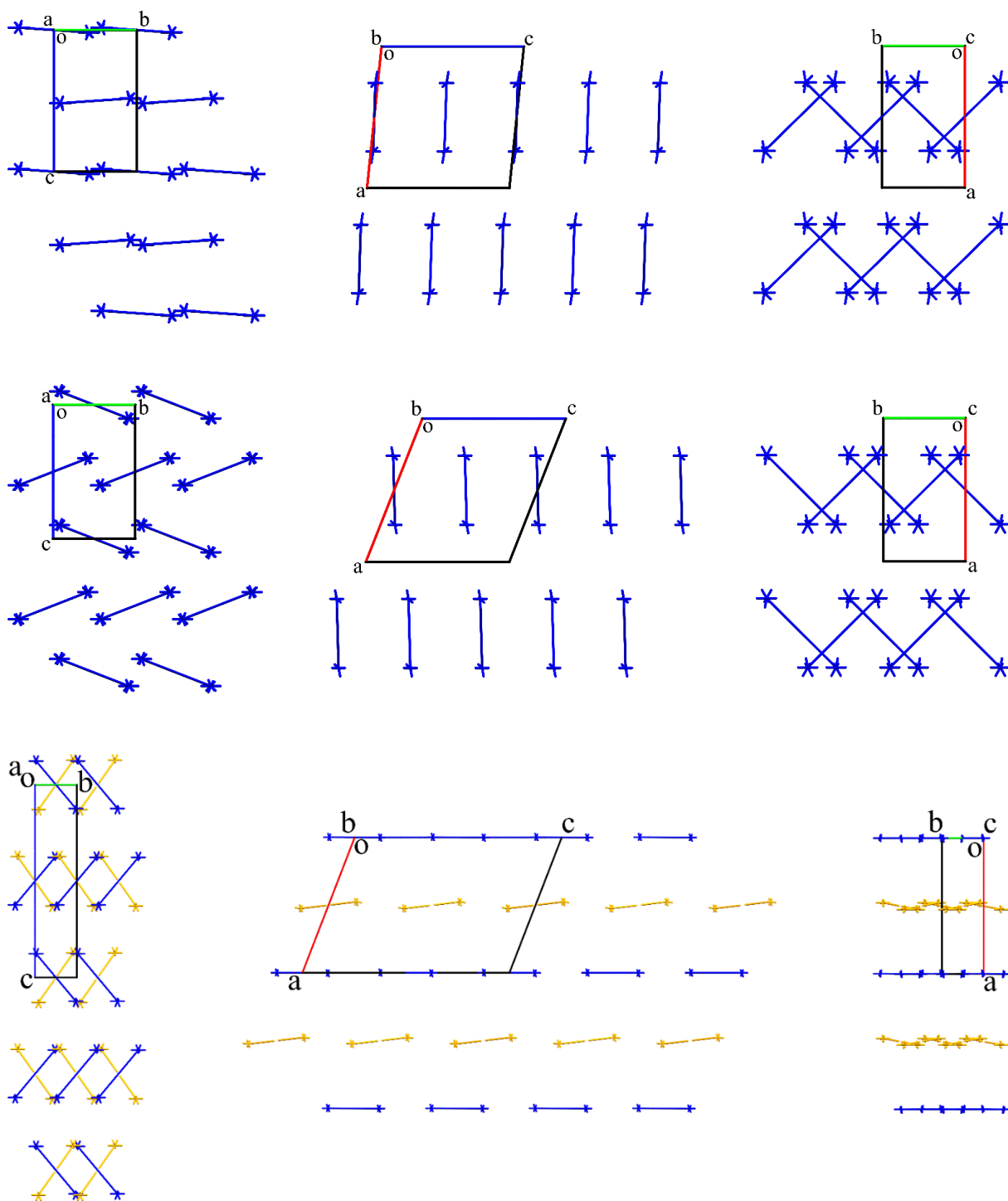


Figure A 4.2. Packing of the energy vector diagrams representing the distribution of monomeric BUs in the crystals of aspirin polymorphs I (at the top), II (in the middle), IV (at the bottom). The projections in the  $a$  (on the right),  $b$  (in the middle),  $c$  (on the left) crystallographic directions are represented.

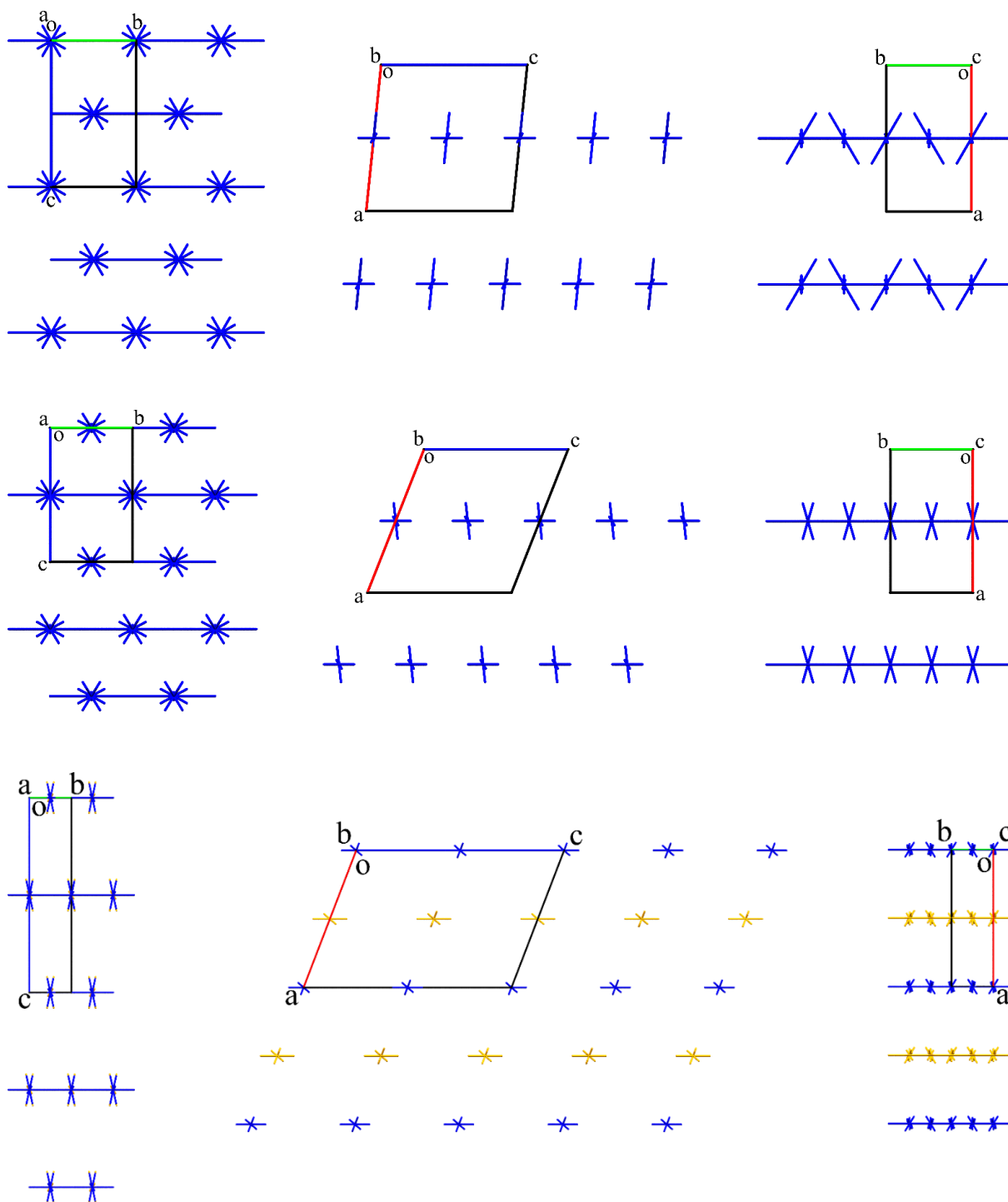


Figure A 4.3. Packing of the energy vector diagrams representing the distribution of dimeric BUs in the crystals of aspirin polymorphs I (at the top), II (in the middle), IV (at the bottom). The projections in the  $a$  (on the right),  $b$  (in the middle),  $c$  (on the left) crystallographic directions are represented.

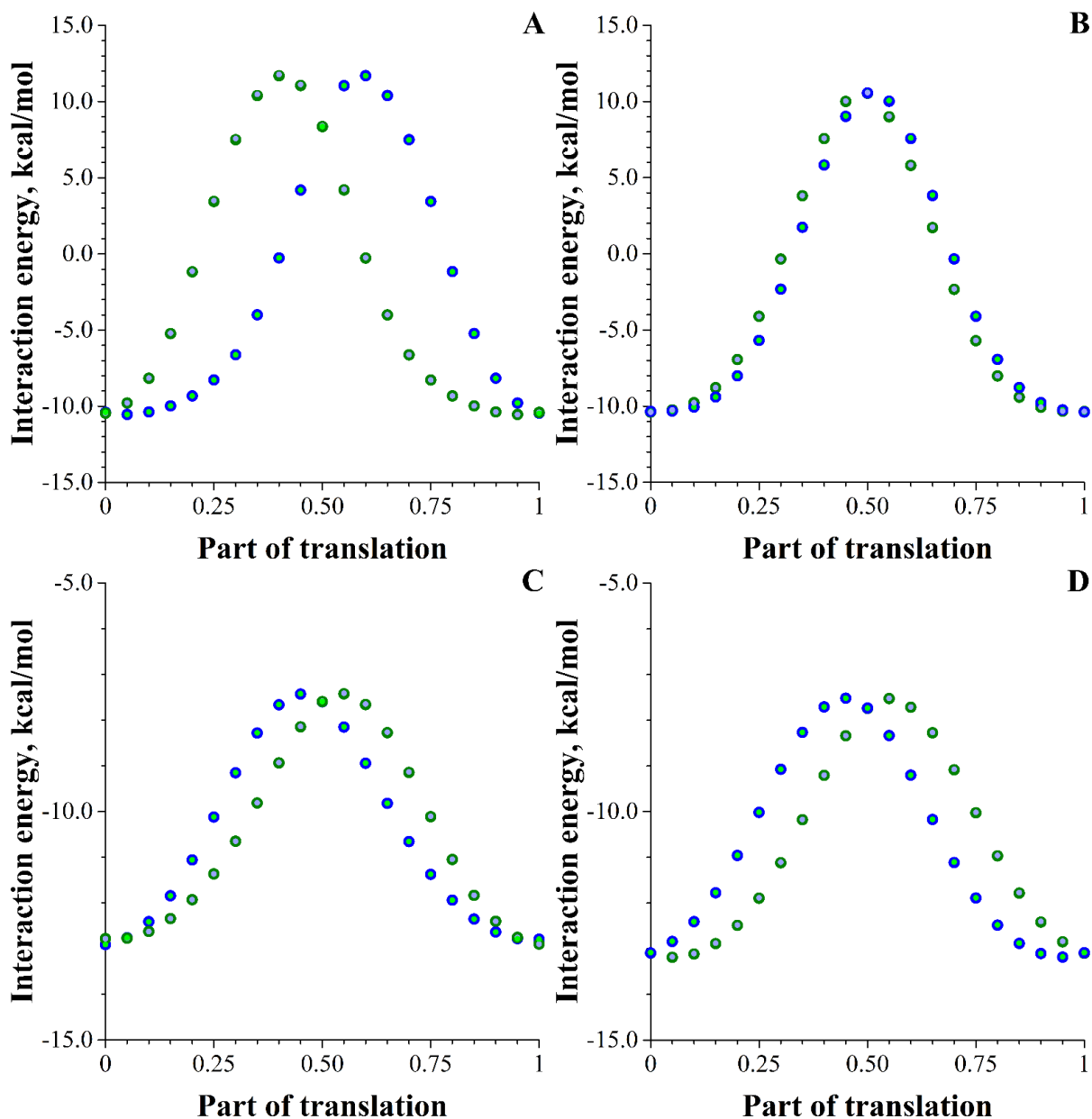


Figure A 4.4. Interaction energy profile for the shifts of different symmetric equivalents of dimeric BUs along the (100) layers in the [010] direction. Blue and pale blue dots correspond to the shifts of the initial dimeric BUs along the BSM<sub>2</sub> with higher (big) or lower (small) coordinate by the [100] direction respectively, olive and green dots are for the shifts of the dimeric BUs rotated by 2<sub>1</sub>-screw axes once belonging to the polymorphic forms: I (A); II (B); IV, AA-BU as a basic element (C); IV, BB-BU as a basic element (D).

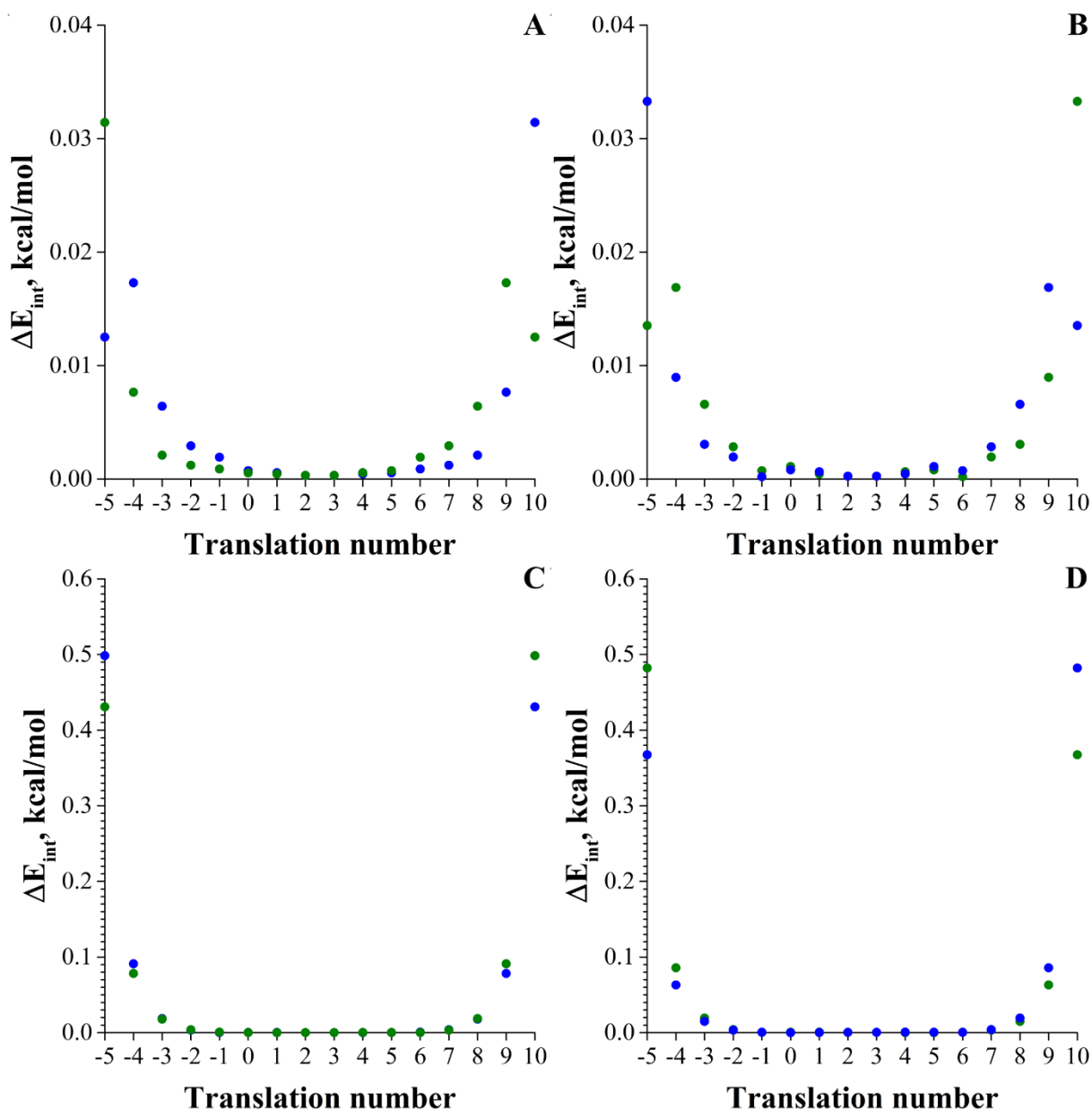


Figure A 4.5. Interaction energy deviations occurring between the symmetrically equivalent positions of the dimeric BU as a mobile part (its initial disposition is in blue, disposition rotated by  $2_1$ -screw axes once is in olive) during the transitions from the edge to the center beside the neighboring (100) layer between the -5th and 10th positions in the [010] direction for the polymorphic forms: I (A); II (B); IV, AA-BU as a basic element (C); IV, BB-BU as a basic element (D).

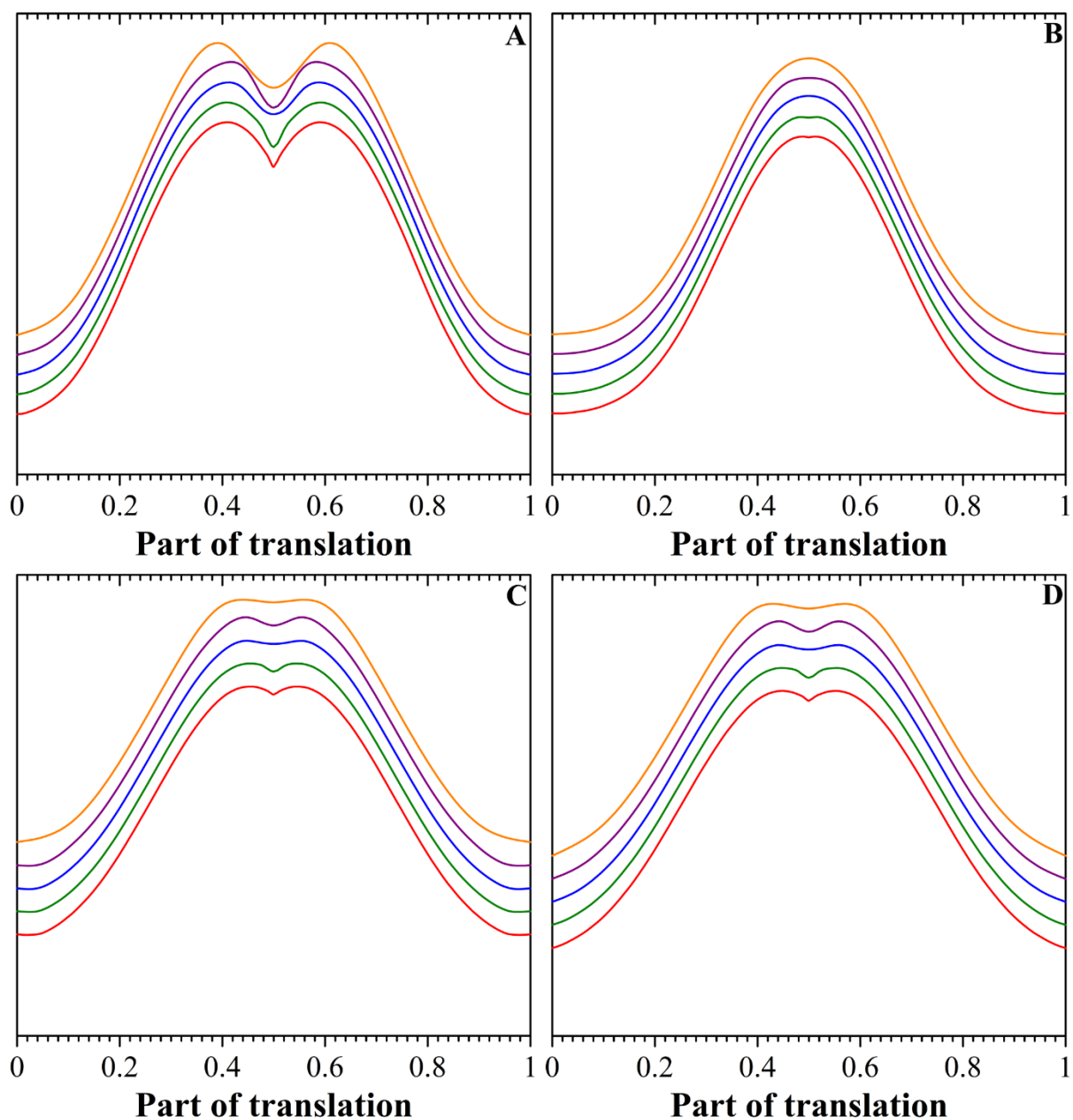


Figure A 4.6. Profile of the interaction energy between the dimeric mobile part and the neighboring (100) layer during the translation between the equivalent positions in the [010] direction with the step size of 1/100 (in red), 1/50 (olive), 1/25 (blue), 1/20 (purple), 1/10 (orange) of the corresponding distance for the polymorphic forms: I (A); II (B); IV, AA-BU as a basic element (C); IV, BB-BU as a basic element (D).

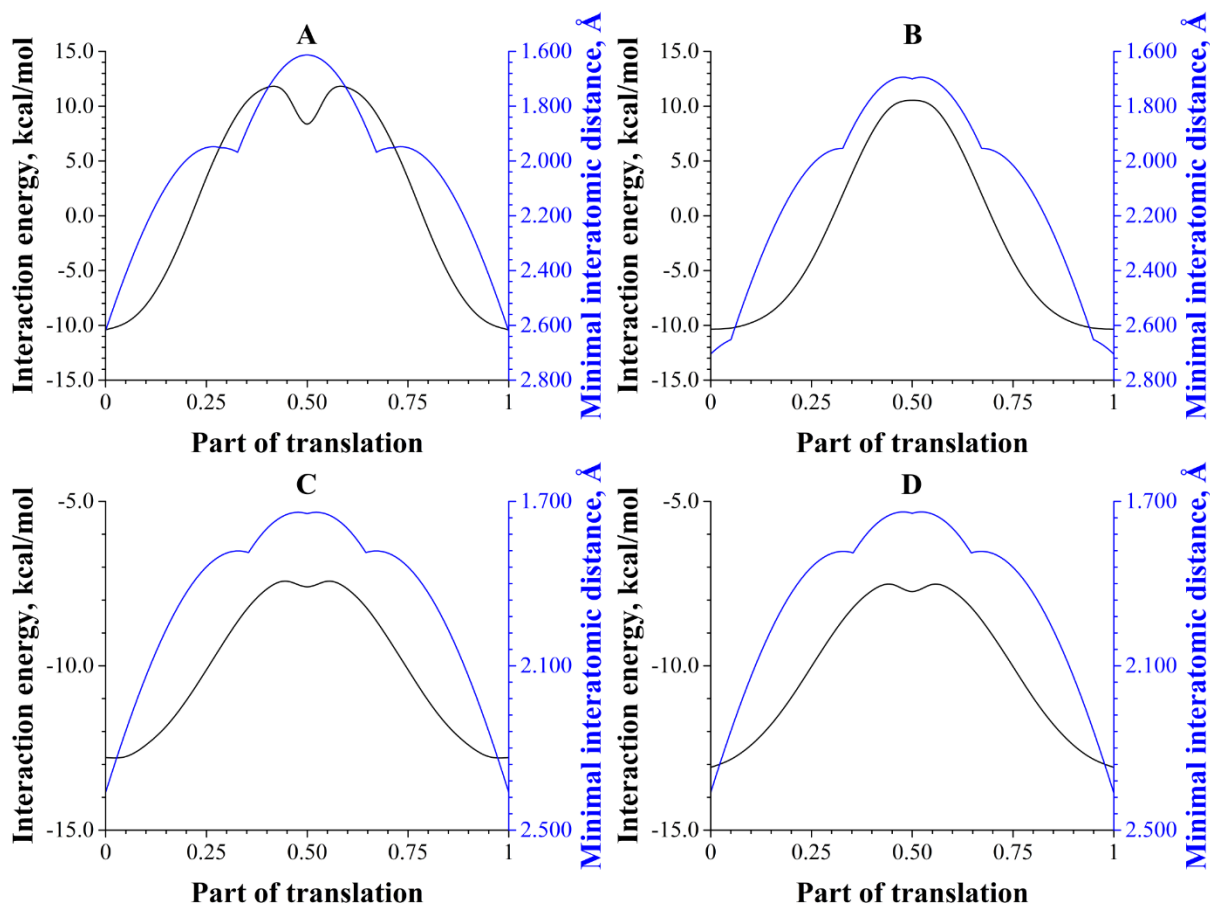


Figure A 4.7. Profiles of the interaction energy (black) and minimal interatomic distance (blue) between the dimeric mobile part and the neighboring (100) layer in the [010] direction for the polymorphic forms: I (A); II (B); IV, AA-BU as a basic element (C); IV, BB-BU as a basic element (D).

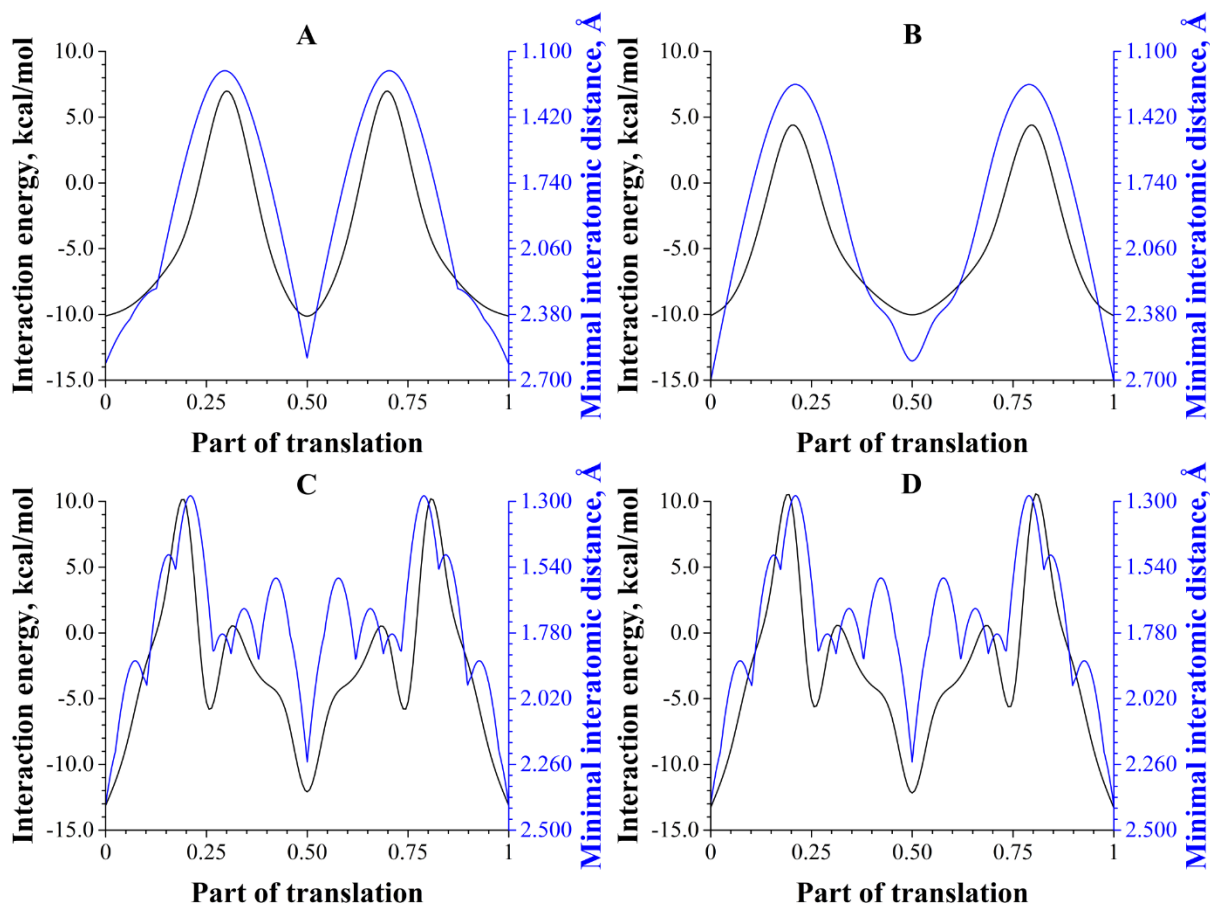


Figure A 4.8. Profiles of the interaction energy (black) and minimal interatomic distance (blue) between the dimeric mobile part and the neighboring (100) layer in the [001] direction for the polymorphic forms: I (A); II (B); IV, AA-BU as a basic element (C); IV, BB-BU as a basic element (D).

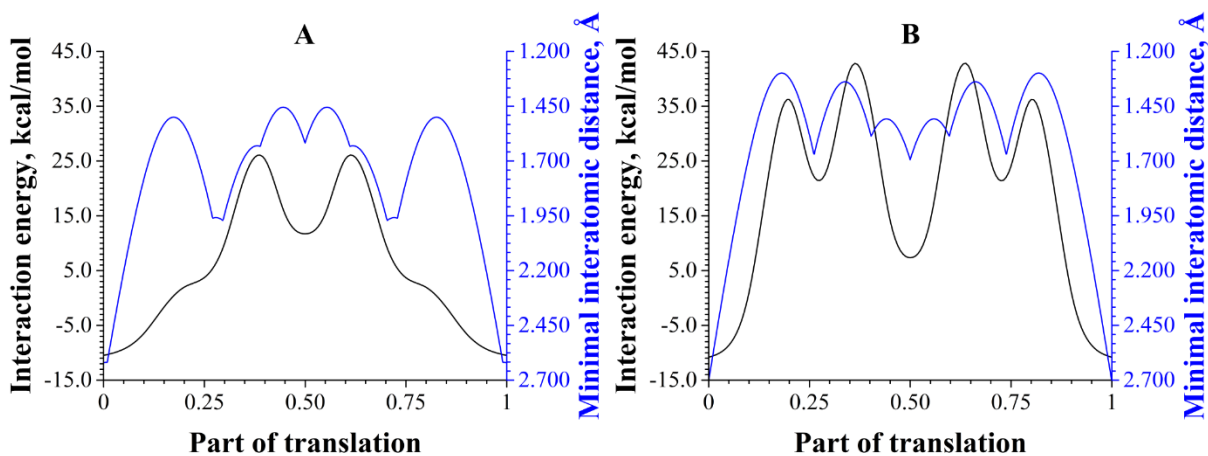


Figure A 4.9. Profiles of the interaction energy (black) and minimal interatomic distance (blue) between the dimeric mobile part and the neighboring (100) layer in the [011] direction for the polymorphic forms I (A) and II (B).

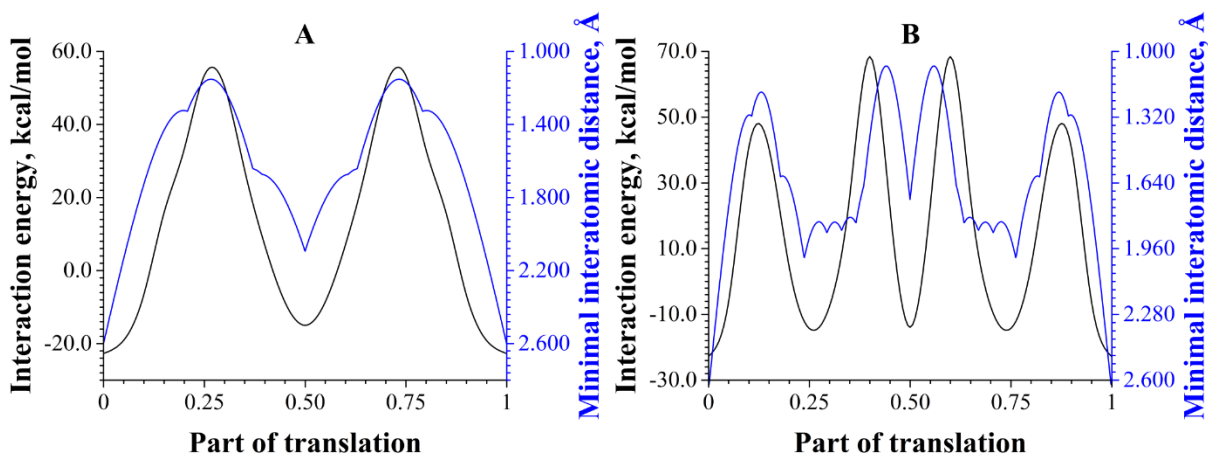


Figure A 4.10. Profiles of the interaction energy (black) and minimal interatomic distance (blue) between the dimeric mobile part and the neighboring (001) layer in the [100] direction for the polymorphic form I (A) and the neighboring (-102) layer in the [201] direction for the polymorphic form II (B) respectively.

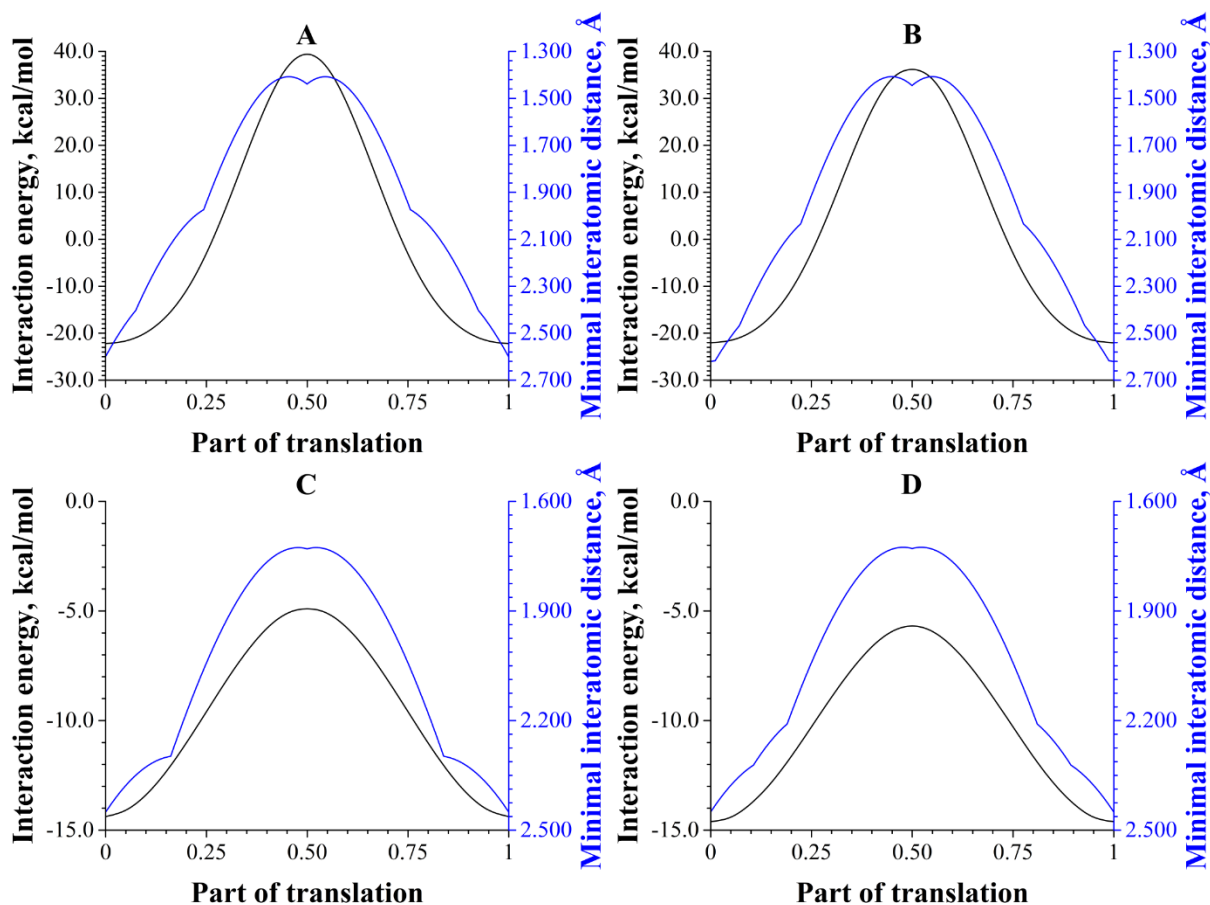


Figure A 4.11. Profiles of the interaction energy (black) and minimal interatomic distance (blue) between the dimeric mobile part and the neighboring (001) layers for the polymorphic forms I (A); IV, AA-BU as a basic element (C); IV, BB-BU as a basic element (D) and the neighboring (-102) layer for the polymorphic form II (B) in the [010] direction respectively.

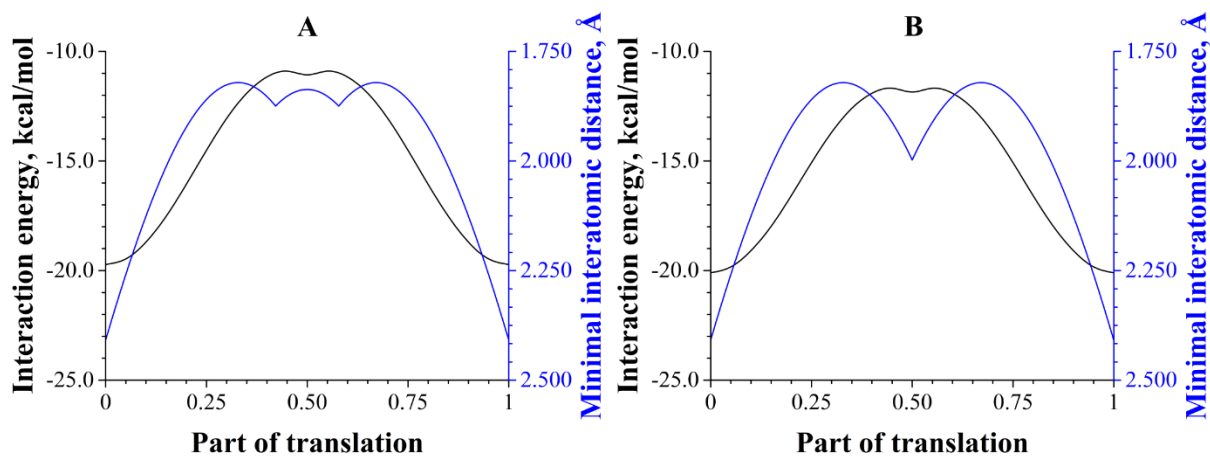


Figure A 4.12. Profiles of the interaction energy (black) and minimal interatomic distance (blue) between the dimeric mobile part and the neighboring (-101) layer in the [010] direction for the polymorphic form IV, AA-BU as a basic element (A) and BB-BU as a basic element (B).

Table A 4.10. Symmetry codes, bounding types, interaction energies and their decomposition terms (kcal/mol) belonging to the basic monomeric building unit and its neighbors, the contributions of the individual interaction energies to the total one (%) in the crystal of piracetam form II at the ambient pressure.

Dimer	Symmetry operation	Interaction	$E_{int}^{Gaussian}$ , kcal/mol	Contribution to the total $E_{int}^{Gaussian}$ , %	$E_{int}^{GAMMESS}$ , kcal/mol	Contribution to the total $E_{int}^{GAMMESS}$ , %	$E_{EX}^{GAMMESS}$ , kcal/mol	$E_{REP}^{GAMMESS}$ , kcal/mol	$E_{ES}^{GAMMESS}$ , kcal/mol	$E_{POL}^{GAMMESS}$ , kcal/mol	$E_{ES+POL}^{GAMMESS}$ , kcal/mol	$E_{DISP}^{GAMMESS}$ , kcal/mol
d1	-1+x,-1+y,z	non-specific	-0.5	0.7	-0.6	0.8	3.4	1.5	32.8	-34.7	-1.9	-3.7
d2	-1+x,y,z	N-H...O, 2.00 Å, 160°	-9.9	13.5	-10.4	13.3	8.2	12.9	21.4	-41.5	-20.0	-11.5
d3	-x,-1-y,-z	non-specific	-0.7	1.0	-0.8	1.0	0.9	0.4	31.9	-32.8	-0.9	-1.1
d4	-x,-y,-1-z	non-specific	-8.8	12.0	-9.4	12.0	14.0	6.7	28.2	-43.1	-14.9	-15.2
d5	-x,-y,-z	non-specific	-7.0	9.6	-7.8	10.0	10.7	5.6	27.4	-39.9	-12.5	-11.6
d6	-x,1-y,-1-z	2*C-H...O, 2.33 Å, 155°	-7.9	10.8	-8.7	11.1	6.8	7.0	24.4	-38.6	-14.2	-8.3
d7	1-x,-y,-z	non-specific	-4.4	6.0	-4.8	6.1	8.0	3.3	30.5	-37.9	-7.4	-8.7
d8	1-x,1-y,-1-z	non-specific	-2.0	2.7	-2.1	2.7	1.3	0.3	31.7	-33.8	-2.1	-1.7
d9	1-x,1-y,-z	2*N-H...O, 1.95 Å, 169°	-15.3	20.9	-15.7	20.1	5.5	23.0	11.8	-44.6	-32.8	-11.4
d10	1+x,1+y,z	non-specific	-0.5	0.7	-0.6	0.8	3.4	1.5	32.8	-34.7	-1.9	-3.7
d11	1+x,y,z	N-H...O, 2.00 Å, 160°	-9.9	13.5	-10.4	13.3	8.2	12.9	21.4	-41.5	-20.0	-11.5
d12	x,-1+y,z	non-specific	-3.1	4.2	-3.5	4.5	7.1	3.9	30.7	-37.3	-6.6	-7.8
d13	x,1+y,z	non-specific	-3.1	4.2	-3.5	4.5	7.1	3.9	30.7	-37.3	-6.6	-7.8

Table A 4.11. Symmetry codes, bounding types, interaction energies and their decomposition terms (kcal/mol) belonging to the basic monomeric building unit and its neighbors, the contributions of the individual interaction energies to the total one (%) in the crystal of piracetam form II under the pressure of 0.45 GPa.

Dimer	Symmetry operation	Interaction	$E_{\text{int}}^{\text{Gaussian}}$ , kcal/mol	Contribution to the total $E_{\text{int}}^{\text{Gaussian}}$ , %	$E_{\text{int}}^{\text{GAMMESS}}$ , kcal/mol	Contribution to the total $E_{\text{int}}^{\text{GAMMESS}}$ , %	$E_{\text{EX}}^{\text{GAMMESS}}$ , kcal/mol	$E_{\text{REP}}^{\text{GAMMESS}}$ , kcal/mol	$E_{\text{ES}}^{\text{GAMMESS}}$ , kcal/mol	$E_{\text{POL}}^{\text{GAMMESS}}$ , kcal/mol	$E_{\text{ES+POL}}^{\text{GAMMESS}}$ , kcal/mol	$E_{\text{DISP}}^{\text{GAMMESS}}$ , kcal/mol
d1	-1+x,-1+y,z	non-specific	-0.5	0.7	-0.6	0.8	3.0	1.3	33.4	-35.2	-1.8	-3.2
d2	-1+x,y,z	N-H...O, 2.11 Å, 152°	-9.6	13.2	-10.2	13.0	8.2	10.3	22.6	-40.6	-18.0	-10.6
d3	-x,-1-y,2-z	non-specific	-0.8	1.1	-0.8	1.0	0.7	0.3	32.3	-33.3	-1.0	-0.9
d4	-x,-y,1-z	non-specific	-10.0	13.7	-10.8	13.7	14.5	8.0	27.7	-45.0	-17.3	-16.0
d5	-x,-y,2-z	non-specific	-7.8	10.7	-8.8	11.2	11.0	6.4	27.0	-41.2	-14.1	-12.0
d6	-x,1-y,1-z	2*C-H...O, 2.36 Å, 153°	-8.8	12.1	-9.7	12.3	7.1	6.2	24.4	-39.1	-14.7	-8.3
d7	1-x,-y,2-z	non-specific	-4.9	6.7	-5.2	6.6	8.1	3.6	30.9	-39.0	-8.1	-8.8
d8	1-x,1-y,1-z	non-specific	-1.9	2.6	-1.9	2.4	1.3	0.4	32.5	-34.5	-2.0	-1.6
d9	1-x,1-y,2-z	2*N-H...O, 2.06 Å, 165°	-12.6	17.3	-13.0	16.5	6.6	16.0	15.8	-41.0	-25.2	-10.4
d10	1+x,1+y,z	non-specific	-0.5	0.7	-0.6	0.8	3.0	1.3	33.4	-35.2	-1.7	-3.2
d11	1+x,y,z	N-H...O, 2.11 Å, 152°	-9.6	13.2	-10.2	13.0	8.2	10.3	22.6	-40.6	-18.0	-10.6
d12	x,-1+y,z	non-specific	-3.0	4.1	-3.4	4.3	6.7	3.9	31.2	-37.8	-6.6	-7.4
d13	x,1+y,z	non-specific	-3.0	4.1	-3.4	4.3	6.7	3.9	31.2	-37.8	-6.6	-7.4

Table A 4.12. Symmetry codes, bounding types, interaction energies and their decomposition terms (kcal/mol) belonging to the basic monomeric building unit and its neighbors, the contributions of the individual interaction energies to the total one (%) in the crystal of piracetam form V under the pressure of 0.7 GPa.

Dimer	Symmetry operation	Interaction	$E_{\text{int}}^{\text{Gaussian}}$ , kcal/mol	Contribution to the total $E_{\text{int}}^{\text{Gaussian}}$ , %	$E_{\text{int}}^{\text{GAMESS}}$ , kcal/mol	Contribution to the total $E_{\text{int}}^{\text{GAMESS}}$ , %	$E_{\text{EX}}^{\text{GAMESS}}$ , kcal/mol	$E_{\text{REP}}^{\text{GAMESS}}$ , kcal/mol	$E_{\text{ES}}^{\text{GAMESS}}$ , kcal/mol	$E_{\text{POL}}^{\text{GAMESS}}$ , kcal/mol	$E_{\text{ES+POL}}^{\text{GAMESS}}$ , kcal/mol	$E_{\text{DISP}}^{\text{GAMESS}}$ , kcal/mol
d1	-1+x,-1+y,z	non-specific	-0.4	0.5	-0.6	0.7	3.6	1.9	33.4	-35.7	-2.3	-3.9
d2	-1+x,y,z	N-H...O, 2.13 Å, 153°	-9.4	11.5	-9.8	11.2	7.8	9.1	23.3	-40.1	-16.8	-9.9
d3	1-x,-y,-z	2*N-H...O, 2.04 Å, 165°	-12.6	15.4	-13.0	14.8	6.7	17.0	15.3	-41.3	-25.9	-10.7
d4	1-x,1-y,-z	non-specific	-5.2	6.3	-5.6	6.4	8.6	4.2	30.4	-39.4	-9.0	-9.4
d5	1+x,1+y,z	non-specific	-0.4	0.5	-0.6	0.7	3.6	1.9	33.4	-35.7	-2.3	-3.9
d6	1+x,y,z	N-H...O, 2.13 Å, 153°	-9.4	11.5	-9.8	11.2	7.8	9.1	23.3	-40.1	-16.8	-9.9
d7	2-x,-y,1-z	non-specific	-11.9	14.5	-12.8	14.6	8.0	4.4	23.0	-39.2	-16.2	-8.9
d8	2-x,1-y,-z	non-specific	-7.8	9.5	-8.8	10.0	11.4	7.2	26.7	-41.5	-14.8	-12.5
d9	2-x,1-y,1-z	non-specific	-8.5	10.4	-9.4	10.7	13.8	8.4	29.2	-45.4	-16.2	-15.4
d10	2-x,2-y,-z	non-specific	-1.0	1.2	-1.1	1.3	1.1	0.4	32.2	-33.5	-1.3	-1.2
d11	3-x,-y,1-z	non-specific	3.4 *	4.2 **	3.3 *	3.8 **	0.2	0.0	36.4	-33.3	3.1	-0.0
d12	3-x,1-y,1-z	non-specific	-4.9	6.0	-5.2	5.9	3.8	1.9	29.2	-35.9	-6.7	-4.3
d13	x,-1+y,z	non-specific	-3.5	4.3	-3.9	4.4	7.3	4.5	30.8	-38.3	-7.5	-8.1
d14	x,1+y,z	non-specific	-3.5	4.3	-3.9	4.4	7.3	4.5	30.8	-38.3	-7.5	-8.1

\* Positive value of the interaction energy appearing due to compression.

\*\* All energy values were taken in absolute for the calculation of their contributions due to crystal symmetry.

Table A 4.13. Symmetry codes, bounding types, interaction energies and their decomposition terms (kcal/mol) belonging to the basic monomeric building unit and its neighbors, the contributions of the individual interaction energies to the total one (%) in the crystal of piracetam form V under the pressure of 0.9 GPa.

Dimer	Symmetry operation	Interaction	$E_{\text{int}}^{\text{Gaussian}}$ , kcal/mol	Contribution to the total $E_{\text{int}}^{\text{Gaussian}}$ , %	$E_{\text{int}}^{\text{GAMESS}}$ , kcal/mol	Contribution to the total $E_{\text{int}}^{\text{GAMESS}}$ , %	$E_{\text{EX}}^{\text{GAMESS}}$ , kcal/mol	$E_{\text{REP}}^{\text{GAMESS}}$ , kcal/mol	$E_{\text{ES}}^{\text{GAMESS}}$ , kcal/mol	$E_{\text{POL}}^{\text{GAMESS}}$ , kcal/mol	$E_{\text{ES+POL}}^{\text{GAMESS}}$ , kcal/mol	$E_{\text{DISP}}^{\text{GAMESS}}$ , kcal/mol
d1	-1+x,-1+y,z	non-specific	-0.4	0.5	-0.7	0.8	4.0	2.4	33.3	-36.0	-2.7	-4.4
d2	-1+x,y,z	N-H...O, 2.14 Å, 154°	-9.5	11.4	-10.0	11.1	8.2	9.4	23.2	-40.5	-17.3	-10.4
d3	1-x,-y,-z	2*N-H...O, 2.02 Å, 167°	-12.6	15.2	-13.0	14.4	6.4	19.0	14.4	-41.8	-27.4	-11.0
d4	1-x,1-y,-z	non-specific	-5.1	6.1	-5.7	6.3	9.9	6.1	30.0	-40.6	-10.5	-11.1
d5	1+x,1+y,z	non-specific	-0.4	0.5	-0.7	0.8	4.0	2.4	33.3	-36.0	-2.7	-4.4
d6	1+x,y,z	N-H...O, 2.14 Å, 154°	-9.5	11.4	-10.0	11.1	8.2	9.4	23.2	-40.5	-17.3	-10.4
d7	2-x,-y,1-z	non-specific	-12.6	15.2	-13.6	15.1	9.1	5.8	22.0	-40.2	-18.2	-10.3
d8	2-x,1-y,-z	non-specific	-7.6	9.1	-8.7	9.6	12.4	8.2	26.7	-42.2	-15.6	-13.7
d9	2-x,1-y,1-z	non-specific	-8.7	10.5	-9.8	10.9	14.3	9.2	28.7	-45.9	-17.2	-16.1
d10	2-x,2-y,-z	non-specific	-1.1	1.3	-1.1	1.2	1.4	0.7	32.1	-33.7	-1.6	-1.7
d11	3-x,-y,1-z	non-specific	3.7 *	4.5 **	3.7 *	4.1 **	0.4	0.1	36.8	-33.4	3.4	-0.2
d12	3-x,1-y,1-z	non-specific	-5.1	6.1	-5.5	6.1	4.3	2.5	29.0	-36.3	-7.3	-5.0
d13	x,-1+y,z	non-specific	-3.4	4.1	-3.9	4.3	7.6	5.2	30.6	-38.7	-8.1	-8.6
d14	x,1+y,z	non-specific	-3.4	4.1	-3.9	4.3	7.6	5.2	30.6	-38.7	-8.1	-8.6

\* Positive value of the interaction energy appearing due to compression.

\*\* All energy values were taken in absolute for the calculation of their contributions due to crystal symmetry.

Table A 4.14. Symmetry codes, bounding types, interaction energies and their decomposition terms (kcal/mol) belonging to the basic monomeric building unit and its neighbors, the contributions of the individual interaction energies to the total one (%) in the crystal of piracetam form V under the pressure of 2.5 GPa.

Dimer	Symmetry operation	Interaction	$E_{int}^{Gaussian}$ , kcal/mol	Contribution to the total $E_{int}^{Gaussian}$ , %	$E_{int}^{GAMMESS}$ , kcal/mol	Contribution to the total $E_{int}^{GAMMESS}$ , %	$E_{EX}^{GAMMESS}$ , kcal/mol	$E_{REP}^{GAMMESS}$ , kcal/mol	$E_{ES}^{GAMMESS}$ , kcal/mol	$E_{POL}^{GAMMESS}$ , kcal/mol	$E_{ES+POL}^{GAMMESS}$ , kcal/mol	$E_{DISP}^{GAMMESS}$ , kcal/mol
d1	-1+x,y,z	N-H...O, 2.02 Å, 152°	-9.1	11.4	-9.8	11.0	8.8	14.2	22.0	-42.6	-20.6	-12.1
d2	1-x,-y,-z	2*N-H...O, 1.97 Å, 164°	-11.5	14.4	-11.8	13.2	6.4	22.4	14.2	-43.0	-28.9	-11.7
d3	1-x,1-y,-z	non-specific	-4.9	6.1	-5.9	6.6	11.8	9.7	29.6	-43.1	-13.5	-13.9
d4	1+x,y,z	N-H...O, 2.02 Å, 152°	-9.1	11.4	-9.8	11.0	8.8	14.2	22.0	-42.6	-20.6	-12.1
d5	2-x,-y,1-z	non-specific	-12.9	16.2	-14.3	16.0	11.3	10.4	20.6	-42.9	-22.3	-13.7
d6	2-x,1-y,-z	non-specific	-7.4	9.3	-8.7	9.8	14.3	12.1	26.0	-44.5	-18.5	-16.5
d7	2-x,1-y,1-z	non-specific	-7.6	9.5	-9.6	10.8	15.7	16.7	27.7	-50.1	-22.4	-19.7
d8	2-x,2-y,-z	non-specific	-1.1	1.4	-1.2	1.3	2.0	1.1	32.6	-34.6	-2.0	-2.3
d9	3-x,-y,1-z	non-specific	4.2 *	5.3 **	4.2 *	4.7 **	0.8	0.2	38.0	-34.2	3.7	-0.5
d10	3-x,1-y,1-z	non-specific	-5.6	7.0	-6.1	6.8	5.3	4.1	28.7	-37.8	-9.1	-6.3
d11	x,-1+y,z	non-specific	-3.2	4.0	-3.9	4.4	8.2	7.3	30.4	-40.0	-9.6	-9.8
d12	x,1+y,z	non-specific	-3.2	4.0	-3.9	4.4	8.2	7.3	30.4	-40.0	-9.6	-9.8

\* Positive value of the interaction energy appearing due to compression.

\*\* All energy values were taken in absolute for the calculation of their contributions due to crystal symmetry.

Table A 4.15. Symmetry codes, bounding types, interaction energies and their decomposition terms (kcal/mol) belonging to the basic monomeric building unit and its neighbors, the contributions of the individual interaction energies to the total one (%) in the crystal of piracetam form V under the pressure of 4.0 GPa.

Dimer	Symmetry operation	Interaction	$E_{int}^{Gaussian}$ , kcal/mol	Contribution to the total $E_{int}^{Gaussian}$ , %	$E_{int}^{GAMMESS}$ , kcal/mol	Contribution to the total $E_{int}^{GAMMESS}$ , %	$E_{EX}^{GAMMESS}$ , kcal/mol	$E_{REP}^{GAMMESS}$ , kcal/mol	$E_{ES}^{GAMMESS}$ , kcal/mol	$E_{POL}^{GAMMESS}$ , kcal/mol	$E_{ES+POL}^{GAMMESS}$ , kcal/mol	$E_{DISP}^{GAMMESS}$ , kcal/mol
d1	-1+x,y,z	N-H...O, 2.03 Å, 155°	-9.4	12.0	-10.2	11.4	9.4	15.2	21.9	-43.8	-21.9	-13.0
d2	1-x,-y,-z	2*N-H...O, 1.92 Å, 167°	-11.7	14.9	-12.0	13.4	5.9	26.8	12.3	-44.8	-32.4	-12.2
d3	1-x,1-y,-z	non-specific	-4.2	5.4	-5.6	6.3	12.8	13.5	29.1	-45.1	-16.0	-15.9
d4	1+x,y,z	N-H...O, 2.03 Å, 155°	-9.4	12.0	-10.2	11.4	9.4	15.2	21.9	-43.8	-21.9	-13.0
d5	2-x,-y,1-z	non-specific	-13.0	16.6	-14.6	16.3	12.2	14.7	19.0	-44.7	-25.8	-15.7
d6	2-x,1-y,-z	non-specific	-6.8	8.7	-8.2	9.2	15.7	15.9	25.5	-46.4	-20.9	-18.8
d7	2-x,1-y,1-z	non-specific	-7.0	8.9	-9.5	10.6	15.8	22.1	26.4	-52.5	-26.0	-21.3
d8	2-x,2-y,-z	non-specific	-1.1	1.4	-1.3	1.5	2.5	1.6	32.8	-35.2	-2.5	-2.9
d9	3-x,-y,1-z	non-specific	4.7*	6.0**	4.7*	5.3**	1.1	0.3	38.8	-34.8	4.0	-0.7
d10	3-x,1-y,1-z	non-specific	-5.6	7.2	-6.2	6.9	5.8	5.2	28.7	-38.7	-10.1	-7.1
d11	x,-1+y,z	non-specific	-2.7	3.4	-3.5	3.9	8.4	8.9	30.5	-40.9	-10.4	-10.4
d12	x,1+y,z	non-specific	-2.7	3.4	-3.5	3.9	8.4	8.9	30.5	-40.9	-10.4	-10.4

\* Positive value of the interaction energy appearing due to compression.

\*\* All energy values were taken in absolute for the calculation of their contributions due to crystal symmetry.

Table A 4.16. Symmetry codes, bounding types, interaction energies (kcal/mol) of the basic dimeric building unit with its neighbors, the contributions of the individual interaction energies to the total one (%) in the crystal of piracetam form II at the ambient pressure.

Dimer of dimers	Symmetry operation	Interaction	$E_{\text{int}}$ , kcal/mol	Contribution to the total interaction energy, %
dd1	-1+x,-1+y,-1+z	non-specific	-8.5	8.0
dd2	-1+x,-1+y,z	non-specific	-7.1	6.7
dd3	-1+x,-2+y,z	non-specific	-0.5	0.5
dd4	-1+x,y,-1+z	2*C-H...O, 2.33 Å, 155°	-7.0	6.6
dd5	-1+x,y,z	2*N-H...O, 2.00 Å, 160°	-18.4	17.3
dd6	1+x,1+y,1+z	non-specific	-8.5	8.0
dd7	1+x,1+y,z	non-specific	-7.1	6.7
dd8	1+x,2+y,z	non-specific	-0.5	0.5
dd9	1+x,y,1+z	2*C-H...O, 2.33 Å, 155°	-7.0	6.6
dd10	1+x,y,z	2*N-H...O, 2.00 Å, 160°	-18.4	17.3
dd11	x,-1+y,z	non-specific	-10.4	9.8
dd12	x,1+y,z	non-specific	-10.4	9.8
dd13	x,y,-1+z	non-specific	-1.2	1.1
dd14	x,y,1+z	non-specific	-1.2	1.1

Table A 4.17. Symmetry codes, bounding types, interaction energies (kcal/mol) of the basic dimeric building unit with its neighbors, the contributions of the individual interaction energies to the total one (%) in the crystal of piracetam form II under the pressure of 0.45 GPa.

Dimer of dimers	Symmetry operation	Interaction	$E_{int}$ , kcal/mol	Contribution to the total interaction energy, %
dd1	-x,-1-y,2-z	non-specific	-0.5	0.5
dd2	-x,-y,1-z	non-specific	-9.6	8.6
dd3	-x,-y,2-z	non-specific	-8.1	7.3
dd4	-x,1-y,1-z	2*C-H...O, 2.36 Å, 153°	-7.7	6.9
dd5	-x,1-y,2-z	2*N-H...O, 2.11 Å, 152°	-17.9	16.1
dd6	1-x,-y,2-z	non-specific	-10.6	9.5
dd7	1-x,1-y,1-z	non-specific	-1.1	1.0
dd8	1-x,1-y,3-z	non-specific	-1.1	1.0
dd9	1-x,2-y,2-z	non-specific	-10.6	9.5
dd10	2-x,1-y,2-z	2*N-H...O, 2.11 Å, 152°	-17.9	16.1
dd11	2-x,1-y,3-z	2*C-H...O, 2.36 Å, 153°	-7.7	6.9
dd12	2-x,2-y,2-z	non-specific	-8.1	7.3
dd13	2-x,2-y,3-z	non-specific	-9.6	8.6
dd14	2-x,3-y,2-z	non-specific	-0.5	0.5

Table A 4.18. Symmetry codes, bounding types, interaction energies (kcal/mol) of the basic dimeric building unit with its neighbors, the contributions of the individual interaction energies to the total one (%) in the crystal of piracetam form V under the pressure of 0.7 GPa.

Dimer of dimers	Symmetry operation	Interaction	$E_{\text{int}}$ , kcal/mol	Contribution to the total interaction energy, %
dd1	-1+x,-1+y,-1+z	non-specific	-8.1	6.4
dd2	-1+x,-1+y,z	non-specific	-7.8	6.1
dd3	-1+x,-2+y,z	non-specific	-0.7	0.5
dd4	-1+x,y,-1+z	non-specific	-10.0	7.8
dd5	-1+x,y,z	2* N-H...O, 2.13 Å, 153°	-17.3	13.6
dd6	-2+x,-1+y,-1+z	non-specific	-4.7	3.7
dd7	-2+x,y,-1+z	non-specific	3.2*	2.5**
dd8	1+x,1+y,1+z	non-specific	-8.1	6.4
dd9	1+x,1+y,z	non-specific	-7.8	6.1
dd10	1+x,2+y,z	non-specific	-0.7	0.5
dd11	1+x,y,1+z	non-specific	-10.0	7.8
dd12	1+x,y,z	2* N-H...O, 2.13 Å, 153°	-17.3	13.6
dd13	2+x,1+y,1+z	non-specific	-4.7	3.7
dd14	2+x,y,1+z	non-specific	3.2*	2.5**
dd15	x,-1+y,z	non-specific	-11.9	9.3
dd16	x,1+y,z	non-specific	-11.9	9.3

\* Positive value of the interaction energy appearing due to compression.

\*\* All energy values were taken in absolute for the calculation of their contributions due to crystal symmetry.

Table 4.19. Symmetry codes, bounding types, interaction energies (kcal/mol) of the basic dimeric building unit with its neighbors, the contributions of the individual interaction energies to the total one (%) in the crystal of piracetam form V under the pressure of 0.9 GPa.

Dimer of dimers	Symmetry operation	Interaction	$E_{\text{int}}$ , kcal/mol	Contribution to the total interaction energy, %
dd1	-1+x,-1+y,-1+z	non-specific	-8.4	6.4
dd2	-1+x,-1+y,z	non-specific	-7.6	5.8
dd3	-1+x,-2+y,z	non-specific	-0.8	0.6
dd4	-1+x,y,-1+z	non-specific	-10.6	8.1
dd5	-1+x,y,z	2* N-H...O, 2.14 Å, 154°	-17.6	13.5
dd6	-2+x,-1+y,-1+z	non-specific	-5.0	3.8
dd7	-2+x,y,-1+z	non-specific	3.5*	2.7**
dd8	1+x,1+y,1+z	non-specific	-8.4	6.4
dd9	1+x,1+y,z	non-specific	-7.6	5.8
dd10	1+x,2+y,z	non-specific	-0.8	0.6
dd11	1+x,y,1+z	non-specific	-10.6	8.1
dd12	1+x,y,z	2* N-H...O, 2.14 Å, 154°	-17.6	13.5
dd13	2+x,1+y,1+z	non-specific	-5.0	3.8
dd14	2+x,y,1+z	non-specific	3.5*	2.7**
dd15	x,-1+y,z	non-specific	-11.7	9.0
dd16	x,1+y,z	non-specific	-11.7	9.0

\* Positive value of the interaction energy appearing due to compression.

\*\* All energy values were taken in absolute for the calculation of their contributions due to crystal symmetry.

Table 4.20. Symmetry codes, bounding types, interaction energies (kcal/mol) of the basic dimeric building unit with its neighbors, the contributions of the individual interaction energies to the total one (%) in the crystal of piracetam form V under the pressure of 2.5 GPa.

Dimer of dimers	Symmetry operation	Interaction	$E_{\text{int}}$ , kcal/mol	Contribution to the total interaction energy, %
dd1	-1+x,-1+y,-1+z	non-specific	-7.3	5.8
dd2	-1+x,-1+y,z	non-specific	-6.6	5.3
dd3	-1+x,-2+y,z	non-specific	-0.8	0.6
dd4	-1+x,y,-1+z	non-specific	-10.7	8.5
dd5	-1+x,y,z	2*N-H...O, 2.02 Å, 152°	-16.8	13.4
dd6	-2+x,-1+y,-1+z	non-specific	-5.4	4.3
dd7	-2+x,y,-1+z	non-specific	4.0*	3.2**
dd8	1+x,1+y,1+z	non-specific	-7.3	5.8
dd9	1+x,1+y,z	non-specific	-6.6	5.3
dd10	1+x,2+y,z	non-specific	-0.8	0.6
dd11	1+x,y,1+z	non-specific	-10.7	8.5
dd12	1+x,y,z	2*N-H...O, 2.02 Å, 152°	-16.8	13.4
dd13	2+x,1+y,1+z	non-specific	-5.4	4.3
dd14	2+x,y,1+z	non-specific	4.0*	3.2**
dd15	x,-1+y,z	non-specific	-11.1	8.9
dd16	x,1+y,z	non-specific	-11.1	8.9

\* Positive value of the interaction energy appearing due to compression.

\*\* All energy values were taken in absolute for the calculation of their contributions due to crystal symmetry.

Table 4.21. Symmetry codes, bounding types, interaction energies (kcal/mol) of the basic dimeric building unit with its neighbors, the contributions of the individual interaction energies to the total one (%) in the crystal of piracetam form V under the pressure of 4.0 GPa.

Dimer of dimers	Symmetry operation	Interaction	$E_{\text{int}}$ , kcal/mol	Contribution to the total interaction energy, %
dd1	-1+x,-1+y,-1+z	non-specific	-6.6	5.4
dd2	-1+x,-1+y,z	non-specific	-5.5	4.5
dd3	-1+x,-2+y,z	non-specific	-0.8	0.7
dd4	-1+x,y,-1+z	non-specific	-10.7	8.8
dd5	-1+x,y,z	2*N-H...O, 2.03 Å, 155°	-17.5	14.4
dd6	-2+x,-1+y,-1+z	non-specific	-5.5	4.5
dd7	-2+x,y,-1+z	non-specific	4.4*	3.6**
dd8	1+x,1+y,1+z	non-specific	-6.6	5.4
dd9	1+x,1+y,z	non-specific	-5.5	4.5
dd10	1+x,2+y,z	non-specific	-0.8	0.7
dd11	1+x,y,1+z	non-specific	-10.7	8.8
dd12	1+x,y,z	2*N-H...O, 2.03 Å, 155°	-17.5	14.4
dd13	2+x,1+y,1+z	non-specific	-5.5	4.5
dd14	2+x,y,1+z	non-specific	4.4*	3.6**
dd15	x,-1+y,z	non-specific	-9.7	8.0
dd16	x,1+y,z	non-specific	-9.7	8.0

\* Positive value of the interaction energy appearing due to compression.

\*\* All energy values were taken in absolute for the calculation of their contributions due to crystal symmetry.

Table 4.22. Minimal interatomic distances and errors of their determination (with different step sizes notified in brackets) in comparison to the high-precision computation with a step size of 1/1000 of a translation occurring for the displacements of the dimeric building units in different crystallographic directions.

Shift direction	Minimal interatomic distance, Å					
	II		V			
	Ambient pressure	0.45 GPa	0.7 GPa	0.9 GPa	2.5 GPa	4.0 GPa
[1 0 0] (0 0 1)	1.718 ±		2.005 ±	1.962 ±	1.878 ±	1.835 ±
	0.012 (1/5)		0.006 (1/5)	0.006 (1/5)	0.007 (1/5)	0.003 (1/5)
	0.012 (1/10)	1.839 ±	0.006 (1/10)	0.006 (1/10)	0.007 (1/10)	0.003 (1/10)
	0.004 (1/20)	0.000 (any)	0.006 (1/20)	0.006 (1/20)	0.006 (1/20)	0.003 (1/20)
	0.001 (1/25)		0.003 (1/25)	0.003 (1/25)	0.002 (1/25)	0.003 (1/25)
	0.001 (1/50)		0.000 (1/50)	0.000 (1/50)	0.000 (1/50)	0.000 (1/50)
[0 1 0] (0 0 1)	1.388 ±	1.244 ±	1.427 ±	1.347 ±	1.180 ±	1.157 ±
	0.104 (1/5)	0.144 (1/5)	0.098 (1/5)	0.112 (1/5)	0.137 (1/5)	0.139 (1/5)
	0.005 (1/10)	0.001 (1/10)	0.003 (1/10)	0.002 (1/10)	0.001 (1/10)	0.000 (1/10)
	0.005 (1/20)	0.001 (1/20)	0.003 (1/20)	0.002 (1/20)	0.001 (1/20)	0.000 (1/20)
	0.000 (1/25)	0.003 (1/25)	0.000 (1/25)	0.001 (1/25)	0.003 (1/25)	0.004 (1/25)
	0.000 (1/50)	0.001 (1/50)	0.000 (1/50)	0.001 (1/50)	0.001 (1/50)	0.000 (1/50)
[1 1 0] (0 0 1)			1.275 ±	1.161 ±	0.956 ±	0.837 ±
			0.165 (1/5)	0.183 (1/5)	0.226 (1/5)	0.238 (1/5)
	1.486 ±	1.394 ±	0.019 (1/10)	0.019 (1/10)	0.016 (1/10)	0.021 (1/10)
	0.000 (any)	0.002 (any)	0.019 (1/20)	0.019 (1/20)	0.016 (1/20)	0.021 (1/20)
			0.001 (1/25)	0.000 (1/25)	0.000 (1/25)	0.000 (1/25)
		0.001 (1/50)	0.000 (1/50)	0.000 (1/50)	0.000 (1/50)	
[1 0 0] (0 -1 1)	1.101 ±	1.327 ±	1.177 ±	1.133 ±	0.991 ±	0.924 ±
	0.016 (1/5)	0.013 (1/5)	0.053 (1/5)	0.043 (1/5)	0.049 (1/5)	0.048 (1/5)
	0.016 (1/10)	0.013 (1/10)	0.034 (1/10)	0.043 (1/10)	0.048 (1/10)	0.048 (1/10)
	0.008 (1/20)	0.006 (1/20)	0.001 (1/20)	0.000 (1/20)	0.000 (1/20)	0.000 (1/20)
	0.002 (1/25)	0.002 (1/25)	0.004 (1/25)	0.002 (1/25)	0.002 (1/25)	0.002 (1/25)
	0.002 (1/50)	0.002 (1/50)	0.000 (1/50)	0.002 (1/50)	0.002 (1/50)	
[0 1 1] (0 -1 1) *	-	-	-	-	-	-
[1 1 1] (0 -1 1) *	-	-	-	-	-	-

Table 4.22 Continue.

Shift direction	Minimal interatomic distance, Å					
	II		V			
	Ambient pressure	0.45 GPa	0.7 GPa	0.9 GPa	2.5 GPa	4.0 GPa
	1.101 ±	1.327 ±	1.177 ±	1.133 ±	0.991 ±	0.924 ±
	0.016 (1/5)	0.013 (1/5)	0.053 (1/5)	0.043 (1/5)	0.049 (1/5)	0.048 (1/5)
[1 0 0]	0.016 (1/10)	0.013 (1/10)	0.034 (1/10)	0.043 (1/10)	0.048 (1/10)	0.048 (1/10)
(0 1 0)	0.008 (1/20)	0.006 (1/20)	0.001 (1/20)	0.000 (1/20)	0.000 (1/20)	0.000 (1/20)
	0.002 (1/25)	0.002 (1/25)	0.004 (1/25)	0.002 (1/25)	0.002 (1/25)	0.002 (1/25)
	0.002 (1/50)	0.001 (1/50)	0.000 (1/50)	0.002 (1/50)	0.002 (1/50)	0.002 (1/50)
[0 0 1]	-	-	-	-	-	-
(0 1 0) *	-	-	-	-	-	-
[1 0 1]	-	-	-	-	-	-
(0 1 0) *	-	-	-	-	-	-

\* Displacements are sterically hindered (overlap of the motile and fixed parts during movement).

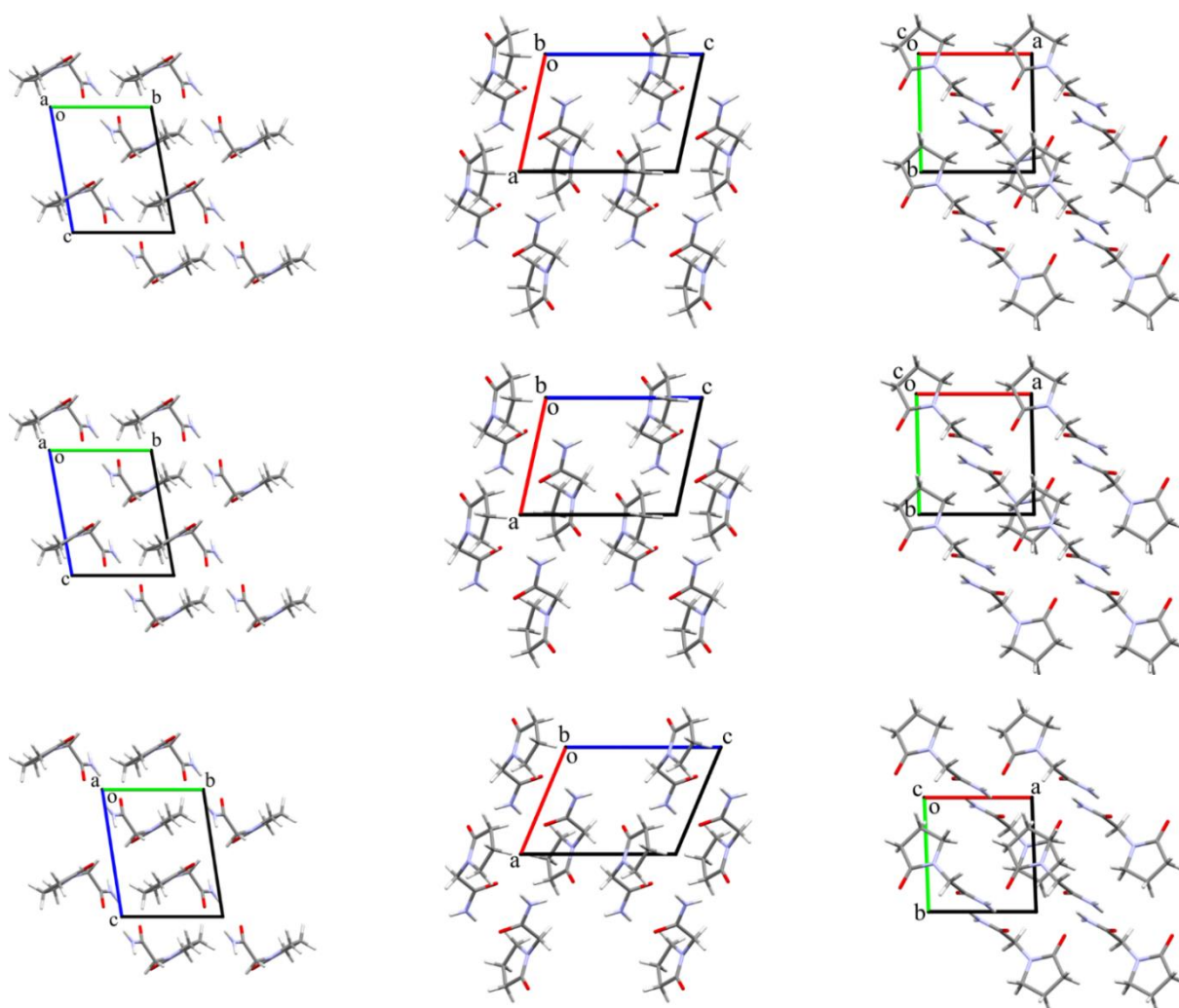


Figure A 4.13. Packing of the molecules in the crystals of piracetam polymorphs II at ambient pressure (at the top) and under the pressure of 0.45 GPa (in the middle) and V under the pressure of 0.7 GPa (at the bottom). The projections in *a* (on the right), *b* (in the middle), *c* (on the left) crystallographic directions are represented.

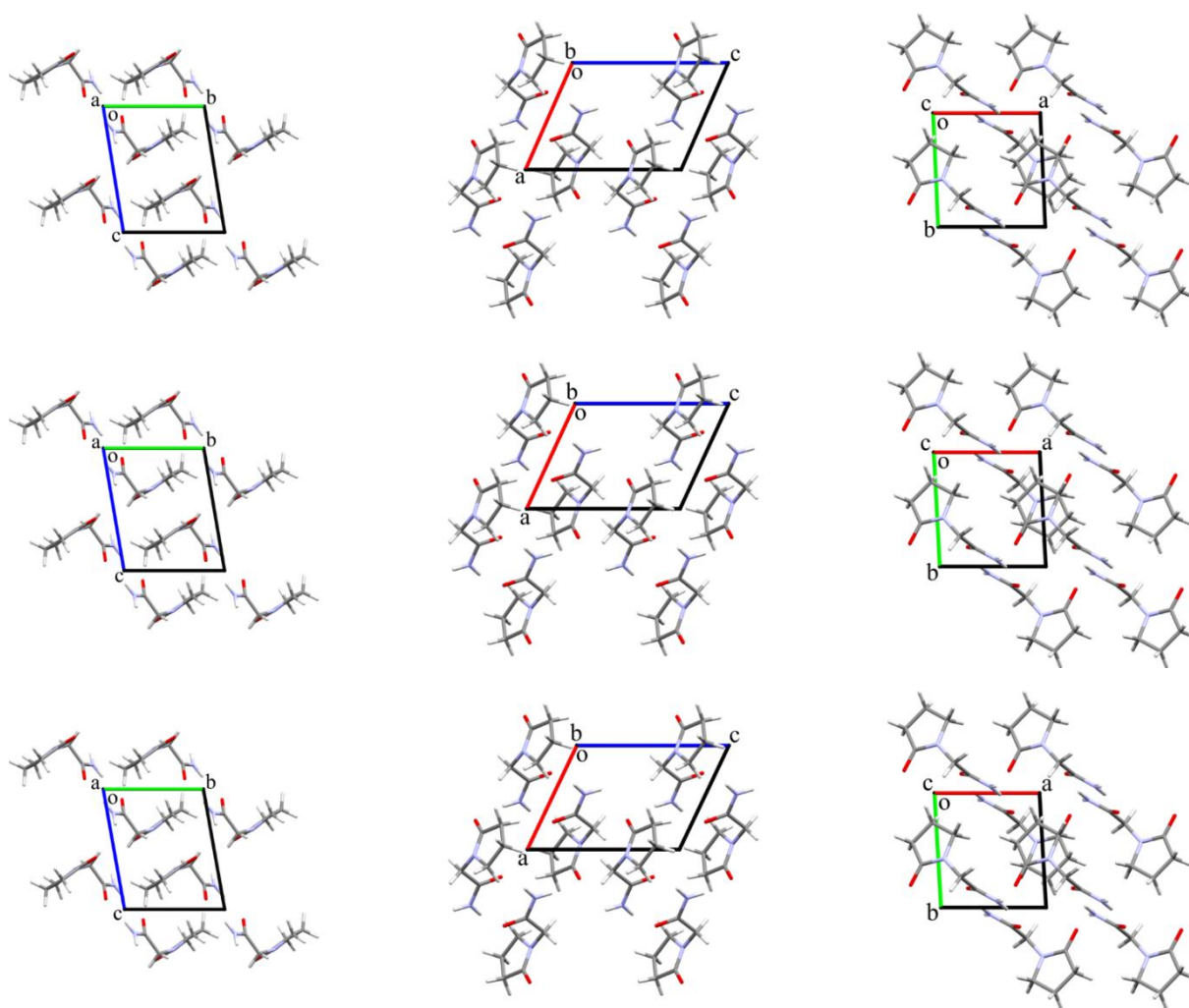


Figure A 4.14. Packing of the molecules in the crystals of piracetam polymorph V under pressures of 0.9 GPa (at the top), 2.5 GPa (in the middle) and 4.0 GPa (at the bottom). The projections in *a* (on the right), *b* (in the middle), *c* (on the left) crystallographic directions are represented.

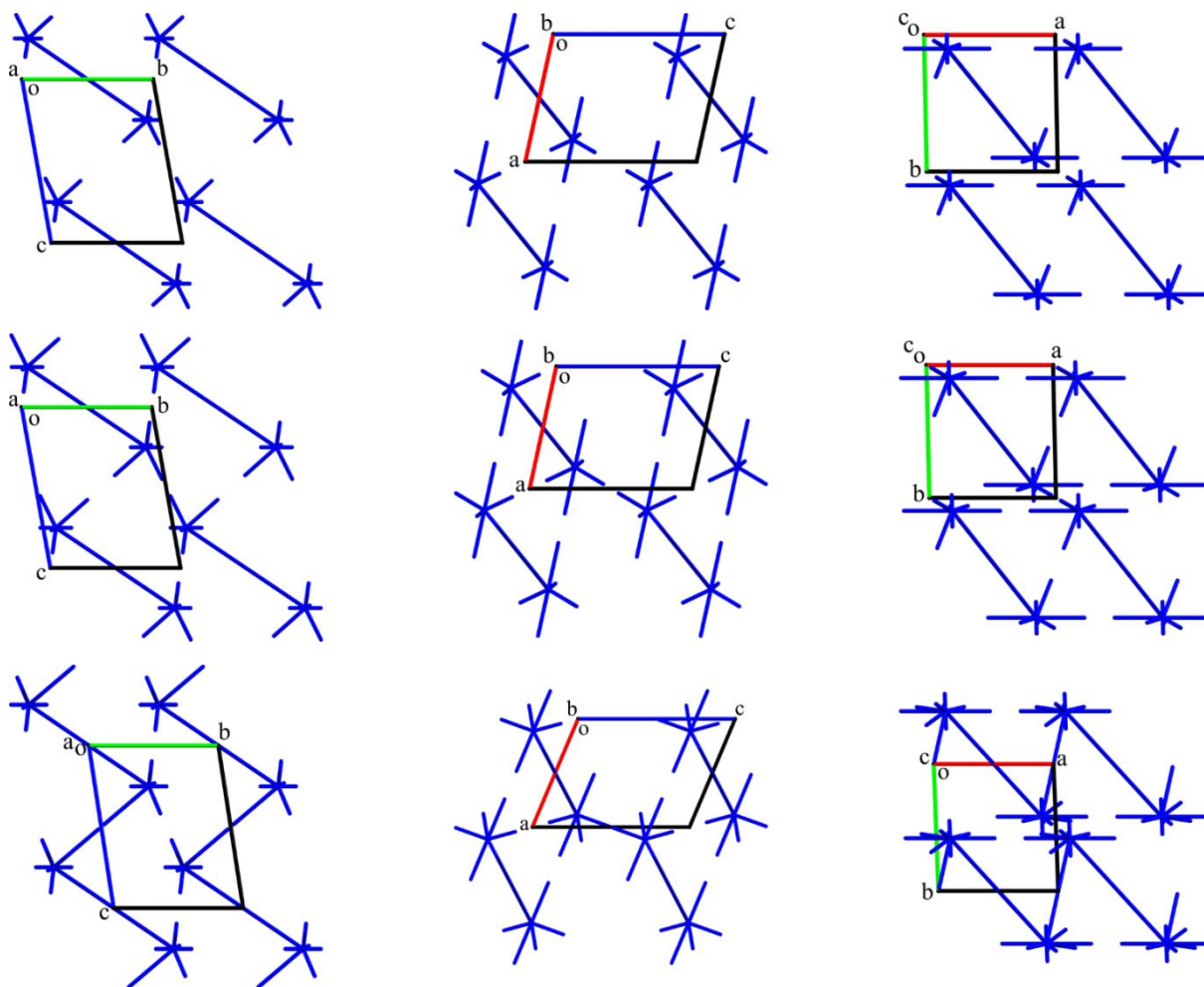


Figure A 4.15. Packing of the energy vector diagrams representing the distribution of monomeric building units in the crystals of piracetam polymorphs II at ambient pressure (at the top) and under the pressure of 0.45 GPa (in the middle) and V under the pressure of 0.7 GPa (at the bottom). The projections in  $a$  (on the right),  $b$  (in the middle),  $c$  (on the left) crystallographic directions are represented.

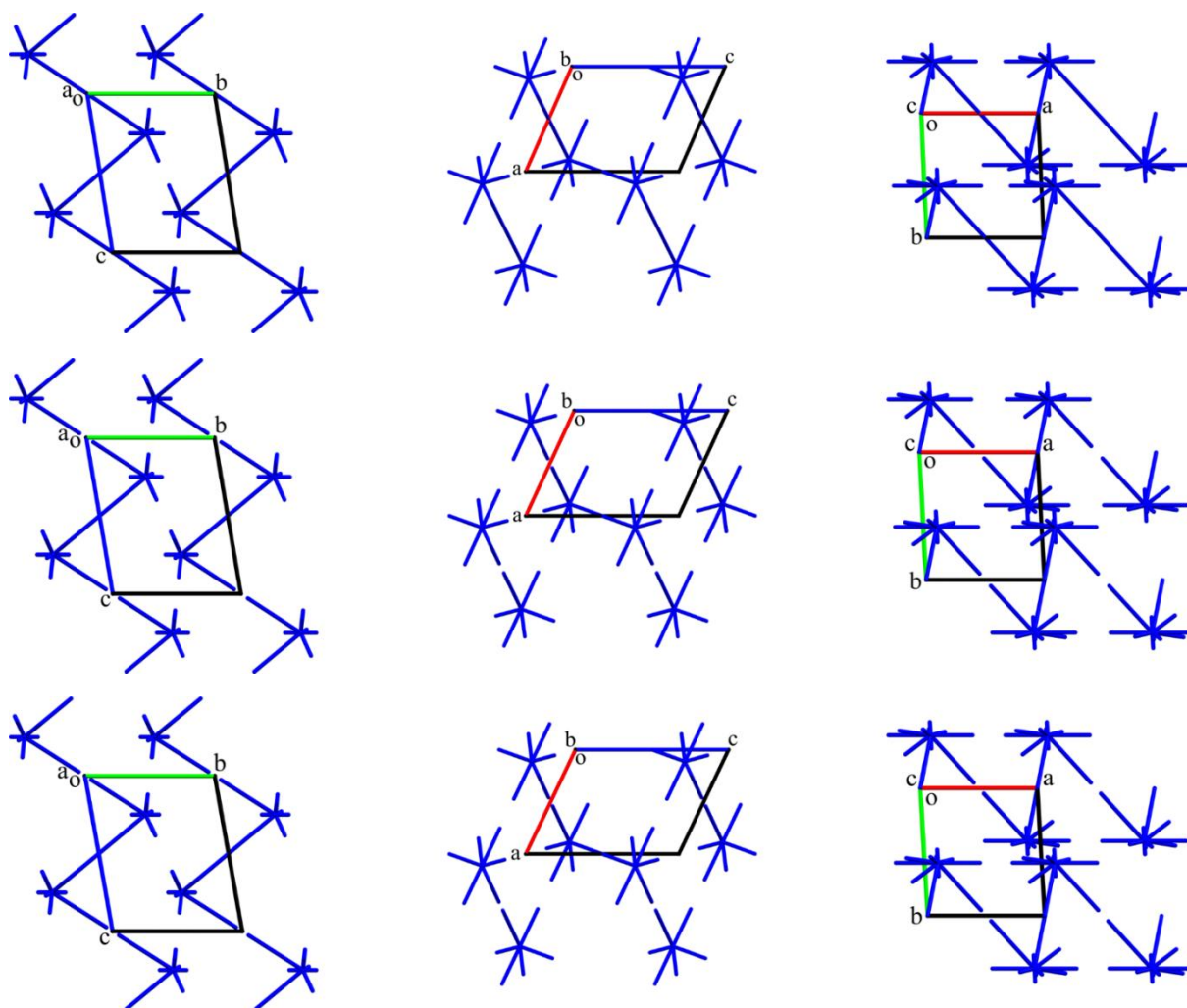


Figure A 4.16. Packing of the energy vector diagrams representing the distribution of monomeric building units in the crystals of piracetam polymorph V under pressures of 0.9 GPa (at the top), 2.5 GPa (in the middle) and 4.0 GPa (at the bottom). The projections in *a* (on the right), *b* (in the middle), *c* (on the left) crystallographic directions are represented.

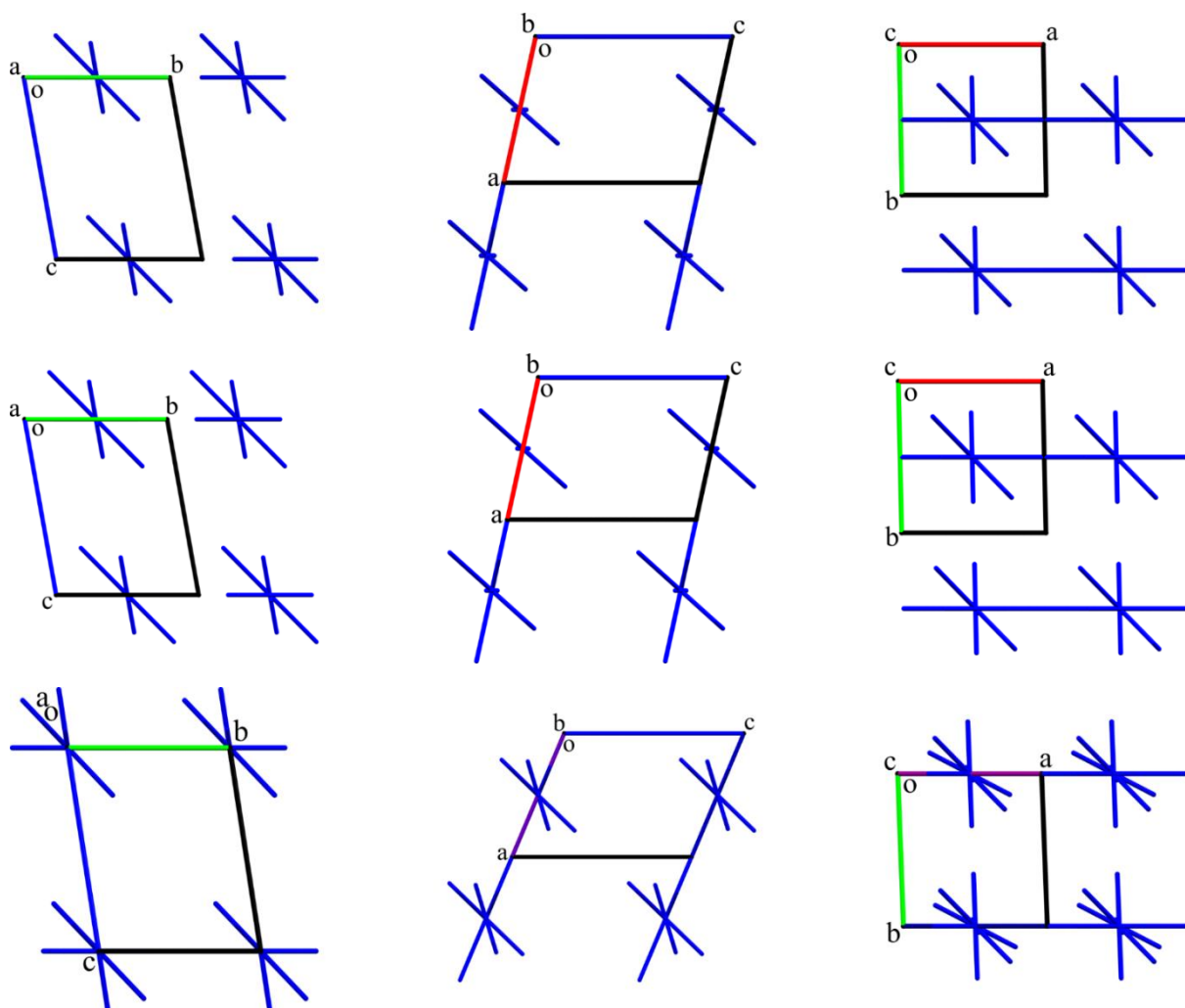


Figure A 4.17. Packing of the energy vector diagrams representing the distribution of dimeric building units in the crystals of piracetam polymorphs II at ambient pressure (at the top) and under the pressure of 0.45 GPa (in the middle) and V under the pressure of 0.7 GPa (at the bottom). The projections in *a* (on the right), *b* (in the middle), *c* (on the left) crystallographic directions are represented.

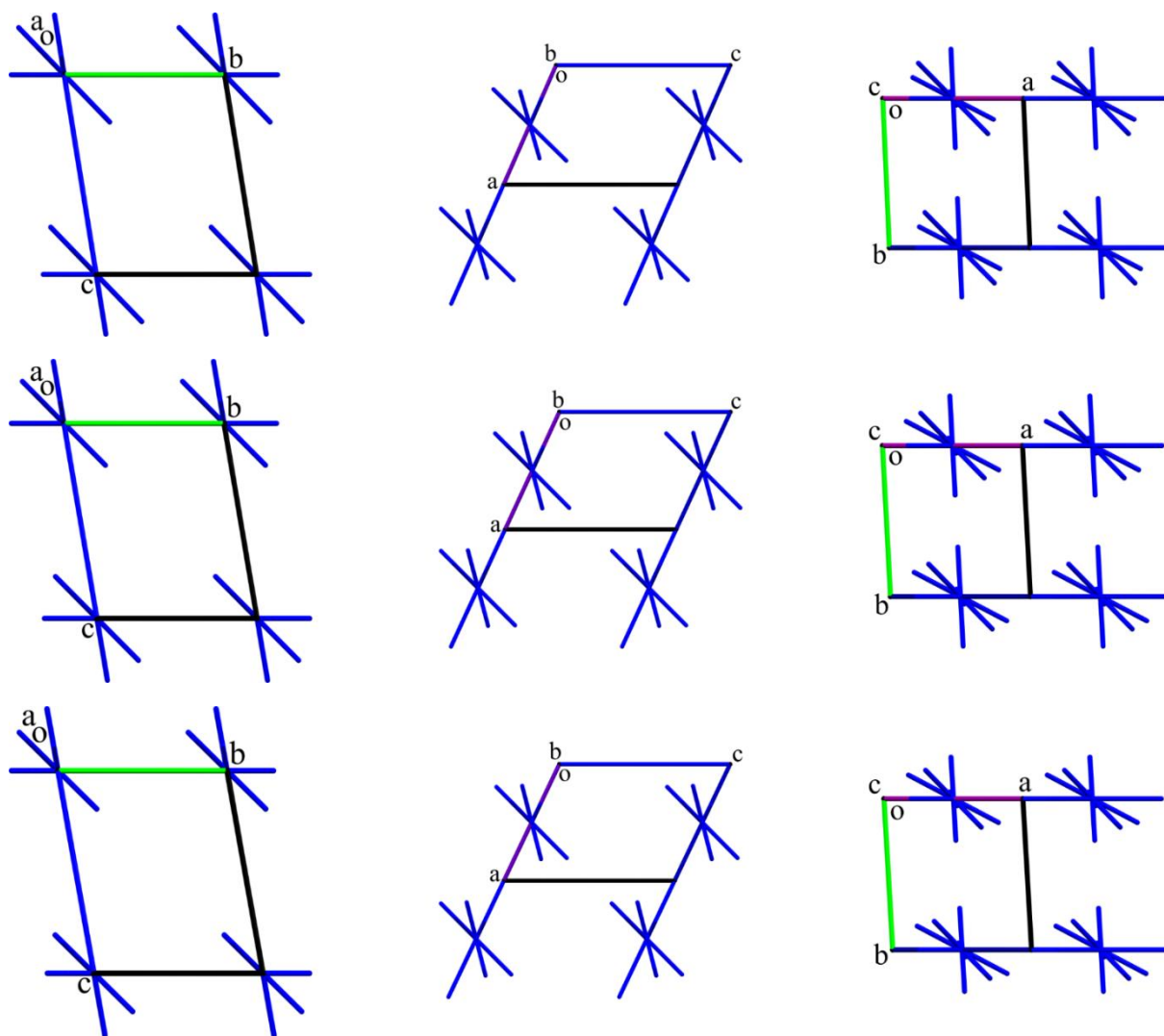


Figure A 4.18. Packing of the energy vector diagrams representing the distribution of dimeric building units in the crystals of piracetam polymorph V under pressures of 0.9 GPa (at the top), 2.5 GPa (in the middle) and 4.0 GPa (at the bottom). The projections in *a* (on the right), *b* (in the middle), *c* (on the left) crystallographic directions are represented.

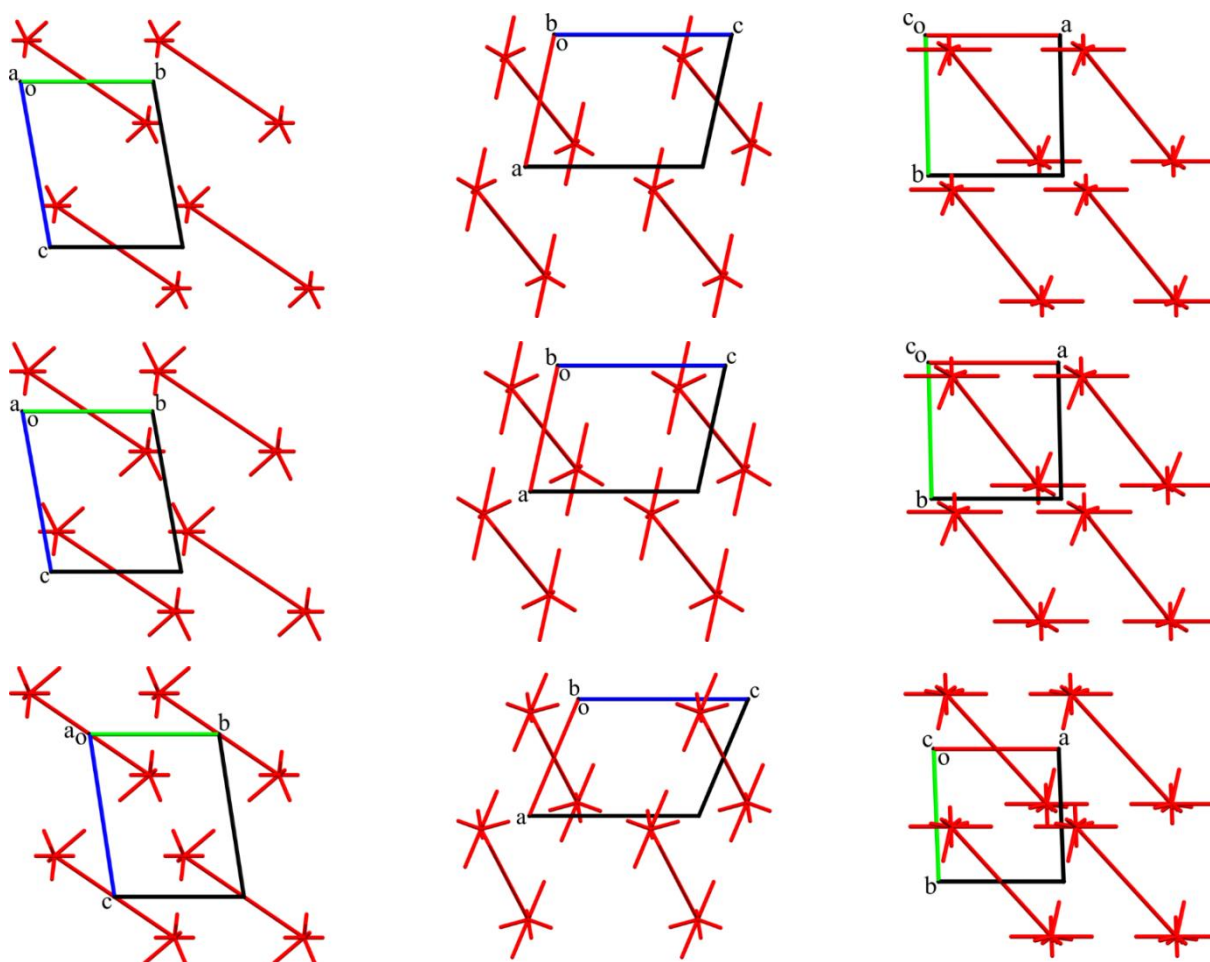


Figure A 4.19. Packing of the energy vector diagrams based on the sum of electrostatic and polarization terms subtracted from LMOEDA representing the distribution of monomeric building units in the crystals of piracetam polymorphs II at ambient pressure (at the top) and under the pressure of 0.45 GPa (in the middle) and V under the pressure of 0.7 GPa (at the bottom). The projections in  $a$  (on the right),  $b$  (in the middle),  $c$  (on the left) crystallographic directions are represented.

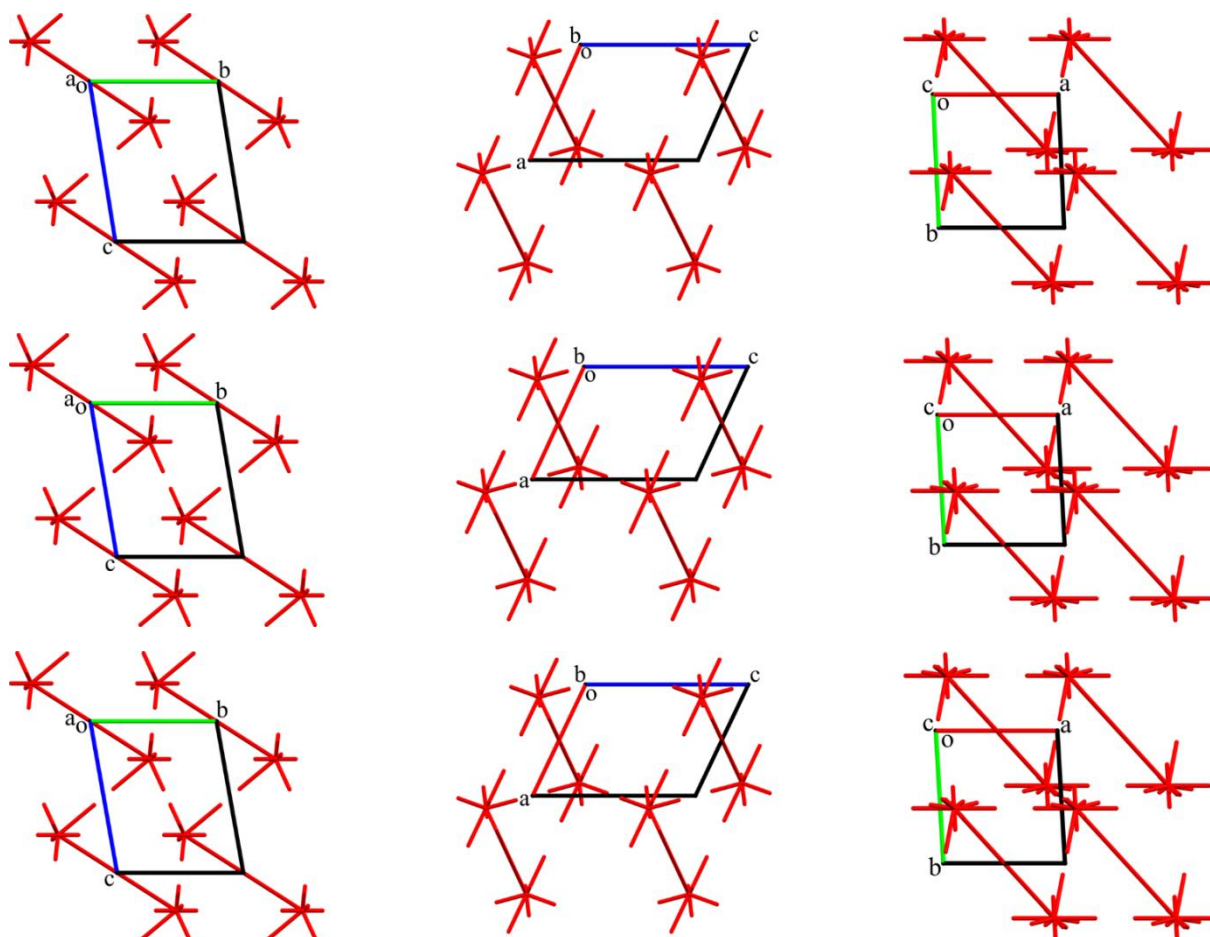


Figure A 4.20. Packing of the energy vector diagrams based on the sum of electrostatic and polarization terms subtracted from LMOEDA representing the distribution of monomeric building units in the crystals of piracetam polymorph V under pressures of 0.9 GPa (at the top), 2.5 GPa (in the middle) and 4.0 GPa (at the bottom). The projections in  $a$  (on the right),  $b$  (in the middle),  $c$  (on the left) crystallographic directions are represented.

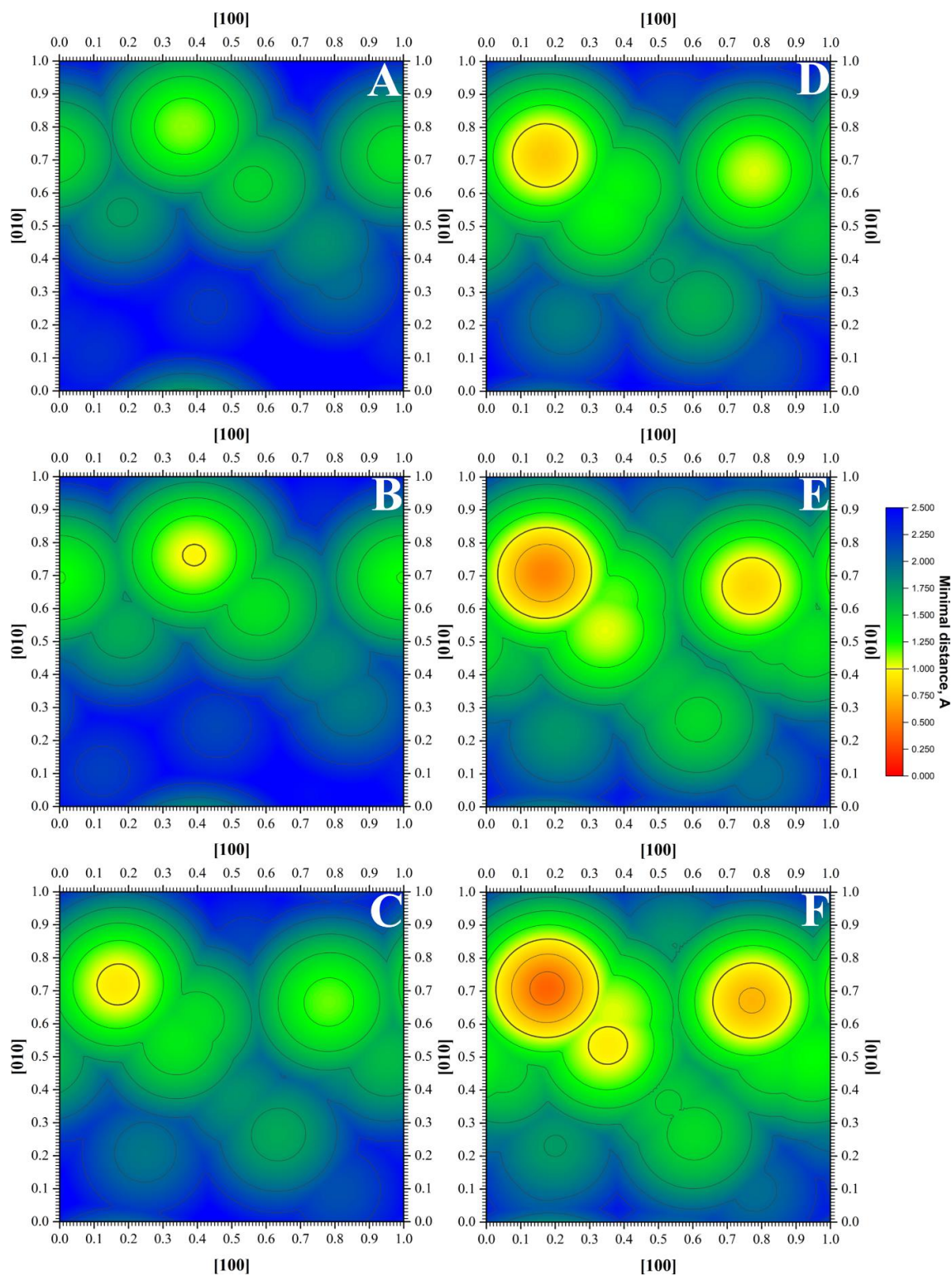


Figure A 4.21. Maps of the minimal interatomic distances ( $\text{\AA}$ ) during the shear of the dimeric motile part in relation to the fixed one in (001) plane ([100] and [010] directions of shift) in the crystals of piracetam polymorphic forms II at ambient pressure (A) and under the pressure of 0.45 GPa (B) and V under pressures of 0.7 (C), 0.9 (D), 2.5 (E) and 4.0 GPa (F). Bold contour surrounds zones with interatomic distances shorter than 1  $\text{\AA}$ .

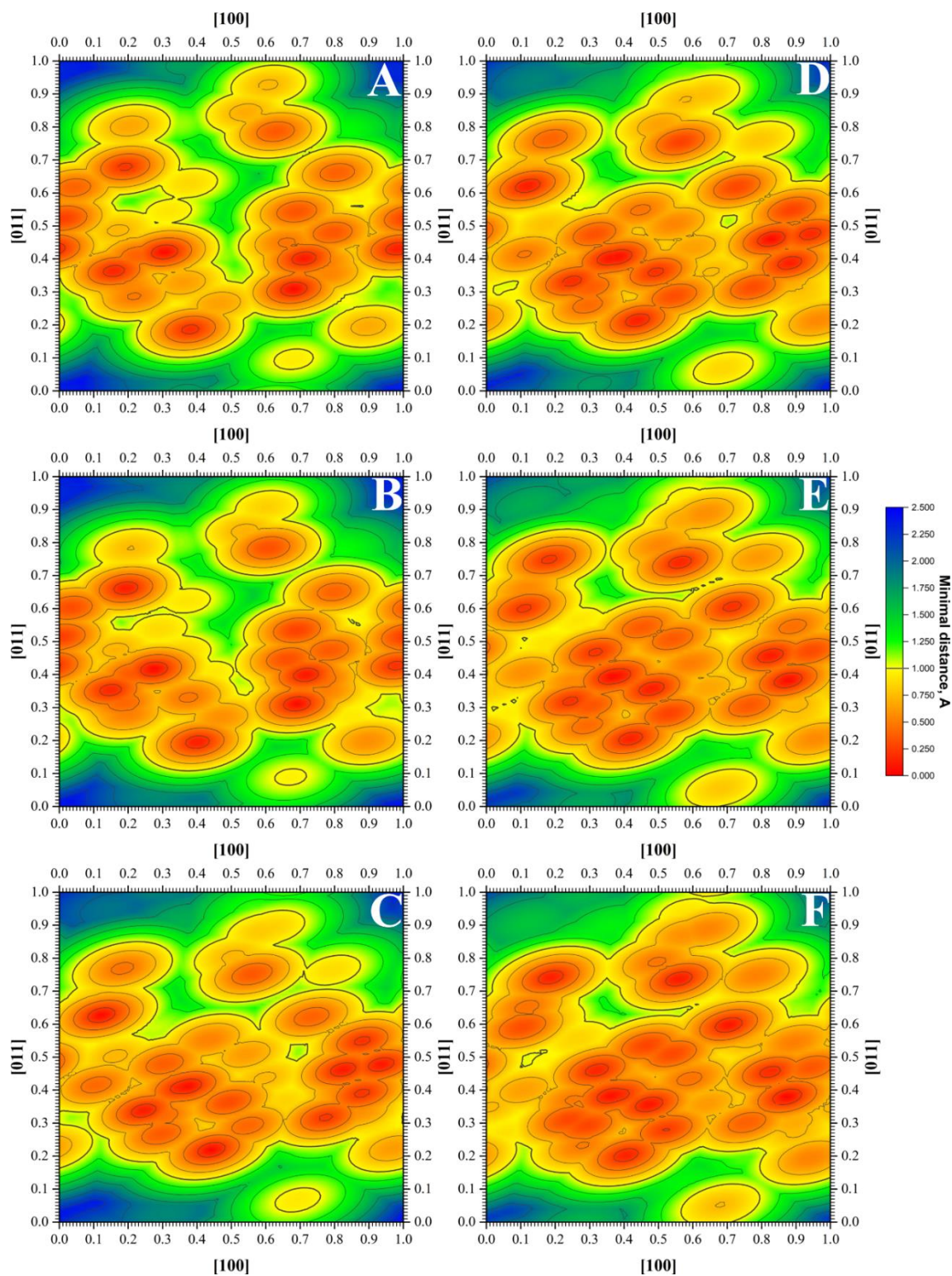


Figure A 4.22. Maps of the minimal interatomic distances ( $\text{\AA}$ ) during the shear of the dimeric motile part in relation to the fixed one in (0-11) plane ([100] and [011] directions of shift) in the crystals of piracetam polymorphic forms II at ambient pressure (A) and under the pressure of 0.45 GPa (B) and V under pressures of 0.7 (C), 0.9 (D), 2.5 (E) and 4.0 GPa (F). Bold contour surrounds zones with interatomic distances shorter than 1  $\text{\AA}$ .

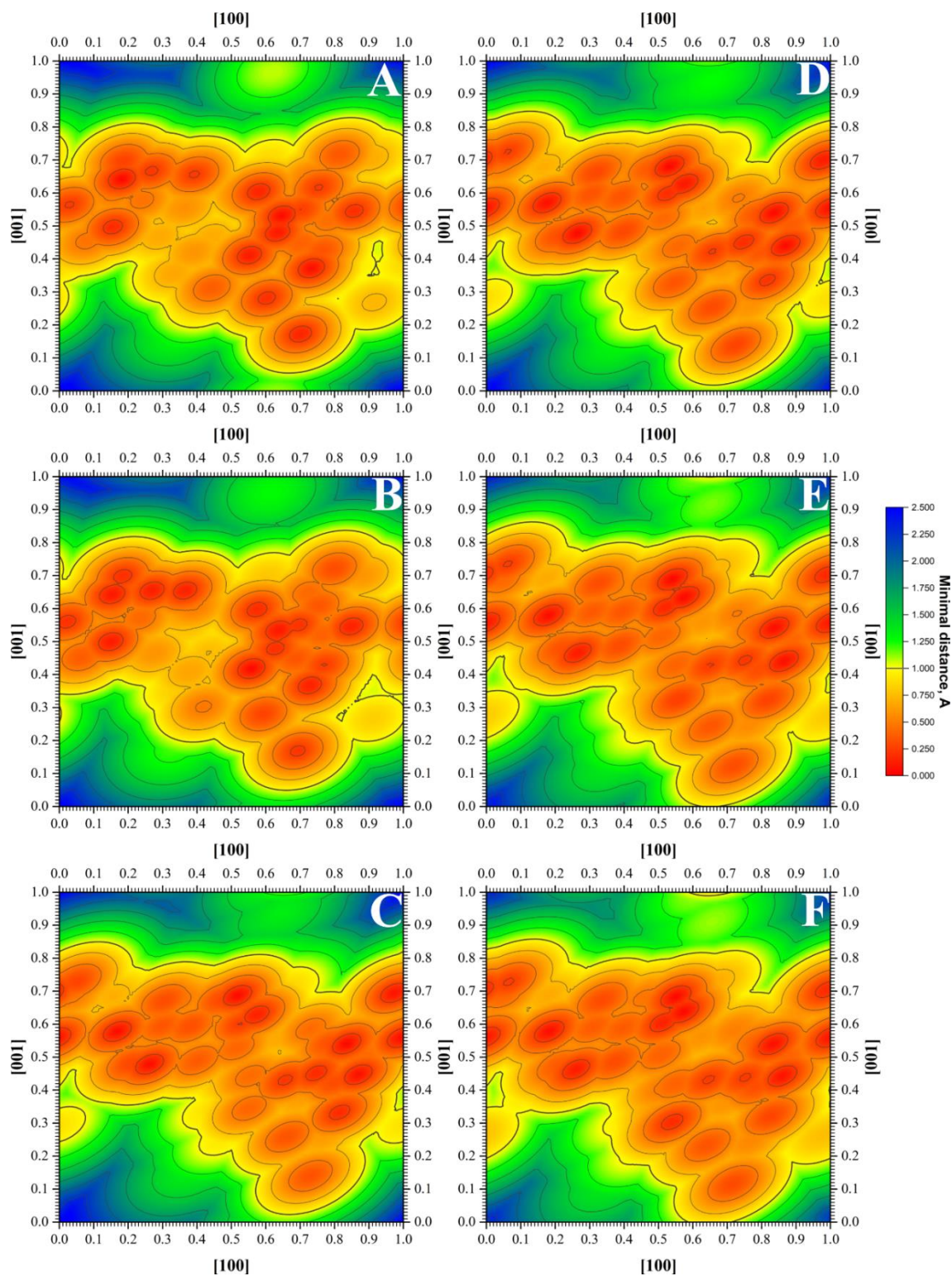


Figure A 4.23. Maps of the minimal interatomic distances ( $\text{\AA}$ ) during the shear of the dimeric motile part in relation to the fixed one in (010) plane ([100] and [001] directions of shift) in the crystals of piracetam polymorphic forms II at ambient pressure (A) and under the pressure of 0.45 GPa (B) and V under pressures of 0.7 (C), 0.9 (D), 2.5 (E) and 4.0 GPa (F). Bold contour surrounds zones with interatomic distances shorter than 1  $\text{\AA}$ .

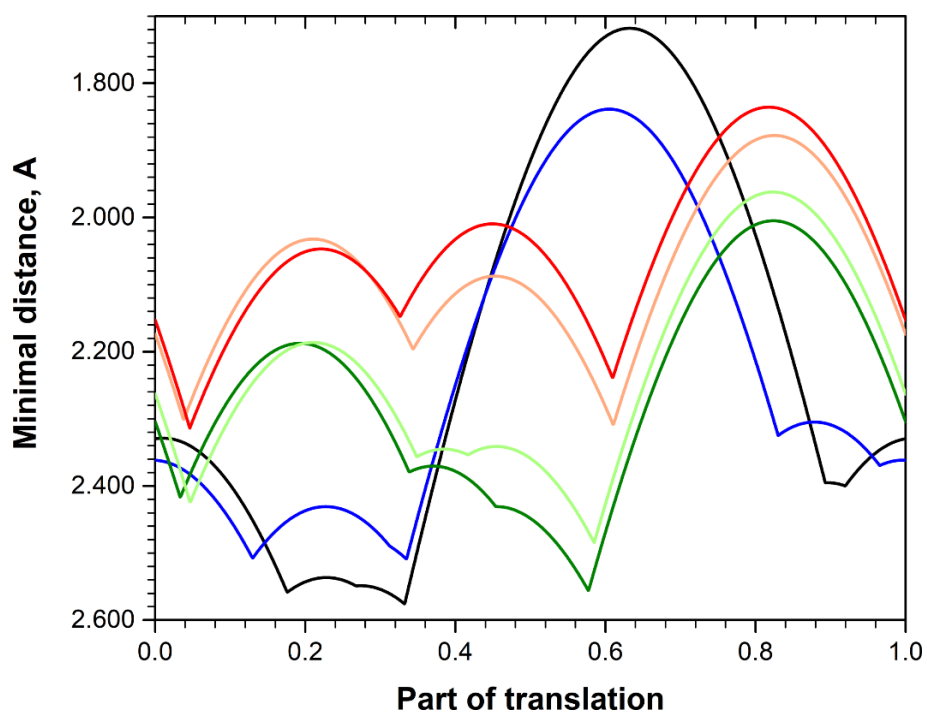


Figure A 4.24. Minimal interatomic distances ( $\text{\AA}$ ) between the dimeric motile part and (001) neighboring layer scanned with a step size of 1/1000 of a [100] translation in the crystals of piracetam polymorphic forms II at ambient pressure (in black) and under the pressure of 0.45 GPa (in blue) and V under pressures of 0.7 (in olive), 0.9 (in lite green), 2.5 (in peach) and 4.0 GPa (in red).

Table A 4.23. Symmetry codes, binding types, interaction energies of the monomeric building unit with neighboring ones ( $E_{\text{int}}$ , kcal/mol) and the contribution of these energies to the total interaction energy (%) in the crystal of ibuprofen form I under ambient pressure.

Dimer	Symmetry operation	$E_{\text{int}}$ , kcal/mol	Contribution to the total interaction energy, %	Interaction
d1	1-x,-1/2+y,3/2-z	-1.8	3.0	non-specific
d2	1-x,-y,1-z	-11.5	18.9	O-H...O, 1.85 Å, 176°
d3	1-x,1-y,1-z	-5.8	9.6	non-specific
d4	1-x,1/2+y,3/2-z	-1.8	3.0	non-specific
d5	2-x,-1/2+y,1/2-z	-2.2	3.6	non-specific
d6	2-x,1-y,1-z	-3.7	6.1	non-specific
d7	2-x,1/2+y,1/2-z	-2.2	3.6	non-specific
d8	2-x,2-y,1-z	-1.7	2.8	non-specific
d9	x,-1+y,z	-2.7	4.4	non-specific
d10	x,1/2-y,-1/2+z	-6.5	10.6	C-H... $\pi$ , 2.86 Å, 166°
d11	x,1/2-y,1/2+z	-6.5	10.6	C-H... $\pi$ , 2.86 Å, 166°
d12	x,1+y,z	-2.7	4.4	non-specific
d13	x,3/2-y,-1/2+z	-6.0	9.8	non-specific
d14	x,3/2-y,1/2+z	-6.0	9.8	non-specific

Table A 4.24. Symmetry codes, binding types, interaction energies of the monomeric building unit with neighboring ones ( $E_{\text{int}}$ , kcal/mol) and the contribution of these energies to the total interaction energy (%) in the crystal of ibuprofen form II under ambient pressure.

Dimer	Symmetry operation	$E_{\text{int}}$ , kcal/mol	Contribution to the total interaction energy, %	Interaction
d1	$x, 1/2-y, -1/2+z$	-1.7	2.4	non-specific
d2	$x, -1+y, z$	-5.5	8.1	C...H, 2.88 Å
d3	$x, 1/2-y, 1/2+z$	-1.7	2.4	non-specific
d4	$x, 3/2-y, -1/2+z$	-2.4	3.5	H...H, 2.16 Å
d5	$1-x, -1/2+y, 1/2-z$	-4.9	7.2	C-H... $\pi$ , 2.80 Å, 172°
d6	$1-x, 1-y, 1-z$	-26.3	38.8	O-H...O, 1.53 Å, 176°
d7	$x, 3/2-y, 1/2+z$	-2.4	3.5	H...H, 2.16 Å
d8	$x, 1+y, z$	-5.5	8.1	C...H, 2.88 Å
d9	$1-x, 1/2+y, 1/2-z$	-4.9	7.2	C-H... $\pi$ , 2.80 Å, 172°
d10	$1-x, 2-y, 1-z$	-2.2	3.3	non-specific
d11	$2-x, -y, -z$	-0.9	1.3	non-specific
d12	$2-x, 1-y, -z$	-1.2	1.8	H...H, 2.35 Å
d13	$2-x, -1/2+y, 1/2-z$	-4.1	6.1	C...H, 2.81 Å
d14	$2-x, 1/2+y, 1/2-z$	-4.1	6.1	C...H, 2.81 Å

Table A 4.25. Symmetry codes, binding types, interaction energies of the monomeric building unit with neighboring ones ( $E_{\text{int}}$ , kcal/mol) and the contribution of these energies to the total interaction energy (%) in the crystal of ibuprofen form I under pressure of 0.23 GPa.

Dimer	Symmetry operation	$E_{\text{int}}$ , kcal/mol	Contribution to the total interaction energy, %	Interaction
d1	$x, -1+y, z$	-2.9	4.6	non-specific
d2	$x, 1+y, z$	-2.9	4.6	non-specific
d3	$1-x, -1/2+y, 3/2-z$	-1.9	3.1	non-specific
d4	$1-x, 1/2+y, 3/2-z$	-1.9	3.1	non-specific
d5	$2-x, -1/2+y, 1/2-z$	-2.2	3.6	non-specific
d6	$2-x, 1/2+y, 1/2-z$	-2.2	3.6	non-specific
d7	$1-x, -y, 1-z$	-10.9	17.7	O-H...O, 1.80 Å, 176°
d8	$1-x, 1-y, 1-z$	-5.6	9.1	non-specific
d9	$2-x, 1-y, 1-z$	-4.0	6.5	non-specific
d10	$2-x, 2-y, 1-z$	-1.9	3.1	non-specific
d11	$x, 1/2-y, -1/2+z$	-6.5	10.6	C-H... $\pi$ , 2.77 Å, 165°
d12	$x, 1/2-y, 1/2+z$	-6.5	10.6	C-H... $\pi$ , 2.77 Å, 165°
d13	$x, 3/2-y, -1/2+z$	-6.1	10.0	non-specific
d14	$x, 3/2-y, 1/2+z$	-6.1	10.0	non-specific

Table A 4.26. Symmetry codes, binding types, interaction energies of the monomeric building unit with neighboring ones ( $E_{\text{int}}$ , kcal/mol) and the contribution of these energies to the total interaction energy (%) in the crystal of ibuprofen form I under pressure of 0.60 GPa.

Dimer	Symmetry operation	$E_{\text{int}}$ , kcal/mol	Contribution to the total interaction energy, %	Interaction
d1	$x, -1+y, z$	-3.0	4.6	non-specific
d2	$x, 1+y, z$	-3.0	4.6	non-specific
d3	$1-x, -1/2+y, 3/2-z$	-2.0	3.1	non-specific
d4	$1-x, 1/2+y, 3/2-z$	-2.0	3.1	non-specific
d5	$2-x, -1/2+y, 1/2-z$	-2.5	3.8	non-specific
d6	$2-x, 1/2+y, 1/2-z$	-2.5	3.8	non-specific
d7	$1-x, -y, 1-z$	-10.9	16.8	O-H...O, 1.82 Å, 173°
d8	$1-x, 1-y, 1-z$	-5.8	8.9	non-specific
d9	$2-x, 1-y, 1-z$	-4.2	6.5	non-specific
d10	$2-x, 2-y, 1-z$	-2.0	3.2	non-specific
d11	$x, 1/2-y, -1/2+z$	-6.6	10.3	C-H... $\pi$ , 2.69 Å, 164°
d12	$x, 1/2-y, 1/2+z$	-6.6	10.3	C-H... $\pi$ , 2.69 Å, 164°
d13	$x, 3/2-y, -1/2+z$	-6.8	10.5	non-specific
d14	$x, 3/2-y, 1/2+z$	-6.8	10.5	non-specific

Table A 4.27. Symmetry codes, binding types, interaction energies of the monomeric building unit with neighboring ones ( $E_{\text{int}}$ , kcal/mol) and the contribution of these energies to the total interaction energy (%) in the crystal of ibuprofen form I under pressure of 0.80 GPa.

Dimer	Symmetry operation	$E_{\text{int}}$ , kcal/mol	Contribution to the total interaction energy, %	Interaction
d1	$x, -1+y, z$	-3.1	4.6	non-specific
d2	$x, 1+y, z$	-3.1	4.6	non-specific
d3	$1-x, -1/2+y, 3/2-z$	-2.0	3.0	non-specific
d4	$1-x, 1/2+y, 3/2-z$	-2.0	3.0	non-specific
d5	$2-x, -1/2+y, 1/2-z$	-2.6	3.9	non-specific
d6	$2-x, 1/2+y, 1/2-z$	-2.6	3.9	non-specific
d7	$1-x, -y, 1-z$	-11.8	17.6	O-H...O, 1.78 Å, 172°
d8	$1-x, 1-y, 1-z$	-5.7	8.5	non-specific
d9	$2-x, 1-y, 1-z$	-4.4	6.6	non-specific
d10	$2-x, 2-y, 1-z$	-2.1	3.2	H...H, 2.34 Å
d11	$x, 1/2-y, -1/2+z$	-6.7	10.0	C-H... $\pi$ , 2.65 Å, 166°
d12	$x, 1/2-y, 1/2+z$	-6.7	10.0	C-H... $\pi$ , 2.65 Å, 166°
d13	$x, 3/2-y, -1/2+z$	-7.0	10.5	C...H, 2.85 Å
d14	$x, 3/2-y, 1/2+z$	-7.0	10.5	C...H, 2.85 Å

Table A 4.28. Symmetry codes, binding types, interaction energies of the monomeric building unit with neighboring ones ( $E_{\text{int}}$ , kcal/mol) and the contribution of these energies to the total interaction energy (%) in the crystal of ibuprofen form I under pressure of 0.88 GPa.

Dimer	Symmetry operation	$E_{\text{int}}$ , kcal/mol	Contribution to the total interaction energy, %	Interaction
d1	$x, -1+y, z$	-3.2	4.7	non-specific
d2	$x, 1+y, z$	-3.2	4.7	non-specific
d3	$1-x, -1/2+y, 3/2-z$	-2.0	3.0	non-specific
d4	$1-x, 1/2+y, 3/2-z$	-2.0	3.0	non-specific
d5	$2-x, -1/2+y, 1/2-z$	-2.6	3.8	non-specific
d6	$2-x, 1/2+y, 1/2-z$	-2.6	3.8	non-specific
d7	$1-x, -y, 1-z$	-12.1	18.0	O-H...O, 1.82 Å, 172°
d8	$1-x, 1-y, 1-z$	-5.6	8.3	non-specific
d9	$2-x, 1-y, 1-z$	-4.4	6.6	non-specific
d10	$2-x, 2-y, 1-z$	-2.2	3.2	non-specific
d11	$x, 1/2-y, -1/2+z$	-6.6	9.8	C-H... $\pi$ , 2.68 Å, 164°; C...H, 2.88 Å
d12	$x, 1/2-y, 1/2+z$	-6.6	9.8	C-H... $\pi$ , 2.68 Å, 164°; C...H, 2.88 Å
d13	$x, 3/2-y, -1/2+z$	-7.1	10.6	C...H, 2.85 Å
d14	$x, 3/2-y, 1/2+z$	-7.1	10.6	C...H, 2.85 Å

Table A 4.29. Symmetry codes, binding types, interaction energies of the monomeric building unit with neighboring ones ( $E_{\text{int}}$ , kcal/mol) and the contribution of these energies to the total interaction energy (%) in the crystal of ibuprofen form I under pressure of 1.70 GPa.

Dimer	Symmetry operation	$E_{\text{int}}$ , kcal/mol	Contribution to the total interaction energy, %	Interaction
d1	$x, -1+y, z$	-3.2	4.7	non-specific
d2	$x, 1+y, z$	-3.2	4.7	non-specific
d3	$1-x, -1/2+y, 3/2-z$	-2.1	3.1	non-specific
d4	$1-x, 1/2+y, 3/2-z$	-2.1	3.1	non-specific
d5	$2-x, -1/2+y, 1/2-z$	-2.6	3.8	H...H, 2.21 Å
d6	$2-x, 1/2+y, 1/2-z$	-2.6	3.8	H...H, 2.21 Å
d7	$1-x, -y, 1-z$	-12.2	17.9	O-H...O, 1.80 Å, 170°
d8	$1-x, 1-y, 1-z$	-5.6	8.1	non-specific
d9	$2-x, 1-y, 1-z$	-4.7	6.9	non-specific
d10	$2-x, 2-y, 1-z$	-2.3	3.4	H...H, 2.28 Å
d11	$x, 1/2-y, -1/2+z$	-6.3	9.3	C-H... $\pi$ , 2.63 Å, 163°; C...H, 2.80 Å
d12	$x, 1/2-y, 1/2+z$	-6.3	9.3	C-H... $\pi$ , 2.63 Å, 163°; C...H, 2.80 Å
d13	$x, 3/2-y, -1/2+z$	-7.5	10.9	C...H, 2.72 Å
d14	$x, 3/2-y, 1/2+z$	-7.5	10.9	C...H, 2.72 Å

Table A 4.30. Symmetry codes, binding types, interaction energies of the monomeric building unit with neighboring ones ( $E_{\text{int}}$ , kcal/mol) and the contribution of these energies to the total interaction energy (%) in the crystal of ibuprofen form I under pressure of 1.89 GPa.

Dimer	Symmetry operation	$E_{\text{int}}$ , kcal/mol	Contribution to the total interaction energy, %	Interaction
d1	$x, -1+y, z$	-3.2	4.9	non-specific
d2	$x, 1+y, z$	-3.2	4.9	non-specific
d3	$1-x, -1/2+y, 3/2-z$	-2.0	3.0	non-specific
d4	$1-x, 1/2+y, 3/2-z$	-2.0	3.0	non-specific
d5	$2-x, -1/2+y, 1/2-z$	-2.7	4.0	H...H, 2.23 Å
d6	$2-x, 1/2+y, 1/2-z$	-2.7	4.0	H...H, 2.23 Å
d7	$1-x, -y, 1-z$	-10.7	16.1	O-H...O, 1.77 Å, 170°
d8	$1-x, 1-y, 1-z$	-5.3	8.0	O-H...O, 2.43 Å, 125°
d9	$2-x, 1-y, 1-z$	-4.7	7.1	non-specific
d10	$2-x, 2-y, 1-z$	-2.3	3.4	H...H, 2.22 Å
d11	$x, 1/2-y, -1/2+z$	-6.4	9.5	C-H... $\pi$ , 2.55 Å, 164°; C...H, 2.81 Å
d12	$x, 1/2-y, 1/2+z$	-6.4	9.5	C-H... $\pi$ , 2.55 Å, 164°; C...H, 2.81 Å
d13	$x, 3/2-y, -1/2+z$	-7.5	11.2	C...H, 2.70 Å
d14	$x, 3/2-y, 1/2+z$	-7.5	11.2	C...H, 2.70 Å

Table A 4.31. Symmetry codes, binding types, interaction energies of the monomeric building unit with neighboring ones ( $E_{\text{int}}$ , kcal/mol) and the contribution of these energies to the total interaction energy (%) in the crystal of ibuprofen form I under pressure of 2.32 GPa.

Dimer	Symmetry operation	$E_{\text{int}}$ , kcal/mol	Contribution to the total interaction energy, %	Interaction
d1	$x, -1+y, z$	-3.2	4.9	non-specific
d2	$x, 1+y, z$	-3.2	4.9	non-specific
d3	$1-x, -1/2+y, 3/2-z$	-2.0	3.1	non-specific
d4	$1-x, 1/2+y, 3/2-z$	-2.0	3.1	non-specific
d5	$2-x, -1/2+y, 1/2-z$	-2.7	4.0	H...H, 2.19 Å
d6	$2-x, 1/2+y, 1/2-z$	-2.7	4.0	H...H, 2.19 Å
d7	$1-x, -y, 1-z$	-11.7	17.5	O-H...O, 1.80 Å, 168°
d8	$1-x, 1-y, 1-z$	-5.4	8.1	O-H...O, 2.43 Å, 124°
d9	$2-x, 1-y, 1-z$	-4.8	7.1	non-specific
d10	$2-x, 2-y, 1-z$	-2.4	3.5	H...H, 2.22 Å
d11	$x, 1/2-y, -1/2+z$	-5.8	8.7	C-H... $\pi$ , 2.48 Å, 164°; C...H, 2.73 Å;
d12	$x, 1/2-y, 1/2+z$	-5.8	8.7	C-H... $\pi$ , 2.48 Å, 164°; C...H, 2.73 Å
d13	$x, 3/2-y, -1/2+z$	-7.5	11.3	C...H, 2.70 Å, 2.88 Å; H...H, 2.33 Å
d14	$x, 3/2-y, 1/2+z$	-7.5	11.3	C...H, 2.70 Å, 2.88 Å; H...H, 2.33 Å

Table A 4.32. Symmetry codes, binding types, interaction energies of the monomeric building unit with neighboring ones ( $E_{\text{int}}$ , kcal/mol) and the contribution of these energies to the total interaction energy (%) in the crystal of ibuprofen form I under pressure of 2.65 GPa.

Dimer	Symmetry operation	$E_{\text{int}}$ , kcal/mol	Contribution to the total interaction energy, %	Interaction
d1	$x, -1+y, z$	-3.2	5.0	non-specific
d2	$x, 1+y, z$	-3.2	5.0	non-specific
d3	$1-x, -1/2+y, 3/2-z$	-1.9	3.0	non-specific
d4	$1-x, 1/2+y, 3/2-z$	-1.9	3.0	non-specific
d5	$2-x, -1/2+y, 1/2-z$	-2.6	4.1	H...H, 2.16 Å, 2.34 Å
d6	$2-x, 1/2+y, 1/2-z$	-2.6	4.1	H...H, 2.16 Å, 2.34 Å
d7	$1-x, -y, 1-z$	-10.0	15.5	O-H...O, 1.78 Å, 168°
d8	$1-x, 1-y, 1-z$	-5.2	8.0	O-H...O, 2.41 Å, 124°
d9	$2-x, 1-y, 1-z$	-4.8	7.5	non-specific
d10	$2-x, 2-y, 1-z$	-2.4	3.7	H...H, 2.22 Å
d11	$x, 1/2-y, -1/2+z$	-5.9	9.1	C-H... $\pi$ , 2.54 Å, 162°; C...H, 2.73 Å; C...C, 3.41 Å
d12	$x, 1/2-y, 1/2+z$	-5.9	9.1	C-H... $\pi$ , 2.54 Å, 162°; C...H, 2.73 Å; C...C, 3.41 Å
d13	$x, 3/2-y, -1/2+z$	-7.5	11.6	C...H, 2.60 Å, 2.83 Å; H...H, 2.32 Å
d14	$x, 3/2-y, 1/2+z$	-7.5	11.6	C...H, 2.60 Å, 2.83 Å; H...H, 2.32 Å

Table A 4.33. Symmetry codes, binding types, interaction energies of the monomeric building unit with neighboring ones ( $E_{\text{int}}$ , kcal/mol) and the contribution of these energies to the total interaction energy (%) in the crystal of ibuprofen form I under pressure of 3.46 GPa.

Dimer	Symmetry operation	$E_{\text{int}}$ , kcal/mol	Contribution to the total interaction energy, %	Interaction
d1	$x, -1+y, z$	-3.3	5.1	C...C, 3.40 Å
d2	$x, 1+y, z$	-3.3	5.1	C...C, 3.40 Å
d3	$1-x, -1/2+y, 3/2-z$	-1.9	3.0	non-specific
d4	$1-x, 1/2+y, 3/2-z$	-1.9	3.0	non-specific
d5	$2-x, -1/2+y, 1/2-z$	-2.5	3.9	H...H, 2.10 Å, 2.31 Å; C...H, 2.85 Å, 2.88 Å
d6	$2-x, 1/2+y, 1/2-z$	-2.5	3.9	H...H, 2.10 Å, 2.31 Å; C...H, 2.85 Å, 2.88 Å
d7	$1-x, -y, 1-z$	-11.9	18.4	O-H...O, 1.76 Å, 167°
d8	$1-x, 1-y, 1-z$	-5.0	7.7	O-H...O, 2.41 Å, 123°
d9	$2-x, 1-y, 1-z$	-4.9	7.6	non-specific
d10	$2-x, 2-y, 1-z$	-2.4	3.7	H...H, 2.15 Å; C...H, 2.87 Å
d11	$x, 1/2-y, -1/2+z$	-5.1	7.9	C-H... $\pi$ , 2.43 Å, 163°; C...H, 2.63 Å; C...C, 3.31 Å, 3.39 Å
d12	$x, 1/2-y, 1/2+z$	-5.1	7.9	C-H... $\pi$ , 2.43 Å, 163°; C...H, 2.63 Å; C...C, 3.31 Å, 3.39 Å
d13	$x, 3/2-y, -1/2+z$	-7.4	11.5	C...H, 2.53 Å, 2.75 Å, 2.85 Å; H...H, 2.27 Å, 2.32 Å
d14	$x, 3/2-y, 1/2+z$	-7.4	11.5	C...H, 2.53 Å, 2.75 Å, 2.85 Å; H...H, 2.27 Å, 2.32 Å

Table A 4.34. Symmetry codes, binding types, interaction energies of the monomeric building unit with neighboring ones ( $E_{\text{int}}$ , kcal/mol) and the contribution of these energies to the total interaction energy (%) in the crystal of ibuprofen form I under pressure of 4.00 GPa.

Dimer	Symmetry operation	$E_{\text{int}}$ , kcal/mol	Contribution to the total interaction energy, %	Interaction
d1	$x, -1+y, z$	-3.2	5.1	C...C, 3.33 Å; C...H, 2.86 Å
d2	$x, 1+y, z$	-3.2	5.1	C...C, 3.33 Å; C...H, 2.86 Å
d3	$1-x, -1/2+y, 3/2-z$	-1.9	3.0	non-specific
d4	$1-x, 1/2+y, 3/2-z$	-1.9	3.0	non-specific
d5	$2-x, -1/2+y, 1/2-z$	-2.5	4.1	H...H, 2.11 Å, 2.29 Å; C...H, 2.84 Å
d6	$2-x, 1/2+y, 1/2-z$	-2.5	4.1	H...H, 2.11 Å, 2.29 Å; C...H, 2.84 Å
d7	$1-x, -y, 1-z$	-9.9	15.9	O-H...O, 1.74 Å, 167°
d8	$1-x, 1-y, 1-z$	-5.1	8.3	O-H...O, 2.39 Å, 124°; O-H...O, 2.41 Å, 122°
d9	$2-x, 1-y, 1-z$	-4.9	7.9	non-specific
d10	$2-x, 2-y, 1-z$	-2.4	3.9	H...H, 2.13 Å; C...H, 2.84 Å
d11	$x, 1/2-y, -1/2+z$	-5.0	8.0	C-H... $\pi$ , 2.40 Å, 163°; C...H, 2.61 Å; C...C, 3.31 Å, 3.34 Å
d12	$x, 1/2-y, 1/2+z$	-5.0	8.0	C-H... $\pi$ , 2.40 Å, 163°; C...H, 2.61 Å; C...C, 3.31 Å, 3.34 Å
d13	$x, 3/2-y, -1/2+z$	-7.3	11.7	C...H, 2.50 Å, 2.76 Å, 2.85 Å, 2.86 Å; H...H, 2.25 Å, 2.25 Å
d14	$x, 3/2-y, 1/2+z$	-7.3	11.7	C...H, 2.50 Å, 2.76 Å, 2.85 Å, 2.86 Å; H...H, 2.25 Å, 2.25 Å

Table A 4.35. Symmetry codes, binding types, interaction energies of the dimeric building unit with neighboring ones ( $E_{\text{int}}$ , kcal/mol) and the contribution of these energies to the total interaction energy (%) in the crystal of ibuprofen form I under ambient pressure.

Dimer	Symmetry operation	$E_{\text{int}}$ , kcal/mol	Contribution to the total interaction energy, %	Interaction
d1	-x,-1-y,1-z	-3.8	3.8	non-specific
d2	-x,-1/2+y,3/2-z	-2.2	2.2	non-specific
d3	-x,-2-y,1-z	-1.7	1.7	non-specific
d4	-x,1/2+y,3/2-z	-2.2	2.2	non-specific
d5	1-x,-1-y,1-z	-10.7	10.6	non-specific
d6	1-x,-1/2+y,1/2-z	-8.8	8.8	C-H... $\pi$ , 2.86 Å, 166°
d7	1-x,-1/2+y,3/2-z	-8.8	8.8	C-H... $\pi$ , 2.86 Å, 166°
d8	1-x,-3/2+y,1/2-z	-6.0	6.0	non-specific
d9	1-x,-3/2+y,3/2-z	-6.0	6.0	non-specific
d10	1-x,1-y,1-z	-10.7	10.6	non-specific
d11	1-x,1/2+y,1/2-z	-8.8	8.8	C-H... $\pi$ , 2.86 Å, 166°
d12	1-x,1/2+y,3/2-z	-8.8	8.8	C-H... $\pi$ , 2.86 Å, 166°
d13	1-x,3/2+y,1/2-z	-6.0	6.0	non-specific
d14	1-x,3/2+y,3/2-z	-6.0	6.0	non-specific
d15	2-x,-1/2+y,1/2-z	-2.2	2.2	non-specific
d16	2-x,1-y,1-z	-3.8	3.8	non-specific
d17	2-x,1/2+y,1/2-z	-2.2	2.2	non-specific
d18	2-x,2-y,1-z	-1.7	1.7	non-specific

Table A 4.36. Symmetry codes, binding types, interaction energies of the dimeric building unit with neighboring ones ( $E_{\text{int}}$ , kcal/mol) and the contribution of these energies to the total interaction energy (%) in the crystal of ibuprofen form II under ambient pressure.

Dimer	Symmetry operation	$E_{\text{int}}$ , kcal/mol	Contribution to the total interaction energy, %	Interaction
d1	$-x, -1/2+y, 3/2-z$	-4.2	5.2	C...H, 2.81 Å
d2	$-x, 1/2+y, 3/2-z$	-4.2	5.2	C...H, 2.81 Å
d3	$-1+x, y, 1+z$	-1.2	1.5	H...H, 2.35 Å
d4	$-1+x, 1+y, 1+z$	-0.9	1.1	non-specific
d5	$-x, -1/2+y, 1/2-z$	-8.4	10.4	C-H... $\pi$ , 2.80 Å, 172°, H...H, 2.16 Å
d6	$x, -1+y, z$	-13.2	16.2	C...H, 2.88 Å
d7	$1-x, -1/2+y, 3/2-z$	-8.4	10.4	C-H... $\pi$ , 2.80 Å, 172°, H...H, 2.16 Å
d8	$1-x, 1/2+y, 1/2-z$	-8.4	10.4	C-H... $\pi$ , 2.80 Å, 172°, H...H, 2.16 Å
d9	$1-x, 1/2+y, 3/2-z$	-8.4	10.4	C-H... $\pi$ , 2.80 Å, 172°, H...H, 2.16 Å
d10	$x, 1+y, z$	-13.2	16.2	C...H, 2.88 Å
d11	$1+x, -1+y, -1+z$	-0.9	1.1	non-specific
d12	$2-x, -1/2+y, 1/2-z$	-4.2	5.2	C...H, 2.81 Å
d13	$1+x, y, -1+z$	-1.2	1.5	H...H, 2.35 Å
d14	$2-x, 1/2+y, 1/2-z$	-4.2	5.2	C...H, 2.81 Å

Table A 4.37. Symmetry codes, binding types, interaction energies of the dimeric building unit with neighboring ones ( $E_{\text{int}}$ , kcal/mol) and the contribution of these energies to the total interaction energy (%) in the crystal of ibuprofen form I under pressure of 0.23 GPa.

Dimer	Symmetry operation	$E_{\text{int}}$ , kcal/mol	Contribution to the total interaction energy, %	Interaction
d1	-1+x,-2+y,z	-1.9	1.9	non-specific
d2	-1+x,-1+y,z	-4.1	3.9	non-specific
d3	x,-1+y,z	-10.8	10.5	non-specific
d4	x,-3/2-y,-1/2+z	-6.2	6.0	non-specific
d5	x,-3/2-y,1/2+z	-6.2	6.0	non-specific
d6	x,-1/2-y,-1/2+z	-8.9	8.7	C-H... $\pi$ , 2.77 Å, 165°
d7	x,-1/2-y,1/2+z	-8.9	8.7	C-H... $\pi$ , 2.77 Å, 165°
d8	x,1+y,z	-10.8	10.5	non-specific
d9	-1+x,-1/2-y,1/2+z	-2.2	2.2	non-specific
d10	-1+x,1/2-y,1/2+z	-2.2	2.2	non-specific
d11	x,1/2-y,-1/2+z	-8.9	8.7	C-H... $\pi$ , 2.77 Å, 165°
d12	x,1/2-y,1/2+z	-8.9	8.7	C-H... $\pi$ , 2.77 Å, 165°
d13	1+x,-1/2-y,-1/2+z	-2.2	2.2	non-specific
d14	1+x,1/2-y,-1/2+z	-2.2	2.2	non-specific
d15	1+x,1+y,z	-4.1	3.9	non-specific
d16	1+x,2+y,z	-1.9	1.9	non-specific
d17	x,3/2-y,-1/2+z	-6.2	6.0	non-specific
d18	x,3/2-y,1/2+z	-6.2	6.0	non-specific

Table A 4.38. Symmetry codes, binding types, interaction energies of the dimeric building unit with neighboring ones ( $E_{\text{int}}$ , kcal/mol) and the contribution of these energies to the total interaction energy (%) in the crystal of ibuprofen form I under pressure of 0.60 GPa.

Dimer	Symmetry operation	$E_{\text{int}}$ , kcal/mol	Contribution to the total interaction energy, %	Interaction
d1	-1+x,-2+y,z	-2.1	1.9	non-specific
d2	-1+x,-1+y,z	-4.3	3.9	non-specific
d3	x,-1+y,z	-11.2	10.2	non-specific
d4	x,-3/2-y,-1/2+z	-6.9	6.3	non-specific
d5	x,-3/2-y,1/2+z	-6.9	6.3	non-specific
d6	x,-1/2-y,-1/2+z	-9.2	8.4	C-H... $\pi$ , 2.69 Å, 164°
d7	x,-1/2-y,1/2+z	-9.2	8.4	C-H... $\pi$ , 2.69 Å, 164°
d8	x,1+y,z	-11.2	10.2	non-specific
d9	-1+x,-1/2-y,1/2+z	-2.5	2.3	non-specific
d10	-1+x,1/2-y,1/2+z	-2.5	2.3	non-specific
d11	x,1/2-y,-1/2+z	-9.2	8.4	C-H... $\pi$ , 2.69 Å, 164°
d12	x,1/2-y,1/2+z	-9.2	8.4	C-H... $\pi$ , 2.69 Å, 164°
d13	1+x,-1/2-y,-1/2+z	-2.5	2.3	non-specific
d14	1+x,1/2-y,-1/2+z	-2.5	2.3	non-specific
d15	1+x,1+y,z	-4.3	3.9	non-specific
d16	1+x,2+y,z	-2.1	1.9	non-specific
d17	x,3/2-y,-1/2+z	-6.9	6.3	non-specific
d18	x,3/2-y,1/2+z	-6.9	6.3	non-specific

Table A 4.39. Symmetry codes, binding types, interaction energies of the dimeric building unit with neighboring ones ( $E_{\text{int}}$ , kcal/mol) and the contribution of these energies to the total interaction energy (%) in the crystal of ibuprofen form I under pressure of 0.80 GPa.

Dimer	Symmetry operation	$E_{\text{int}}$ , kcal/mol	Contribution to the total interaction energy, %	Interaction
d1	$x, -1+y, z$	-11.3	10.0	non-specific
d2	$x, 1+y, z$	-11.3	10.0	non-specific
d3	$x, -1/2-y, 1/2+z$	-9.3	8.3	C-H... $\pi$ , 2.65 Å, 166°
d4	$x, 1/2-y, 1/2+z$	-9.3	8.3	C-H... $\pi$ , 2.65 Å, 166°
d5	$1+x, -1/2-y, -1/2+z$	-2.6	2.4	non-specific
d6	$1+x, 1/2-y, -1/2+z$	-2.6	2.4	non-specific
d7	$1+x, 1+y, z$	-4.5	4.0	non-specific
d8	$1+x, 2+y, z$	-2.1	1.9	H...H, 2.34 Å
d9	$x, 1/2-y, -1/2+z$	-9.3	8.3	C-H... $\pi$ , 2.65 Å, 166°
d10	$x, 3/2-y, -1/2+z$	-7.1	6.4	C...H, 2.85 Å
d11	$x, 3/2-y, 1/2+z$	-7.1	6.4	C...H, 2.85 Å
d12	$-1+x, -2+y, z$	-2.1	1.9	H...H, 2.34 Å
d13	$-1+x, -1+y, z$	-4.5	4.0	non-specific
d14	$x, -3/2-y, -1/2+z$	-7.1	6.4	C...H, 2.85 Å
d15	$x, -3/2-y, 1/2+z$	-7.1	6.4	C...H, 2.85 Å
d16	$x, -1/2-y, -1/2+z$	-9.3	8.3	C-H... $\pi$ , 2.65 Å, 166°
d17	$-1+x, -1/2-y, 1/2+z$	-2.6	2.4	non-specific
d18	$-1+x, 1/2-y, 1/2+z$	-2.6	2.4	non-specific

Table A 4.40. Symmetry codes, binding types, interaction energies of the dimeric building unit with neighboring ones ( $E_{\text{int}}$ , kcal/mol) and the contribution of these energies to the total interaction energy (%) in the crystal of ibuprofen form I under pressure of 0.88 GPa.

Dimer	Symmetry operation	$E_{\text{int}}$ , kcal/mol	Contribution to the total interaction energy, %	Interaction
d1	-1+x,-2+y,z	-2.2	1.9	non-specific
d2	-1+x,-1+y,z	-4.5	4.0	non-specific
d3	x,-1+y,z	-11.3	10.1	non-specific
d4	x,-3/2-y,-1/2+z	-7.2	6.4	C...H, 2.85 Å
d5	x,-3/2-y,1/2+z	-7.2	6.4	C...H, 2.85 Å
d6	x,-1/2-y,-1/2+z	-9.2	8.2	C-H... $\pi$ , 2.68 Å, 164°; C...H, 2.88 Å
d7	x,-1/2-y,1/2+z	-9.2	8.2	C-H... $\pi$ , 2.68 Å, 164°; C...H, 2.88 Å
d8	x,1+y,z	-11.3	10.1	non-specific
d9	-1+x,-1/2-y,1/2+z	-2.6	2.3	non-specific
d10	-1+x,1/2-y,1/2+z	-2.6	2.3	non-specific
d11	x,1/2-y,-1/2+z	-9.2	8.2	C-H... $\pi$ , 2.68 Å, 164°; C...H, 2.88 Å
d12	x,1/2-y,1/2+z	-9.2	8.2	C-H... $\pi$ , 2.68 Å, 164°; C...H, 2.88 Å
d13	1+x,-1/2-y,-1/2+z	-2.6	2.3	non-specific
d14	1+x,1/2-y,-1/2+z	-2.6	2.3	non-specific
d15	1+x,1+y,z	-4.5	4.0	non-specific
d16	1+x,2+y,z	-2.2	1.9	non-specific
d17	x,3/2-y,-1/2+z	-7.2	6.4	C...H, 2.85 Å
d18	x,3/2-y,1/2+z	-7.2	6.4	C...H, 2.85 Å

Table A 4.41. Symmetry codes, binding types, interaction energies of the dimeric building unit with neighboring ones ( $E_{\text{int}}$ , kcal/mol) and the contribution of these energies to the total interaction energy (%) in the crystal of ibuprofen form I under pressure of 1.70 GPa.

Dimer	Symmetry operation	$E_{\text{int}}$ , kcal/mol	Contribution to the total interaction energy, %	Interaction
d1	-1+x,-2+y,z	-2.3	2.0	H...H, 2.28 Å
d2	-1+x,-1+y,z	-4.8	4.2	non-specific
d3	x,-1+y,z	-11.3	9.9	non-specific
d4	x,-3/2-y,-1/2+z	-7.6	6.6	C...H, 2.72 Å
d5	x,-3/2-y,1/2+z	-7.6	6.6	C...H, 2.72 Å
d6	x,-1/2-y,-1/2+z	-9.2	8.0	C-H... $\pi$ , 2.63 Å, 163°; C...H, 2.80 Å
d7	x,-1/2-y,1/2+z	-9.2	8.0	C-H... $\pi$ , 2.63 Å, 163°; C...H, 2.80 Å
d8	x,1+y,z	-11.3	9.9	non-specific
d9	-1+x,-1/2-y,1/2+z	-2.7	2.3	H...H, 2.21 Å
d10	-1+x,1/2-y,1/2+z	-2.7	2.3	H...H, 2.21 Å
d11	x,1/2-y,-1/2+z	-9.2	8.0	C-H... $\pi$ , 2.63 Å, 163°; C...H, 2.80 Å
d12	x,1/2-y,1/2+z	-9.2	8.0	C-H... $\pi$ , 2.63 Å, 163°; C...H, 2.80 Å
d13	1+x,-1/2-y,-1/2+z	-2.7	2.3	H...H, 2.21 Å
d14	1+x,1/2-y,-1/2+z	-2.7	2.3	H...H, 2.21 Å
d15	1+x,1+y,z	-4.8	4.2	non-specific
d16	1+x,2+y,z	-2.3	2.0	H...H, 2.28 Å
d17	x,3/2-y,-1/2+z	-7.6	6.6	C...H, 2.72 Å
d18	x,3/2-y,1/2+z	-7.6	6.6	C...H, 2.72 Å

Table A 4.42. Symmetry codes, binding types, interaction energies of the dimeric building unit with neighboring ones ( $E_{\text{int}}$ , kcal/mol) and the contribution of these energies to the total interaction energy (%) in the crystal of ibuprofen form I under pressure of 1.89 GPa.

Dimer	Symmetry operation	$E_{\text{int}}$ , kcal/mol	Contribution to the total interaction energy, %	Interaction
d1	$x, -1+y, z$	-11.2	9.8	O-H...O, 2.43 Å, 125°
d2	$x, 1+y, z$	-11.2	9.8	O-H...O, 2.43 Å, 125°
d3	$x, -1/2-y, 1/2+z$	-9.1	8.0	C-H... $\pi$ , 2.55 Å, 164°; C...H, 2.81 Å
d4	$x, 1/2-y, 1/2+z$	-9.1	8.0	C-H... $\pi$ , 2.55 Å, 164°; C...H, 2.81 Å
d5	$1+x, -1/2-y, -1/2+z$	-2.7	2.4	H...H, 2.23 Å
d6	$1+x, 1/2-y, -1/2+z$	-2.7	2.4	H...H, 2.23 Å
d7	$1+x, 1+y, z$	-4.8	4.2	non-specific
d8	$1+x, 2+y, z$	-2.3	2.0	H...H, 2.22 Å
d9	$x, 1/2-y, -1/2+z$	-9.1	8.0	C-H... $\pi$ , 2.55 Å, 164°; C...H, 2.81 Å
d10	$x, 3/2-y, -1/2+z$	-7.6	6.6	C...H, 2.70 Å
d11	$x, 3/2-y, 1/2+z$	-7.6	6.6	C...H, 2.70 Å
d12	$-1+x, -2+y, z$	-2.3	2.0	H...H, 2.22 Å
d13	$-1+x, -1+y, z$	-4.8	4.2	non-specific
d14	$x, -3/2-y, -1/2+z$	-7.6	6.6	C...H, 2.70 Å
d15	$x, -3/2-y, 1/2+z$	-7.6	6.6	C...H, 2.70 Å
d16	$x, -1/2-y, -1/2+z$	-9.1	8.0	C-H... $\pi$ , 2.55 Å, 164°; C...H, 2.81 Å
d17	$-1+x, -1/2-y, 1/2+z$	-2.7	2.4	H...H, 2.23 Å
d18	$-1+x, 1/2-y, 1/2+z$	-2.7	2.4	H...H, 2.23 Å

Table A 4.43. Symmetry codes, binding types, interaction energies of the dimeric building unit with neighboring ones ( $E_{\text{int}}$ , kcal/mol) and the contribution of these energies to the total interaction energy (%) in the crystal of ibuprofen form I under pressure of 2.32 GPa.

Dimer	Symmetry operation	$E_{\text{int}}$ , kcal/mol	Contribution to the total interaction energy, %	Interaction
d1	$x, -1+y, z$	-11.2	9.9	O-H...O, 2.43 Å, 124°
d2	$x, 1+y, z$	-11.2	9.9	O-H...O, 2.43 Å, 124°
d3	$x, -1/2-y, 1/2+z$	-8.6	7.7	C-H... $\pi$ , 2.48 Å, 164°; C...H, 2.73 Å
d4	$x, 1/2-y, 1/2+z$	-8.6	7.7	C-H... $\pi$ , 2.48 Å, 164°; C...H, 2.73 Å
d5	$1+x, -1/2-y, -1/2+z$	-2.7	2.4	H...H, 2.19 Å
d6	$1+x, 1/2-y, -1/2+z$	-2.7	2.4	H...H, 2.19 Å
d7	$1+x, 1+y, z$	-4.9	4.3	non-specific
d8	$1+x, 2+y, z$	-2.4	2.1	H...H, 2.22 Å
d9	$x, 1/2-y, -1/2+z$	-8.6	7.7	C-H... $\pi$ , 2.48 Å, 164°; C...H, 2.73 Å
d10	$x, 3/2-y, -1/2+z$	-7.6	6.8	C...H, 2.70 Å, 2.88 Å; H...H, 2.33 Å
d11	$x, 3/2-y, 1/2+z$	-7.6	6.8	C...H, 2.70 Å, 2.88 Å; H...H, 2.33 Å
d12	$-1+x, -2+y, z$	-2.4	2.1	H...H, 2.22 Å
d13	$-1+x, -1+y, z$	-4.9	4.3	non-specific
d14	$x, -3/2-y, -1/2+z$	-7.6	6.8	C...H, 2.70 Å, 2.88 Å; H...H, 2.33 Å
d15	$x, -3/2-y, 1/2+z$	-7.6	6.8	C...H, 2.70 Å, 2.88 Å; H...H, 2.33 Å
d16	$x, -1/2-y, -1/2+z$	-8.6	7.7	C-H... $\pi$ , 2.48 Å, 164°; C...H, 2.73 Å
d17	$-1+x, -1/2-y, 1/2+z$	-2.7	2.4	H...H, 2.19 Å
d18	$-1+x, 1/2-y, 1/2+z$	-2.7	2.4	H...H, 2.19 Å

Table A 4.44. Symmetry codes, binding types, interaction energies of the dimeric building unit with neighboring ones ( $E_{\text{int}}$ , kcal/mol) and the contribution of these energies to the total interaction energy (%) in the crystal of ibuprofen form I under pressure of 2.65 GPa.

Dimer	Symmetry operation	$E_{\text{int}}$ , kcal/mol	Contribution to the total interaction energy, %	Interaction
d1	-1+x,-2+y,z	-2.4	2.1	H...H, 2.22 Å
d2	-1+x,-1+y,z	-4.9	4.4	non-specific
d3	x,-1+y,z	-11.0	9.8	O-H...O, 2.41 Å, 124°
d4	x,-3/2-y,-1/2+z	-7.6	6.7	C...H, 2.60 Å, 2.83 Å; H...H, 2.32 Å
d5	x,-3/2-y,1/2+z	-7.6	6.7	C...H, 2.60 Å, 2.83 Å; H...H, 2.32 Å
d6	x,-1/2-y,-1/2+z	-8.7	7.7	C-H... $\pi$ , 2.54 Å, 162°; C...H, 2.73 Å; C...C, 3.41 Å
d7	x,-1/2-y,1/2+z	-8.7	7.7	C-H... $\pi$ , 2.54 Å, 162°; C...H, 2.73 Å; C...C, 3.41 Å
d8	x,1+y,z	-11.0	9.8	O-H...O, 2.41 Å, 124°
d9	-1+x,-1/2-y,1/2+z	-2.7	2.4	H...H, 2.16 Å, 2.34 Å
d10	-1+x,1/2-y,1/2+z	-2.7	2.4	H...H, 2.16 Å, 2.34 Å
d11	x,1/2-y,-1/2+z	-8.7	7.7	C-H... $\pi$ , 2.54 Å, 162°; C...H, 2.73 Å; C...C, 3.41 Å
d12	x,1/2-y,1/2+z	-8.7	7.7	C-H... $\pi$ , 2.54 Å, 162°; C...H, 2.73 Å; C...C, 3.41 Å
d13	1+x,-1/2-y,-1/2+z	-2.7	2.4	H...H, 2.16 Å, 2.34 Å
d14	1+x,1/2-y,-1/2+z	-2.7	2.4	H...H, 2.16 Å, 2.34 Å
d15	1+x,1+y,z	-4.9	4.4	non-specific
d16	1+x,2+y,z	-2.4	2.1	H...H, 2.22 Å
d17	x,3/2-y,-1/2+z	-7.6	6.7	C...H, 2.60 Å, 2.83 Å; H...H, 2.32 Å
d18	x,3/2-y,1/2+z	-7.6	6.7	C...H, 2.60 Å, 2.83 Å; H...H, 2.32 Å

Table A 4.45. Symmetry codes, binding types, interaction energies of the dimeric building unit with neighboring ones ( $E_{\text{int}}$ , kcal/mol) and the contribution of these energies to the total interaction energy (%) in the crystal of ibuprofen form I under pressure of 3.46 GPa.

Dimer	Symmetry operation	$E_{\text{int}}$ , kcal/mol	Contribution to the total interaction energy, %	Interaction
d1	-1+x,-2+y,z	-2.4	2.2	H...H, 2.15 Å; C...H, 2.87 Å
d2	-1+x,-1+y,z	-5.0	4.6	non-specific
d3	x,-1+y,z	-10.8	10.0	O-H...O, 2.41 Å, 123°; C...C, 3.40 Å
d4	x,-3/2-y,-1/2+z	-7.5	7.0	C...H, 2.53 Å, 2.75 Å, 2.85 Å; H...H, 2.27 Å, 2.32 Å
d5	x,-3/2-y,1/2+z	-7.5	7.0	C...H, 2.53 Å, 2.75 Å, 2.85 Å; H...H, 2.27 Å, 2.32 Å
d6	x,-1/2-y,-1/2+z	-7.9	7.3	C-H... $\pi$ , 2.43 Å, 163°; C...H, 2.63 Å; C...C, 3.31 Å, 3.39 Å
d7	x,-1/2-y,1/2+z	-7.9	7.3	C-H... $\pi$ , 2.43 Å, 163°; C...H, 2.63 Å; C...C, 3.31 Å, 3.39 Å
d8	x,1+y,z	-10.8	10.0	O-H...O, 2.41 Å, 123°; C...C, 3.40 Å
d9	-1+x,-1/2-y,1/2+z	-2.5	2.3	H...H, 2.10 Å, 2.31 Å; C...H, 2.85 Å, 2.88 Å
d10	-1+x,1/2-y,1/2+z	-2.5	2.3	H...H, 2.10 Å, 2.31 Å; C...H, 2.85 Å, 2.88 Å
d11	x,1/2-y,-1/2+z	-7.9	7.3	C-H... $\pi$ , 2.43 Å, 163°; C...H, 2.63 Å; C...C, 3.31 Å, 3.39 Å
d12	x,1/2-y,1/2+z	-7.9	7.3	C-H... $\pi$ , 2.43 Å, 163°; C...H, 2.63 Å; C...C, 3.31 Å, 3.39 Å
d13	1+x,-1/2-y,-1/2+z	-2.5	2.3	H...H, 2.10 Å, 2.31 Å; C...H, 2.85 Å, 2.88 Å
d14	1+x,1/2-y,-1/2+z	-2.5	2.3	H...H, 2.10 Å, 2.31 Å; C...H, 2.85 Å, 2.88 Å
d15	1+x,1+y,z	-5.0	4.6	non-specific
d16	1+x,2+y,z	-2.4	2.2	H...H, 2.15 Å; C...H, 2.87 Å
d17	x,3/2-y,-1/2+z	-7.5	7.0	C...H, 2.53 Å, 2.75 Å, 2.85 Å; H...H, 2.27 Å, 2.32 Å
d18	x,3/2-y,1/2+z	-7.5	7.0	C...H, 2.53 Å, 2.75 Å, 2.85 Å; H...H, 2.27 Å, 2.32 Å

Table A 4.46. Symmetry codes, binding types, interaction energies of the dimeric building unit with neighboring ones ( $E_{\text{int}}$ , kcal/mol) and the contribution of these energies to the total interaction energy (%) in the crystal of ibuprofen form I under pressure of 4.00 GPa.

Dimer	Symmetry operation	$E_{\text{int}}$ , kcal/mol	Contribution to the total interaction energy, %	Interaction
d1	-1+x,-2+y,z	-2.4	2.3	H...H, 2.13 Å; C...H, 2.84 Å
d2	-1+x,-1+y,z	-5.1	4.7	non-specific
d3	x,-1+y,z	-10.8	10.0	O-H...O, 2.39 Å, 124°; O-H...O, 2.41 Å, 122°; C...C, 3.33 Å; C...H, 2.86 Å
d4	x,-3/2-y,-1/2+z	-7.4	6.9	C...H, 2.50 Å, 2.76 Å, 2.85 Å, 2.86 Å; H...H, 2.25 Å, 2.25 Å
d5	x,-3/2-y,1/2+z	-7.4	6.9	C...H, 2.50 Å, 2.76 Å, 2.85 Å, 2.86 Å; H...H, 2.25 Å, 2.25 Å
d6	x,-1/2-y,-1/2+z	-7.8	7.2	C-H... $\pi$ , 2.40 Å, 163°; C...H, 2.61 Å; C...C, 3.31 Å, 3.34 Å
d7	x,-1/2-y,1/2+z	-7.8	7.2	C-H... $\pi$ , 2.40 Å, 163°; C...H, 2.61 Å; C...C, 3.31 Å, 3.34 Å
d8	x,1+y,z	-10.8	10.0	O-H...O, 2.39 Å, 124°; O-H...O, 2.41 Å, 122°; C...C, 3.33 Å; C...H, 2.86 Å
d9	-1+x,-1/2-y,1/2+z	-2.6	2.4	H...H, 2.11 Å, 2.29 Å; C...H, 2.84 Å
d10	-1+x,1/2-y,1/2+z	-2.6	2.4	H...H, 2.11 Å, 2.29 Å; C...H, 2.84 Å
d11	x,1/2-y,-1/2+z	-7.8	7.2	C-H... $\pi$ , 2.40 Å, 163°; C...H, 2.61 Å; C...C, 3.31 Å, 3.34 Å
d12	x,1/2-y,1/2+z	-7.8	7.2	C-H... $\pi$ , 2.40 Å, 163°; C...H, 2.61 Å; C...C, 3.31 Å, 3.34 Å
d13	1+x,-1/2-y,-1/2+z	-2.6	2.4	H...H, 2.11 Å, 2.29 Å; C...H, 2.84 Å
d14	1+x,1/2-y,-1/2+z	-2.6	2.4	H...H, 2.11 Å, 2.29 Å; C...H, 2.84 Å
d15	1+x,1+y,z	-5.1	4.7	non-specific
d16	1+x,2+y,z	-2.4	2.3	H...H, 2.13 Å; C...H, 2.84 Å
d17	x,3/2-y,-1/2+z	-7.4	6.9	C...H, 2.50 Å, 2.76 Å, 2.85 Å, 2.86 Å; H...H, 2.25 Å, 2.25 Å
d18	x,3/2-y,1/2+z	-7.4	6.9	C...H, 2.50 Å, 2.76 Å, 2.85 Å, 2.86 Å; H...H, 2.25 Å, 2.25 Å

Table A 4.47. Minimal interatomic distances and absolute deviation (AD) of their determination for the different step sizes in comparison to the high-precision computation with a step size of 1/1000 of a translation occurring during the displacement of the dimeric building units in polymorph I and monomeric building units in polymorph II of ibuprofen along [001] and [010] directions of layers laying in (100) plane.

Shift direction	Step size (Part of a translation)	Minimal interatomic distance $\pm$ AD, Å											
		I		II		I							
		Ambient pressure		Ambient pressure		0.23 GPa		0.60 GPa		0.80 GPa		0.88 GPa	
[010] (100)	0.20	0.360	0.055	0.275	0.381	0.025	0.497	0.265 $\beta$ $\pm$ 0.051	1.126 $\pm$ 0.002	0.446 $\beta$ $\pm$ 0.033	0.234 $\beta$ $\pm$ 0.064	0.543 $\beta$ $\pm$ 0.025	0.096 $\beta$ $\pm$ 0.107
	0.10	0.082	0.023	0.038	0.074	0.025	0.107						
	0.05	0.008	0.006	0.004	0.005	0.017	0.003						
	0.04	0.008	0.000	0.004	0.005	0.000	0.003						
	0.02	0.039	0.010	0.009	0.042	0.082	0.055						
[001] (100)	0.20	0.039	0.010	0.009	0.042	0.082	0.055	1.548 $\pm$ 0.011	1.206 $\delta$ $\pm$ 0.003	1.450 $\pm$ 0.009	1.286 $\pm$ 0.014	1.182 $\pm$ 0.002	1.189 $\pm$ 0.009
	0.10	0.039	0.003	0.009	0.042	0.082	0.055						
	0.05	0.002	0.001	0.009	0.003	0.001	0.001						
	0.04	0.002	0.001	0.009	0.003	0.001	0.001						
	0.02	0.002	0.001	0.009	0.003	0.001	0.001						
Shift direction	Step size (Part of a translation)	Minimal interatomic distance (AD), Å											
		I											
		1.70 GPa		1.89 GPa		2.32 GPa		2.65 GPa		3.46 GPa		4.00 GPa	
[010] (100)	0.20	0.306	0.264	0.116	0.034	0.051	0.038	0.153 $\beta$ $\pm$ 0.054	0.195 $\beta$ $\pm$ 0.044	0.243 $\beta$ $\pm$ 0.024	0.285 $\beta$ $\pm$ 0.016	0.156 $\beta$ $\pm$ 0.051	0.207 $\beta$ $\pm$ 0.038
	0.10	0.054	0.044	0.024	0.016	0.051	0.038						
	0.05	0.000	0.000	0.003	0.004	0.051	0.038						
	0.04	0.000	0.000	0.003	0.001	0.000	0.000						
	0.02	0.106	0.103	0.132	0.157	0.206	0.195						
[001] (100)	0.20	0.106	0.103	0.126	0.112	0.097	0.118	1.017 $\pm$ 0.001	0.966 $\pm$ 0.001	0.907 $\pm$ 0.000	0.863 $\pm$ 0.001	0.747 $\pm$ 0.007	0.697 $\pm$ 0.003
	0.10	0.003	0.002	0.006	0.012	0.025	0.019						
	0.05	0.003	0.002	0.005	0.002	0.000	0.001						
	0.04	0.003	0.002	0.005	0.002	0.000	0.001						
	0.02	0.003	0.002	0.005	0.002	0.000	0.001						

$\beta$  Movements in the directions are improbable from the topological point of view because of the molecules overlapping during the translations.

$\delta$  The shift direction [010] for the layers family parallel to plane (102) is shown instead of [001] (100) for the polymorphic form II of ibuprofen.

Table A 4.48. Minimal differences between the interatomic distances and the corresponding sums of van der Waals radii ( $\delta$ ) and absolute deviation (AD) of their determination for the different step sizes in comparison to the high-precision computation with a step size of 1/1000 of a translation occurring during the displacement of the dimeric building units in polymorph I and monomeric building units in polymorph II of ibuprofen along [001] and [010] directions of layers laying in (100) plane.

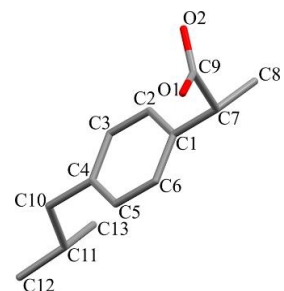
Shift direction	Step size (Part of a translation)	$\delta \pm AD, \text{\AA}$							
		I		II		I			
		Ambient pressure		Ambient pressure		0.23 GPa	0.60 GPa	0.80 GPa	0.88 GPa
[010] (100)	0.20	0.169	0.055	0.089	0.158	0.131	0.193		
	0.10	0.000	0.023	0.000	0.000	0.000	0.000		
	0.05	-2.107 <sup><math>\beta</math></sup>	-1.054 <sup><math>\gamma</math></sup>	-2.093 <sup><math>\beta</math></sup>	-2.200 <sup><math>\beta</math></sup>	-2.352 <sup><math>\beta</math></sup>	-2.300 <sup><math>\beta</math></sup>		
	0.04	$\pm$	$\pm$	$\pm$	$\pm$	$\pm$	$\pm$		
	0.02	0.010	0.006	0.009	0.010	0.011	0.011		
[001] (100)	0.20	0.000	0.000	0.000	0.000	0.000	0.000		
	0.10	0.039	0.010	0.009	0.042	0.082	0.055		
	0.05	0.039	0.003	0.009	0.042	0.082	0.055		
	0.04	-0.632 $\pm$	-0.974 <sup><math>\delta</math></sup> $\pm$	-0.730 $\pm$	-0.894 $\pm$	-0.998 $\pm$	-0.991 $\pm$		
	0.02	0.011	0.003	0.009	0.014	0.002	0.009		
[010] (100)	0.20	0.002	0.001	0.009	0.003	0.001	0.001		
	0.10	0.002	0.001	0.009	0.003	0.001	0.001		
	0.05	0.002	0.001	0.009	0.003	0.001	0.001		
	0.04	0.002	0.001	0.009	0.003	0.001	0.001		
	0.02	0.002	0.001	0.001	0.003	0.001	0.001		
Shift direction	Step size (Part of a translation)	$\delta \pm AD, \text{\AA}$							
		I							
		1.70 GPa	1.89 GPa	2.32 GPa	2.65 GPa	3.46 GPa	4.00 GPa		
[010] (100)	0.20	0.118	0.168	0.090	0.085	0.051	0.124		
	0.10	0.000	0.000	0.000	0.000	0.003	0.000		
	0.05	-2.449 <sup><math>\beta</math></sup>	-2.499 <sup><math>\beta</math></sup>	-2.522 <sup><math>\beta</math></sup>	-2.557 <sup><math>\beta</math></sup>	-2.634 <sup><math>\beta</math></sup>	-2.669 <sup><math>\beta</math></sup>		
	0.04	$\pm$	$\pm$	$\pm$	$\pm$	$\pm$	$\pm$		
	0.02	0.000	0.000	0.013	0.013	0.016	0.014		
[001] (100)	0.20	0.000	0.000	0.000	0.000	0.000	0.000		
	0.10	0.109	0.103	0.132	0.157	0.206	0.195		
	0.05	0.109	0.103	0.126	0.112	0.097	0.118		
	0.04	-1.163 <sup><math>\gamma</math></sup>	-1.214 <sup><math>\gamma</math></sup>	-1.273 <sup><math>\gamma</math></sup>	-1.317 <sup><math>\gamma</math></sup>	-1.433 <sup><math>\gamma</math></sup>	-1.483 <sup><math>\gamma</math></sup>		
	0.02	$\pm$	$\pm$	$\pm$	$\pm$	$\pm$	$\pm$		
		0.000	0.001	0.000	0.001	0.007	0.003		
		0.003	0.002	0.006	0.012	0.025	0.019		
		0.003	0.002	0.005	0.002	0.000	0.001		

<sup>$\beta$</sup>  Movements in the directions are improbable from the topological point of view because of the molecules overlapping during the translations.

<sup>$\gamma$</sup>  Probability of movements in the directions are very low because of the compression of material / molecules rapprochement.

<sup>$\delta$</sup>  The shift direction [010] for the layers family parallel to plane (102) is shown instead of [001] (100) for the polymorphic form II of ibuprofen.

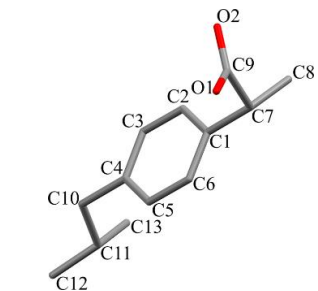
Table A 4.49. Comparison of the covalent bond lengths in experimental and optimized structures of the polymorphic modification I of ibuprofen in the range from ambient pressure to 4 GPa. The bond lengths, which do not coincide according to the  $3\sigma$  (99.7%) rule, are marked with asterisk.



Bond length in optimized (experimental) structure, Å

Covalent bond	Ambient pressure	0.23 GPa	0.60 GPa	0.80 GPa	0.88 GPa	1.70 GPa
O1–C9	1.307 (1.319) *	1.310 (1.319)	1.316 (1.317)	1.288 (1.317) *	1.294 (1.317)	1.284 (1.314) *
O2=C9	1.216 (1.245) *	1.220 (1.245)	1.228 (1.245)	1.226 (1.245)	1.226 (1.246)	1.234 (1.245)
C9–C7	1.512 (1.515)	1.520 (1.516)	1.500 (1.513)	1.510 (1.513)	1.500 (1.512)	1.490 (1.508)
C7–C8	1.527 (1.529)	1.570 (1.528)	1.540 (1.526)	1.530 (1.526)	1.540 (1.525)	1.530 (1.524)
C7–C1	1.522 (1.525)	1.510 (1.526)	1.480 (1.525)	1.460 (1.523) *	1.420 (1.523) *	1.480 (1.521)
C1–C2 (ar)	1.385 (1.400) *	1.360 (1.400)	1.370 (1.399)	1.450 (1.398) *	1.420 (1.399)	1.360 (1.397) *
C2–C3 (ar)	1.380 (1.394) *	1.320 (1.394)	1.390 (1.393)	1.390 (1.392)	1.340 (1.393)	1.460 (1.391) *
C3–C4 (ar)	1.381 (1.400) *	1.410 (1.400)	1.400 (1.399)	1.380 (1.400)	1.440 (1.398) *	1.360 (1.398) *
C4–C5 (ar)	1.384 (1.404) *	1.350 (1.404)	1.400 (1.404)	1.360 (1.403) *	1.370 (1.403) *	1.390 (1.403)
C5–C6 (ar)	1.386 (1.395)	1.390 (1.395)	1.390 (1.395)	1.370 (1.394)	1.370 (1.394)	1.380 (1.393)
C6–C1 (ar)	1.382 (1.400) *	1.420 (1.400)	1.380 (1.400)	1.400 (1.400)	1.400 (1.400)	1.370 (1.398)
C4–C10	1.512 (1.504)	1.460 (1.505)	1.520 (1.503)	1.490 (1.502)	1.530 (1.502)	1.520 (1.499)
C10–C11	1.524 (1.544) *	1.550 (1.544)	1.480 (1.543) *	1.500 (1.541) *	1.510 (1.541) *	1.540 (1.539)
C11–C13	1.515 (1.529) *	1.490 (1.529)	1.520 (1.529)	1.570 (1.529) *	1.560 (1.528) *	1.520 (1.526)
C11–C12	1.518 (1.529)	1.470 (1.528)	1.450 (1.527) *	1.490 (1.528)	1.480 (1.527)	1.520 (1.525)

Table A 4.49 (Continue).



Bond length in optimized (experimental) structure, Å

Covalent bond	1.89 GPa	2.32 GPa	2.65 GPa	3.46 GPa	4.00 GPa
O1–C9	1.320 (1.312)	1.301 (1.314)	1.330 (1.313)	1.280 (1.309) *	1.293 (1.309) *
O2=C9	1.230 (1.247)	1.239 (1.245)	1.236 (1.246)	1.250 (1.246)	1.228 (1.246) *
C9–C7	1.500 (1.508)	1.490 (1.504)	1.450 (1.503) *	1.470 (1.500) *	1.480 (1.499) *
C7–C8	1.530 (1.523)	1.550 (1.522)	1.600 (1.521) *	1.580 (1.518) *	1.540 (1.517) *
C7–C1	1.470 (1.520)	1.510 (1.518)	1.450 (1.518) *	1.500 (1.515)	1.490 (1.514) *
C1–C2 (ar)	1.400 (1.396)	1.390 (1.397)	1.380 (1.396)	1.370 (1.395) *	1.410 (1.394) *
C2–C3 (ar)	1.400 (1.391)	1.440 (1.389)	1.440 (1.389)	1.410 (1.389) *	1.330 (1.389) *
C3–C4 (ar)	1.400 (1.398)	1.380 (1.397)	1.370 (1.396)	1.400 (1.395)	1.420 (1.395) *
C4–C5 (ar)	1.400 (1.403)	1.430 (1.403)	1.410 (1.402)	1.410 (1.402)	1.440 (1.400) *
C5–C6 (ar)	1.360 (1.393)	1.360 (1.393)	1.340 (1.392)	1.330 (1.391) *	1.330 (1.392) *
C6–C1 (ar)	1.380 (1.398)	1.400 (1.397)	1.400 (1.397)	1.390 (1.395)	1.400 (1.393)
C4–C10	1.480 (1.500)	1.450 (1.498)	1.500 (1.497)	1.430 (1.496) *	1.430 (1.495) *
C10–C11	1.530 (1.540)	1.552 (1.537)	1.560 (1.537)	1.540 (1.535)	1.550 (1.535) *
C11–C13	1.540 (1.527)	1.530 (1.527)	1.520 (1.527)	1.510 (1.525)	1.520 (1.524)
C11–C12	1.510 (1.524)	1.520 (1.523)	1.520 (1.522)	1.560 (1.520) *	1.530 (1.518)

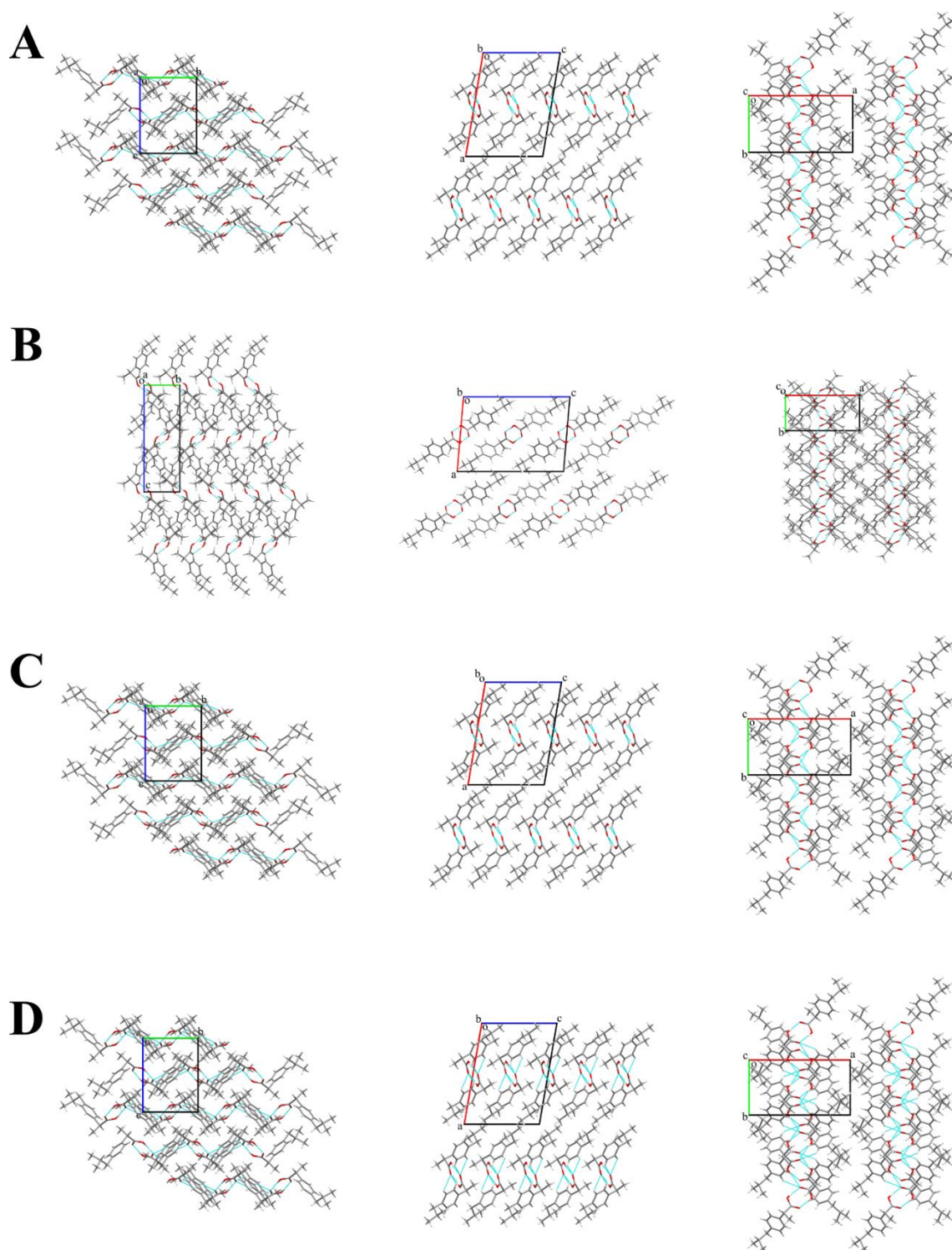


Figure A 4.25. Packing of the molecules in the crystals of ibuprofen polymorphs I (A) and II (B) at ambient pressure and polymorph I under the pressure of 0.23 (C) and 0.60 GPa (D). The projections in  $a$  (on the right),  $b$  (in the middle),  $c$  (on the left) crystallographic directions are represented.

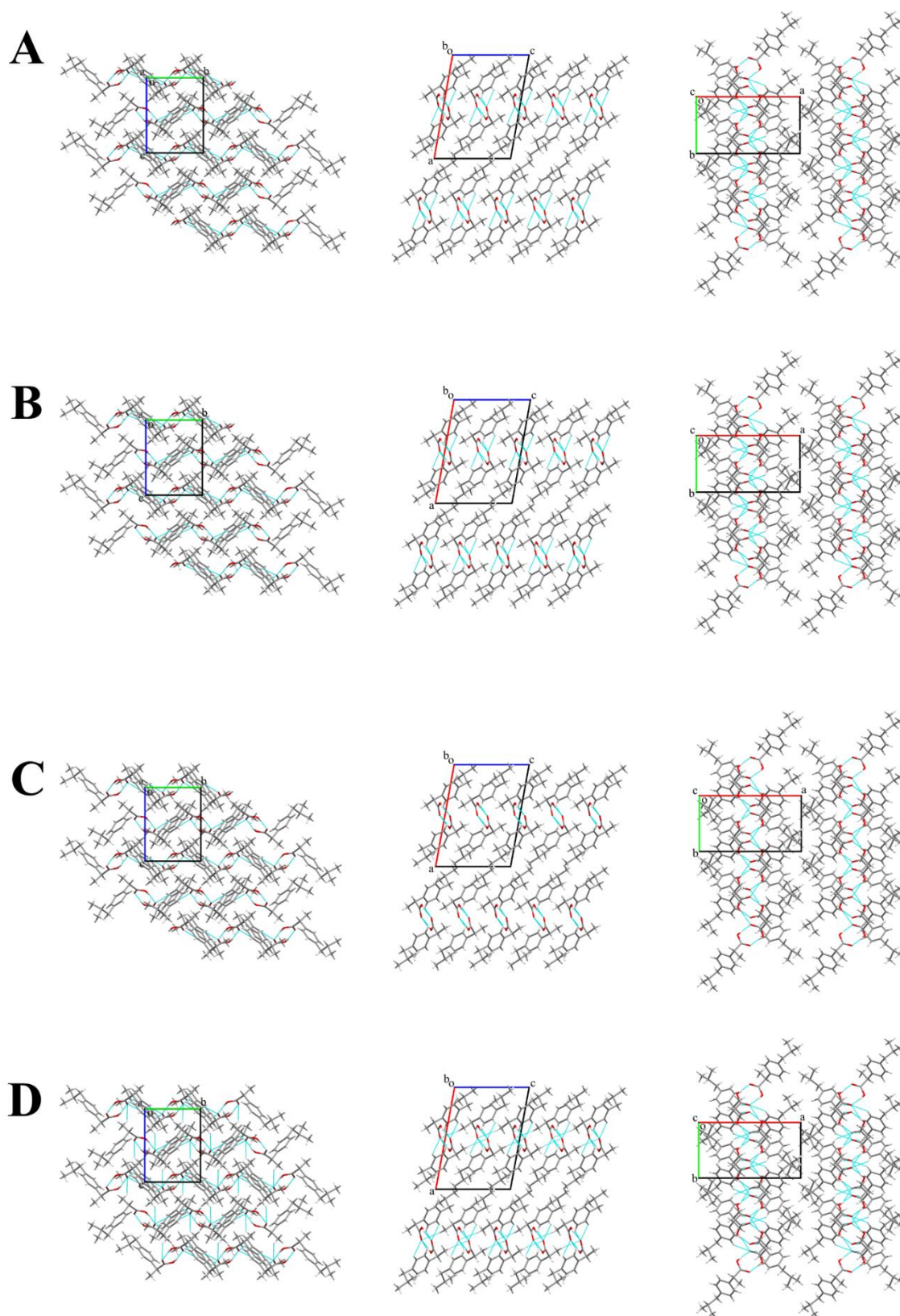


Figure A 4.26. Packing of the molecules in the crystals of ibuprofen polymorph I under the pressure of 0.80 (A), 0.88 (B), 1.70 (C) and 1.89 GPa (D). The projections in  $a$  (on the right),  $b$  (in the middle),  $c$  (on the left) crystallographic directions are represented.

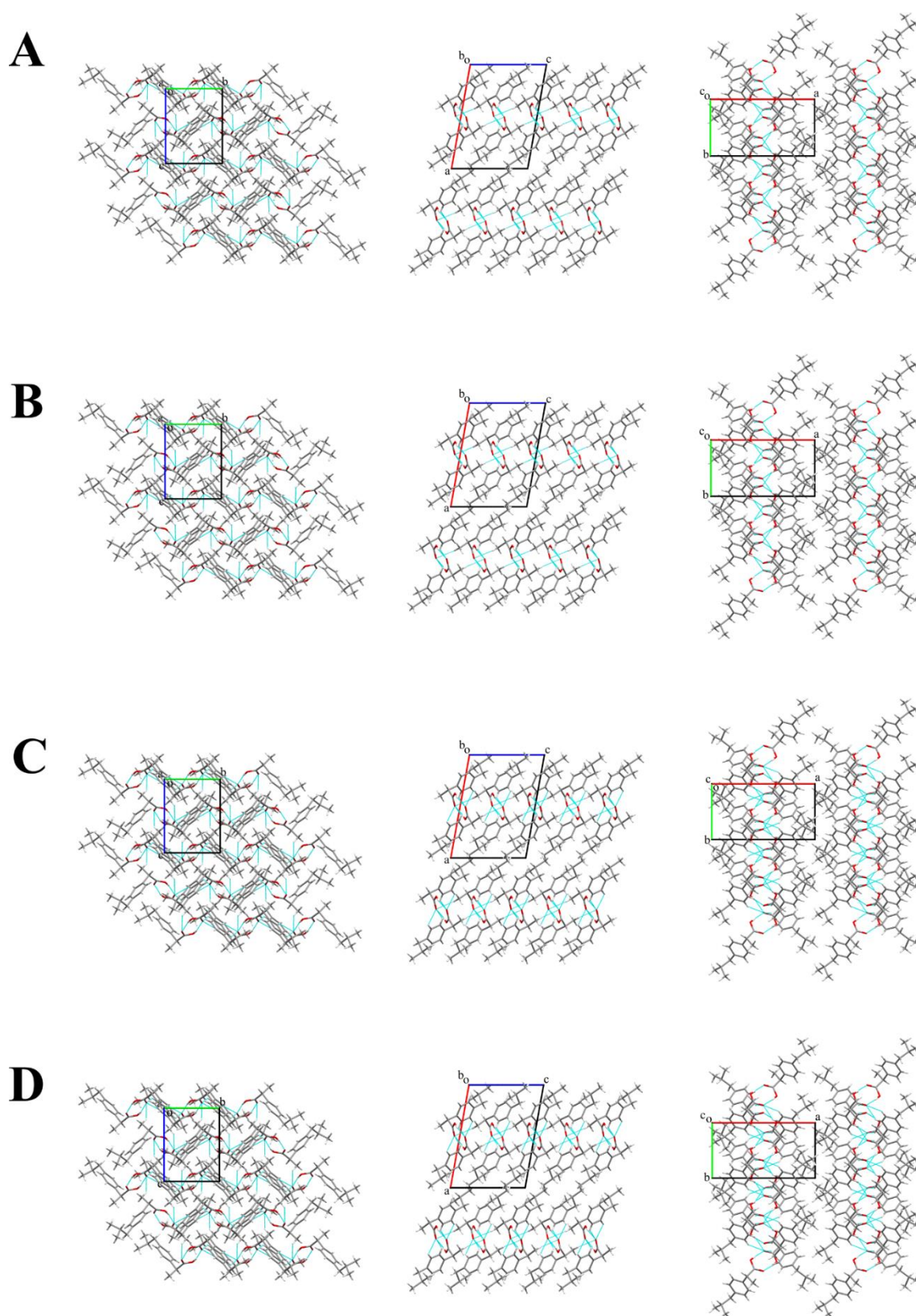


Figure A 4.27. Packing of the molecules in the crystals of ibuprofen polymorph I under the pressure of 2.32 (A), 2.65 (B), 3.46 (C) and 4.00 GPa (D). The projections in  $a$  (on the right),  $b$  (in the middle),  $c$  (on the left) crystallographic directions are represented.

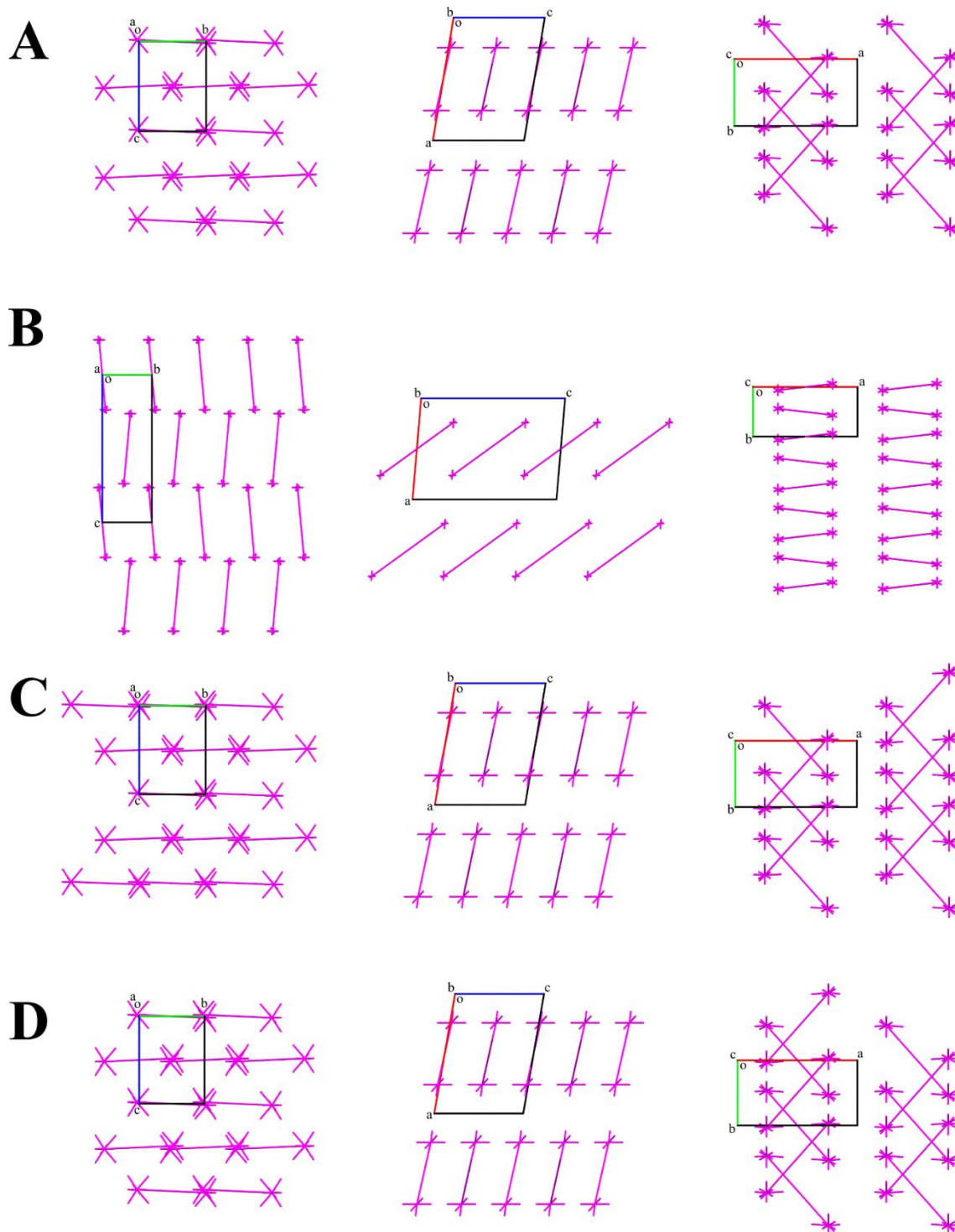


Figure A 4.28. Packing of the energy vector diagrams representing the pairwise interaction energy distribution of monomeric building units in the crystals of ibuprofen polymorphs I (A) and II (B) at ambient pressure and polymorph I under the pressure of 0.23 (C) and 0.60 GPa (D). The projections in  $a$  (on the right),  $b$  (in the middle),  $c$  (on the left) crystallographic directions are represented.

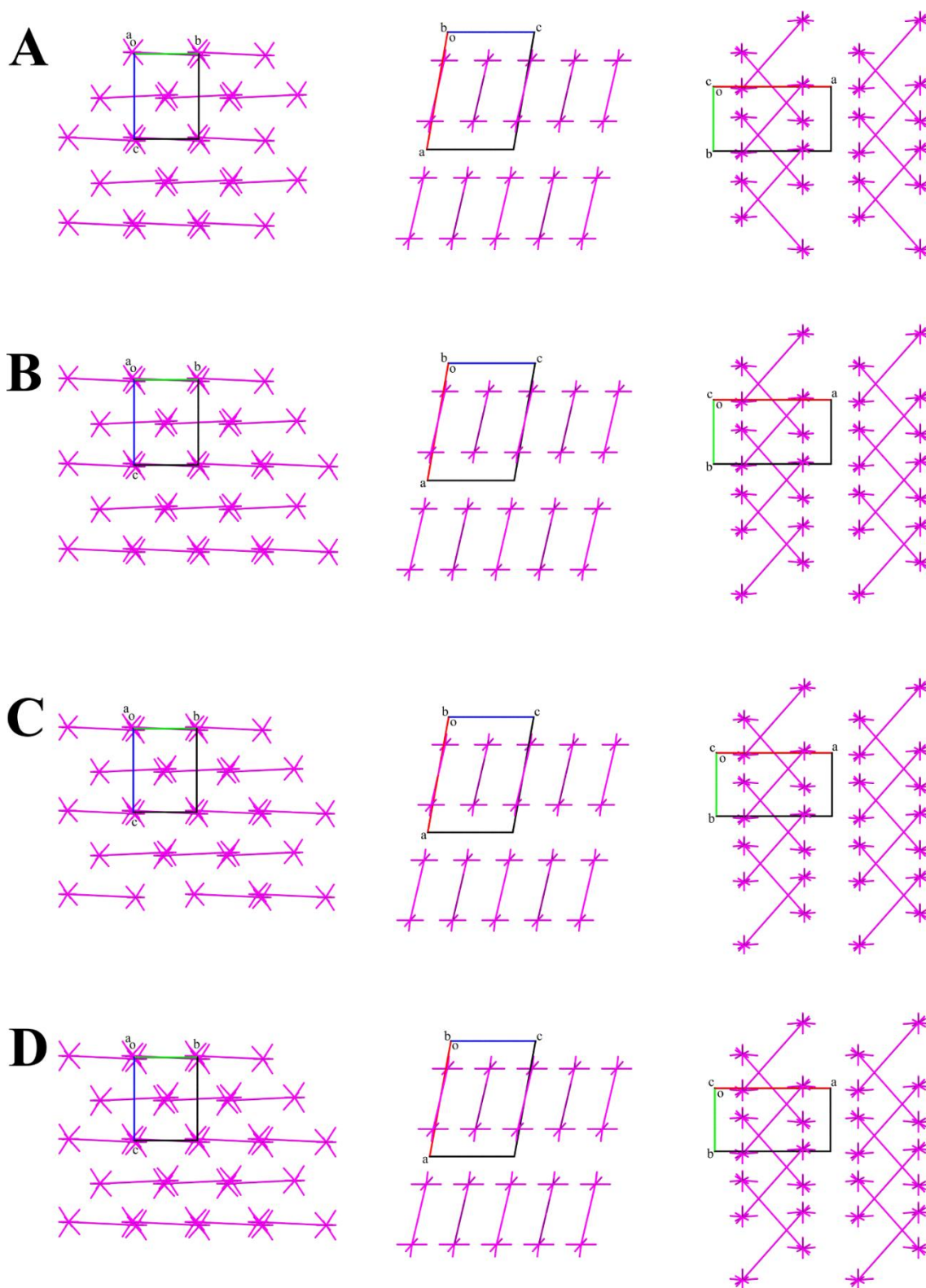


Figure A 4.29. Packing of the energy vector diagrams representing the pairwise interaction energy distribution of monomeric building units in the crystals of ibuprofen polymorph I under the pressure of 0.80 (A), 0.88 (B), 1.70 (C) and 1.89 GPa (D). The projections in  $a$  (on the right),  $b$  (in the middle),  $c$  (on the left) crystallographic directions are represented.

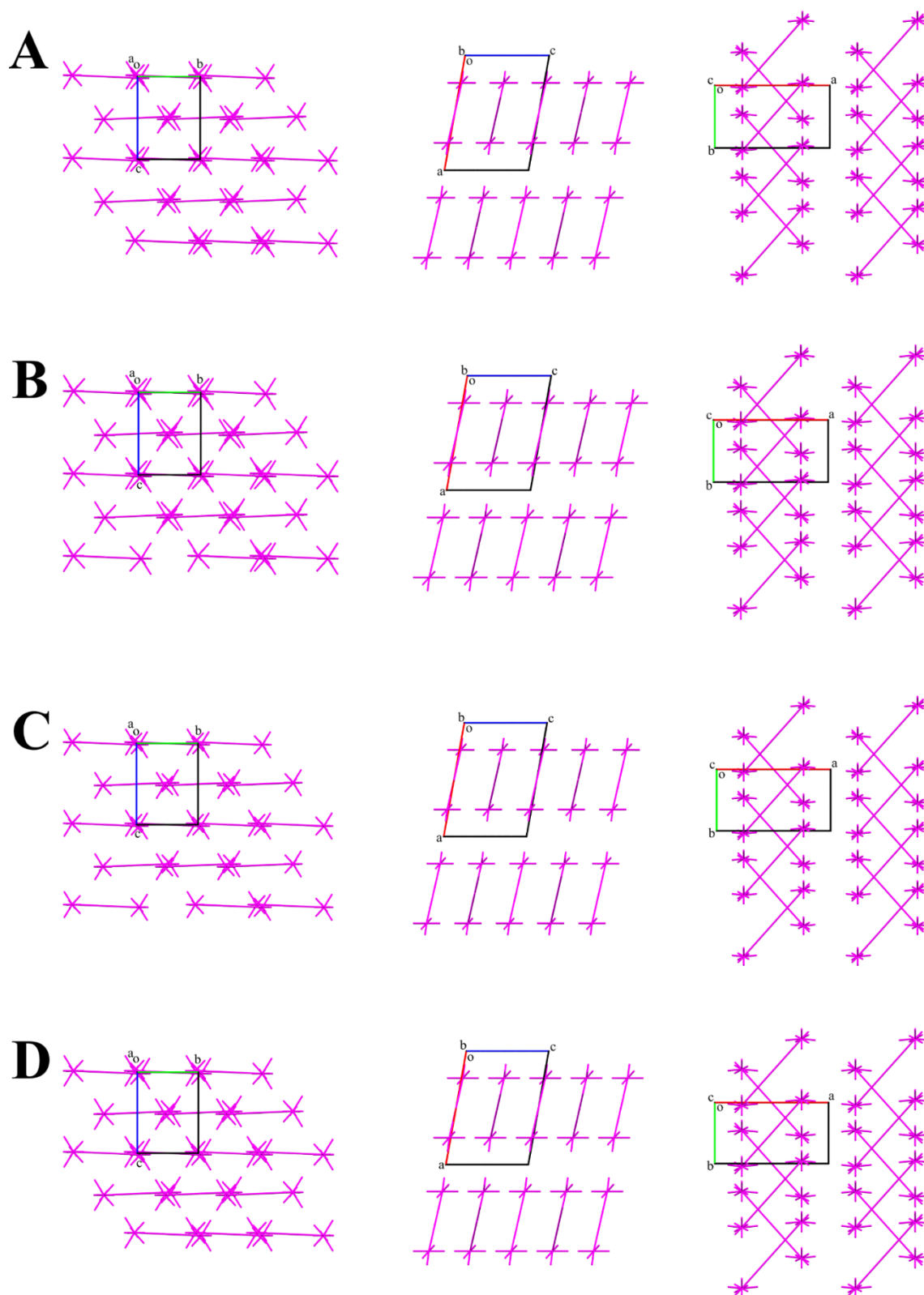


Figure A 4.30. Packing of the energy vector diagrams representing the pairwise interaction energy distribution of monomeric building units in the crystals of ibuprofen polymorph I under the pressure of 2.32 (A), 2.65 (B), 3.46 (C) and 4.00 GPa (D). The projections in  $a$  (on the right),  $b$  (in the middle),  $c$  (on the left) crystallographic directions are represented.

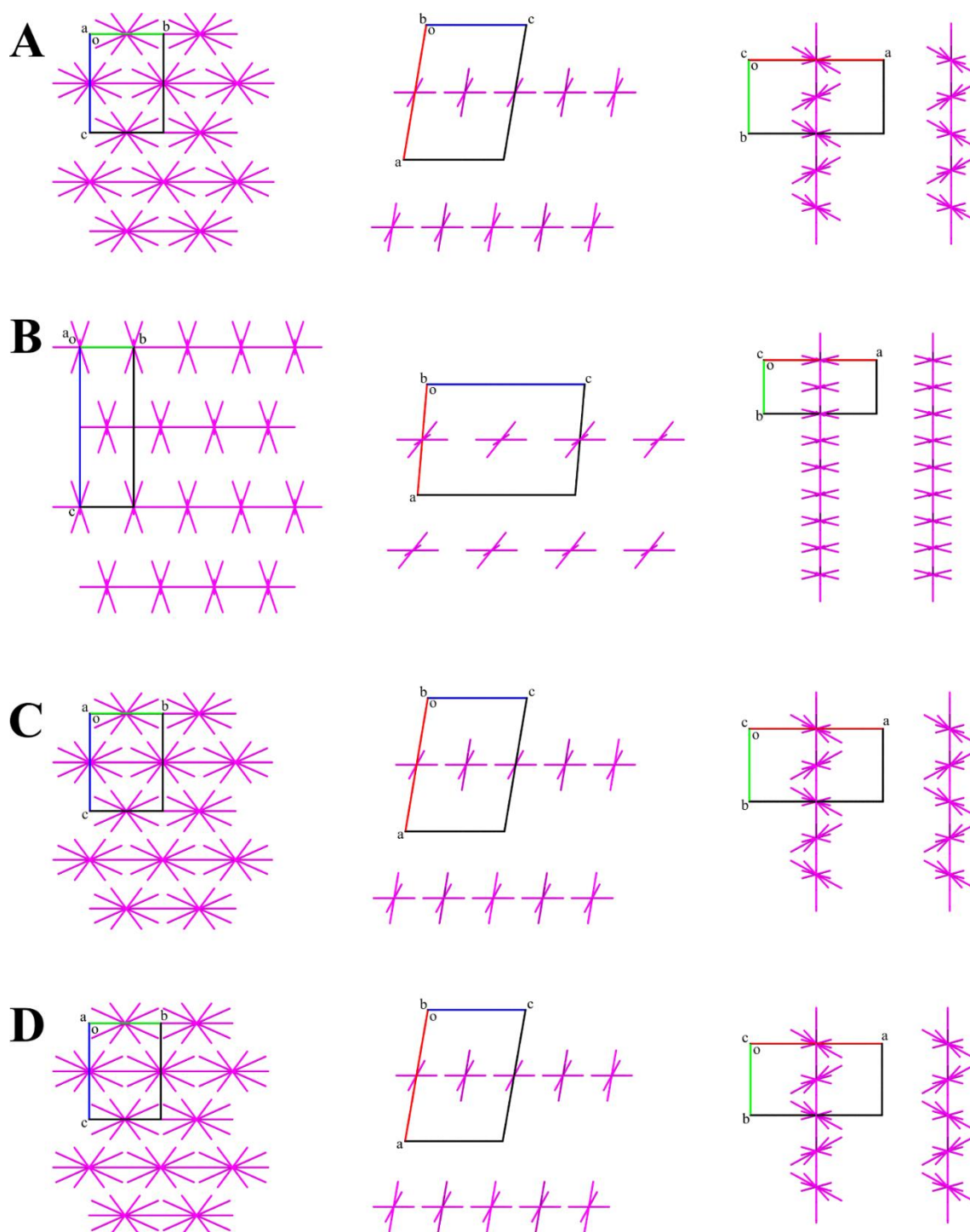


Figure A 4.31. Packing of the energy vector diagrams representing the pairwise interaction energy distribution of dimeric building units in the crystals of ibuprofen polymorphs I (A) and II (B) at ambient pressure and polymorph I under the pressure of 0.23 (C) and 0.60 GPa (D). The projections in  $a$  (on the right),  $b$  (in the middle),  $c$  (on the left) crystallographic directions are represented.

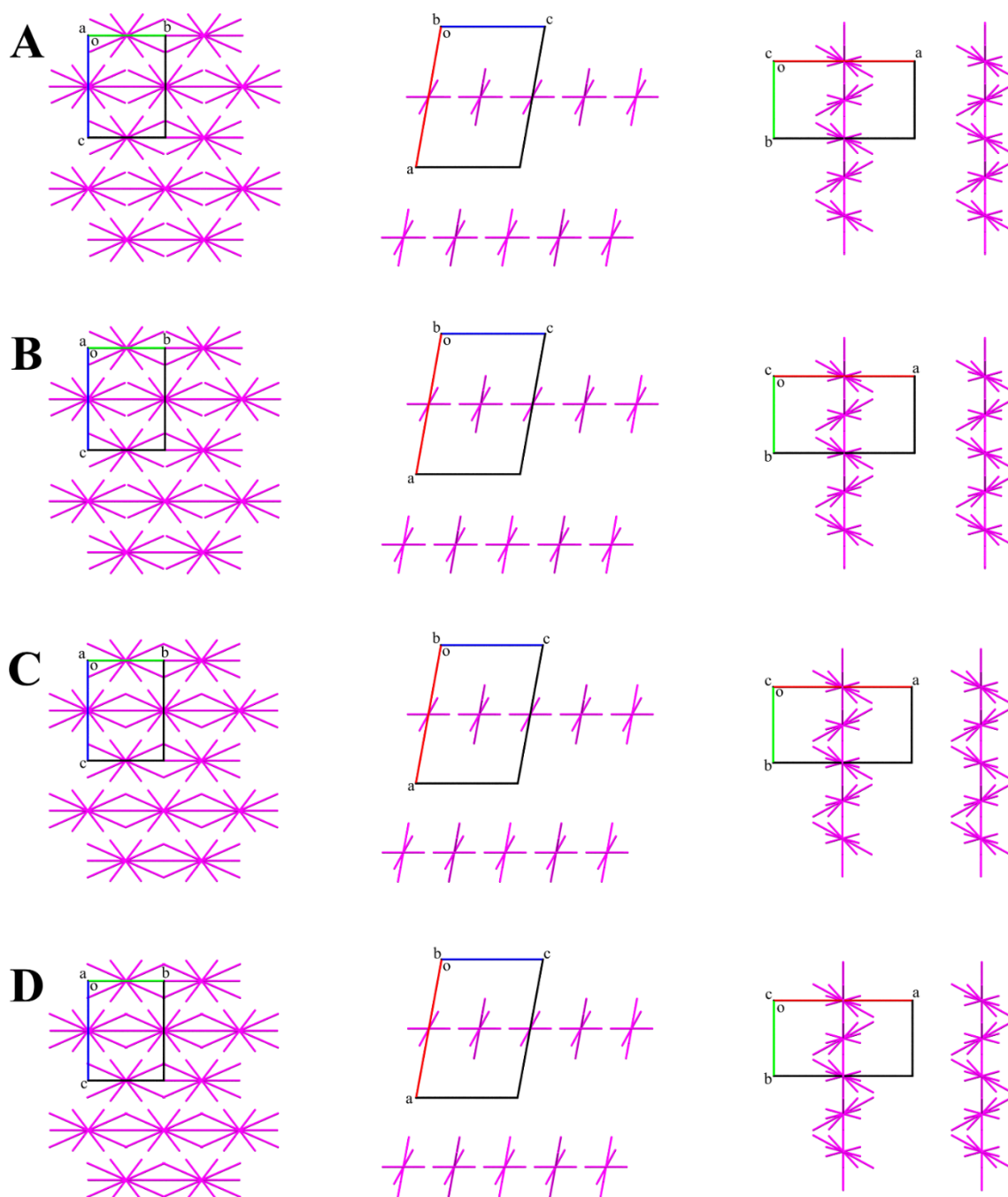


Figure A 4.32. Packing of the energy vector diagrams representing the pairwise interaction energy distribution of dimeric building units in the crystals of ibuprofen polymorph I under the pressure of 0.80 (A), 0.88 (B), 1.70 (C) and 1.89 GPa (D). The projections in  $a$  (on the right),  $b$  (in the middle),  $c$  (on the left) crystallographic directions are represented.

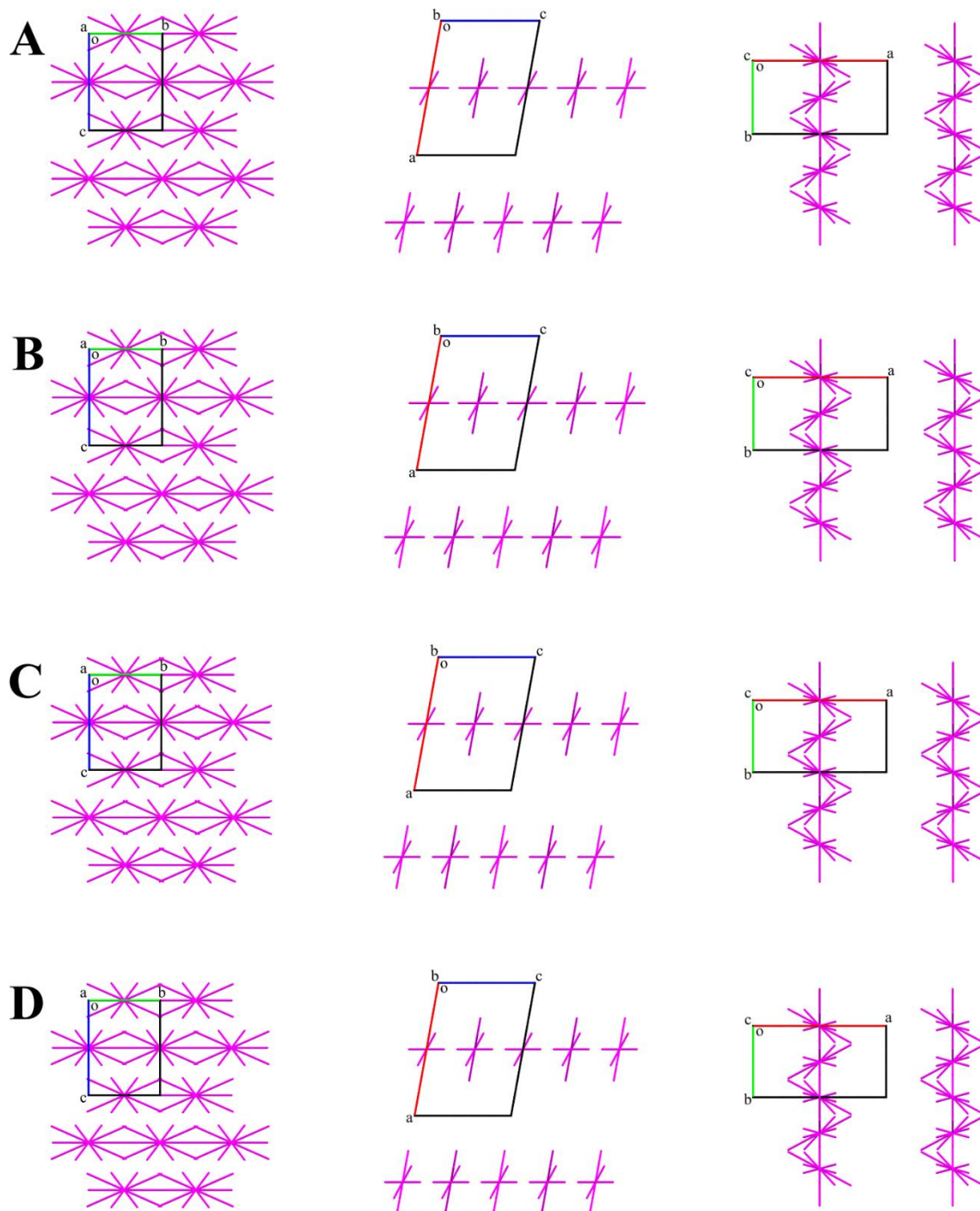


Figure A 4.33. Packing of the energy vector diagrams representing the pairwise interaction energy distribution of dimeric building units in the crystals of ibuprofen polymorph I under the pressure of 2.32 (A), 2.65 (B), 3.46 (C) and 4.00 GPa (D). The projections in  $a$  (on the right),  $b$  (in the middle),  $c$  (on the left) crystallographic directions are represented.

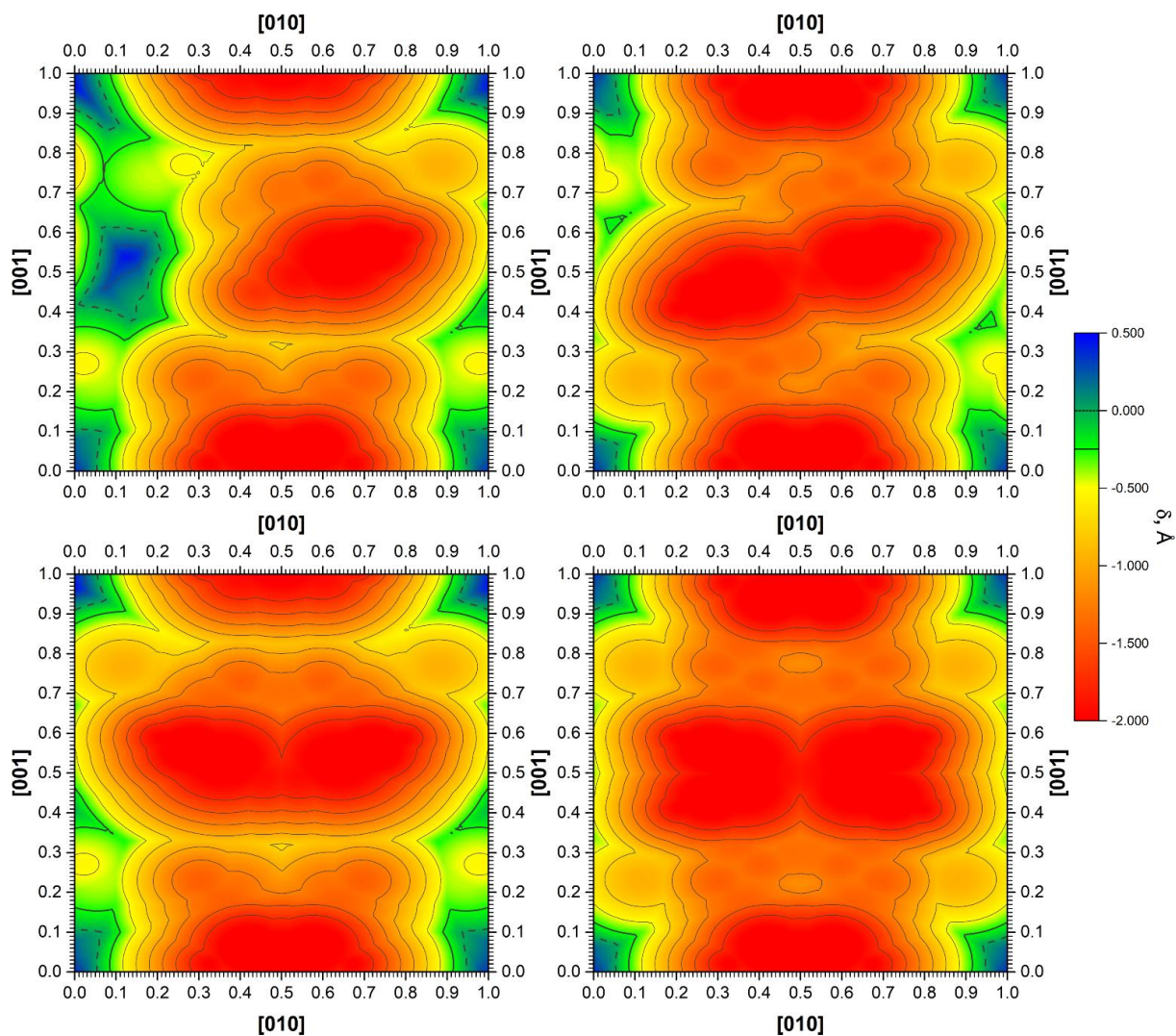


Figure A 4.34. Maps of  $\delta$  ( $\text{\AA}$ ) occurring during the shear of the dimeric motile part in relation to the fixed one in (100) plane ([010] and [001] directions of shift) in the crystals of ibuprofen polymorphic form I at ambient pressure for the following cases: motile dimer symmetry is not considered (at the top) and both rotated equivalents in the motile part are taken into account (at the bottom) for the systems with one (on the left) and two neighboring layers (on the right). Dashed contour surrounds the zones without the shortening of interatomic distances below the corresponding sum of van der Waals radii ( $\delta$ ). Bold contour surrounds zones with  $\delta$  smaller than  $-0.25 \text{ \AA}$ .

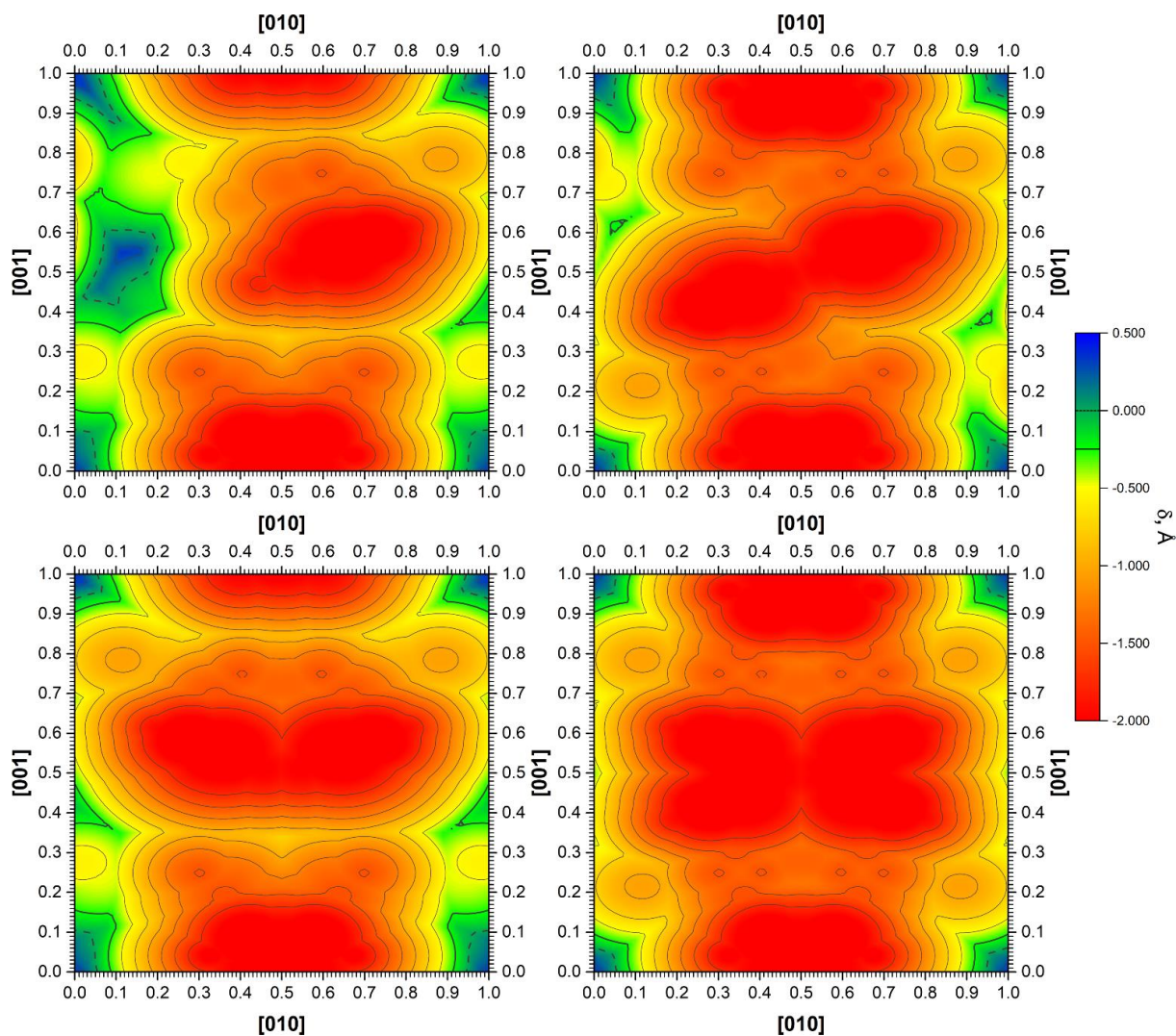


Figure A 4.35. Maps of  $\delta$  ( $\text{\AA}$ ) occurring during the shear of the dimeric motile part in relation to the fixed one in (100) plane ([010] and [001] directions of shift) in the crystals of ibuprofen polymorphic form I under the pressure of 0.23 GPa for the following cases: motile dimer symmetry is not considered (at the top) and both rotated equivalents in the motile part are taken into account (at the bottom) for the systems with one (on the left) and two neighboring layers (on the right). Dashed contour surrounds the zones without the shortening of interatomic distances below the corresponding sum of van der Waals radii ( $\delta$ ). Bold contour surrounds zones with  $\delta$  smaller than  $-0.25 \text{ \AA}$ .

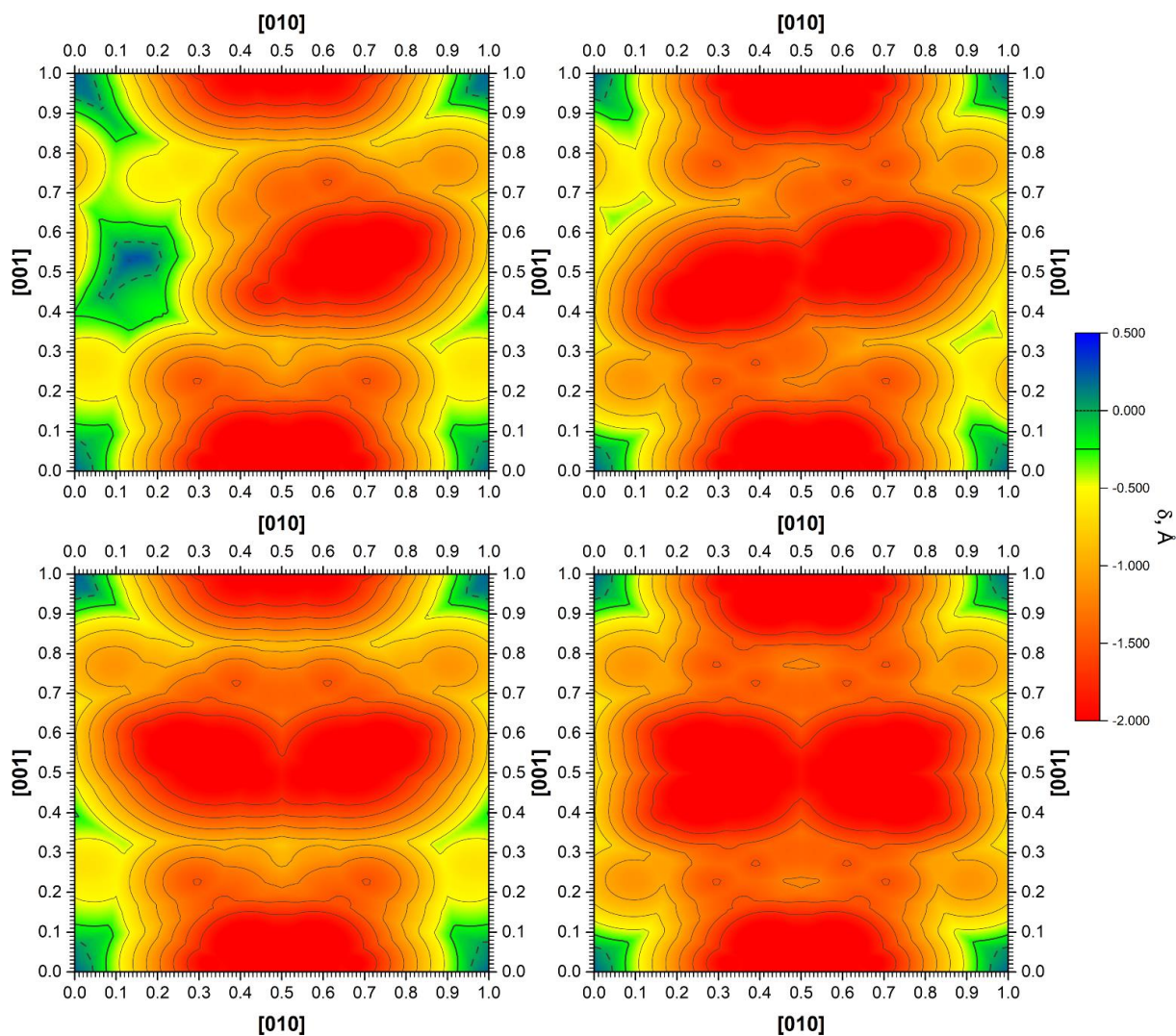


Figure A 4.36. Maps of  $\delta$  ( $\text{\AA}$ ) occurring during the shear of the dimeric motile part in relation to the fixed one in (100) plane ([010] and [001] directions of shift) in the crystals of ibuprofen polymorphic form I under the pressure of 0.60 GPa for the following cases: motile dimer symmetry is not considered (at the top) and both rotated equivalents in the motile part are taken into account (at the bottom) for the systems with one (on the left) and two neighboring layers (on the right). Dashed contour surrounds the zones without the shortening of interatomic distances below the corresponding sum of van der Waals radii ( $\delta$ ). Bold contour surrounds zones with  $\delta$  smaller than  $-0.25 \text{ \AA}$ .

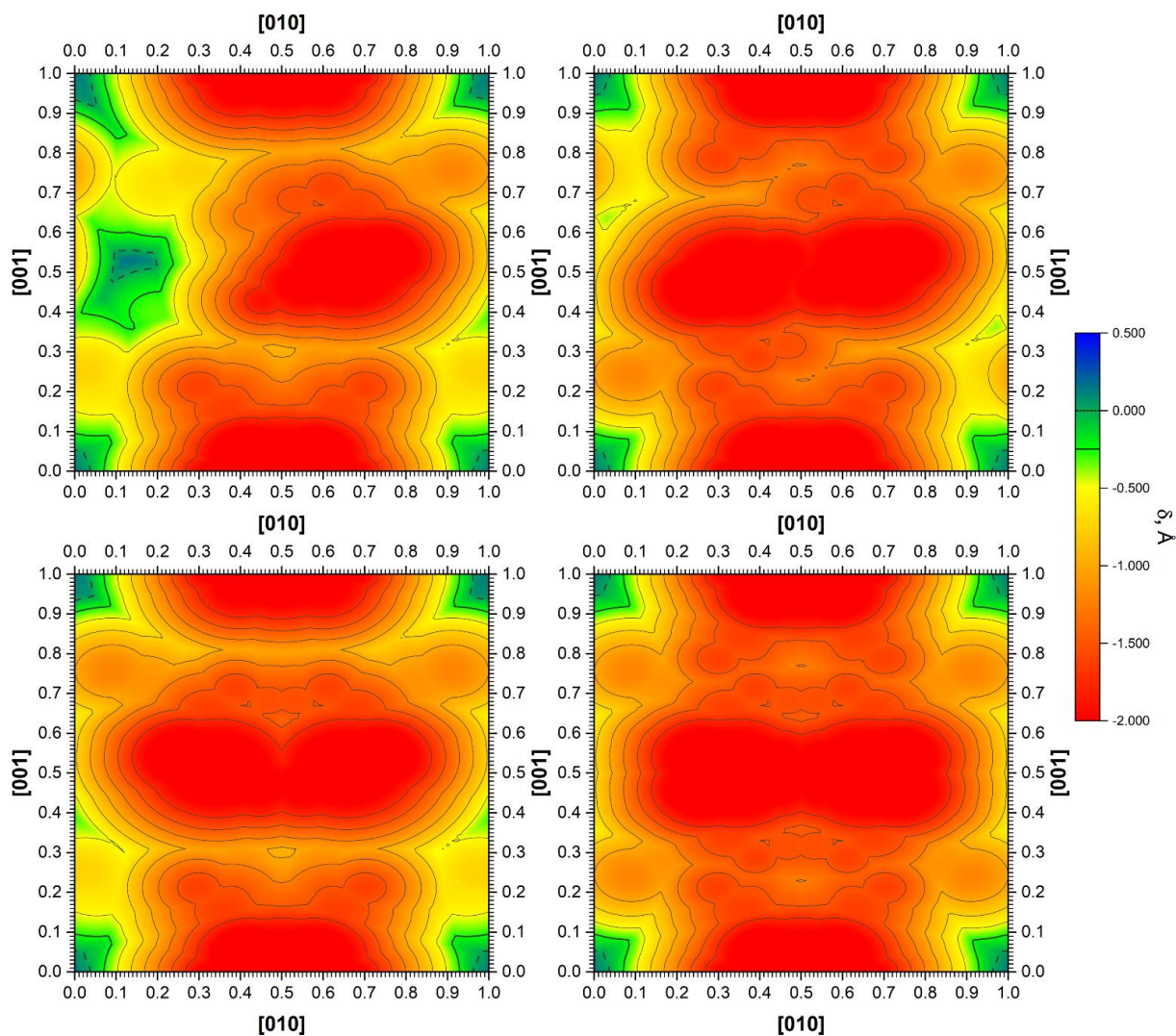


Figure A 4.37. Maps of  $\delta$  ( $\text{\AA}$ ) occurring during the shear of the dimeric motile part in relation to the fixed one in (100) plane ([010] and [001] directions of shift) in the crystals of ibuprofen polymorphic form I under the pressure of 0.80 GPa for the following cases: motile dimer symmetry is not considered (at the top) and both rotated equivalents in the motile part are taken into account (at the bottom) for the systems with one (on the left) and two neighboring layers (on the right). Dashed contour surrounds the zones without the shortening of interatomic distances below the corresponding sum of van der Waals radii ( $\delta$ ). Bold contour surrounds zones with  $\delta$  smaller than  $-0.25 \text{ \AA}$ .

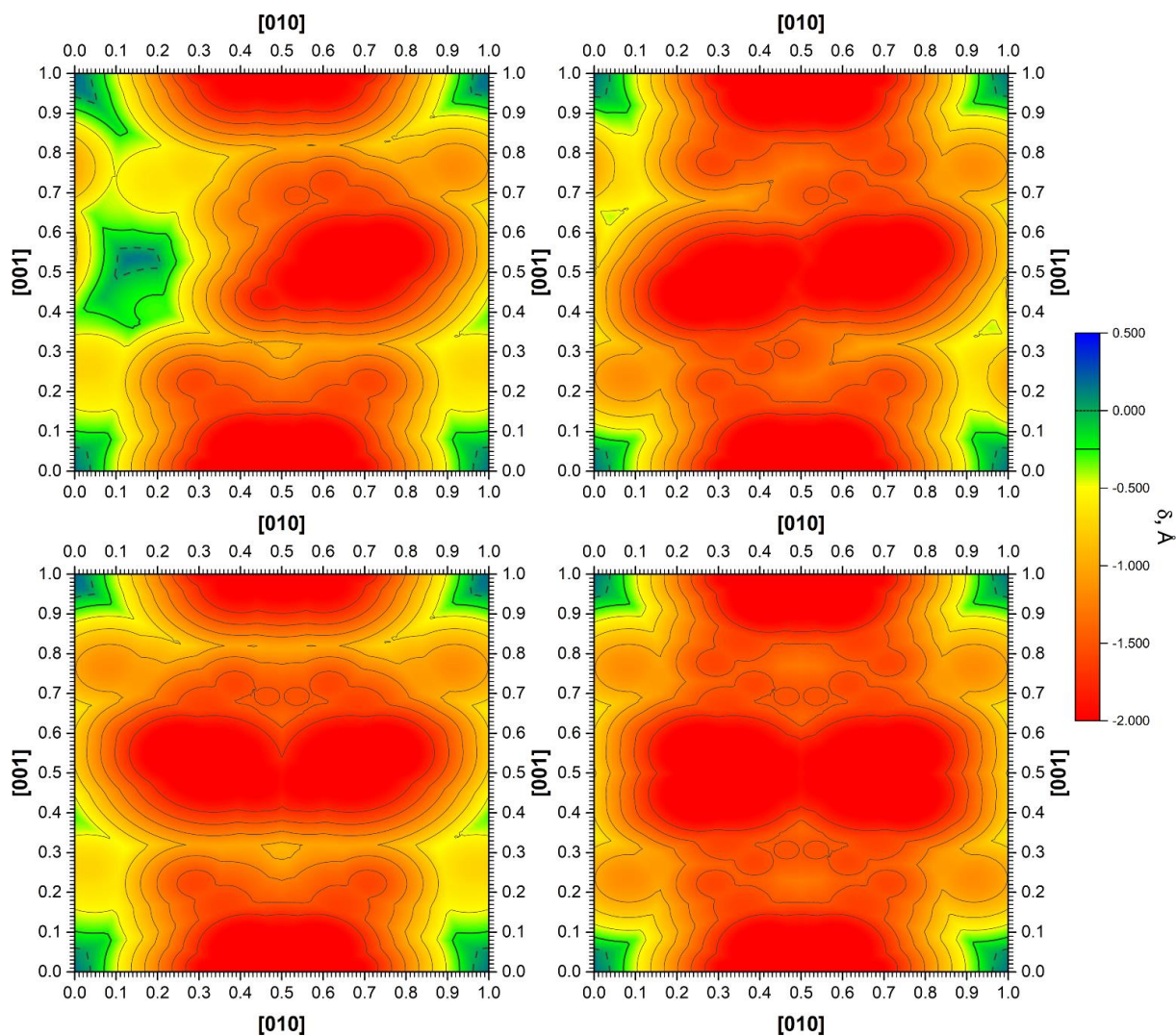


Figure A 4.38. Maps of  $\delta$  ( $\text{\AA}$ ) occurring during the shear of the dimeric motile part in relation to the fixed one in (100) plane ([010] and [001] directions of shift) in the crystals of ibuprofen polymorphic form I under the pressure of 0.88 GPa for the following cases: motile dimer symmetry is not considered (at the top) and both rotated equivalents in the motile part are taken into account (at the bottom) for the systems with one (on the left) and two neighboring layers (on the right). Dashed contour surrounds the zones without the shortening of interatomic distances below the corresponding sum of van der Waals radii ( $\delta$ ). Bold contour surrounds zones with  $\delta$  smaller than  $-0.25 \text{ \AA}$ .

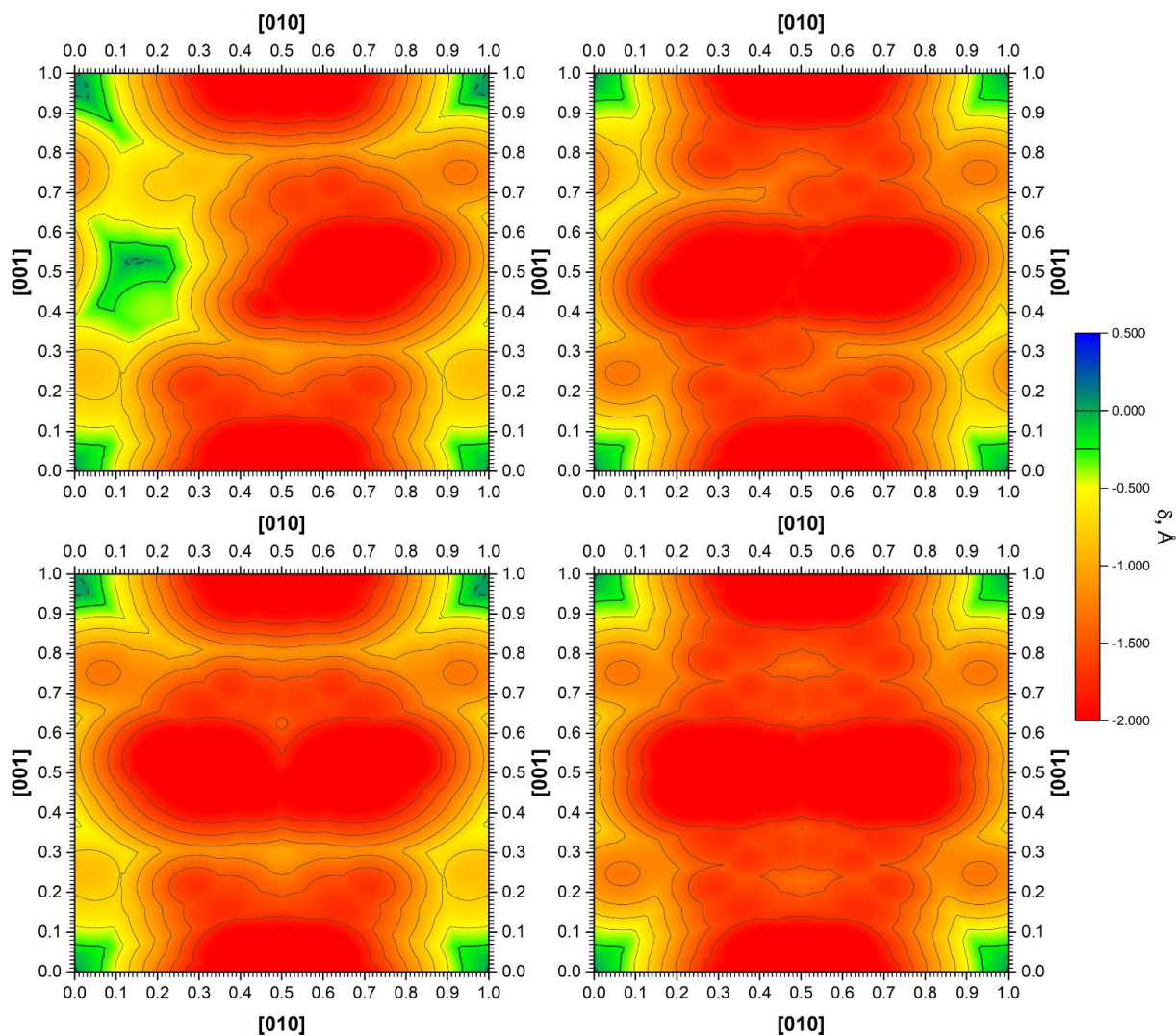


Figure A 4.39. Maps of  $\delta$  ( $\text{\AA}$ ) occurring during the shear of the dimeric motile part in relation to the fixed one in (100) plane ([010] and [001] directions of shift) in the crystals of ibuprofen polymorphic form I under the pressure of 1.70 GPa for the following cases: motile dimer symmetry is not considered (at the top) and both rotated equivalents in the motile part are taken into account (at the bottom) for the systems with one (on the left) and two neighboring layers (on the right). Dashed contour surrounds the zones without the shortening of interatomic distances below the corresponding sum of van der Waals radii ( $\delta$ ). Bold contour surrounds zones with  $\delta$  smaller than  $-0.25 \text{ \AA}$ .

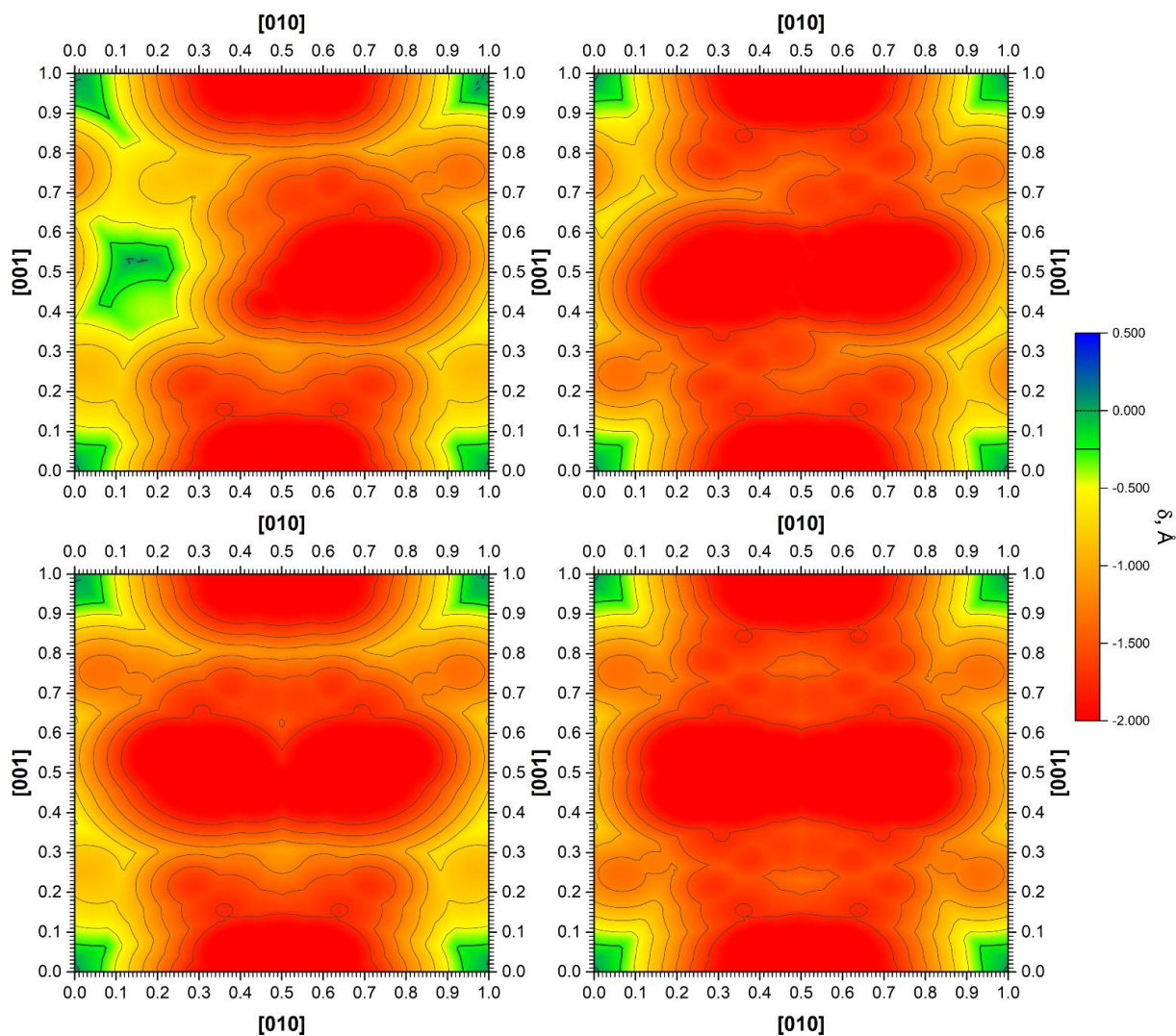


Figure A 4.40. Maps of  $\delta$  ( $\text{\AA}$ ) occurring during the shear of the dimeric motile part in relation to the fixed one in (100) plane ([010] and [001] directions of shift) in the crystals of ibuprofen polymorphic form I under the pressure of 1.89 GPa for the following cases: motile dimer symmetry is not considered (at the top) and both rotated equivalents in the motile part are taken into account (at the bottom) for the systems with one (on the left) and two neighboring layers (on the right). Dashed contour surrounds the zones without the shortening of interatomic distances below the corresponding sum of van der Waals radii ( $\delta$ ). Bold contour surrounds zones with  $\delta$  smaller than  $-0.25 \text{ \AA}$ .

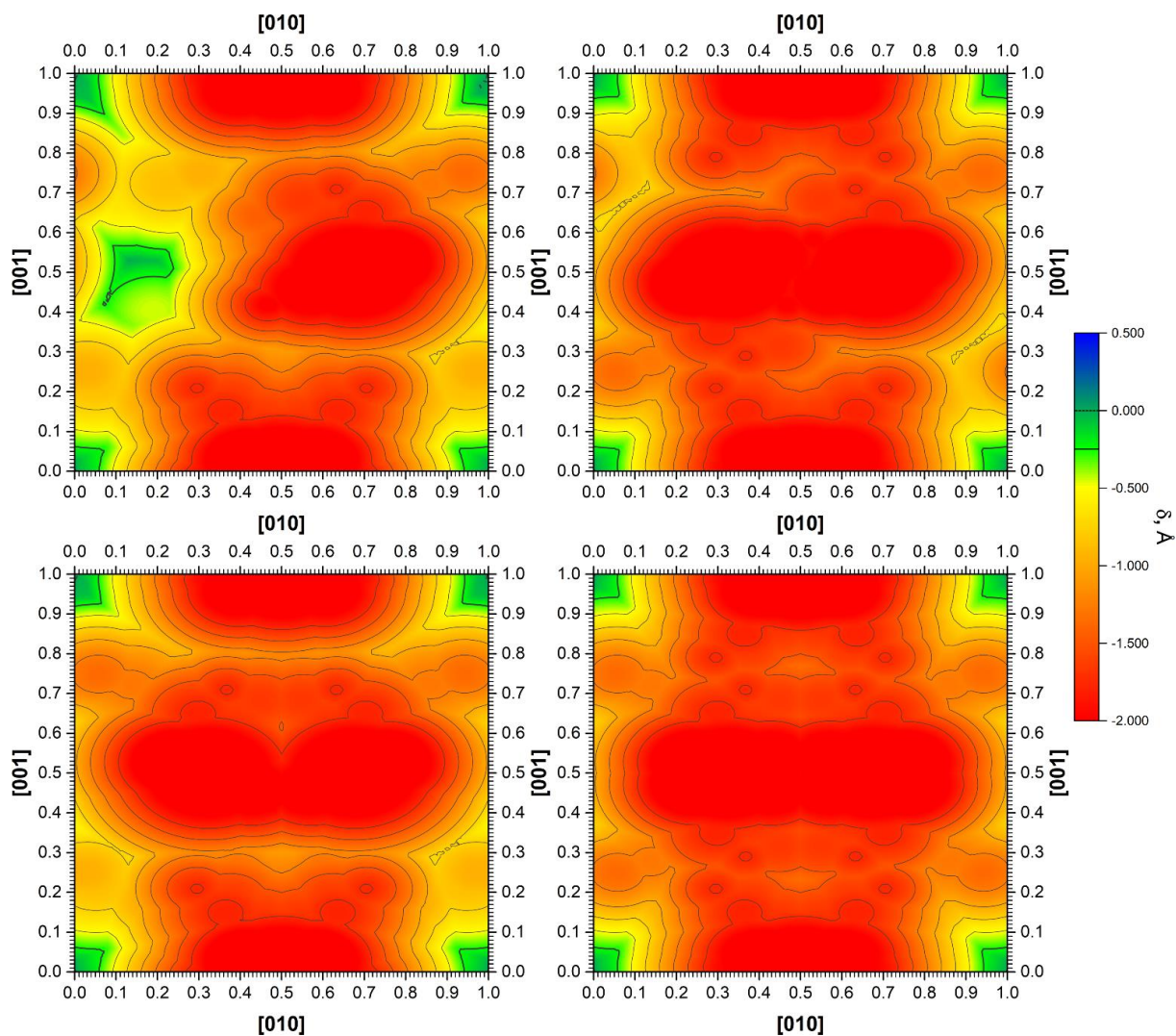


Figure A 4.41. Maps of  $\delta$  ( $\text{\AA}$ ) occurring during the shear of the dimeric motile part in relation to the fixed one in (100) plane ([010] and [001] directions of shift) in the crystals of ibuprofen polymorphic form I under the pressure of 2.32 GPa for the following cases: motile dimer symmetry is not considered (at the top) and both rotated equivalents in the motile part are taken into account (at the bottom) for the systems with one (on the left) and two neighboring layers (on the right). Dashed contour surrounds the zones without the shortening of interatomic distances below the corresponding sum of van der Waals radii ( $\delta$ ). Bold contour surrounds zones with  $\delta$  smaller than  $-0.25 \text{ \AA}$ .

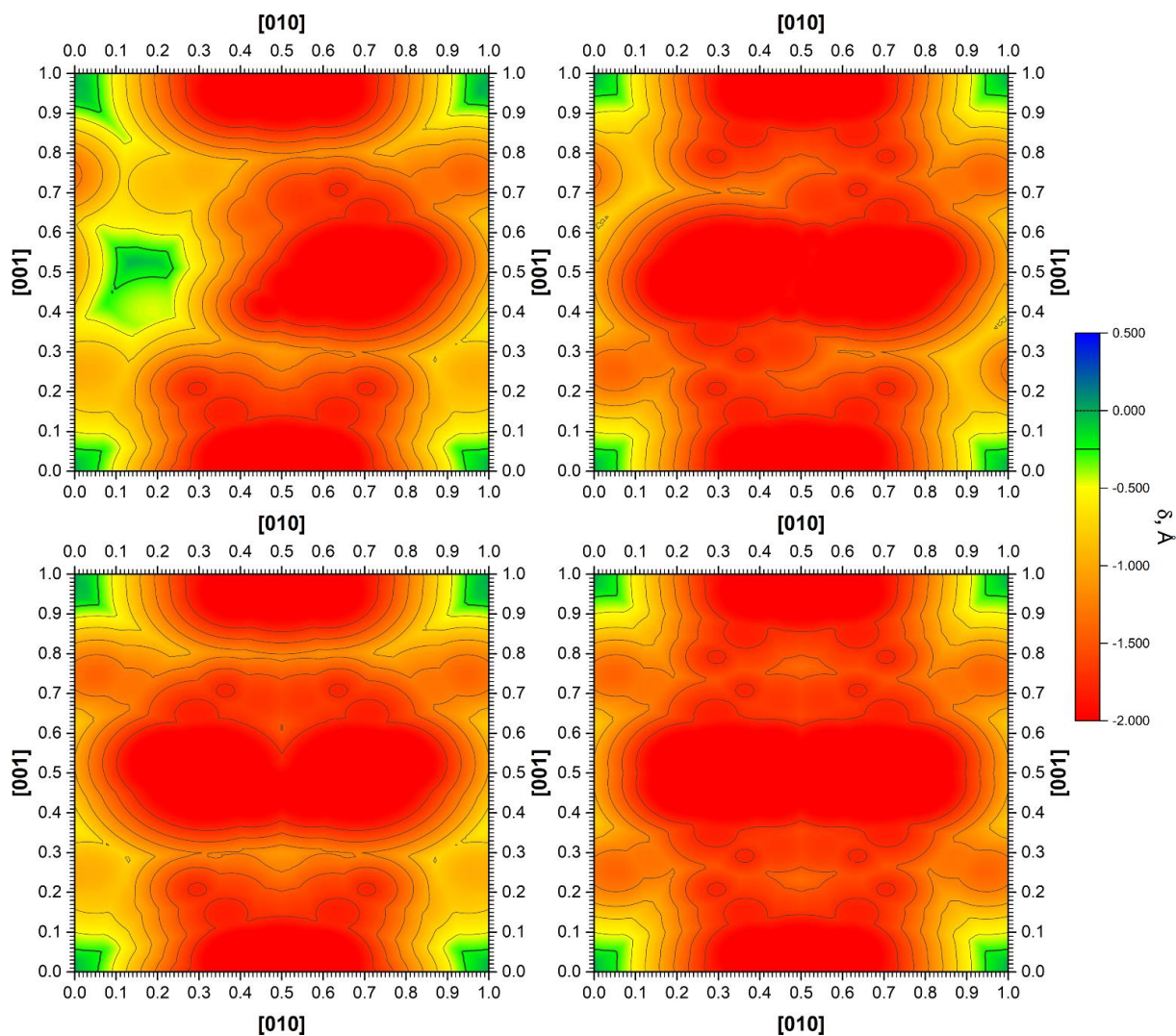


Figure A 4.42. Maps of  $\delta$  ( $\text{\AA}$ ) occurring during the shear of the dimeric motile part in relation to the fixed one in (100) plane ([010] and [001] directions of shift) in the crystals of ibuprofen polymorphic form I under the pressure of 2.65 GPa for the following cases: motile dimer symmetry is not considered (at the top) and both rotated equivalents in the motile part are taken into account (at the bottom) for the systems with one (on the left) and two neighboring layers (on the right). Dashed contour surrounds the zones without the shortening of interatomic distances below the corresponding sum of van der Waals radii ( $\delta$ ). Bold contour surrounds zones with  $\delta$  smaller than  $-0.25 \text{ \AA}$ .

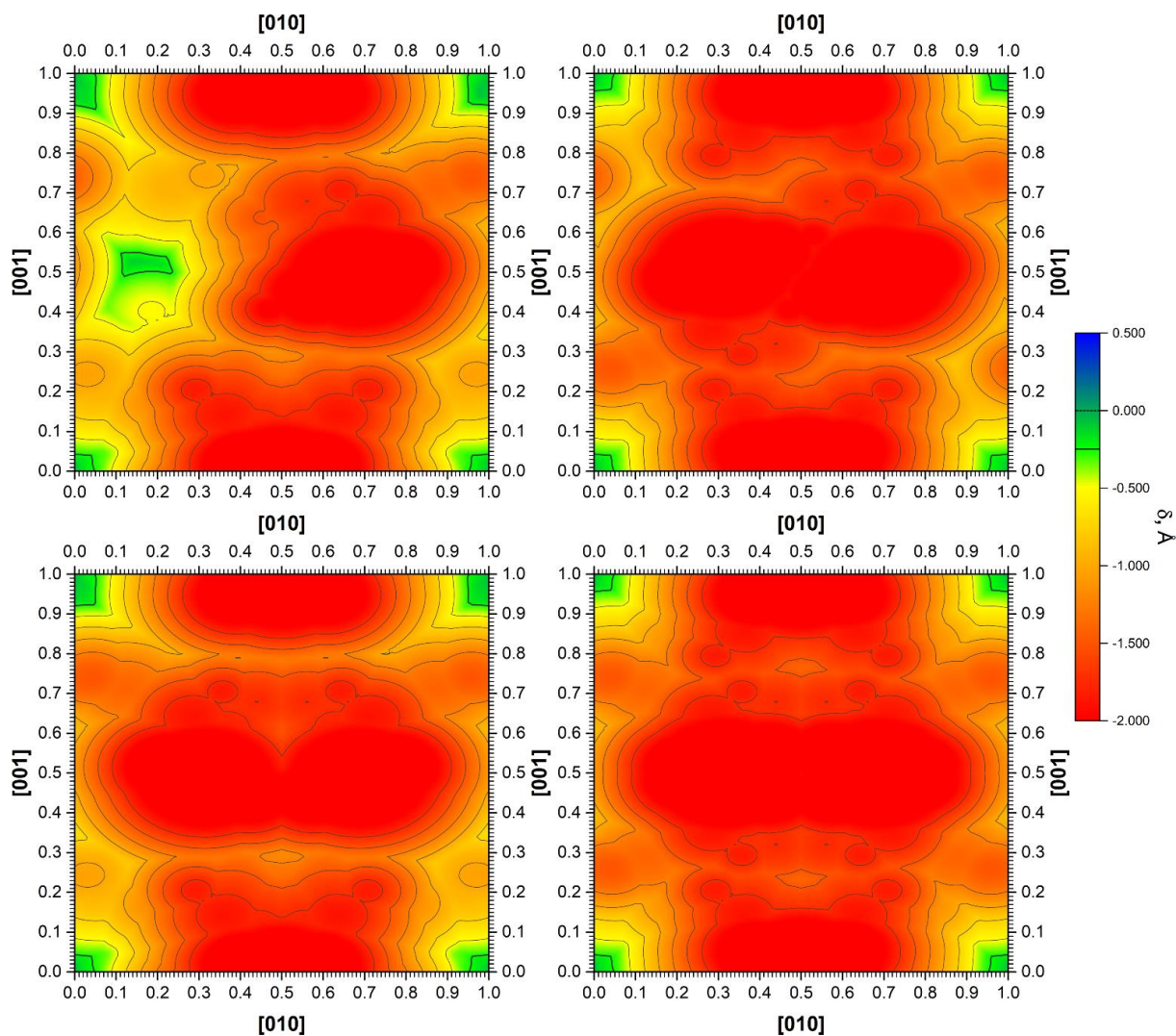


Figure A 4.43. Maps of  $\delta$  ( $\text{\AA}$ ) occurring during the shear of the dimeric motile part in relation to the fixed one in (100) plane ([010] and [001] directions of shift) in the crystals of ibuprofen polymorphic form I under the pressure of 3.46 GPa for the following cases: motile dimer symmetry is not considered (at the top) and both rotated equivalents in the motile part are taken into account (at the bottom) for the systems with one (on the left) and two neighboring layers (on the right). Dashed contour surrounds the zones without the shortening of interatomic distances below the corresponding sum of van der Waals radii ( $\delta$ ). Bold contour surrounds zones with  $\delta$  smaller than  $-0.25 \text{ \AA}$ .

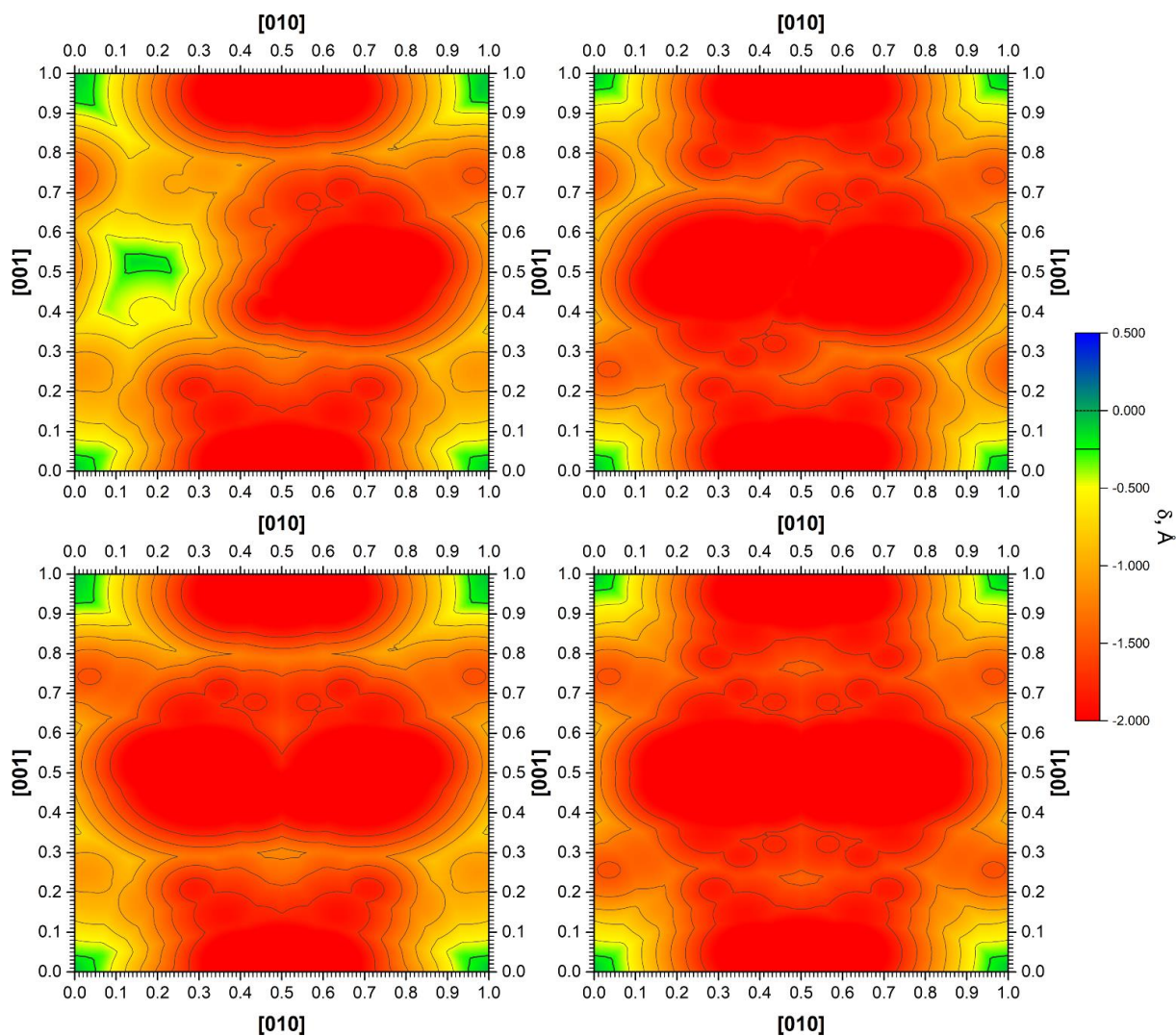


Figure A 4.44. Maps of  $\delta$  ( $\text{\AA}$ ) occurring during the shear of the dimeric motile part in relation to the fixed one in (100) plane ([010] and [001] directions of shift) in the crystals of ibuprofen polymorphic form I under the pressure of 4.00 GPa for the following cases: motile dimer symmetry is not considered (at the top) and both rotated equivalents in the motile part are taken into account (at the bottom) for the systems with one (on the left) and two neighboring layers (on the right). Dashed contour surrounds the zones without the shortening of interatomic distances below the corresponding sum of van der Waals radii ( $\delta$ ). Bold contour surrounds zones with  $\delta$  smaller than  $-0.25 \text{ \AA}$ .

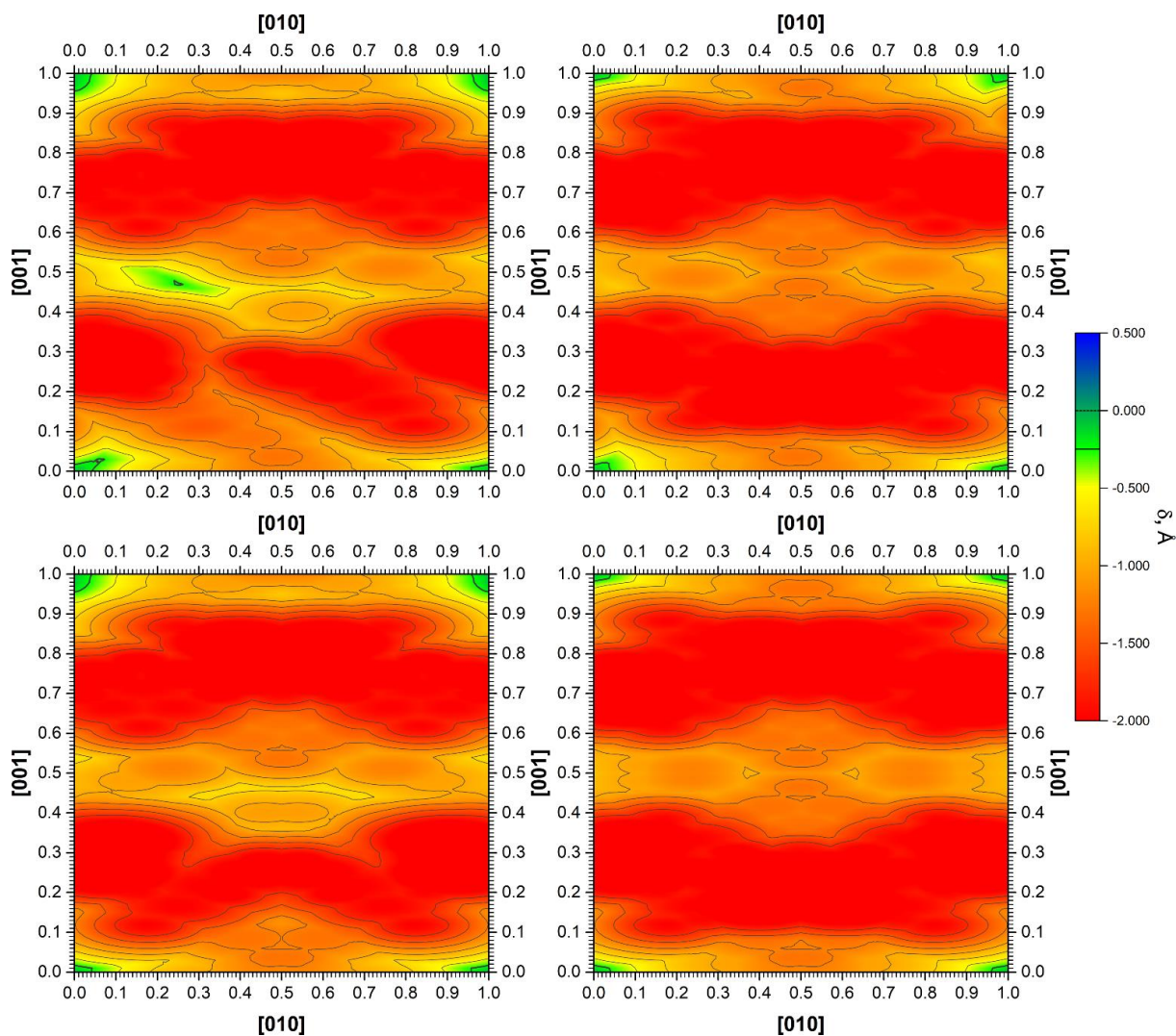


Figure A 4.45. Maps of  $\delta$  (Å) occurring during the shear of the dimeric motile part in relation to the fixed one in (100) plane ([010] and [001] directions of shift) in the crystals of ibuprofen polymorphic form II at ambient pressure for the following cases: motile dimer symmetry is not considered (at the top) and both rotated equivalents in the motile part are taken into account (at the bottom) for the systems with one (on the left) and two neighboring layers (on the right). Dashed contour surrounds the zones without the shortening of interatomic distances below the corresponding sum of van der Waals radii ( $\delta$ ). Bold contour surrounds zones with  $\delta$  smaller than  $-0.25$  Å.

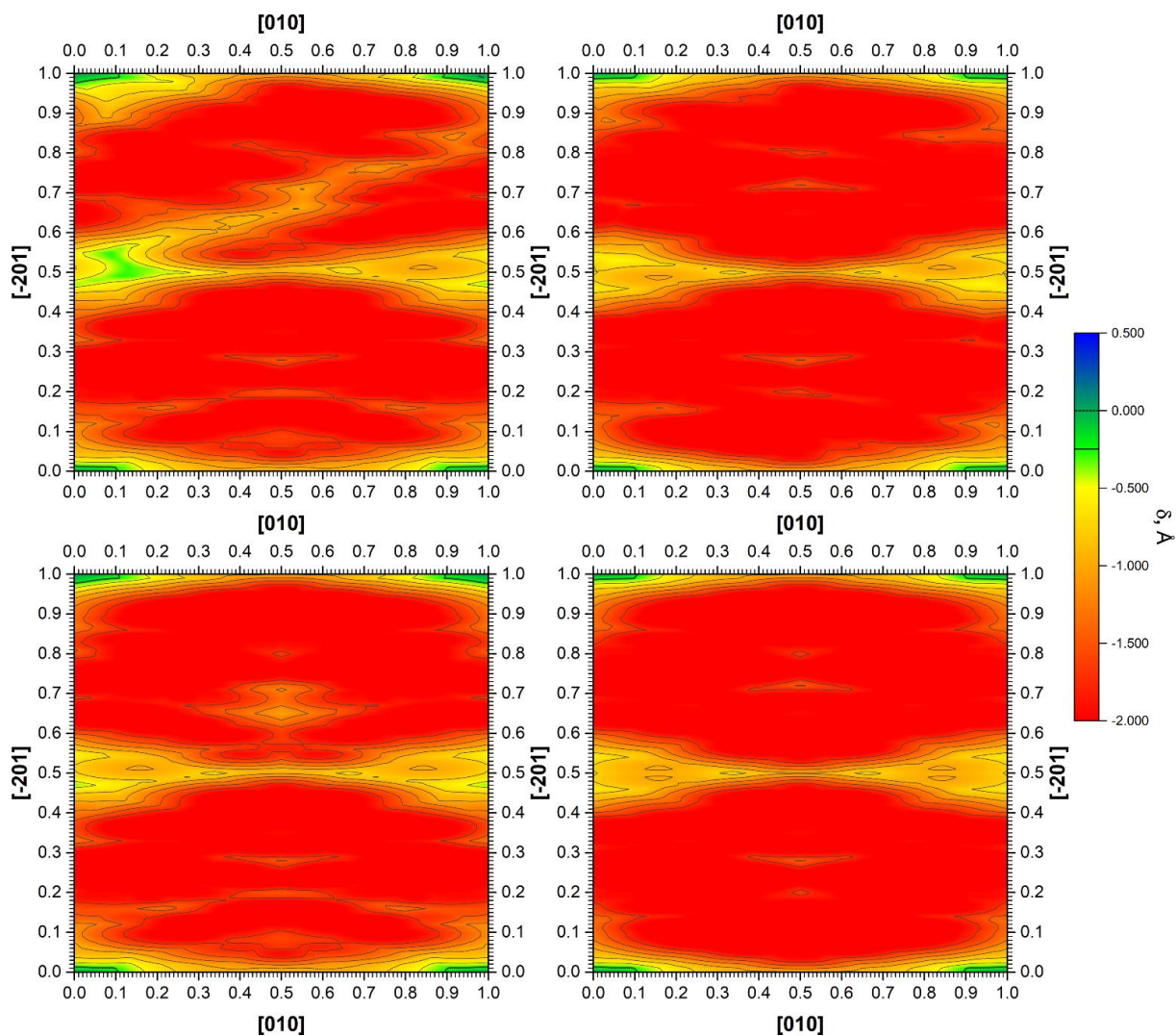


Figure A 4.46. Maps of  $\delta$  (Å) occurring during the shear of the dimeric motile part in relation to the fixed one in (102) plane ([010] and [-201] directions of shift) in the crystals of ibuprofen polymorphic form II at ambient pressure for the following cases: motile dimer symmetry is not considered (at the top) and both rotated equivalents in the motile part are taken into account (at the bottom) for the systems with one (on the left) and two neighboring layers (on the right). Dashed contour surrounds the zones without the shortening of interatomic distances below the corresponding sum of van der Waals radii ( $\delta$ ). Bold contour surrounds zones with  $\delta$  smaller than  $-0.25$  Å.

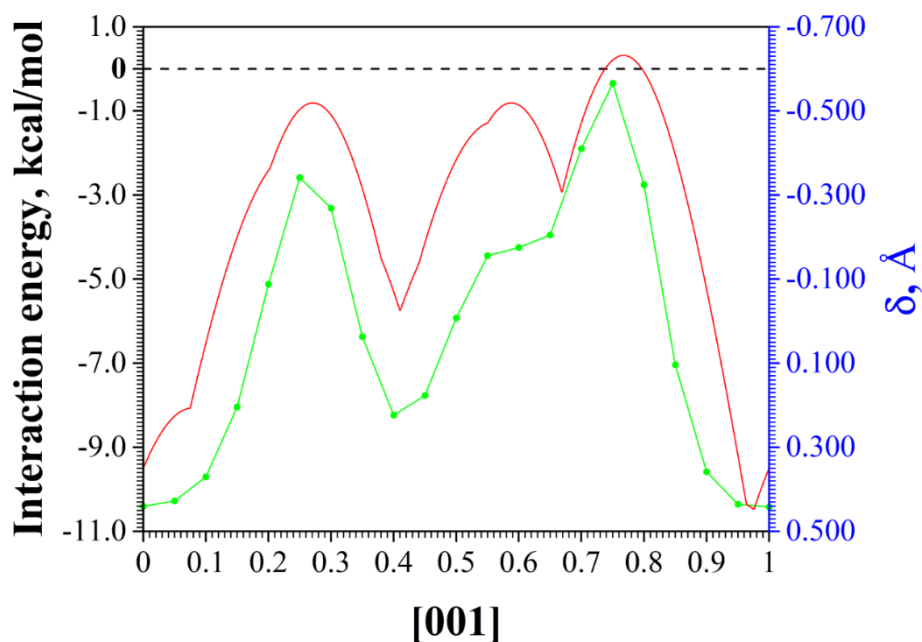


Figure A 4.47. Profiles of interaction energy (in bright green) and topological parameter  $\delta$  (in red) occurring during the shear of the dimeric building unit(s) along the direction [001] in parallel to a neighboring layer (100) with lower coordinate  $a$  in the crystals of the polymorphic modification I of ibuprofen under ambient pressure. The line of zero energy is marked as the black dashed one.

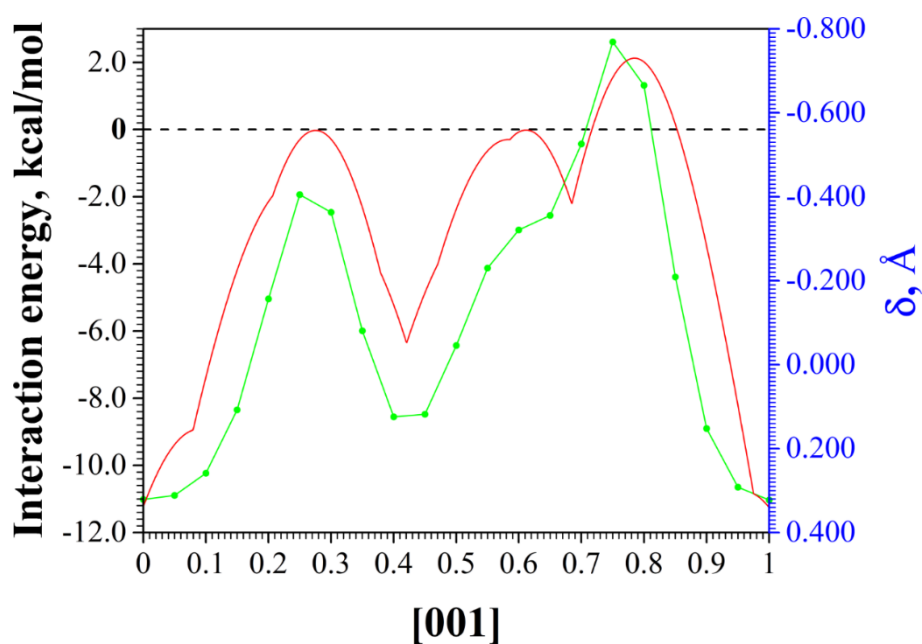


Figure A 4.48. Profiles of interaction energy (in bright green) and topological parameter  $\delta$  (in red) occurring during the shear of the dimeric building unit(s) along the direction [001] in parallel to a neighboring layer (100) with lower coordinate  $a$  in the crystals of the polymorphic modification I of ibuprofen at the pressure of 0.23 GPa. The line of zero energy is marked as the black dashed one.

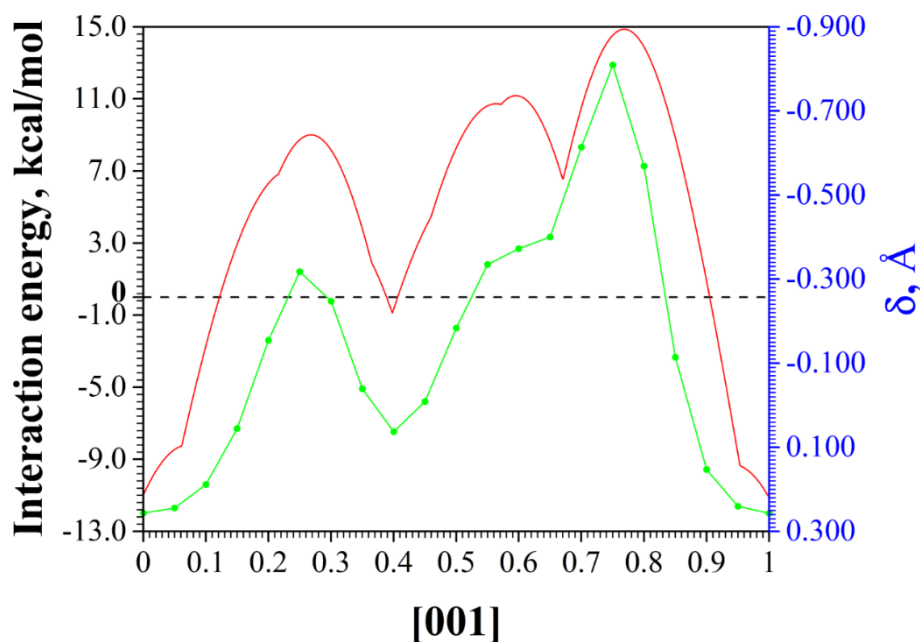


Figure A 4.49. Profiles of interaction energy (in bright green) and topological parameter  $\delta$  (in red) occurring during the shear of the dimeric building unit(s) along the direction [001] in parallel to a neighboring layer (100) with lower coordinate  $a$  in the crystals of the polymorphic modification I of ibuprofen at the pressure of 0.60 GPa. The line of zero energy is marked as the black dashed one.

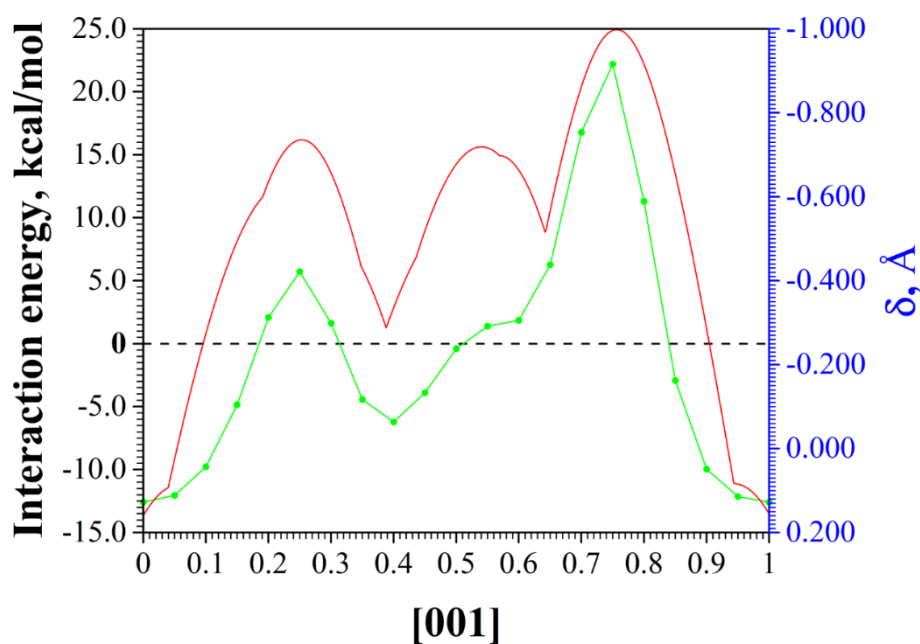


Figure A 4.50. Profiles of interaction energy (in bright green) and topological parameter  $\delta$  (in red) occurring during the shear of the dimeric building unit(s) along the direction [001] in parallel to a neighboring layer (100) with lower coordinate  $a$  in the crystals of the polymorphic modification I of ibuprofen at the pressure of 0.80 GPa. The line of zero energy is marked as the black dashed one.

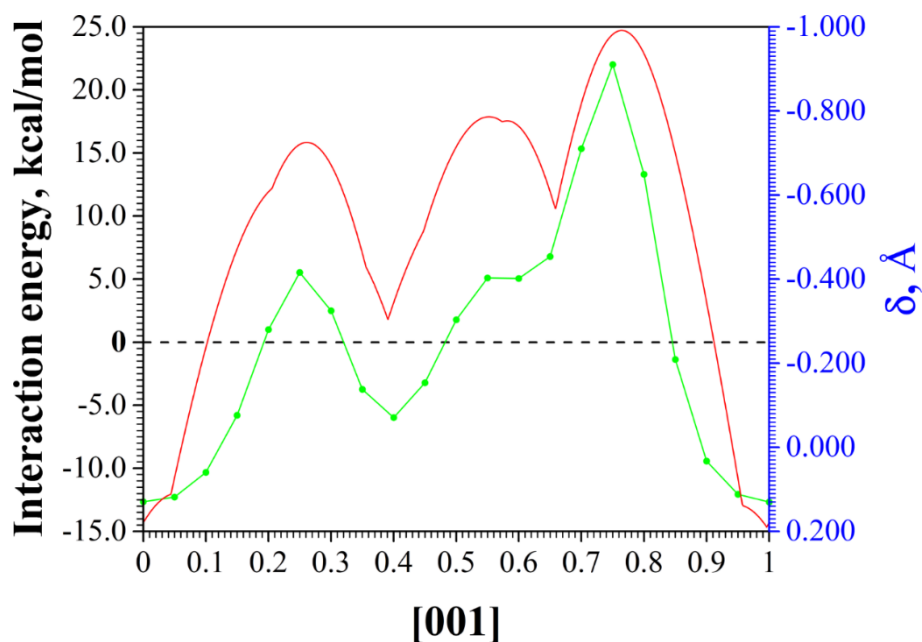


Figure A 4.51. Profiles of interaction energy (in bright green) and topological parameter  $\delta$  (in red) occurring during the shear of the dimeric building unit(s) along the direction [001] in parallel to a neighboring layer (100) with lower coordinate  $a$  in the crystals of the polymorphic modification I of ibuprofen at the pressure of 0.88 GPa. The line of zero energy is marked as the black dashed one.

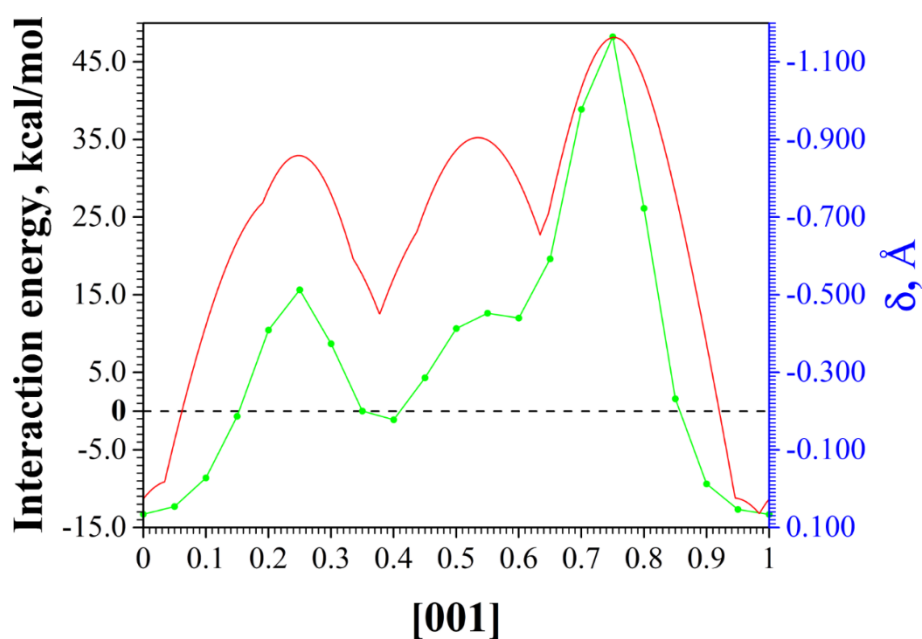


Figure A 4.52. Profiles of interaction energy (in bright green) and topological parameter  $\delta$  (in red) occurring during the shear of the dimeric building unit(s) along the direction [001] in parallel to a neighboring layer (100) with lower coordinate  $a$  in the crystals of the polymorphic modification I of ibuprofen at the pressure of 1.70 GPa. The line of zero energy is marked as the black dashed one.

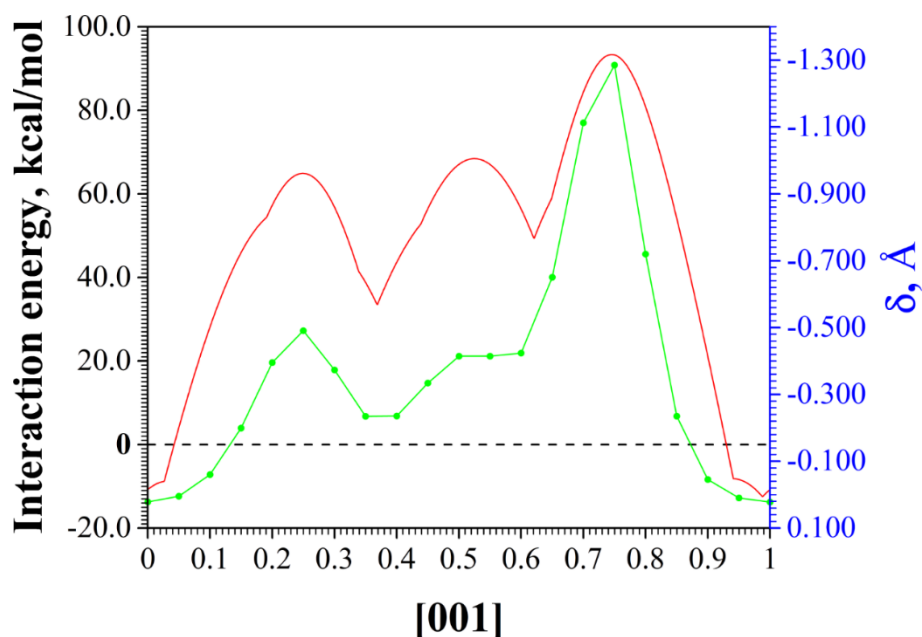


Figure A 4.53. Profiles of interaction energy (in bright green) and topological parameter  $\delta$  (in red) occurring during the shear of the dimeric building unit(s) along the direction  $[001]$  in parallel to a neighboring layer (100) with lower coordinate  $a$  in the crystals of the polymorphic modification I of ibuprofen at the pressure of 2.65 GPa. The line of zero energy is marked as the black dashed one.

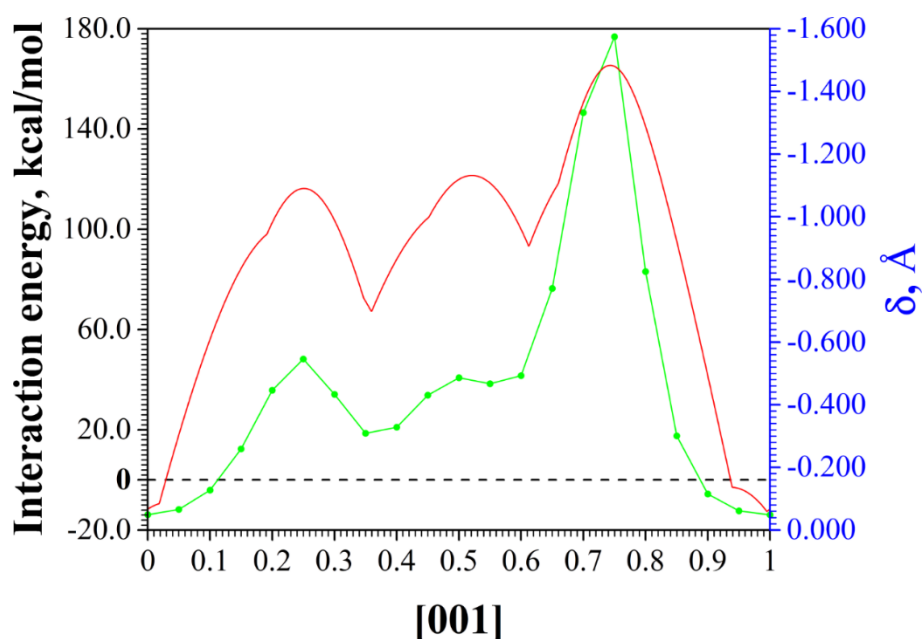


Figure A 4.54. Profiles of interaction energy (in bright green) and topological parameter  $\delta$  (in red) occurring during the shear of the dimeric building unit(s) along the direction  $[001]$  in parallel to a neighboring layer (100) with lower coordinate  $a$  in the crystals of the polymorphic modification I of ibuprofen at the pressure of 4.00 GPa. The line of zero energy is marked as the black dashed one.

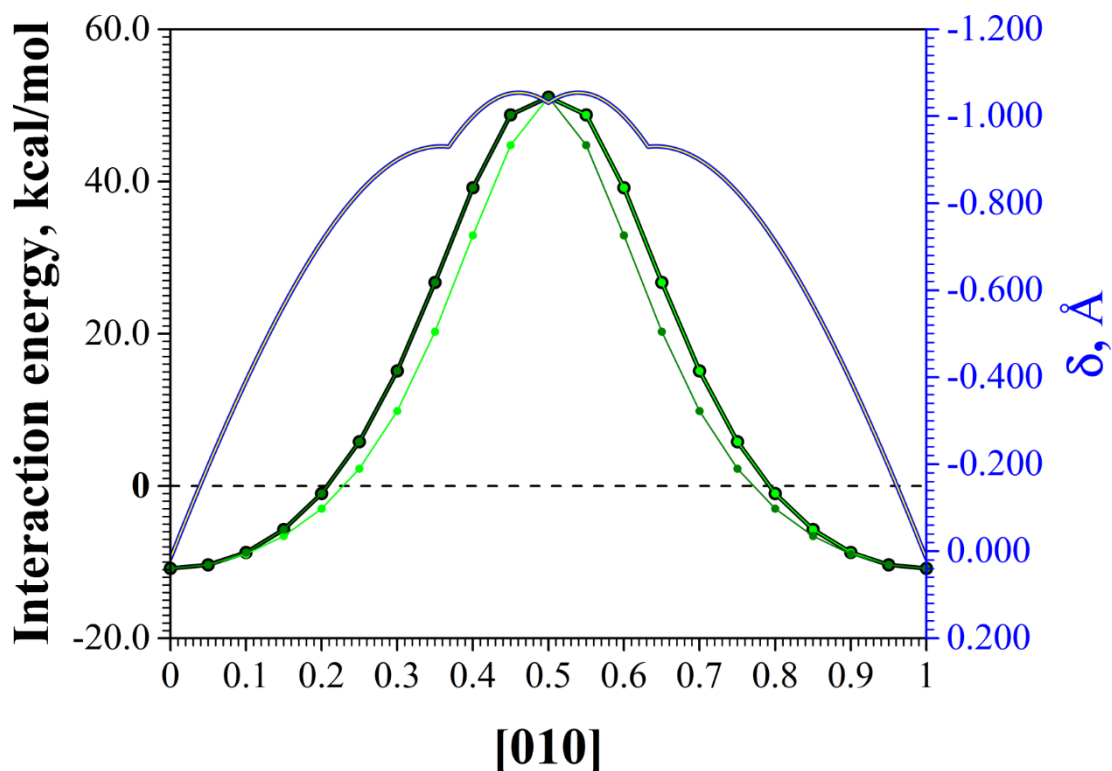


Figure A 4.55. Profiles of interaction energy (in bright green and olive for different symmetric equivalents, black for their overlap) and topological parameter  $\delta$  (in blue and yellow, similar for equivalents and their overlap) occurring during the shear of the dimeric building unit(s) along the direction [010] in parallel to a neighboring layer (100) with lower coordinate  $a$  in the crystals of the polymorphic modification II of ibuprofen. The line of zero energy is marked as the black dashed one.

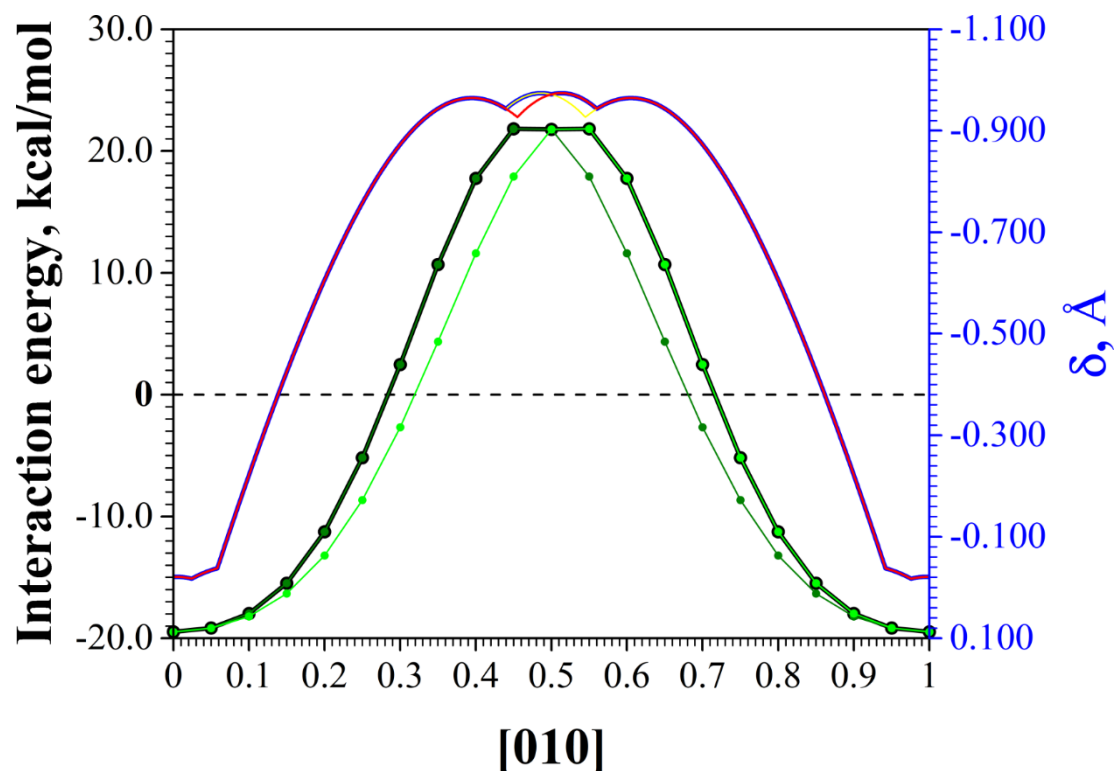


Figure A 4.56. Profiles of interaction energy (in bright green and olive for different symmetric equivalents, black for their overlap) and topological parameter  $\delta$  (in red and yellow for different symmetric equivalents, blue for their overlap) occurring during the shear of the dimeric building unit(s) along the direction [010] in parallel to a neighboring layer (102) with lower coordinate  $a$  in the crystals of the polymorphic modification II of ibuprofen. The line of zero energy is marked as the black dashed one.

## Conclusions and perspectives

Current thesis presents new suggestions in the field of solving important problems of the pharmaceutical industry, namely, the controllable synthesis of the most suitable polymorphic form and control of polymorphism of active pharmaceutical ingredients during the processing.

Chapter 3 of this thesis discusses the different possibilities of controlling the solid phases of mefenamic acid, carbamazepine and co-crystal of mefenamic acid with nicotinamide obtained during recrystallization from supercritical carbon dioxide. Two methods are proposed for this:

- Control of polymorphism of active pharmaceutical ingredient through an equilibrium of the solid phase with a solution of biologically active molecules in supercritical carbon dioxide by means of *in situ* vibrational spectroscopy (infrared and Raman).
- Analysis of crystalline phases after extraction from supercritical carbon dioxide.

The first method was used to synthesize polymorphic modifications of mefenamic acid and carbamazepine. Based on the established equilibria between the conformations in solution and in a solid sample, the parameters of state of such systems, required for obtaining pure polymorphic modifications of the aforementioned active pharmaceutical ingredients, have been proposed. Spectra of solutions of individual conformers were obtained, which are necessary to crystallize pure stable modifications I and III of mefenamic acid and carbamazepine respectively and their metastable forms II and I. They can be used as references in the synthesis of the desired polymorphic modifications or as an additional tool that increases the reproducibility of methods of their synthesis.

The second method is not new itself, being the most common method for controlling polymorphism. However, it is not possible without the presence of strictly verified reference powder patterns, vibrational spectra or thermal

analysis curves of the desired polymorphic modification. We have proposed a technique for the growth of high-quality single crystals directly from a solution of bioactive molecules in supercritical carbon dioxide using the example of a co-crystal of mefenamic acid and nicotinamide. Single crystals can be used to easily determine the crystal structure of the resulting product. As a consequence, the calculated and experimental reference powder patterns for the exactly same conditions of crystallization can be obtained and, further, the spectral and thermal data collections can be formed.

Chapter 4 of the dissertation examines the possibilities of analyzing and predicting polymorphic transitions in the processing and storage of already crystallized solid phases. Polymorphic modifications of many substances during mechanical processing such as grinding or tableting or long-term storage are able to change their structure. This is especially true for the desired metastable forms with higher solubility, manufacturability, etc. Thus, a tool capable of predicting the stability of crystalline modification in various manufacturing processes is essential for the pharmaceutical industry.

We propose a multi-step approach based on the quantum-chemical calculation of the energies of interactions between the basic structural motives of the crystal structure during displacement. It allows one to estimate the directions of the simplest shear deformation in any molecular crystal, whose structure is known, and also to reveal possible polymorphic transformations. Our methodology minimizes the number of calculations required and consists of the following steps:

1. Evaluation of the structure of crystals in terms of pairwise interaction energy in order to identify the preferred slip planes.
2. Analysis of the topological characteristics of separated layers to identify the fundamentally possible directions for their mutual shift.
3. Quantum-chemical calculation of the shift energy profiles for the displacement of building units along the layers in the identified directions

in the crystal structure, determination of local extrema of the interaction energy during translation and shift energy barriers.

This approach was tested for the first time on a well-studied aspirin polymorphic forms I and II. A correlation was found between our calculations and an abundant base of experimental studies of mechanical properties. Low stability of the metastable phase IV of aspirin was also predicted from its crystal structure.

The second object for method verification and development was piracetam, whose reversible polymorphic transformation was studied in detail using high-pressure experiments in a diamond anvil cell. The signs of a future polymorphic transition can be observed under ambient conditions. They are the appearance of a local minimum on a shear energy profile and its accessibility from the original position of molecules in a crystal (small shear energy barrier). It was also found that the following two ratios of the components of pairwise interaction energy are important for the possibility of a polymorphic transition:

- Attraction (the sum of electrostatic, polarization and dispersion) and repulsion (the sum of repulsion and exchange).
- Hydrogen bonding (the sum of electrostatic and polarization) and dispersion.

The last active pharmaceutical ingredient studied by us, ibuprofen, does not exhibit a polymorphic transition upon compression, although it can undergo transformation to amorphous state upon grinding with mesoporous silica. The reasons for such behavior, as well as the various types of shear deformation, were considered. Four possible types of shear in the crystal structure were formulated. Optimal conditions, more precisely, low pressure, were proposed to achieve the displacement of layers in the structure of polymorph I of ibuprofen due to low shift energy barriers. The directions that are difficult to reach during the compression along the normal to the crystal surface were also noticed. Thus, the grinding can be actually called optimal for the polymorphic transformation of ibuprofen.

Taken together, the results of the present thesis create the basis for reliable control of the polymorphism of active pharmaceutical ingredients at all stages of the production of dosage forms and can be used for the further development of the pharmaceutical industry. For example, like this:

- Formation of databases of X-ray, spectral and thermal data of individual polymorphic forms, as well as spectra of the corresponding conformations of bioactive molecules in various solvents, in particular supercritical CO<sub>2</sub>, to simplify the control over the pharmaceutical production.
- Analysis and prediction of probable solid-state polymorphic transitions and mechanical properties of individual polymorphic modifications used in pharmaceutical production by means of quantum-chemical calculations.
- Acquisition of metastable polymorphic modifications of active pharmaceutical ingredients and the creation of stable dosage forms based on them by combining supercritical solvent-free crystallization technology and excluding the formation of new phases during processing using the proposed computational approach.